RECHARGE UNCERTAINTY ANALYSIS OF MAJOR AQUIFERS IN TEXAS

A Thesis

By

AARON PENA RODRIGUEZ

Submitted to the Office of Graduate and Professional Studies of
Texas A&M University
in partial fulfillment of the requirements of the degree of

MASTER OF SCIENCE

Chair of Committee, Gretchen R. Miller
Committee Members, Ronald Kaiser
Hongbin Zhan
Head of Department, Ronald Kaiser

May 2020

Major Subject: Water Management and Hydrological Sciences

ABSTRACT

While the reduction of the groundwater available volume in the state of Texas of urban, agricultural, and industrial use has been dealt with in different ways, the first step is to assess the current and future behavior of the aquifers that supply it. For this the Texas Water Development Board created the Groundwater Availability models. This paper studies the recharge data used to build them and how the sensitivity to changes in recharge of each aquifer can affect the available groundwater statewide to point to interest aquifers that need a more in-depth recharge analysis. The reported recharge in the models was variated from 50% to 150% to determine changes in head, stored volume, and overall baseflow. The normalized variations where then compared to select the most and least recharge sensitive aquifers to perform a recharge surge reflecting that of hurricane Harvey (1000% normal recharge) in the Gulf Coast Center (Houston, Texas) to determine the behavior when subjected to atypical recharge events.

Given the great geohydrological variability, not only inside the aquifers, but between the analyzed aquifers, the changes in head, volume, and baseflow do not only follow the greatest increase in recharge. The Hueco Mesilla Bolson aquifer experienced the least absolute change in mean head (0.0003% of normal head), paired with the lowest absolute change in recharge ($0.004 m^{-1} y^{-1}$). However, the Edwards Balcones Fault Zone Springs (near San Antonio, Texas) experiences the largest absolute change in recharge ($0.370 m^{-1} y^{-1}$), but the Gulf Coast North experienced the largest absolute change in mean head (42% of normal head).

While the differences in composition and size of the aquifers make a complete comparison difficult, the most sensitive aquifers, determined by the linear model to which head and stored volume were subjected to, were determined to be the Trinity North and the Edwards Trinity Plateau for respectively. These two can be the focus of subsequent and more localized studies to determine the feasibility of the recharge driven strategies to increase the groundwater availability of Texas.

ACKNOWLEDGEMENTS

I would like to thank to my committee chair and advisor Dr. Gretchen R. Miller, for her unwavering guidance, support, understanding, and encouragement through the course of this research and my stay at Texas A&M College Station. Also, to my committee members, Dr. Ronald Kaiser and Dr. Hongbin Zhan, for their input and support that helped me complete this research.

To the Water Management and Hydrological Sciences department heads, Dr. Ronald Kaiser and Dr. John R. Giardino and the program coordinator Dr. C. Prakash Khedun, thank you for their support along my Master's Program.

Thanks to Shirley Wade, at the Texas Water Development Board for sharing the Groundwater Availability Models, without which this research wouldn't have been possible.

Thanks to Elise, at Aquaveo Technical Support, for helping me get all the models up to working in GMS.

To my undergrad research group colleagues, Emily Schweizerhof, Camille Sico, and Melanie Latham for adding me with the large data volume to be processed. And my graduate research group colleagues for the feedback necessary to achieve this research.

Thanks also go to my friends and colleagues and the department faculty and staff for making my time at Texas A&M University a great experience.

Finally, thanks to my father, mother, and brother for their always present love, encouragement, and support in this incredible endeavor that was my Master's.

CONTRIBUTORS AND FUNDING SOURCES

Contributors

This work was supervised by a thesis committee consisting of Professor Gretchen R. Miller (advisor and chair) of the Department of Civil Engineering, Professor Ronald Kaiser, of the Department of Recreation, Park and Tourism Sciences, and Professor Hongbin Zhan of the Department of Geology and Geophysics.

The data analyzed for the Edwards Balcones Fault Zone North was conducted by Emily Schweizerhof.

All other work conducted for the thesis was completed by the student independently.

Funding Sources

This work was made in part possible by the funding by BANXICO, under their FIDERH (Fondo para el Desarollo de Recursos Humanos; Human Resources Development Fund) program. Its contents are solely the responsibility of the authors and do not necessarily represent the official views of BANXICO.

Graduate Travel Grant from the Water Management and Hydrological Sciences program to attend AGU 2019 to present this research.

TABLE OF CONTENTS

Page

LIST OF FIGURES

Page

LIST OF TABLES

Page

1. INTRODUCTION

The ability to quantify and predict available groundwater state-wide is a powerful tool used for planning for the future and implies knowing the resources at hand, their distribution, their origin, and what causes changes in said amounts. Currently, the Texas Water Development Board (TWDB) follows the 2017 State Water Plan, which has a 2050 planning horizon. In order to meet the requirements of the Water Plan, the TWDB commissioned the creation and/or updating of a series of computer models of the aquifers in the state (Bruun et al., 2017). These models rely on all the pertinent hydrogeologic properties of the aquifers and on the recharge estimations for each one of them, which vary greatly (George & Mace, 2011). Therefore, a better understanding of the uncertainty surrounding Groundwater Availability Models (GAMs) predictions under uncertain recharge inputs is important for future decision making.

The overall objective of this research is to determine the sensitivity of major GAMs to changes of recharge. The different methods of estimating and modeling recharge and how they are incorporated in the aquifer models will also impact the effect recharge has on the overall behavior of the aquifer. Once determined how each GAM reacts to recharge, the sensitivity of said model can be determined and, when compared to the other models, can be used to ascertain the areas that require a more in-depth analysis from the recharge point of view. Locating areas, or aquifers, that require more study as of to how they react to changes in recharge helps to paint a more accurate picture of the analyzed aquifers and to help achieve the objectives posted in the 2017 Water Plan which points to recharge-type projects as the only feasible alternative to the decrease of groundwater availability (Bruun et al., 2017).

1.1. Texas Groundwater Availability Models

In 1999, the TWDB created/commissioned the GAMs, which were needed due to the size of the Texas (270,000 mi^2), the numerous aquifers within its borders, and the importance of groundwater availability for the sustainable development of the state across the agricultural, urban, and industrial sectors (Bruun et al., 2017). Each one of the models represent a hydrologically distinct segment of an aquifer and is intended as a tool to determine the variability in availability of groundwater across the state. The majority of them have been constructed in MODFLOW using its different versions such as MODFLOW 96, 2000 and Unstructured Grid (USG).

There are currently 19 GAMs for the mayor aquifer systems, each one built in a different moment and updated when important data is collected that can improve the accuracy of the models. Larger aquifers, such as the Carrizo-Wilcox system and the Gulf Coast aquifer have been divided in three distinct sections that run separately. These divisions follow the differences in distinct hydrogeological characteristics of the aquifers but also are a practical decision, since even though a complete model of the whole aquifer could be beneficial, it could be near impossible to run the model, due to its complexity, in standard computers rendering them unusable. Another reason to delineate separate sections of a whole aquifer that are to be modelled separately is data availability. The northern section of the Gulf Coast aquifer encompasses the city of Houston, one of the most important cities not only in the state but in the country and, due to its growth and importance, several studies are taking place around it and more accurate data is available for the model. The central and south sections, however, have less detailed data available and have their own separate

GAM's. Figure 1.1 shows the mayor aquifers that exist in the state and their geographical distribution.

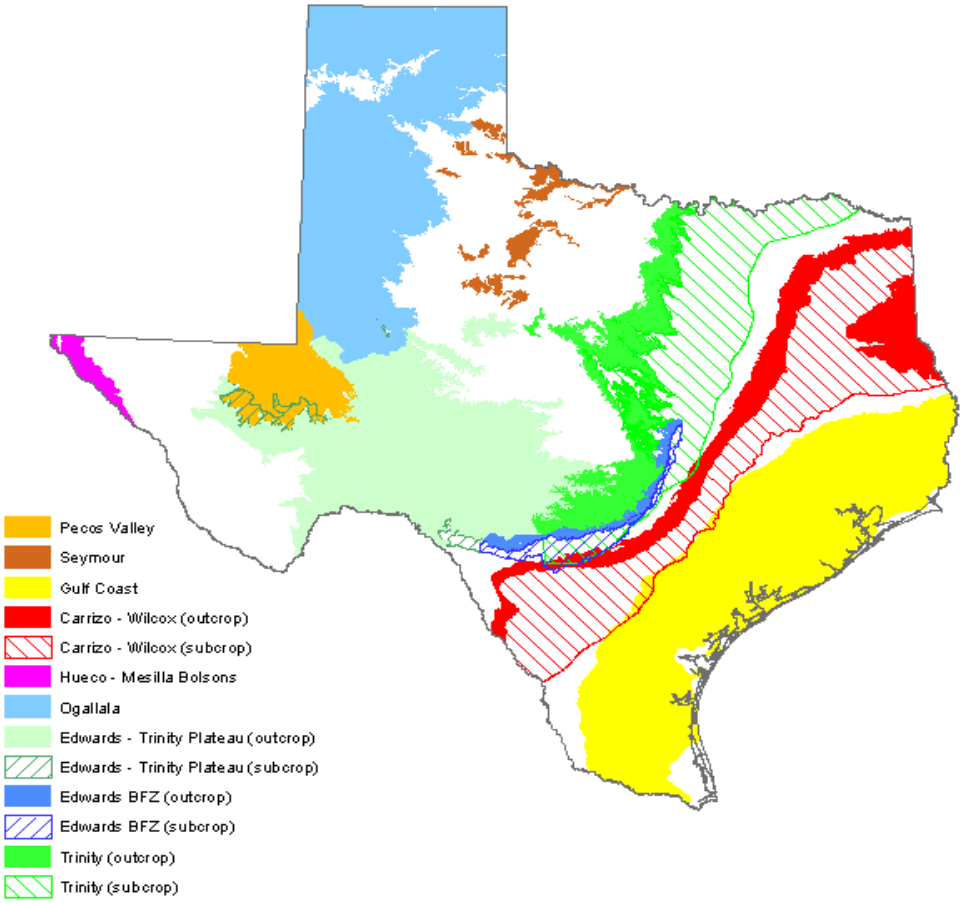

Figure 1.1 Major aquifers in Texas, (George & Mace, 2011)

At its core, each GAM complies parameter sets (hydraulic conductivity, specific yield, specific storage) based on data from its aquifer section and solves the governing groundwater flow equation (GFE) for all the specified cells in the model using an iterative process. Each GAM is constructed of different layers, which are divided in cells and for each cell the partial GFE is solved. Since the models need to predict long-term changes which are transient in nature, each GAM also solves the GFE for a user-determined timeframe and a set number of time steps in said

timeframe. Finally, the iterative process repeats the solving of the whole array of equations at each timestep until convergence is reached; this means, until the solutions encountered satisfy the whole array of equations for a given timestep and then, moves to the next timestep and solves the whole array again taking the previous solution as the new starting point. For a solution to be encountered, an initial state has to be provided to the model and, based on that initial state, the model continues solving the array.

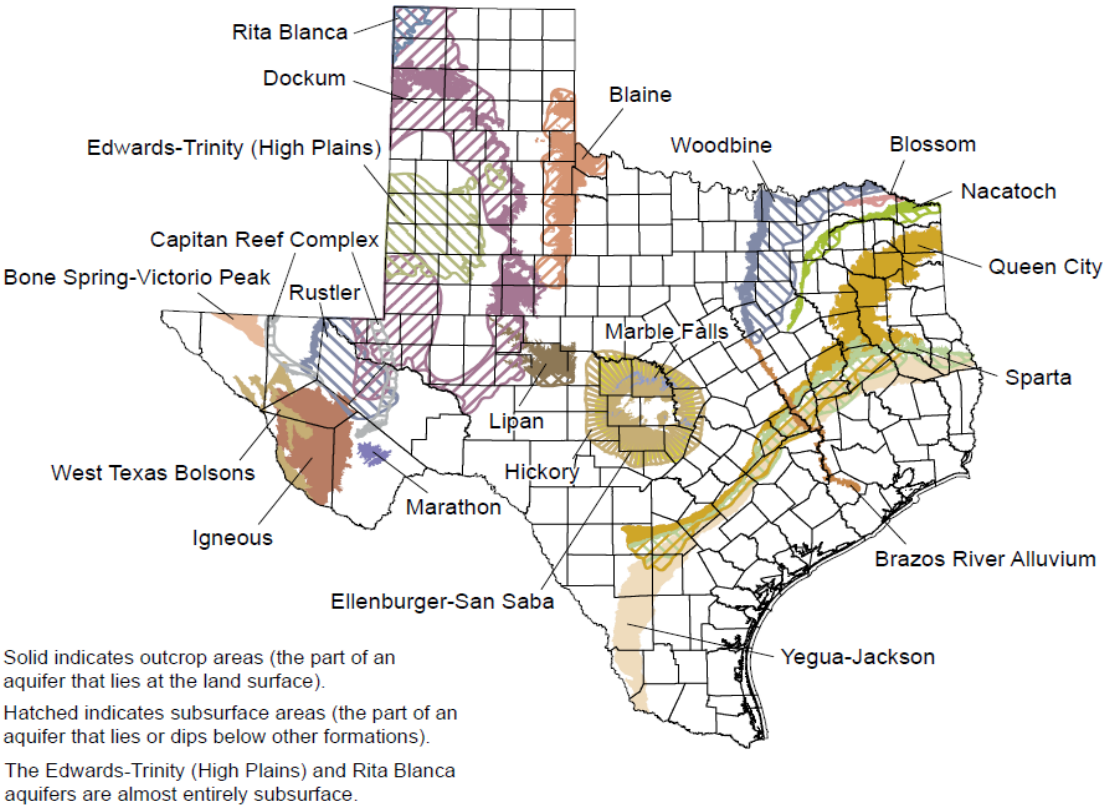

Figure 1.2 Minor aquifers in Texas (George & Mace, 2011)

Alongside the mayor aquifers in the state, figure 1.2 shows the minor aquifers in Texas. Even though they are smaller than the mayor aquifers, their importance both as water supplies and research focus makes them another interest point for this research. The Brazos River Alluvium

Aquifer (BRAA) is the one minor aquifer analyzed for its recharge sensitivity, since it has several interesting characteristics such as the clay compartmentalization created by clay deposits.

1.2. MODFLOW

The Modular Three-Dimensional Finite-Difference Ground-Water Flow Model (MODFLOW) was coded by the USGS in the early 1980's as a tool to solve water-resource problems in the US. (McDonald & Harbaugh, 2003). The idea of a modular program in which each package (module) could be used independently, without affecting the others, opened the door for tailored simulations that could be specific to the problem that was being studied. Said packages could be activated, interchanged, and manipulated independently from each other to reflect the system under study and also allowed the incorporation of new packages along the time to address new problems. The standardization of the format (FORTRAN 66) of the code and the data inputs and outputs also gave the program a great flexibility to be ran in different computer brands and, with the advent of personal computers and the phasing out of mainframes, allowed researchers to obtain standardized data fit for comparison instead of the mismatch of data formats form the myriad of codes that had been used prior to its creation (McDonald & Harbaugh, 2003). Table 1 shows the different MODFLOW version in which the analyzed GAMs were built.

1.2.1. MODFLOW USG

One of the latest additions to MODFLOW was the ability to define an unstructured grid to represent the aquifers in MODFLOW Unstructured-Grid (USG). This grid allows for different cell

sizes along the model which contrasts with the single size and uniform grids from the previous models and this confers the modeler the opportunity to refine the grid in areas of interest to obtain more detailed behavioral data from the model (Panday et al., 2013). A perfect example of its applications, even thought it was coded in the beta of the USG, is the BRAA. The characteristics of this aquifer and the great spatial variability of its characteristics near the Brazos River, requires a finer approach. USG incorporates both the fine detailed modeling of the river banks and flood plain and its immediate interactions with the BRAA and the larger aquifer area to model it as a whole instead of just the regions closest to the river itself.

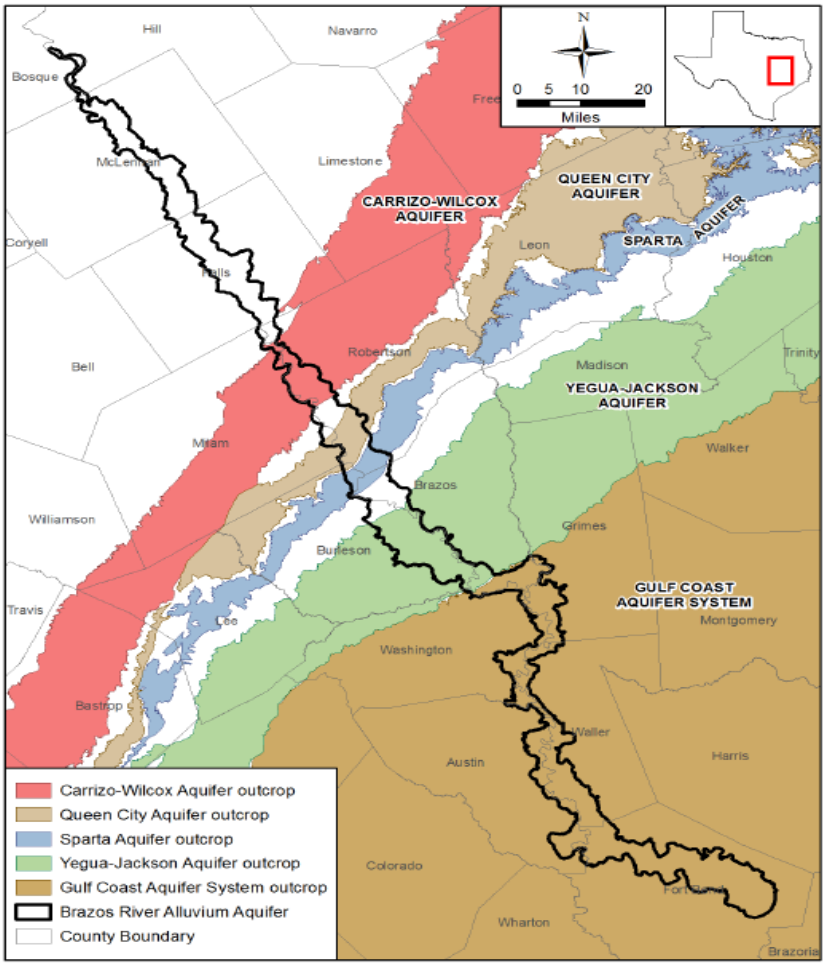

Figure 1.3 BRAA boundaries and mayor aquifers interactions (Ewing et al., 2006)

In a standard MODFLOW model a tradeoff between accuracy and efficiency would had have to be reached, since small enough cells as the ones need near the river would have rendered the model virtually unusable, and large enough cells to cover the extent of the aquifer would mean that the cell size would dilute the effects, reactions, and interactions between the surface and underground sections of the system (Ewing & Jigmond, 2016). For larger aquifers, this tradeoff is avoided by splitting them into several sections to allow for independent and feasible modeling of the quasi-independent sections. For the case of the BRAA's GAM, figure 1.3 shows its location in relation to other mayor aquifers and the different orientation compared to said aquifers.

1.2.2. MODFLOW Packages

As it has been stated before, MODFLOW is comprised of separate and independent packages (modules). These packages address the different "formulators" in the model and are what gives to MODFLOW its versatility. McDonald and Harbaugh (2003) described the "formulators" as the inputs that create the terms into the finite-difference equations that are solved by the program. They all contribute to the overall behavior of the modeled aquifer and can be modified independently to add or subtract information. Furthermore, since they are not dependent from one another, new packages can be added to improve the model or to aid in the post-processing of the obtained data. Some of the packages that were used in this research are the River, Stream, Drain, Recharge, Drain, Reservoir, and Block Centered Flow packages. Given that the main focus in the present is the sensitivity to recharge of the aquifers, the recharge package will be the most used.

1.2.2.1. River Package (RIV)

The river package consists in the introduction of a "river cell" into a node of the grid. This cell is a sink-source inside the model, since it both introduces and extracts water volume out from the system. The parameters that this package needs are: River stage, riverbed conductance, and riverbed bottom elevation (Harbaugh et al., 2000). With this, MODFLOW is able to compute the head coefficient that the river cell will have in a giver time step of the simulation. However, it only calculates leakage between streams and the aquifer systems (Prudic, 1989). To address its limitations, the Stream Package was created and introduced. Both these packages can be used in tandem to simulate a river system and its interactions with the aquifer system using Equations 1.1 or 1.2 depending on the head inside the river cell.

$$QRIV_{nb} = CRIV_{nb}(HRIV_{nb} - h_n), \quad h_n > RBOT_{nb} \tag{1.1}$$

$$QRIV_{nb} = CRIV_{nb}(HRIV_{nb} - RBOT_{nb}), \quad h_n \leq RBOT_{nb} \tag{1.2}$$

Where $QRIV_{nb}$ is the flow between the river and the aquifer; $HRIV_{nb}$ is the water level (stage) in the river; $CRIV_{nb}$ is the hydraulic conductance of the river-aquifer interconnection; h_n is the head at the node in the cell underlying the river reach; $RBOT_{nb}$ and is the river's bottom elevation. MODFLOW provides an acceptable approximation of $CRIV_{nb}$ with Equation 1.3.

$$CRIV_{nb} = \frac{K_{nb}L_{nb}W_{nb}}{b_{nb}} \tag{1.3}$$

Where K_{nb} is the hydraulic conductivity of the riverbed material; L_{nb} is the length of the conductance block; W_{nb} is the river width; and b_{nb} is the thickness of the riverbed layer.

1.2.2.2. Steam Package (STR)

In addition to the leakage that the River Package calculates, the Stream Package has been coded to route flow thorough the streams (streams include rivers, streams, ditches, and canals) (Prudic, 1989). For this porpoise, the package uses Manning's formula and coefficient applied to all of the stages along the stream meandering. Since it not only calculates the leakage, the STR package requires more data that the RIV package; particularly the direction in which the streams flow, the initial or incoming flow from outside the system, the connections between the different streams in the system, and the diversions if they are present. With all this information the STR package not only calculates the leakage inside on out the stream cells, it also routes the water flow along the stream using equations 1.4 and 1.5.

$$QSFR_{nb} = S^*_{SFR,nb} \frac{K_{nb} L_{nb} W_{nb}}{b_{nb}} (HSFR_{nb} - h_n), \quad h_n > SBOT_{nb} \tag{1.4}$$

$$QSFR_{nb} = S^*_{SFR,nb} \frac{K_{nb} L_{nb} W_{nb}}{b_{nb}} (HSFR_{nb} - SBOT_{nb}), \quad h_n \leq SBOT_{nb} \tag{1.5}$$

Where $QSFR_{nb}$ is the flow between the aquifer and the stream, $S^*_{SFR,nb}$ is a cubic saturation function, K_{nb} is the hydraulic conductivity of the sediments underlying the reach, L_{nb} is the length of the reach in the cell, W_{nb} is the width of the reach, b_{nb} is the thickness of the reach streambed

sediments, $HSFR_{nb}$ is the simulated stage un the reach, h_n is the head at the node underlying the reach, and $SBOT_{nb}$ is the bottom elevation of the streambed sediments. $S^*_{SFR,nb}$ varies from 0 to 1 for the stream depths ranging from 0 to a small value above the top of the streambed, respectively. In this approach, transient leakage across the streambed sediments could change, depending on both the stream stage and the aquifer head calculated during the time step. The RIV Package requires that the conductance term ($\frac{KWL}{b}$) be specified for the streambed sediments. In the SFR Package, the conductance term is calculated from the hydraulic conductivity, stream width, stream length, and streambed sediment thickness.

1.2.2.3. Recharge (RCH)

Along with the Evapotranspiration package and other layer data packages, the Recharge package represents a source or sink of water in all the cells of the model's first layer. It represents the input of water due to precipitations to the aquifer and, if present in a multi-layer model, operates in the top cell of each column (equation 1.6). Its effects, as all the other source/sink packages is quantified in the head coefficient of the groundwater flow equations.

$$QR_{nb} = I_{nb} M_{nb} A_n \tag{1.6}$$

Where QR_{nb} is the recharge flow rate applied to the node n; I_{nb} is the recharge flux applicable to the map area, A_n , of the cell; M_{nb} and is the area multiplier that can be used to scale M_{nb}.

Being this the most used package, as it controls the recharge along the whole aquifer modelled, it is also important to point out to the Multiplier and Use Previous tools present in GMS. While MODFLOW natively requires a separate Multiplier Package, in GMS this functionality is incorporated one step before the coefficients are calculated and this, only affects the data inside the model without changing any data files in the process.

1.3. GMS

While MODFLOW is a command-line program (built in FORTRAN and operated from a DOS command-line window), some graphic interphases have been built for it. One of them is the Groundwater Modeling System (GMS) from Aquaveo ® (Aquaveo Inc., 2017). This graphic interphase allows the user to create and manipulate the MODFLOW models in a more user-friendly way without having an in-depth knowledge for MODFLOW and its programing. The versions used for this research were GMS 10.3 and 10.4 since the update came out mid-project. In some cases, such as the BRAA, the version of MODFLOW USG in which it was constructed (MODFLOW USG beta) is not compatible with GMS (even though GMS supports USG) and the model had to be run in its command-line form.

1.4. Recharge estimations

Recharge plays an important role in the behavior and availability of groundwater for the state, as such it is the focus of this research; however, there are several methods for estimating the recharge in the aquifers such as the baseflow separation method, chloride mass balance method,

diffuse, main-channel, and flood flow method, climate estimations method, hydrograph separation method, and gage stations method.

Allison and Hughes (1978) describe the use of chlorine (Cl^-) as a suitable method to estimate recharge to aquifers since its increase in concentration (due to evaporation) gives better results than the use of tritium. Chlorine, as tritium, is a naturally occurrent element of precipitation and its mass balance can be used to estimate recharge in a method known as Chlorine Mass Balance. With the known concentration of chlorine in the groundwater and the concentration in the precipitation, the influx can be calculated to determine the recharge rate of an aquifer. This method can also be used with a different tracer, such as tritium, but the uncertainties related with this tracer, such as the requirement of detailed precipitation time series data and the recreation of tritium un the vadose zone (Li et al., 2019), plus the low concentrations of it both in precipitation and groundwater and the need of a spectrometer for accurate measurements, leads chlorine to be a more widely used method in the Texas aquifers.

A similar method to determine recharge is the Total Dissolved Solids (TDS) Mass Balance. Similarly, to the Chlorine mass balance, the TDS mass balance relies in the estimation or recharge by measuring the changes in the concentration of a tracer in the groundwater known the input it receives from precipitation (infiltration).

Both mass balance methods, apart from relying in accurate measurements of the concentration both in the groundwater and precipitation, are based in the assumption that the groundwater system has reached a steady state. This state can take from 20 to 400 years (Allison & Hughes, 1978) to be reached and needs a long time of accurate measurements or the availability

of a long and accurate historical record of concentration readings that is not always available. Another problem with the balance methods, pointed out by Allison and Hughes (1978) and Li et al. (2019), is that these methods are susceptible to changes in the land use; since they require long term data and concentration measurements, changes in the land use will affect its accuracy and can take several years to be reflected in the calculated recharge.

The climate estimation methods consist in the use of precipitation and its correlation with recharge to estimate, based on previous recharge and precipitation data, the recharge present in the aquifer. Mohan et al. (2018) created a global empirical model to estimate recharge form climatological and land use information obtaining Precipitation, and Potential Evapotranspiration as the most influential meteorological factors in the groundwater recharge phenomena. From their findings, it can be deducted that recharge can be estimated with meteorological data but, for a local usage, the model needs to be calibrated with historical data. This method, with the Percentage of Precipitation also used in some of the GAMs (the Edwards Balcones Fault Zone North), relies in accurate precipitation data to estimate recharge.

The third group of methods used are the flow methods. They rely in the accurate measurement of the flow in channels, rivers, and streams along the aquifer to determine both diffuse and localized recharge. With the precipitation in the aquifer and the exit flow from its recharge area, they can estimate both the diffuse recharge that occurs from precipitation-runoff and the localized infiltration taking place in the riverbeds. A balance between the input (precipitation) and the flow at a gage station estimates the total recharge to the aquifer which can then be distributed using precipitation as a base since precipitation data is more prevalent.

All the recharge estimation methods rely in some or other historical dataset to determine the recharge to the aquifers and, while when provided with the appropriate data the mass balance methods can be more accurate, the need for long records of accurate historical data of precipitation and recharge (potential evapotranspiration and tracer concentration in some cases) makes them unfeasible to be applied in some cases. Added to the need of data, the uncertainties inherent to the estimation methods, even if the uncertainty of the data estimation and measurement of the parent data for them is not taken into account, produce a value of most probable recharge for the aquifers. Due to this, it is important to analyses how the aquifers react to higher or lower recharge than the estimated one, which is just a good estimate. The obtained sensitivity information helps not only with the better understanding of the aquifers and their behavior, but with the proofing of the accuracy of the recharge data used to create the GAMs since it highlights the possible shortcomings it can have.

1.5. Study areas

Given the reliance of the state on the different aquifers (George & Mace, 2011) as a water source for different activities (urban, agricultural, and industrial), the recharge sensitivity analysis was conducted in eight aquifers: seven mayor and one minor (BRAA). The mayor aquifers analyzed were: Ogallala, Gulf Coast, Carrizo-Wilcox, Hueco-Mesilla Bolson, Edwards-Trinity Plateau, Edwards Balcones Fault Zone, and Trinity. The number of geohydrological sections and GAMs in which each aquifer is divided (Table 1.1), the hydraulic characteristics of each section (Table 1.2) and the recharge estimation method used to determine the recharge and the mean recharge along the aquifer (Table 1.3) are the initial step to the analysis of the GAMs. While the

mentioned aquifers provide more than 85% of the available groundwater volume state wide, the BRAA was included as well due to its characteristics. Being an alluvial aquifer created by the meandering and deposits of the Brazos River, it has a unique morphology that renders it an interest aquifer from the sensitivity point of view to assess how alluvial aquifers with compartmentalization react to changes in recharge.

The Hueco-Mesilla aquifer is located in the west of the state and serves as a water source to El Paso, TX. It is recharged by mountain front recharge and seepage from the Rio Grande. Since it has a low hydraulic conductivity (Heywood & Yager, 2003) and high pumping rates due to the growth of the city of El Paso, recharge is slow to reach the water table and when it does, it distributes slowly along the aquifer. Precipitation in this area is low as well, contributing to the low recharge of the aquifer but, since it lies outside of any GCD's the recharge data used to generate its GAM is estimated from climate variations assuming a linear correlation of precipitation to recharge (Heywood & Yager, 2003).

Two overlaying geological formations (the Wilcox group and the overlaying Carrizo formation) constitute the Carrizo-Wilcox hydrological unit known as the Carrizo-Wilcox aquifer. It extends from the Rio Grande diagonally north-east to Arkansas and Louisiana and is conformed of local sand interbedded with graven and clay (Young et al., 2018). Its great hydraulic conductivity variability and eight layers, as well as its narrow-strip form, required the creation of three GAM's to model it. Each one of these sections, though interconnected in reality, are modelled separately with its own set of parameters that originated from the several metropolitan and agricultural areas that depend on it for water such as the Bryan-College Station region. The conductivity varies greatly, from 0.5 m d^{-1} (Schorr & Zivic, 2018)in the north to 13.7m d^{-1} in the

central section (Young et al., 2018), the recharge has been estimated with chlorine tracer and calibration in the northern and central section, respectively.

Deemed one of the most important aquifers in the state (and in the neighboring states of Kansas, Colorado, Oklahoma, Wyoming, South Dakota, Nebraska and New Mexico), the Ogallala aquifer provides groundwater for agriculture in the northern region of the state making it a vital part of the state's economy. In Texas alone, 95% of the water extracted from the Ogallala is used in agriculture (George & Mace, 2011). Being this important, the data available for this aquifer is extensive, tracer methods and calibration have been used to calculate the recharge along the aquifer. Overlaying the Edwards-Trinity formation, the sandy Ogallala formation has a great hydraulic conductivity 4.5 m d^{-1} to 20.7 m d^{-1} (Dutton et al., 2001) creates an imbalance when paired with the low recharge in the aquifer and the high pumping rate to which the aquifer is subjected.

Underlaying the Ogallala formation, the Edwards-Trinity formation contains the Edwards-Trinity Plateau aquifer. Consisting of limestone and dolomite from the Edwards group and sands from the Trinity group, the aquifer has a good secondary porosity (faulted and fractured limestone) with and average to low hydraulic conductivity that ranges from 0.7 m d^{-1} to 2.6m d^{-1} (Anaya & Jones, 2009). In regards to recharge, both hydrograph separation and chlorine tracer methods have been used to estimate it producing data with a good certainty along the aquifer.

Originated form similar limestone formations than the Edwards-Trinity, the Edwards Balcones Fault Zone (Scanlon et al.) is a narrow aquifer that extends diagonally in the central section of the state. Being a highly permeable aquifer, springs are common along it. This is also

reflected by its high hydraulic conductivity in certain sections and aided by fractures that allow for rapid water movement. It is the primary water source of the city of San Antonio, and the city has conducted several studies of the aquifer to ensure that this supply is not interrupted. When subjected to heavy pumping, the water table drops significantly but, due to the great permeability, it recovers when the proper recharge presents itself. Because of this, several recharge studies have been conducted, concentrated in the section corresponding to San Antonio where a sensitivity analysis has been conducted to determine the parameters that affect the water availability the most (Lindgren et al., 2004) as well as tracer studies to estimate the recharge.

Being an alluvial aquifer, the Brazos River Alluvium Aquifer extends along the Brazos River and has 79 miles of width and 350 miles of length. Since it was created by deposits from the Brazos River, it is composed by beds and lenses of coarser materials embedded in fine materials with an irregular, complex, and everchanging geometry. This makes it a poor water source and thus a minor aquifer. Given that its composition is sands and gravels, the hydraulic conductivity is high and the recharge has been estimated to be low. The gaining river only helps to reduce the net recharge to the aquifer since any recharge flows into the river in almost all its length.

The Trinity aquifer is a system of several small hydrologically interconnected aquifers (Toll et al., 2018) such as :Antlers, Glen Rose, Paluxy, Twin Mountains, Travis Peak, Hensell, and Hosston and is one of the most municipally important aquifers in the state and also one with the larges head declines due to pumping. The recharge is low and the formations in which the aquifers exist are not the best for water movement.

Due to its importance as a costal aquifer and with the added complexity of saline intrusion, the Gulf Coast aquifer is the last major aquifer that this project will discuss. The great variation of formations in it correspond to the, as in the case of the Trinity, existence of several aquifers within this group designated Gulf Coast aquifer. As such, the group also has a great hydraulic conductivity variation along all of it from 0.015 m d^{-1} to 3.2 m d^{-1} in the north and south sections respectively (Scanlon et al., 2011). When looking to recharge, the estimation was conducted for the whole system with the chlorine tracer method and was found to vary from 0.17 m yr^{-1} in the north to 0.0254 m yr^{-1} in the south.

Table 1.1 Aquifers of Interest and their GAMs sections

Aquifer	Number of sections	Sections	Associated TWDB report
Brazos River Alluvium Aquifer (BRAA)	1	Brazos River Alluvium Aquifer GAM	(Ewing & Jigmond, 2016) (Ewing et al., 2006)
Gulf Coast	3	Gulf Coast Aquifer System (northern portion) GAM Gulf Coast Aquifer System (central portion) GAM Gulf Coast Aquifer System (southern portion) GAM	(Scanlon et al., 2011) (Kasmarek & Robinson, 2004) (A. H. Chowdhury et al., 2004) (A. Chowdhury & Mace, 2007)
Carrizo-Wilcox	3	Carrizo-Wilcox Aquifer (northern portion) GAM Carrizo-Wilcox Aquifer (central portion) GAM Carrizo-Wilcox Aquifer (southern portion) GAM	(Schorr & Zivic, 2018) (Young et al., 2018) (Deeds et al., 2003)
Hueco-Mesilla Bolsons	1	Hueco-Mesilla Bolsons Aquifer GAM	(Heywood & Yager, 2003)
Ogallala	2	Ogallala Aquifer (northern portion) GAM Ogallala Aquifer (southern portion) GAM	(Dutton et al., 2001) (Blandford et al., 2003)
Edwards-Trinity (Plateau)	1	Edwards-Trinity (Plateau) and Pecos Valley Aquifers GAM	(Anaya & Jones, 2009)
Edwards (Balcones Fault Zone)	3	Edwards BFZ Aquifer (northern segment) GAM Edwards BFZ Aquifer (Barton Springs segment) GAM Edwards BFZ Aquifer (San Antonio segment) GAM	(Jones, 2003) (Scanlon et al., 2001) (Lindgren et al., 2004)
Trinity	2	Trinity (northern portion) and Woodbine Aquifers GAM Trinity (Hill Country) Aquifer GAM	(Kelley et al., 2014) (Toll et al., 2018)

Table 1.2 Hydraulic characteristics of the studied GAM reports

Aquifer	NS	Section	Average Hydraulic Conductivity (ft d^{-1})	Average Storativity (1 ft^{-1})	Average Specific Yield (-)
BRAA	1	BRAA	108.1 (1.57 – 1000)	0.04 – 0.1	0.15
Gulf Coast	3	North	0.05 ($4.0x10^{-3}$ - 39.91)	$1.5x10^{-5}$ – $8.7x10^{-5}$	0.0004-0.1
		Central	3.8 (1 – 7)	$1.5x10^{-5}$ – $1.5x10^{-6}$	0.005-0.05
		South	10.5 (0.5 – 27)	$1.5x10^{-5}$ –$1.5x10^{-6}$	0.01-0.0005
Carrizo-Wilcox	3	North	1.6 (0.00012-5.5)	$4.12x10^{-6}$ ($3x10^{-6}$– $5.50x10^{-6}$)	0.10 (0.1-0.3)
		Central	42.13 (322 – 0.2)	$1.29x10^{-4}$ ($5.1x10^{-7}$ – $6.4x10^{-4}$)	0.13 (0.08-0.2)
		South	25.2 (11.8-55.8)	$15.1x10^{-6}$ ($1x10^{-7}$ – $1x10^{-4}$)	0.2 (0.15-0.29)
Hueco-Mesilla Bolsons	1		32.8 (3.3 – 164.0)	$22.9x10^{-6}$ ($6.6x10^{-6}$ – $3.3x10^{-5}$)	0.178 (0.173 – 0.184)
Ogallala	2	North	14.8 (5 – 44)	NA	0.18 (0.05-0.3)
		South	68 (10 – 150)	NA	0.156 (0.04- 0.25)
Edwards-Trinity (Plateau)	1		5.58 (2.5 – 8.6)	$5x10^{-7}$ – $2x10^{-4}$	$4.5x10^{-3}$ ($5x10^{-4}$ – 0.2)
Edwards (Balcones Fault Zone)	3	North	9 (0.01 – 30 000)	$5x10^{-7}$ – $5x10^{-5}$	(0.0005-0.05)
		Barton Springs	0.6 (0.4 – 75.3)	0.00025 - 0.00045	0.017 (0.001 - 0.023)
		San Antonio Region	11.3 (0.28 – 34)	$5.0x10^{-7}$ – $5x10^{-6}$	0.08 (0.005 – 0.15)
Trinity	2	North	2.2 (0.87 – 3.75)	NA	0.17
		Hill County	1.6 (0.5 – 2.5)	10^{-7} – 10^{-5}	0.055 (0.0003-0.1)

Table 1.3 MODFLOW version, year of creation, recharge value, and recharge estimation method

Aquifer	Original Model	Year of Creation	Mean Recharge	Estimation Method	Citation
BRAA	MF USG	2012	0.74 in yr^{-1}	Base Flow Separation	(TWDB, 2012)
Gulf Coast	MF 96	2003	6.8 in yr^{-1}	Chloride mass balance	(TWDB, 2003d)
	MF 96	2004	3.1 in yr^{-1}	Chloride mass balance	(TWDB, 2004c)
	MF 96	2007	0.1 in yr^{-1}	Chloride mass balance	(TWDB, 2007)
Carrizo Wilcox	MF 96 QS	2003	5 in yr^{-1}	Chloride mass balance	(TWDB, 2003b)
	MF 96 QS	2003	5.3 in yr^{-1}	Calibrated data	(TWDB, 2003a)
	MF 96 QS	2003	2.7 in yr^{-1}	Main-channel flow	(TWDB, 2003c)
Hueco Mesilla	MF 96	2001	0.8 in yr^{-1}	Climate estimations	(TWDB, 2003e)
Ogallala	MF 96	2001	0.4 in yr^{-1}	Chloride mass balance	(TWDB, 2001)
	MF 96	2003	0.3 in yr^{-1}	Chloride mass balance	(TWDB, 2003f)
ETP	MF 96	2004	1.6 in yr^{-1}	Chloride mass balance	(TWDB, 2004a)
Edwards BFZ	MF 96	2003	0.37 in yr^{-1}	Percentage of Precipitation (20%)	(TWDB, 2003d)
	MF DCM	2008	0.24 in yr^{-1}	Gage stations	(TWDB, 2008)
	GWSIM-IV	2004	0.22 in yr^{-1}	Gage stations	(TWDB, 2004b)
Trinity	MF NWT	2014	1.6 in yr^{-1}	Total Dissolved Solids balance	(Kelley et al., 2014)
	MF 2000	2018	0.12 in yr^{-1}	Moisture and Precipitation balance	(Toll et al., 2018)

The main objective of this research is to aid in the completion of the Desired Future Conditions (DFC) outlined in the Water Plan by the TWDB. Since the plan focuses on recharge-driven efforts to address the groundwater availability problems, knowing the areas where these

efforts can have the greater effect in the availability levels is of great importance. The present recharge analysis of the different aquifers in the state contributes to that idea. Based on the available information of the aquifers, their GAMs, and the methods used to estimate recharge in them, the following set of hypotheses was developed:

- *For all the GAMs studied, the modeled head difference under typical recharge conditions (baseline) and alternate scenarios (higher and lower rates), will be linearly correlated to the change in recharge. However, said linear tendency will be limited by an upper and a lower threshold value beyond which the aquifers will not respond to changes in recharge.*
- *Surface water reaches within the aquifer boundaries, both losing and gaining, will be impacted by the variation in recharge. The losing reaches will see their contribution to the aquifer increased as the recharge decreases in a linear tendency correlated with said recharge variation.*
- *The northwest aquifers will be less sensitive to recharge than the southeast aquifers since they are made of finer materials that allow for slower water movement.*
- *Aquifers with sub-crops, like the Carrizo-Wilcox, Trinity, and Edwards BFZ, will have a slower response to the change in recharge.*

Even if the aquifer models react in different ways than the anticipated, their behavior will yield important information about the areas that will benefit the most of applied recharge-increasing techniques to obtain the greater effect to the aquifers.

2. UNCERTAINTY OF TEXAS GROUDWATER AVAILABILITY MODELS TO VARIATIONS IN RECHARGE RATES

2.1. Chapter Summary

The variably of recharge in the aquifers of the state of Texas is an important part of the groundwater availability for urban, agricultural, and industrial uses state wide. The present study variates recharge from 50% to 150% of the original Texas Water Development Board's Groundwater Availability Models (GAMs) recharge in 10% increments to determine their sensitivity. In general, the confined aquifers, such as the Trinity, Edwards Balcones Fault Zone, and Carrizo-Wilcox, obtained an average head increase of 1.6% per 10% recharge increase while the unconfined aquifers, such as the Gulf Coast, Ogallala, and Edwards Trinity Plateau, presented an average head increase of 2.9%. Even though the mean head follows a linear trend in regards to recharge in all the aquifers, some of them (Trinity Hill and Ogallala South) have a non-linear response at the beginning of the recharge range (50% to 80%). A similar non-linear response is also present in the baseflow and stored water volume of the GAMs, with the majority of them starting to plateau near the high recharge range (130% to 150%). Even though there are some deviations, all the parameters (hydraulic head, river baseflow, and stored water volume) were fitted to a linear model with high r^2 (>0.9) which follows this studies hypothesis that the response of the GAMs will be linear to variations in recharge. The data also suggest the presence of thresholds in the high recharge range, but those were not found inside the study per view.

The impact of the changing Texas hydroclimate, and of short-term increases in recharge (less than a year), was addressed with surges of 1000% the original recharge in the first year of simulation of the Trinity North and the Edwards Balcones Fault Zone San Antonio GAMs. While the Edwards Balcones Fault Zone dissipated the increase of hydraulic head in 10 years, the Trinity North stored the extra water volume in its matrix well after the end of the simulation (50 years). These results can help with the management of the new and more variable (both in frequency and intensity) recharge regime for the state and its groundwater availability.

2.2. Introduction

The Texas Water Development Board (TWDB), in its 2012 state water plan (Vaughan et al., 2012), outlines projections for the water supply in the state: a decrease of 30% (from 9.9 billion to 7 billion cubic meters) from 2010 to 2060 in groundwater and an increase of only 6% (10.2 billion to 11.1 billion cubic meters) in the surface water supply. In the current adopted 2017 Texas State Water Plan (Bruun et al., 2017), the revised figures show that, in 2020, the total availability of surface and groundwater is 4% lower than the projected in the 2012 plan (Bruun et al., 2017). This reduction in the available groundwater and the increase in the demand will strain the water supply state-wide taking aquifers, such as the Ogallala, closer to complete depletion. An important part of the availability of groundwater is the replenishment of the used volume in the exploited aquifers, the recharge received from exterior sources, being it natural or artificial.

Aquifer recharge is one of the more important factors when trying to determine the future behavior of an aquifer and the future available volume of water that can be extracted without

endangering it. The properties and characteristics of an aquifer, such as hydraulic conductivity and geology, are constant over time. However, recharge, pumping, surface to groundwater interactions, are not constant and can vary greatly in short periods of time due to climatological or land use changes. Kumar (2012) notes that, although the effects of climate change can be more directly observed in surface water resources, the decrease of quantity and quality of the groundwater supply is of great importance for management and planning for the future. Recharge is one of the most important affected but uncertain parts of said availability, and the role groundwater plays in every aspect of the modern life, 51% irrigation, 28% municipal, 12% manufacturing, 9% others (Bruun et al., 2017). It is high uncertainty; the present sensitivity analysis helps to point out the areas of the state where projects of artificial recharge and natural recharge increase would be more feasible.

While some of the characteristics and properties of the eight studied aquifers have been determined to a high degree of confidence (in comparison with the recharge data available), such as hydraulic conductivity, porosity, and boundaries, recharge, in most cases must be estimated by a variety of methods. Mass balance methods, such as chlorine and total dissolved solids balance, are used in a large section of the aquifers (Gulf Coast, Ogallala). These balances allow the estimation of the recharge that enters an aquifer with high accuracy (Allison & Hughes, 1978) and have been around for a long time with different tracer elements such as tritium and chlorine. Flow balance methods, such as hydrograph separation and gage stations in rivers, are another set of methods used to estimate the volume of recharge being received by an aquifer. Killian et al. (2019) reports the use of the hydrograph separation as an adequate method to estimate the surface to subsurface water interactions and proposes that changes in baseflow can be used as a proxy for groundwater levels in some aquifers. Climatological estimations are another group of used

recharge estimation methods. While the mass balance can be performed in several points along the interest aquifer (Dassi, 2010) to obtain a detailed picture of the recharge state of the aquifer, the flow balance methods can only produce an estimation of the total volume recharged in the interest basin. The distribution of the recharge along the area of the aquifers has to be performs using climatological data, such as precipitation, and its spatial and temporal distribution as a base for the recharge distribution. Within the climatological methods, the estimation of recharge solely from precipitation and other climatic variables has been attempted. Mohan et al. (2018) created a global empirical model to estimate recharge form climatological and land use information obtaining precipitation, and potential evapotranspiration as the most influential meteorological factors in the groundwater recharge phenomena.

Along the eight aquifers analyzed (shown in Figure 2.1), the method of recharge estimation varies, not only from aquifer to aquifer, but form section to section. Given the size of the aquifers, and the limited power and computing time, to make the TWDB's Groundwater Availability Models (GAMs) a feasible and useful tool, some aquifers have been partitioned in distinct hydrogeological sections. All this sections work as an independent model with its own initial and boundary conditions to allow the modelers and the TWDB to estimate the behavior of the aquifers along the run time of the models, which finishes in 2050, as a tool to accomplish the goals delineated in the current 2017 water plan (Bruun et al., 2017). A total of 16 GAMs were analyzed encompassing the following aquifers: Ogallala, Gulf Coast, Carrizo-Wilcox, Edwards-Trinity Plateau, Edwards Balcones Fault Zone, Trinity, Hueco Mesilla Bolson, and Brazos River Alluvium Aquifer being only the last one a minor aquifer in the state. The first seven aquifers represent 87% of the current groundwater supply of the state (Vaughan et al., 2012) and, while the BRAA is not

a great source of groundwater, its complexity and geological formation (with clay lenses and compartmentalization due to the Brazos River deposits) it is an aquifer of interest in regards to the challenges of modeling.

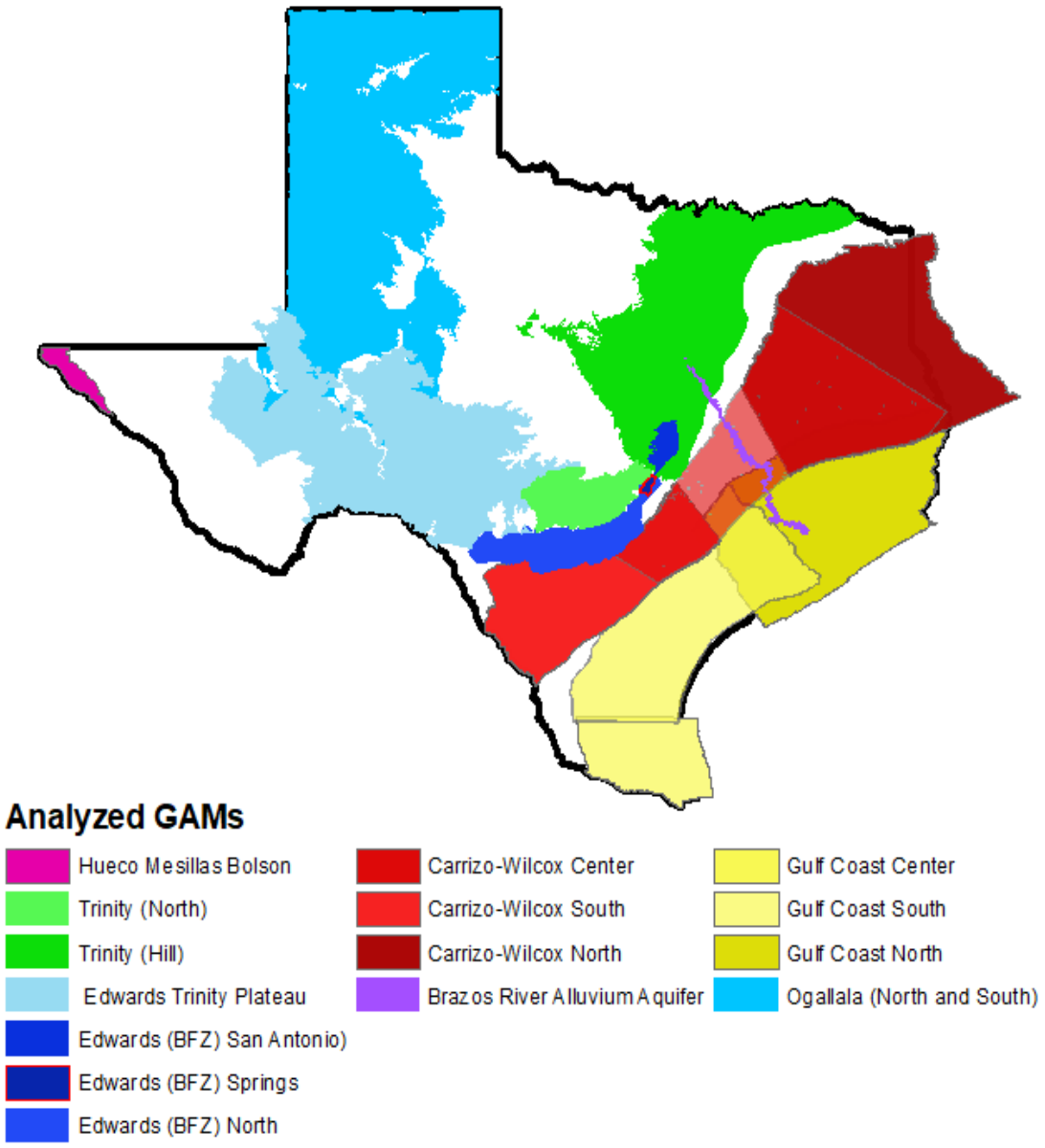

Figure 2.1 Aquifers of interest and the GAMs in which they are separated for modeling purpose

With the importance of recharge as the source of the stored water in the aquifer's matrix, and the heavy reliance of not only Texas but the U.S. as a whole on groundwater, such as the Ogallala aquifer that supports one-sixth of the worlds grain production (Frankel, 2018), determining how changes in recharge levels affect the current and future conditions in the aquifers is an important step towards the better understanding of the water supply problem in Texas.

The specific objectives of this paper are:

- To assess the response that mayor Texas aquifers have to variations in recharge, based on modeled changes in head, stored water volume, and river baseflow.
- To determine the correlation of recharge variation to the changes in aquifer characteristics, the sensitivity of each one of them to said changes in recharge and the trend they show. (linear, exponential or otherwise).
- To outline priority data needs for Texas Groundwater Availability Models
- To identify which aquifers could benefit the most of existing planned recharge improvement projects and future artificial recharge initiatives.

The behavior of the aquifers will also suggest where artificial recharge projects may have the greatest chance to improve the groundwater availability and, in some cases such as the Gulf Coast aquifer where limitations to pumping have already been enacted, help assess if the aquifers are recovering. To accomplish the stated objectives the following set of hypotheses was developed:

- *For all the GAMs studied, the modeled head difference under typical recharge conditions (baseline) and alternate scenarios (higher and lower rates), will be linearly correlated to the change in recharge. However, said linear tendency will*

be limited by an upper and a lower threshold value beyond which the aquifers will not respond to changes in recharge.

- *Surface water reaches within the aquifer boundaries, both losing and gaining, will be impacted by the variation in recharge. The losing reaches will see their contribution to the aquifer increased as the recharge decreases in a linear tendency correlated with said recharge variation.*
- *The northwest aquifers will be less sensitive to recharge than the southeast aquifers since they are made of finer materials that allow for slower water movement.*
- *Aquifers with sub-crops, like the Carrizo-Wilcox, Trinity, and Edwards BFZ, will have a slower response to the change in recharge.*

Even if the aquifer models react in different ways than the anticipated, their behavior will yield important information about the areas that will benefit the most of applied recharge-increasing techniques to obtain the greater effect to the aquifers.

2.3. Methods

The GAMs used in this study (Table 1.1) were obtained directly from the TWDB and represent the models adopted and distributed by the state for management purposes. Some groundwater conservation districts (GCDs) have adopted their own model versions, which may or may not be publicly available. Additionally, we note the methods for constructing and obtaining the data can differ significantly between the models. Although all were commissioned by the TWDB, their development spans a 20-year time period and more than 5 consulting practices.

2.3.1. Model Inputs and Settings

Here, we explain the methods we used to re-run the models, which were largely consistent, with the exception of the BRAA, which we will discuss later in this section. After obtaining the GAMs for all the aquifers of interest (16 GAMs across 8 aquifers), they were translated to run in the GMS pre- and post-processor package (Aquaveo Inc., 2017) and translated to MODFLOW 2000 as appropriate. In some cases, direct translation presented issues, such as the Gulf Coast South, which was originally written in PMWIN. When necessary, selected files were rewritten for compatibility with the GMS software package. Model instances used in this project have been made available via the Hydroshare repository system (Pena Rodriguez, 2019).

In order to test the response of the aquifers in head, stored water volume and river baseflow, recharge values across the entire period were varied from 50% to 150% of the original recharge rate, in 10% increments, using the GMS's "multiplier" feature. This resulted in a total of 11 simulations per GAM, and a total 176 across the project. The solvers Preconditioned Conjugate-Gradient and Strongly Implicit Procedure were used, convergence criteria was set to obtain no lower than 0.003 m head change criteria, and 1 ft3/day cross the entire simulation. Clock times for the models ranged from 0.5 to 3.1 hours.

The BRAA model. The most recent of any of the GAMs, was originally created in a beta version of MODFLOW-USG, which allows for different sizes of cells all along the aquifer without the need of extending said different sizes to the rest of the aquifer. This irregular grid feature is necessary for resolving fine scale details near the river while keeping computations tractable across the larger domain. Unfortunately, while GMS supports MODFLOW-USG, its beta version is

incompatible. Given that, all the recharge data (the 11 different recharge values for the 3 layers of the aquifer) were manually computed using MATLAB 2016a (MATLAB, 2016), and then each scenario was run separately in the native DOS environment of MODFLOW-USG-beta.

2.3.2. Model Output and Post Processing

One of the outputs of GMS (and MODFLOW) is the head in each one of the cells that comprise the modeled aquifer. This, however, is not suitable for a variability comparison of the different recharge scenarios to which each aquifer was subjected to since it only shows the head for each recharge level. To address this, MATLAB was used to post-process the data obtained from GMS and create head variation maps of all the GAMs for each one of the recharge scenarios compared to the normal recharge used in the model (baseline).

To analyze the baseflow to the rivers and the impact of the variation in recharge (from 50% to 150%) the Flow Budget tool of GMS was used. In some cases, like the Hueco Mesilla Bolson aquifer, only one river transverses the aquifer: the Rio Grande. For other GAMs, like the Gulf Coast Center aquifer, its GAM includes eight basins and rivers: Brazos River, Colorado River, Guadalupe River, Lavaca River, Nueces River, Nueces-Rio Grande Basin, San Antonio River, and San Antonio-Nueces Basin. In addition to calculating the river baseflow, the same tool was used to calculate the changes in stored water volume in the aquifer's matrices.

With the obtained data of the stored water volume, the baseflow, and head variation along all the GAMs and their respective recharge multipliers, a linear regression to the recharge

multipliers was performed in MATLAB To better appreciate the different tendencies that the data follows, they were normalized to the mean of the normal recharge (100%).

Using the correlation data and the mean head in each GAM, two of them were selected to perform a surge in recharge at the beginning of the modeling period. This surge was of 10 times the normal recharge for the first year of the modeled stress periods. The two models, Trinity North and Edwards BFZ San Antonio, were selected for being the most and least sensitive to recharge respectively. Once the surge was performed, the data was compared with the normal recharge mean heads of the respective GAMs as a baseline comparison. The difference between the baseline and the perturbed data were plotted and analyzed. Additionally, the Gulf Coast North aquifer was also subjected to an increase in recharge. Said surge was the simulation of Hurricane Harvey in its touchdown in Texas on august 2017. Rainfall data obtained from the TexMesonet website (TexMesonet, 2019) for the Scholes International Airport at Galveston (KGLS) station with precipitation data from 2017 and 2016. The daily precipitation data was used to estimate the percentual increase originated by Harvey day by day. This increase was used as a multiplier for the month of August 2017 in the GMS Gulf Coast North GAM in order to analyze the reaction of the aquifer to a high increase in recharge in a short period of time (one month).

2.4. Results

The GAMs simulations ran in GMS and MOFLOW-USG yielded important data to better understand the behavior of the aquifers when subjected to changes in the recharge levels they are

subjected to. Said results have been separated in 3 separate sections to better address them separated.

2.4.1. Hydraulic Head and Total Stored Volume

Once all the simulations of the GAMs were run, their mean change was compared to the one obtained with the normal recharge to obtain the percent change (see Table 2.1). In some cases, such as the Carrizo-Wilcox South the response of the aquifer's section was of the same magnitude in both directions (± 1.2%) showing the linear tendency of mean head relating to recharge. In other cases, such as the Gulf Coast South, the increase of mean head is of smaller absolute magnitude (+17.4%) than the decrease with 50% recharge (-18.2%).

The higher mean head variations (Table 2.1) were the ones corresponding to the Trinity North (±48.6%) and the Gulf Coast North (±42.2%) i.e. variation of 0.972% for each 1% change in recharge. Both the most reactive aquifers have a low hydraulic conductivity (0.00064 m hr^{-1} for the Gulf Coast North and 0.047 m hr^{-1} for the Trinity North) and the slower horizontal and vertical movement of water creates the increased head. The least sensitive GAM is the Hueco Mesilla Bolson aquifer, with a relation of mean head change of 0.000006% for each 1% change in recharge.

The comparison between the different recharge rates (from 50% to 150% in 10% increments) created several figures that can be seen in Appendix A. The Brazos River Alluvium Aquifer (BRAA) in the smaller (50%) and larger (150%) recharge levels in two of its layers (one and three) since layer one and layer two are equal in area (Figure 2.1).

Table 2.1 GAMs recharge, range, mean head with the percentual increase and decrease for 50 and 150 percent recharge, the reported recharge for each GAM, and the classification to which each GAM belongs according to its hydraulic head reaction to the changes in recharge

GAM	*Report Recharge ($m\ yr^{-1}$)*	*Model Recharge ($m\ yr^{-1}$)*	*Range*	*Mean Head (m)*	*Percent Decrease*	*Percent Increase*	*Classification*
BRAA	0.019	0.431	± 0.216	84	-8.10%	8.60%	HS, SC
CWN	0.127	0.084	± 0.042	67	-5.80%	4.30%	HS, C/U
CWC	0.135	0.079	± 0.039	72	-2.00%	2.30%	C/U
CWS	0.069	0.056	± 0.028	118	-1.20%	1.20%	Di, C/U
GCN	0.173	0.102	± 0.051	103	-42.20%	42.10%	BD, Di
GCC	0.079	0.123	± 0.062	46	-3.30%	3.80%	HS, Di
GCS	0.003	0.009	± 0.004	25	-18.20%	17.40%	HS, Di
OGN	0.01	0.029	± 0.015	935	-0.20%	0.20%	Di, C/U
OGS	0.008	0.032	± 0.016	1052	-0.30%	0.30%	Di, PB
BFZN	0.009	0.413	± 0.206	204	-2.70%	1.90%	Di
BFZSP	0.006	0.740	± 0.370	161	-5.60%	3.70%	BD
BFZSA	0.006	0.292	± 0.146	238	-0.01%	0.01%	HS
HMB	0.02	0.007	± 0.004	357	-0.0003%	0.0003%	HS
TRH	0.041	0.45	± 0.225	419	-4.00%	2.60%	Di
TRN	0.003	0.052	± 0.026	1423	-48.60%	48.60%	C/U
ETP	0.041	0.057	± 0.028	647	-5.90%	5.50%	Di

Where, HS is hot spots inside the GAM where the response is concentrated; SC is subsurface connectivity of the GAM with underlying or overlying formation; C/U is confined/unconfined differentiation of the response of a GAM depending if the section is confined or unconfined; Di is the diffuse response of the aquifer with a evenly spread increase of head near the average increase of the whole GAM; BD is boundary disconnect that isolates some sections of the GAM due to geological formations; and PB is political boundaries that limit the available data.

Some sections of the aquifer's top layer (a and b in Figure 2.3) reflect the similar increases and decreases in head while some sections show different responses to the increase and decrease

of recharge. For the case of the third layer (c and d in Figure 2.3) the difference is more evident in the top of the aquifer model: negligible increases (around 0.5 m) present in layer one compared to small decreases (around 2m) in layer three. The greater changes in head, represented by the dark red (decrease) and dark blue (increase), locate the sections of the aquifer that are the most sensitive to recharge.

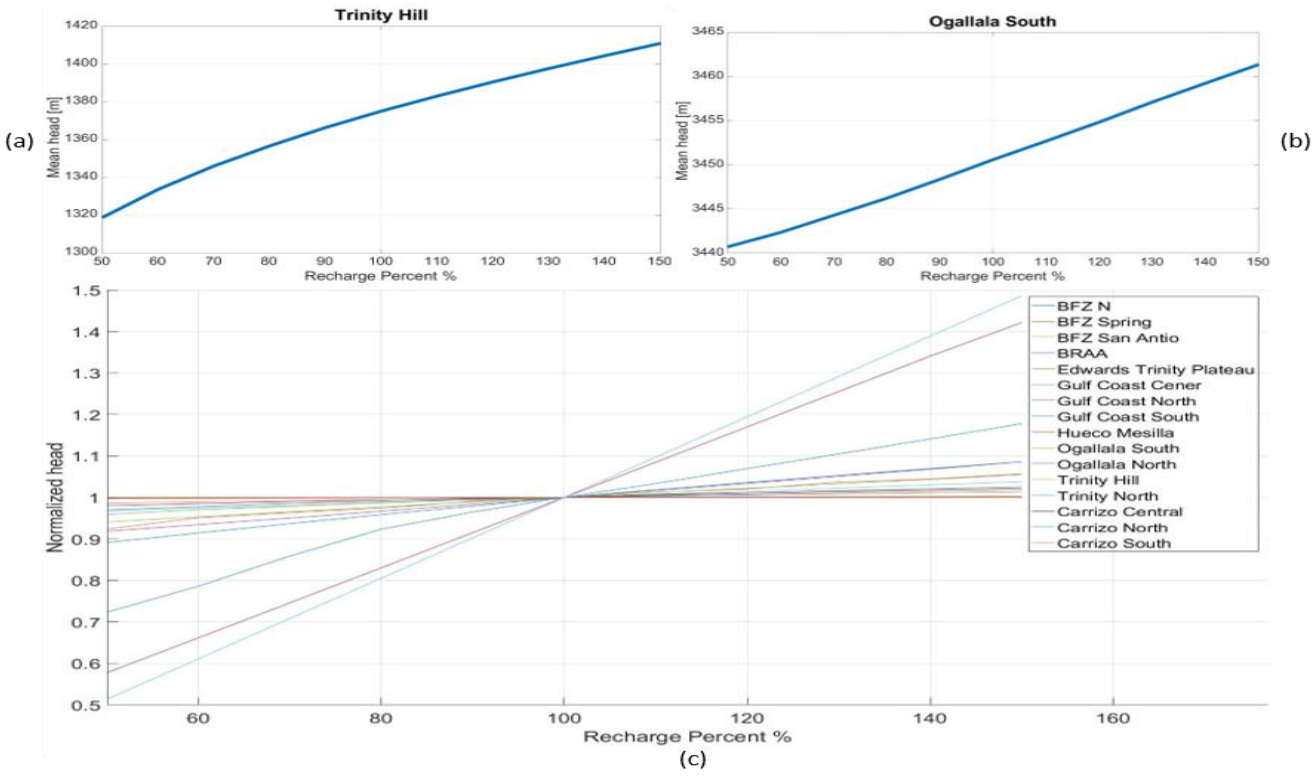

Figure 2.2 (a) Trinity Hill's GAM mean head response to recharge increase (b) Ogallala South's GAM mean head response to recharge increase (c) GAMs normalized mean head response to increase in recharge (50% to 150% original recharge)

While the spatial distribution of the increase in head along the GAMs was addressed, the overall trend of said increase (Figure 2.2) reflects the response of the aquifers to changes in recharge. In the majority of cases, the increase of mean head follows a linear trend (Figure 2.2 c) but in some ones, such as the Trinity Hill and the Ogallala South, the tendency is slightly non-

linear. For the case of the Trinity Hill (Figure 2.2 a) the initial response (from 50 % to 60% of the original recharge) is steeper but, as the recharge increase, the mean head increase "slows down". The Ogallala South (Figure 2.2 b) presents slight concave up tendency before 90% original recharge and a linear tendency between 90% and 140% where the concavity changes to down and starts to tend to the same plateau present in all the GAMs.

(a)

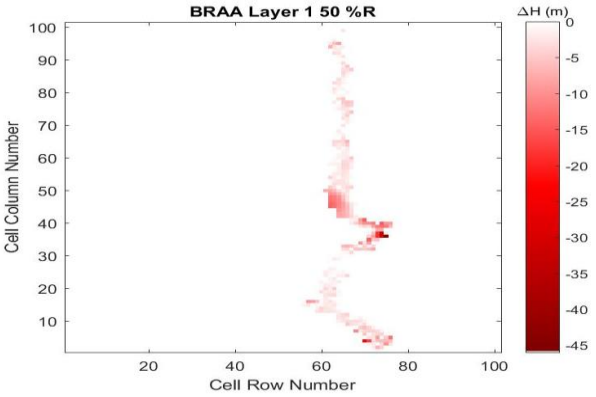

(c)

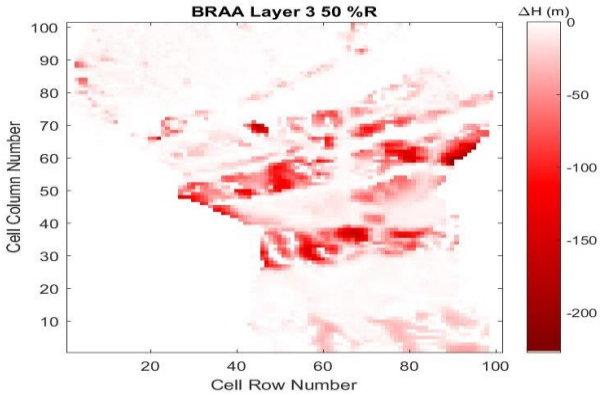

(b)

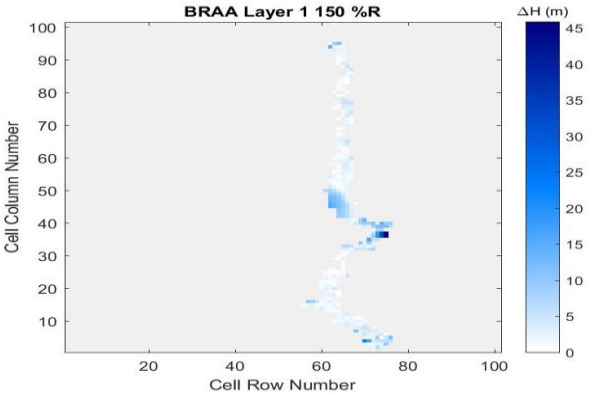

(d)

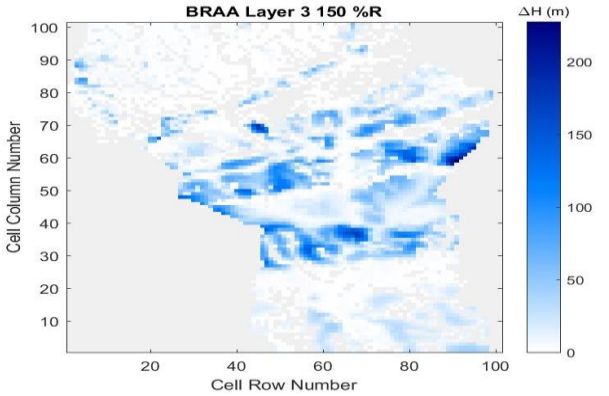

Figure 2.3 Brazos River Alluvium Aquifer head change to baseline: (a) Layer 1 with 50% normal recharge, (b) Layer 1 with 150% normal recharge (c) Layer 3 with 50% normal recharge (d) Layer3 with 150% normal recharge

The classification (Table 2.1) of each GAM show that in some aquifers, such as the Gulf Coast Aquifer (Gulf Coast North, Center, and South GAMs) the diffuse increase of head is shared between all the sections of the aquifer. In contrast, the Carrizo-Wilcox shares the C/U classification

(Confined/Unconfined) of an aquifer with a subcrop and an outcrop but has one section with hot spots (HS) and other with diffuse (Di) response.

2.4.2. River baseflow and correlation to recharge

Given the great number of rivers in each GAM and the number of GAMs, the complete set of graphs is located in Appendix A. In the case of the Carrizo-Wilcox South (Figure 2.4), a threshold appears near the low recharge levels. The baseflow to the river remains almost constant for the three first recharge levels (50%, 60%, and 70%) and then starts to increase in a geometrical manner.

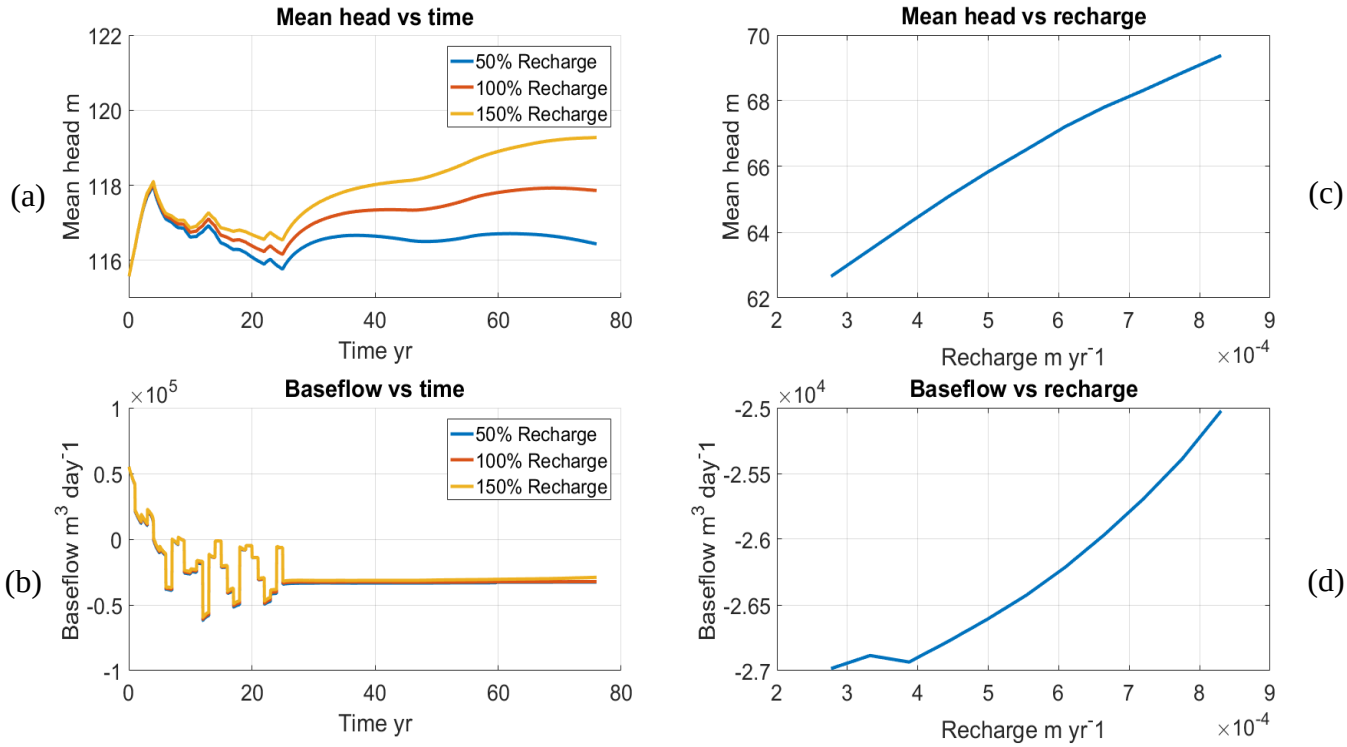

Figure 2.4 Carrizo-Wilcox South Atascosa River (a) mean head versus time for three recharge levels, (b) baseflow versus time for three recharge levels, (c) mean head versus recharge, and (d) baseflow versus recharge

For other rivers, such as the Trinity River in the sections that traverses the Carrizo-Wilcox Central section, the threshold appears in the higher recharge rates plateauing the change in baseflow at 12 million cubic meters when the equilibrium is reached in the aquifer and it stops responding to increases in recharge. Another scenario encountered is the Brazos River in the BRAA's GAM, which stays relatively constant at 1.1 million cubic meters but also presents an increasing linear tendency with an increase of 14.2% from the original recharge value.

All the rivers contained within the GAMs experience an increase in the baseflow from the aquifers. While the increase of head (Figure 2.4 c) is continuous, a clear plateau appears as the recharge increases. However, the baseflow follows an exponential tendency (Figure 2.4 d).

While the increase in baseflow to the rivers follows the increase in recharge and head, each river reacts in a different manner. The Nueces River, in the section comprised within the Trinity Hill, follows linear tendency (Figure 2.5 e). Both the Upper Trinity River and the Sabine River (Carrizo Wilcox North) follow a slightly exponential trend (Figure 2.5 c and a respectively). The Rio Grande River (Hueco Mesilla Bolson) and the Lavaca River (Gulf Coast Central) present a plateau (Figure 2.5 b and d respectively) when the highest recharge levels are reached (140% to 150% original recharge). However, the Brazos River (Edwards Balcones Fault Zone North) presents a concave down trend that then phases into a linear trend implying a rapid response to the first increase in recharge, and a posterior linear tendency. This same linear tendency is present in the majority of the rivers in the GAMs (Appendix A).

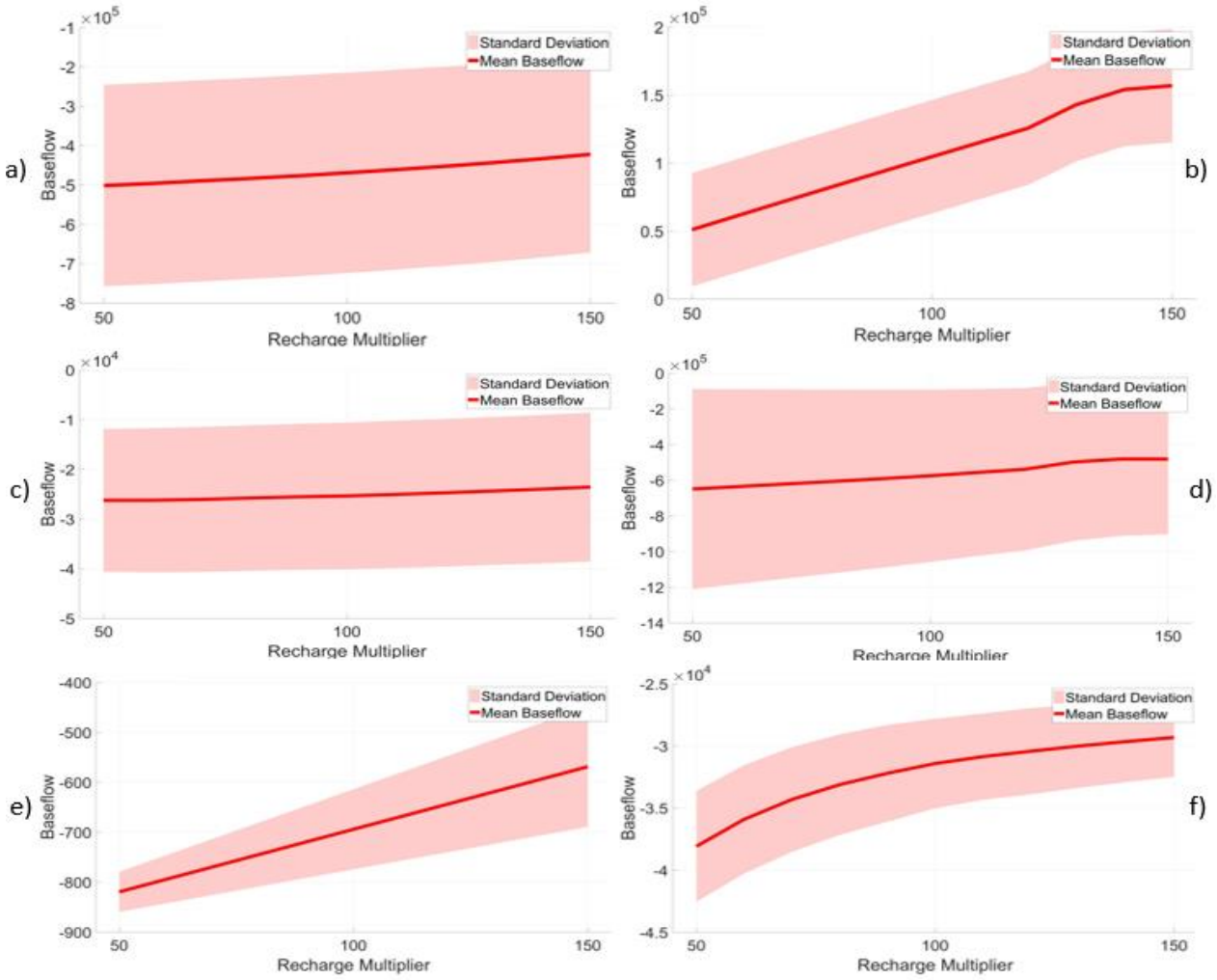

Figure 2.5 River baseflow and Standard deviation for: a) Sabine River in the Carrizo Wilcox North's GAM, b) Rio Grande River in the Hueco Mesilla Bolson's GAM, c) Upper Trinity River in the Carrizo Wilcox North's GAM, d) Lavaca River in the Gulf Coast Central's GAM, e) Nueces River in the Trinity Hill's GAM, and f) Brazos River in the Edwards Balcones Fault Zone North's GAM

Even though all the GAMs have a linear response to changes in stored water volume and mean head, the slope of the linear model, which reflects the sensitivity to recharge for each one, they all have a different value (Table 2.2). The Hueco Mesilla Bolson (HMB) is the least sensitive to recharge with a slope of $7x10^{-5}$, and the Trinity North (TRN) is the most sensitive to recharge (m=1382.8) in regards of mean head. In the case of the variation of the stored volume in the aquifer,

the sensitivity of it to changes in recharge is similar with the HMB and TRN being the least and most sensitive to recharge. Although the "b" term in the models shows only the intercept with the y axis (mean head or stored volume variation) the slope "m" of the linear model reflects the sensitivity to recharge of each GAM and can be used to determine the most and least sensitive aquifer section.

Table 2.2 Mean head and stored water volume correlation to recharge under a linear model

GAM	*Mean Head*			*Stored Water Volume*		
	b	m	r^2	b	m	r^2
BRAA	70.1	14.1	0.999	-2.51E+11	-1.22E+10	0.996
CWN	68.8	3.1	0.997	2.46E+11	-6.10E+10	0.999
CWC	59.6	6.7	0.992	4.09E+10	-2.60E+10	0.995
CWS	115	2.8	0.999	5.41E+11	-5.38E+09	0.999
GCN	43.1	3.3	0.999	2.86E+10	-1.09E+09	0.954
GCC	15.9	87.3	0.999	1.01E+10	-4.30E+09	0.995
GCS	16	8.6	0.999	2.35E+09	-1.40E+09	0.999
OGN	931.5	3.4	0.999	2.44E+11	-3.60E+10	0.999
OGS	1045.4	6.4	0.999	1.92E+11	-6.10E+10	0.999
BFZN	194.3	9.2	0.989	26842262	-3.30E+07	0.990
BFZSA	237.9	0.1	0.999	97727451	-2.20E+07	0.988
BFZSP	145.9	14.4	0.988	1.39E+09	-3.10E+10	0.999
HMB	1170.5	7.00E-05	0.993	-1.00E+09	-190.72	0.982
TRH	391	27	0.985	6.13E+08	-6.70E+08	0.984
TRN	39.8	1382.8	0.999	5.32E+09	-7.00E+10	0.999
ETP	573.1	73.2	0.999	3.97E+11	-1.90E+11	0.997

In the case of the baseflow and its correlation to recharge, each one of the rivers in each GAM was linearly regressed to recharge to obtain a linear model to which the data better fits and all the models obtained models were analyzed (Table 2.3). For all the models a good fit was accomplished with an r^2 of over 0.9 for all cases. For some of the aquifers the slope "m" of the linear model to which they were fitted, is significantly smaller when compared with the slopes

obtained for the linear models of mean head and stored volume variation (Table 2.1 and Table 2.2 respectively). However, contrary to those cases, some of the slopes in the baseflow correlation to recharge models are negative showing a decrease of the baseflow towards rivers form the aquifer. For the most part of the recharge range in the models, the slope is positive but all of the positive slopes tend to a maximum level and start to plateau.

The changing sign of "m" (the slope) for the different rivers present in the same GAM is also notable, since the same changes in recharge along a specific aquifer have different effects in the baseflow experienced by the rivers that exist within it (Table 2.3). Such is the case of the Gulf Coast South GAM, where the Nueces and Rio Grande rivers have contrary signs even though they both form part of the same aquifer system. For other aquifers, such as the Carrizo-Wilcox, all the rivers in a determined section present the same sign and thus, behave in the same way to changes in recharge.

The baseflow for each river allowed the classification of the rivers based on their behavior when compared with the change in recharge (Table 2.3 and Table 2.3 Cont.): An asymptotic (ASY) behavior, such as the one experienced by the Brazos River inside the Edwards BFZ North GAM (Figure 2.5 f); an Linear (LIN) behavior such as the one experienced by the Nueces River in the Trinity Hill's GAM (Figure 2.5 e); an inflexion (INF) behavior present in the Lavaca River in the Gulf Coast Central's GAM (Figure 2.5 d) which consist in an exponential (EXP) behavior in the lower recharge range (50%-80%) that becomes a threshold (THR) behavior in the higher recharge range (130%-150%); and a combined multiple behavior that combines linear and threshold behavior (MLT).

Table 2.3 Linear relationship between baseflow and river recharge across GAMs and their classification

GAM	*River*	*b*	*m*	*r²*	*Classification*
BFZN	Brazos	1.284	-0.003	0.904	ASY
	Colorado	1.732	-0.006	0.934	ASY
BRAA	Brazos	0.834	0.002	0.998	LIN
ETP	Rio Grande	-0.303	0.013	0.999	LIN
	Colorado	-0.485	0.015	0.99	THR
	Nueces	-0.661	0.017	0.986	INF
	Guadalupe	-0.271	0.013	0.989	THR
	San Antonio	-0.596	0.016	0.991	THR
CWC	San Antonio	10.473	-0.095	0.999	LIN
	Guadalupe	-0.157	0.012	0.99	THR
	Colorado	0.527	0.005	0.988	THR
	Brazos	0.557	0.004	0.991	THR
	Trinity	0.612	0.004	0.992	THR
	Neches	0.639	0.004	0.992	THR
CWN	Lower Trinity	1.292	-0.003	0.996	EXP
	Neches	1.317	-0.003	0.998	EXP
	Saline	1.161	-0.002	0.989	EXP
	Red-Saline	2.956	-0.02	0.999	LIN
	Big Cypress-Sulphur	1.235	-0.002	0.999	EXP
	Upper Trinity	1.1	-0.001	0.971	EXP
CWS	Rio Grande	1.244	-0.002	0.999	LIN
	Nueces	1.283	-0.003	0.997	EXP
	San Antonio	13.347	-0.125	0.999	EXP
	Guadalupe	0.086	0.009	0.999	LIN
	Bastrop	0.563	0.004	0.999	LIN
HMB	Rio Grande	-0.045	0.011	0.996	THR

Table 2.3 Linear relationship between baseflow and river recharge across GAMs and their classification. (Continued)

GAM	*River*	*b*	*m*	*r²*	*Classification*
GCC	Brazos	3.887	-0.029	0.999	LIN
	Colorado	1.378	-0.004	0.986	INF
	Lavaca	1.3	-0.003	0.98	INF
	Guadalupe	-1.727	0.028	0.989	THR
	San Antonio	0.406	0.006	0.999	LIN
	San Antonio-Nueces	-0.621	0.016	0.999	LIN
	Nueces	0.501	0.005	0.999	LIN
	Nueces-Rio Grande	-0.873	0.019	0.999	LIN
GCN	Nueces	1.361	-0.004	0.999	LIN
	San Antonio	0.1	0.009	0.991	THR
	Guadalupe	-1.623	0.026	0.988	ASY
	Colorado	0.361	0.006	0.992	THR
GCS	Nueces	1.315	-0.003	0.999	LIN
	Rio Grande	-0.62	0.017	0.99	THR
OGN	Canadian	0.574	0.004	0.999	LIN
	Red	0.822	0.002	0.999	LIN
OGS	Brazos	0.999	0	0.973	LIN
	Red	1	0	0.998	LIN
	Canadian	0.991	0	0.994	EXP
TRH	Nueces	1.361	-0.004	0.999	LIN
	San Antonio	0.1	0.009	0.991	MLT
	Guadalupe	-1.623	0.026	0.988	ASY
	Colorado	0.361	0.006	0.992	ASY
TRN	Colorado	-0.043	0.01	0.999	LIN
	Brazos	-0.117	0.011	0.99	THR
	Trinity	-0.069	0.011	0.991	THR
	Red	0.037	0.01	0.992	ASY

Since each river passes through several GAMs and each GAM's baseflow data could yield a different behavior for the section of the river that crosses it, each river has several sections with different classifications (Figure 2.6).

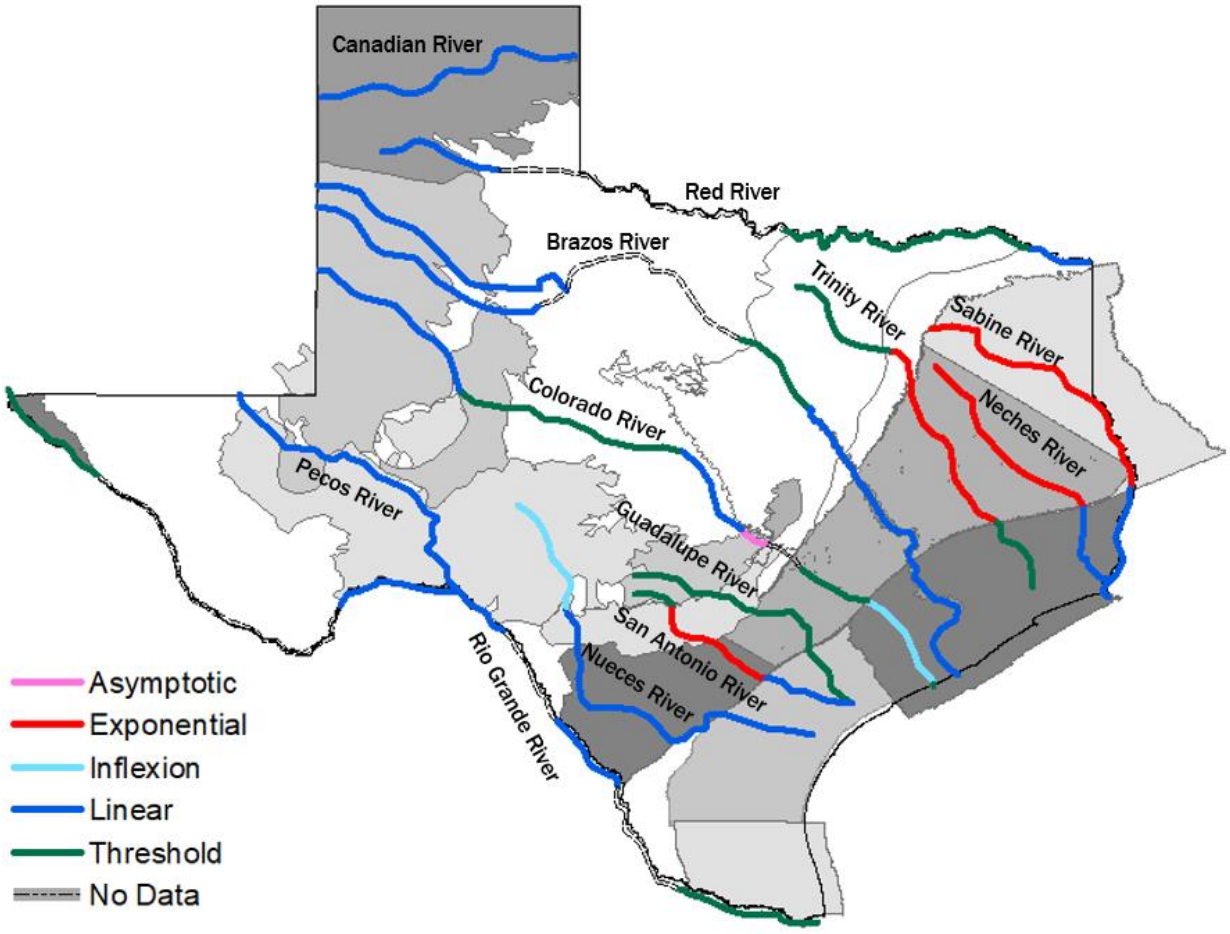

Figure 2.6 River classification from their baseflow behavior inside each GAM

2.4.3. Surge of recharge.

The increase of recharge (10 times the original recharge) over the first year of the models in the most and least sensitive aquifers (Trinity North and Edwards BFZ San Antonio GAMs)

reflects the sensitivity of the aquifers. While the Trinity North takes more that the model's runtime to revert back to the non-recharge state (<50 years), the Edwards BFZ San Antonio follows the same mean head trend after only 10 years. The magnitude of the difference between the baseline and the perturbed (surge of recharge) scenarios is also important since the Trinity Hill presents an increase of around 260 m though out the simulation while the Edwards BFZ San Antonio only presents an increase of less than a meter (0.6 m at the beginning of the simulation).

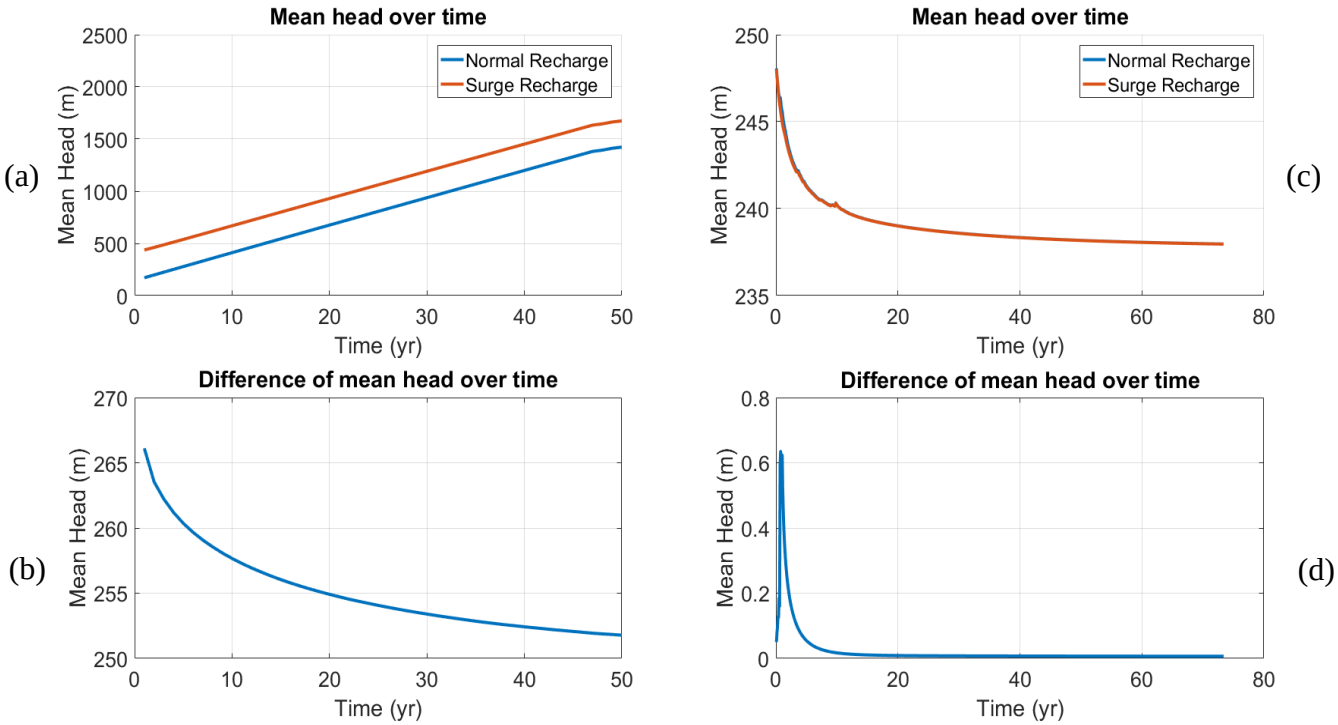

Figure 2.7 (a) Mean head of the two different recharge scenarios versus time in the Trinity North GAM, (b) dissipation of the increased mean head versus time in the Trinity North GAM, (c) Mean head of the two different recharge scenarios versus time in the Edwards BFZ San Antonio GAM, (d) dissipation of the increased mean head versus time in the Edwards BFZ San Antonio GAM,

The top graphs (a and c in Figure 2.6) show the change in head with the normal recharge (blue) and the perturbed recharge (orange). The lower two graphs (b and d in Figure 2.6) show how the difference between the baseline (100% recharge) and the perturbed (1000% recharge) and

how it changes along the length of the GAMs runtime. The Edwards BFZ San Antonio GAM stabilizes relatively quickly (10 years), compared to the Trinity North GAM (>50 years).

For the case of the Gulf Cost North aquifer subjected to the recharge increase represented by Harvey (August 2017), the recharge multiplier for the month of August 2017 in the GAM was of 11 times. This originated an initial head increase of 18.9 m at the beginning of September 2017 which started to decrease immediately. By the end of the simulation time (December 2050) only a head difference of 1.6 m remained.

2.5. Discussion

Even though there exists a difference between the reported mean recharge values and the mean recharge values used in the GAMs (Table 2.1), the difference is due to the way said mean recharge value was calculated in both cases. In the case of the reported value, the majority of the reports show the mean value of recharge along the aquifer for the known stress periods and for a year only. In the case of the value reported from the models, the value is the mean of each one of the stress periods averaged throughout the entire aquifer, and the entire length of the model.

While the recharge variability (from 50% to 150%) was applied to all the GAMs, the actual increase recharge value depended in the normal recharge reported in the models. As such, the lowest recharge variation of 0.004 m-1y-1 corresponds to the Hueco-Mesilla Bolson's GAM and this yielded the smallest increase in mean head of the study (0.0003% of the normal mean head). However, the same cannot be said for the case of the largest recharge level (Edwards BFZ Springs)

which did not experienced the highest changes in mean head. In the case of the Trinity North, it has a relatively high specific yield (0.17) which implies that, even though the Gulf Coast North increases its mean head almost the same percentual amount, the actual stored volume inside the Trinity North is larger. It is important to note that, even though the hydraulic conductivity of the Trinity North is higher than that of the Gulf Coast North, the underlying layers are composed of less permeable materials (0.01 m hr^{-1}) that create a slower water movement and thus contribute to the higher water level in the top layer. This quality, of different layers behaving in different manners along the same GAM, is greatly exemplified in the BRAA's GAM. The two presented layers (1 and 3) have a significant difference in the head variation from the baseline (Figure 2.3). Layer one (shows a variation of ±45 meters while layer three presents a variation of ± 200 meters. Since the head variation is obtained with the difference form the analyzed recharge level (50% and 150% in this case) to the baseline of the GAM (100% recharge) the variation is due only to the change in recharge. It can be seen in both recharge scenarios for layer three (c and d in Figure 2.3) that the grater changes take place in areas away from the layer one outline and also, they follow a different directionality (transversal to the river flow Northwest to Southeast). The BRAA's GAM was constructed under MODFLOW USG, and as such, the first and second layer have a smaller grid cell size, 1/8 of the cells in layer 3 (Ewing & Jigmond, 2016), furthermore the third layer extends well beyond the river's banks and receives recharge in a large area (Figure 2.6). Given that, and the clay and silt that the river deposited in the first and second layer, this creates a hydraulic isolation between the second and third layer which contributes to the different behaviors seen in the model.

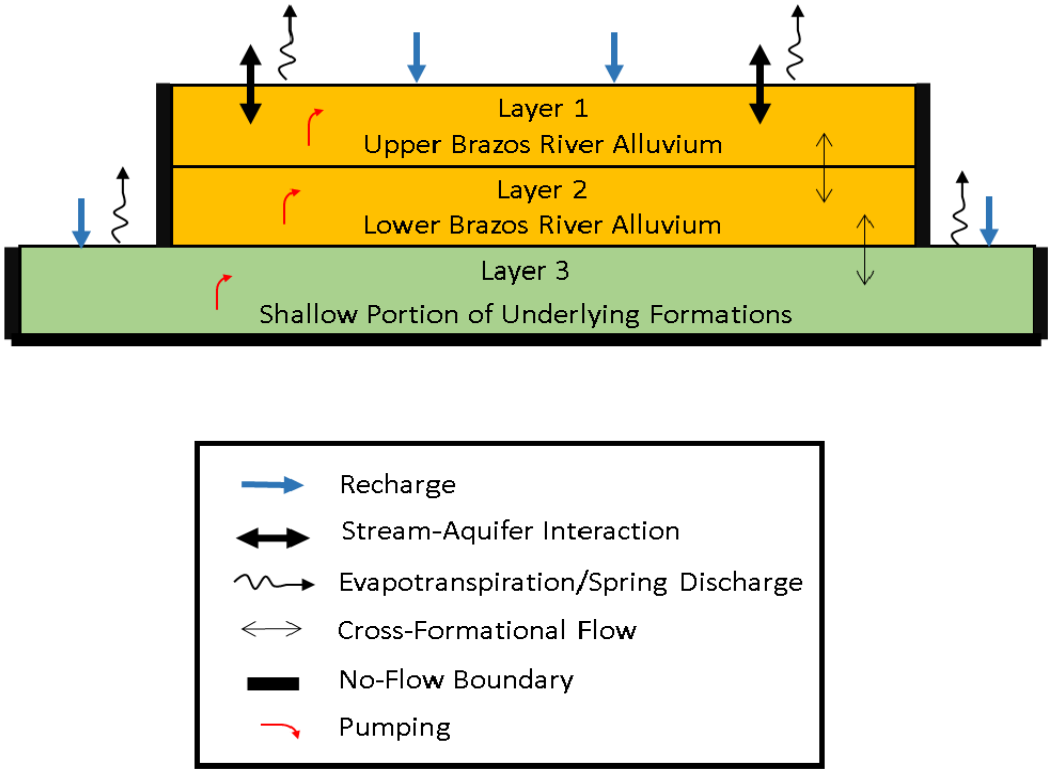

Figure 2.8 Brazos River Alluvial Aquifer Conceptual Model (Ewing & Jigmond, 2016)

This same difference in behavior can be appreciated in the streams and rivers flowing throughout the GAMs (Figure 2.5). Since the mean baseflow values are generated with the whole of the river taken into account and not differentiating between gaining and losing sections within the aquifer, the mean baseflow value gives a rough estimate of the effect of changes in recharge on the rivers. Moreover, some sections of the same river are determined as "rivers" (under MODFLOW's river package) and others are classified as "streams" (under MODFLOW's stream package) a true comparison is not feasible since the geographical location of the riverbeds was used to determine which cells, both river and stream, belonged to each river. For that reason, the baseflow data, while presenting a good idea of the behavior of the rivers with the changes in

recharge, is an estimator and not a true value and is used to determine the relation to recharge changes and not to estimate the real baseflow value.

The obtained models (linear regressions), to which the data was fitted to, present a linear tendency in all the analyzed GAMs (Table 2.2) and, while there is a variability in the coefficient of determination r^2 between them, it is considered that the data follows the linear models in a good way, i.e. the linear models explain the GMS calculated data. Known the linear tendency of the data, it is important to note that several GAMs also present a high threshold in mean head. It is important to note that, while it would be possible to find the value of recharge at which all the aquifers stop responding to increases in recharge (their recharge threshold level) it would just be a mathematical thought experiment since in nature even an increase of 50% recharge from the normal recharge for a sustained period of time is not likely, moreover an increase of 100% or more. Even though it wouldn't be feasible to assume or expect a recharge increase of more than 50% the normal recharge for the whole run-time of the model, some of the analyzed models were subjected to a greater recharge level. This was done to gain a better understanding of the aquifers behavior when they are subjected to a short-term (compared to the total model's run-time) increase in recharge.

In regard to the stored volume variation in the GAMs (Table 2.2), the magnitude of the slopes are higher when compared to the ones form the linear models of mean head, but the linear tendency is also present. All of them are negative with the highest in magnitude being again the Trinity North's GAM and the smallest in magnitude being the Hueco Mesilla Bolson's GAM. The negative direction of the slope signifies, since the stored volume is calculated for the aquifer as a

whole with the difference between the input to storage and the output to storage (i.e. the difference between the volume that enters the soil matrix minus the one that leaves the soil matrix), that the volume extracted from the aquifer as a whole decreases with the increase of recharge. The output of stored volume is due baseflow, pumping, evapotranspiration, and connections with other formations and, in some cases, such as the Hueco Mesilla Bolson, the change in the stored volume change is minimal compared to the other aquifers (-381.4 m^3 per percentage point of recharge increase).

For the case of the baseflow data and its correlation to changes in recharge under a linear model, each one of the rivers in each one of the GAMs was separated to perform one linear regression for each one of them. While all the models have a high determination coefficient ($r^2>0.9$) in some cases, such as the Brazos and Colorado rivers in the Edwards Balcones Fault Zone North where the determination coefficients are 0.904 and 0.934, respectively (Table 2.3). The data, however, shows a greater tendency to plateau near 150% of the normal recharge. This tendency is the origin of the lower r^2 values since the linear model cannot, accurately, represent such tendency. In the case of the Nueces River, in the Gulf Coast North aquifer, the threshold is of around -20 thousand cubic meters per day near 140% recharge. The tendency to a threshold supports the idea that, while the head, stored volume, and baseflow will rise linearly correlated to recharge, all these values will find a ceiling after which they will stop reacting to the increases in recharge. This is the equilibrium point of the aquifer.

Even when an increase of more than 50% in the normal recharge would not be realistic or expected in nature for the whole run time of the models, the surge test offered more information

about the behavior of the aquifers in general to increased recharge rates in short periods of time. As such, the most and least recharge sensitive GAMs (neglecting the Hueco Mesilla Bolson GAM) were subjected to an artificial recharge surge of 10 times the normal recharge. This 1000% recharge was applied for the first year of the Trinity North and the Edwards Balcones Fault Zone San Antonio (Figure 2.6, a and c and b and d respectively). Even though the idea of 1000% the normal recharge to be sustained for a whole year in any scenario is not realistic, the manner in which the recharge (the volume of water that enters the aquifer) gets distributed and its effects in the mean head of the aquifers. While both aquifers tend towards returning to the same mean head level as if the surge in recharge did not happened, the Trinity North does it in a really slow manner and cannot reach it by the time the model ends (end of the stress periods). Contrasting that, the Edwards Balcones Fault Zone San Antonio reaches an almost undisturbed state after 5 years (Figure 2.6). The time difference for the time it takes each aquifer to return to their undisturbed state (3 years compared to >50 years) is due to their different hydrogeologic properties: while the BFZSA aquifer has a hydraulic conductivity and specific storage of 0.14 m hr^{-1} and 0.08 respectively (Lindgren et al., 2004), the TRN has values of 0.028 m hr^{-1} and 0.17 for the same properties (Kelley et al., 2014). This creates a faster water movement along the BFZSA compared to the TRN that diffuses the increased recharged volume quicker. The higher specific yield in the TRN indicates that the soil matrix can store a greater water volume but, paired with a lower hydraulic conductivity, once the porous space has been filled, the movement of it out of the matrix is significantly slower and takes a longer time to distribute the newly entered volume; this causes an uneven distribution of head along the aquifer that takes time to stabilize.

For the case of the Gulf Coast North subjected to Hurricane Harvey, the recharge surge developed in a similar manner to the one performed in the BFZSA GAM: An immediate increase and important head difference which dissipated quicker. By then end of the run time of the model (2050) only a difference of 0.5 m remained. Compared to the 240 m remaining in the BFZSA's GAM at the end of its run time, the recharge surge dissipated faster. This is due to the reduced period during which the recharge was applied (1 month) in comparison with a year in both previous cases. The key differences between the BFZSA and the GCN in regards to hydraulic properties, are that the second has a specific yield ten times smaller (0.02) than the first and a much smaller hydraulic conductivity of 0.00064 m hr^{-1} (Kasmarek, 2013). These differences create an even slower movement of the recharged water volume and, since the specific yield is also significantly smaller, a smaller volume gets stored originating a faster head increase.

Categorizing the GAMs (Table 2.1) depended on the spatial distribution of the increase in head along the GAM. Whereas all the GAMs experience a diffuse increase in head, the encountered hotspots (areas in which the variation of head increase or decrease is significantly greater that its surroundings) in some of them obeys to the spatial variability in hydraulic conductivity of the aquifers. For the case of boundary disconnects, such as the Edwards BFZ Spring, the existence of horizontal flow barriers isolates some sections of the GAM's cells form the interconnecting cells generating localized variation of head that differ from the hotspots. This, because a hotspot was defined as an area with great reactivity to recharge variations, and an isolated area does not have an increased sensitivity to recharge. The differentiation between confined and unconfined aquifers, or sections of the aquifers, is based upon the subcrop and outcrop sections of the aquifer. While a diffuse class an be given to the unconfined (outcrop)

section of the GAM, the confined (subcrop) has a different behavior and as such the GAM was classified as confined/unconfined (C/U).

The categories into which the rivers were classified (Table 2.3) depend upon the tendency of the baseflow and its correlation to the variable recharge values to which each GAM was subjected. While all the rivers have an increase in baseflow as the recharge in the GAM increases, the behavior of each one was classified as exponential, linear, asymptotic, threshold, inflexion, or a combination of two classes. Even when some of the rivers in a GAM are in a different class, such as the San Antonio River in the Carrizo-Wilcox Center GAM that has a linear tendency when all the other rivers have a threshold tendency (Table 2.3), each GAM has a predominant class to which all the rivers belong. In regard to the rivers that transverse more than one GAM, their behavior also changed (Figure 2.6). Since the baseflow from the aquifers depends on the geohydrology, different formations yielded different behaviors for the same river.

The obtained reaction of the most and least recharge sensitive GAMs to the sudden and short termed increase of recharge (first simulation year), show the adaptability of said GAMs to sudden changes to the recharge regime in Texas. The current changing hydroclimate in the state, originated by the eastern movement of the climate boundary (i.e. the country wide boundary between the Arid and Humid climates located around the 100^{th} meridian) due to human generated climate change (Seager et al., 2017), is, and will continue to modify the intensity and frequency of draught and humid years. As such, knowing how the aquifers in the state react to sudden and short termed (less than a year) increases in recharge, will help in the management of groundwater

availability. Said increases in diffuse recharge can be then used to increase the stored water volume in the most sensitive aquifers to ensure a continued water supply.

2.6. Conclusions and Recommendations

The use of models such as the GAMs, to determine and estimate the behavior of aquifers is one of the first steps for planning and management purposes. Jointly, being natural or artificial recharge (for the case of this analysis diffuse), the sole mean thought which groundwater is replenished, the analysis of how said GAMs react to changes in recharge helps to better design and implement conservation and exploitation policies with sustainability in mind. It has been shown that the majority of the analyzed GAMs, and by extension the aquifers they compose, follow a linear trend dependent on recharge in regards to mean head, baseflow to streams and rivers, and variations in stored water volume. These trends, and the slopes their linear models have, depend mainly upon the hydrogeological properties of each aquifer. Looking only at the mean head increases it could be inferred that the aquifers with the greater head gains are the ones that store the larger volume of water but, if the specific yield of said aquifer is taken into account, it can be seen that a high increase in mean head does not reflect, forcefully, a larger stored water volume. For that reason the conjunction of the percent mean head increase and the specific yield point to the North, South, and Central sections of the Carrizo Wilcox aquifer, the North section of the Gulf Coast aquifer, the Springs section of the Edwards Balcones Fault Zone aquifer, and the North section of the Trinity aquifer as the most sensitive and with higher specific yield ones and thus, the aquifers that would benefit the most from the recharge-driven projects outlined in the 2017 Water Plan.

Specific aquifers were identified as the ones that would benefit the most, it is important to point out that the interactions between the different sections and aquifers themselves is, sometimes not completely considered in the creation of the GAMs and, as such, their results have to be further analyzed in the context off the whole groundwater system in which the state depends. As it was stated, of the eight analyzed aquifers, seven of them constitute 87% of the states groundwater supply and should be considered as a complete interdependent system. For the case of the Brazos River Alluvium Aquifer, the modeling using the USG version of MODFLOW, however challenging being the GAM coded for a beta of the program, gave an important insight in the behavior of a complex aquifer and the compartmentalization of alluvial aquifers and how that affects the overall reaction to variations in recharge and how it compares to the other, more homogeneous (in comparison) aquifers. The presence of only one mayor river in this aquifer is also of note since almost all of them contain more than one. As such, the BRAA has only one main source of recharge and baseflow discharge: the Brazos River, whose variation is not only correlated to the recharge, but more directly linked to the head changes in the surrounding (Layer 1 and 2) banks of the river.

The reaction of the aquifers tested with surges in recharge, while outside of the probable range of recharge increase, provide information on how the aquifers would react to sudden and significant increases in recharge during a short (Hurricane Harvey modelled on the Gulf Coast North GAM) or long period of time (a year with 10 times the normal recharge in the Edwards Balcones Fault Zone San Antonio and Trinity North GAMs). While the three aquifers in this category show signs of returning to a non-disturbed state, the differences in their properties originates different timetables for each one of the aquifers (3 years for the Edwards Balcones Fault

Zone San Antonio, more than 50 years for the Trinity North, and 10 years for the Gulf Coast North).

The response of the aquifers to long (small but sustained along the whole runtime of the models) and short term (recharge surges of less than a year) changes of recharge answer to the changing hydroclimate in the state due to the eastern movement of the climate boundary (Seager et al., 2017). The aquifers' reaction to the shot-term changes in recharge helps to understand how and where the extra recharge will be stored in the soil matrix and whether or not it will increase substantially the water availability state wide. Some aquifers will store the added recharge efficiently (Trinity North Figure 2.6 a and b) but others will store it momentarily and then release it back as baseflow or intra-aquifer water movement (Edwards BFZ San Antonio Figure 2.6 c and d) in a short period of time.

The significance of both the obtained results and their proper interpretation being based upon the in-depth knowledge not only of the GAMs and the GUI under which they run (GMS), but of the different information sets that are required for their creation (hydrogeological, meteorological, water usage, surface-groundwater interactions, and groundwater modeling) emphasize the importance of proper data collection. This, since each GAM can only reflect the behavior of an aquifer depending on how accurately the data from which it was created reflects the reality of said aquifer. As such, and since the TWDB relies in the GAMs to the creation of the objectives to be met by the Water Plans (currently the 2017 adopted plan) the update and incorporation of new data to the models should be considered as it would improve the quality of the models and the predicted data they provide.

3. CONCLUSIONS

The obtained data from the models yielded the expected linear models of mean head, stored volume, and baseflow supporting the hypothesis that the aquifers react in a linear way to increases in recharge. The slope of said linear models follows the hydrogeological characteristics of the aquifers themselves, reveling that the predominant factor of said slope is the specific yield. Since a higher specific yield signifies that the aquifer can store more water volume per unit of gained head, an aquifer with a higher specific yield has a greater capacity to store groundwater. Given the importance of the analyzed aquifers as the groundwater supply of the state, the knowledge of which ones react stronger, increase their head higher, and store the greater water volume per unit of increased head is of great importance not only from an academic point of view, and to point the direction of further studies of recharge, but from a management and planning perspective. The aquifers of the North, South, and Central sections of the Carrizo Wilcox aquifer, the North section of the Gulf Coast aquifer, the Springs section of the Edwards Balcones Fault Zone aquifer, and the North section of the Trinity aquifer are clear candidates for the recharge-driven projects proposed and being implemented in the 2017 water plan by the TWDB.

From the geographical perspective, the different aquifers distribute in a way such that their sensitivity to recharge, being dictated not just by the different recharge levels each one receive, but by their hydrogeological properties, it is important to note that, since their geographical location determines the geological formations in which they are imbedded and part of, it also helps to explain the sensitivity they present. Furthermore, the presence of subcrops in some sections of the aquifers, hampers their ability to capture recharge in their whole surface, this reducing their

sensitivity to changes in recharge. Added to the formations, and thus the properties of the aquifers, the presence of rivers also has an important impact in the behavior of the aquifer since they take the role of regulators. The higher the head rises in the aquifer, the more baseflow discharge form it the river receives and, as such the increase in head of the aquifer stabilizes. This can be the Carrizo Wilcox, where the head stabilizes near the 140% recharge and the baseflow towards the river increases more rapidly.

This tendency to stabilization can also be observed with the increased recharge at the beginning of the BFZSA and TRN aquifers. Even though both were subjected to 10 times the normal recharge for one year (the first in the simulation) they experienced different stabilization periods with the TRN never achieving it within the models run time while the BFZSA did accomplished it in less than 10 years. Supporting this behavior as well is the case of the GCN aquifer subjected to the Hurricane Harvey's recharge rates. While the aquifer did not stabilize before the end of the runtime of the model, the difference at that point was of just half a meter.

All the gathered data is of importance in the comprehension of how the aquifers behave when they are subjected to different scenarios, in this case variating recharge, and the important amount of information they can provide for future research projects and the implementation of management strategies in the most indicated aquifers. However, the need of this models and the information they provide sheds light in the differences under which they were created. The different GAMs were commissioned by the TWDB to different companies, and the data used was the one available and pertinent at the time of creation. Some GAMs, such as the Hueco Mesilla created in 2001. Even though its hydrogeologic properties may have not changes in such a

geologically short period of time, the water and land usage data may not be up to date. While the TWDB commissions the actualization of the models periodically, it could also be performed with some guidelines from this research to point out the most important, from the recharge point of view, aquifers to, not just have their GAMs updated, but new recharge and meteorological data collected in order to better reflect the current state of the aquifers.

CITED LITERATURE

Allison, G., & Hughes, M. (1978). The use of environmental chloride and tritium to estimate total recharge to an unconfined aquifer. *Division of Soils, CSIRO, 16*(2), 181-195. doi:https://doi.org/10.1071/SR9780181

Anaya, R., & Jones, I. (2009). Groundwater Availability Model for the Edwards-Trinity (Plateau) and Pecos Valley Aquifers of Texas. *Texas Water Development Board*.

Aquaveo Inc. (2017). Groundwater Modeling System 10.3

Blandford, T. N., Blazer, D. J., Calhoun, K. C., Dutton, A. R., Naing, T., Reedy, R. C., & Scanlon, B. R. (2003). Groundwater Availability of the Southern Ogallala Aquifer in Texas and New Mexico: Numerical Simulations Through 2050. *Texas Water Development Board*.

Bruun, B., Jackson, K., & Lake, P. (2017). *2017 State Water Plan*. Texas Water Development Board

Chowdhury, A., & Mace, R. E. (2007). Groundwater Resource Evaluation and Availability Model of the Gulf Coast Aquifer in the Lower Rio Grande Valley of Texas: Report 368. *Texas Water Development Board.*

Chowdhury, A. H., Wade, S., Mace, R. E., & Ridgeway, C. (2004). Groundwater Availability Model of the Central Gulf Coast Aquifer System: Numerical Simulations through 1999. *Texas Water Development Board, Groundwater Availability Modeling Section*.

Dassi, L. (2010). Use of chloride mass balance and tritium data for estimation of groundwater recharge and renewal rate in an unconfined aquifer from North Africa: a case study from Tunisia. *Environmental Earth Sciences, 60*(4), 861-871. doi:10.1007/s12665-009-0223-1

Deeds, N., Kelley, V., Fryar, D., & Jones, T. (2003). Groundwater Availability Model for the Southern Carrizo-Wilcox Aquifer. *Texas Water Development Board*.

Dutton, A. R., Reedy, R. C., & Mace, R. E. (2001). Saturated Thickness in the Ogallala Aquifer in the Panhandle Water Planning Area-Simulation of 2000 through 2050 Withdrawal Projections. *Bureau of Economic Geology, Panhandle Water Planning Group Panhandle Regional Planning Commission*.

Ewing, J. E., Harding, J. J., & Jones, T. L. (2006). Final Conceptual Model Report for the Brazos River Alluvium Aquifer Groundwater Availability Model. *Texas Water Development Board*.

Ewing, J. E., & Jigmond, M. (2016). Final Numerical Model Report for the Brazos River Alluvium Aquifer Groundwater Availability Model. *Texas Water Development Board*.

Frankel, J. (2018). Crisis on the High Plains: The Loss of America's Largest Aquifer – the Ogallala. *University of Denver Water Law Review at the Sturm College of Law*.

George, P. G., & Mace, R. E. (2011). *Aquifers of Texas: Report 380*. Texas Water Development Board

Harbaugh, A. W., Banta, E. R., Hill, M. C., & McDonald, M. G. (2000). *MODFLOW-2000, The U.S. Geological Survey Modular Ground-Water Model - User Guide to Modularization Concepts and the Ground-Water Flow Process* (2000-92). Retrieved from

Heywood, C. E., & Yager, R. M. (2003). Simulated Ground-Water Flow in the Hueco Bolson, an Alluvial-Basin Aquifer System near El Paso, Texas. *U.S. GEOLOGICAL SURVEY, Water-Resources Investigations Report 02-4108*.

Jones, I. C. (2003). Groundwater Availability Modeling: Northern Segment of the Edwards Aquifer, Texas. *Texas Water Development Board, Report 358*.

Kasmarek, M. C. (2013). Hydrogeology and Simulation of Groundwater Flow and Land-Surface Subsidence in the Northern Part of the Gulf Coast Aquifer System, Texas, 1891–2009. *Harris–Galveston Subsidence District, Fort Bend Subsidence District, Lone Star Groundwater Conservation District, Scientific Investigations Report 2012–5154*.

Kasmarek, M. C., & Robinson, J. L. (2004). Hydrogeology and Simulation of Ground-Water Flow and Land-Surface Subsidence in the Northern Part of the Gulf Coast Aquifer System, Texas. *Texas Water Development Board, Harris-Galveston Coastal Subsidence District, Scientific Investigations Report 2004–5102*.

Kelley, V. A., Ewing, J., Jones, T. L., Young, S. C., Deeds, N., Hamlin, S., Jigmond, M., Harding, J., Pinkard, J., Yan, T. T., Scanlon, B. R., Reedy, B., Beach, J., Davidson, T., & Laughlin, K. (2014). Updated Groundwater Availability Model of the Northern Trinity and Woodbine Aquifers Final Model Report. *North Texas GCD, North Texas GCD, Prarielands GCD, Upper Trinity GCD*.

Killian, C. D., Asquith, W. H., Barlow, J. R. B., Bent, G. C., Kress, W. H., Barlow, P. M., & Schmitz, D. W. (2019). Characterizing groundwater and surface-water interaction using hydrograph-separation techniques and groundwater-level data throughout the Mississippi Delta, USA. *Hydrogeology Journal, 27*(6), 2167-2179. doi:10.1007/s10040-019-01981-6

Kumar, C. P. (2012). Climate Change and Its Impact on Groundwater Resources. *International Journal of Engineering and Science, 1*(5), 43-60.

Li, Z., Jasechko, S., & Si, B. (2019). Uncertainties in tritium mass balance models for groundwater recharge estimation. *Journal of Hydrology, 571*, 150-158. doi:https://doi.org/10.1016/j.jhydrol.2019.01.030

Lindgren, R. J., Dutton, A. R., Hovorka, S. D., Worthingtonl, S. R. H., & Painter, S. (2004). Conceptualization and Simulation of the Edwards Aquifer, San Antonio Region, Texas. *U.S. Department of Defense and Edwards Aquifer Authority, Scientific Investigations Report 2004–5277*.

MATLAB. (2016). MATLAB (Version R2016a). Natick, Massachusetts: The MathWorks Inc.

McDonald, M. G., & Harbaugh, A. W. (2003). The history of MODFLOW. *Ground Water, 41*(2), 280-283. doi:10.1111/j.1745-6584.2003.tb02591.x

Mohan, C., Western, A. W., Wei, Y., & Saft, M. (2018). Predicting groundwater recharge for varying land cover and climate conditions – a global meta-study. *Hydrol. Earth Syst. Sci., 22*(5), 2689-2703. doi:10.5194/hess-22-2689-2018

Panday, S., Langevin, C. D., Niswonger, R. G., Ibaraki, M., & Hughes, J. D. (2013). MODFLOW–USG version 1: An unstructured grid version of MODFLOW for simulating groundwater flow and tightly coupled processes using a control volume finite-difference formulation (Version 1): U.S. Geological Survey Techniques and Methods. Retrieved from https://pubs.usgs.gov/tm/06/a45.

Pena Rodriguez, A. (2019). Hydroshare, *Texas GAMs for recharge uncertainty analysis*. http://www.hydroshare.org/resource/e6642be0023d4269bd882a1a5dfc2593

Prudic, D. E. (1989). *Documentation of a computer program to simulate stream-aquifer relations using a modular, finite-difference, ground-water flow model* (88-729). Retrieved from

Scanlon, B. R., Mace, R. E., Smith, B., Hovorka, S., Dutton, A. R., & Reedy, R. (2001). Groundwater availability of the Barton Springs segment of the Edwards aquifer, Texas: numerical simulations through 2050. *Lower Colorado River Authority under contract number UTA99-0, Bureau of Economic Geology*.

Scanlon, B. R., Reedy, R., Strassberg, G., Huang, Y., & Senay, G. (2011). Estimation of Groundwater Recharge to the Gulf Coast Aquifer in Texas, USA. *Texas Water Development Board*.

Schorr, S., & Zivic, M. (2018). Conceptual model report: groundwater availability model for northern portion of the Queen City, Sparta, and Carrizo-Wilcox aquifers. *Texas Water Development Board*.

Seager, R., Feldman, J., Lis, N., Ting, M., Williams, A. P., Nakamura, J., Liu, H., & Henderson, N. (2017). Whither the 100th Meridian? The once and future physical and human geography of America's arid-humid divide: Part II: The meridian moves east. *Earth Interactions*. Retrieved from https://dx.doi.org/10.1175/EI-D-17-0012.1. doi:10.1175/ei-d-17-0012.1

TexMesonet. (2019). Custom Data Sets. Retrieved from https://www.texmesonet.org/HistoricalData

Toll, N. J., Green, R. T., McGinnis, R. N., Stepchinski, L. M., Nunu, R. R., Walter, G. R., Harding, J., Deeds, N. E., Flores, M. E., & Gulliver, K. D. H. (2018). Conceptual Model Report for the Hill Country Trinity Aquifer Groundwater Availability Model. *Texas Water Development Board*.

TWDB. (2001). *GAM Ogalla Northern Section* Texas Water Development Board Found at http://www.twdb.texas.gov/groundwater/models/gam/ogll_n/ogll_n.asp

TWDB. (2003a). *GAM Carrizo-Wilcox Central Section* Texas Water Development Board Found at http://www.twdb.texas.gov/groundwater/models/gam/czwx_c/czwx_c.asp

TWDB. (2003b). *GAM Carrizo-Wilcox Northern Section*. Texas Water Development Board Found at http://www.twdb.texas.gov/groundwater/models/gam/czwx_n/czwx_n.asp

TWDB. (2003c). *GAM Carrizo-Wilcox Southern Section* Texas Water Development Board Found at http://www.twdb.texas.gov/groundwater/models/gam/czwx_s/czwx_s.asp

TWDB. (2003d). *GAM Gulf Coast North Section*. Texas Water Development Board Found at http://www.twdb.texas.gov/groundwater/models/gam/glfc_n/glfc_n.asp

TWDB. (2003e). *GAM Hueco-Mesilla* Texas Water Development Board Found at http://www.twdb.texas.gov/groundwater/models/gam/hmbl/hmbl.asp

TWDB. (2003f). *GAM Ogallala Southern Section* Texas Water Development Board Found at http://www.twdb.texas.gov/groundwater/models/gam/ogll_s/ogll_s.asp

TWDB. (2004a). *GAM Edwards-Trinity Plateau*. Texas Water Development Board Found at http://www.twdb.texas.gov/groundwater/models/gam/eddt_p/eddt_p.asp

TWDB. (2004b). *GAM Edwards BFZ Southern Section* Texas Water Development Board Found at http://www.twdb.texas.gov/groundwater/models/gam/ebfz_s/ebfz_s.asp

TWDB. (2004c). *GAM Gulf Coast Central Section* Texas Water Development Board Found at http://www.twdb.texas.gov/groundwater/models/gam/glfc_c/glfc_c.asp

TWDB. (2007). *GAM Gulf Coast Southern Section* Texas Water Development Board Found at http://www.twdb.texas.gov/groundwater/models/gam/glfc_s/glfc_s.asp

TWDB. (2008). *GAM Edwards BFZ Cental Section* Texas Water Development Board Found at http://www.twdb.texas.gov/groundwater/models/gam/ebfz_b/ebfz_b.asp

Vaughan, E. G., Crutcher, J. M., W. Labatt II, T., McMahan, L. H., Bradford Jr, B. R., & Cluck, M. (2012). *2012 Water for Texas*. Texas Water Development Board

Young, S., Jigmond, M., Jones, T., & Ewing, T. (2018). Final Report: Groundwater Availability Model for the Central Portion of the Sparta, Queen City, and Carrizo-Wilcox Aquifers. *Texas Water Development Board*.

APENDIX A

River Plots

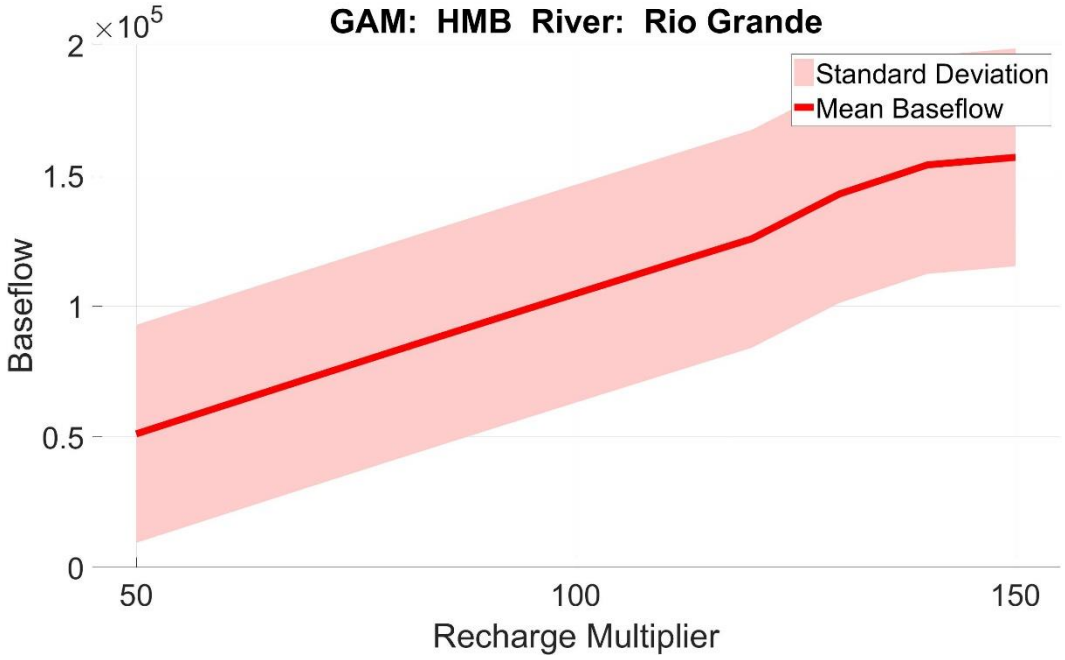

Figure 5. 1 River Baseflow in the Rio Grande River, Hueco Mesilla Bolson GAM

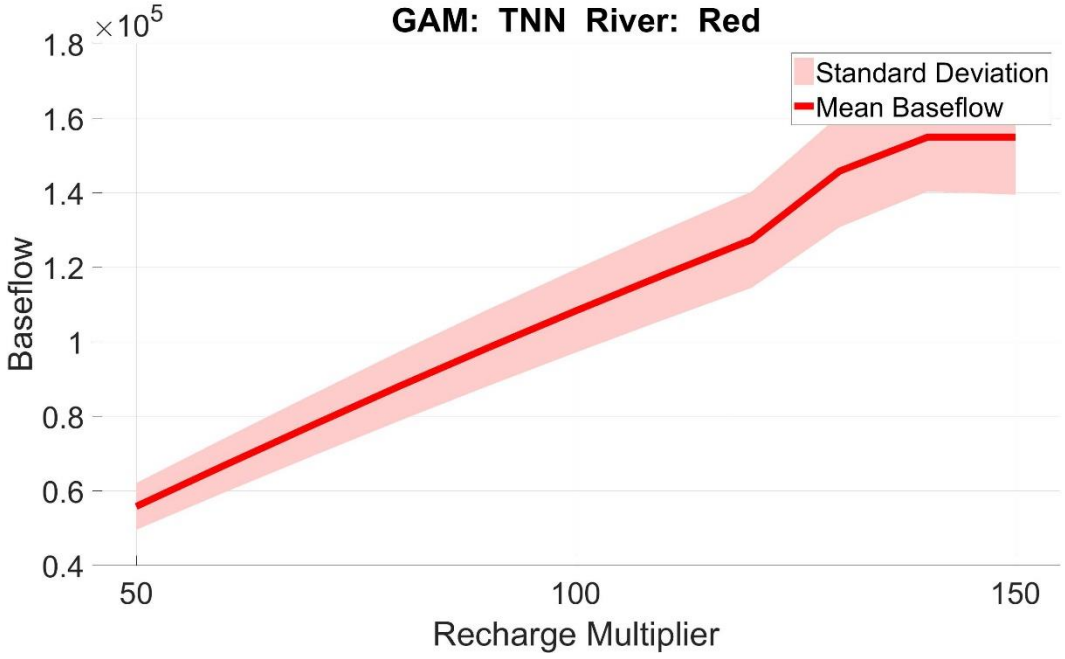

Figure 5. 2 River Baseflow in the Red River, Trinity North GAM

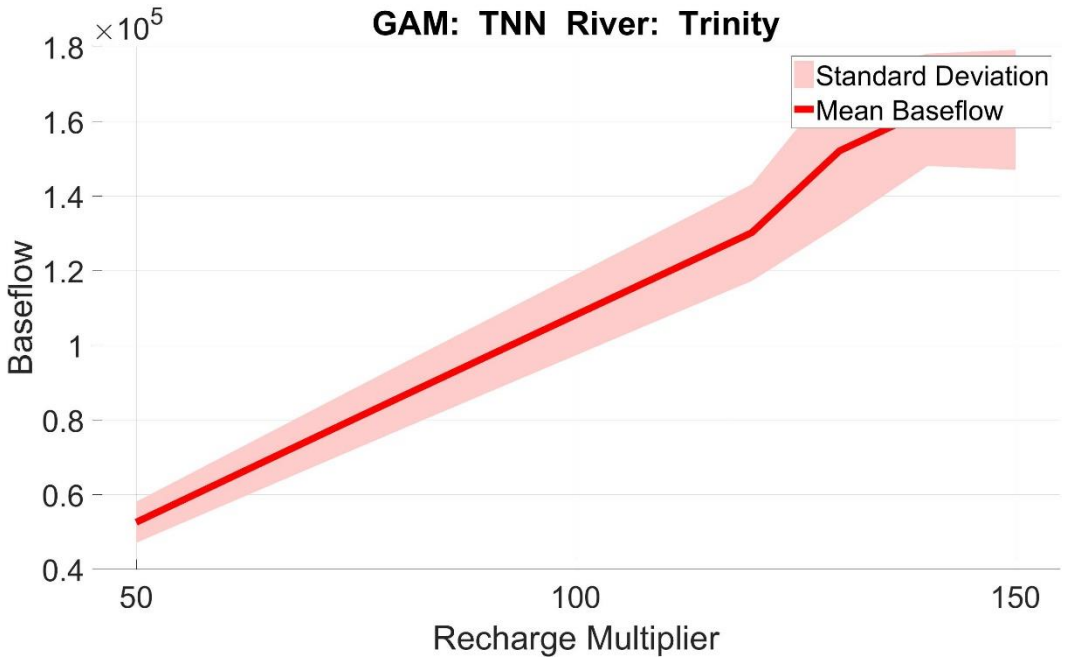

Figure 5. 3 River Baseflow in the Trinity River, Trinity North GAM

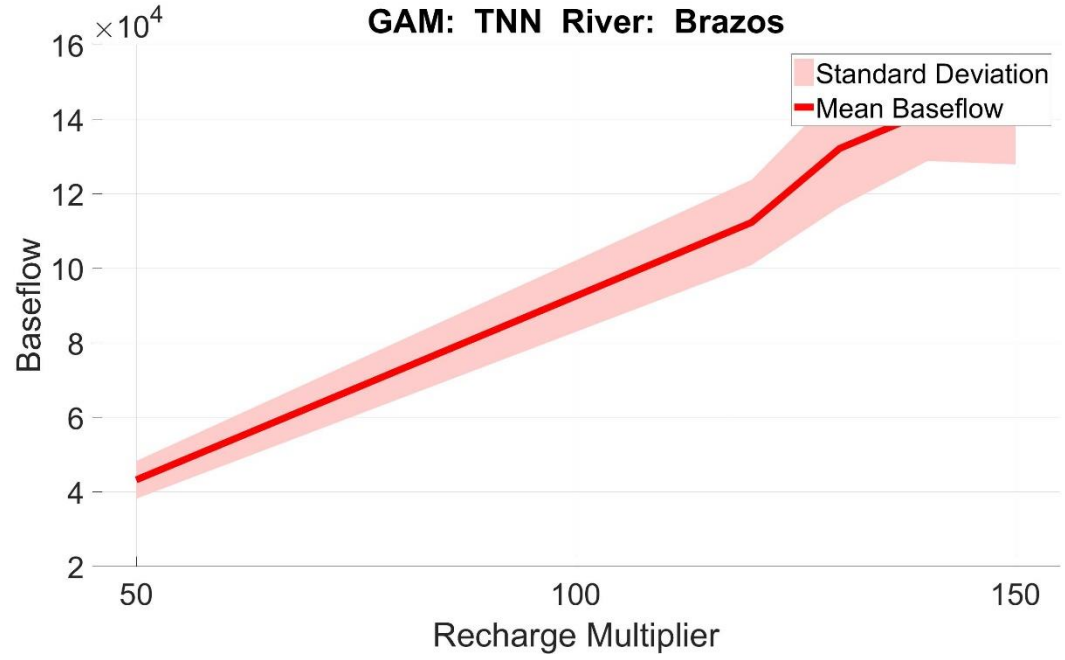

Figure 5. 4 River Baseflow in the Brazos River, Trinity North GAM

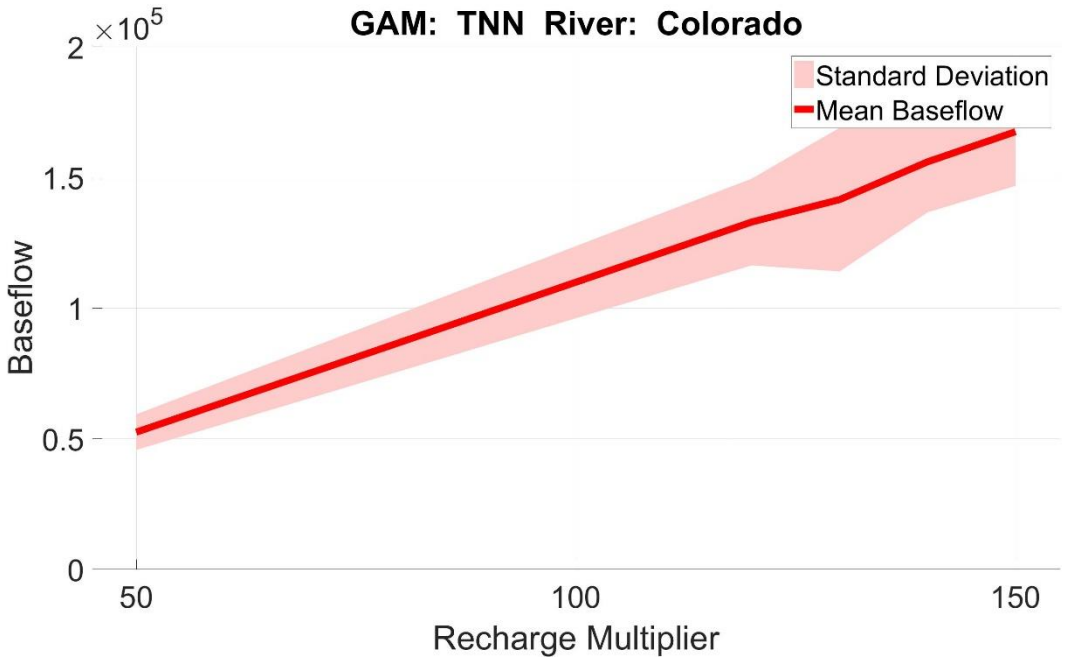

Figure 5. 5 River Baseflow in the Colorado River, Trinity North GAM

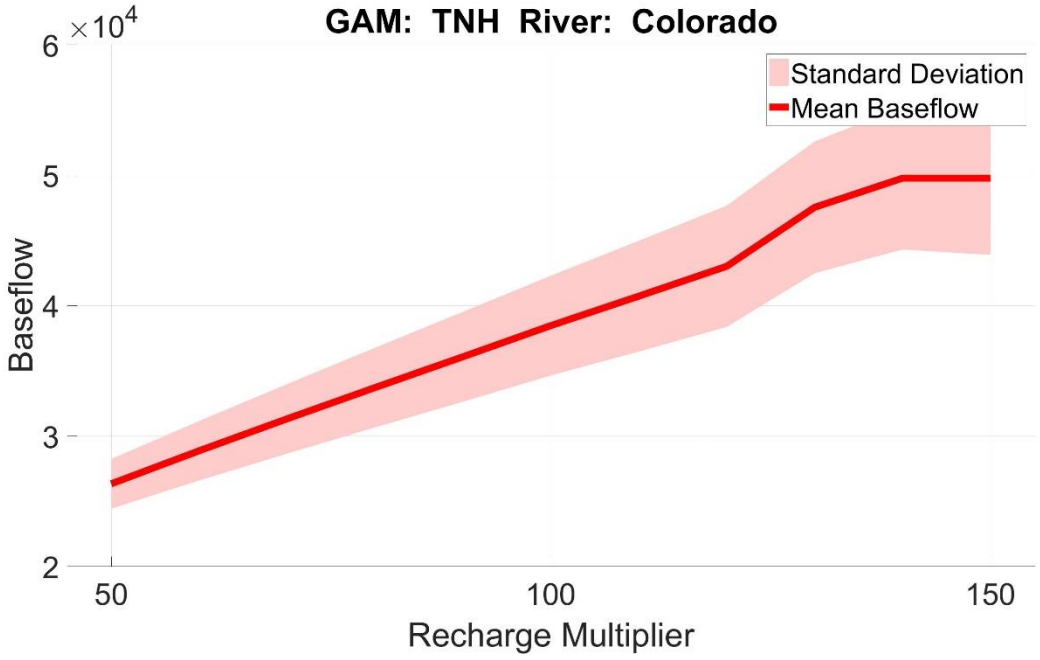

Figure 5. 6 River Baseflow in the Colorado River, Trinity Hill GAM

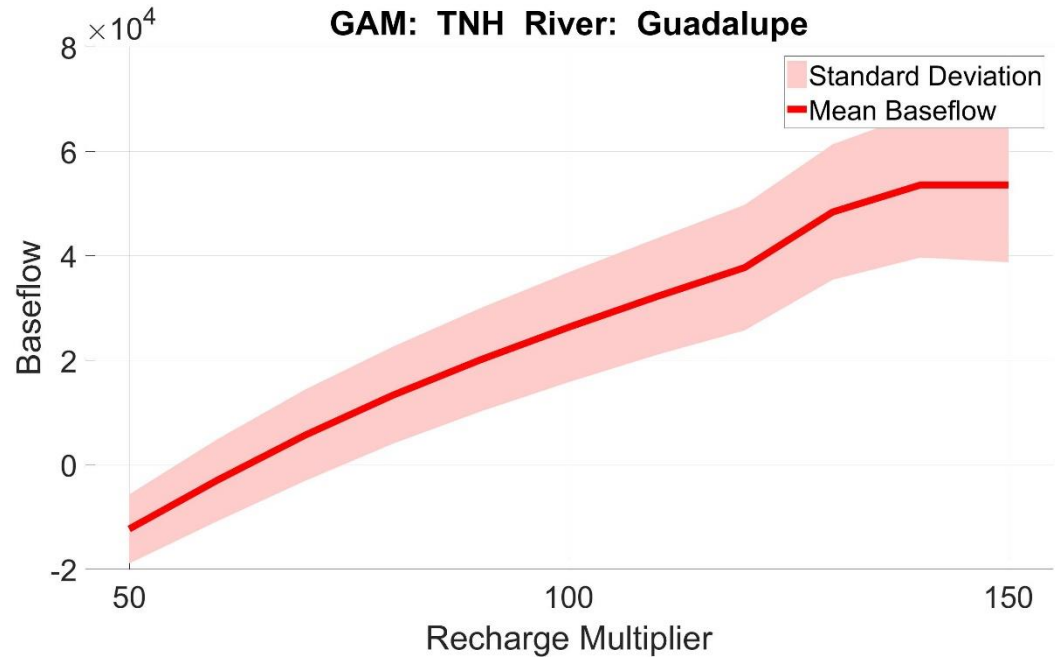

Figure 5. 7 River Baseflow in the Guadalupe River, Trinity Hill GAM

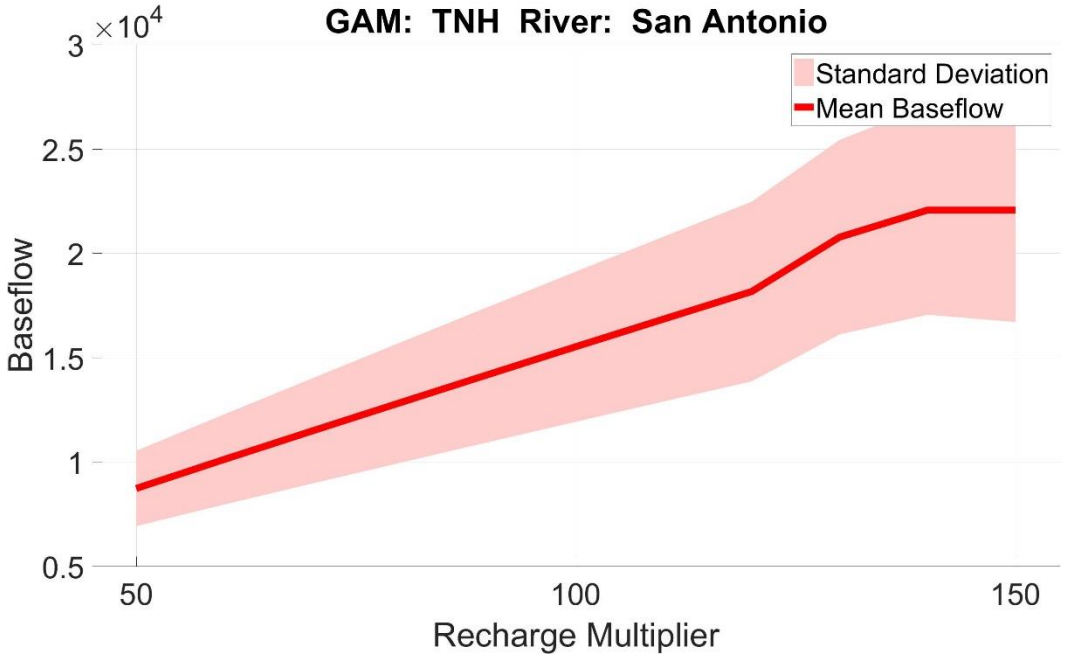

Figure 5. 8 River Baseflow in the San Antonio River, Trinity Hill GAM

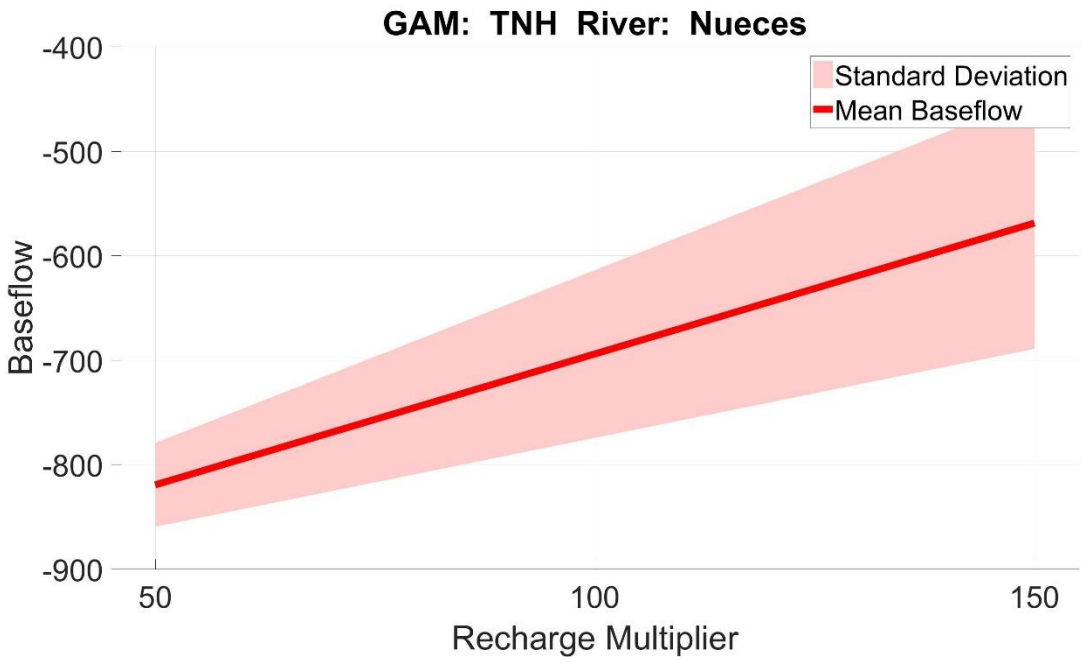

Figure 5. 9 River Baseflow in the Nueces River, Trinity Hill GAM

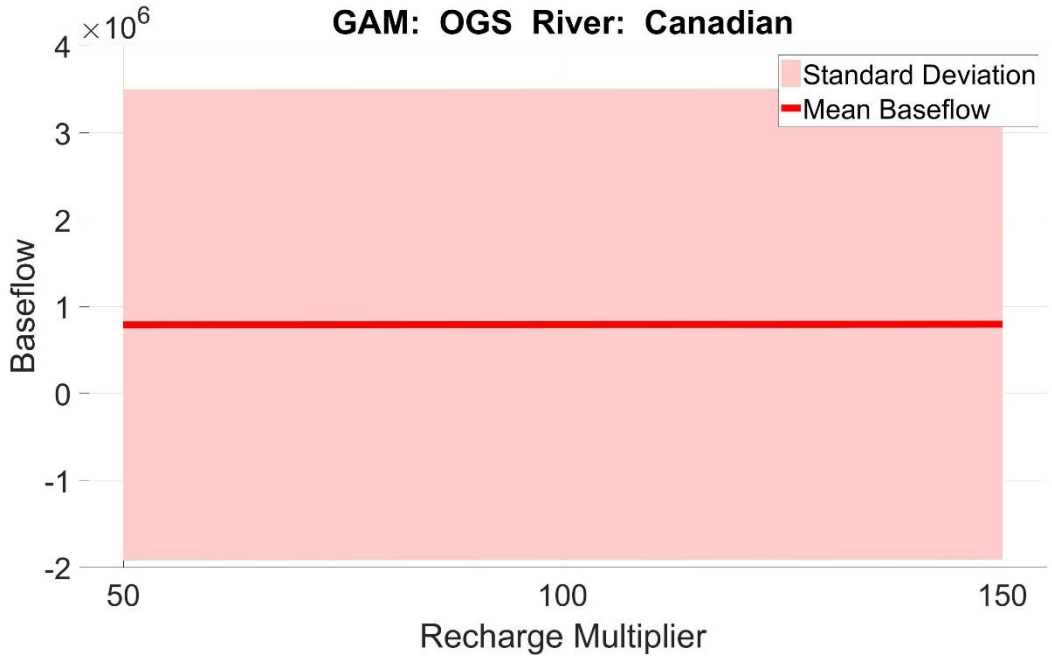

Figure 5. 10 River Baseflow in the Canadian River, Ogallala South GAM

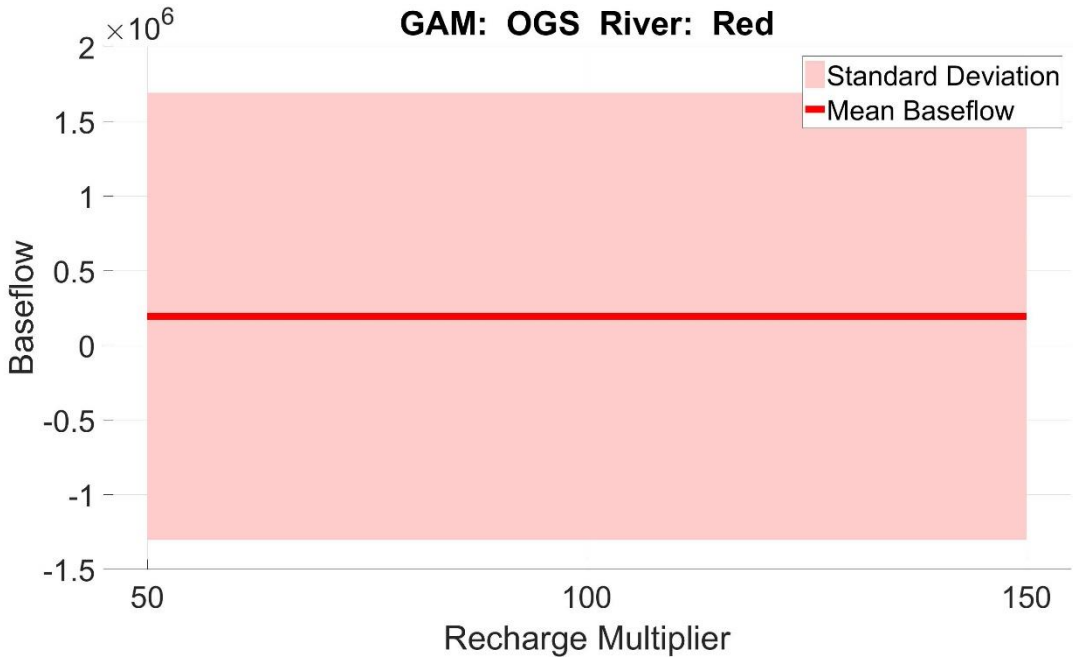

Figure 5. 11 River Baseflow in the Red River, Ogallala South GAM

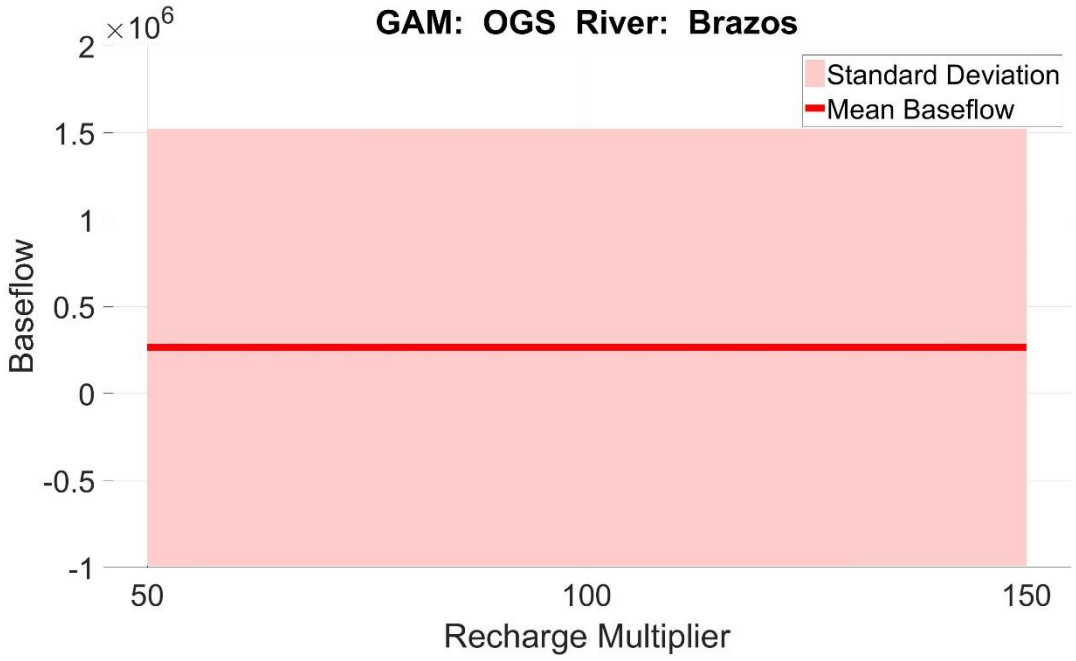

Figure 5. 12 River Baseflow in the Brazos River, Ogallala South GAM

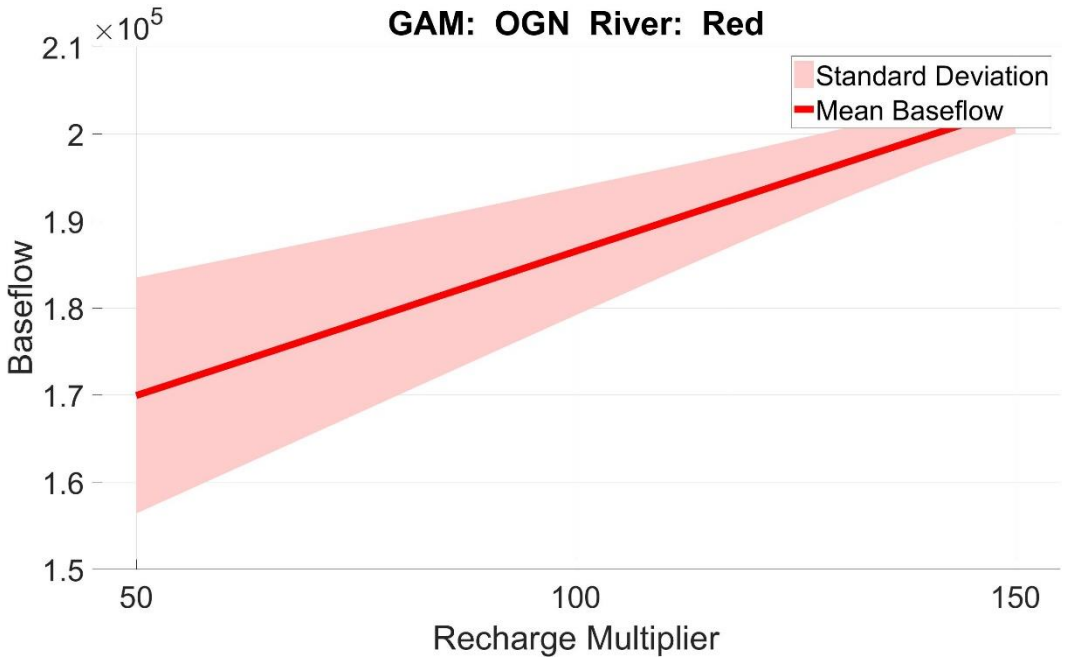

Figure 5. 13 River Baseflow in the Red River, Ogallala North GAM

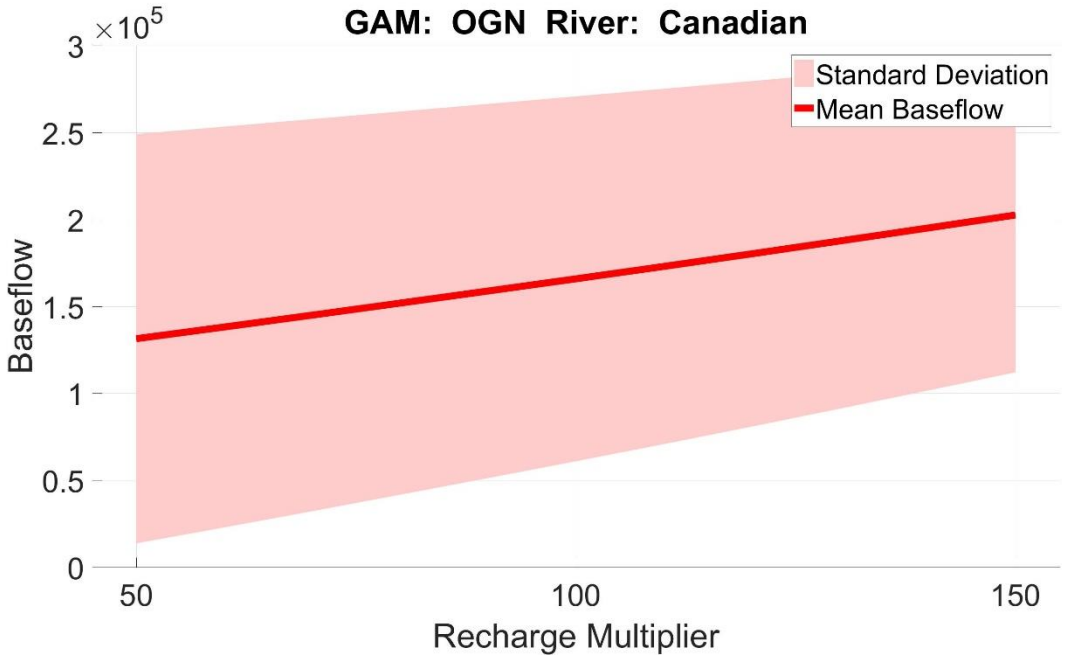

Figure 5. 14 River Baseflow in the Canadian River, Ogallala North GAM

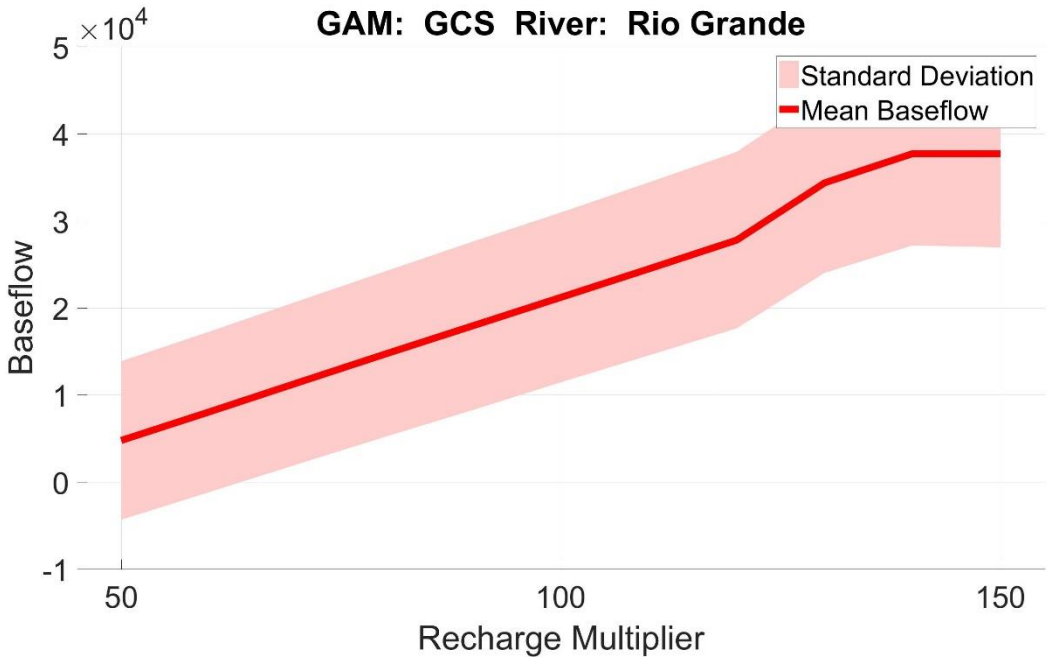

Figure 5. 15 River Baseflow in the Rio Grande River, Gulf Coast South GAM

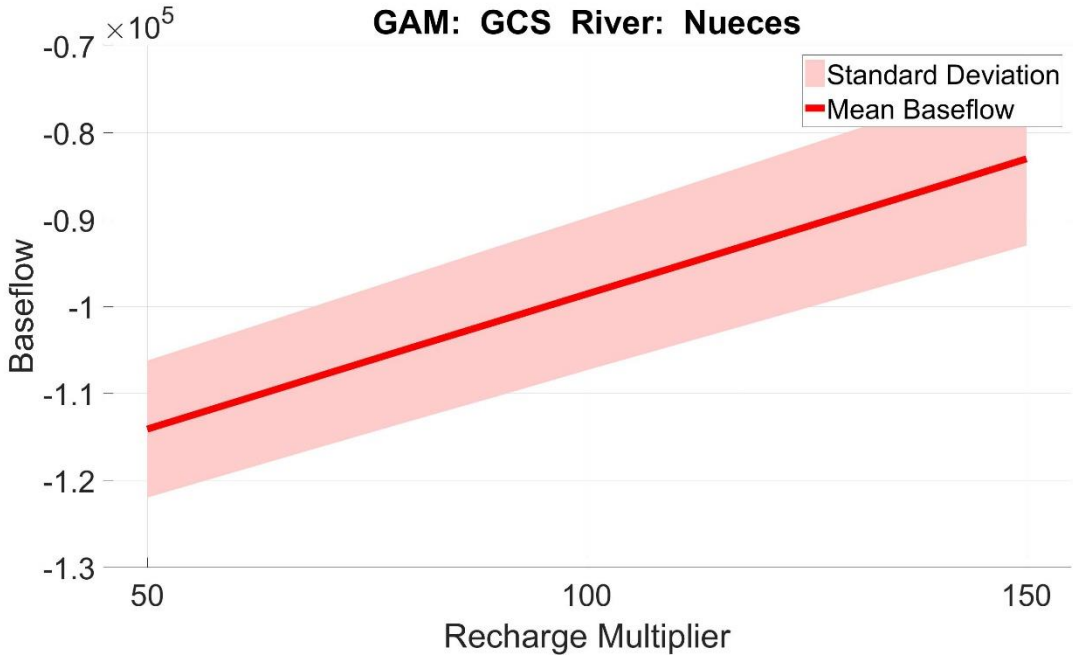

Figure 5. 16 River Baseflow in the Nueces River, Gulf Coast South GAM

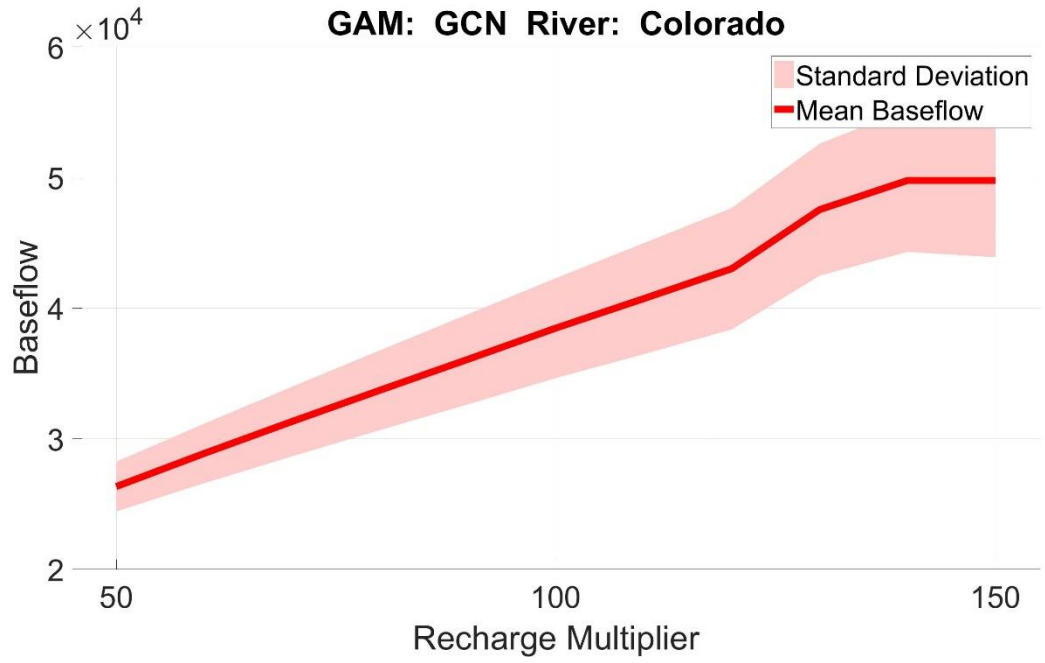

Figure 5. 17 River Baseflow in the Colorado, Gulf Coast North GAM

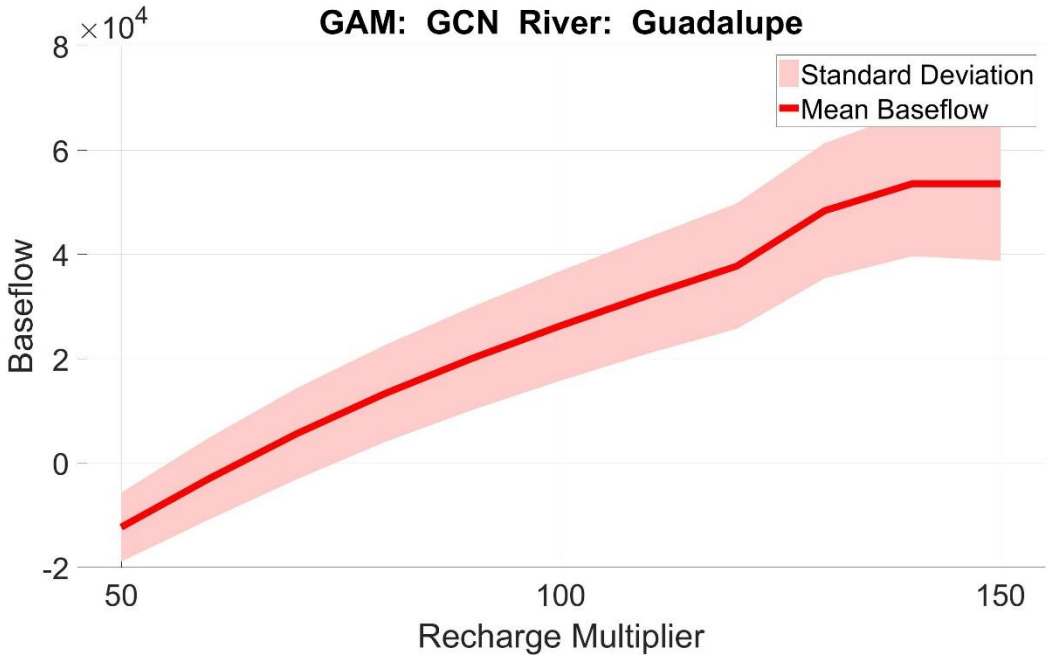

Figure 5. 18 River Baseflow in the Guadalupe River, Gulf Coast North GAM

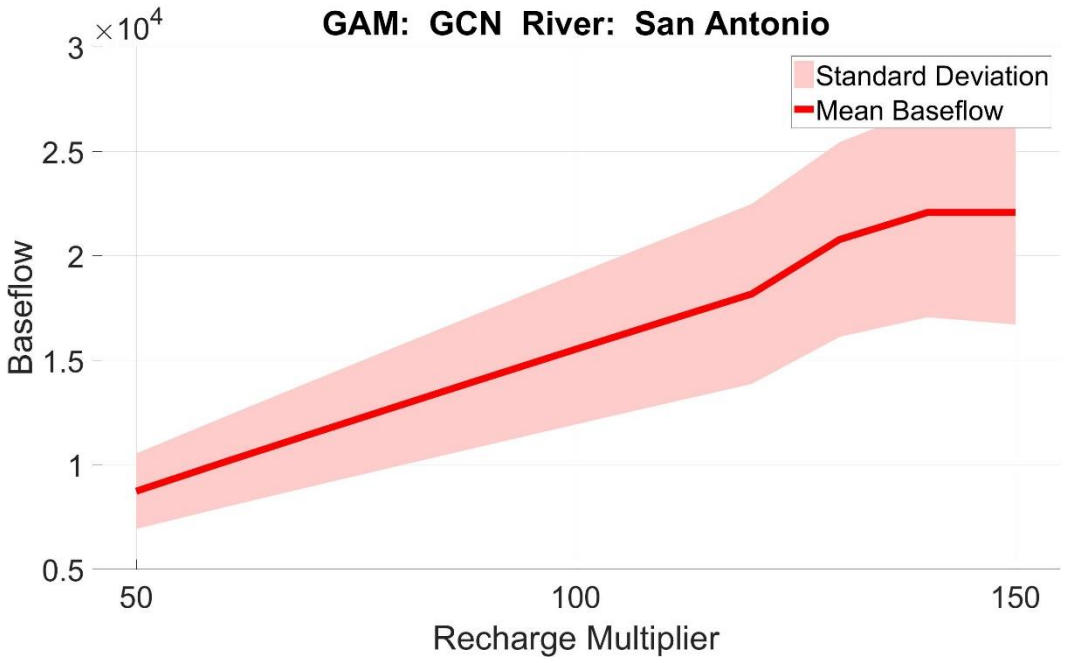

Figure 5. 19 River Baseflow in the San Antonio River, Gulf Coast North GAM

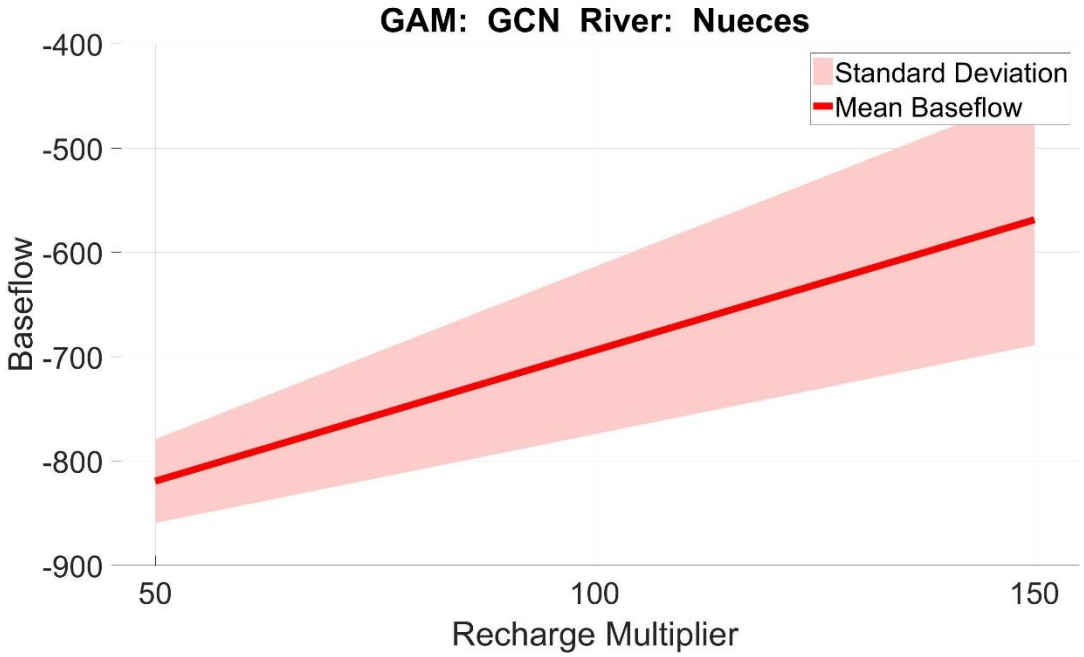

Figure 5. 20 River Baseflow in the Nueces River, Gulf Coast North GAM

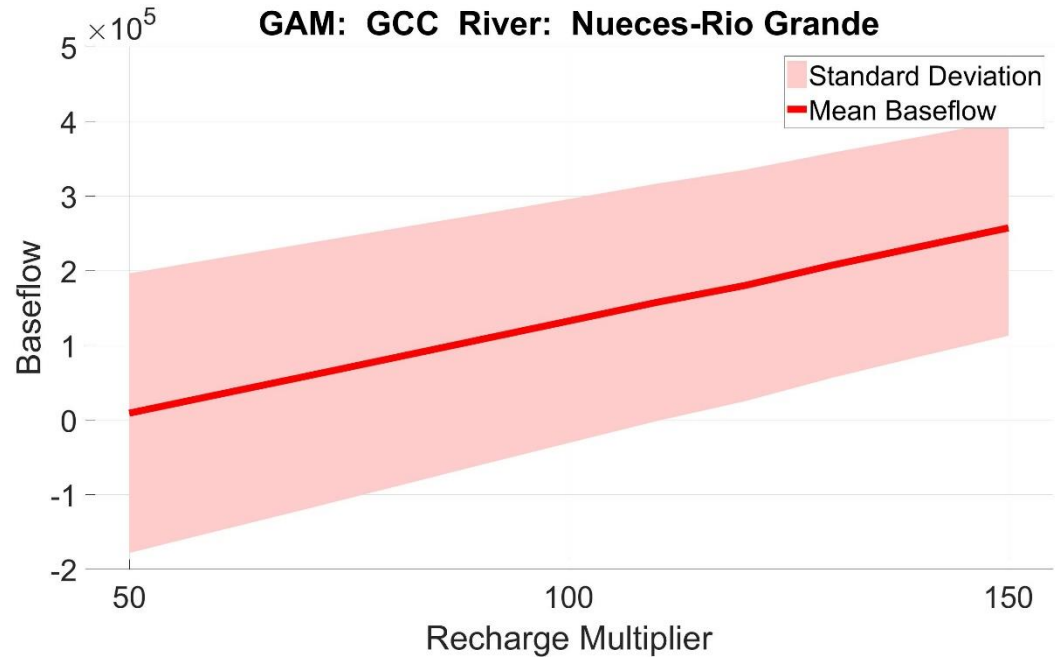

Figure 5. 21 River Baseflow in the Nueces-Rio Grande River, Gulf Coast Center GAM

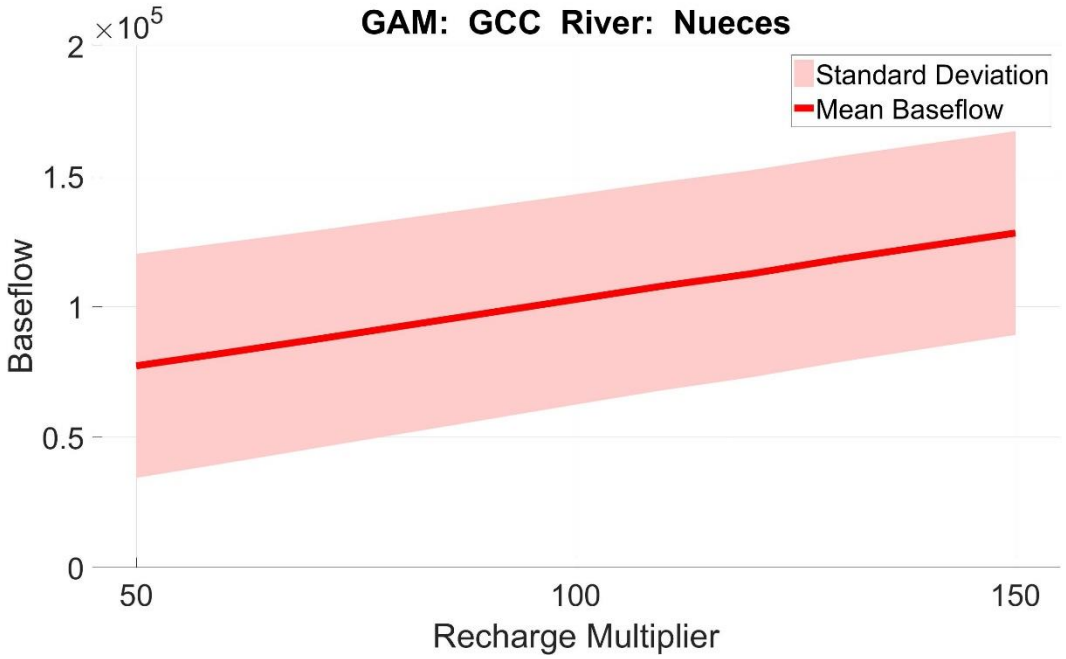

Figure 5. 22 River Baseflow in the Nueces River, Gulf Coast Center GAM

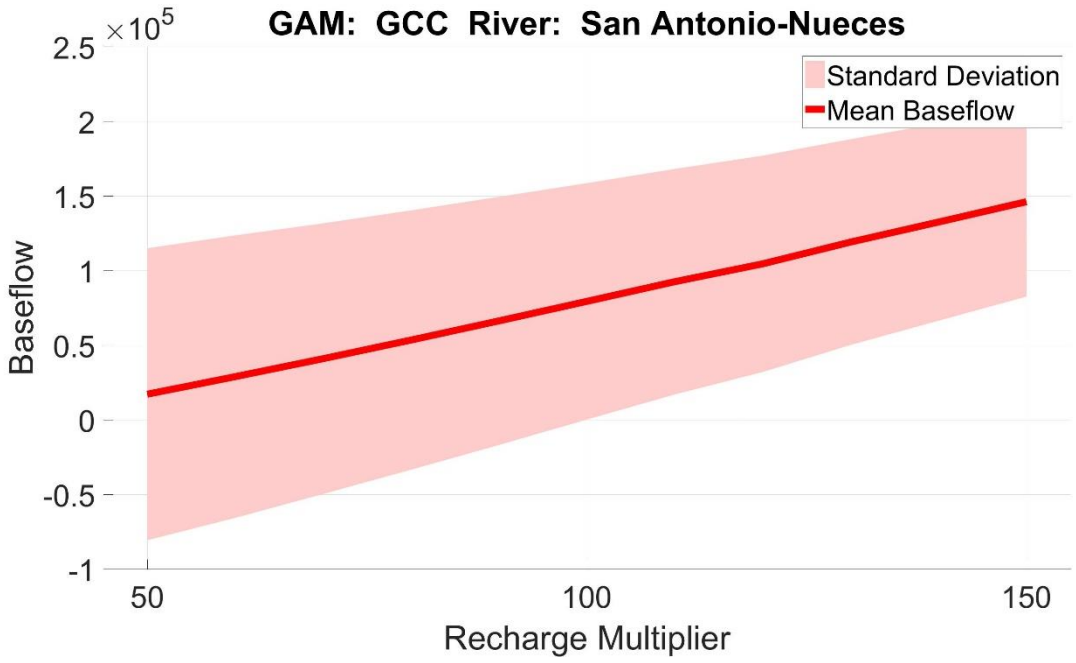

Figure 5. 23 River Baseflow in the San Antonio-Nueces River, Gulf Coast Center GAM

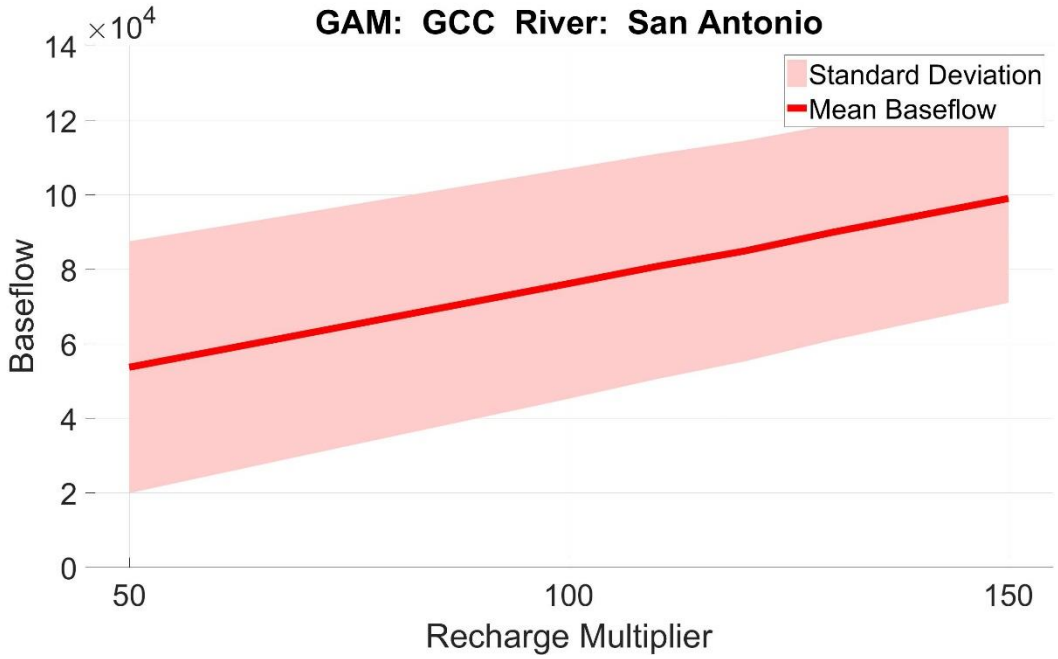

Figure 5. 24 River Baseflow in the San Antonio River, Gulf Coast Center GAM

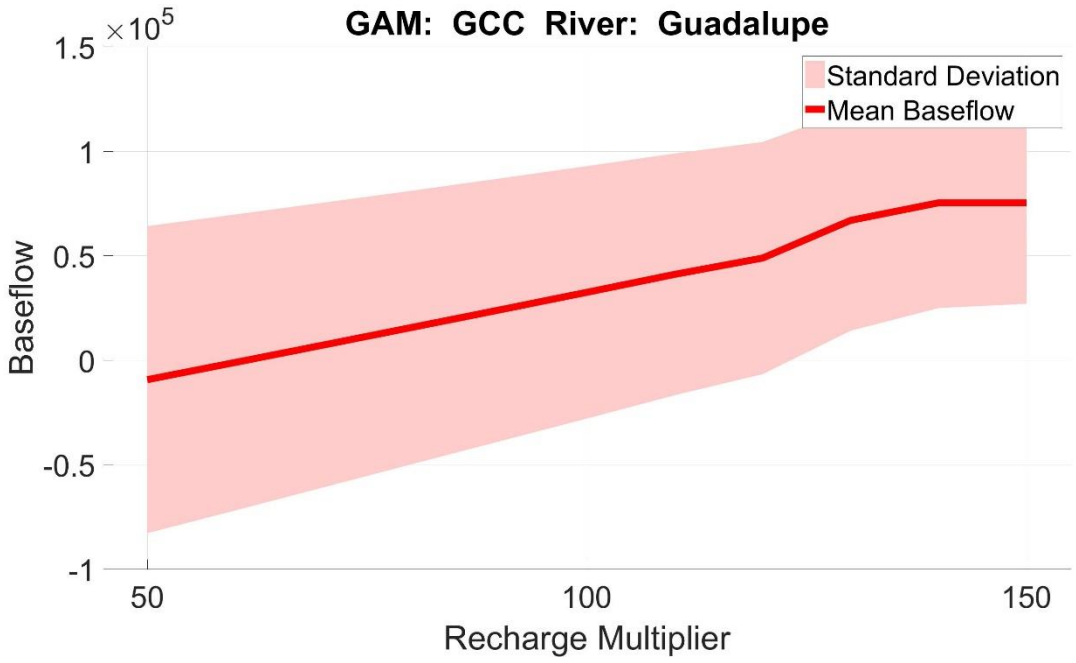

Figure 5. 25 River Baseflow in the Guadalupe River, Gulf Coast Center GAM

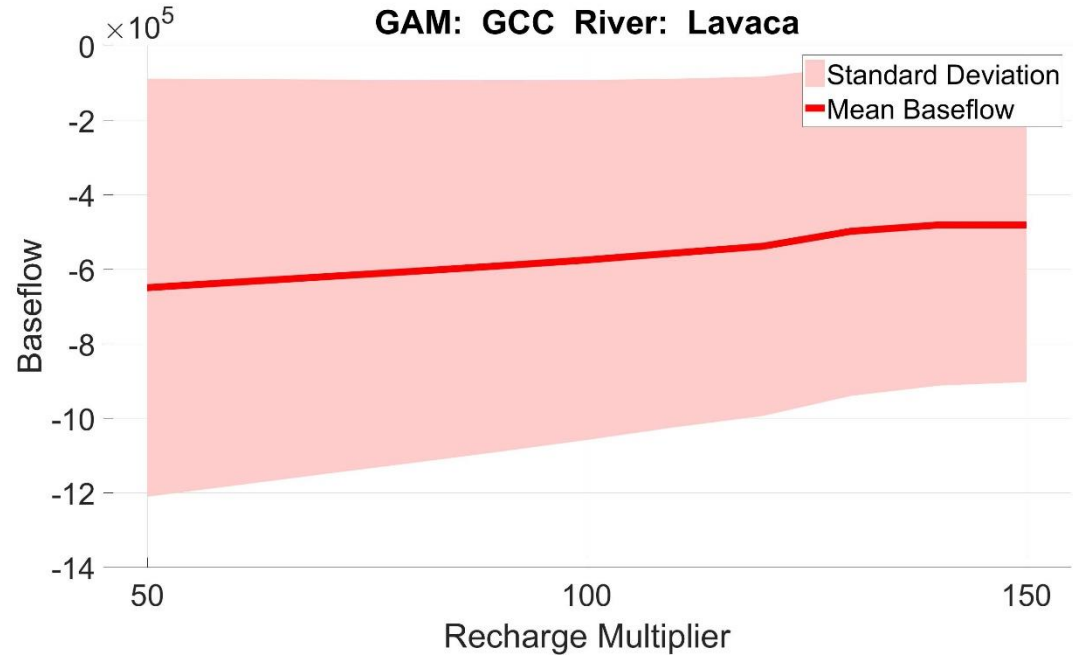

Figure 5. 26 River Baseflow in the Lavaca River, Gulf Coast Center GAM

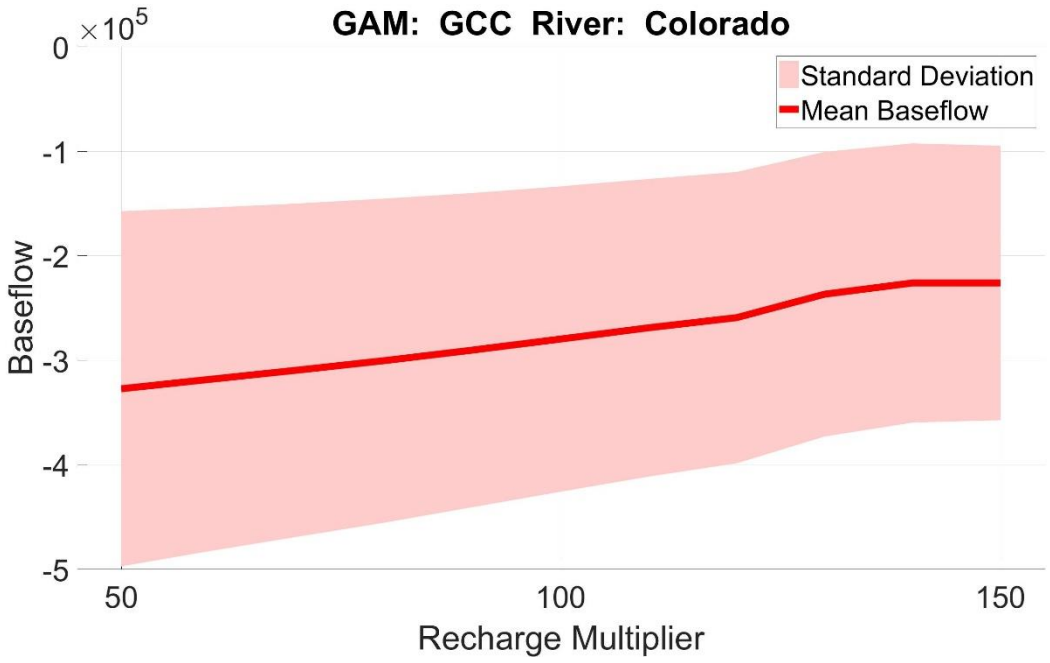

Figure 5. 27 River Baseflow in the Colorado River, Gulf Coast Center GAM

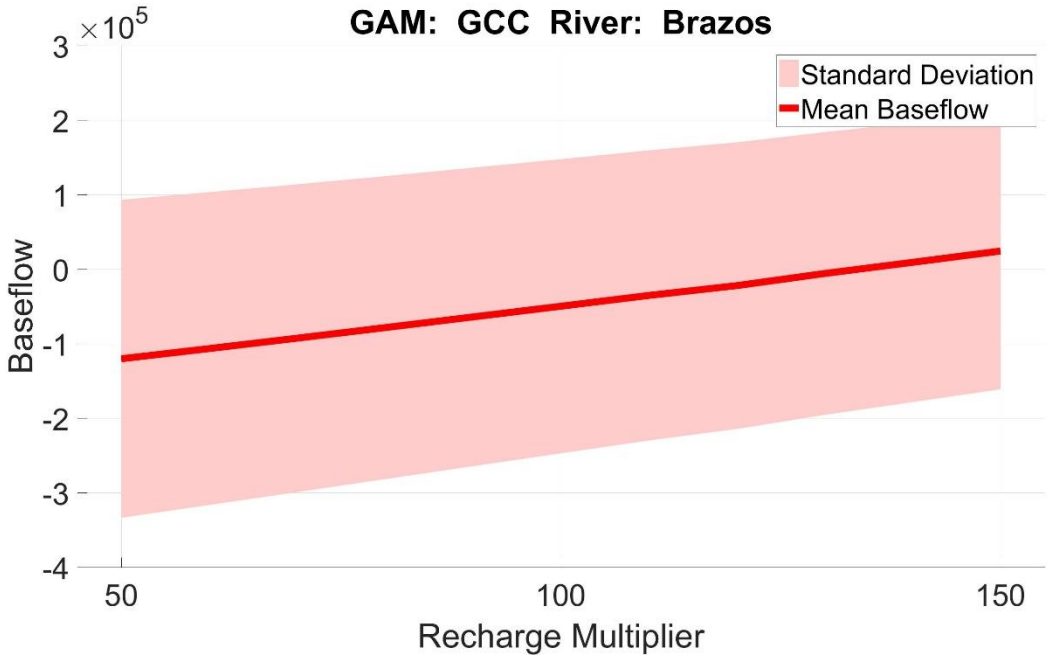

Figure 5. 28 River Baseflow in the Brazos River, Gulf Coast Center GAM

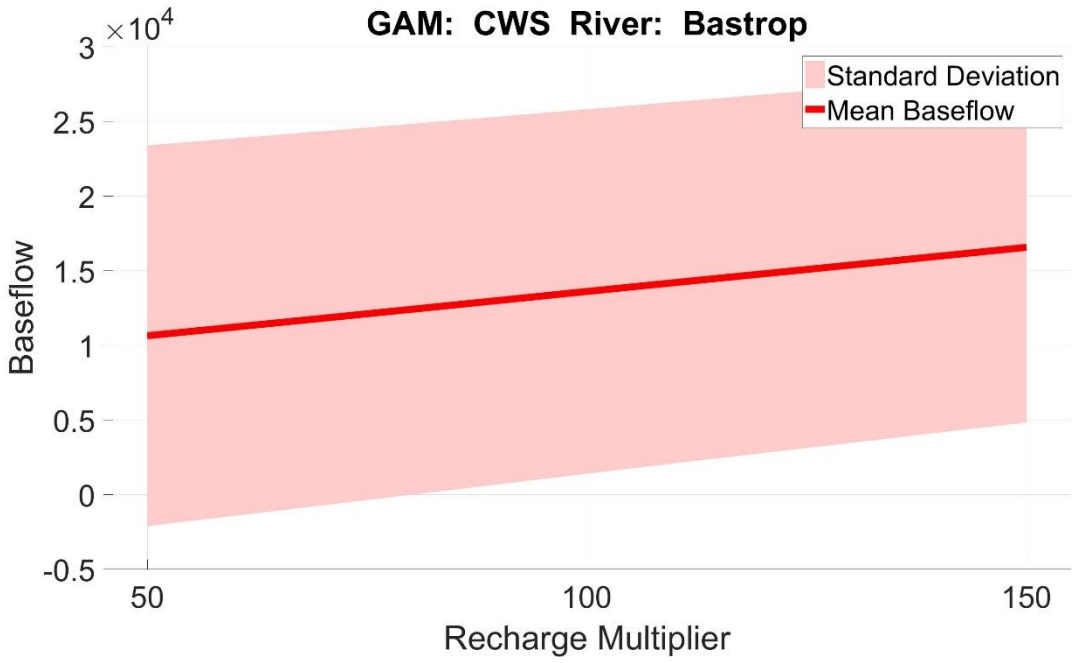

Figure 5. 29 River Baseflow in the Bastrop River, Carrizo-Wilcox South GAM

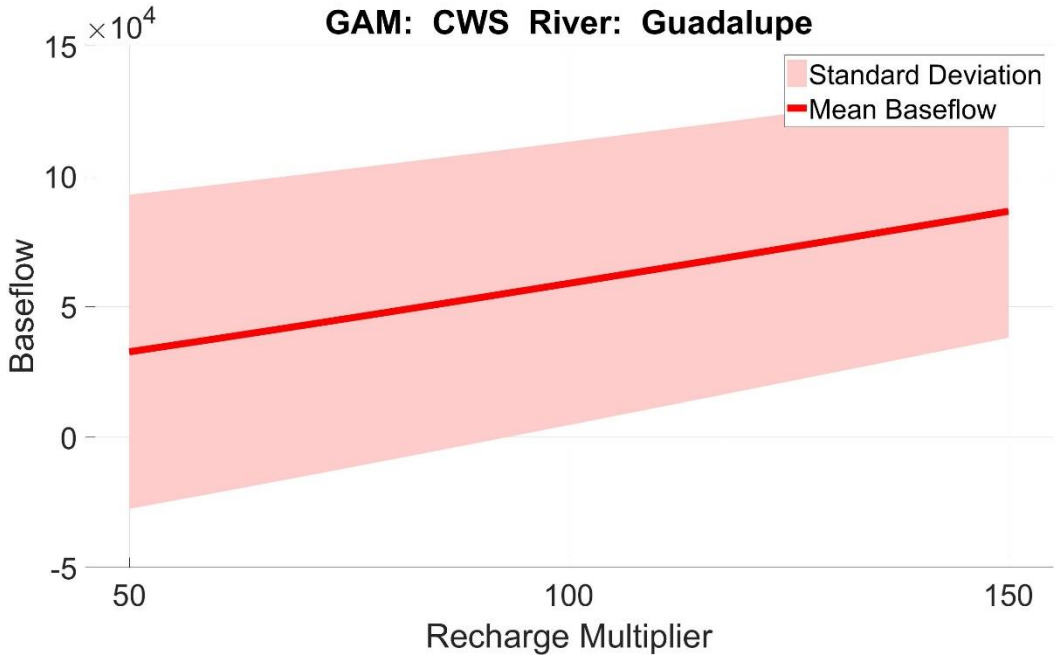

Figure 5. 30 River Baseflow in the Guadalupe River, Carrizo-Wilcox South GAM

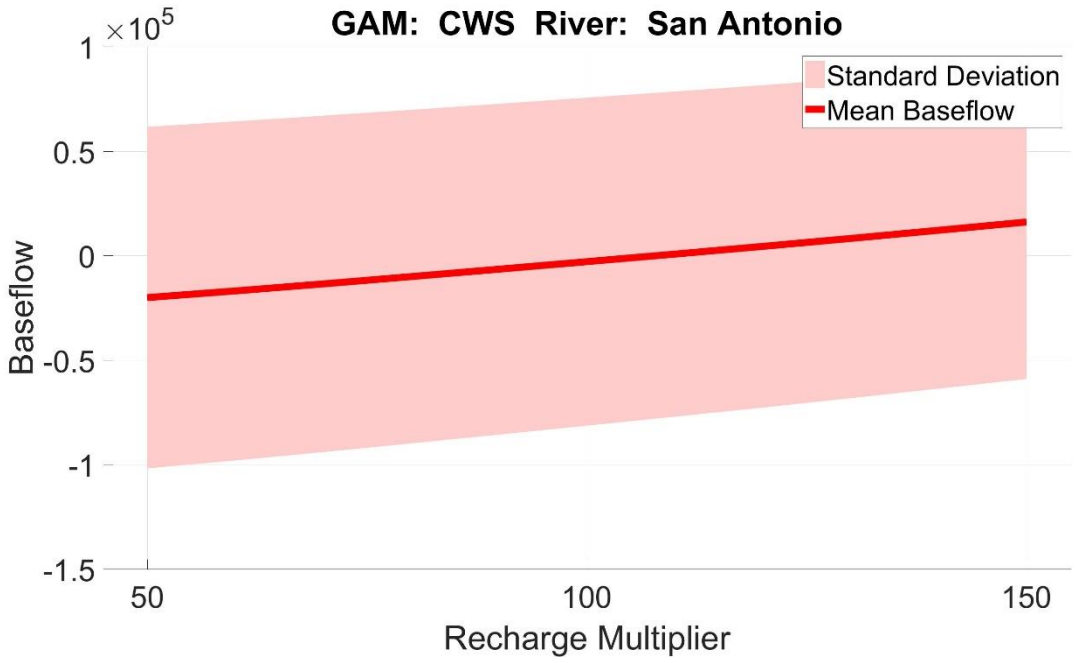

Figure 5. 31 River Baseflow in the San Antonio River, Carrizo-Wilcox South GAM

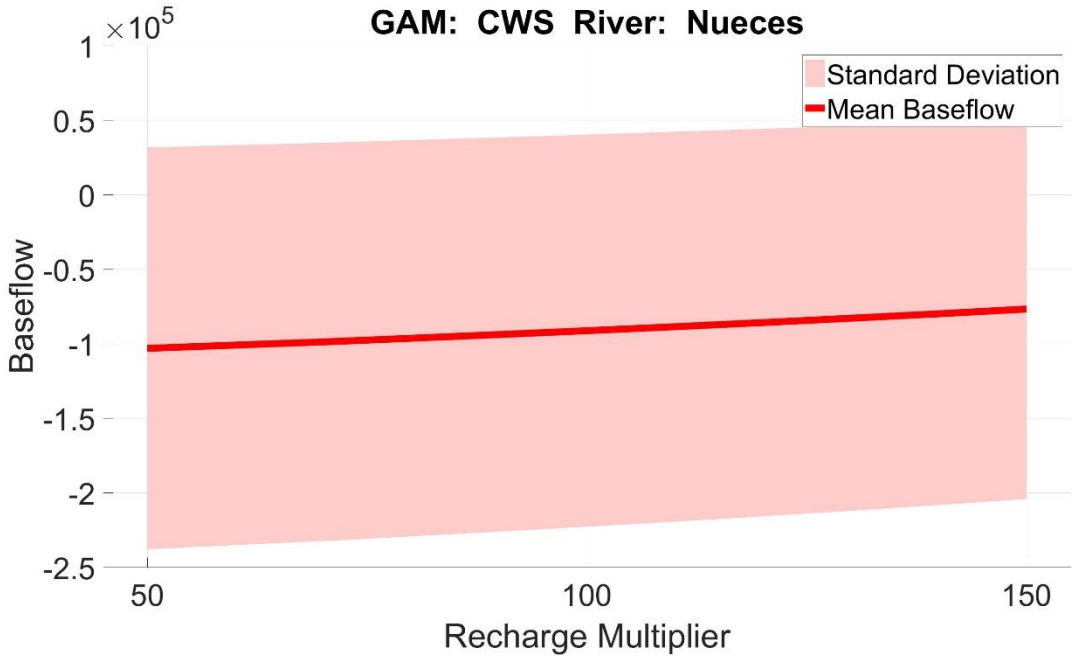

Figure 5. 32 River Baseflow in the Nueces River, Carrizo-Wilcox South GAM

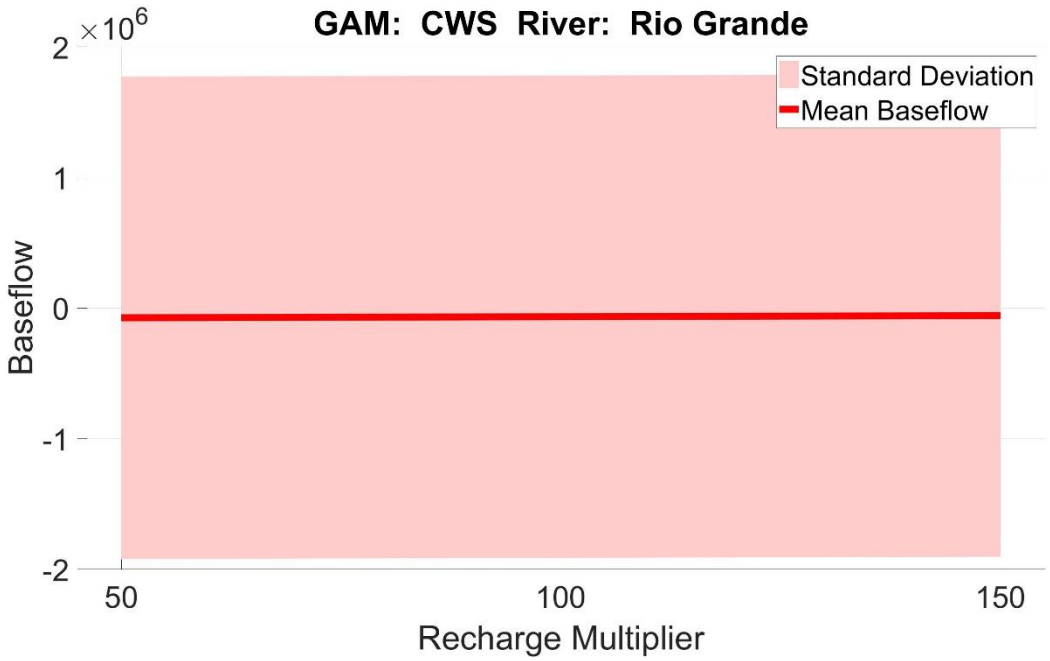

Figure 5. 33 River Baseflow in the Rio Grande River, Carrizo-Wilcox South GAM

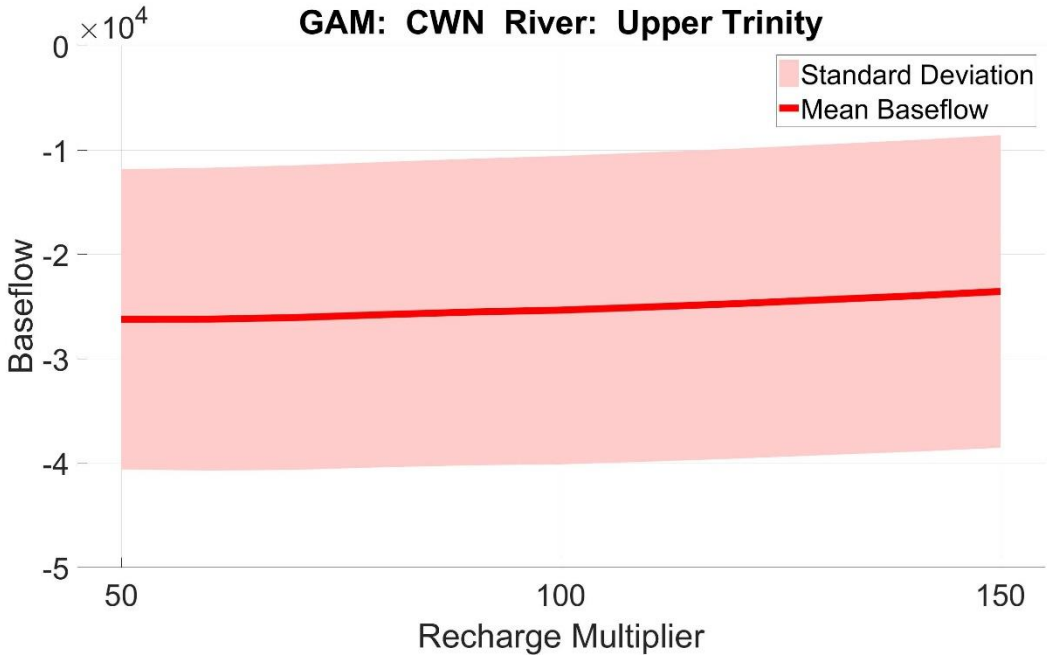

Figure 5. 34 River Baseflow in the Upper Trinity River, Carrizo-Wilcox North GAM

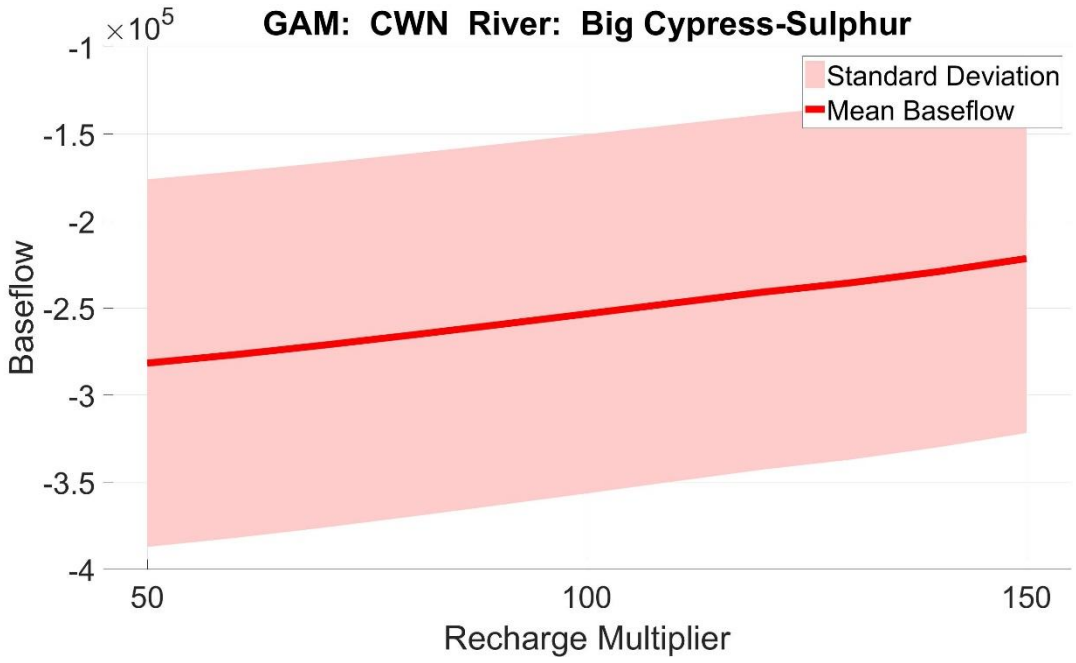

Figure 5. 35 River Baseflow in the Big Cypress-Sulphur River, Carrizo-Wilcox North GAM

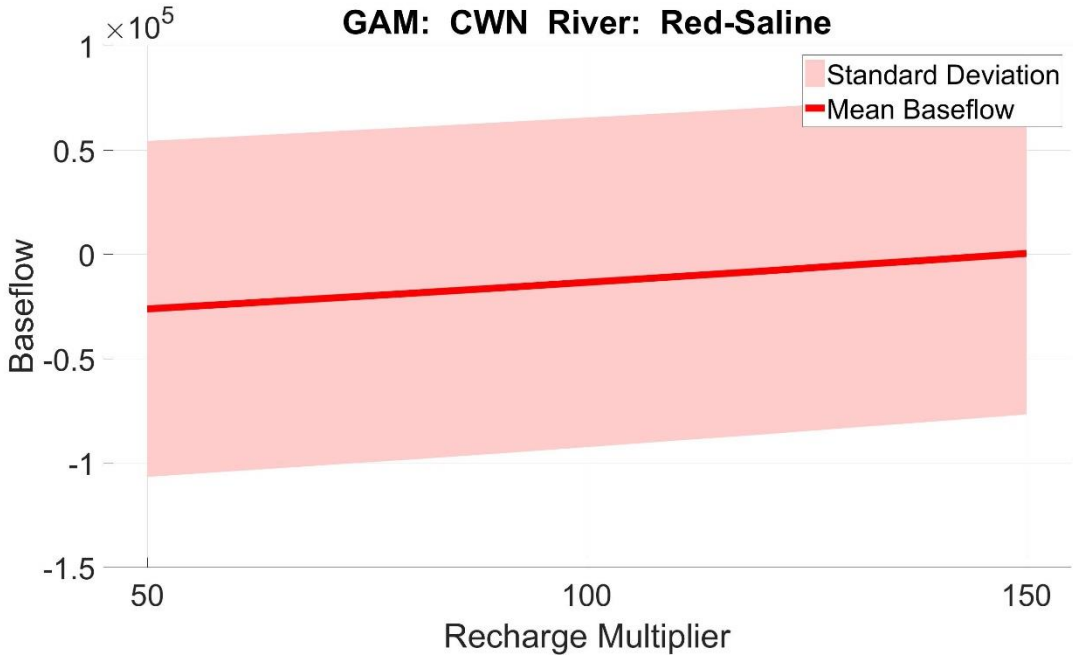

Figure 5. 36 River Baseflow in the Red-Saline River, Carrizo-Wilcox North GAM

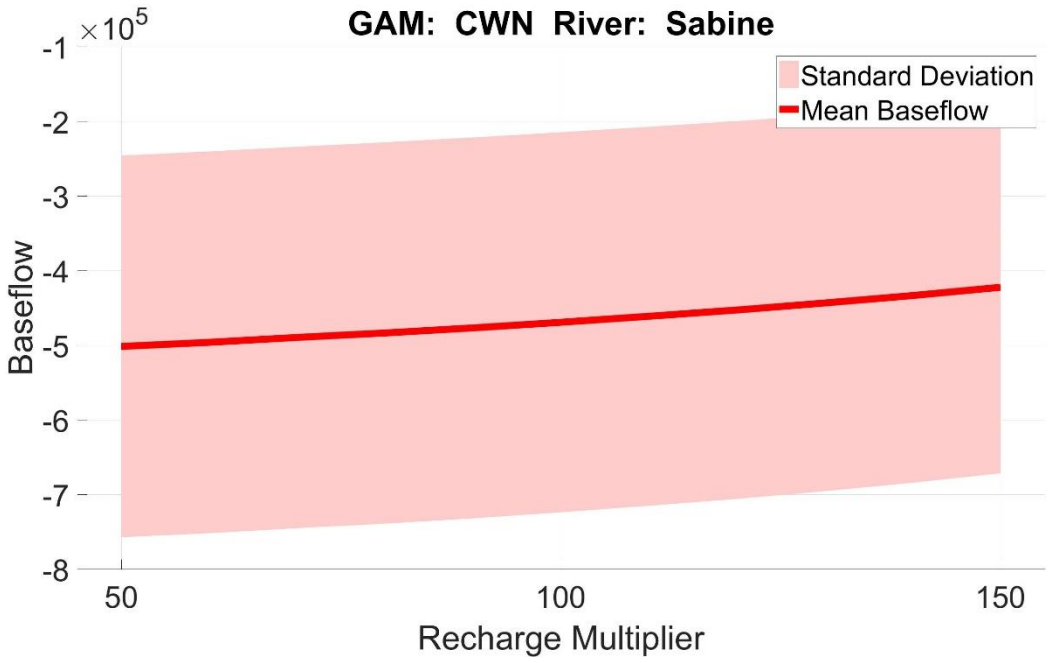

Figure 5. 37 River Baseflow in the Sabine River, Carrizo-Wilcox North GAM

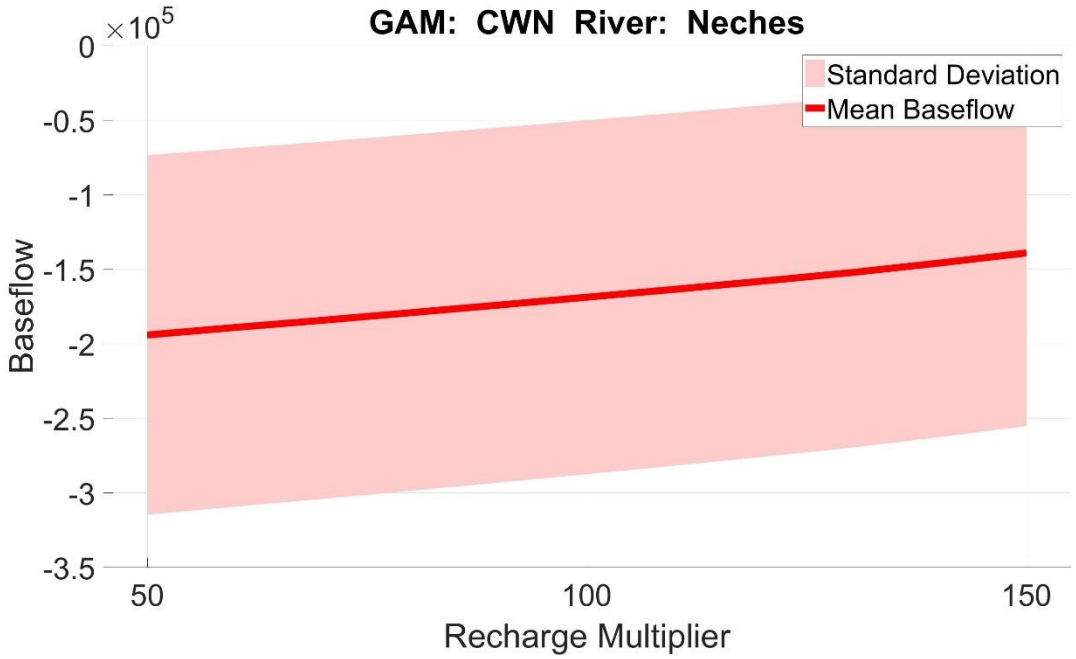

Figure 5. 38 River Baseflow in the Neches River, Carrizo-Wilcox North GAM

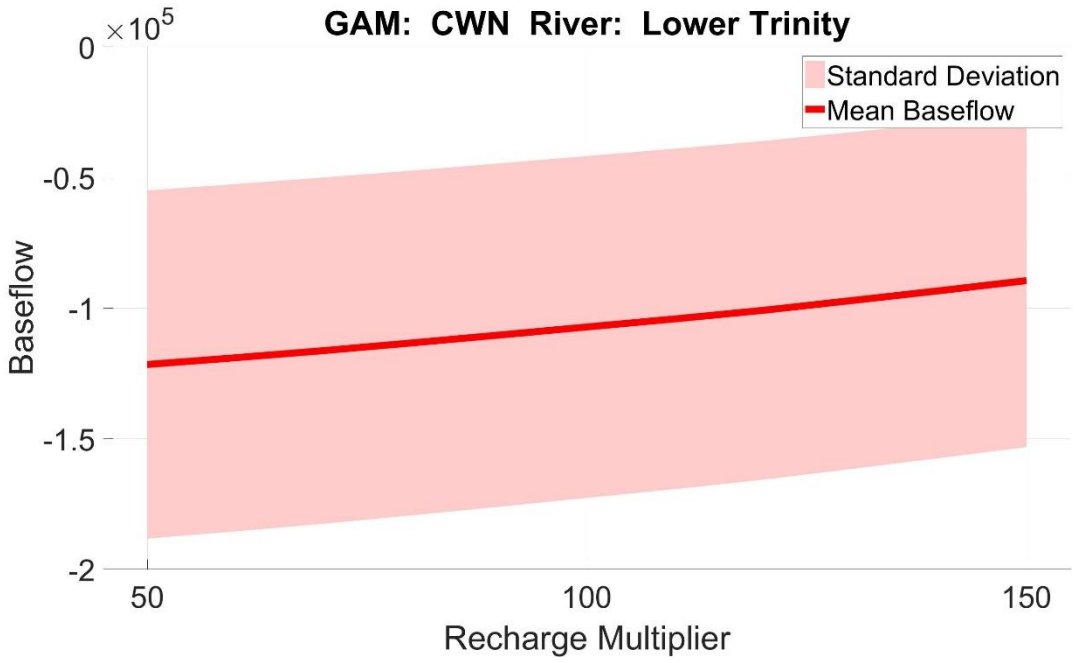

Figure 5. 39 River Baseflow in the Lower Trinity River, Carrizo-Wilcox North GAM

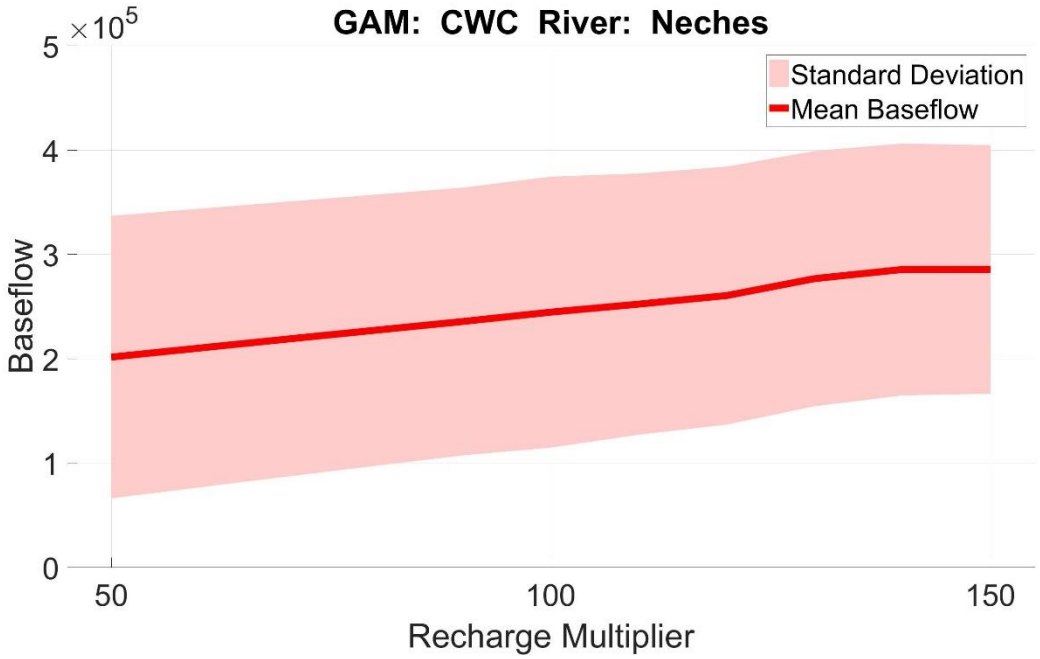

Figure 5. 40 River Baseflow in the Neches River, Carrizo-Wilcox Center GAM

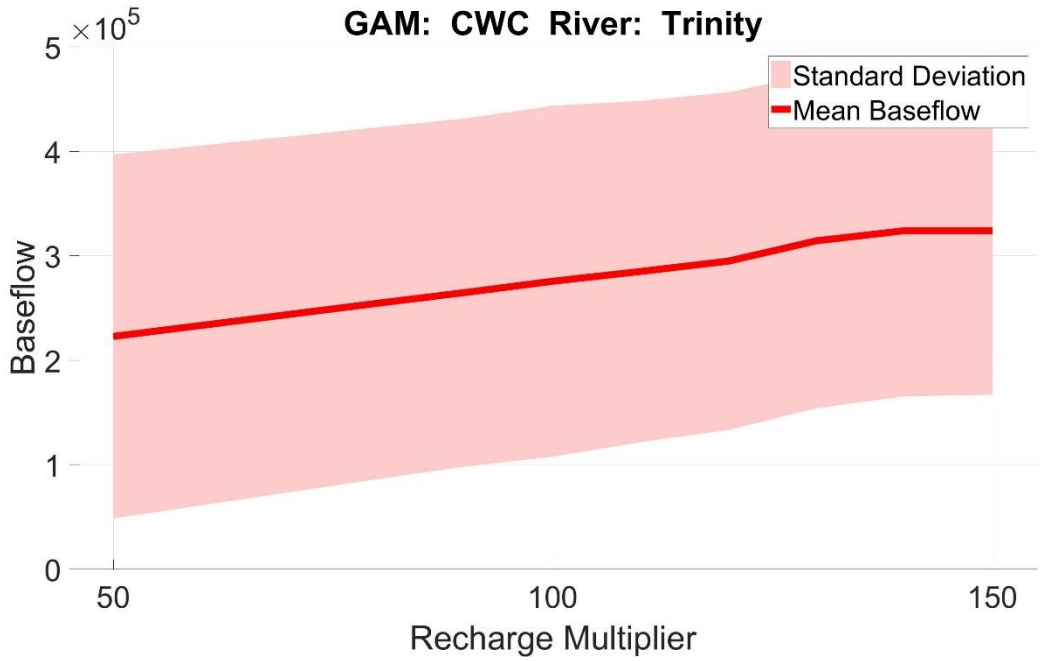

Figure 5. 41 River Baseflow in the Trinity River, Carrizo-Wilcox Center GAM

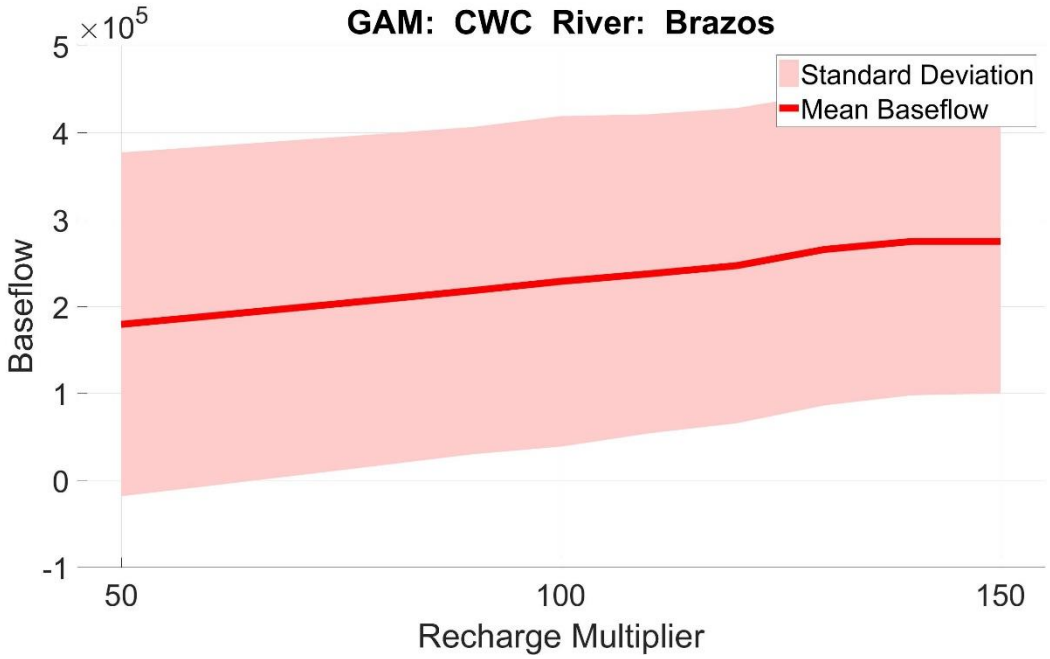

Figure 5. 42 River Baseflow in the Brazos River, Carrizo-Wilcox Center GAM

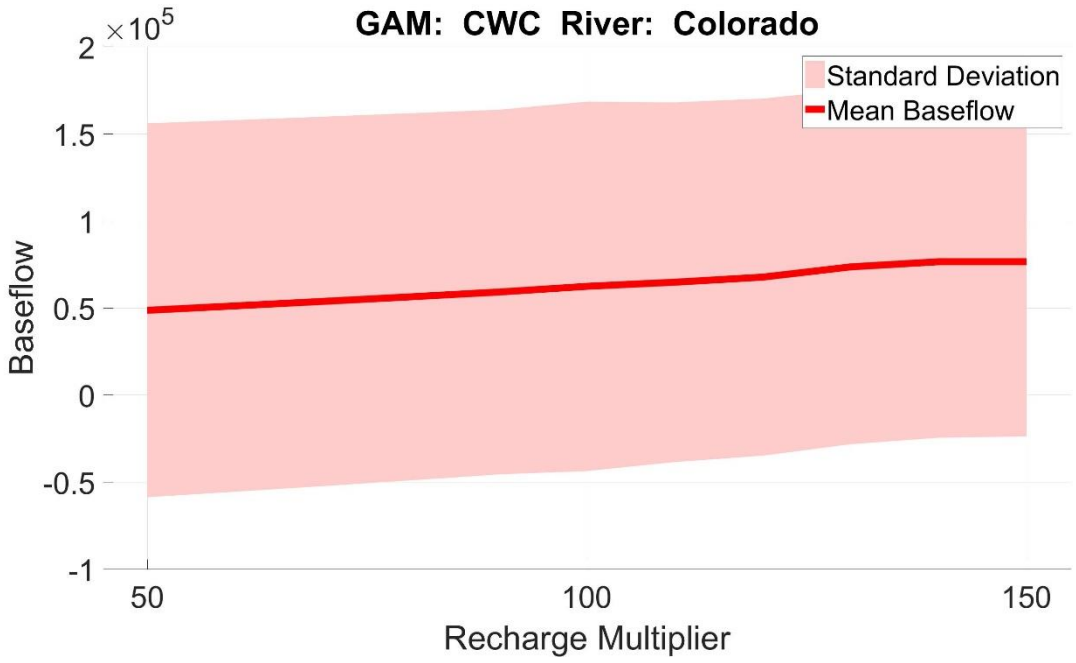

Figure 5. 43 River Baseflow in the Colorado River, Carrizo-Wilcox Center GAM

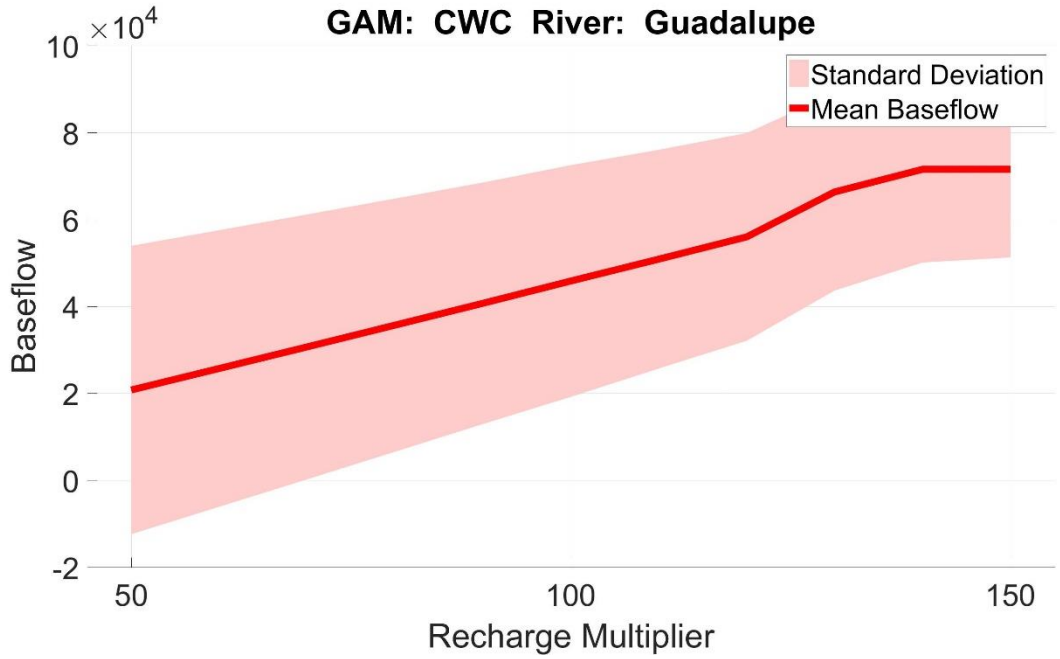

Figure 5. 44 River Baseflow in the Guadalupe River, Carrizo-Wilcox Center GAM

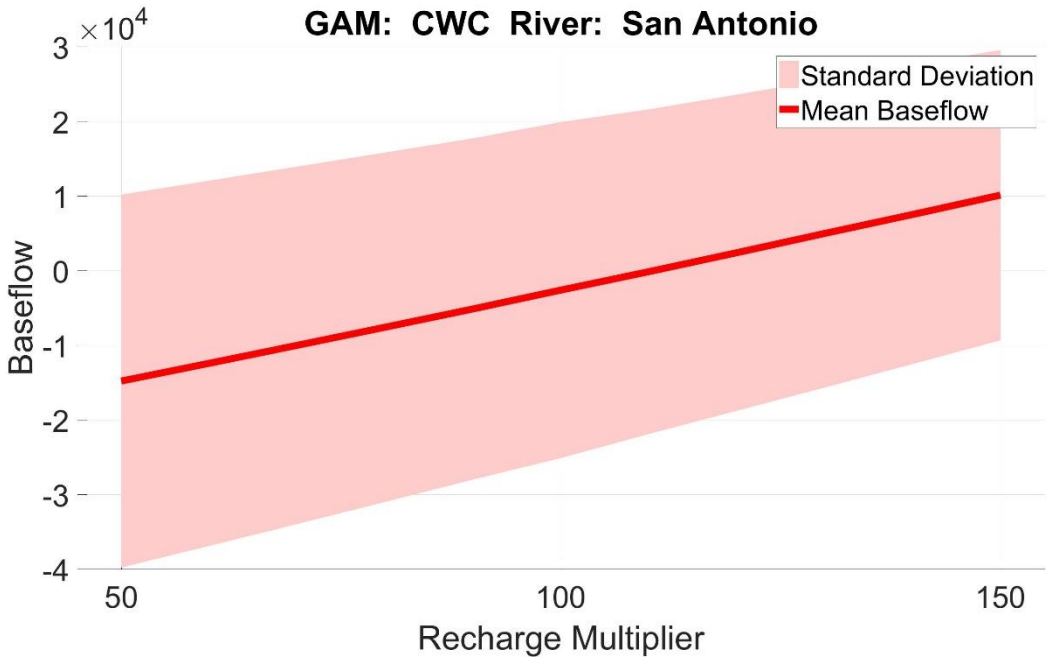

Figure 5. 45 River Baseflow in the San Antonio River, Carrizo-Wilcox Center GAM

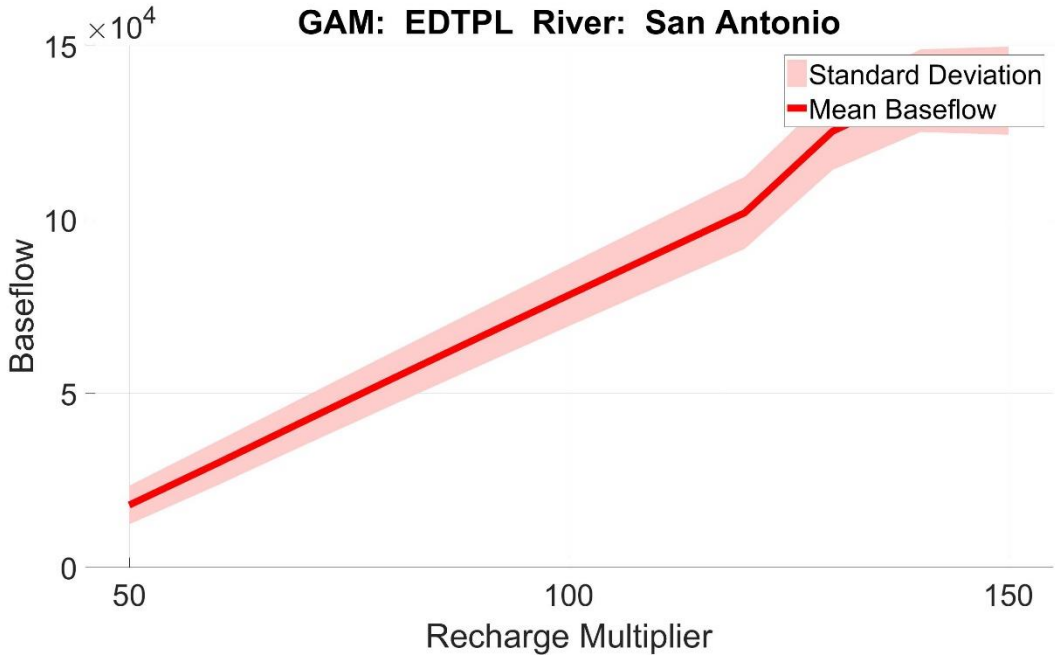

Figure 5. 46 River Baseflow in the San Antonio River, Edwards-Trinity Plateau GAM

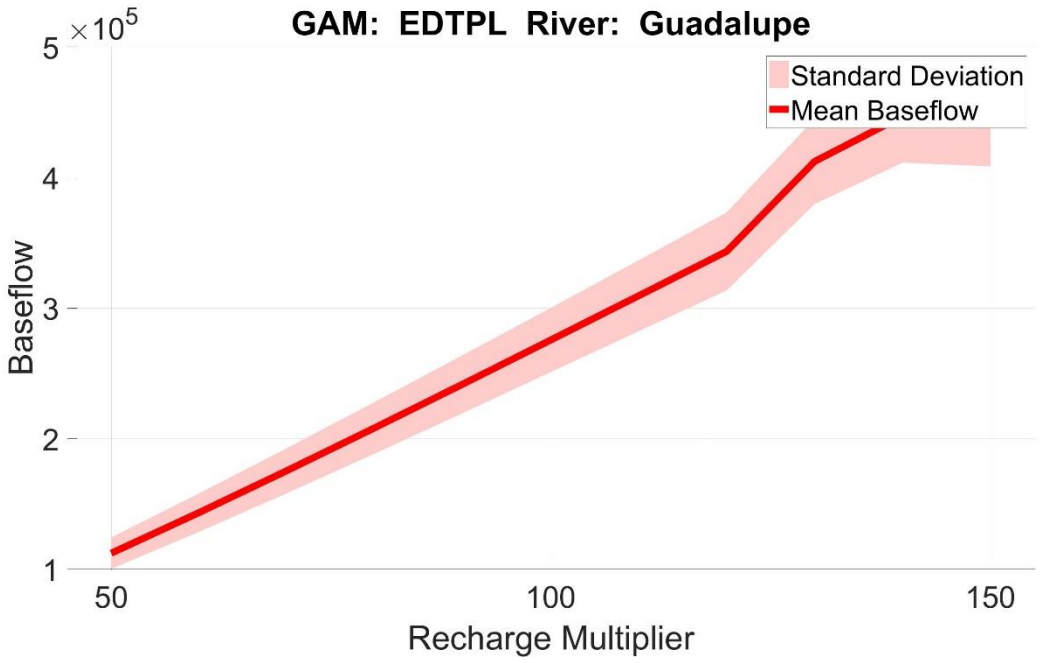

Figure 5. 47 River Baseflow in the Guadalupe River, Edwards-Trinity Plateau GAM

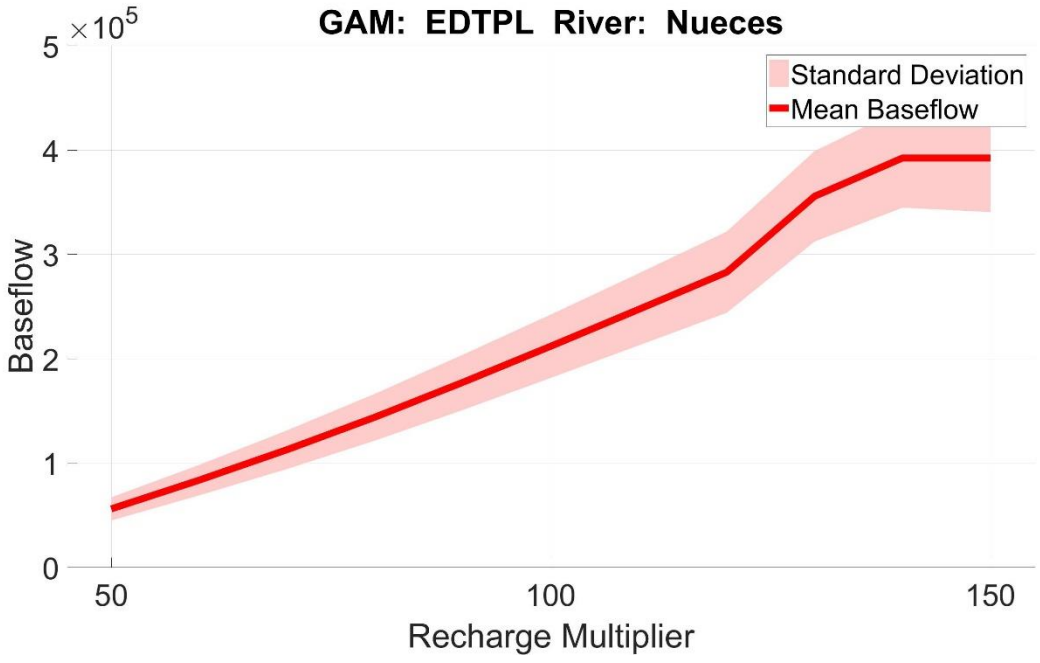

Figure 5. 48 River Baseflow in the Nueces River, Edwards-Trinity Plateau GAM

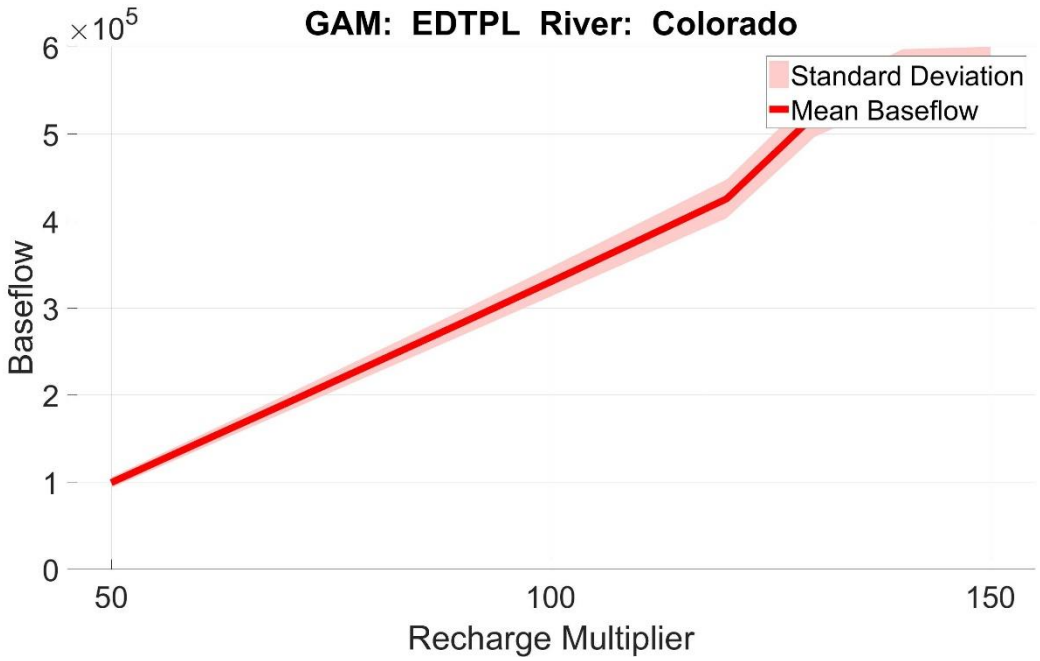

Figure 5. 49 River Baseflow in the Colorado River, Edwards-Trinity Plateau GAM

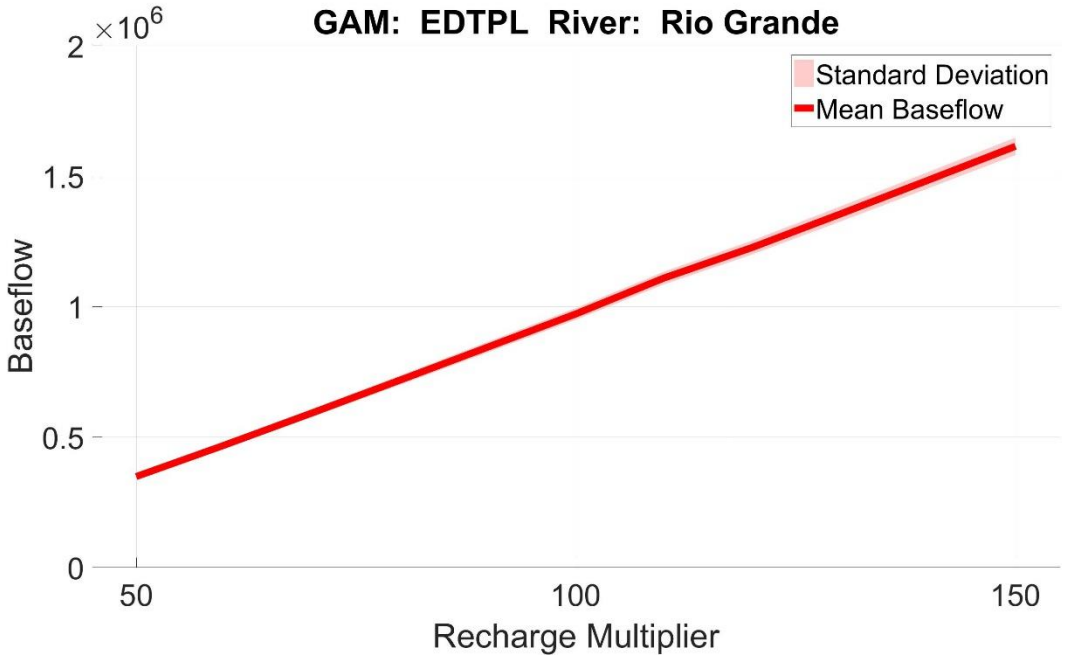

Figure 5. 50 River Baseflow in the Rio Grande River, Edwards-Trinity Plateau GAM

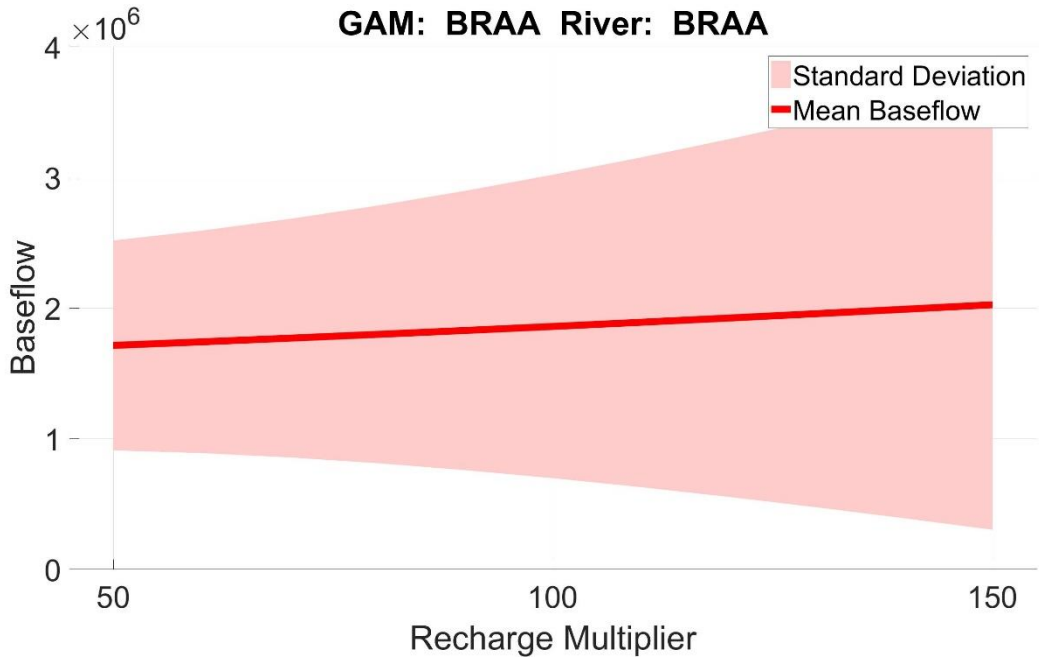

Figure 5. 51 River Baseflow in the Brazos River, Brazos River Alluvium Aquifer GAM

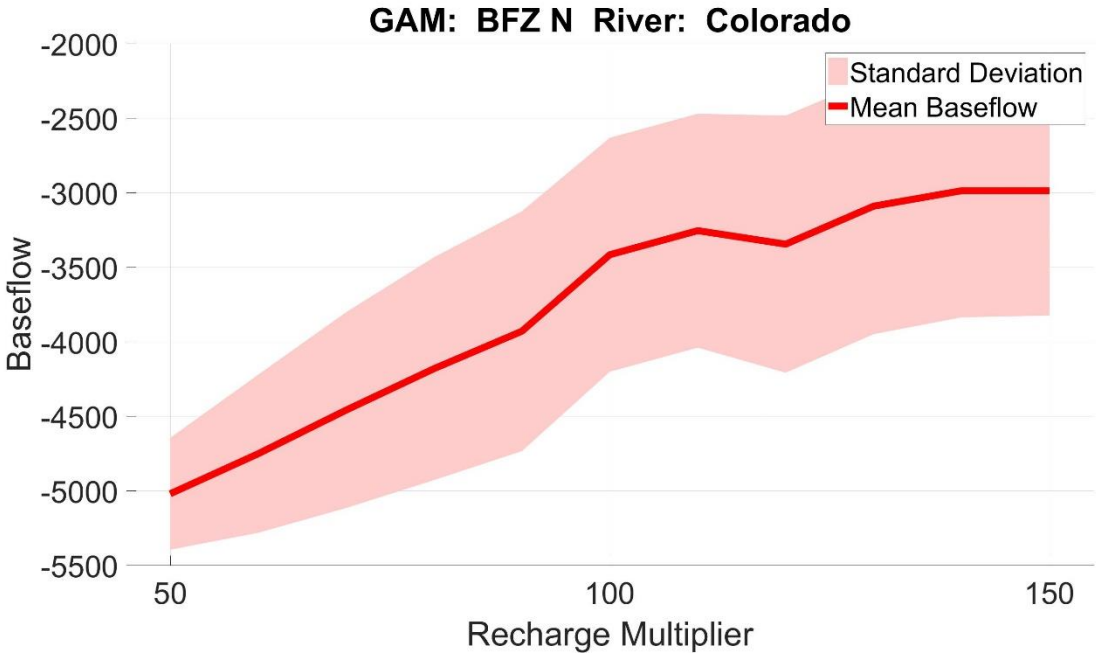

Figure 5. 52 River Baseflow in the Colorado River, Edwards Balcones Fault Zone North GAM

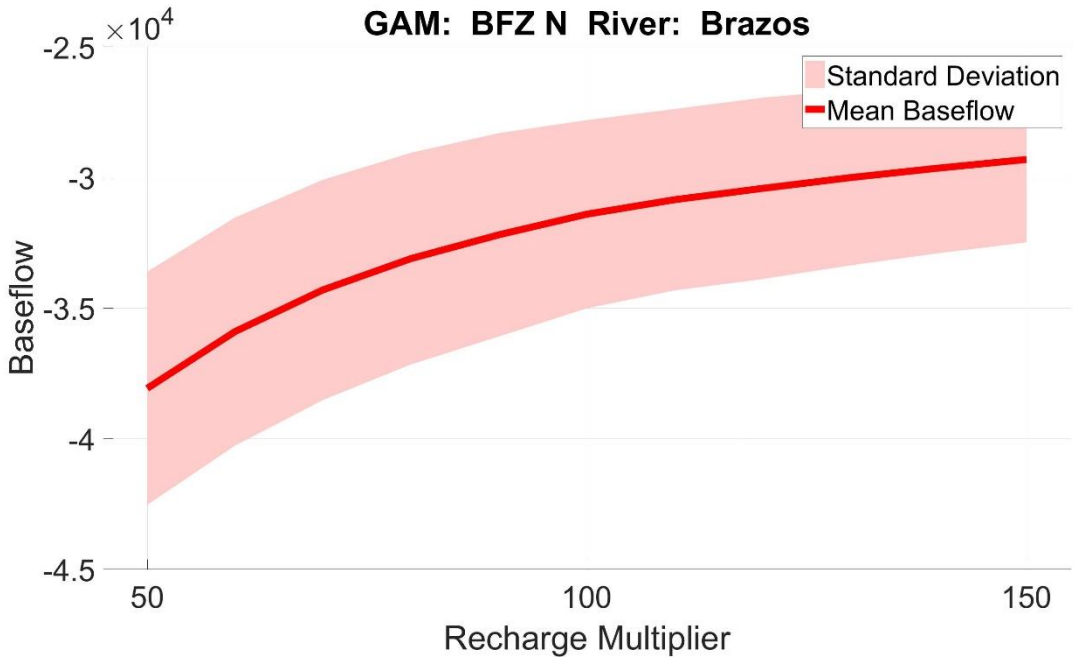

Figure 5. 53 River Baseflow in the Brazos River, Edwards Balcones Fault Zone North GAM

GAMs mean head over time with standard deviation

Head Change Maps

Edwards Balcones Fault Zone North

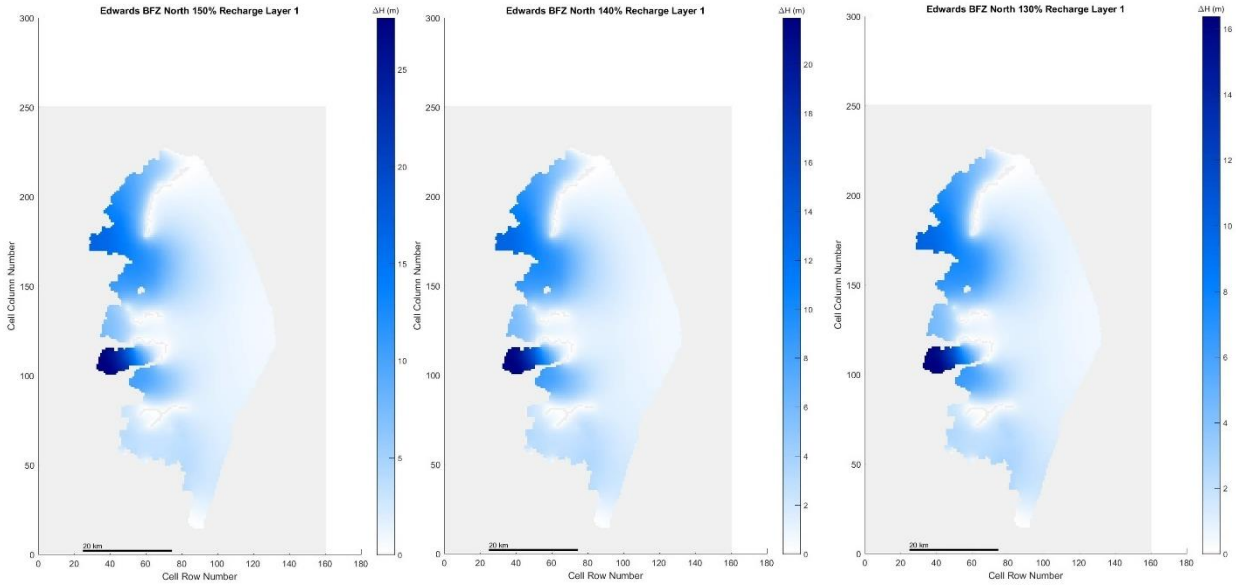

Figure 5. 54 Edwards Balcones Fault Zone North, 150%, 140%, and 130% original recharge hydraulic head spatial distribution

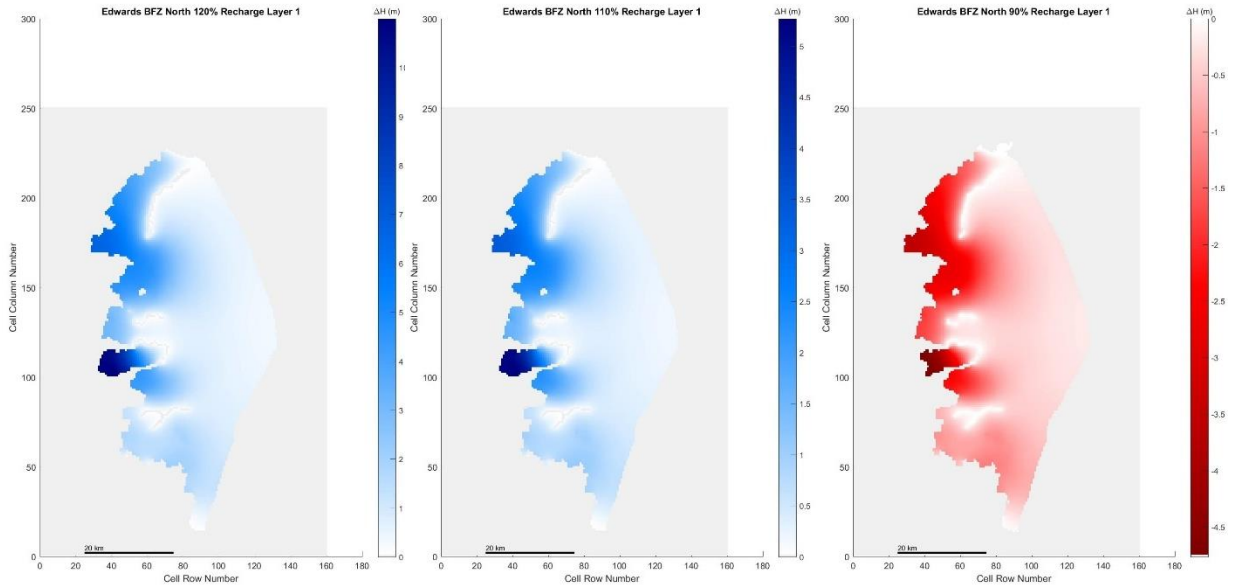

Figure 5. 55 Edwards Balcones Fault Zone North, 120%, 110%, and 90% original recharge hydraulic head spatial distribution

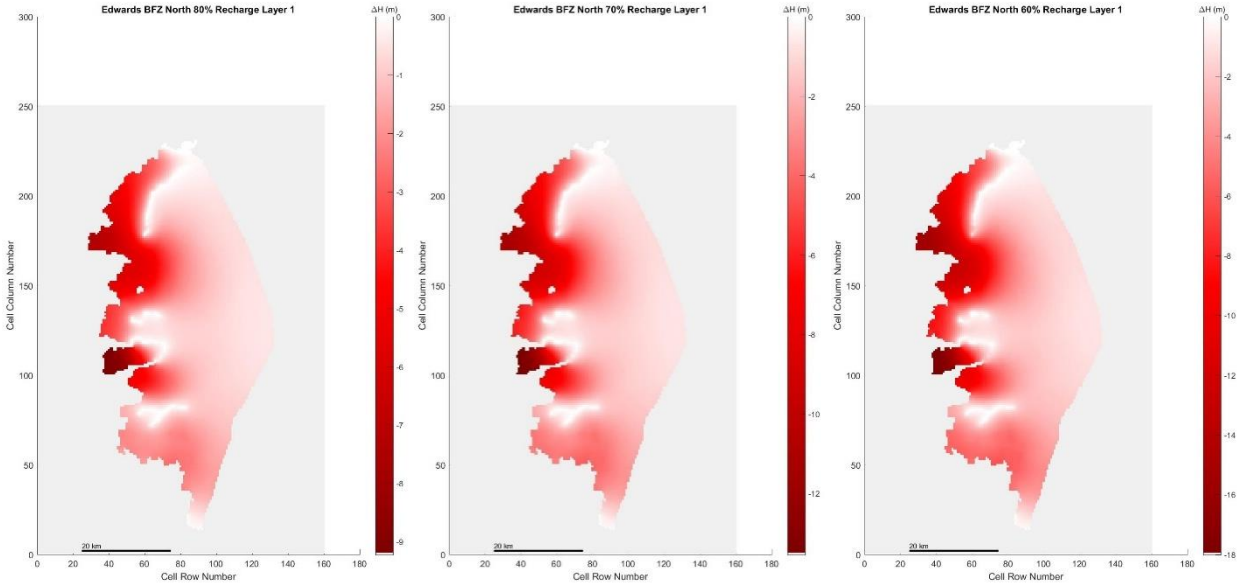

Figure 5. 56 Edwards Balcones Fault Zone North, 80%, 70%, and 60% original recharge hydraulic head spatial distribution

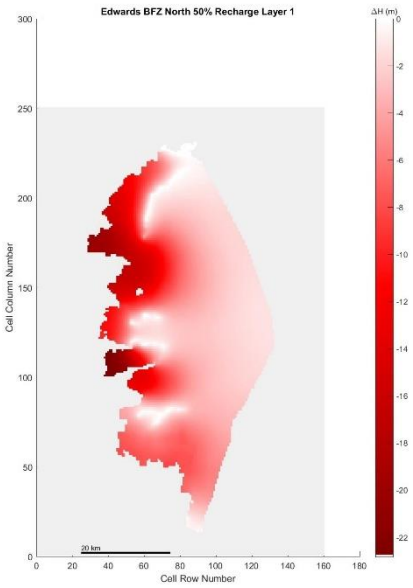

Figure 5. 57 Edwards Balcones Fault Zone North, 50% original recharge hydraulic head spatial distribution

Edwards Balcones Fault Zone San Antonio

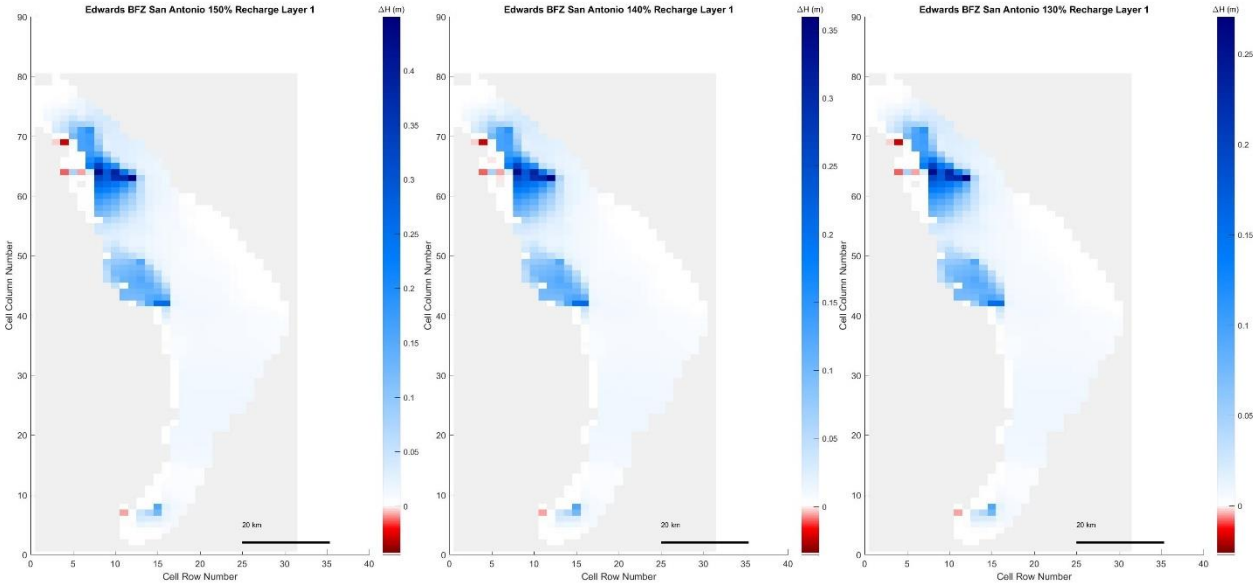

Figure 5. 58 Edwards Balcones Fault Zone San Antonio, 150%, 140%, and 130% original recharge hydraulic head spatial distribution

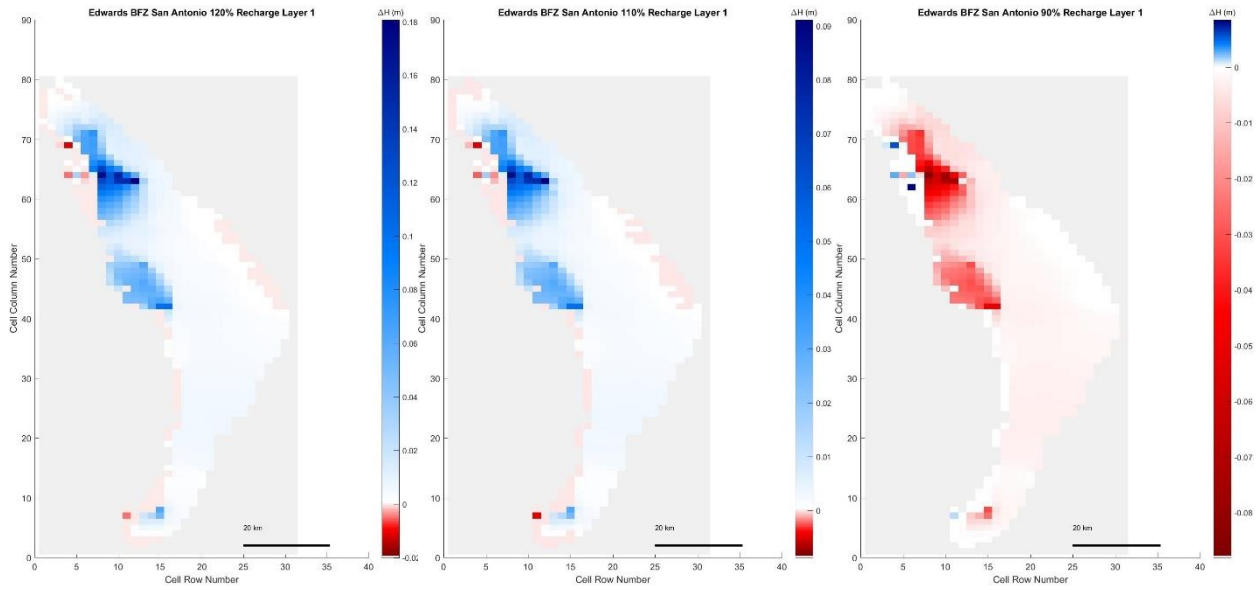

Figure 5. 59 Edwards Balcones Fault Zone San Antonio, 120%, 110%, and 90% original recharge hydraulic head spatial distribution

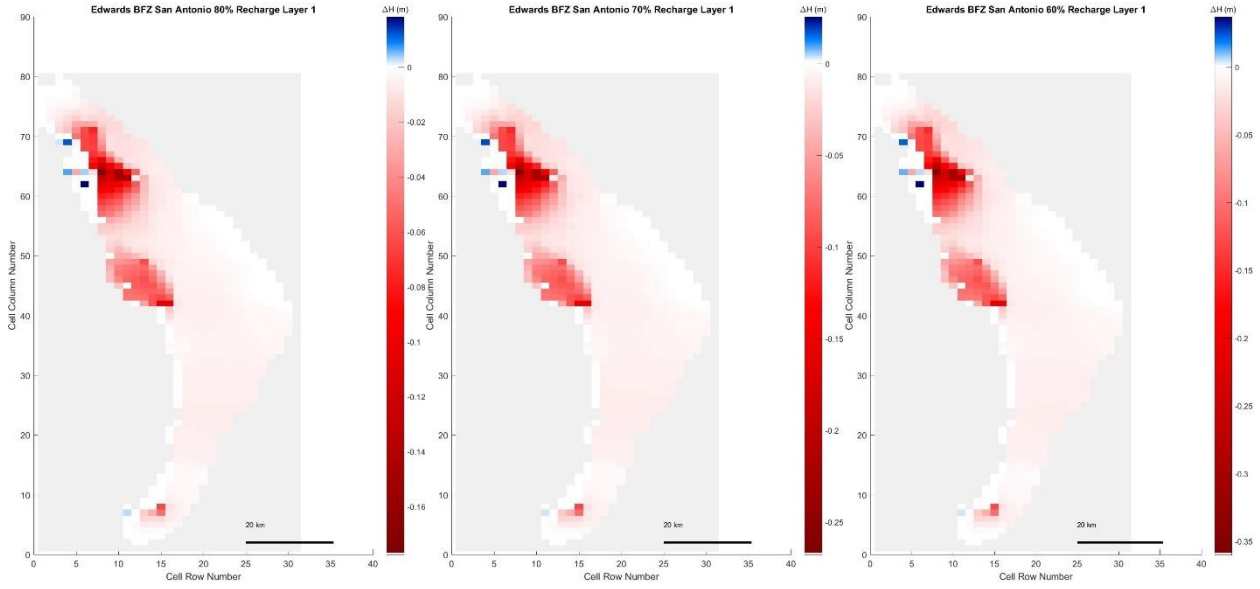

Figure 5. 60 Edwards Balcones Fault Zone San Antonio, 80%, 70%, and 60% original recharge hydraulic head spatial distribution

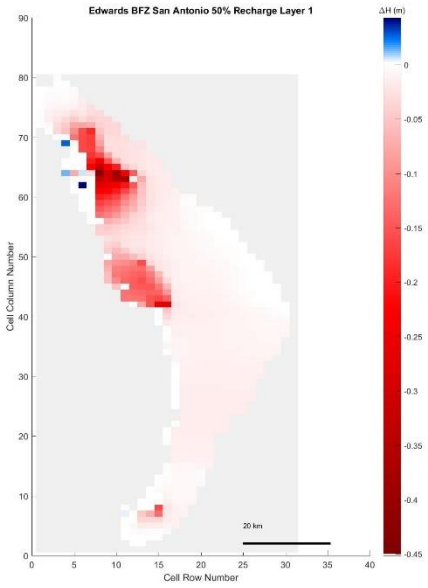

Figure 5. 61 Edwards Balcones Fault Zone San Antonio, 50% original recharge hydraulic head spatial distribution

Edwards Balcones Fault Zone Springs

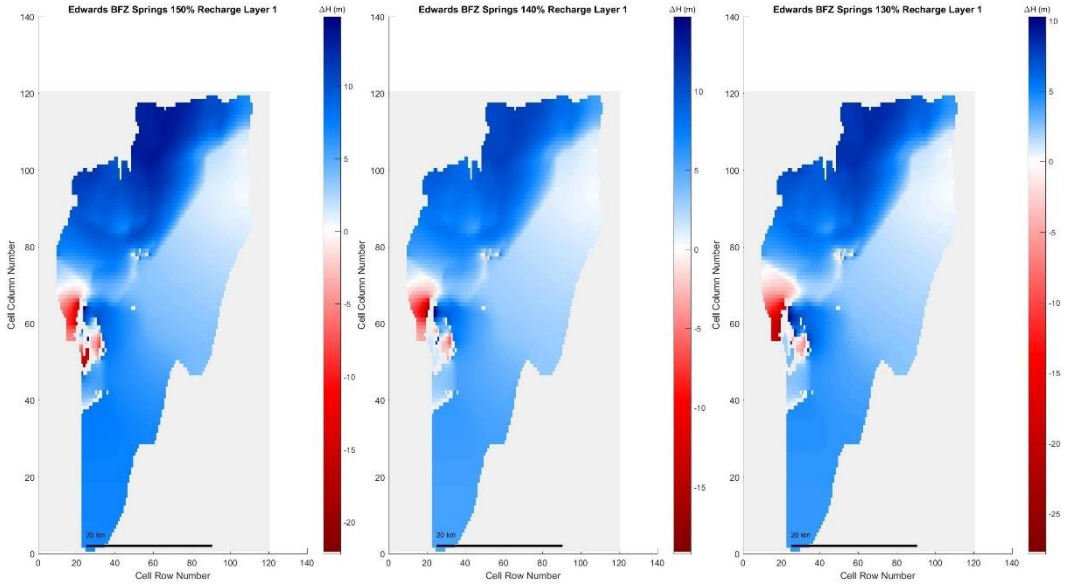

Figure 5. 62 Edwards Balcones Fault Zone Springs, 150%, 140%, and 130% original recharge hydraulic head spatial distribution

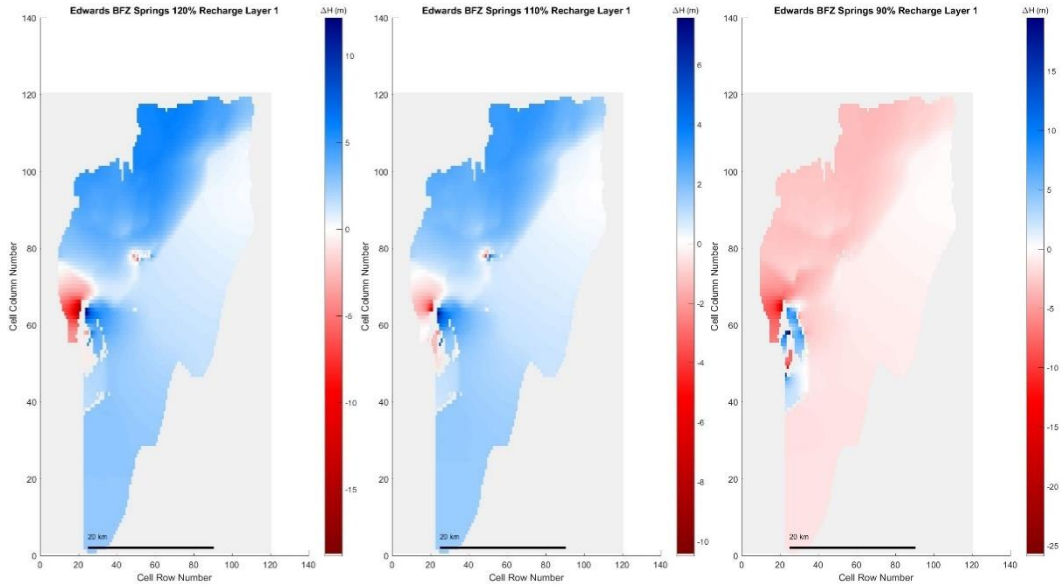

Figure 5. 63 Edwards Balcones Fault Zone Springs, 120%, 110%, and 90% original recharge hydraulic head spatial distribution

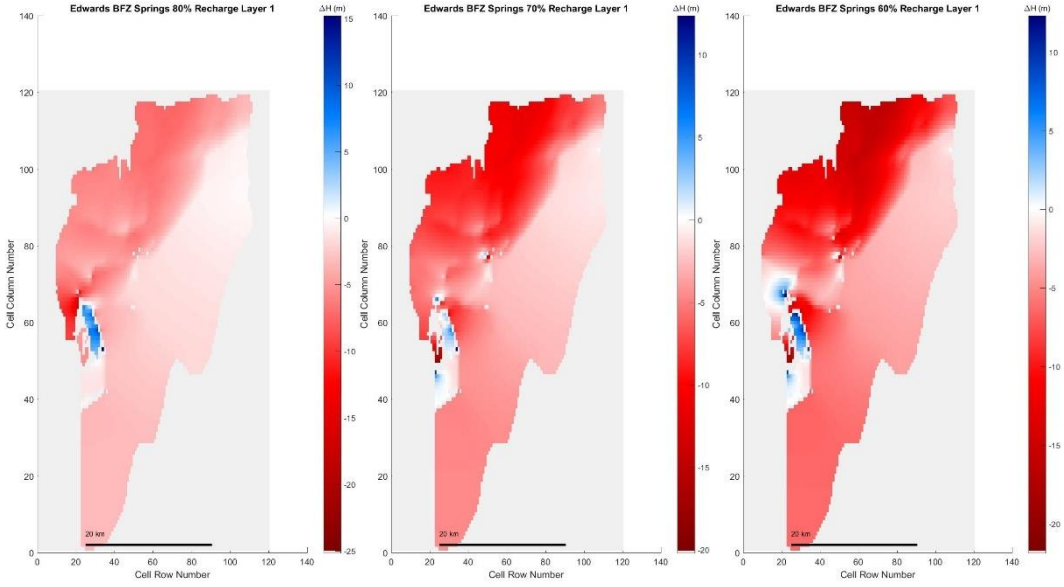

Figure 5. 64 Edwards Balcones Fault Zone Springs, 80%, 70%, and 60% original recharge hydraulic head spatial distribution

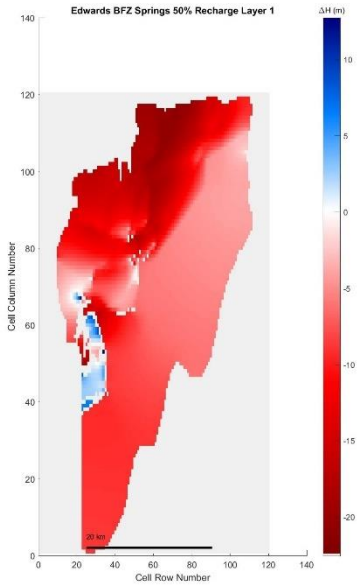

Figure 5. 65 Edwards Balcones Fault Zone Springs, 50% original recharge hydraulic head spatial distribution

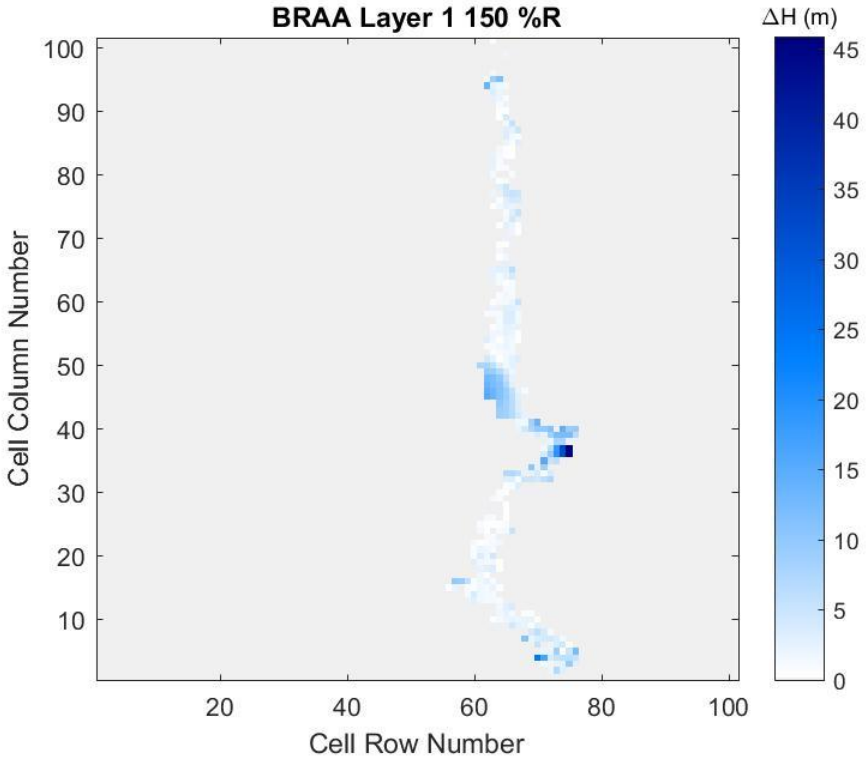

Figure 5. 66 BRAA, 150% original recharge hydraulic head spatial distribution of layer 1

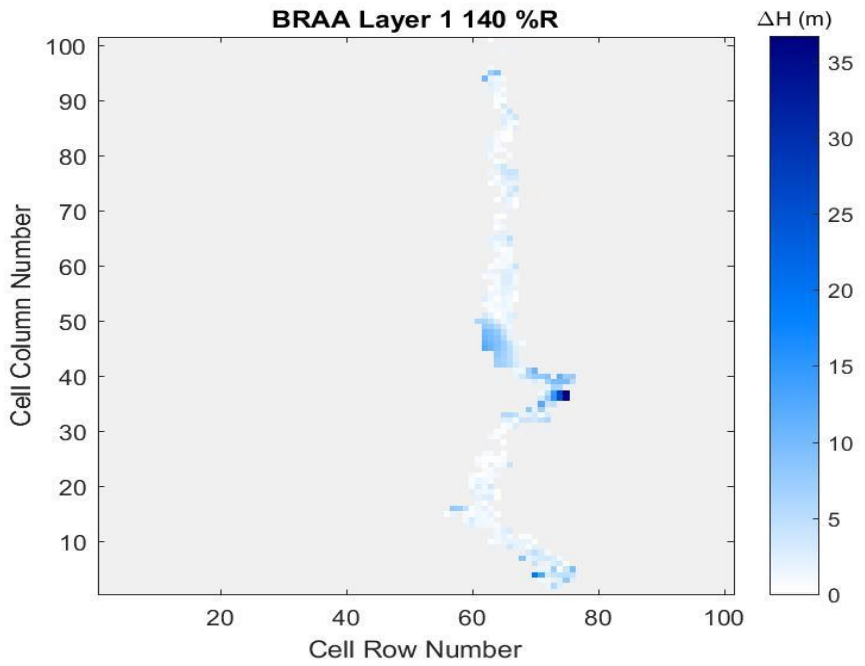

Figure 5. 67 BRAA, 140% original recharge hydraulic head spatial distribution of layer 1

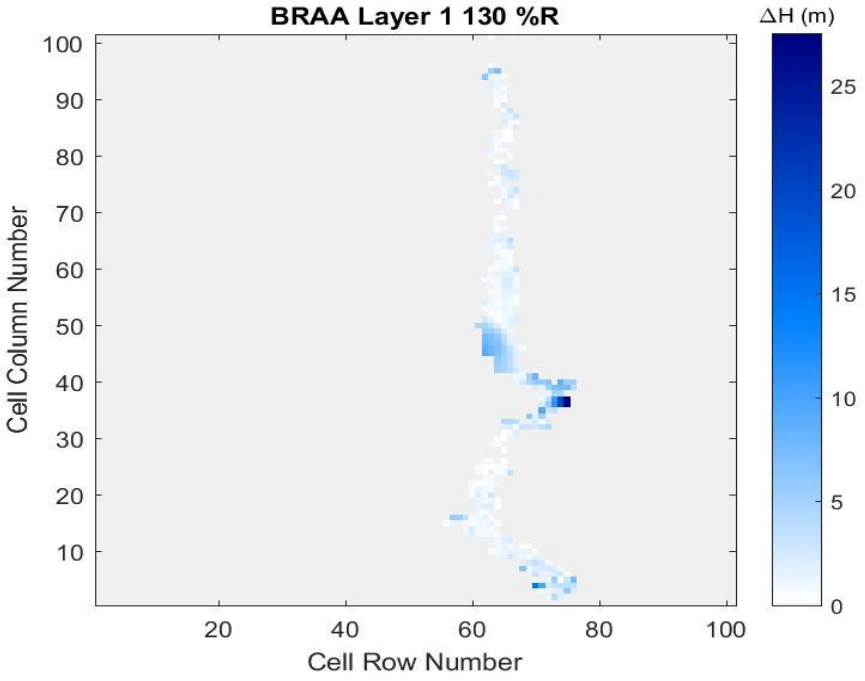

Figure 5. 68 BRAA, 130% original recharge hydraulic head spatial distribution of layer 1

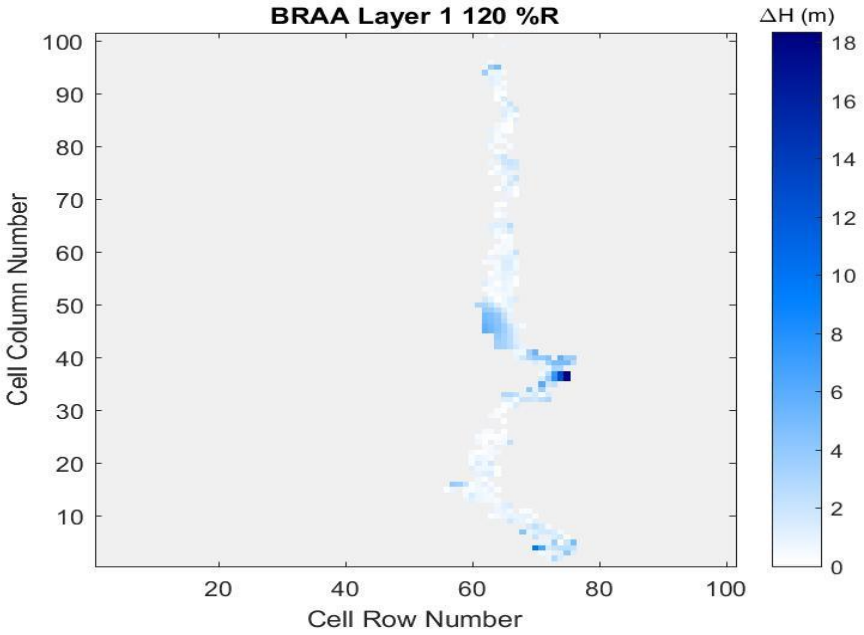

Figure 5. 69 BRAA, 120% original recharge hydraulic head spatial distribution of layer 1

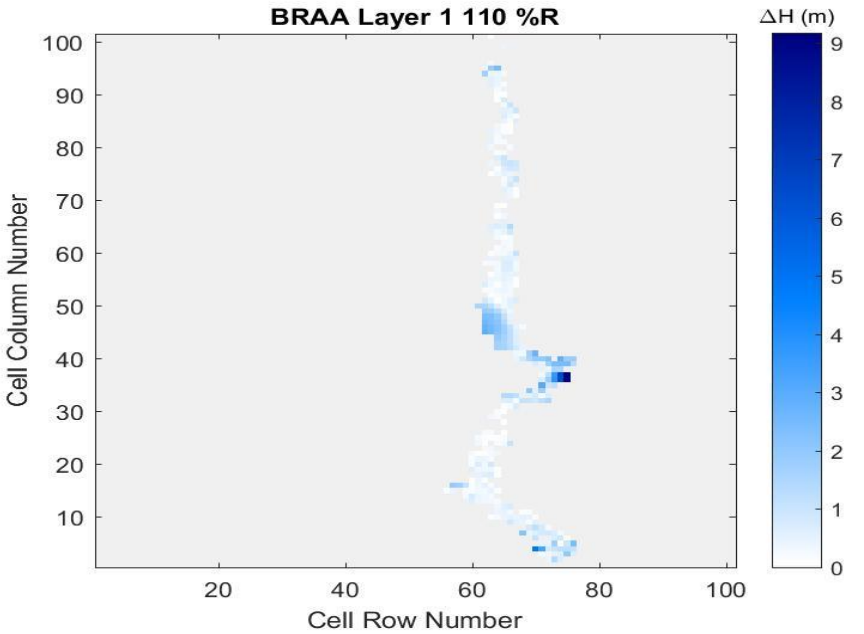

Figure 5. 70 BRAA, 110% original recharge hydraulic head spatial distribution of layer 1

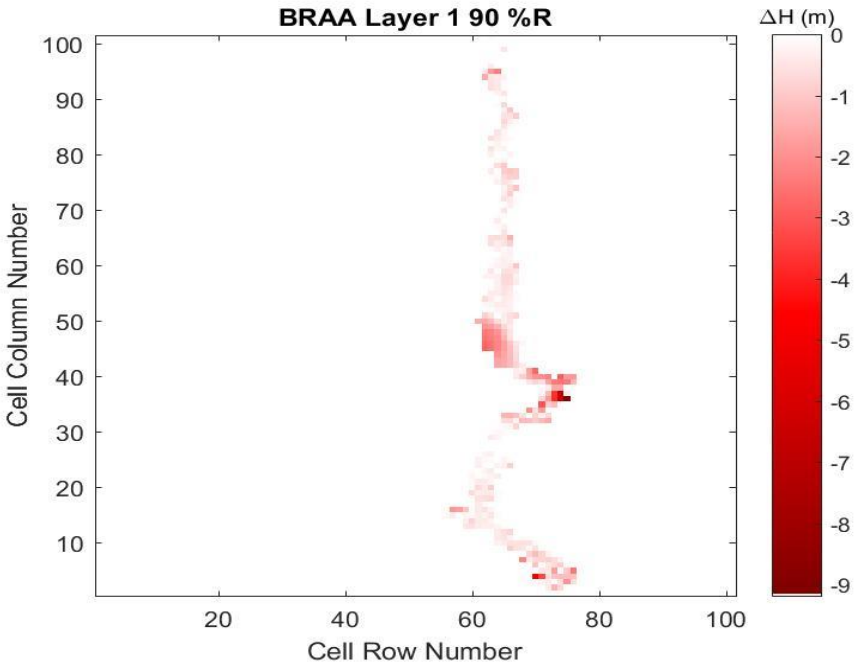

Figure 5. 71 BRAA, 90% original recharge hydraulic head spatial distribution of layer 1

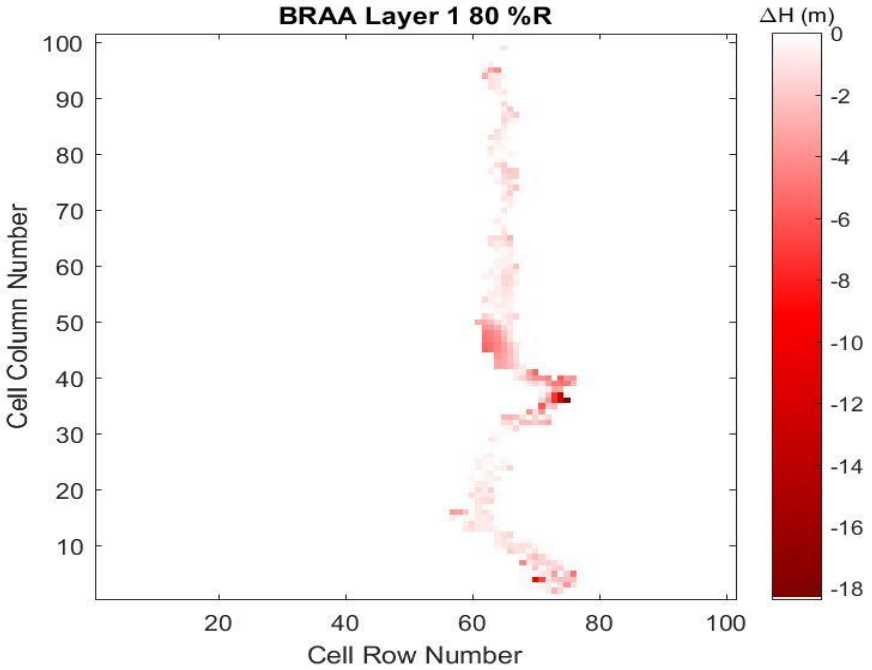

Figure 5. 72 BRAA, 80% original recharge hydraulic head spatial distribution of layer 1

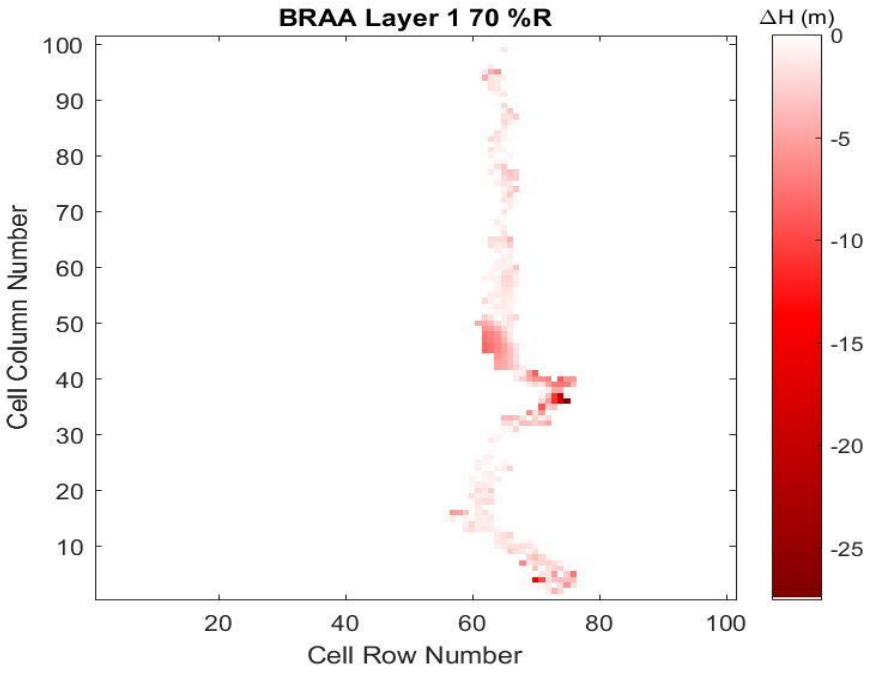

Figure 5. 73 BRAA, 70% original recharge hydraulic head spatial distribution of layer 1

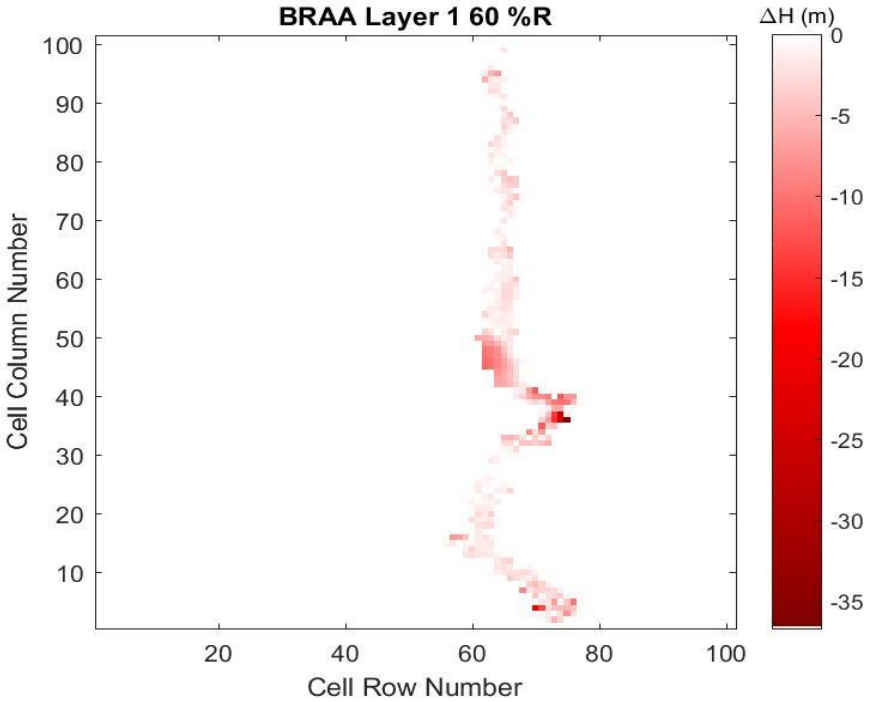

Figure 5. 74 BRAA, 60% original recharge hydraulic head spatial distribution of layer 1

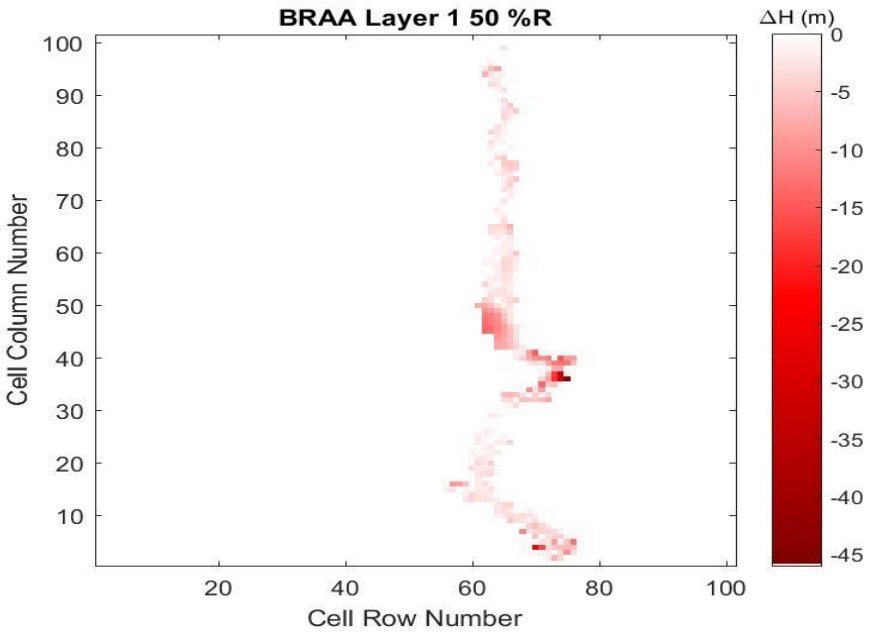

Figure 5. 75 BRAA, 50% original recharge hydraulic head spatial distribution of layer 1

Layer 3

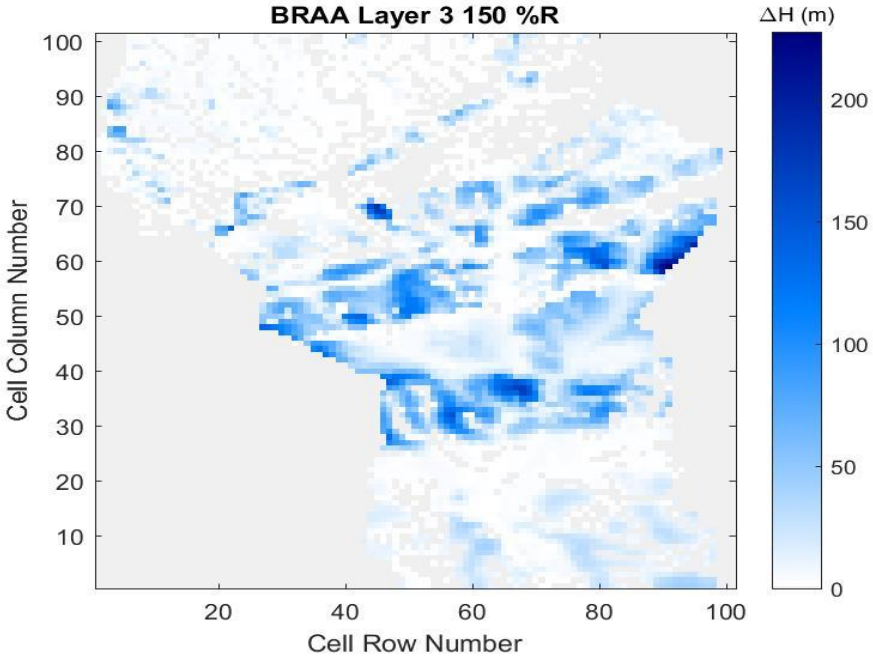

Figure 5. 76 BRAA, 150% original recharge hydraulic head spatial distribution of layer 3

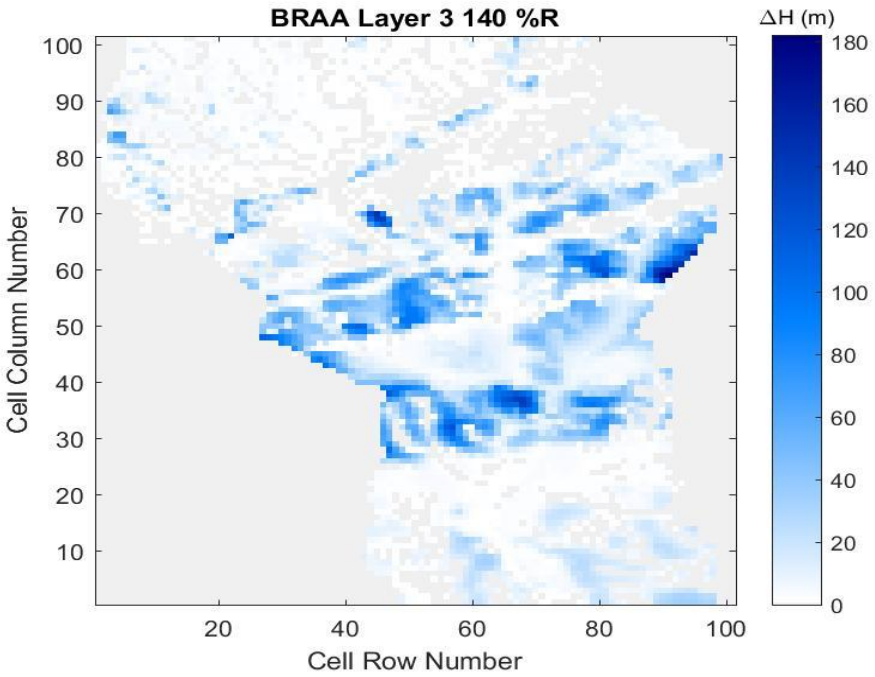

Figure 5. 77 BRAA, 140% original recharge hydraulic head spatial distribution of layer 3

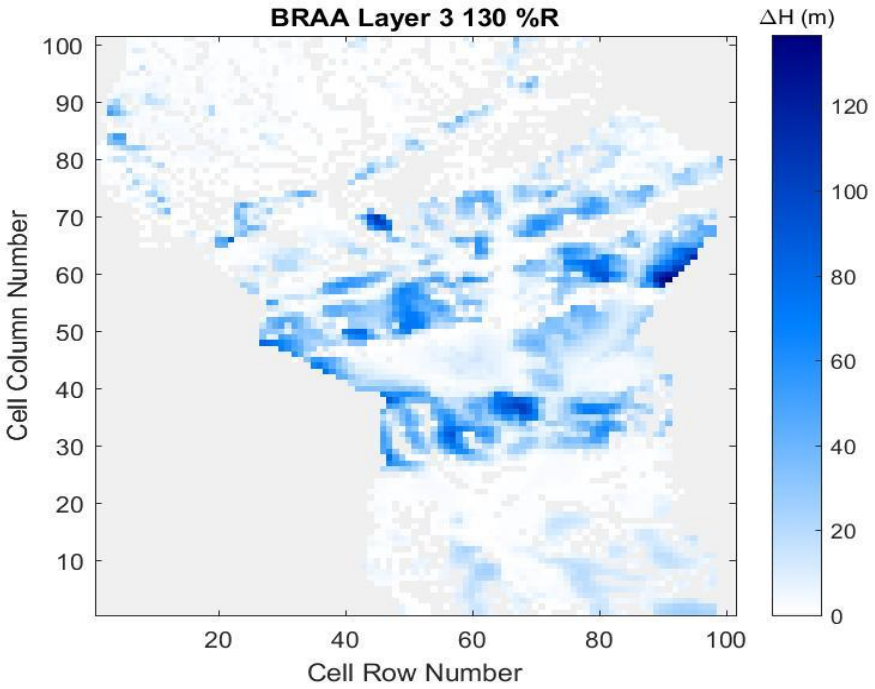

Figure 5. 78 BRAA, 150% original recharge hydraulic head spatial distribution of layer 3

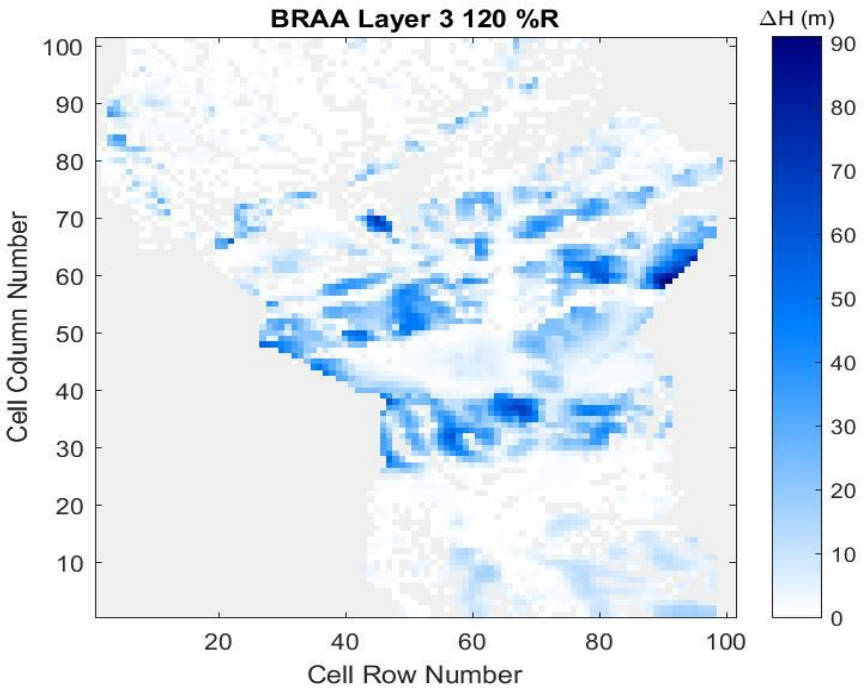

Figure 5. 79 BRAA, 120% original recharge hydraulic head spatial distribution of layer 3

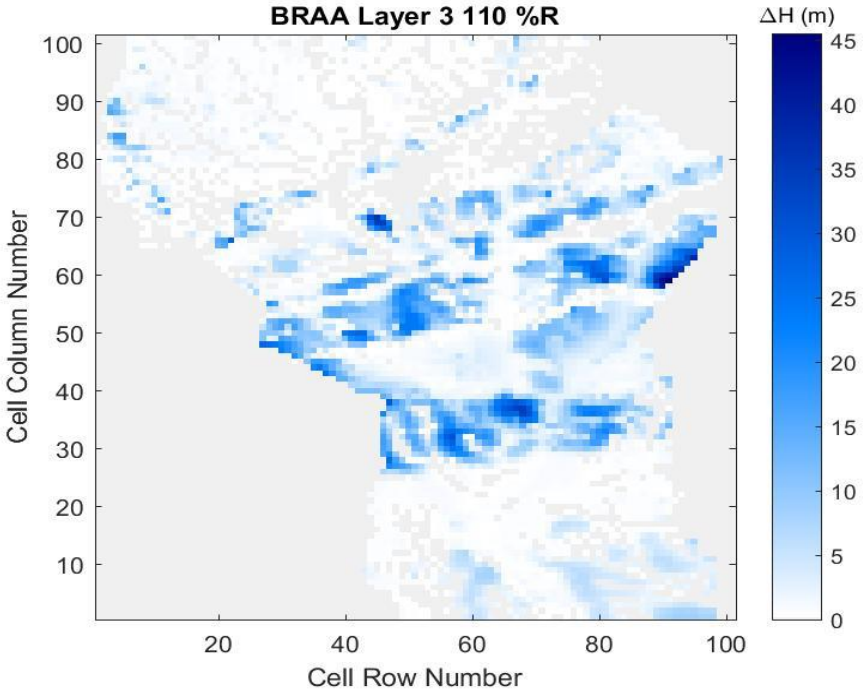

Figure 5. 80 BRAA, 110% original recharge hydraulic head spatial distribution of layer 3

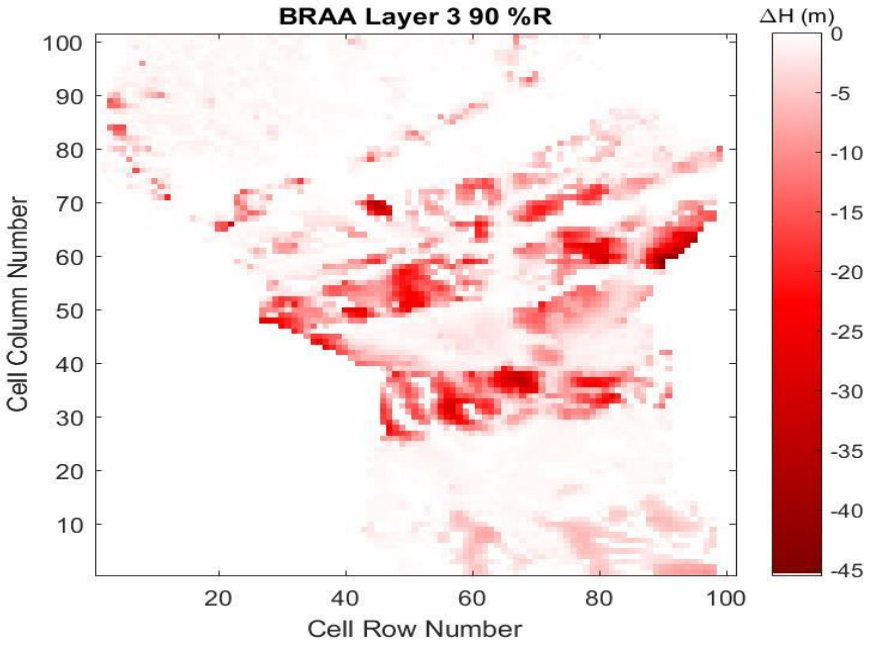

Figure 5. 81 BRAA, 90% original recharge hydraulic head spatial distribution of layer 3

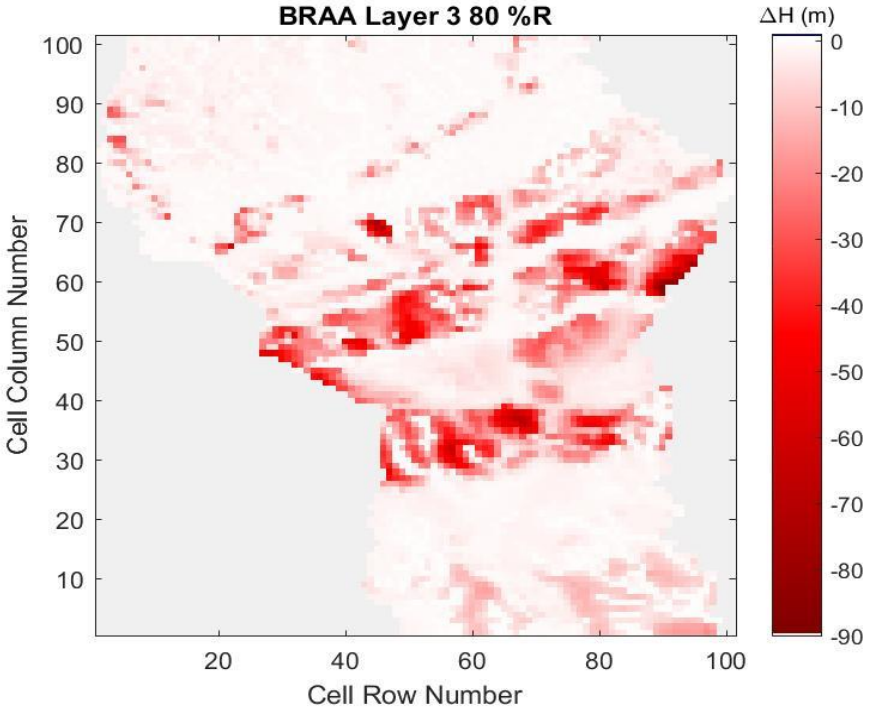

Figure 5. 82 BRAA, 80% original recharge hydraulic head spatial distribution of layer 3

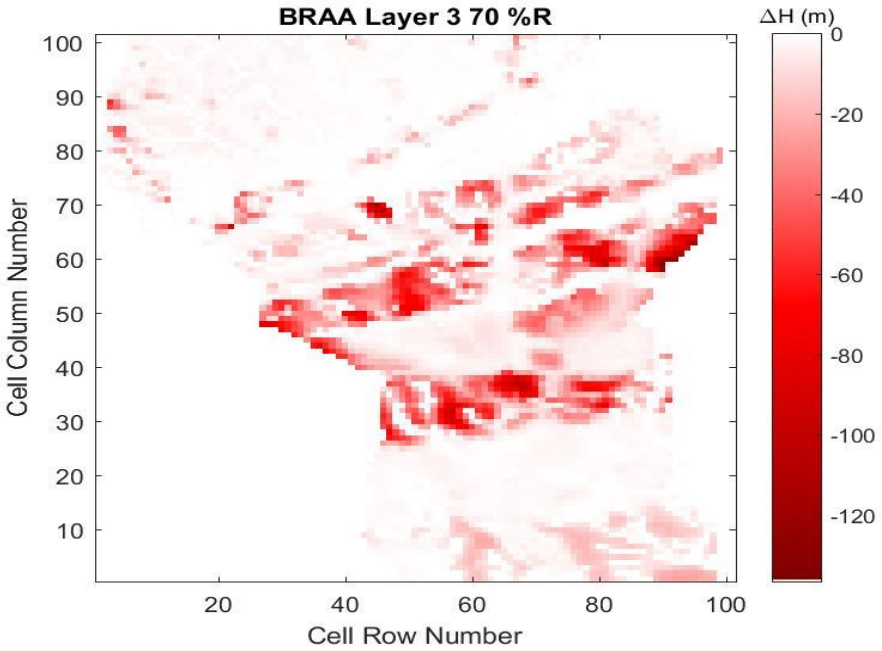

Figure 5. 83 BRAA, 70% original recharge hydraulic head spatial distribution of layer 3

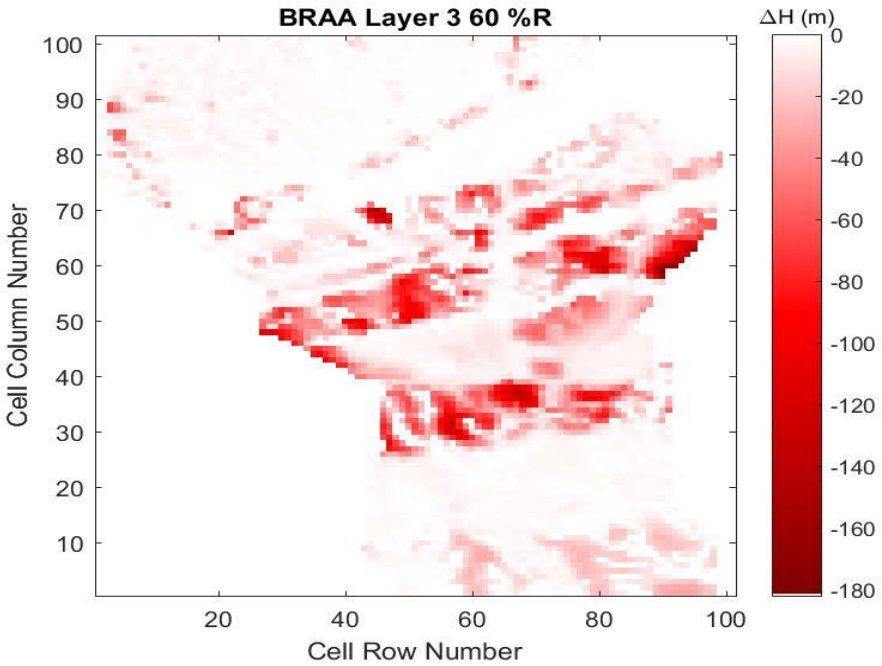

Figure 5. 84 BRAA, 60% original recharge hydraulic head spatial distribution of layer 3

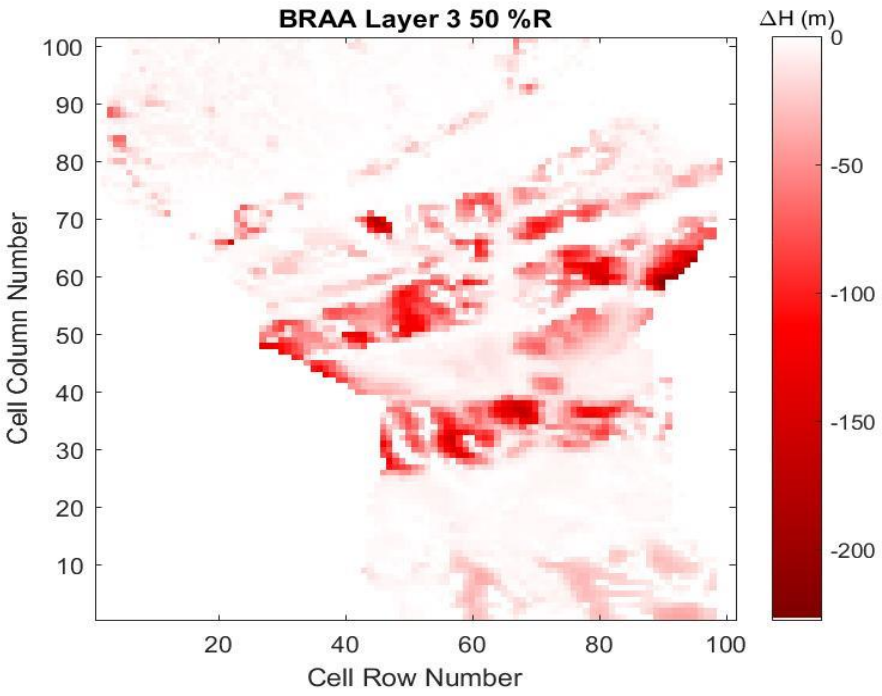

Figure 5. 85 BRAA, 50% original recharge hydraulic head spatial distribution of layer 3

Carrizo-Wilcox Center
Layer 1

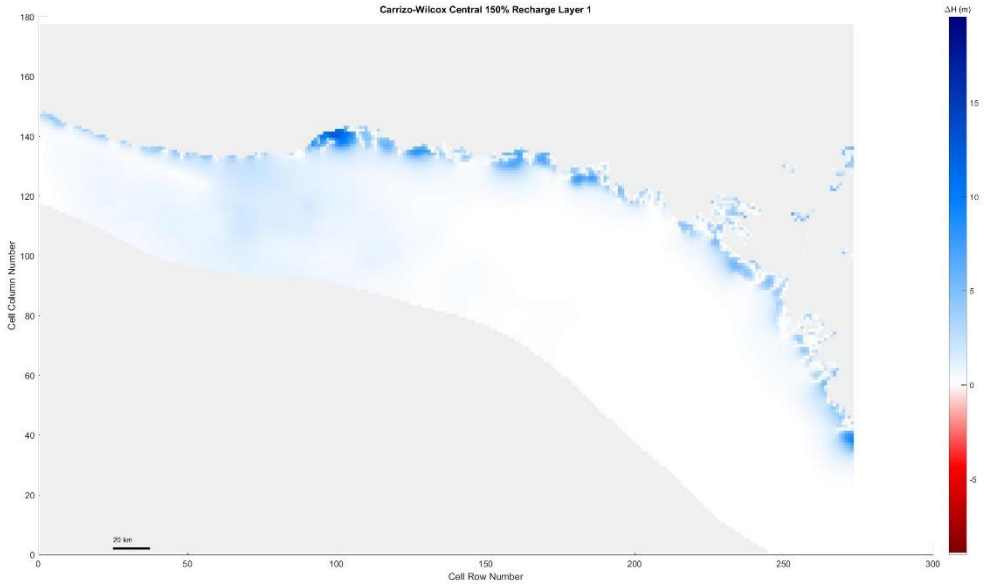

Figure 5. 86 Carrizo-Wilcox Center, 150% original recharge hydraulic head spatial distribution of layer 1

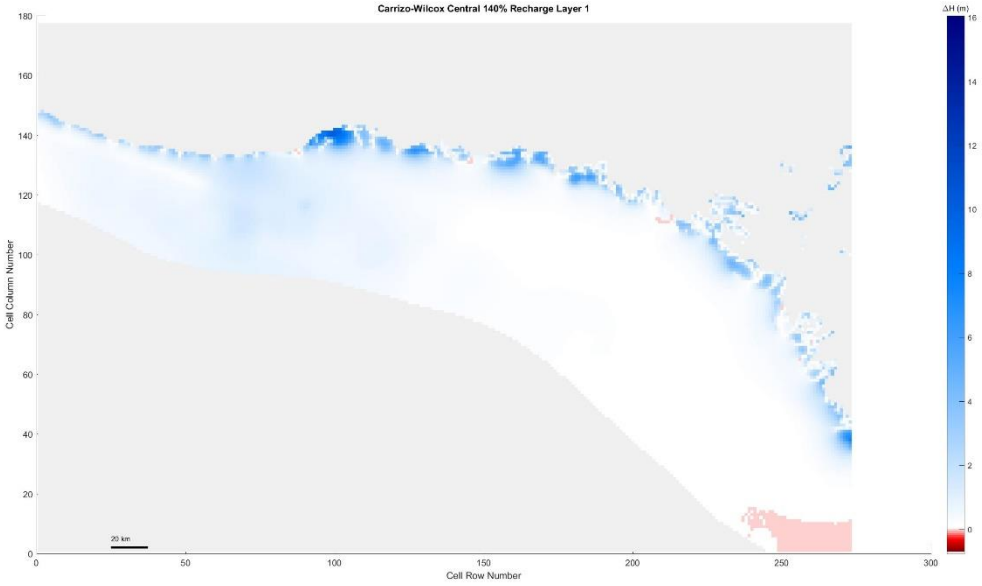

Figure 5. 87 Carrizo-Wilcox Center, 140% original recharge hydraulic head spatial distribution of layer 1

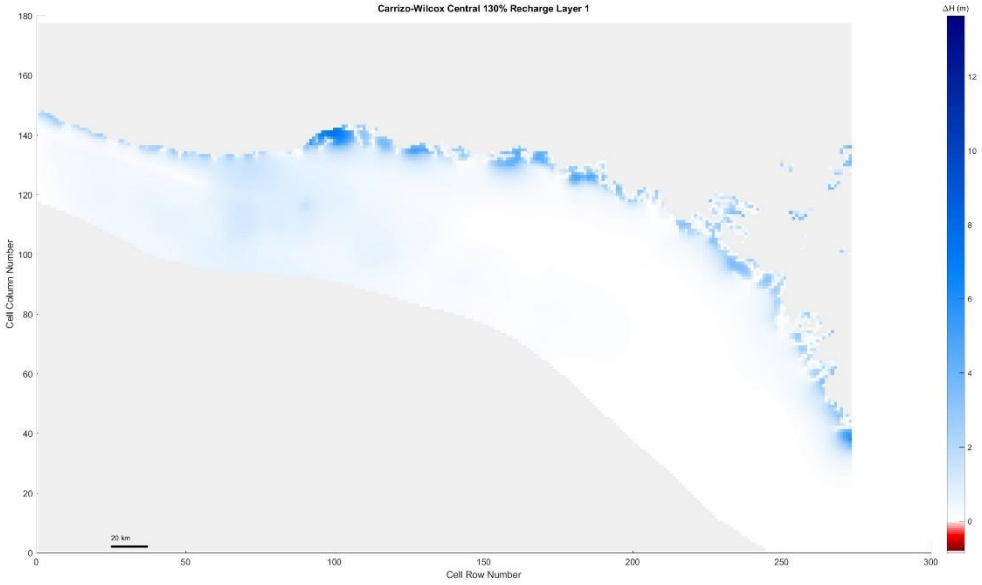

Figure 5. 88 Carrizo-Wilcox Center, 350% original recharge hydraulic head spatial distribution of layer 1

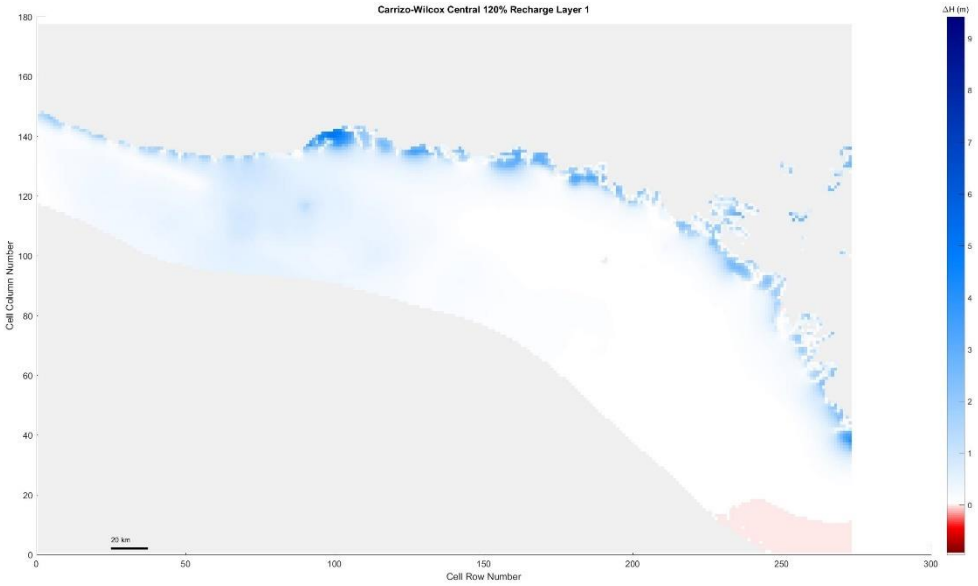

Figure 5. 89 Carrizo-Wilcox Center, 120% original recharge hydraulic head spatial distribution of layer 1

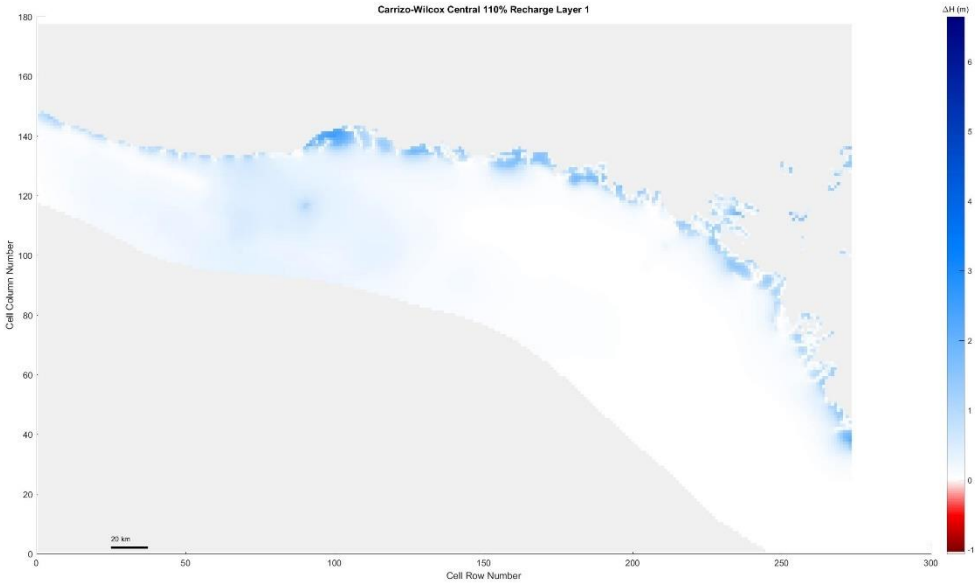

Figure 5. 90 Carrizo-Wilcox Center, 110% original recharge hydraulic head spatial distribution of layer 1

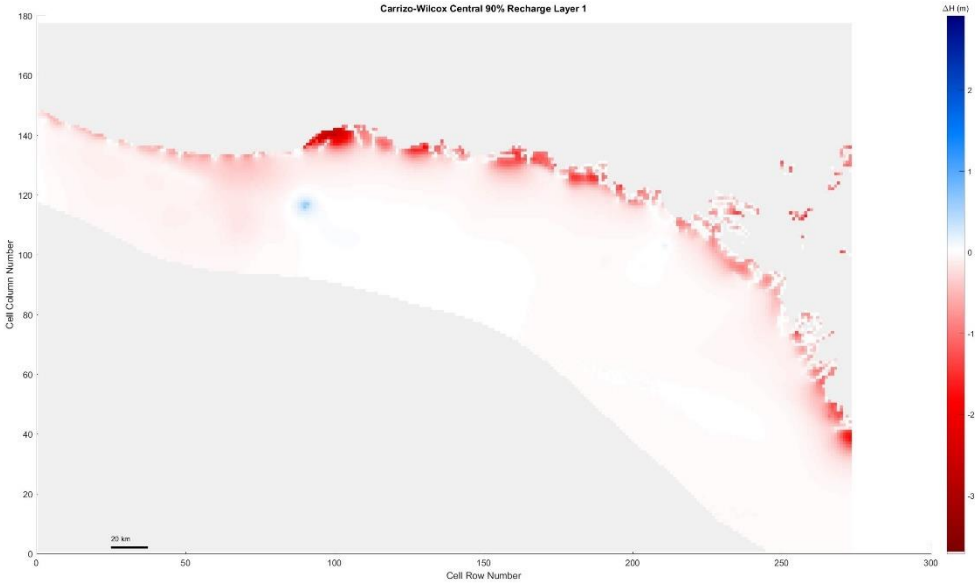

Figure 5. 91 Carrizo-Wilcox Center, 90% original recharge hydraulic head spatial distribution of layer 1

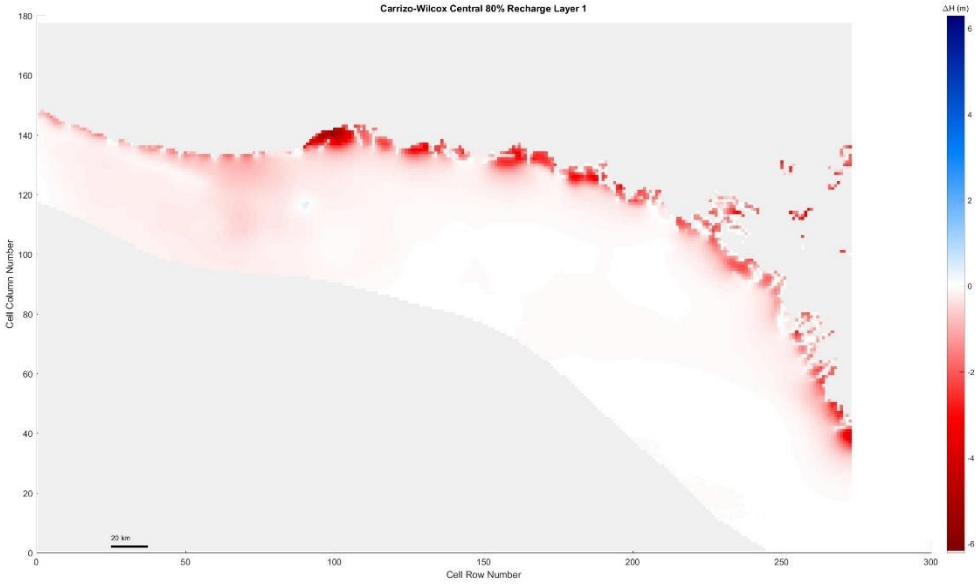

Figure 5. 92 Carrizo-Wilcox Center, 80% original recharge hydraulic head spatial distribution of layer 1

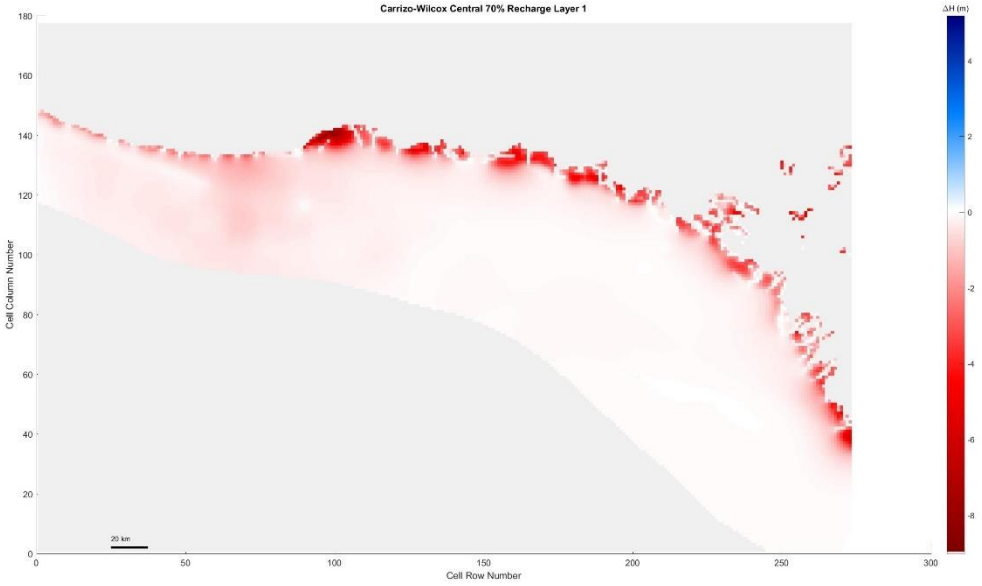

Figure 5. 93 Carrizo-Wilcox Center, 70% original recharge hydraulic head spatial distribution of layer 1

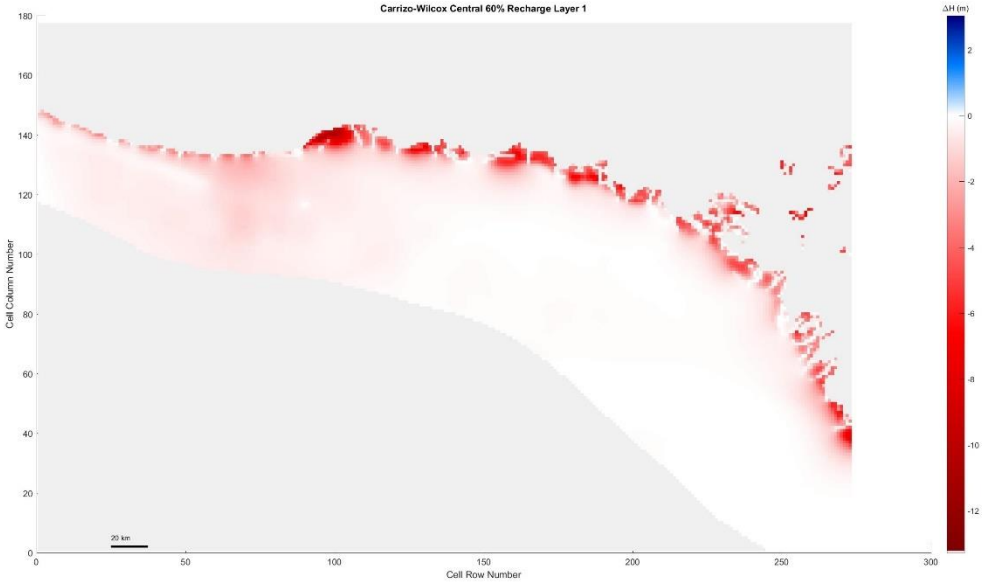

Figure 5. 94 Carrizo-Wilcox Center, 60% original recharge hydraulic head spatial distribution of layer 1

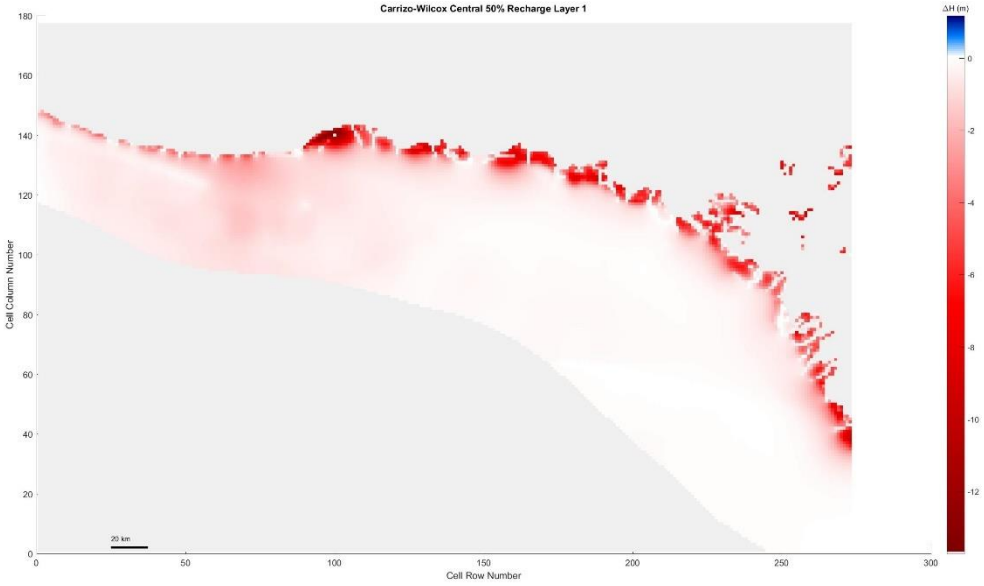

Figure 5. 95 Carrizo-Wilcox Center, 50% original recharge hydraulic head spatial distribution of layer 1

Layer 2

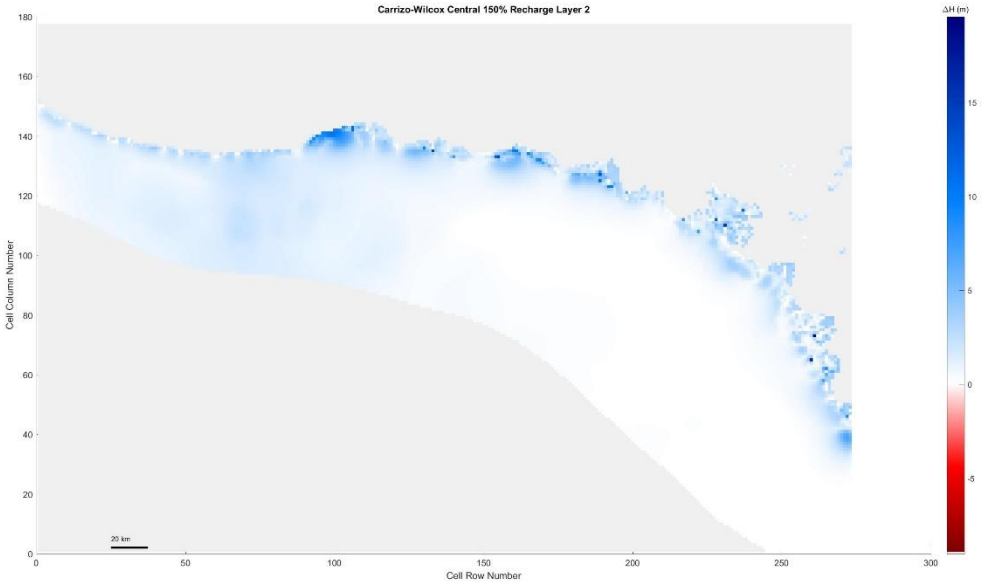

Figure 5. 96 Carrizo-Wilcox Center, 150% original recharge hydraulic head spatial distribution of layer 2

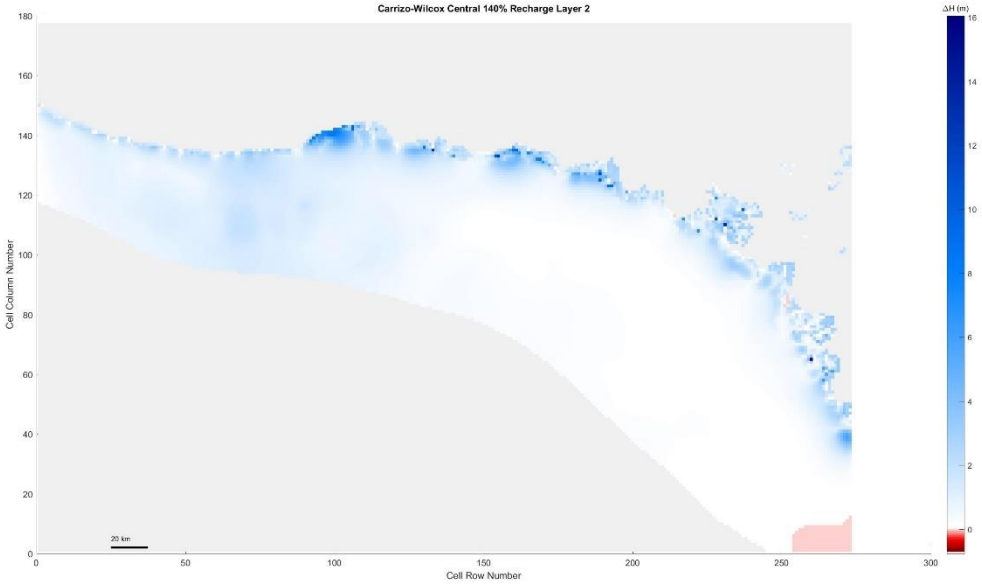

Figure 5. 97 Carrizo-Wilcox Center, 140% original recharge hydraulic head spatial distribution of layer 2

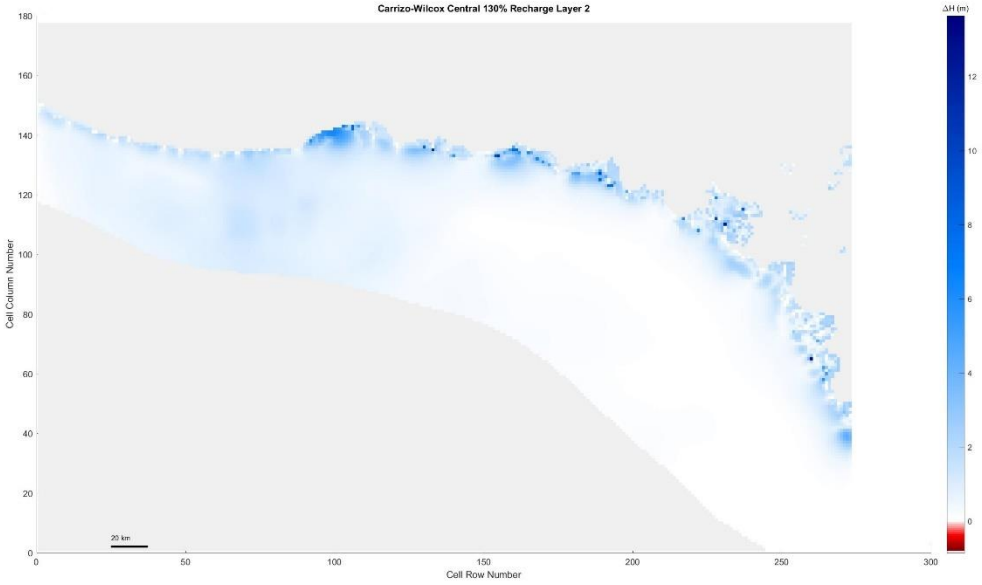

Figure 5. 98 Carrizo-Wilcox Center, 130% original recharge hydraulic head spatial distribution of layer 2

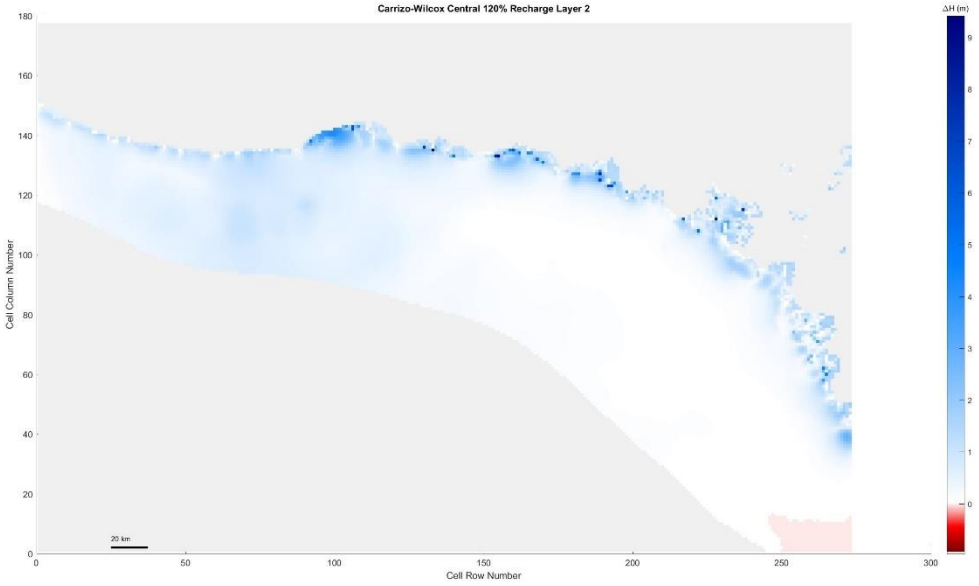

Figure 5. 99 Carrizo-Wilcox Center, 120% original recharge hydraulic head spatial distribution of layer 2

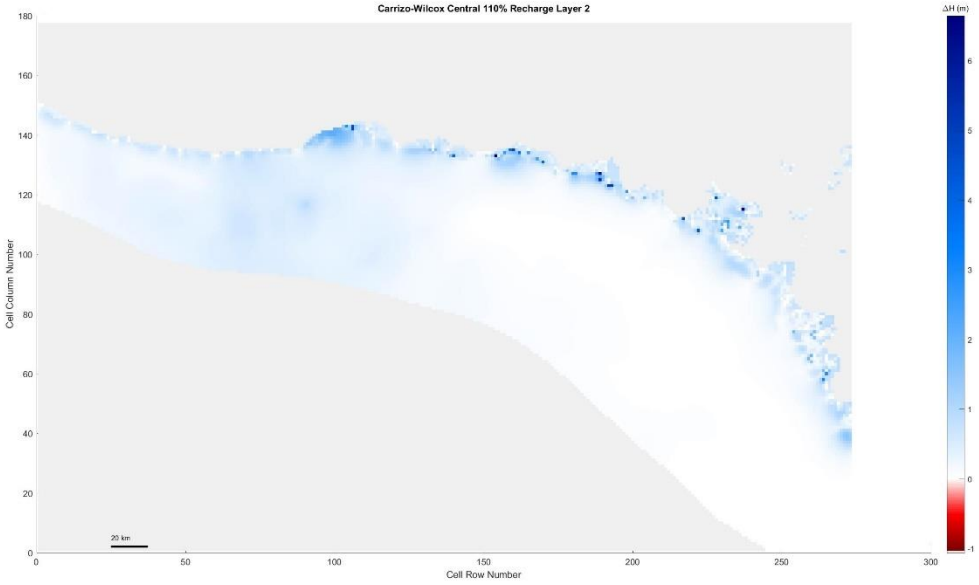

Figure 5. 100 Carrizo-Wilcox Center, 110% original recharge hydraulic head spatial distribution of layer 2

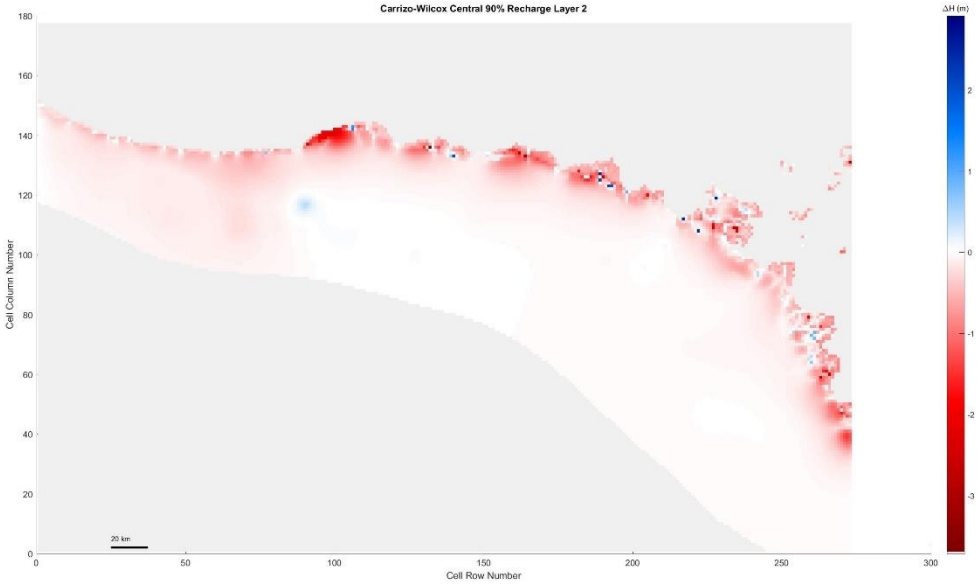

Figure 5. 101 Carrizo-Wilcox Center, 90% original recharge hydraulic head spatial distribution of layer 2

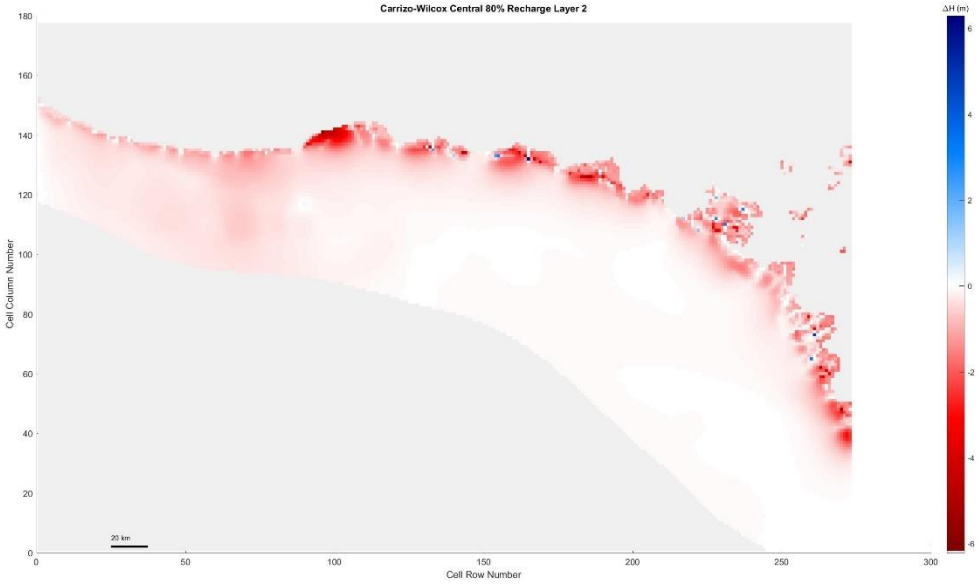

Figure 5. 102 Carrizo-Wilcox Center, 80% original recharge hydraulic head spatial distribution of layer 2

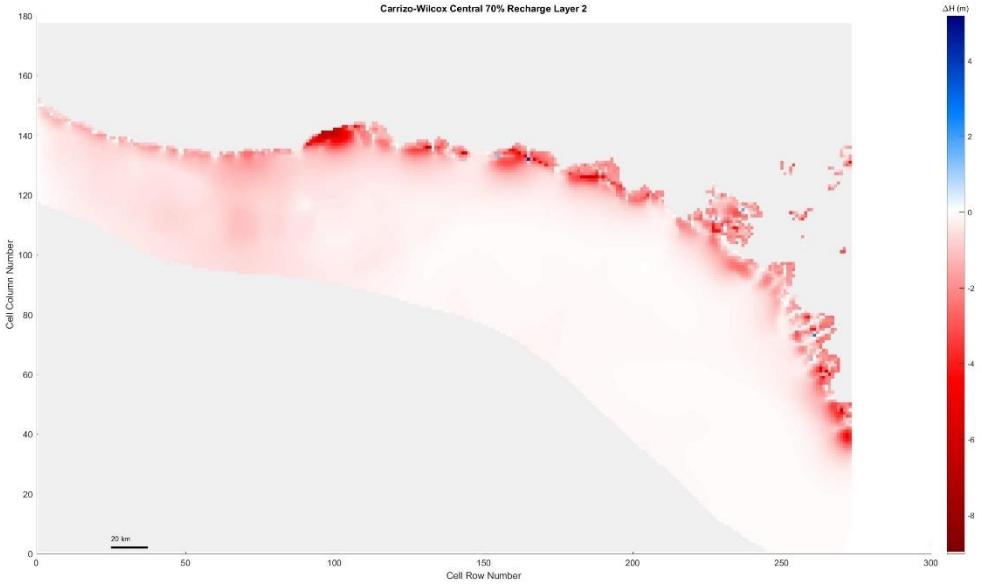

Figure 5. 103 Carrizo-Wilcox Center, 70% original recharge hydraulic head spatial distribution of layer 2

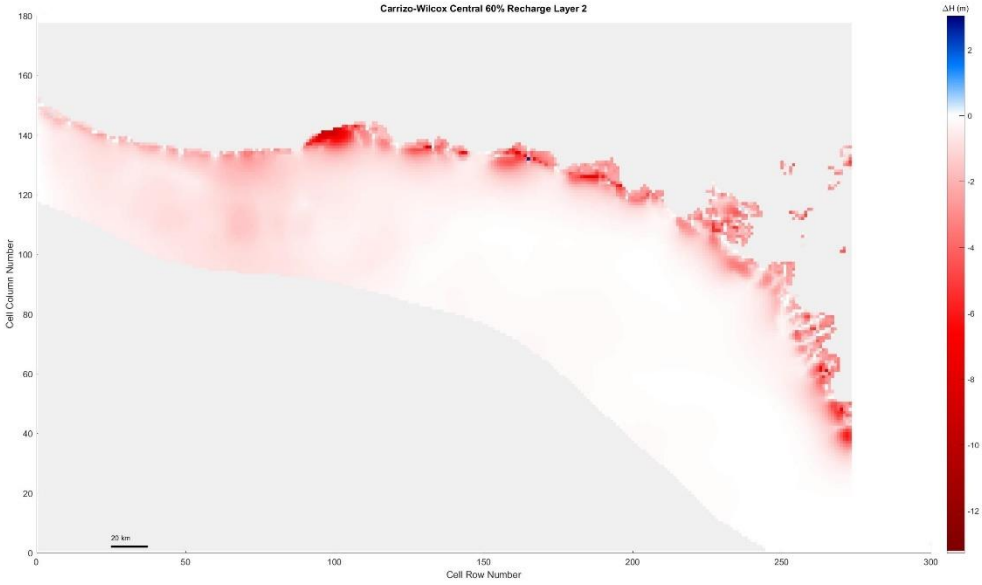

Figure 5. 104 Carrizo-Wilcox Center, 60% original recharge hydraulic head spatial distribution of layer 2

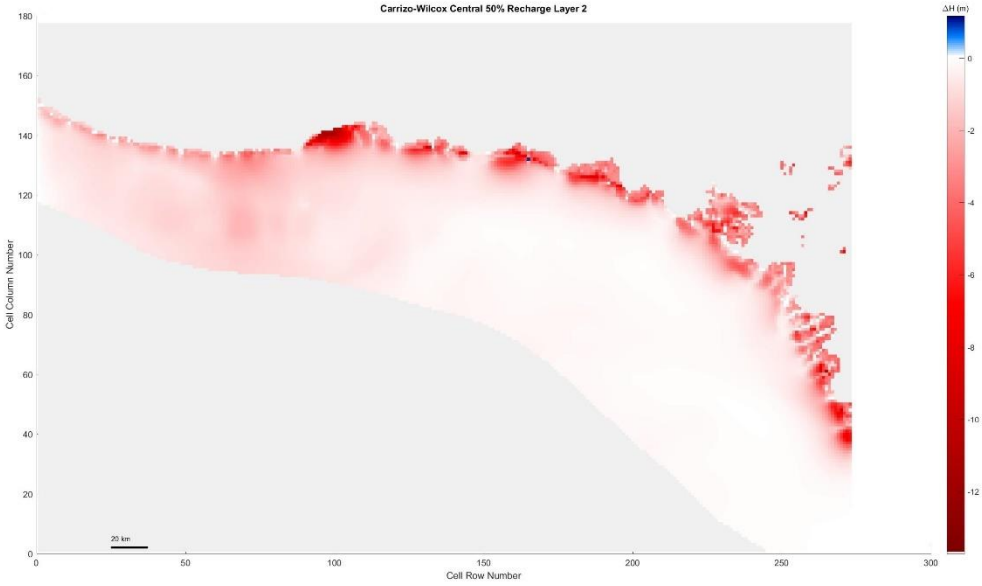

Figure 5. 105 Carrizo-Wilcox Center, 50% original recharge hydraulic head spatial distribution of layer 2

Layer 3

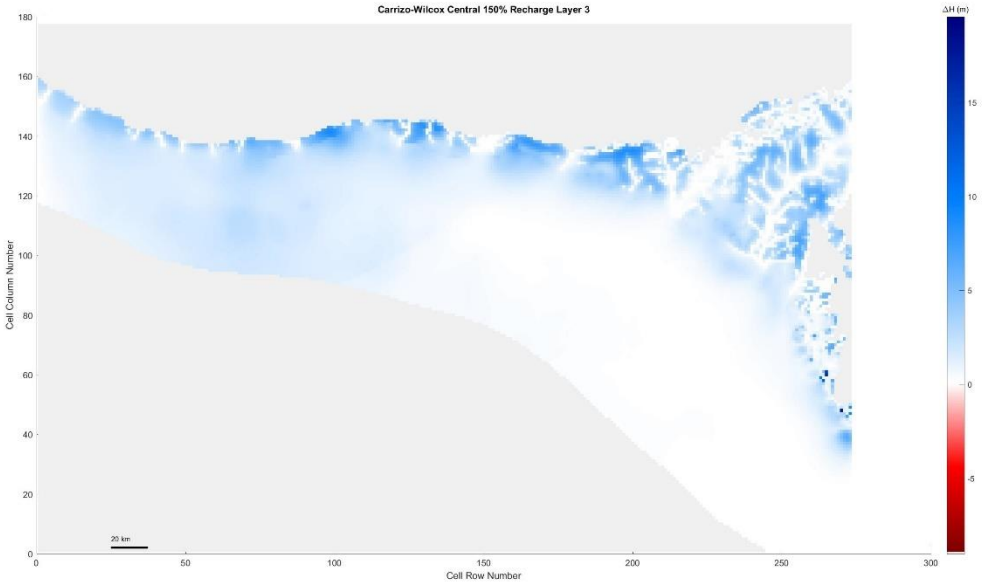

Figure 5. 106 Carrizo-Wilcox Center, 150% original recharge hydraulic head spatial distribution of layer 3

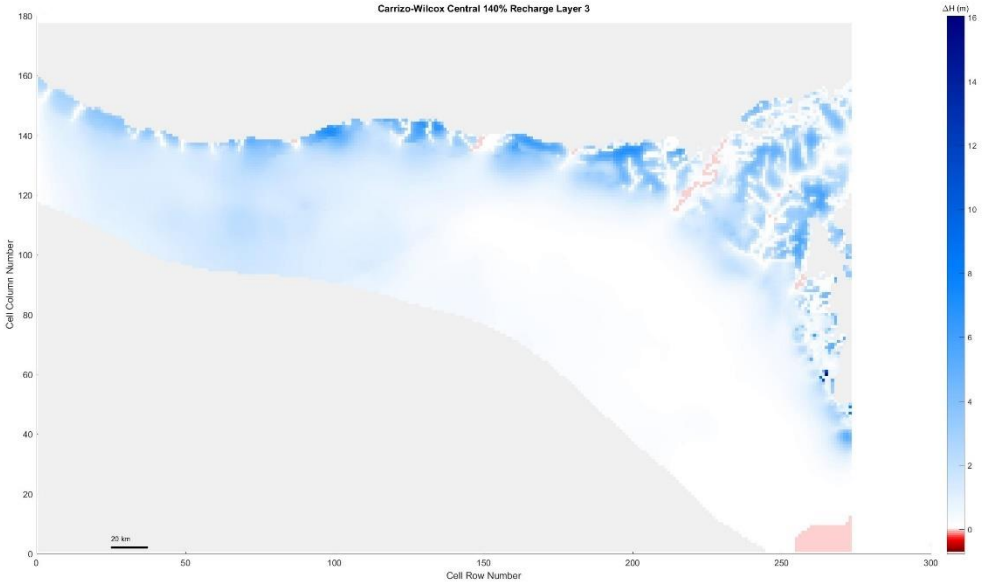

Figure 5. 107 Carrizo-Wilcox Center, 140% original recharge hydraulic head spatial distribution of layer 3

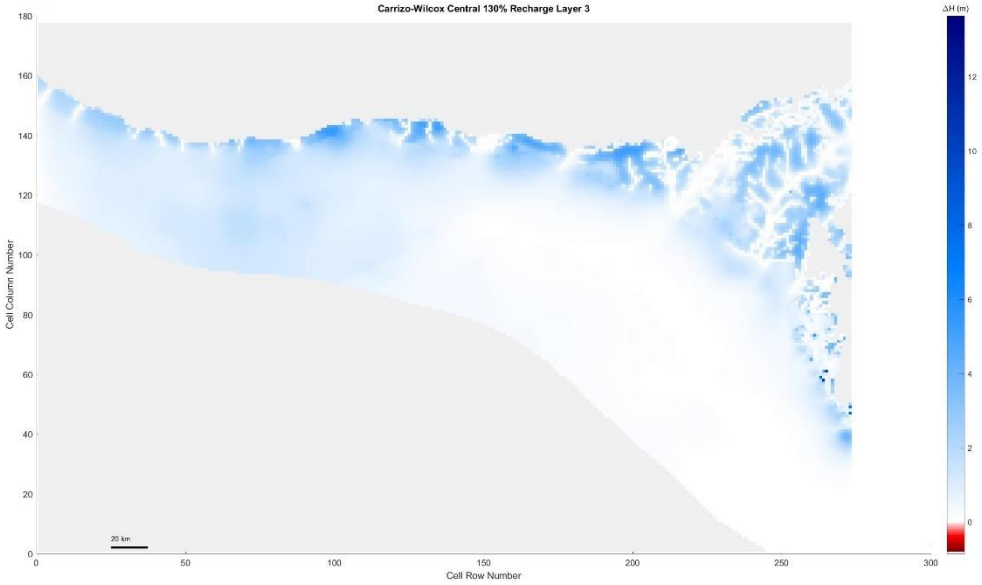

Figure 5. 108 Carrizo-Wilcox Center, 130% original recharge hydraulic head spatial distribution of layer 3

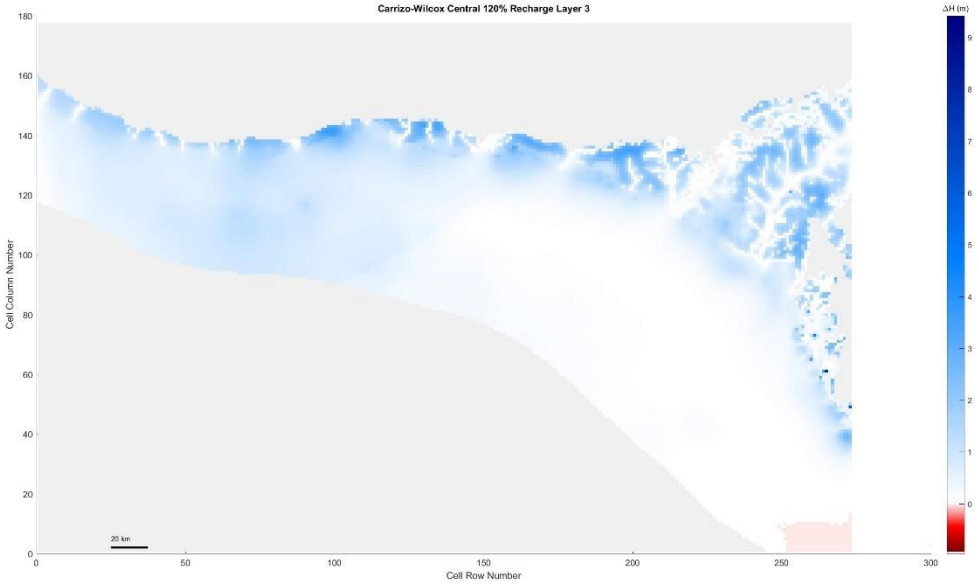

Figure 5. 109 Carrizo-Wilcox Center, 120% original recharge hydraulic head spatial distribution of layer 3

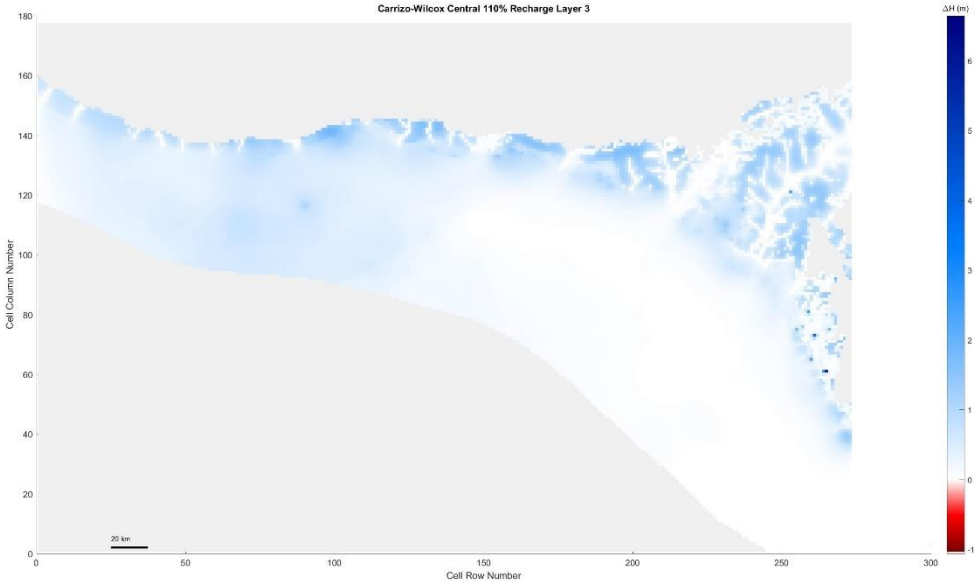

Figure 5. 110 Carrizo-Wilcox Center, 110% original recharge hydraulic head spatial distribution of layer 3

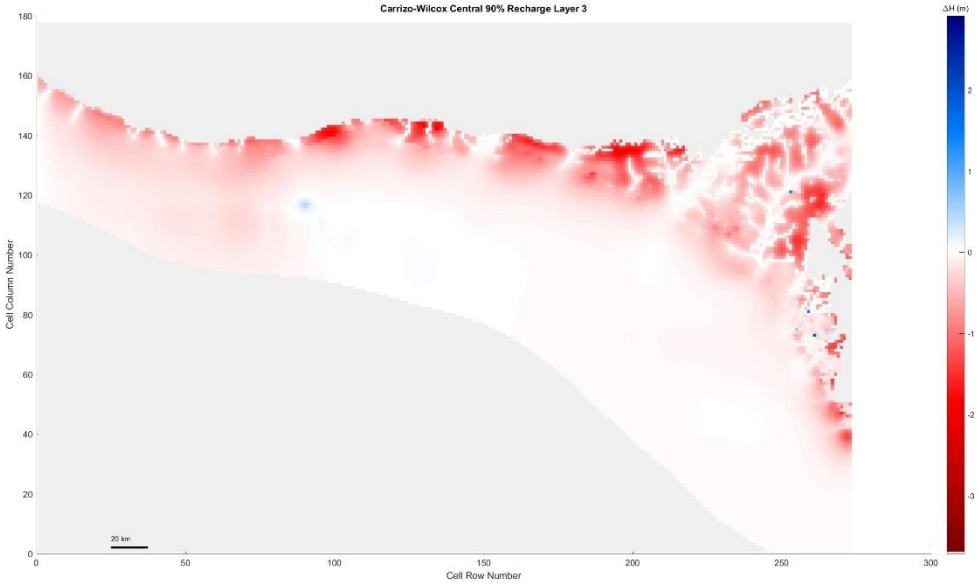

Figure 5. 111 Carrizo-Wilcox Center, 90% original recharge hydraulic head spatial distribution of layer 3

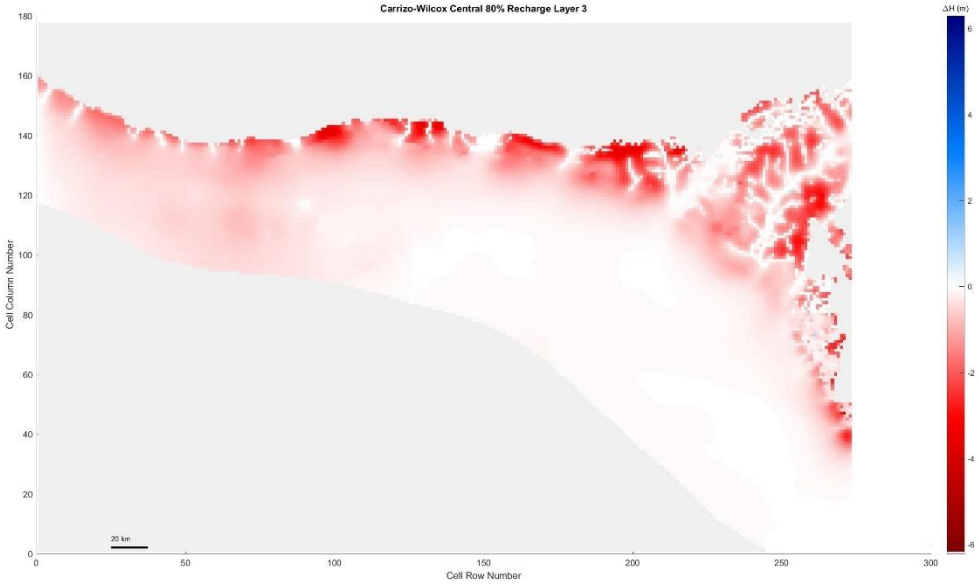

Figure 5. 112 Carrizo-Wilcox Center, 80% original recharge hydraulic head spatial distribution of layer 3

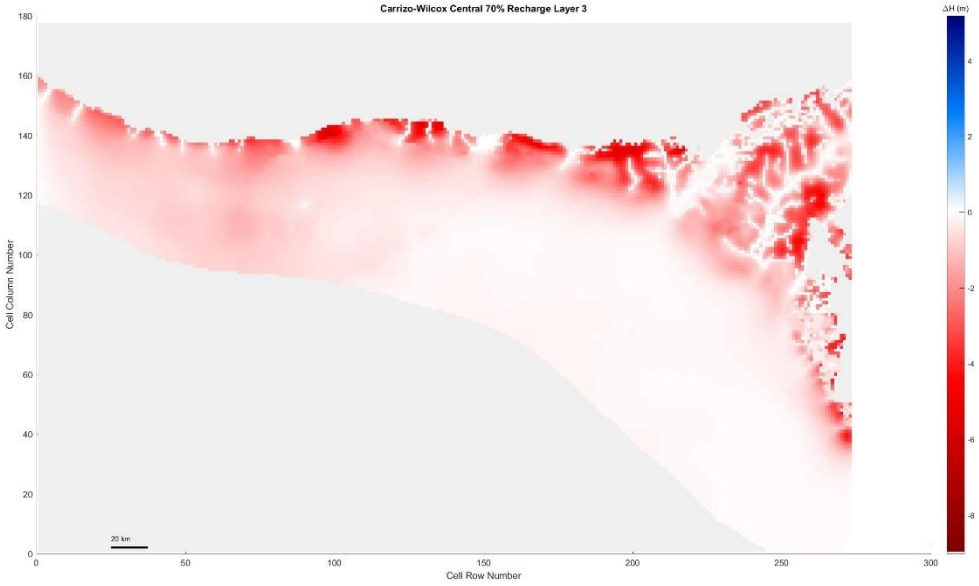

Figure 5. 113 Carrizo-Wilcox Center, 70% original recharge hydraulic head spatial distribution of layer 3

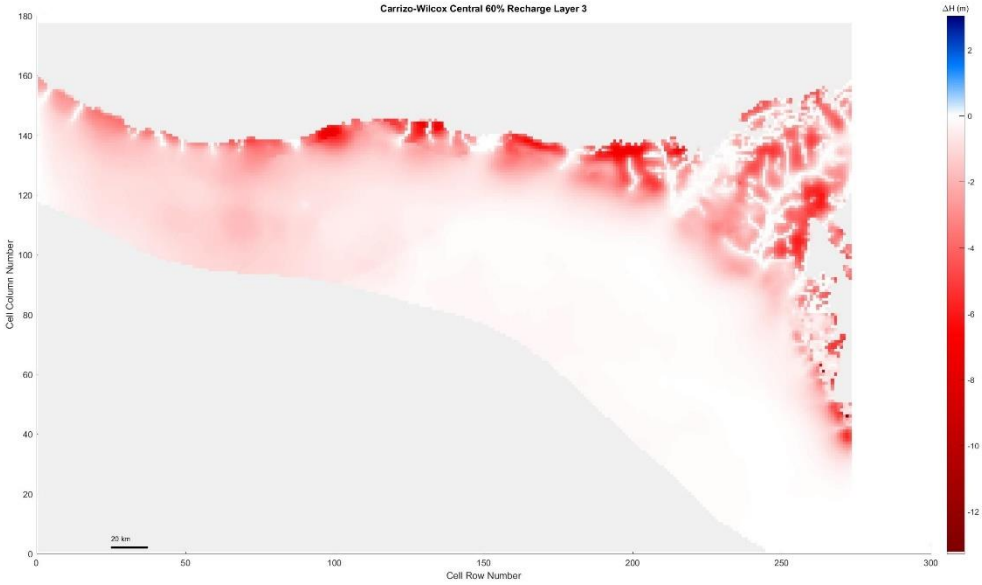

Figure 5. 114 Carrizo-Wilcox Center, 60% original recharge hydraulic head spatial distribution of layer 3

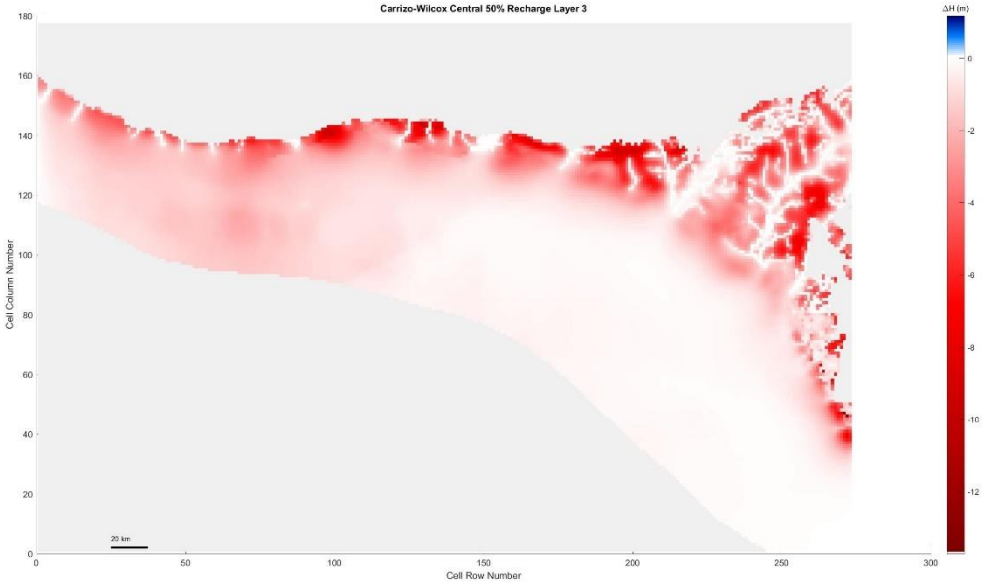

Figure 5. 115 Carrizo-Wilcox Center, 50% original recharge hydraulic head spatial distribution of layer 3

Layer 4

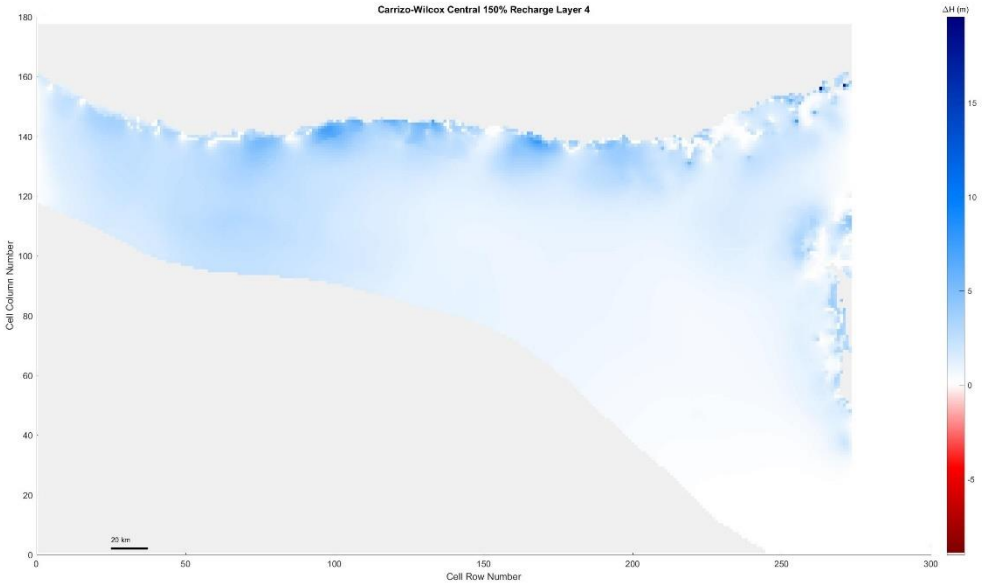

Figure 5. 116 Carrizo-Wilcox Center, 150% original recharge hydraulic head spatial distribution of layer 4

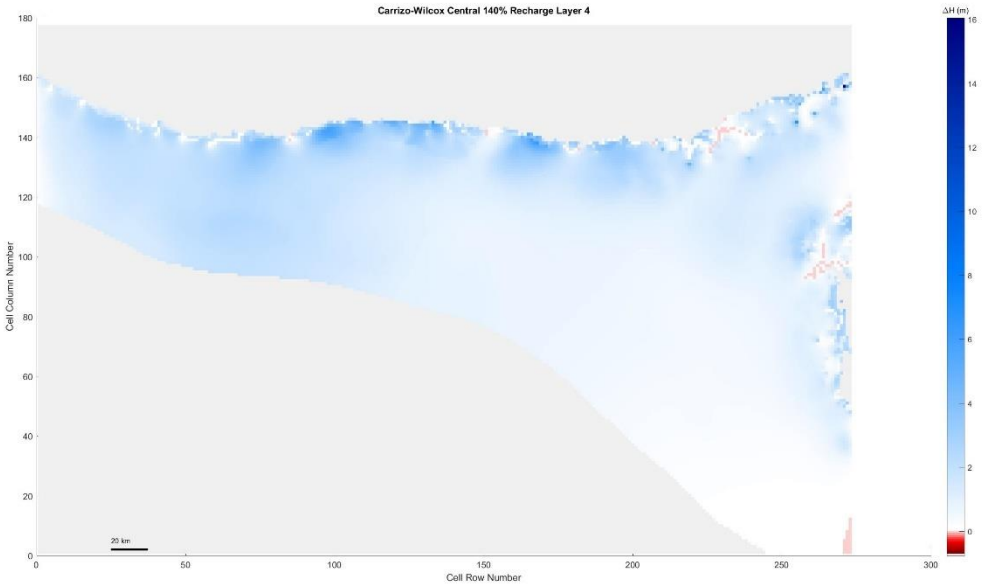

Figure 5. 117 Carrizo-Wilcox Center, 140% original recharge hydraulic head spatial distribution of layer 4

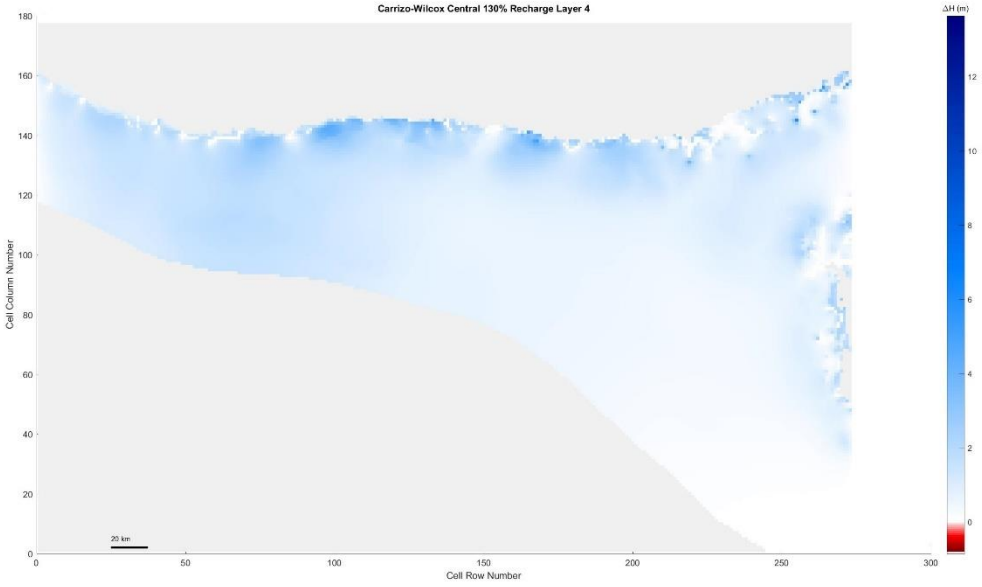

Figure 5. 118 Carrizo-Wilcox Center, 130% original recharge hydraulic head spatial distribution of layer 4

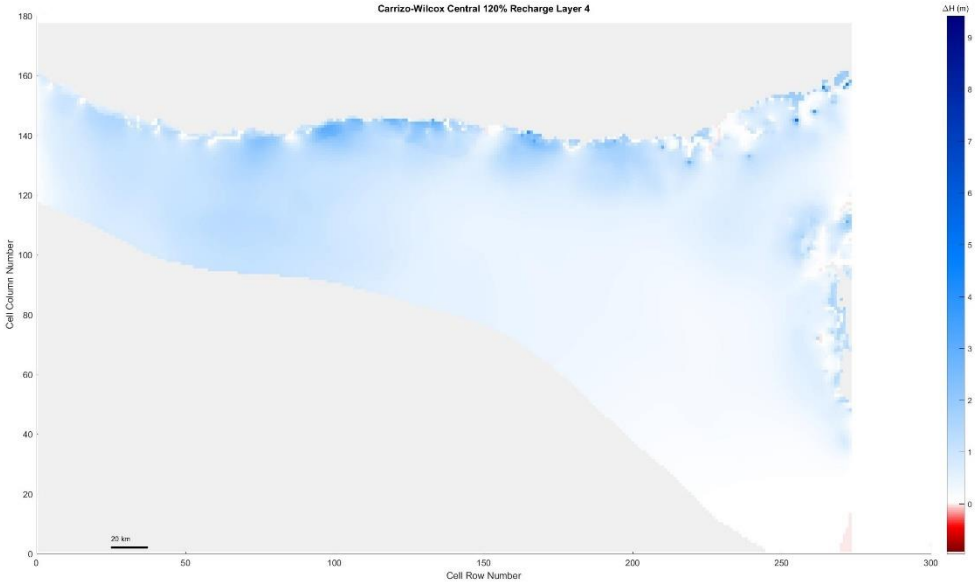

Figure 5. 119 Carrizo-Wilcox Center, 120% original recharge hydraulic head spatial distribution of layer 4

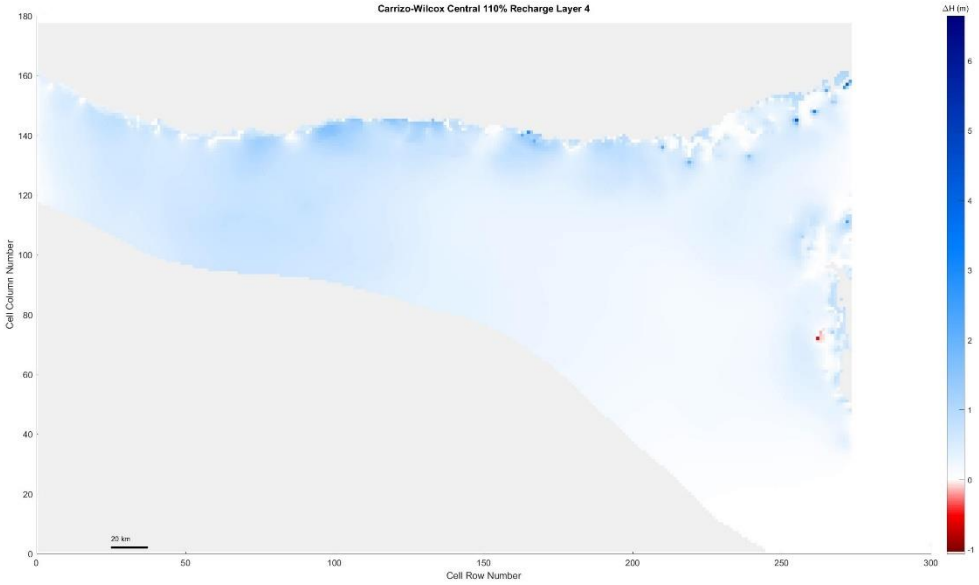

Figure 5. 120 Carrizo-Wilcox Center, 110% original recharge hydraulic head spatial distribution of layer 4

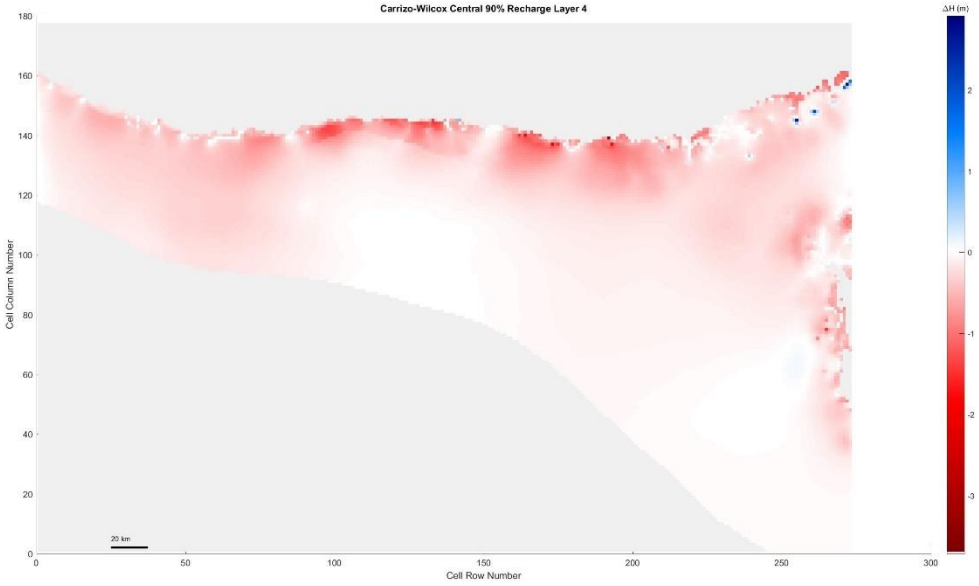

Figure 5. 121 Carrizo-Wilcox Center, 90% original recharge hydraulic head spatial distribution of layer 4

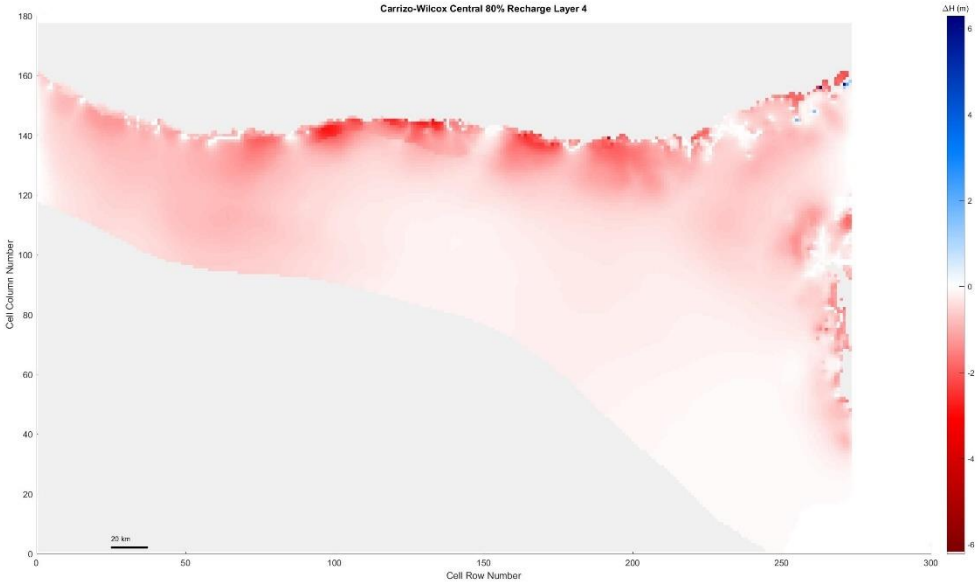

Figure 5. 122 Carrizo-Wilcox Center, 80% original recharge hydraulic head spatial distribution of layer 4

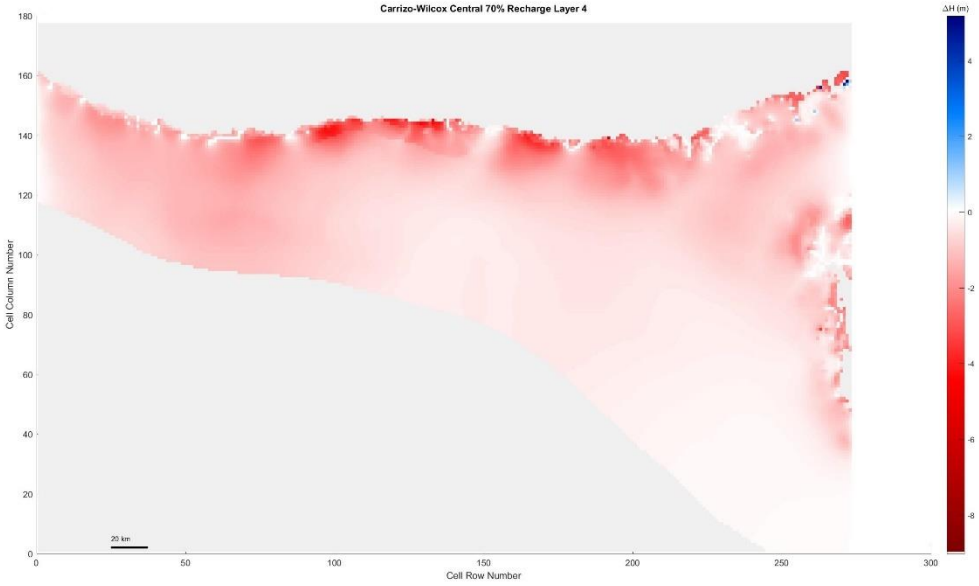

Figure 5. 123 Carrizo-Wilcox Center, 70% original recharge hydraulic head spatial distribution of layer 4

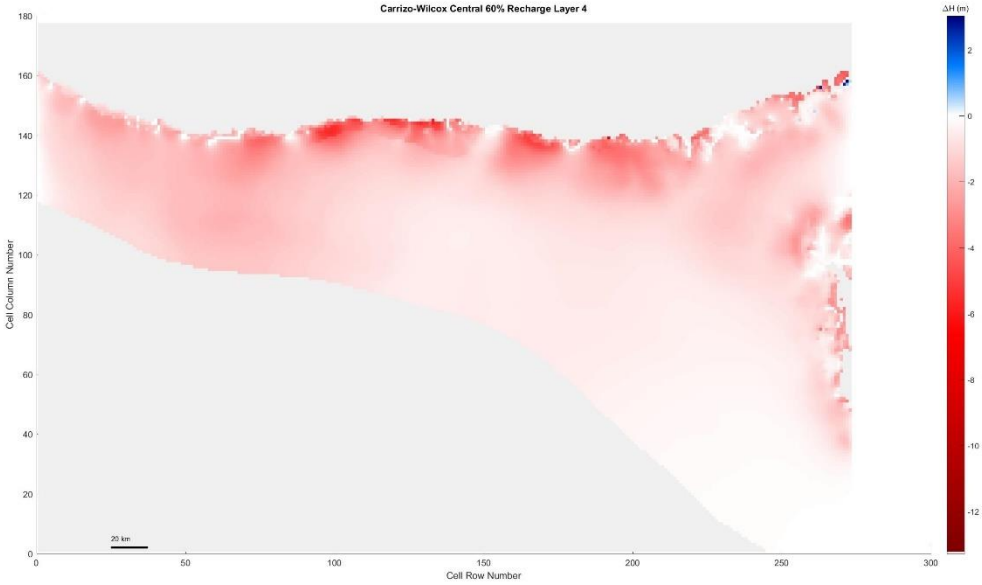

Figure 5. 124 Carrizo-Wilcox Center, 60% original recharge hydraulic head spatial distribution of layer 4

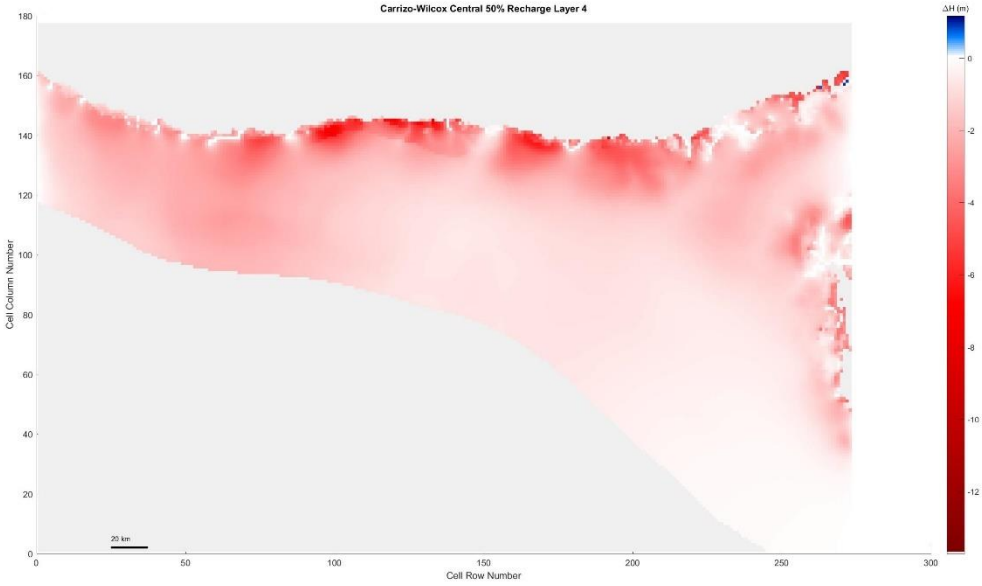

Figure 5. 125 Carrizo-Wilcox Center, 50% original recharge hydraulic head spatial distribution of layer 4

Layer 5

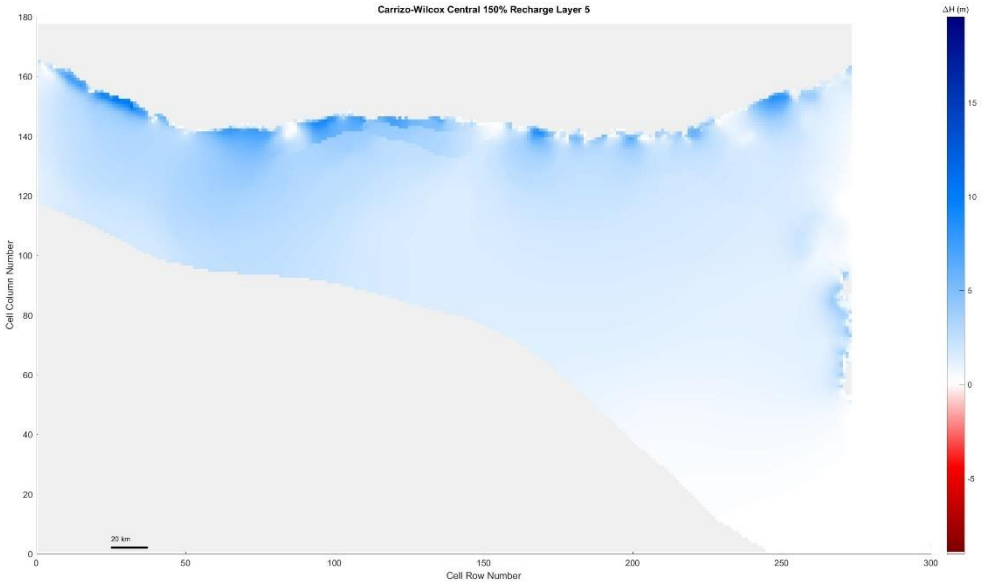

Figure 5. 126 Carrizo-Wilcox Center, 150% original recharge hydraulic head spatial distribution of layer 5

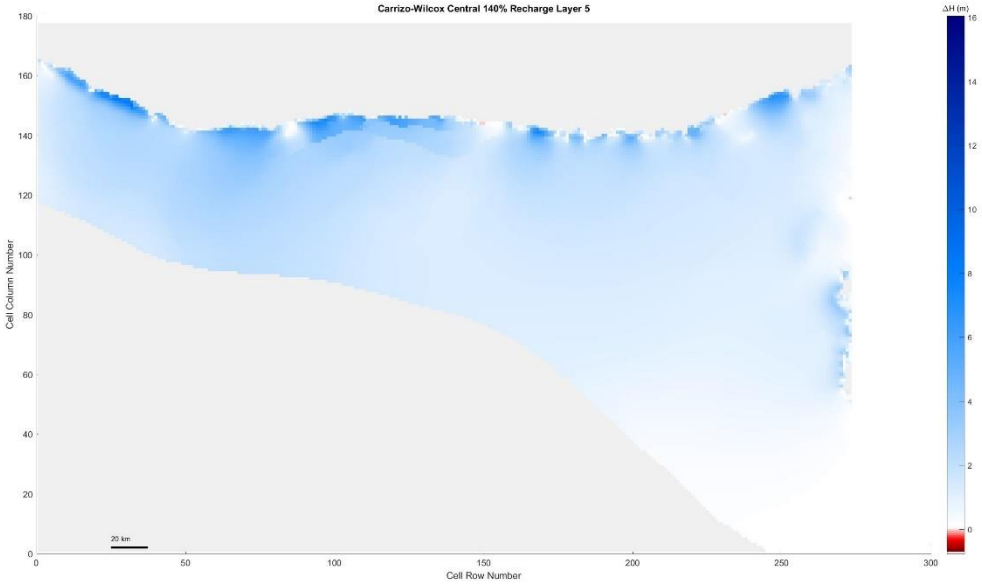

Figure 5. 127 Carrizo-Wilcox Center, 140% original recharge hydraulic head spatial distribution of layer 5

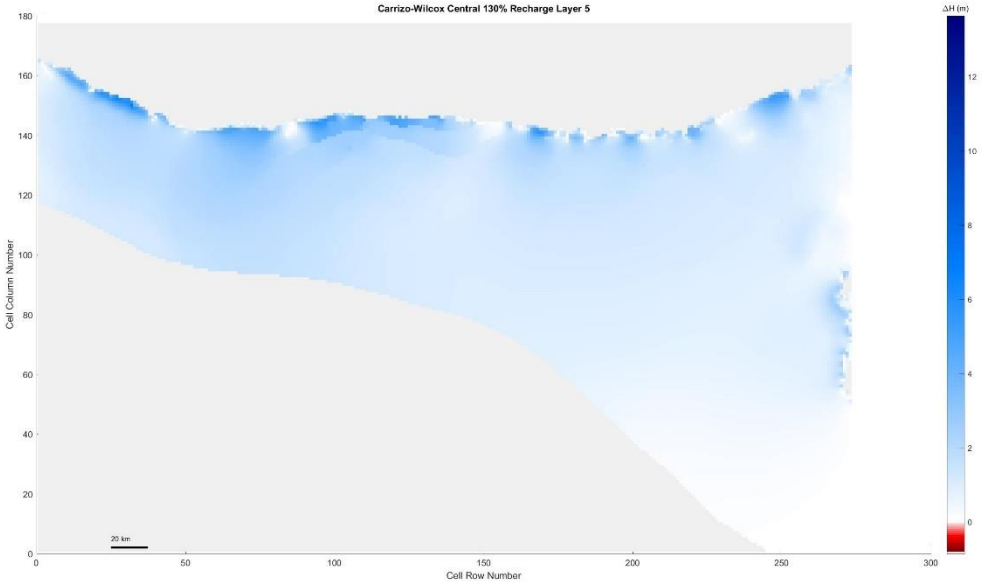

Figure 5. 128 Carrizo-Wilcox Center, 130% original recharge hydraulic head spatial distribution of layer 5

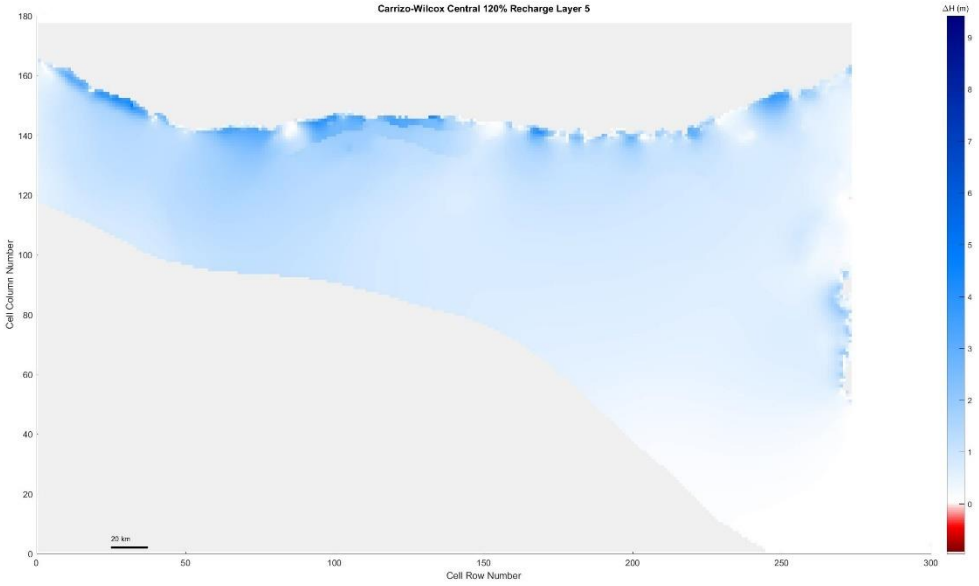

Figure 5. 129 Carrizo-Wilcox Center, 120% original recharge hydraulic head spatial distribution of layer 5

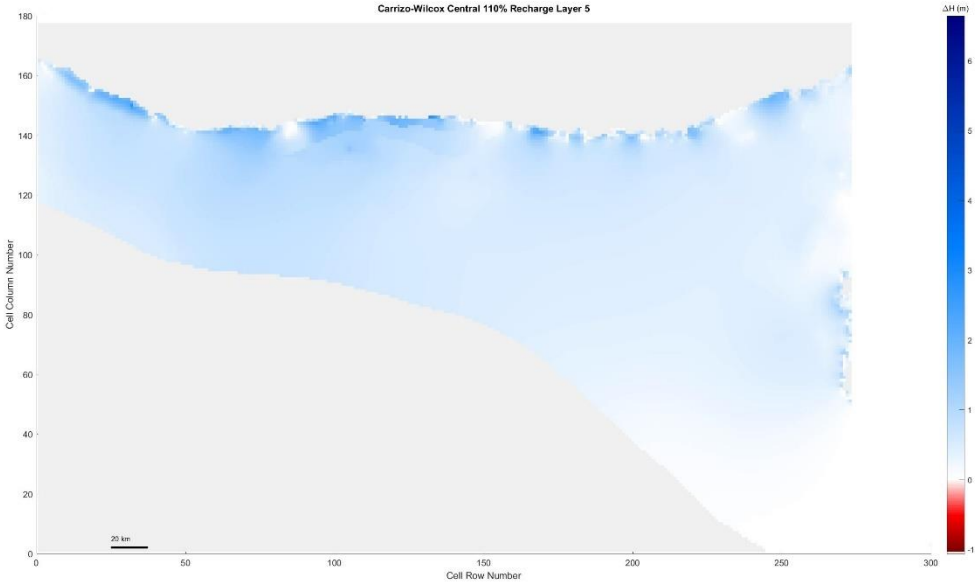

Figure 5. 130 Carrizo-Wilcox Center, 110% original recharge hydraulic head spatial distribution of layer 5

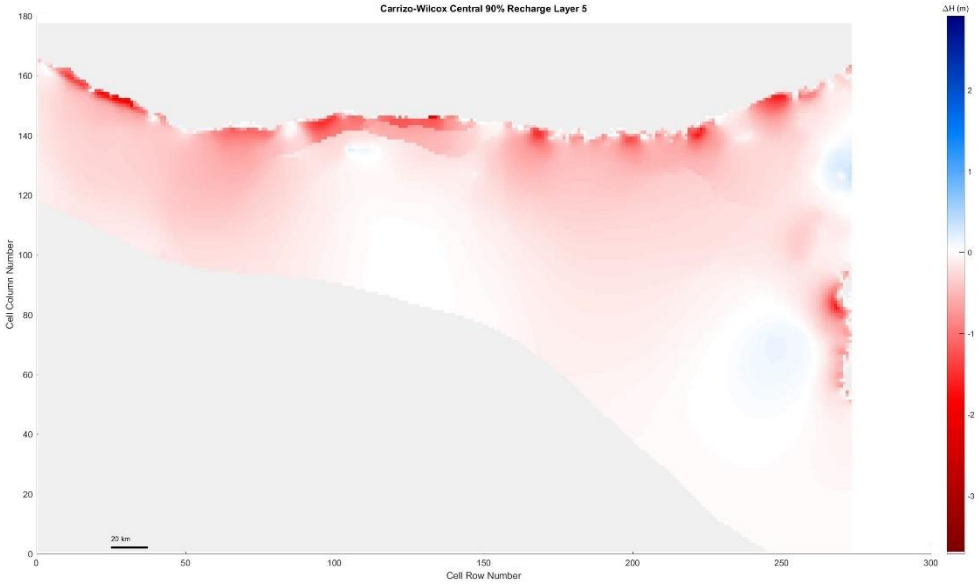

Figure 5. 131 Carrizo-Wilcox Center, 90% original recharge hydraulic head spatial distribution of layer 5

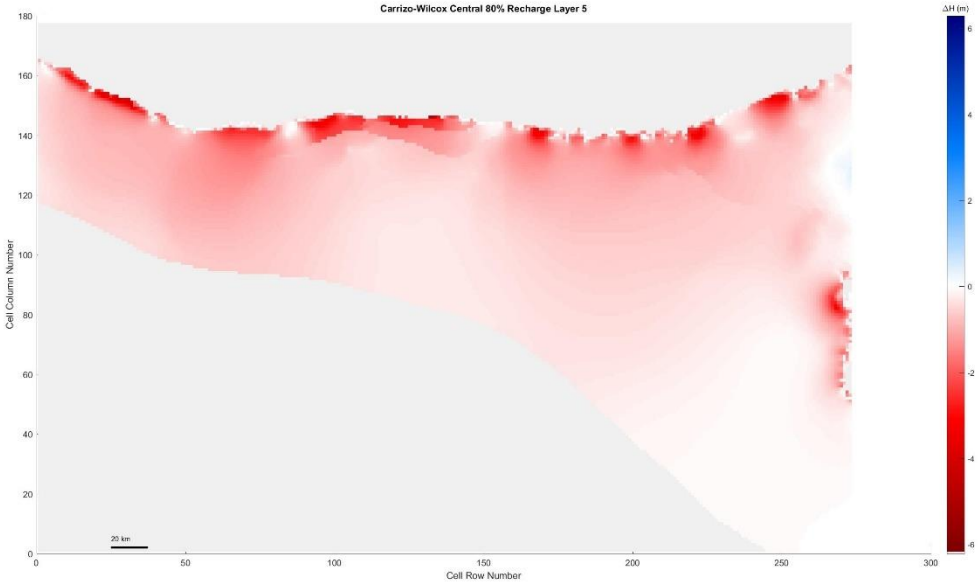

Figure 5. 132 Carrizo-Wilcox Center, 80% original recharge hydraulic head spatial distribution of layer 5

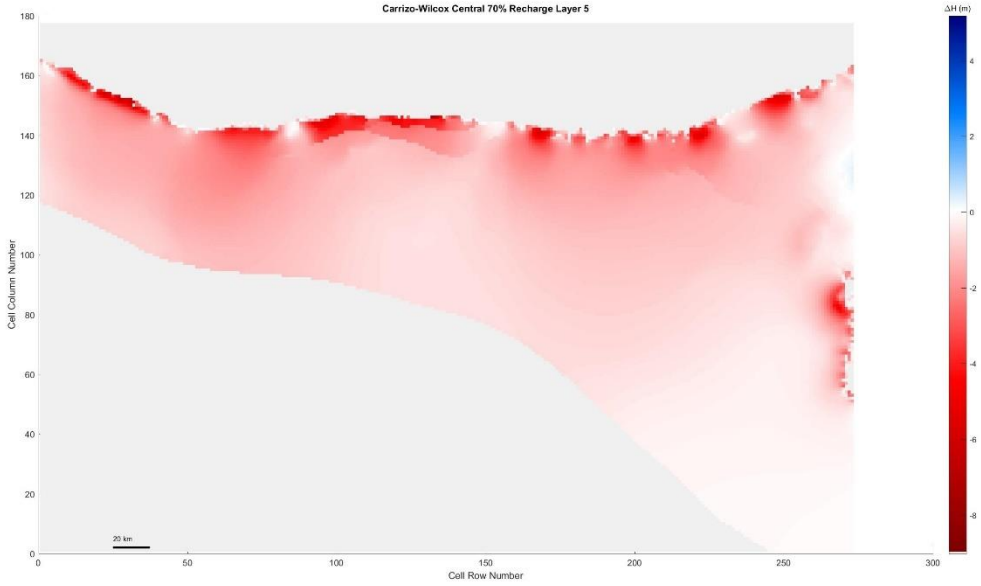

Figure 5. 133 Carrizo-Wilcox Center, 70% original recharge hydraulic head spatial distribution of layer 5

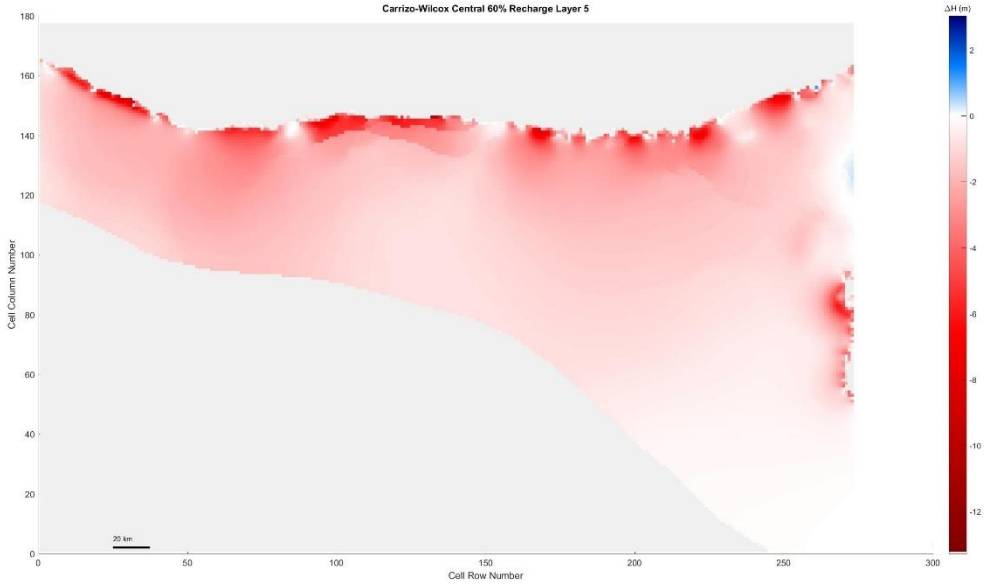

Figure 5. 134 Carrizo-Wilcox Center, 60% original recharge hydraulic head spatial distribution of layer 5

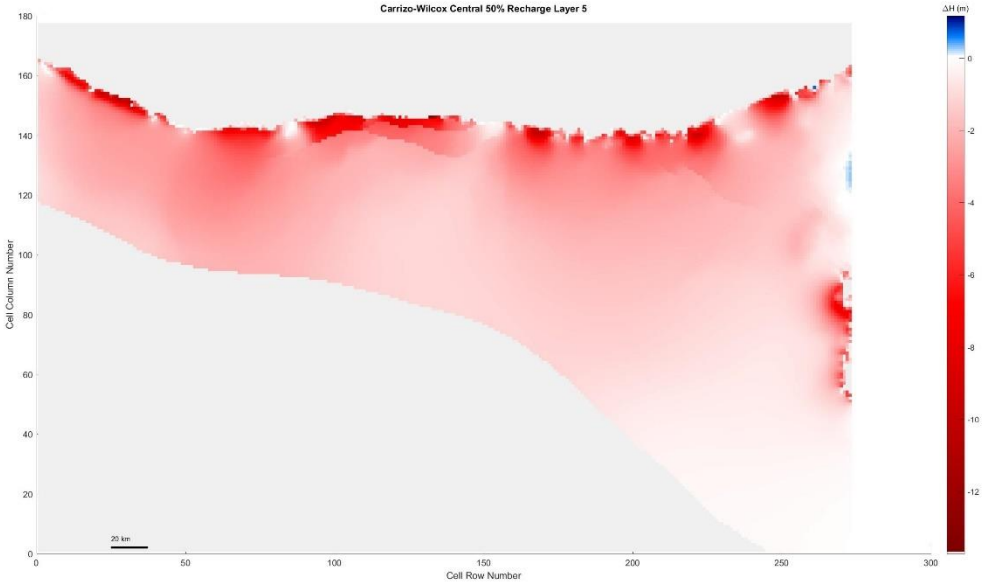

Figure 5. 135 Carrizo-Wilcox Center, 50% original recharge hydraulic head spatial distribution of layer 5

Layer 6

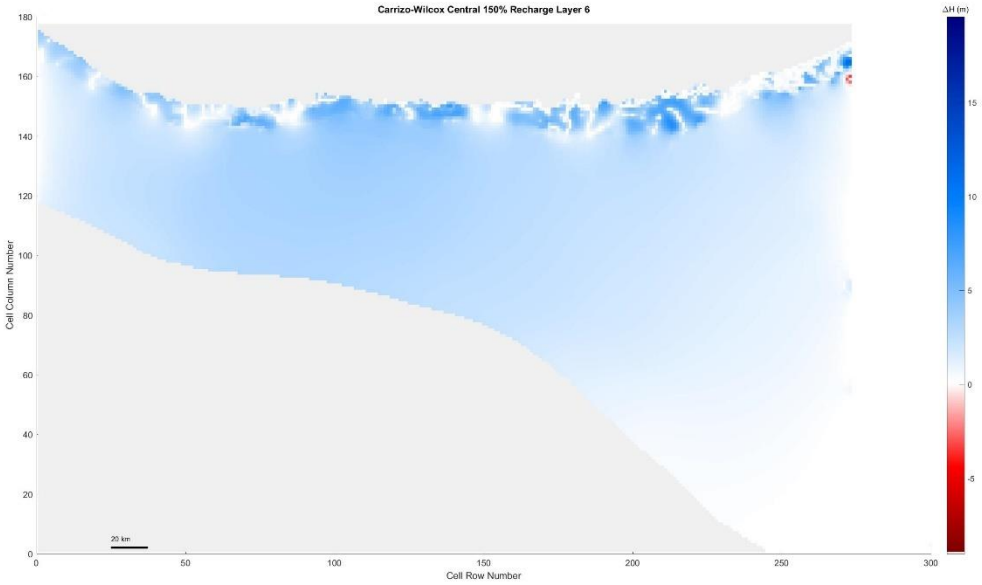

Figure 5. 136 Carrizo-Wilcox Center, 150% original recharge hydraulic head spatial distribution of layer 6

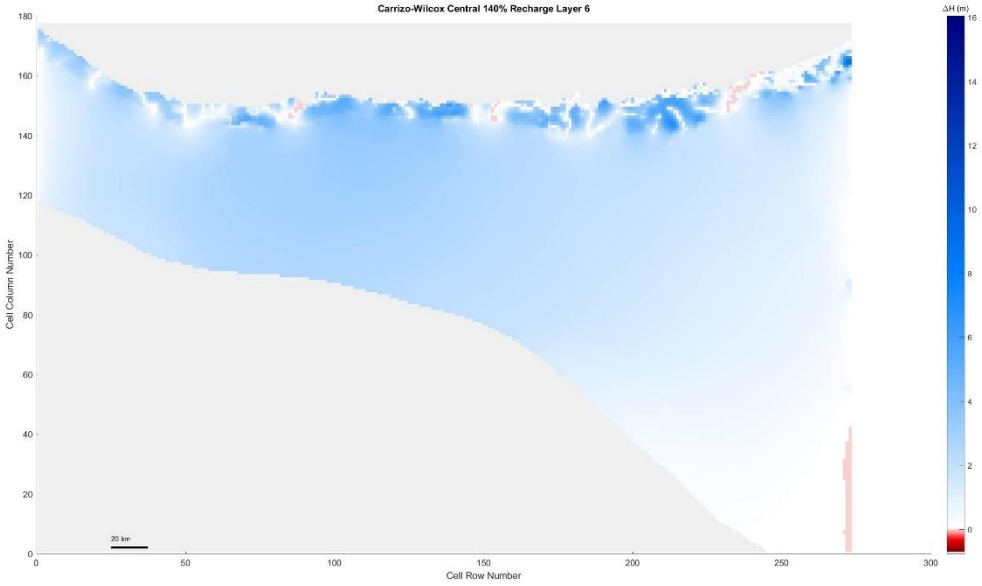

Figure 5. 137 Carrizo-Wilcox Center, 140% original recharge hydraulic head spatial distribution of layer 6

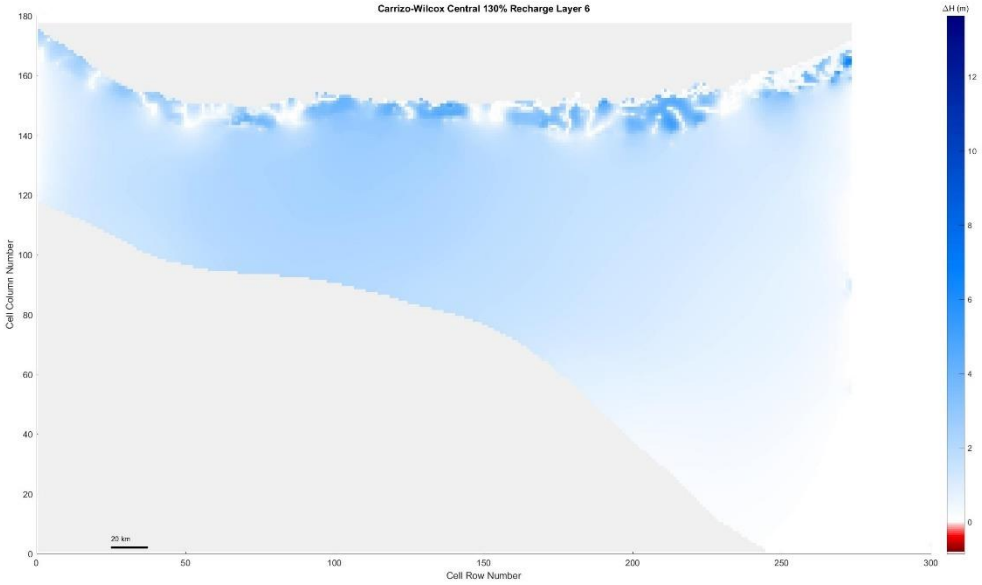

Figure 5. 138 Carrizo-Wilcox Center, 130% original recharge hydraulic head spatial distribution of layer 6

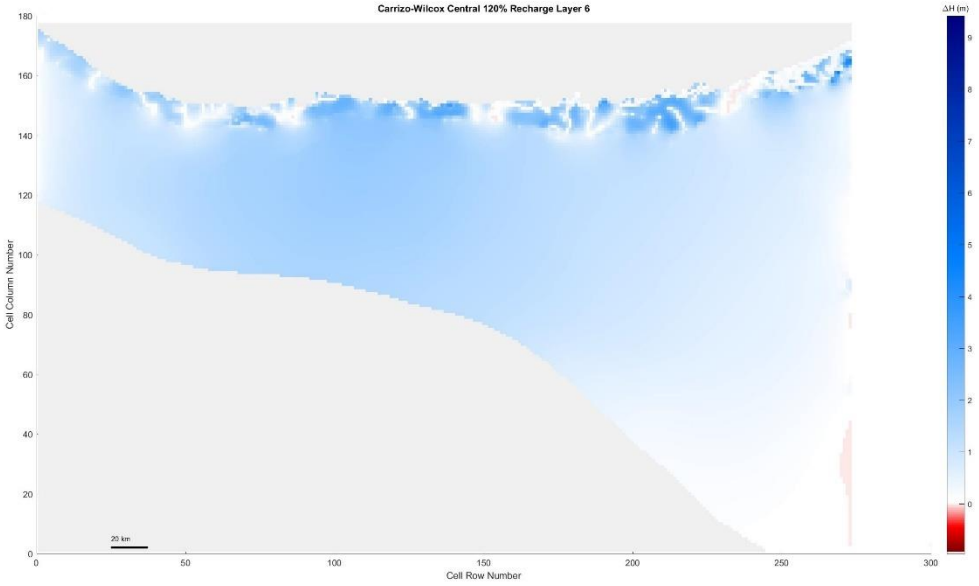

Figure 5. 139 Carrizo-Wilcox Center, 120% original recharge hydraulic head spatial distribution of layer 6

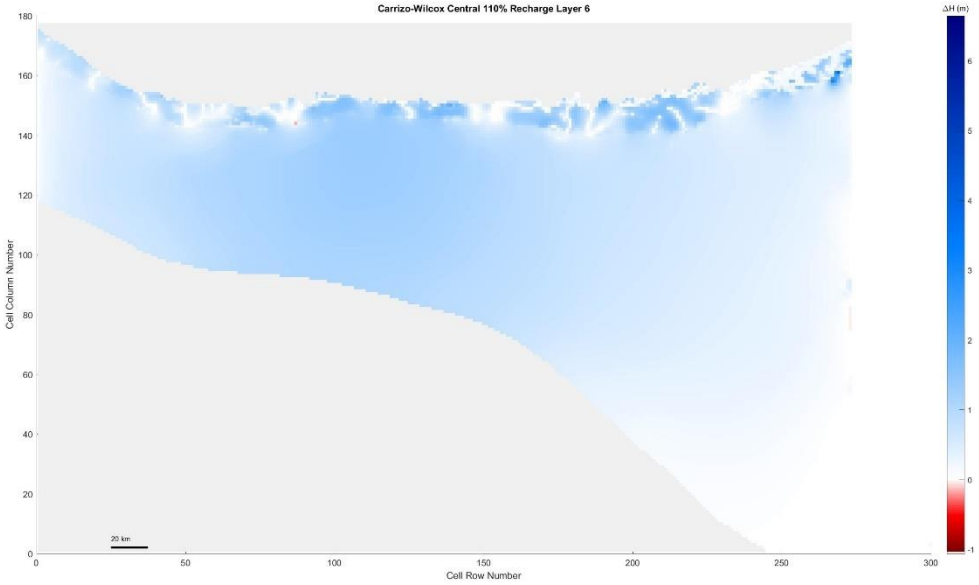

Figure 5. 140 Carrizo-Wilcox Center, 110% original recharge hydraulic head spatial distribution of layer 6

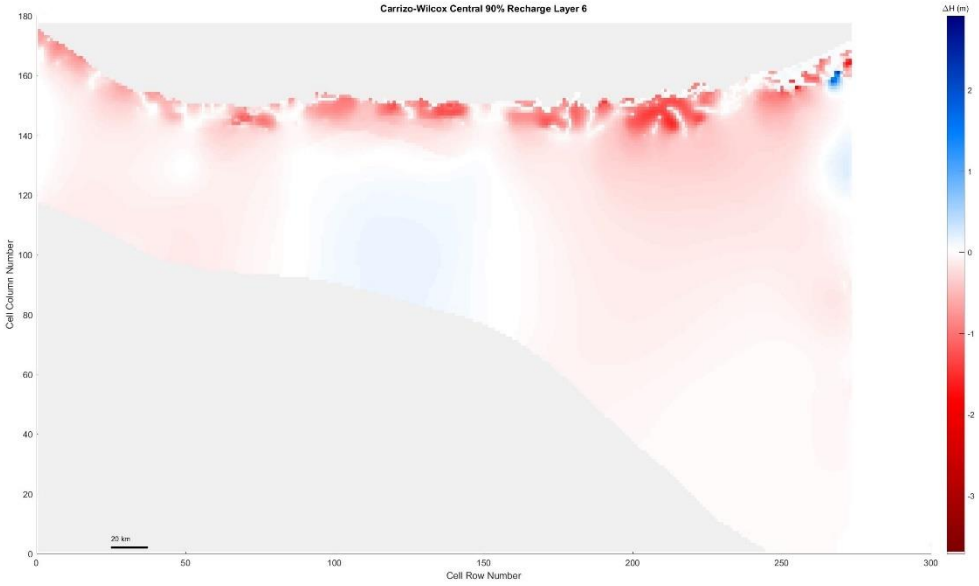

Figure 5. 141 Carrizo-Wilcox Center, 90% original recharge hydraulic head spatial distribution of layer 6

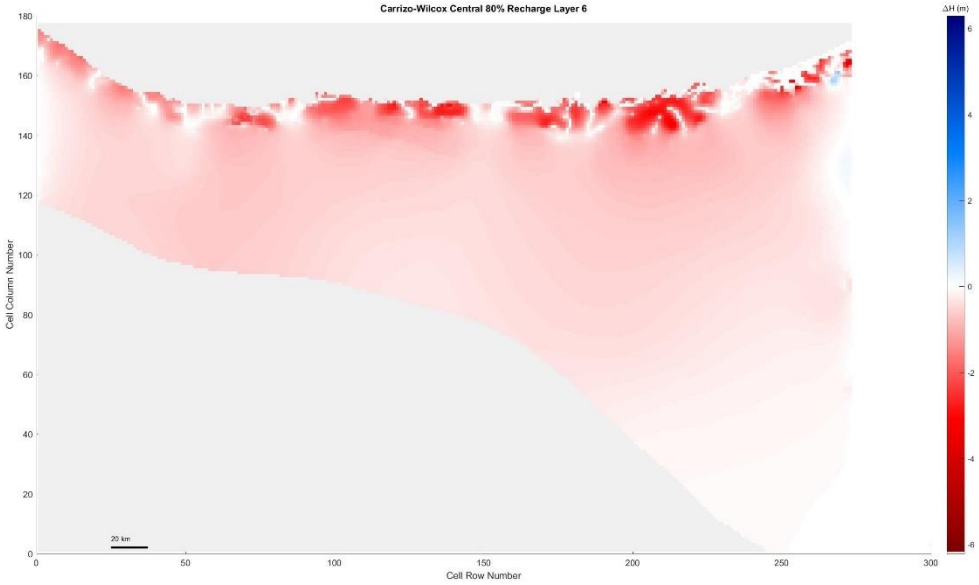

Figure 5. 142 Carrizo-Wilcox Center, 80% original recharge hydraulic head spatial distribution of layer 6

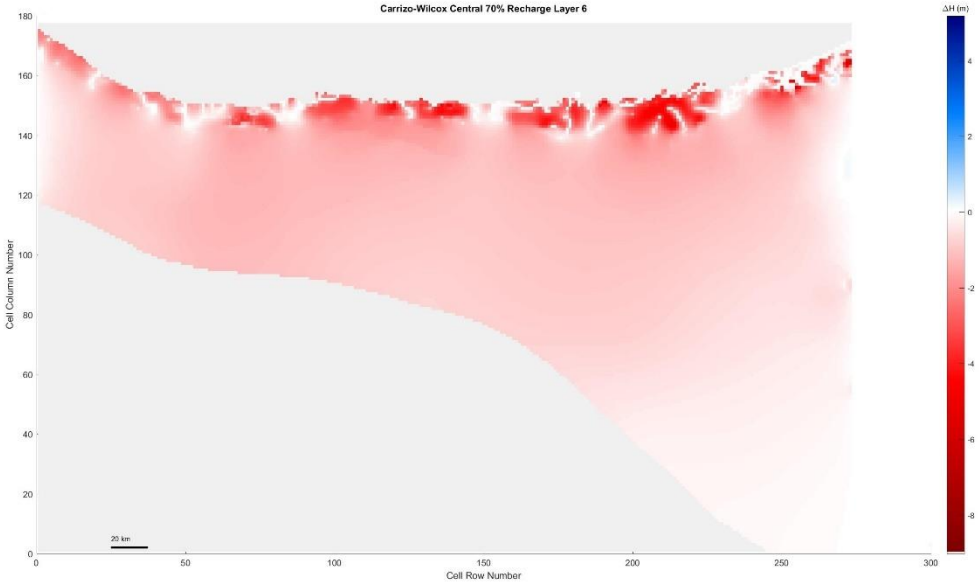

Figure 5. 143 Carrizo-Wilcox Center, 70% original recharge hydraulic head spatial distribution of layer 6

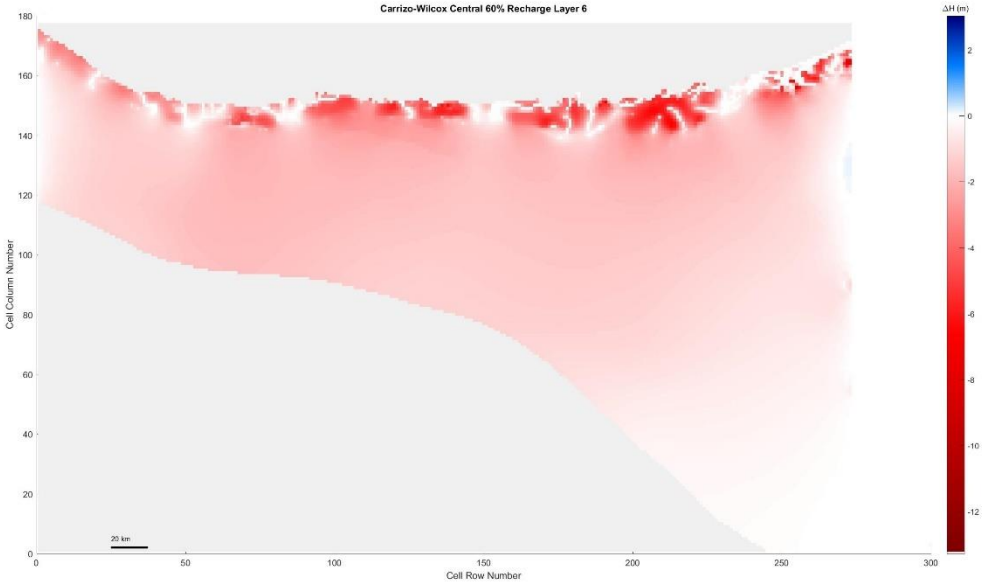

Figure 5. 144 Carrizo-Wilcox Center, 60% original recharge hydraulic head spatial distribution of layer 6

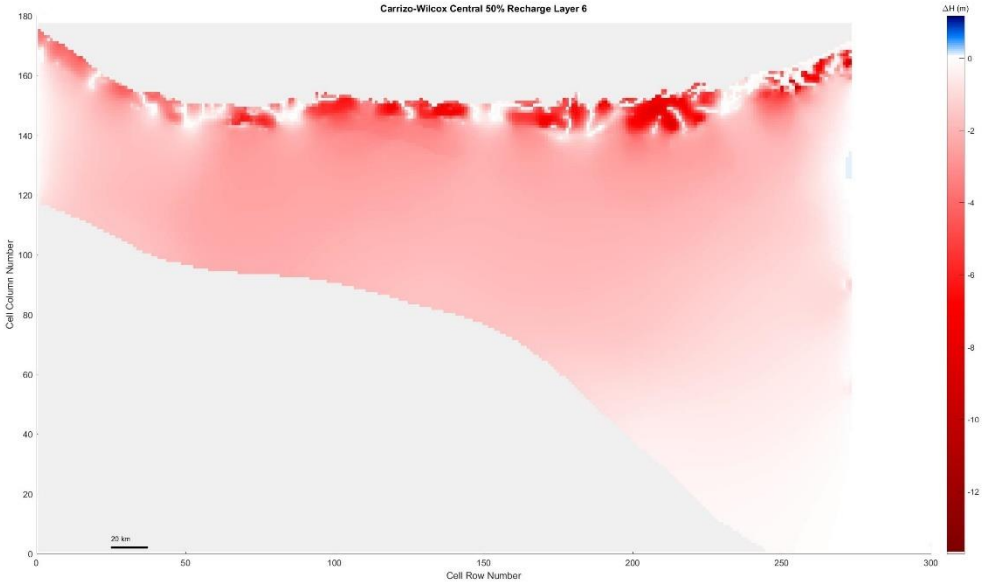

Figure 5. 145 Carrizo-Wilcox Center, 50% original recharge hydraulic head spatial distribution of layer 6

Layer 7

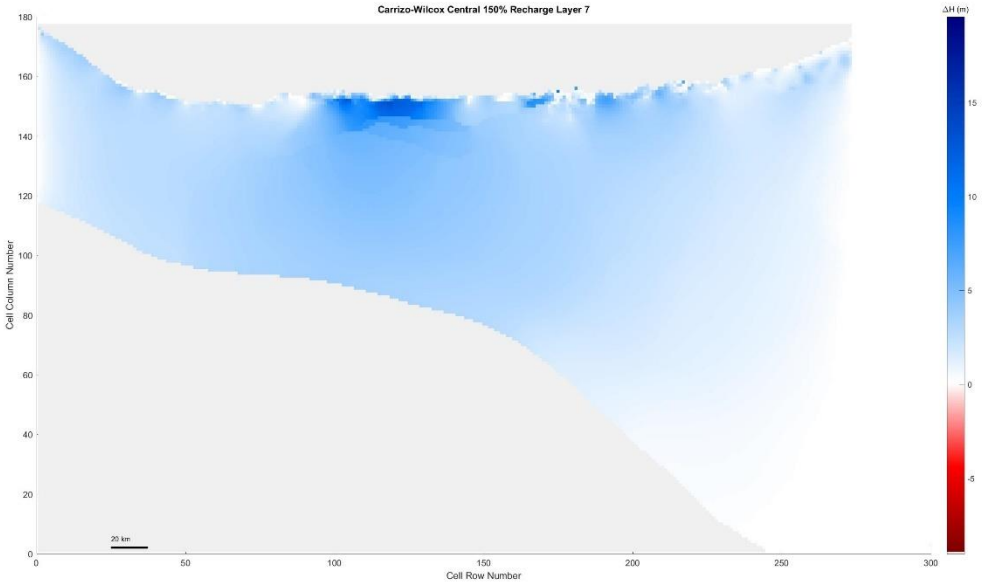

Figure 5. 146 Carrizo-Wilcox Center, 150% original recharge hydraulic head spatial distribution of layer 7

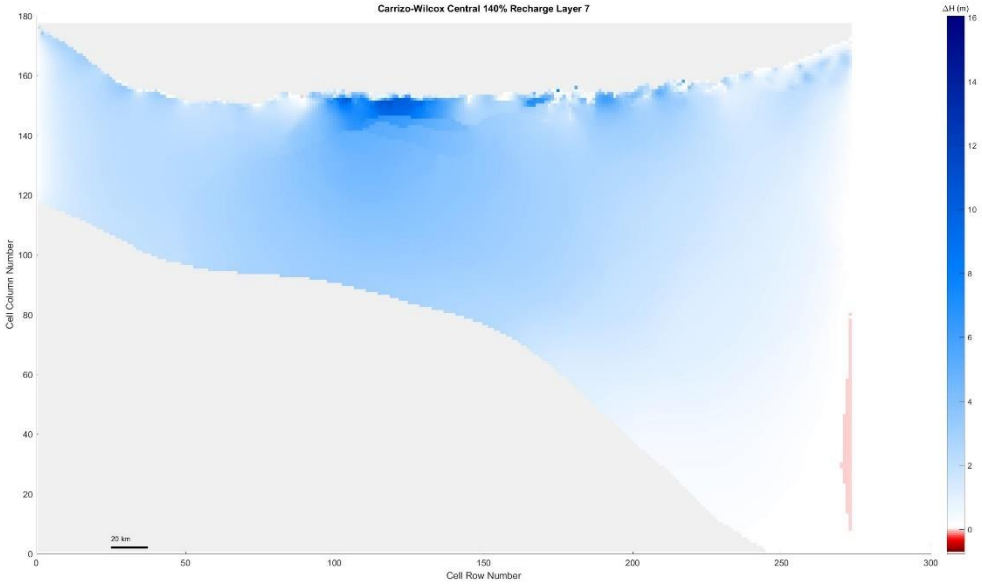

Figure 5. 147 Carrizo-Wilcox Center, 140% original recharge hydraulic head spatial distribution of layer 7

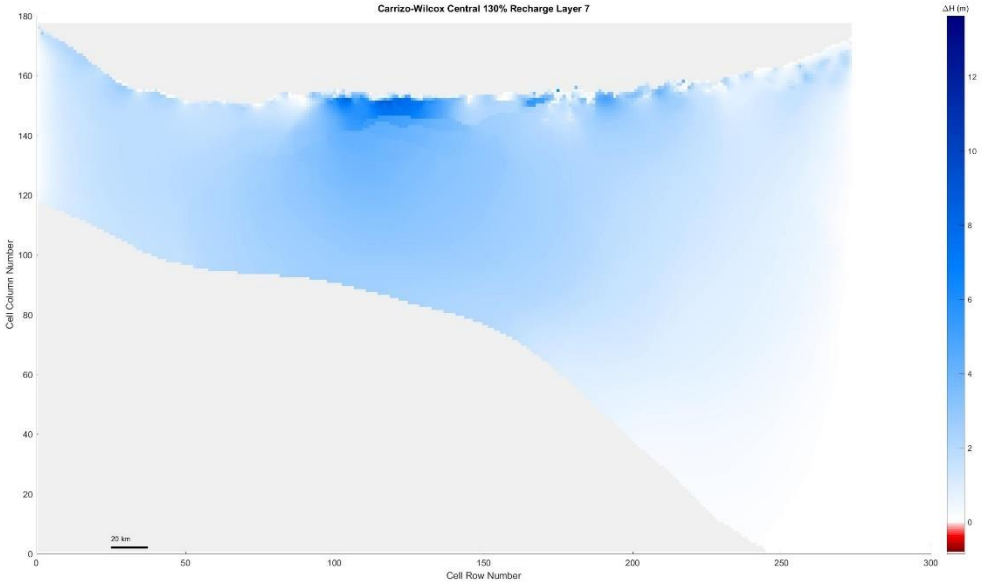

Figure 5. 148 Carrizo-Wilcox Center, 130% original recharge hydraulic head spatial distribution of layer 7

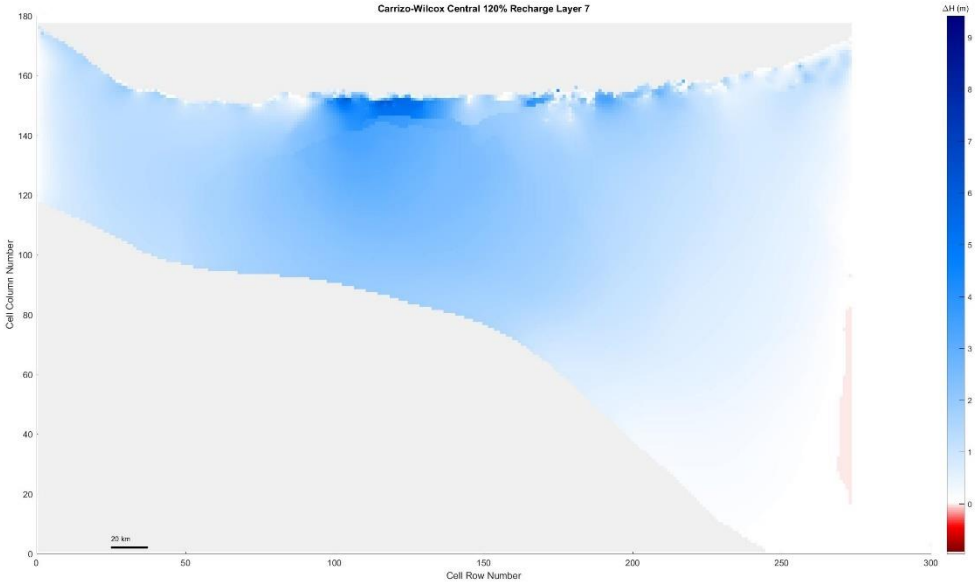

Figure 5. 149 Carrizo-Wilcox Center, 120% original recharge hydraulic head spatial distribution of layer 7

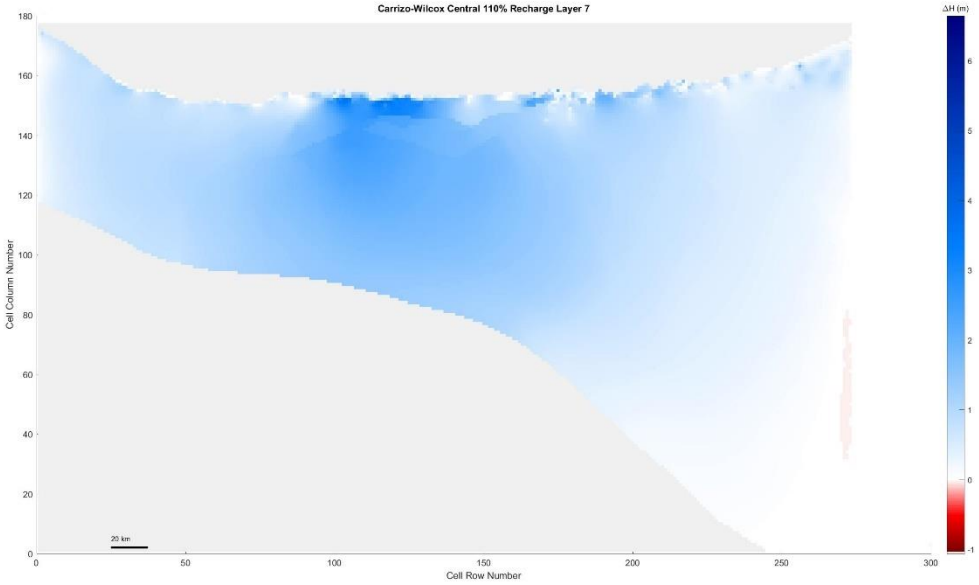

Figure 5. 150 Carrizo-Wilcox Center, 110% original recharge hydraulic head spatial distribution of layer 7

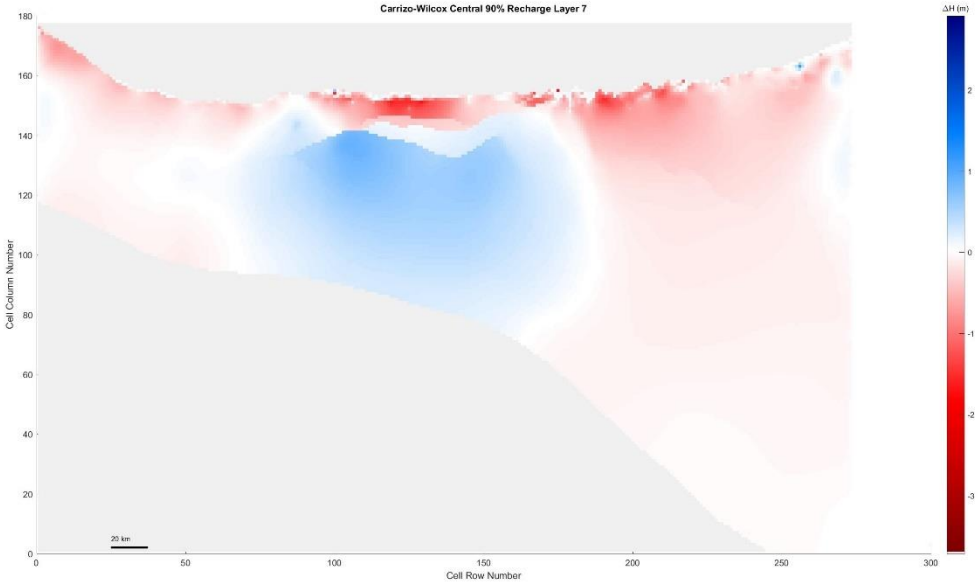

Figure 5. 151 Carrizo-Wilcox Center, 90% original recharge hydraulic head spatial distribution of layer 7

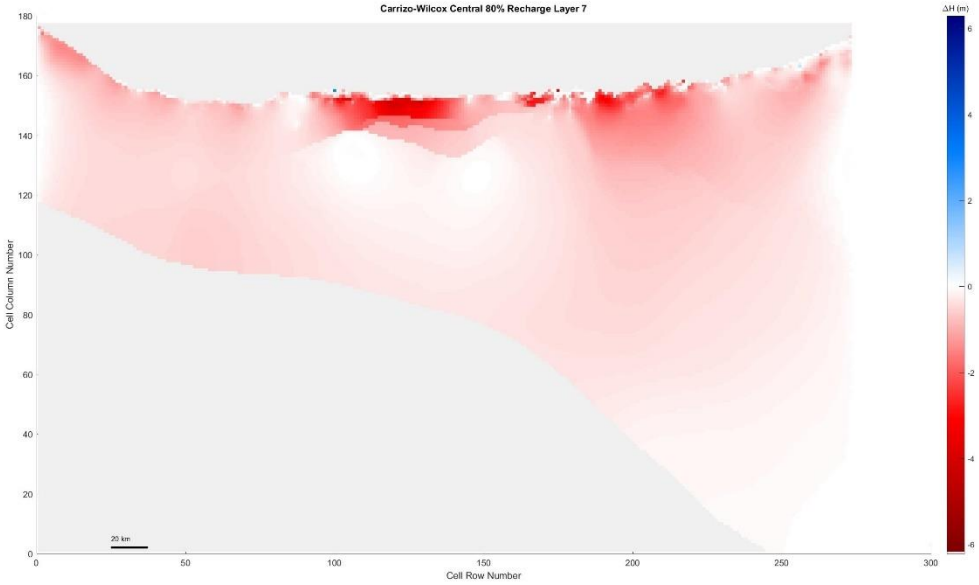

Figure 5. 152 Carrizo-Wilcox Center, 80% original recharge hydraulic head spatial distribution of layer 7

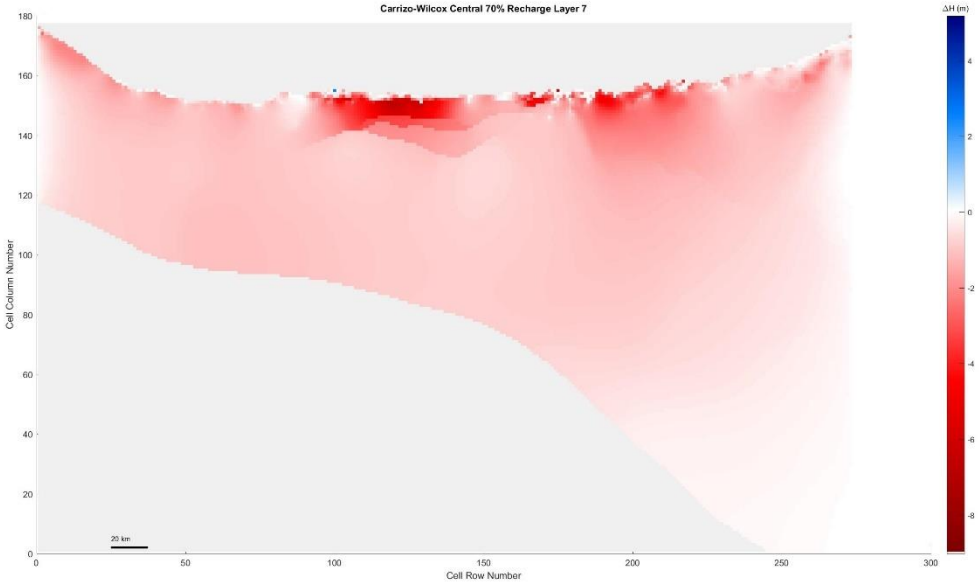

Figure 5. 153 Carrizo-Wilcox Center, 70% original recharge hydraulic head spatial distribution of layer 7

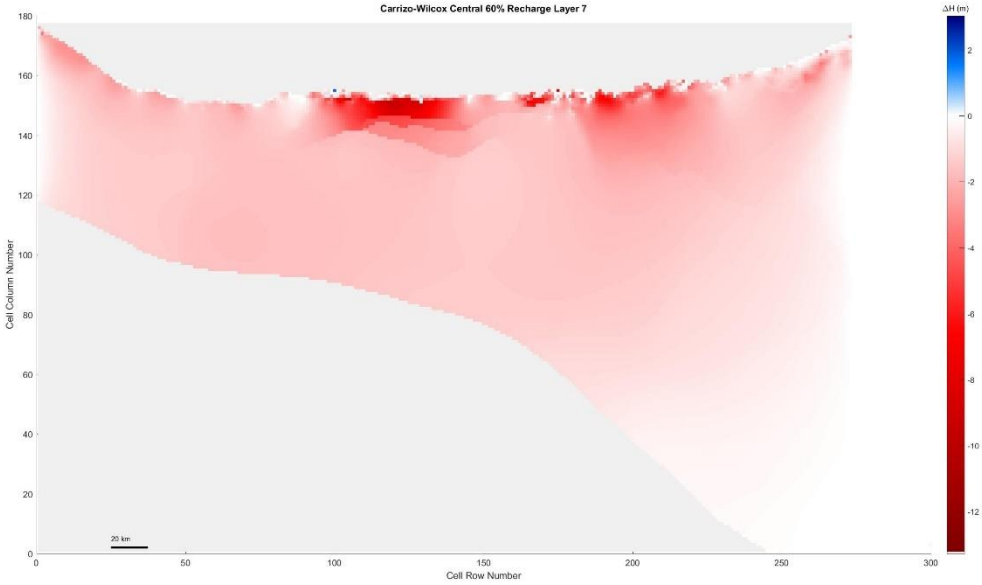

Figure 5. 154 Carrizo-Wilcox Center, 60% original recharge hydraulic head spatial distribution of layer 7

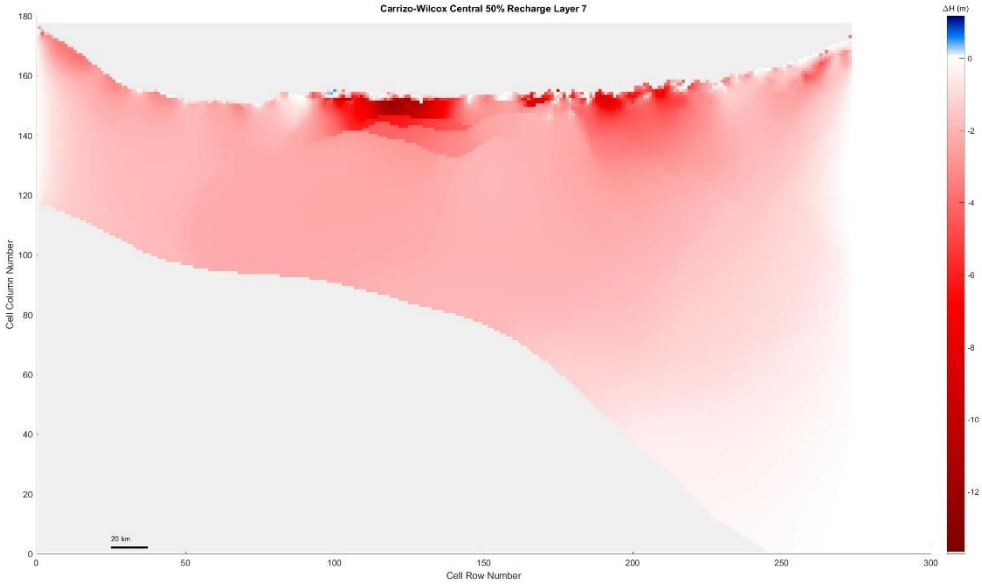

Figure 5. 155 Carrizo-Wilcox Center, 50% original recharge hydraulic head spatial distribution of layer 7

Layer 8

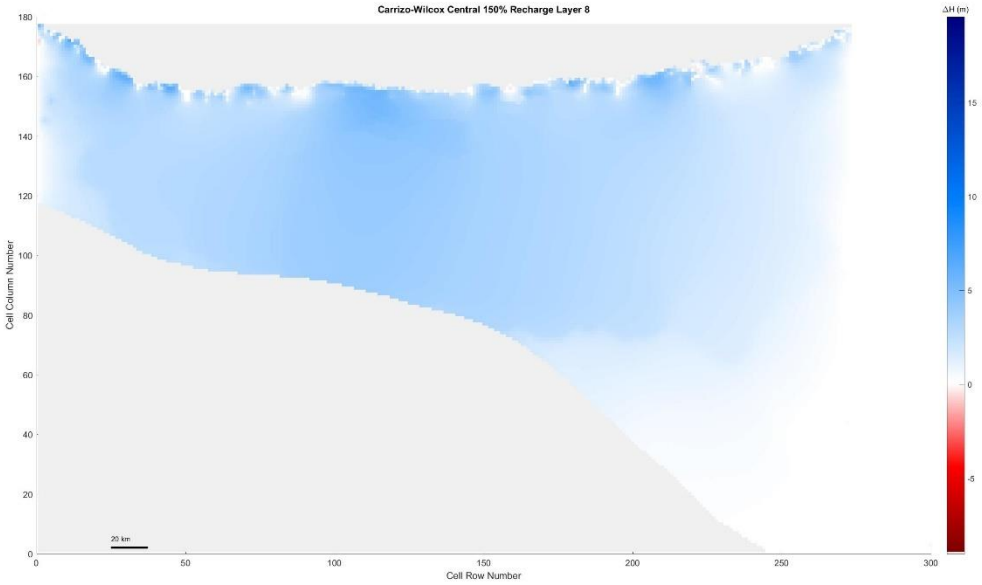

Figure 5. 156 Carrizo-Wilcox Center, 150% original recharge hydraulic head spatial distribution of layer 8

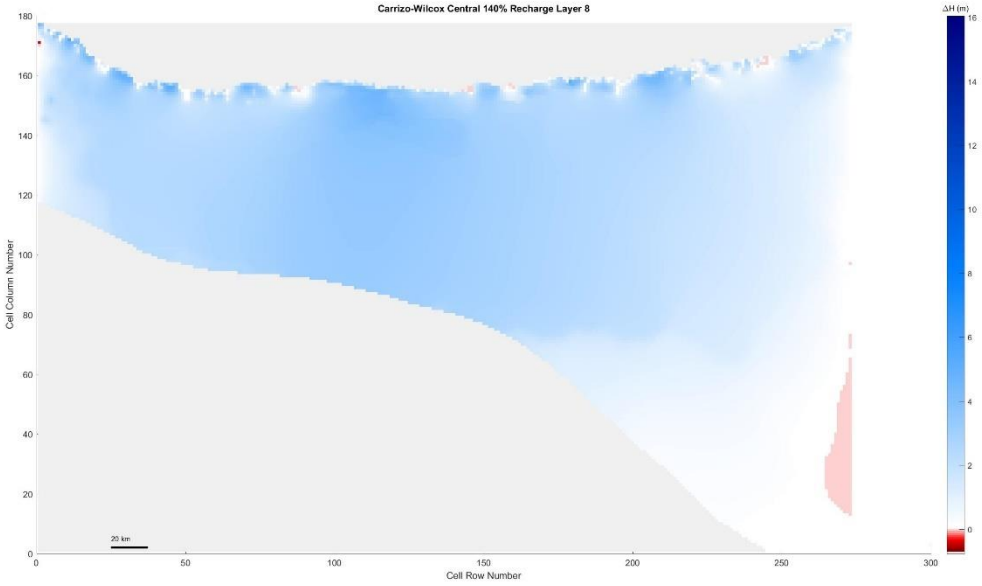

Figure 5. 157 Carrizo-Wilcox Center, 140% original recharge hydraulic head spatial distribution of layer 8

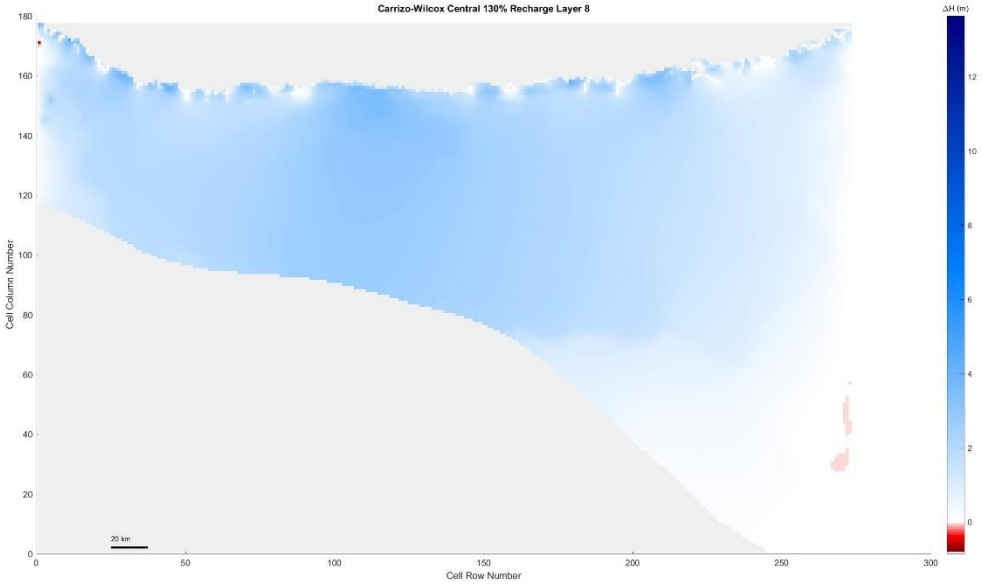

Figure 5. 158 Carrizo-Wilcox Center, 130% original recharge hydraulic head spatial distribution of layer 8

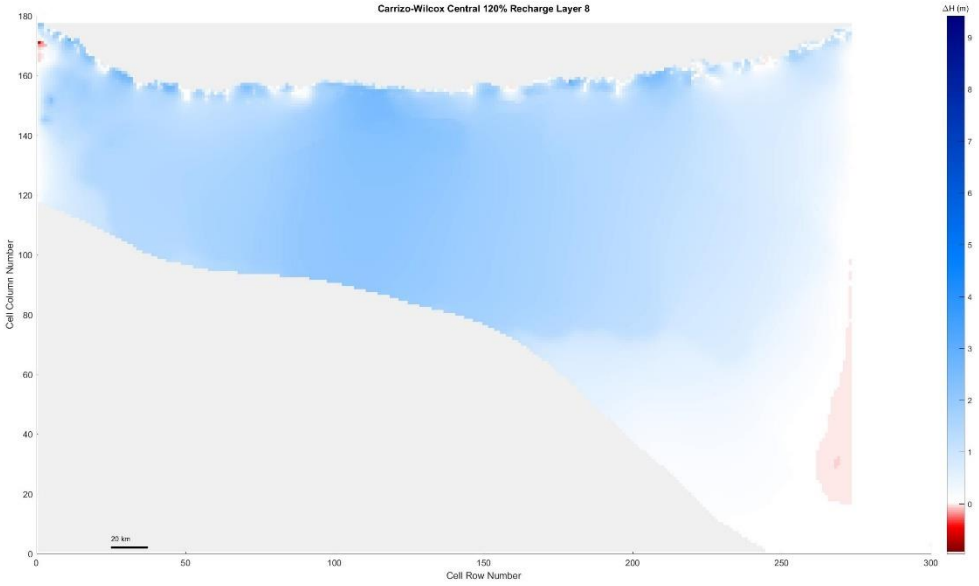

Figure 5. 159 Carrizo-Wilcox Center, 120% original recharge hydraulic head spatial distribution of layer 8

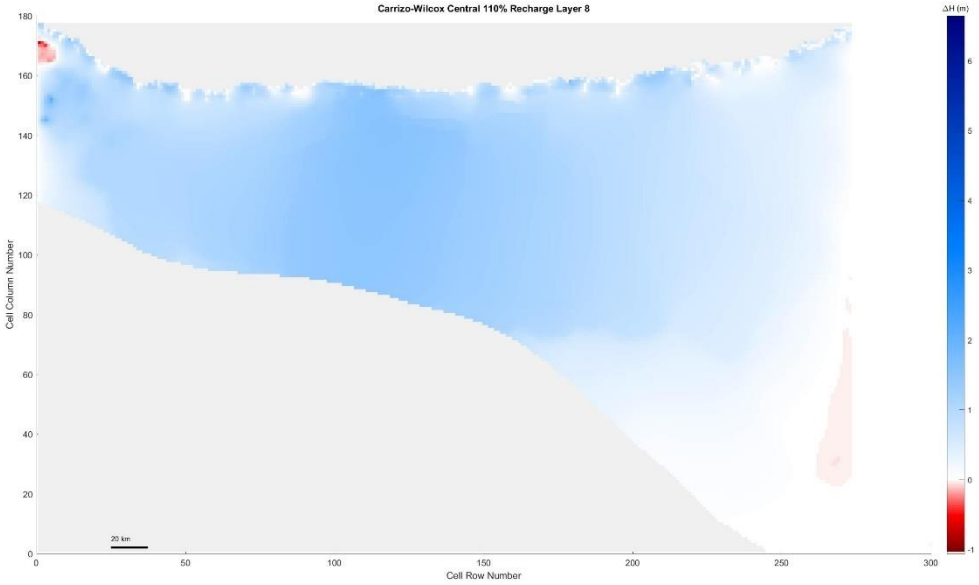

Figure 5. 160 Carrizo-Wilcox Center, 110% original recharge hydraulic head spatial distribution of layer 8

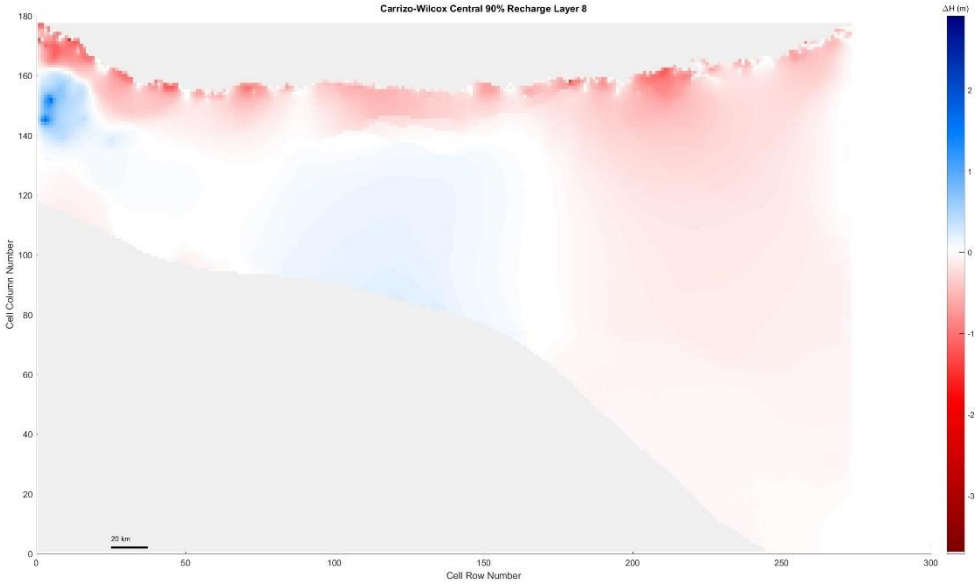

Figure 5. 161 Carrizo-Wilcox Center, 90% original recharge hydraulic head spatial distribution of layer 8

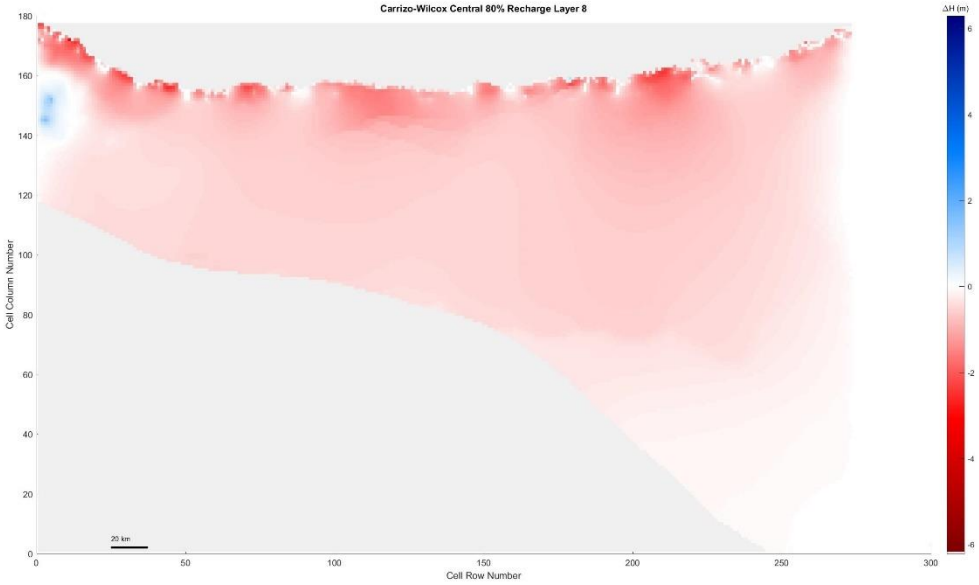

Figure 5. 162 Carrizo-Wilcox Center, 80% original recharge hydraulic head spatial distribution of layer 8

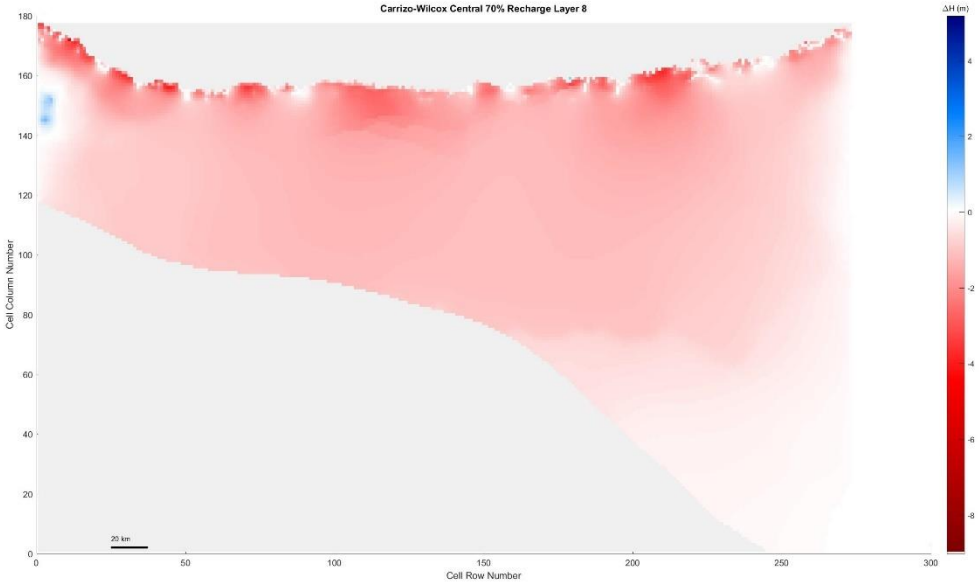

Figure 5. 163 Carrizo-Wilcox Center, 70% original recharge hydraulic head spatial distribution of layer 8

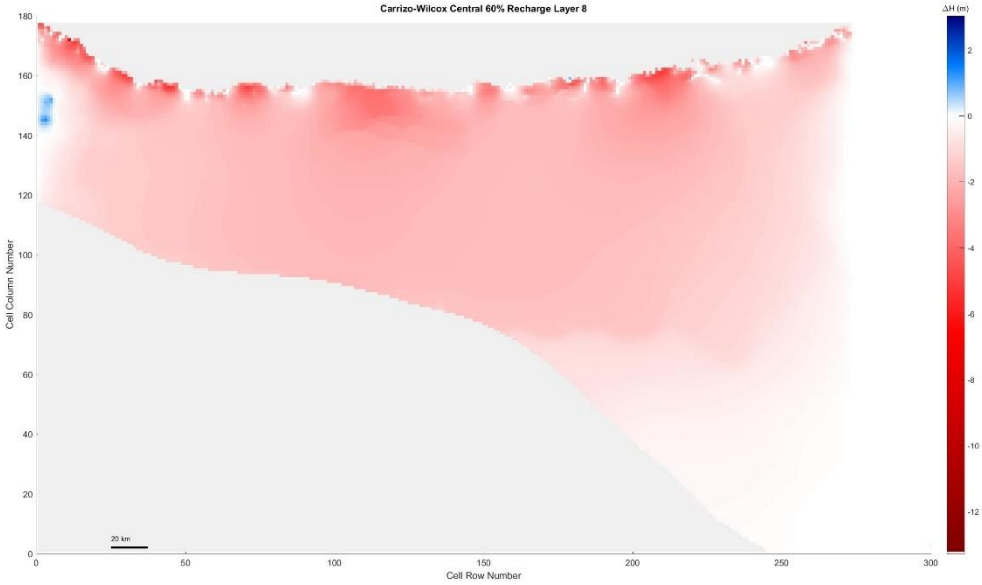

Figure 5. 164 Carrizo-Wilcox Center, 60% original recharge hydraulic head spatial distribution of layer 8

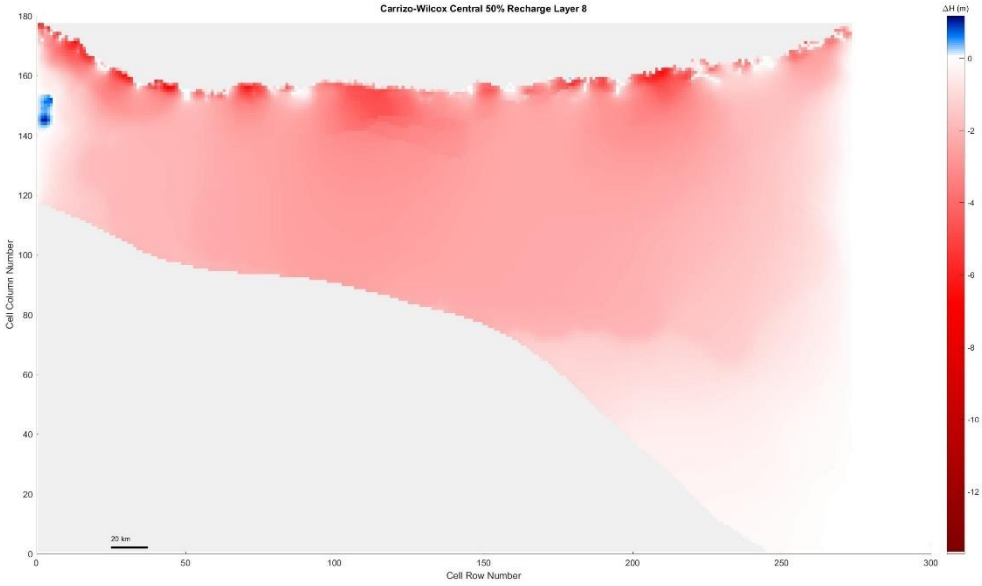

Figure 5. 165 Carrizo-Wilcox Center, 50% original recharge hydraulic head spatial distribution of layer 8

Carrizo-Wilcox North
Layer 1

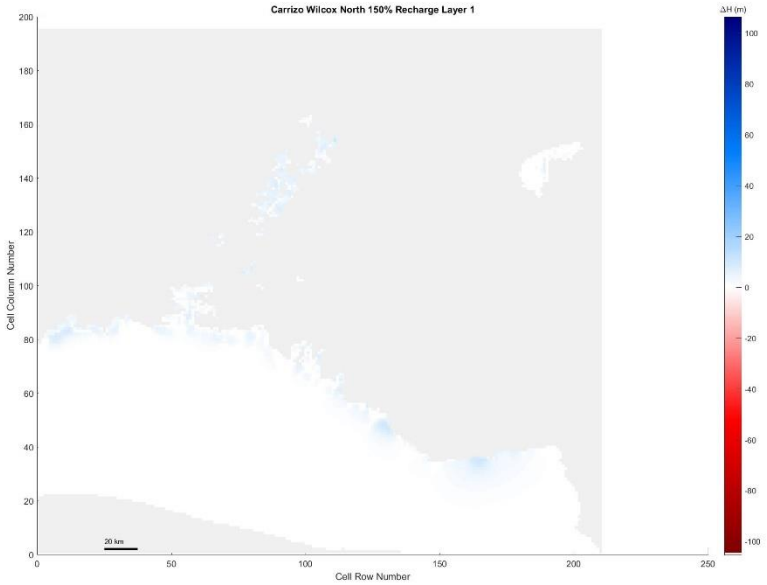

Figure 5. 166 Carrizo-Wilcox North, 150% original recharge hydraulic head spatial distribution of layer 1

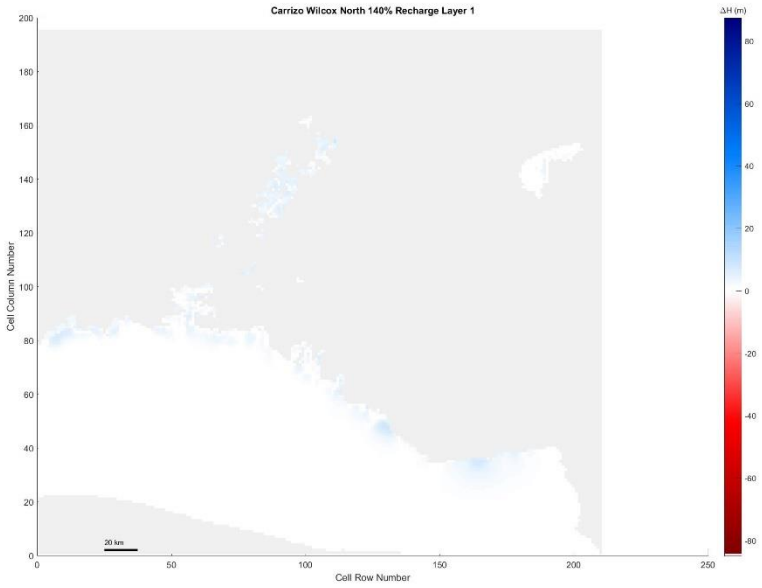

Figure 5. 167 Carrizo-Wilcox North, 140% original recharge hydraulic head spatial distribution of layer 1

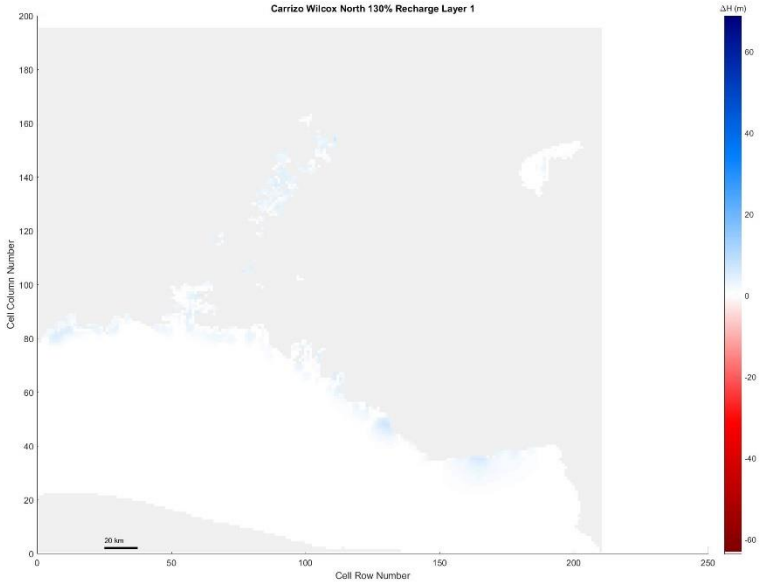

Figure 5. 168 Carrizo-Wilcox North, 130% original recharge hydraulic head spatial distribution of layer 1

Figure 5. 169 Carrizo-Wilcox North, 120% original recharge hydraulic head spatial distribution of layer 1

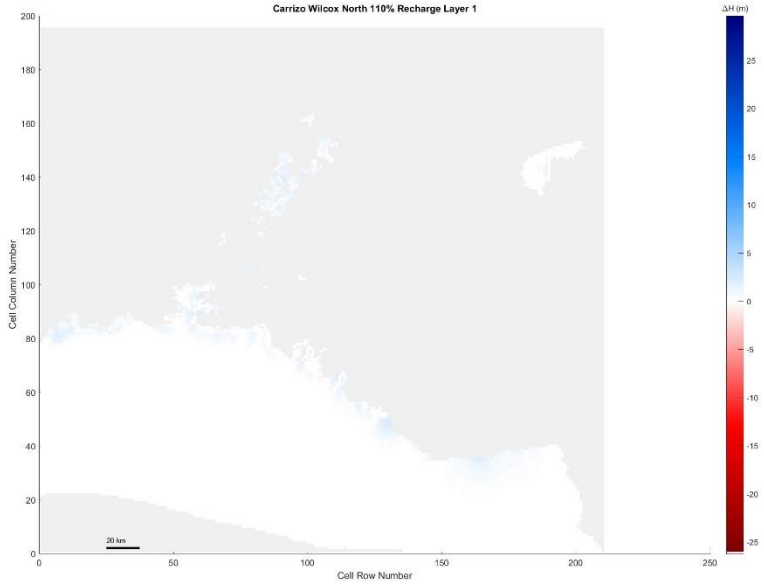

Figure 5. 170 Carrizo-Wilcox North, 110% original recharge hydraulic head spatial distribution of layer 1

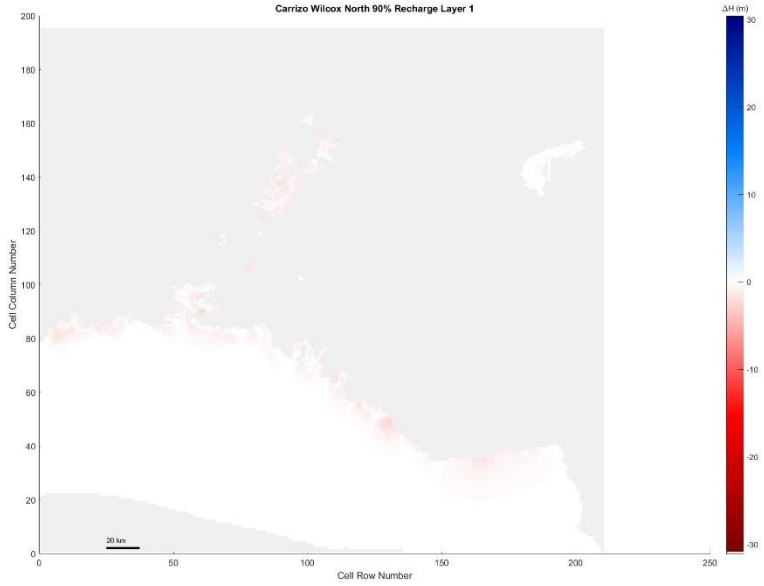

Figure 5. 171 Carrizo-Wilcox North, 90% original recharge hydraulic head spatial distribution of layer 1

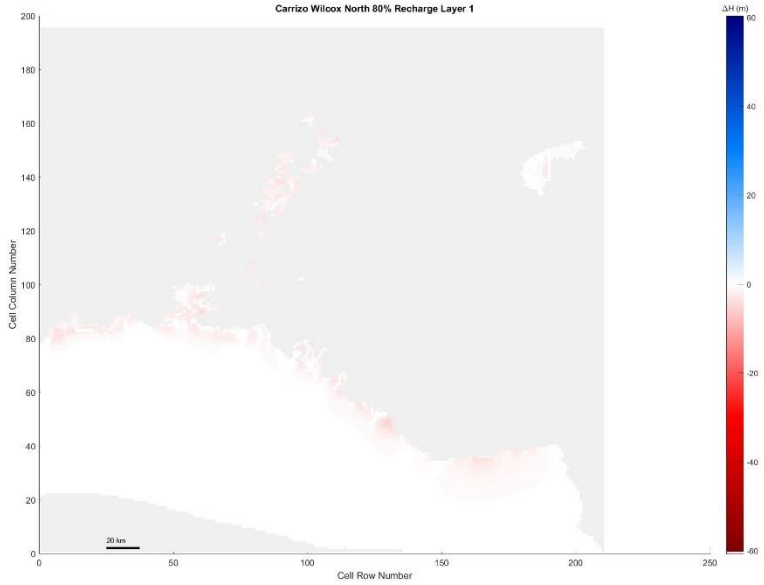

Figure 5. 172 Carrizo-Wilcox North, 80% original recharge hydraulic head spatial distribution of layer 1

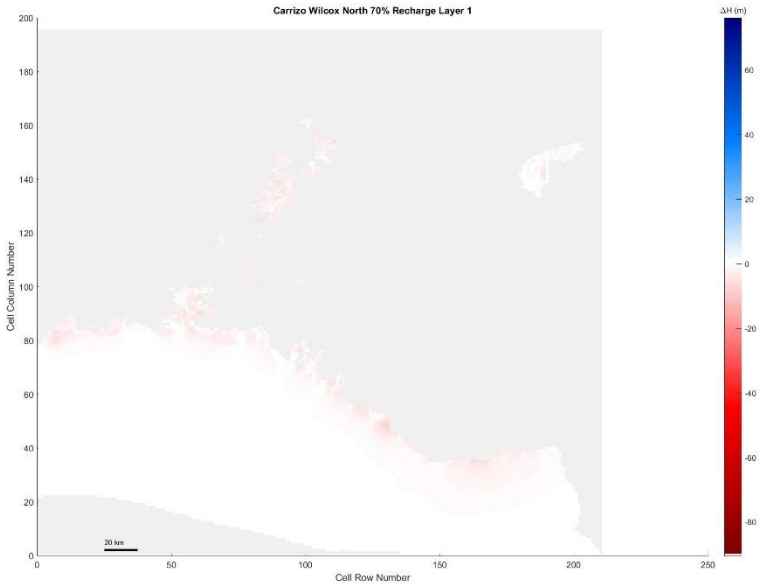

Figure 5. 173 Carrizo-Wilcox North, 70% original recharge hydraulic head spatial distribution of layer 1

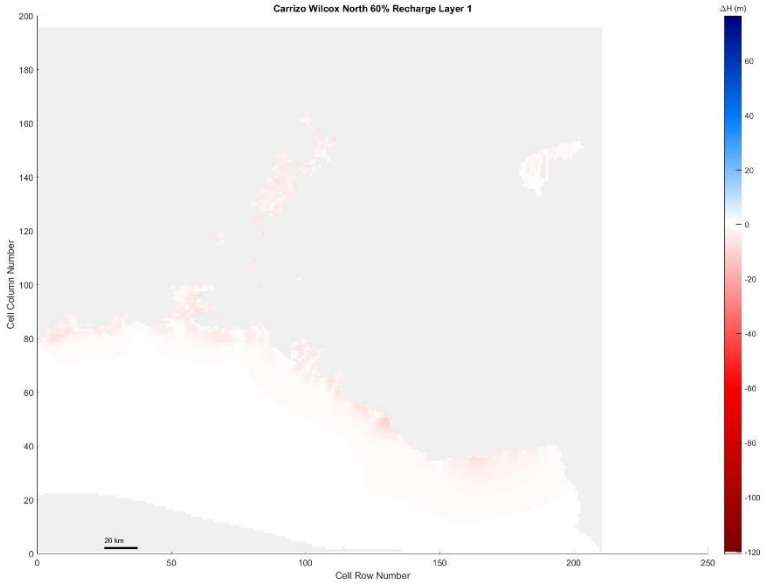

Figure 5. 174 Carrizo-Wilcox North, 60% original recharge hydraulic head spatial distribution of layer 1

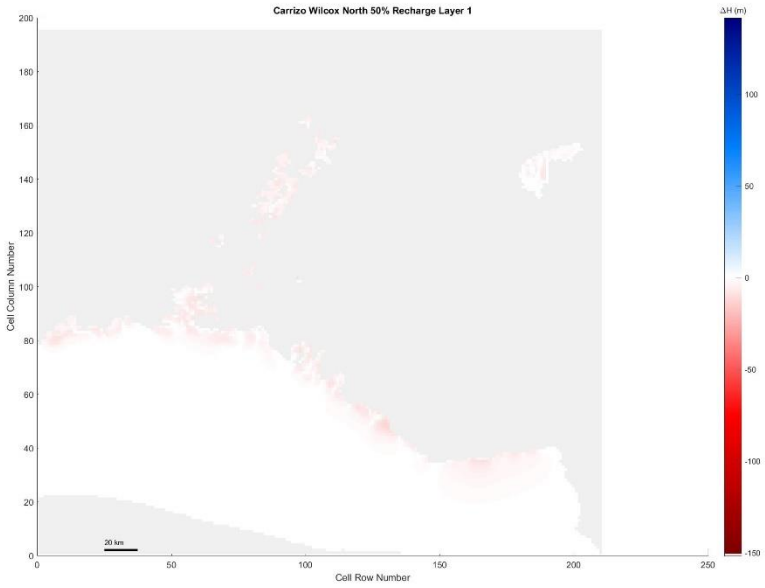

Figure 5. 175 Carrizo-Wilcox North, 50% original recharge hydraulic head spatial distribution of layer 1

Layer 2

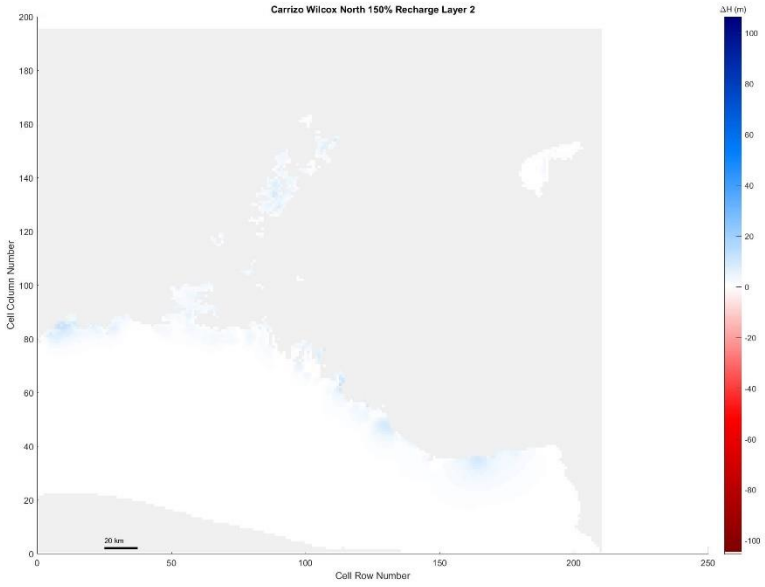

Figure 5. 176 Carrizo-Wilcox North, 150% original recharge hydraulic head spatial distribution of layer 2

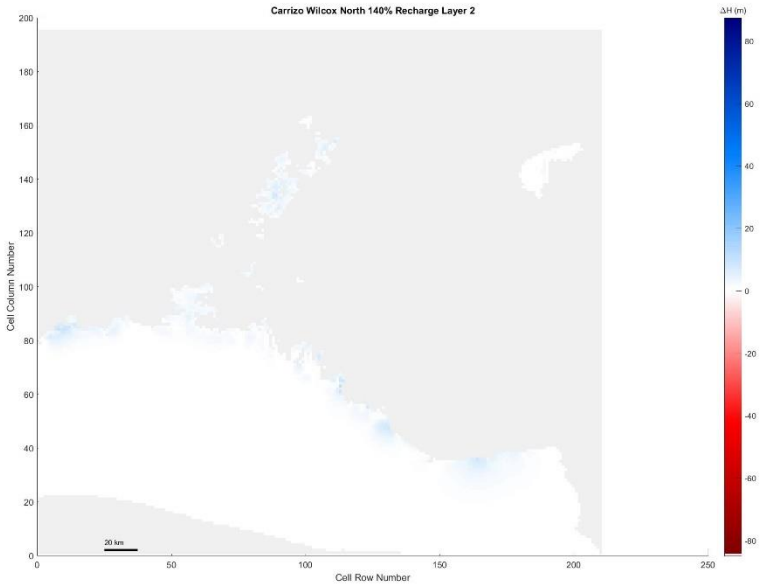

Figure 5. 177 Carrizo-Wilcox North, 140% original recharge hydraulic head spatial distribution of layer 2

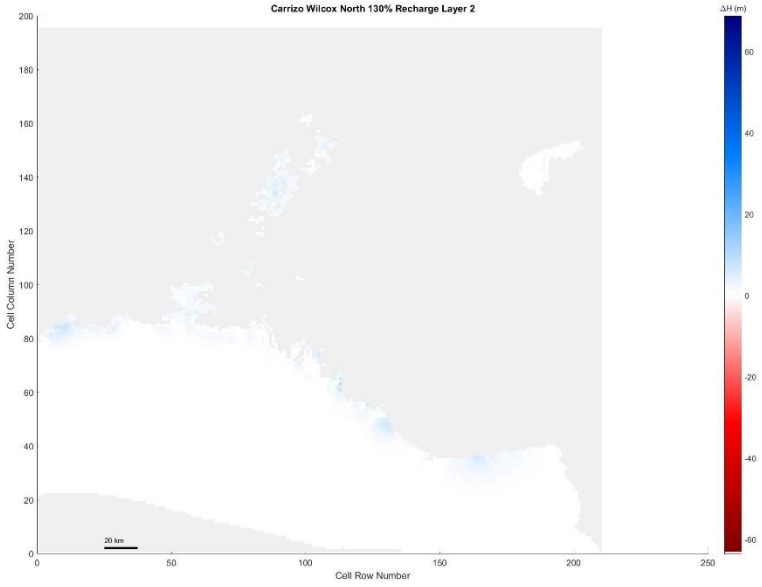

Figure 5. 178 Carrizo-Wilcox North, 130% original recharge hydraulic head spatial distribution of layer 2

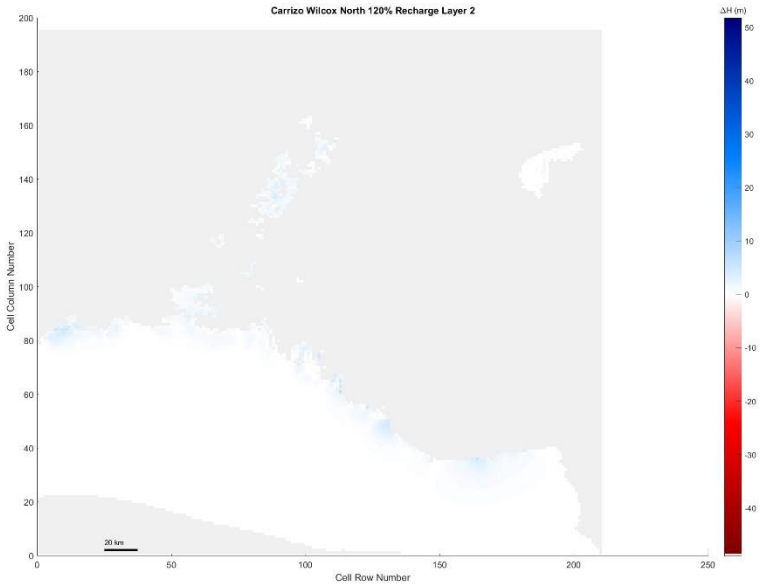

Figure 5. 179 Carrizo-Wilcox North, 120% original recharge hydraulic head spatial distribution of layer 2

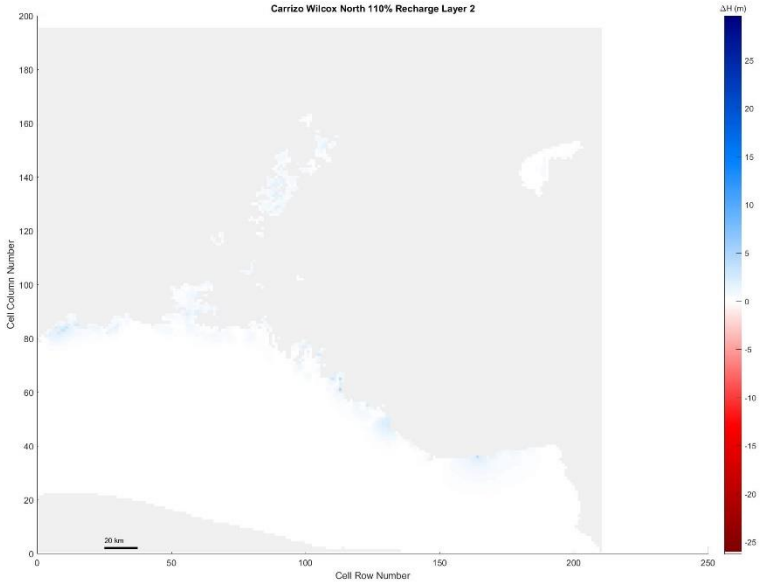

Figure 5. 180 Carrizo-Wilcox North, 110% original recharge hydraulic head spatial distribution of layer 2

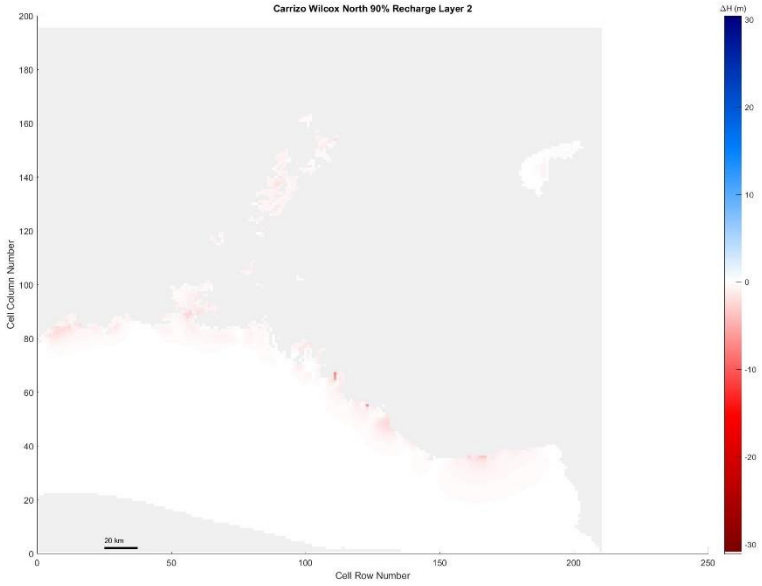

Figure 5. 181 Carrizo-Wilcox North, 90% original recharge hydraulic head spatial distribution of layer 2

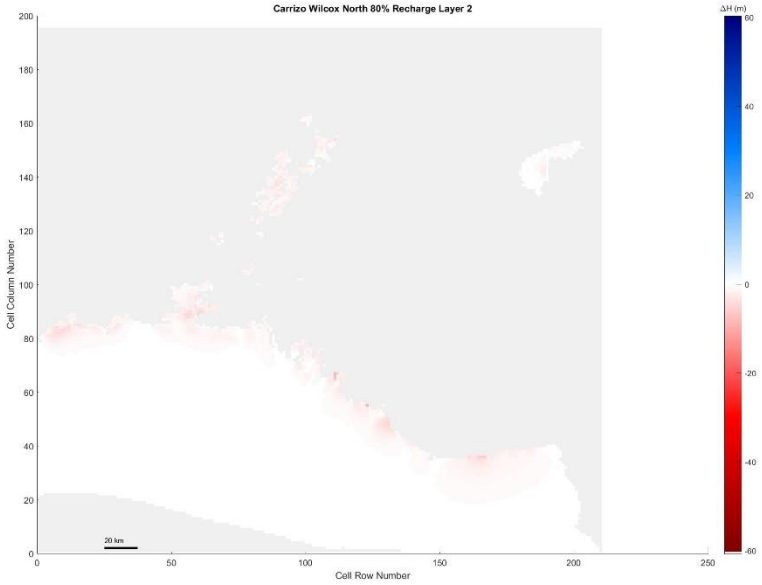

Figure 5. 182 Carrizo-Wilcox North, 80% original recharge hydraulic head spatial distribution of layer 2

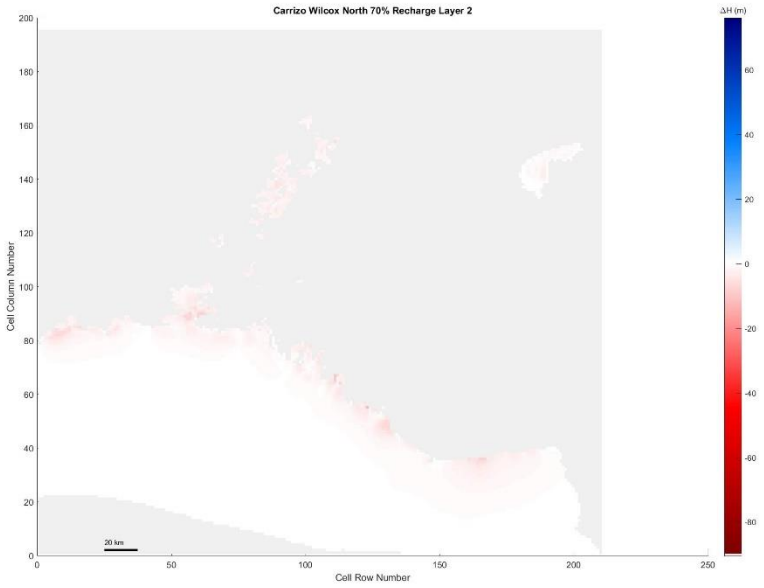

Figure 5. 183 Carrizo-Wilcox North, 70% original recharge hydraulic head spatial distribution of layer 2

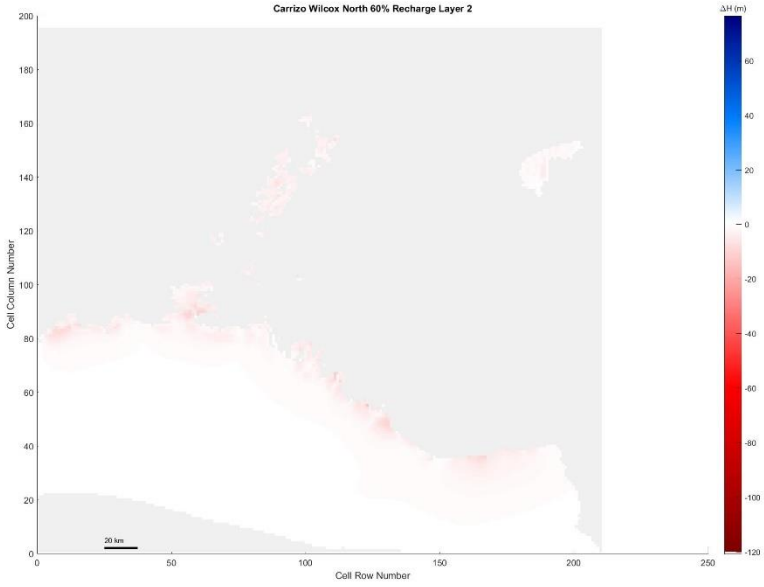

Figure 5. 184 Carrizo-Wilcox North, 60% original recharge hydraulic head spatial distribution of layer 2

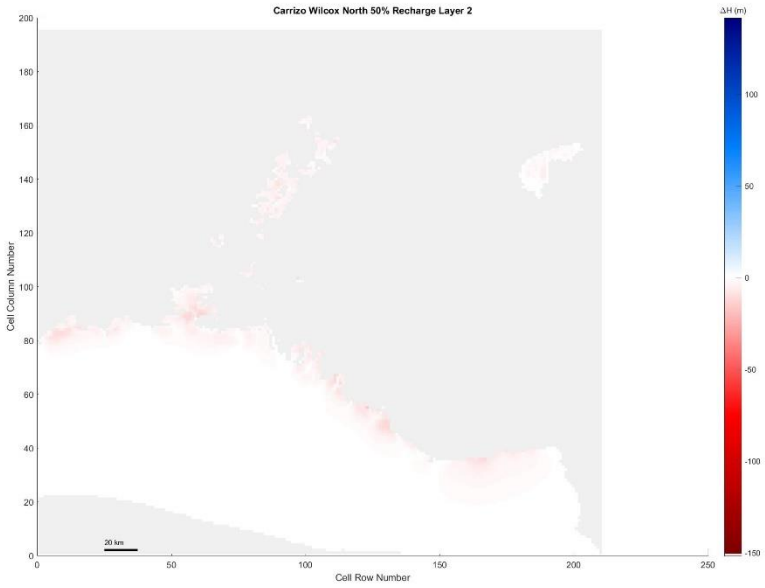

Figure 5. 185 Carrizo-Wilcox North, 50% original recharge hydraulic head spatial distribution of layer 2

Layer 3

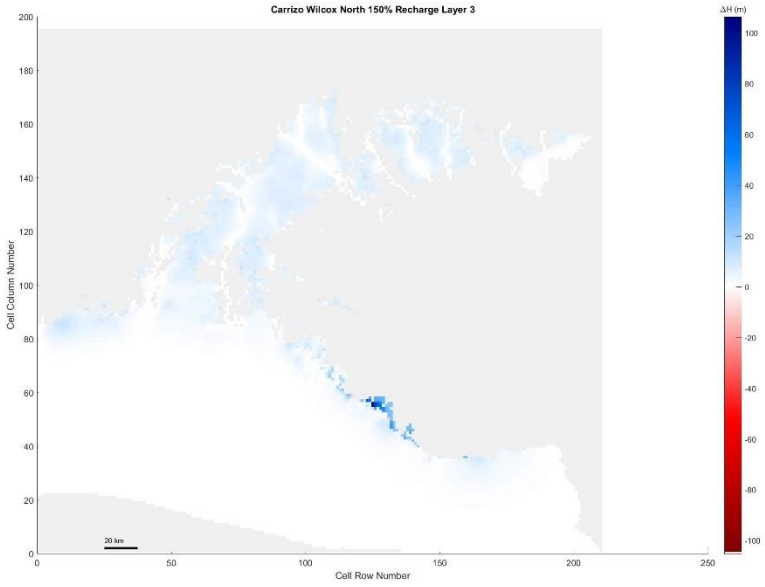

Figure 5. 186 Carrizo-Wilcox North, 150% original recharge hydraulic head spatial distribution of layer 3

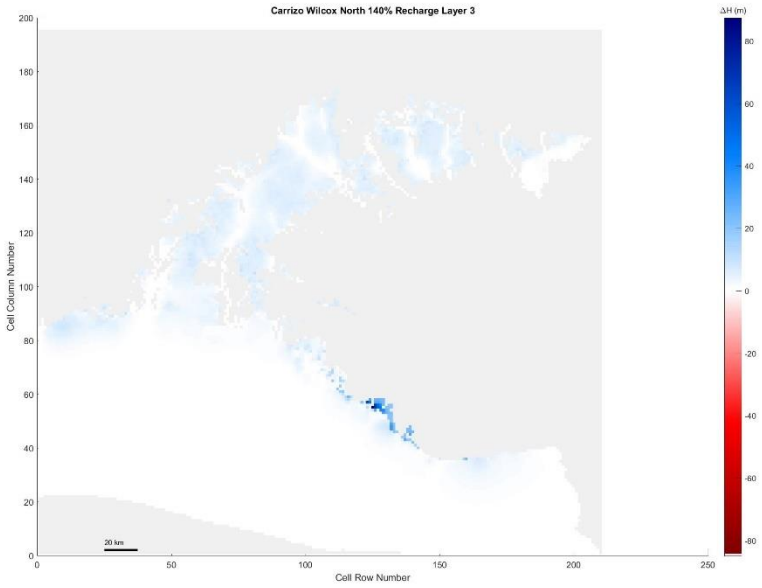

Figure 5. 187 Carrizo-Wilcox North, 140% original recharge hydraulic head spatial distribution of layer 3

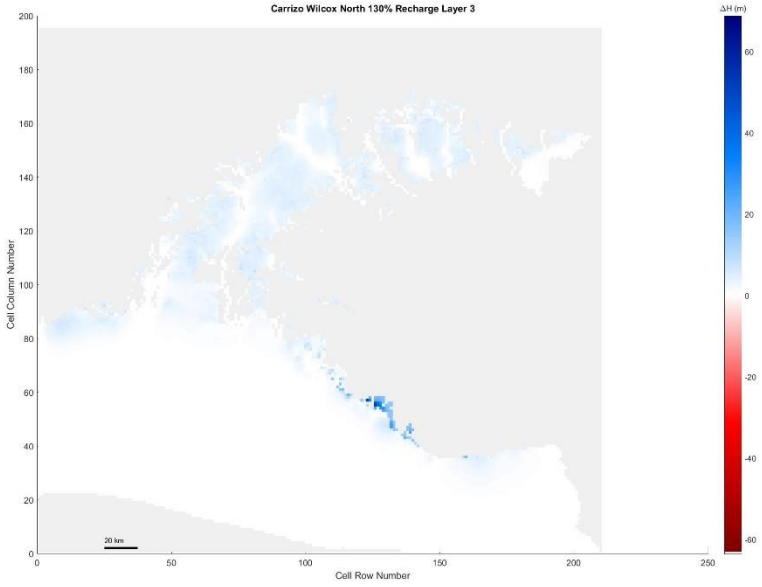

Figure 5. 188 Carrizo-Wilcox North, 130% original recharge hydraulic head spatial distribution of layer 3

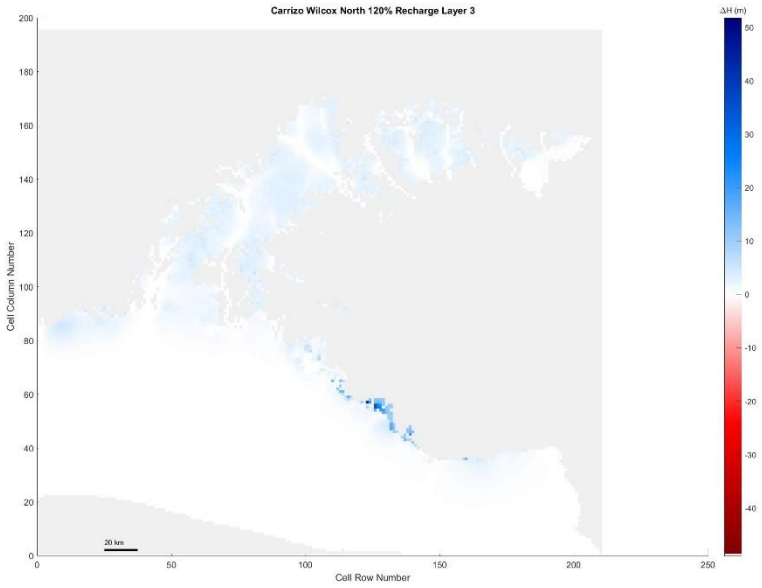

Figure 5. 189 Carrizo-Wilcox North, 120% original recharge hydraulic head spatial distribution of layer 3

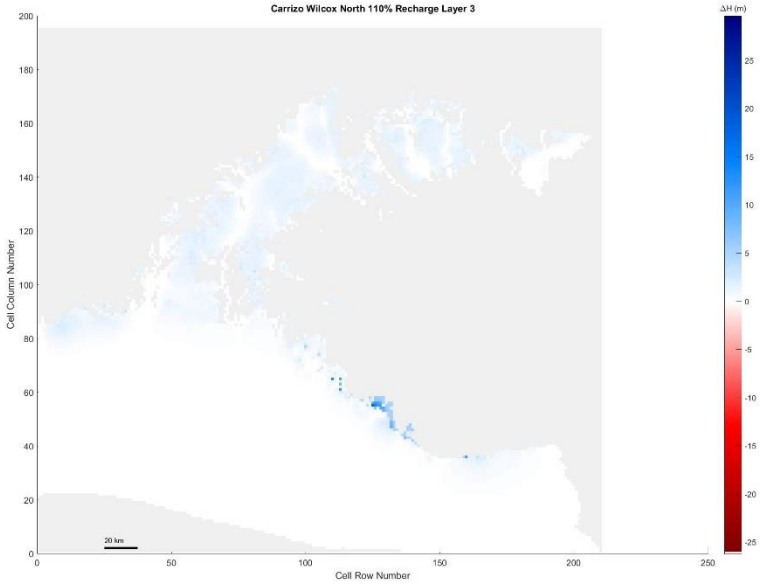

Figure 5. 190 Carrizo-Wilcox North, 110% original recharge hydraulic head spatial distribution of layer 3

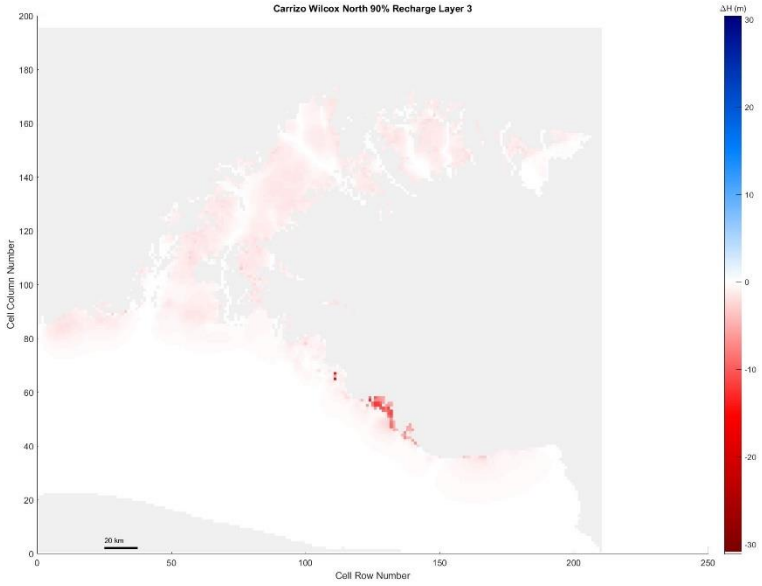

Figure 5. 191 Carrizo-Wilcox North, 90% original recharge hydraulic head spatial distribution of layer 3

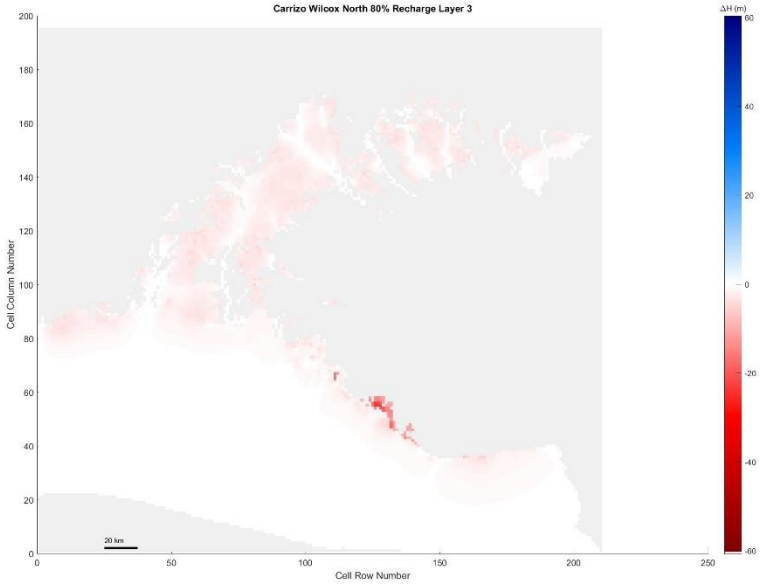

Figure 5. 192 Carrizo-Wilcox North, 80% original recharge hydraulic head spatial distribution of layer 3

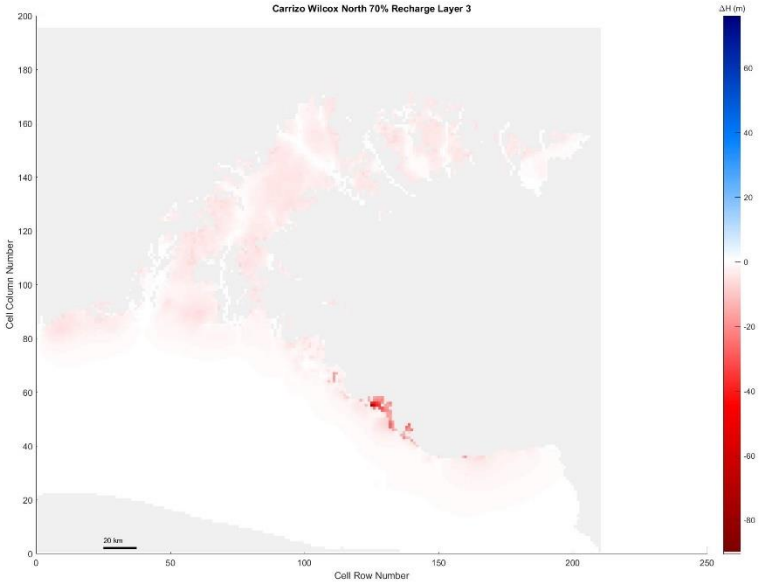

Figure 5. 193 Carrizo-Wilcox North, 70% original recharge hydraulic head spatial distribution of layer 3

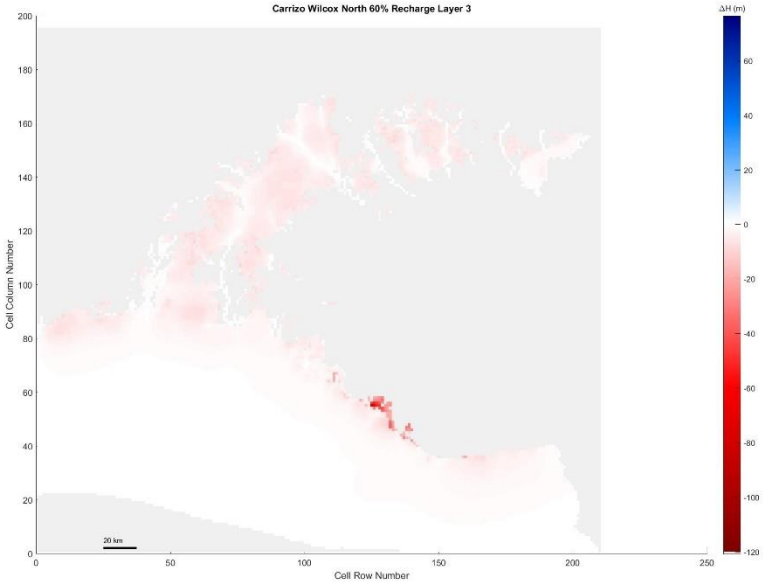

Figure 5. 194 Carrizo-Wilcox North, 60% original recharge hydraulic head spatial distribution of layer 3

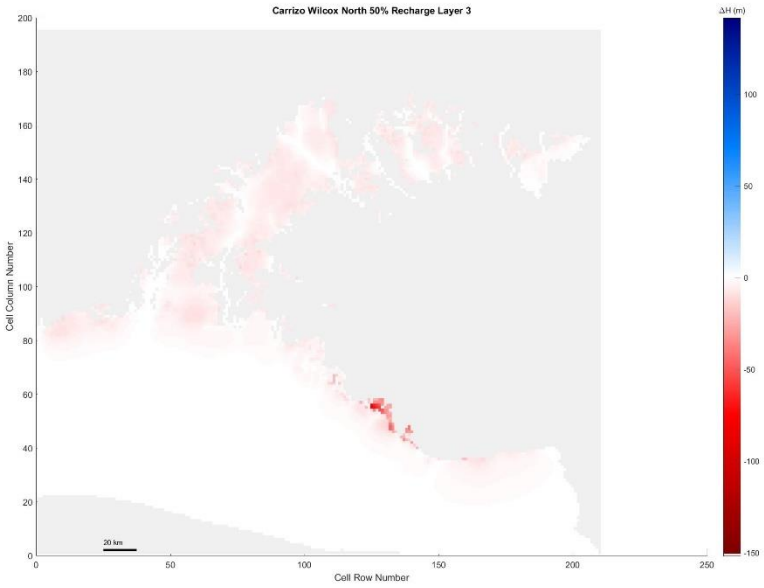

Figure 5. 195 Carrizo-Wilcox North, 50% original recharge hydraulic head spatial distribution of layer 3

Layer 4

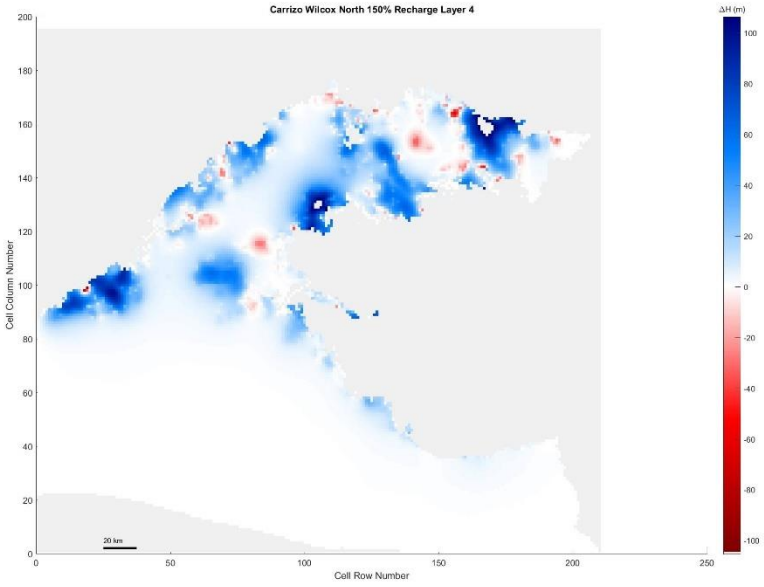

Figure 5. 196 Carrizo-Wilcox North, 150% original recharge hydraulic head spatial distribution of layer 4

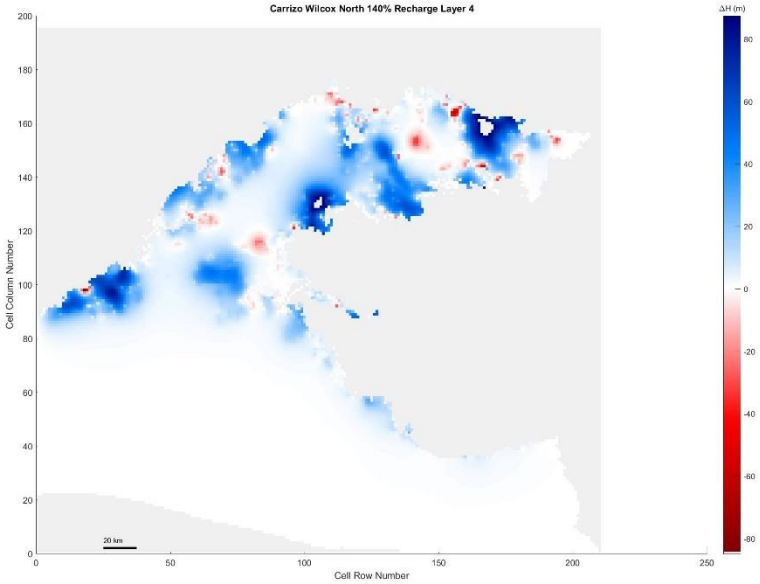

Figure 5. 197 Carrizo-Wilcox North, 140% original recharge hydraulic head spatial distribution of layer 4

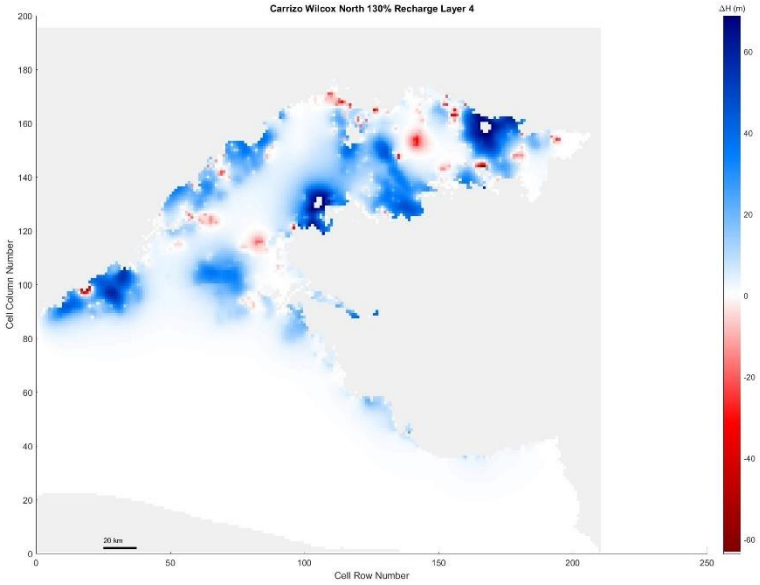

Figure 5. 198 Carrizo-Wilcox North, 130% original recharge hydraulic head spatial distribution of layer 4

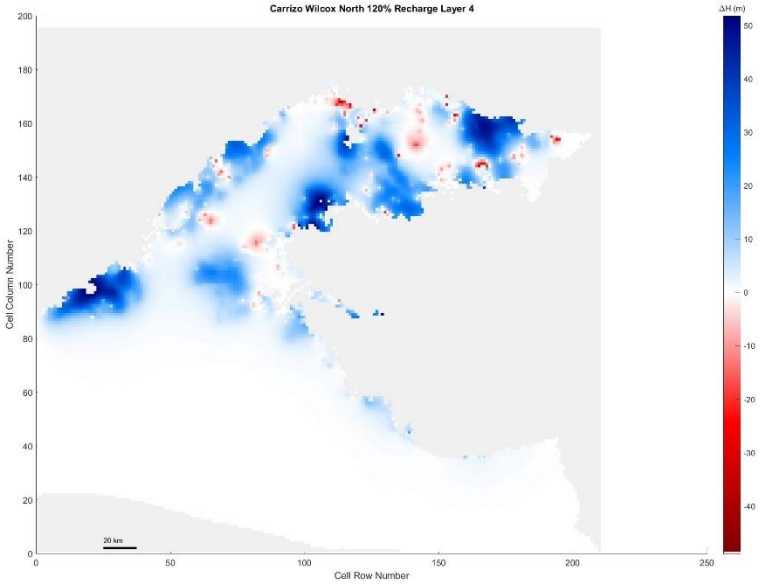

Figure 5. 199 Carrizo-Wilcox North, 120% original recharge hydraulic head spatial distribution of layer 4

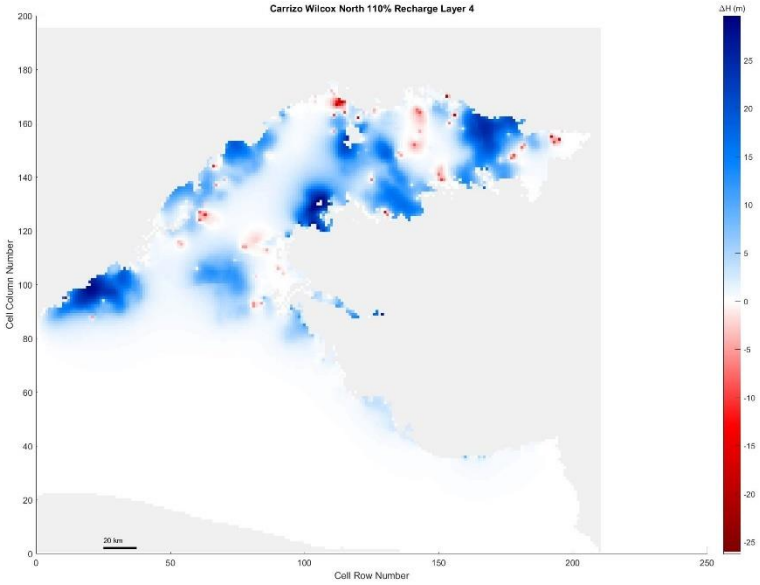

Figure 5. 200 Carrizo-Wilcox North, 110% original recharge hydraulic head spatial distribution of layer 4

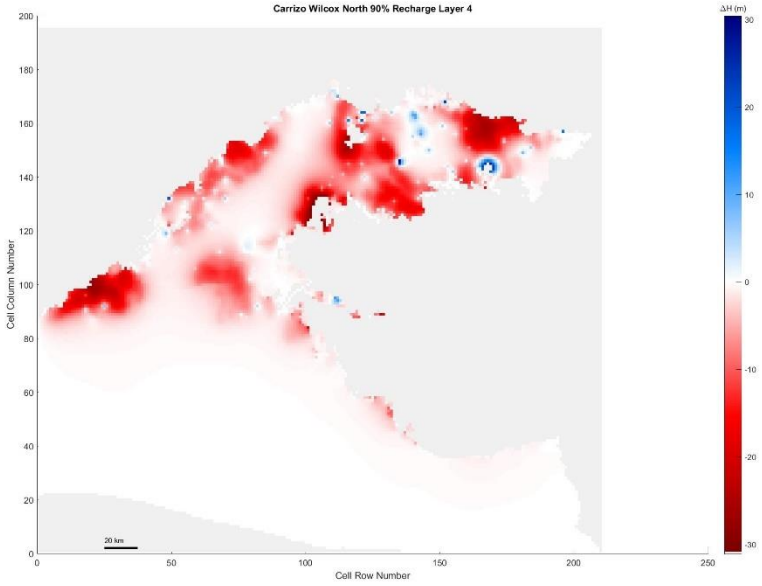

Figure 5. 201 Carrizo-Wilcox North, 90% original recharge hydraulic head spatial distribution of layer 4

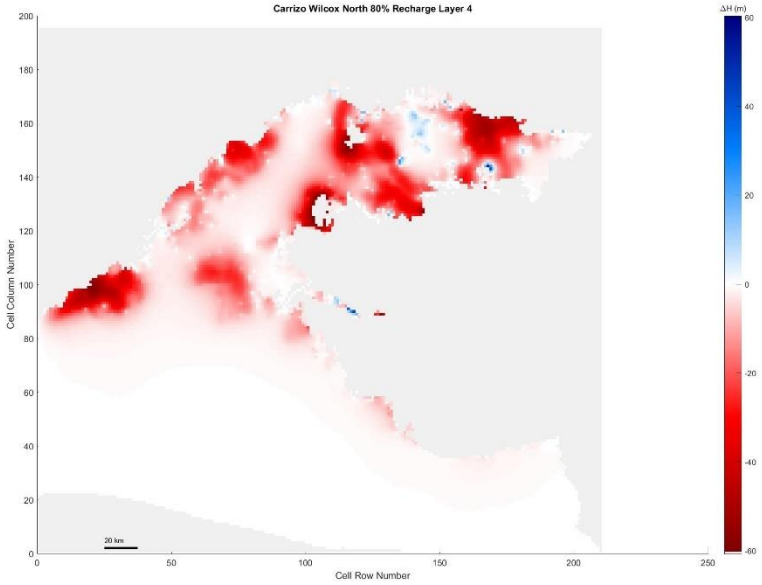

Figure 5. 202 Carrizo-Wilcox North, 80% original recharge hydraulic head spatial distribution of layer 4

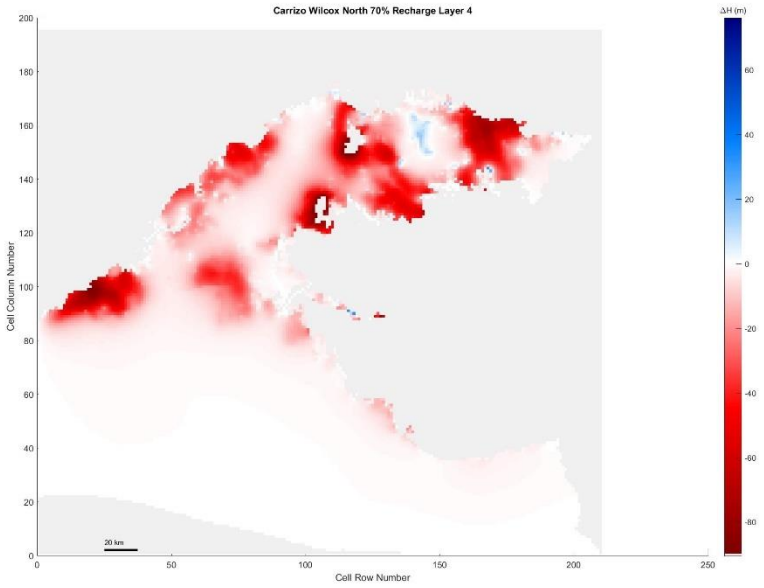

Figure 5. 203 Carrizo-Wilcox North, 70% original recharge hydraulic head spatial distribution of layer 4

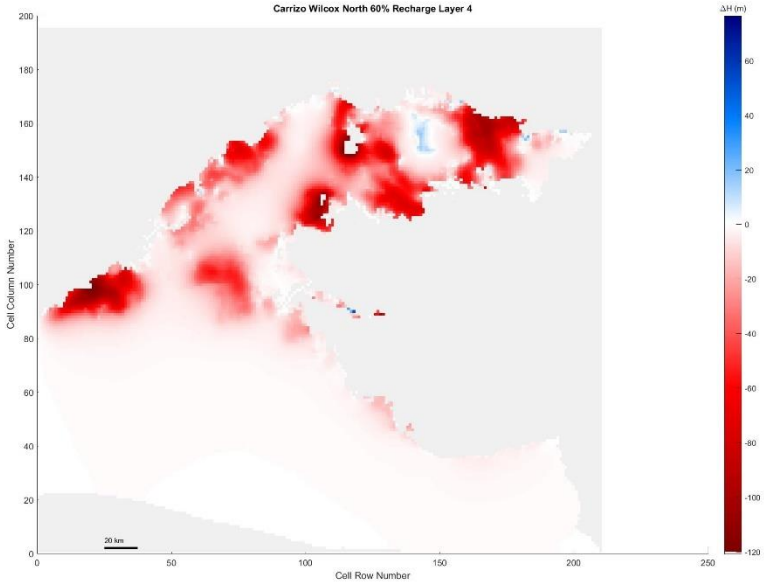

Figure 5. 204 Carrizo-Wilcox North, 60% original recharge hydraulic head spatial distribution of layer 4

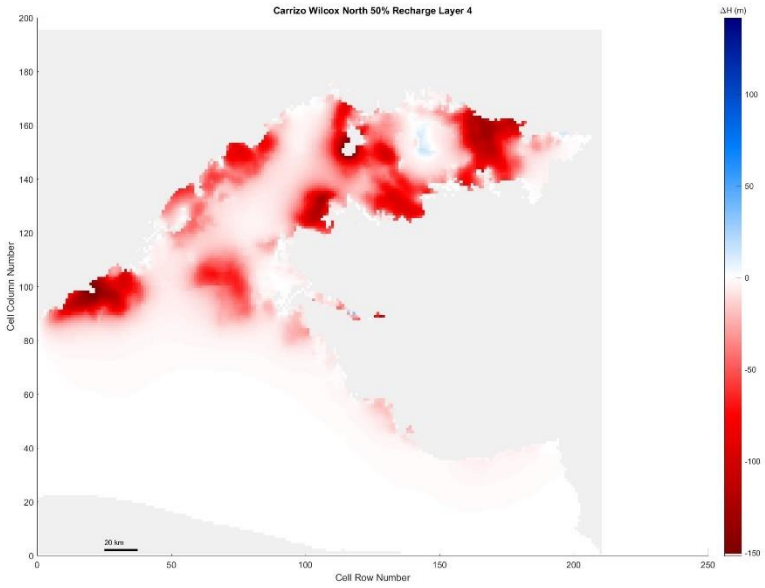

Figure 5. 205 Carrizo-Wilcox North, 50% original recharge hydraulic head spatial distribution of layer 4

Layer 5

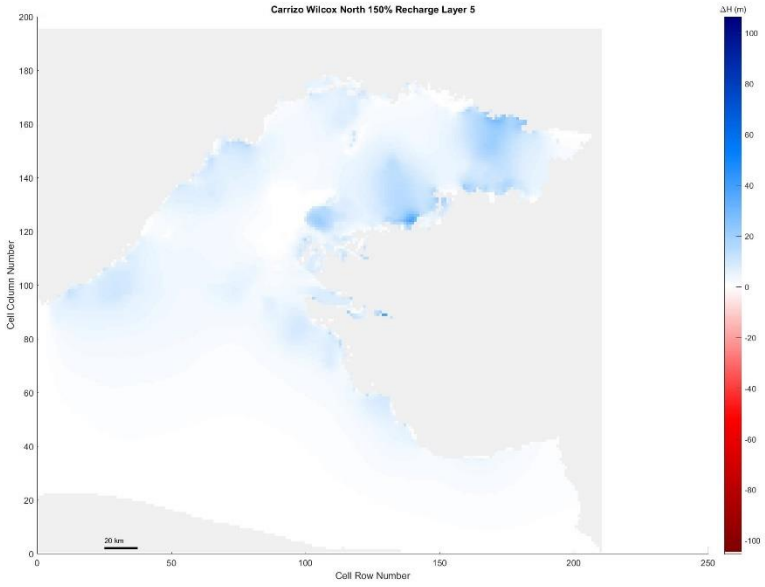

Figure 5. 206 Carrizo-Wilcox North, 150% original recharge hydraulic head spatial distribution of layer 5

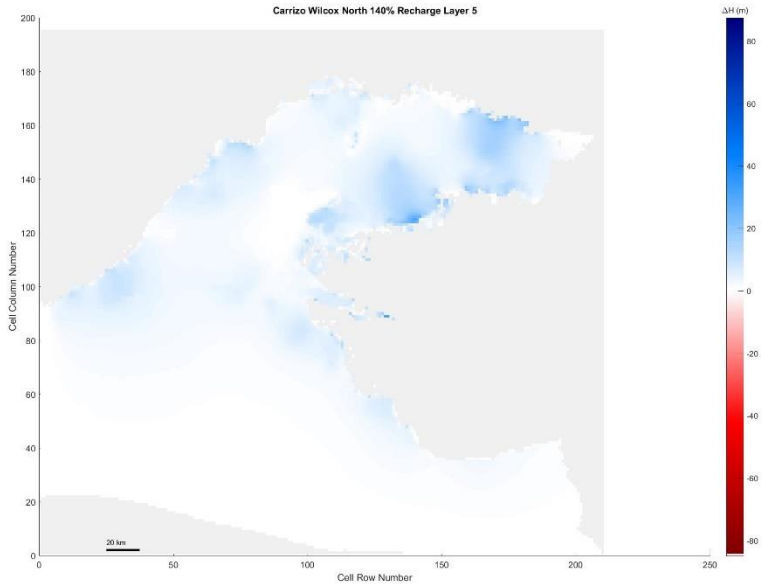

Figure 5. 207 Carrizo-Wilcox North, 140% original recharge hydraulic head spatial distribution of layer 5

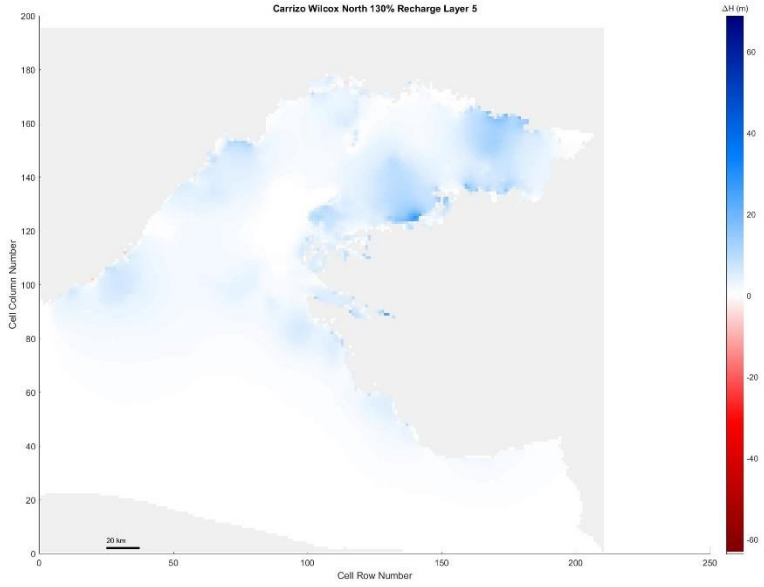

Figure 5. 208 Carrizo-Wilcox North, 130% original recharge hydraulic head spatial distribution of layer 5

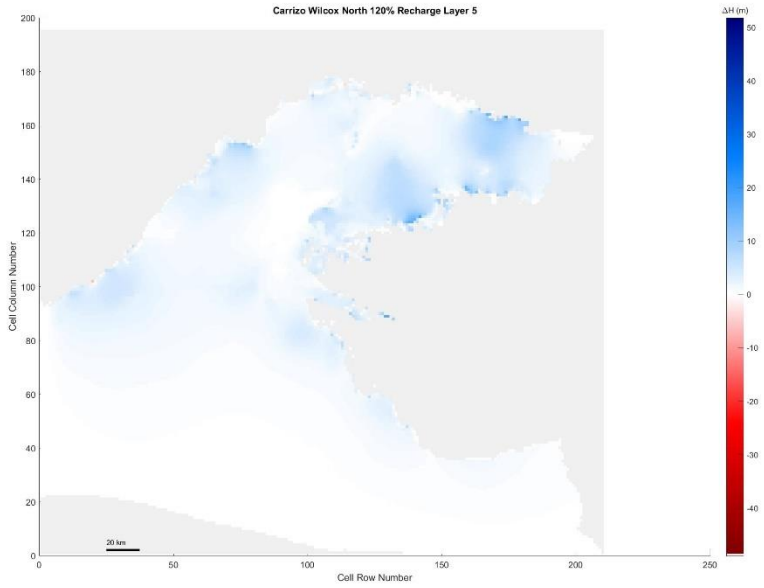

Figure 5. 209 Carrizo-Wilcox North, 120% original recharge hydraulic head spatial distribution of layer 5

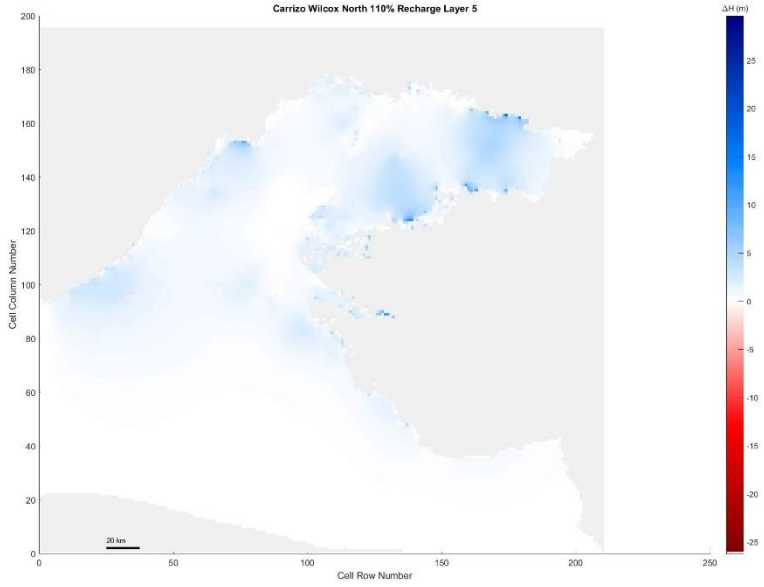

Figure 5. 210 Carrizo-Wilcox North, 110% original recharge hydraulic head spatial distribution of layer 5

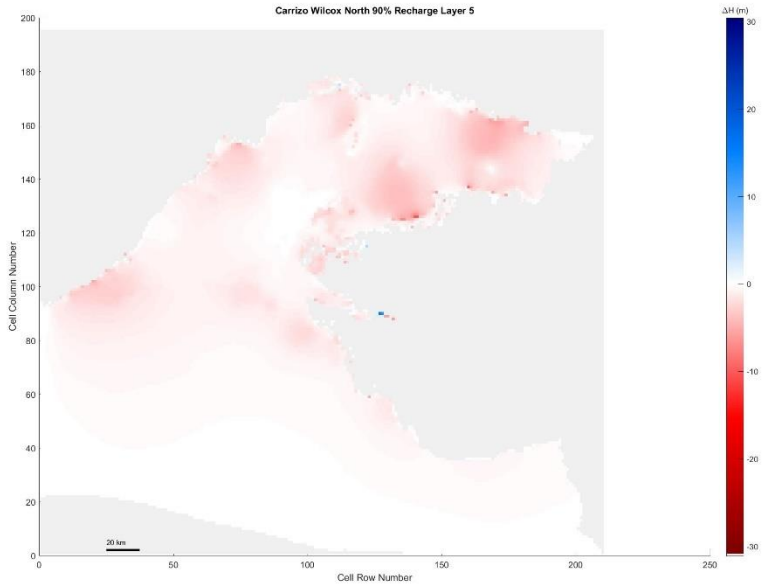

Figure 5. 211 Carrizo-Wilcox North, 90% original recharge hydraulic head spatial distribution of layer 5

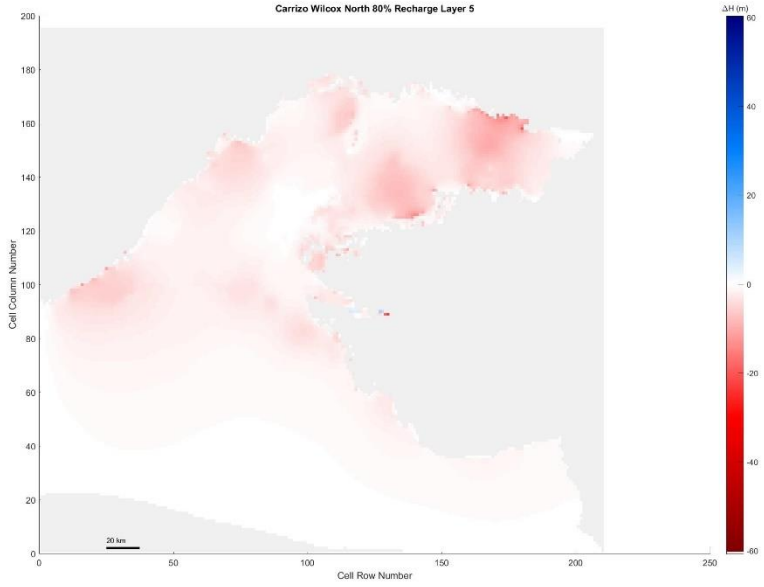

Figure 5. 212 Carrizo-Wilcox North, 80% original recharge hydraulic head spatial distribution of layer 5

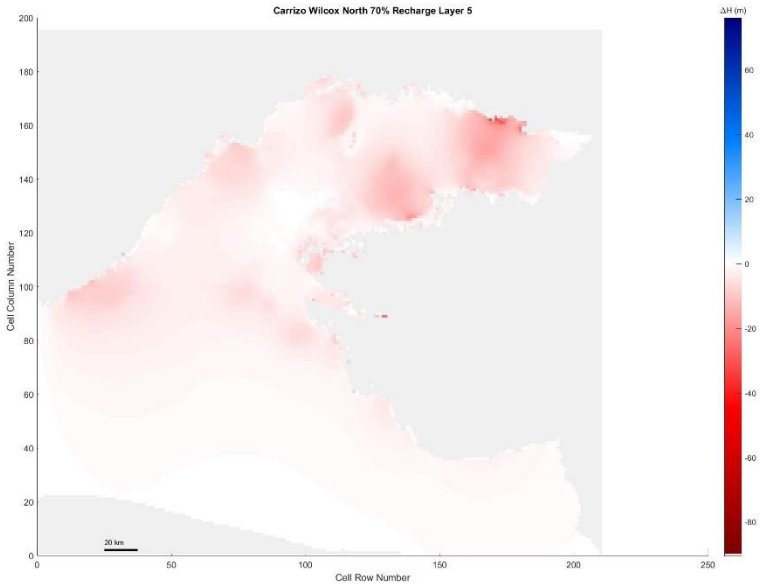

Figure 5. 213 Carrizo-Wilcox North, 70% original recharge hydraulic head spatial distribution of layer 5

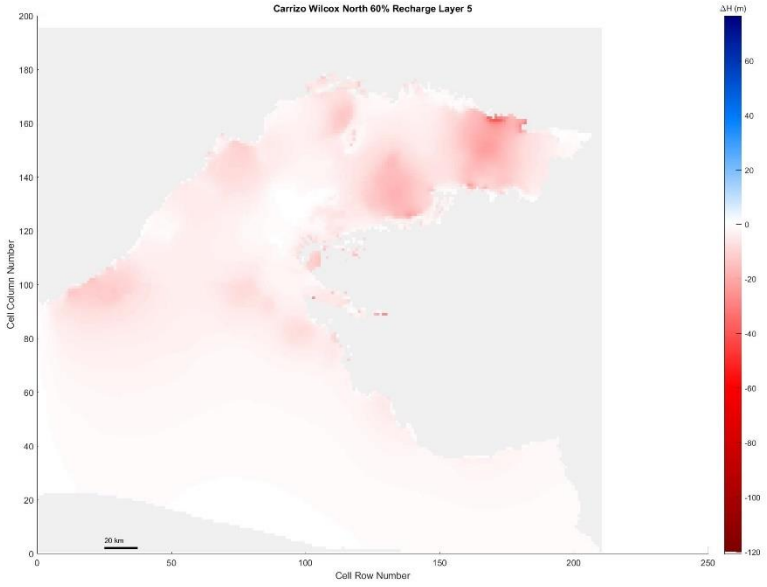

Figure 5. 214 Carrizo-Wilcox North, 60% original recharge hydraulic head spatial distribution of layer 5

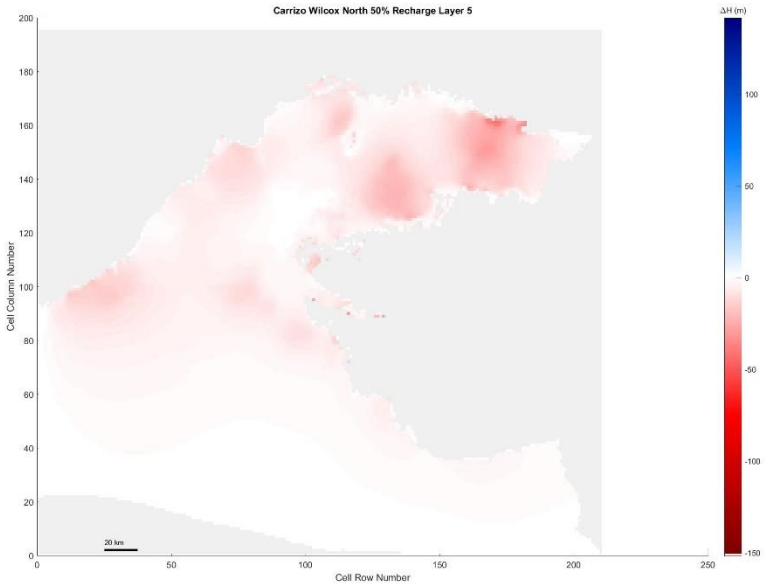

Figure 5. 215 Carrizo-Wilcox North, 50% original recharge hydraulic head spatial distribution of layer 5

Layer 6

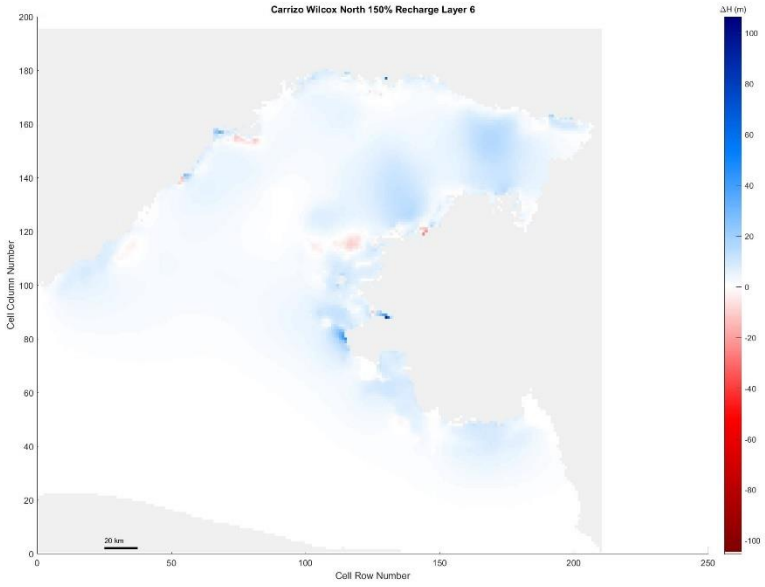

Figure 5. 216 Carrizo-Wilcox North, 150% original recharge hydraulic head spatial distribution of layer 6

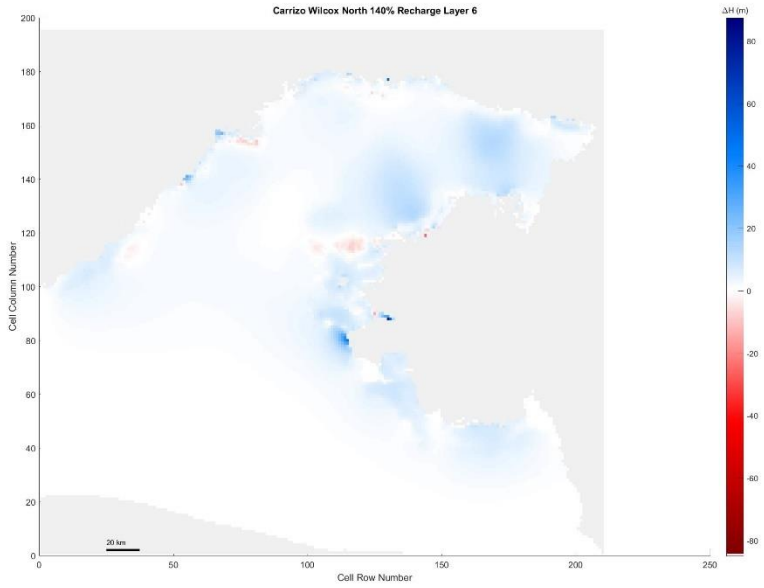

Figure 5. 217 Carrizo-Wilcox North, 140% original recharge hydraulic head spatial distribution of layer 6

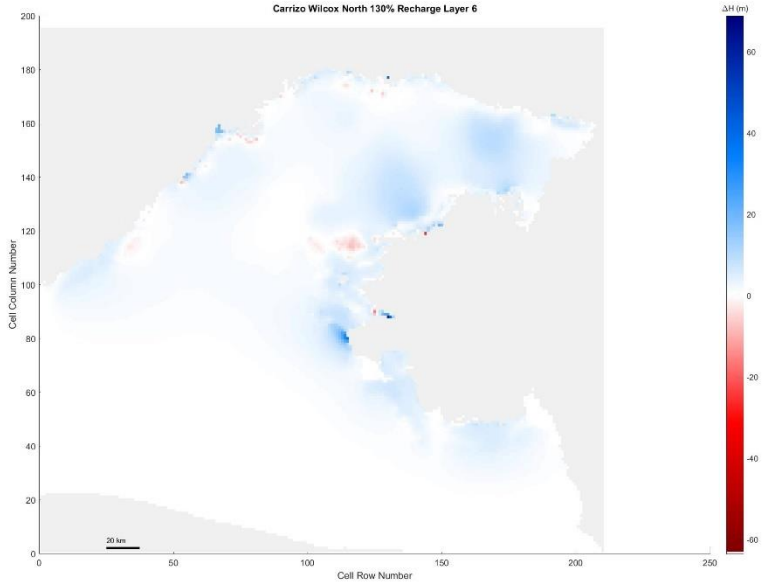

Figure 5. 218 Carrizo-Wilcox North, 130% original recharge hydraulic head spatial distribution of layer 6

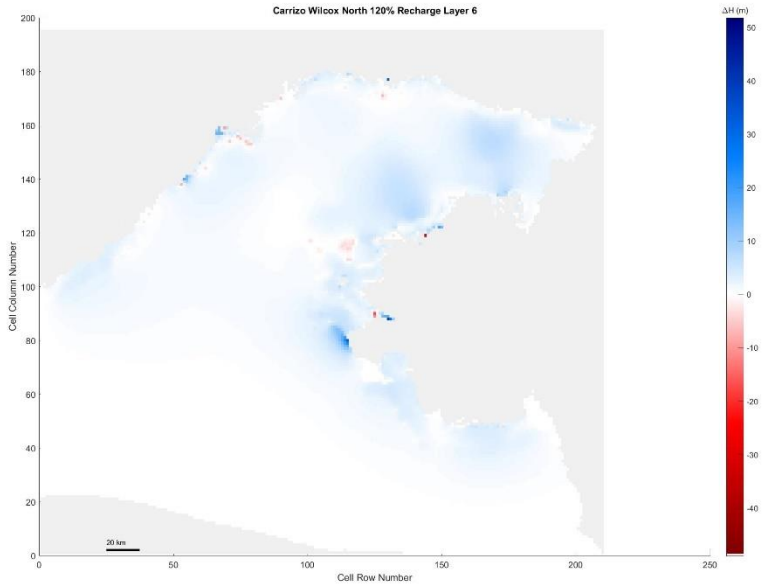

Figure 5. 219 Carrizo-Wilcox North, 120% original recharge hydraulic head spatial distribution of layer 6

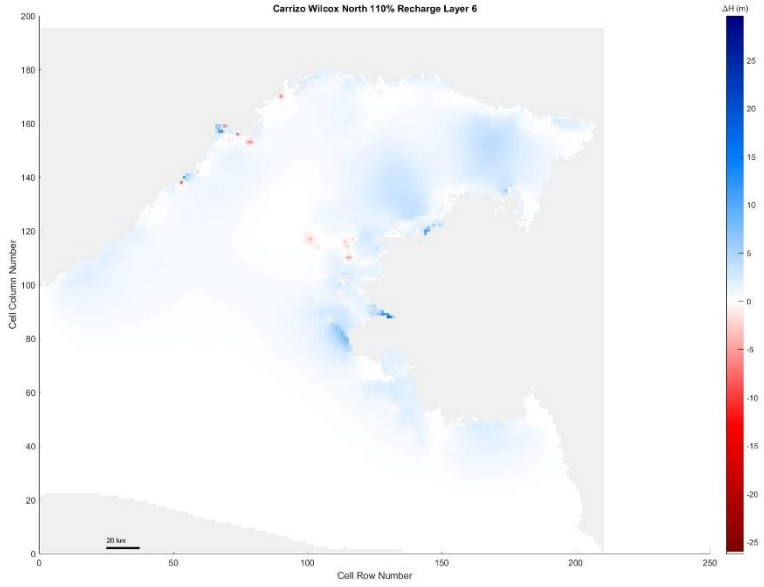

Figure 5. 220 Carrizo-Wilcox North, 110% original recharge hydraulic head spatial distribution of layer 6

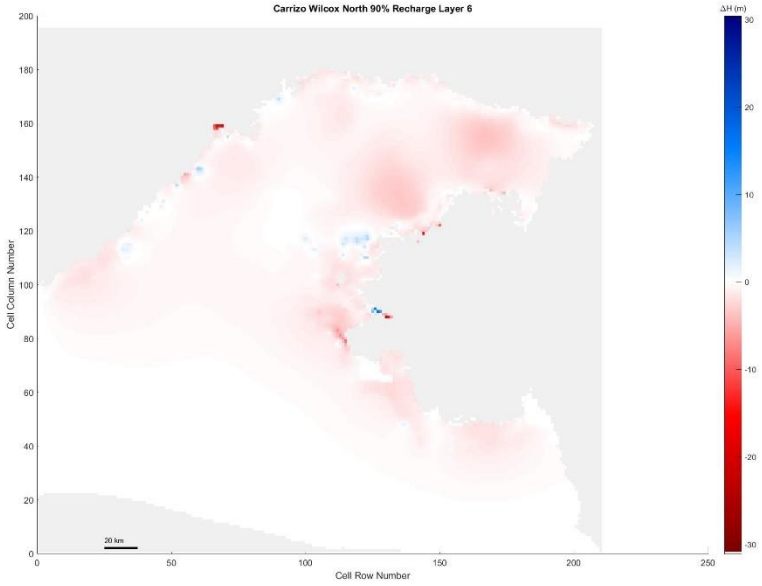

Figure 5. 221 Carrizo-Wilcox North, 90% original recharge hydraulic head spatial distribution of layer 6

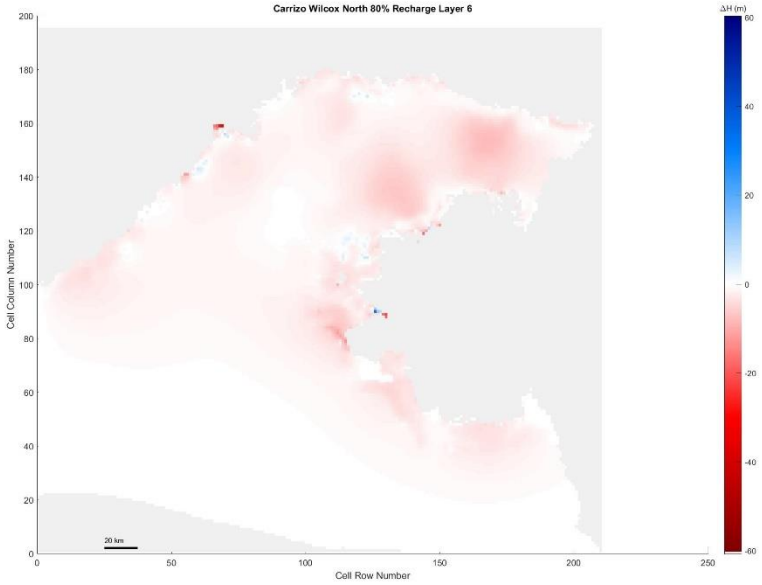

Figure 5. 222 Carrizo-Wilcox North, 80% original recharge hydraulic head spatial distribution of layer 6

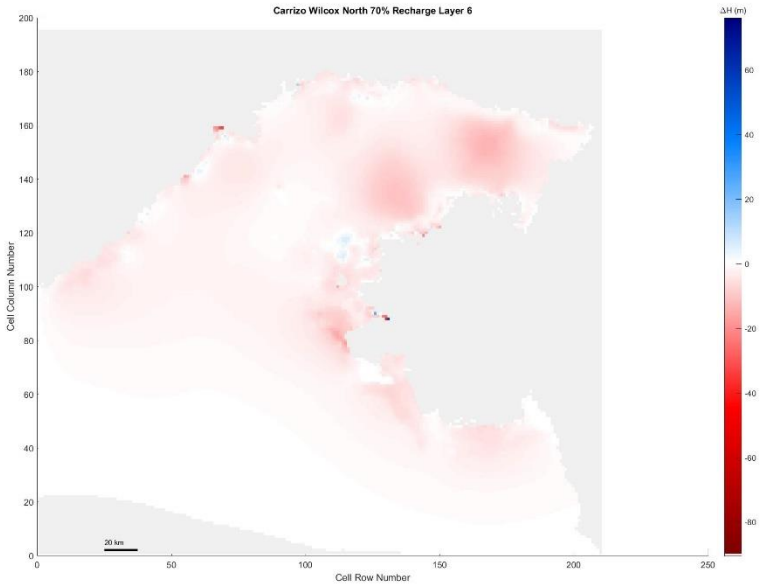

Figure 5. 223 Carrizo-Wilcox North, 70% original recharge hydraulic head spatial distribution of layer 6

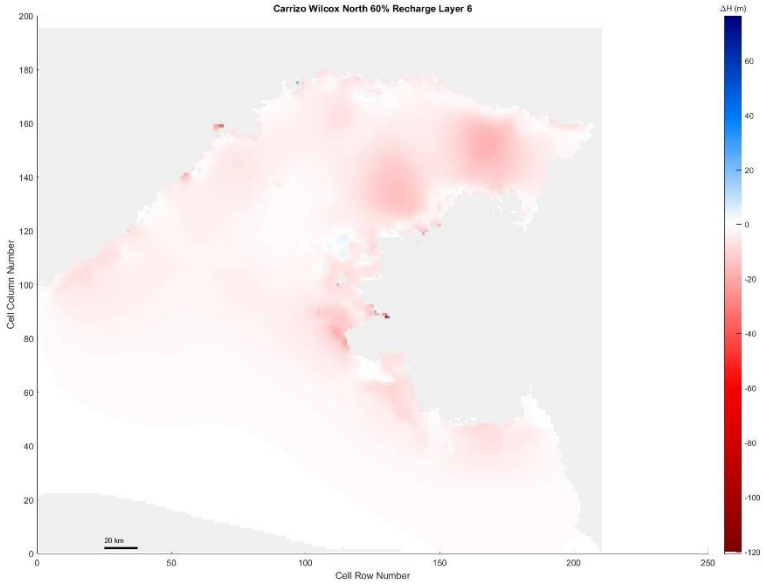

Figure 5. 224 Carrizo-Wilcox North, 60% original recharge hydraulic head spatial distribution of layer 6

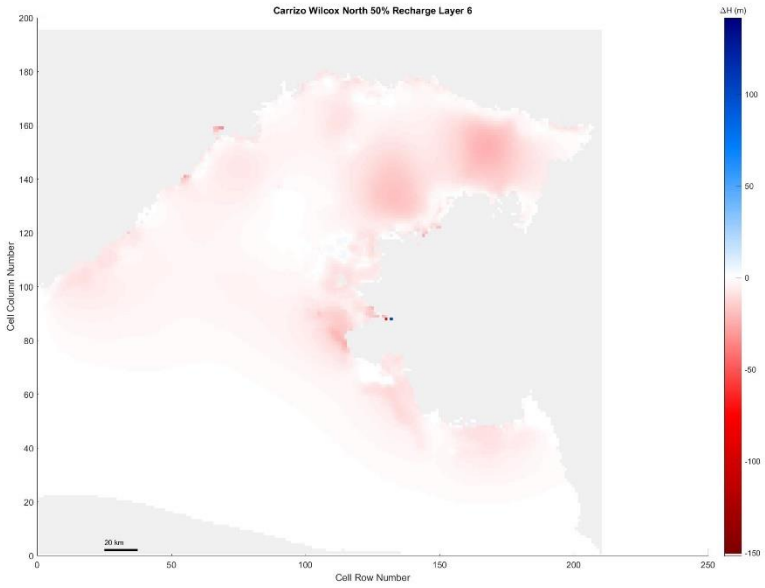

Figure 5. 225 Carrizo-Wilcox North, 50% original recharge hydraulic head spatial distribution of layer 6

Layer 7

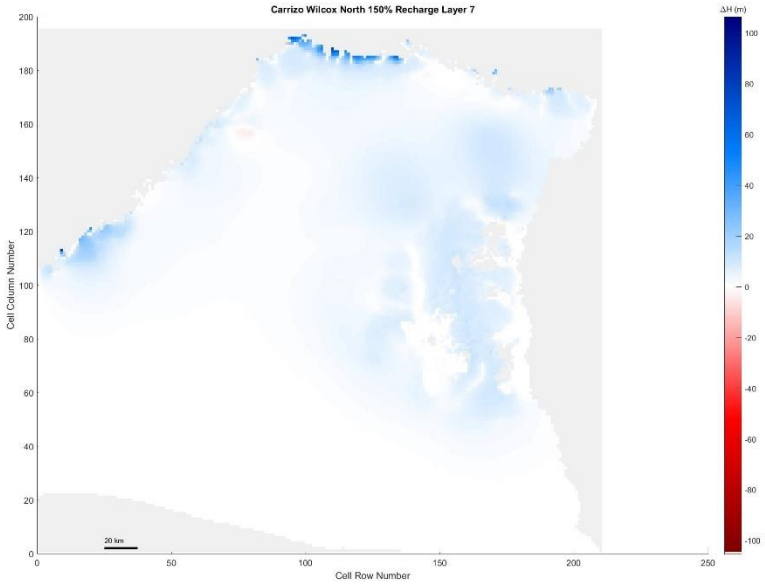

Figure 5. 226 Carrizo-Wilcox North, 150% original recharge hydraulic head spatial distribution of layer 7

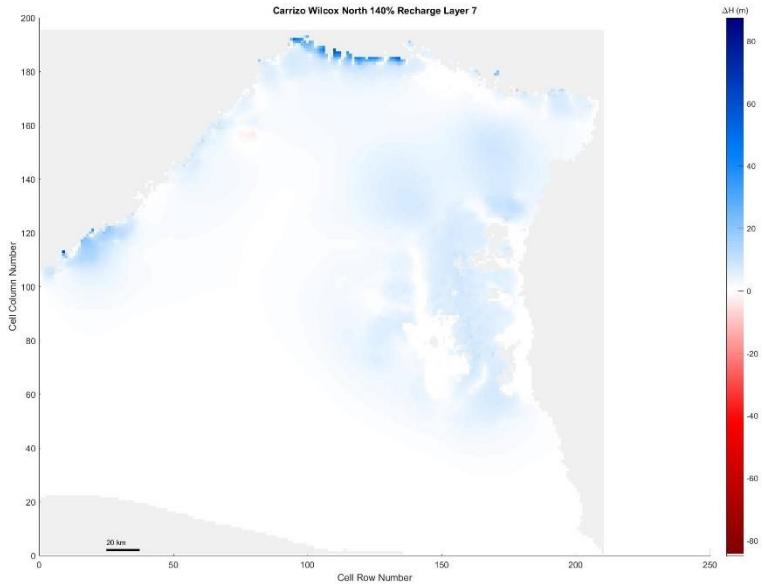

Figure 5. 227 Carrizo-Wilcox North, 140% original recharge hydraulic head spatial distribution of layer 7

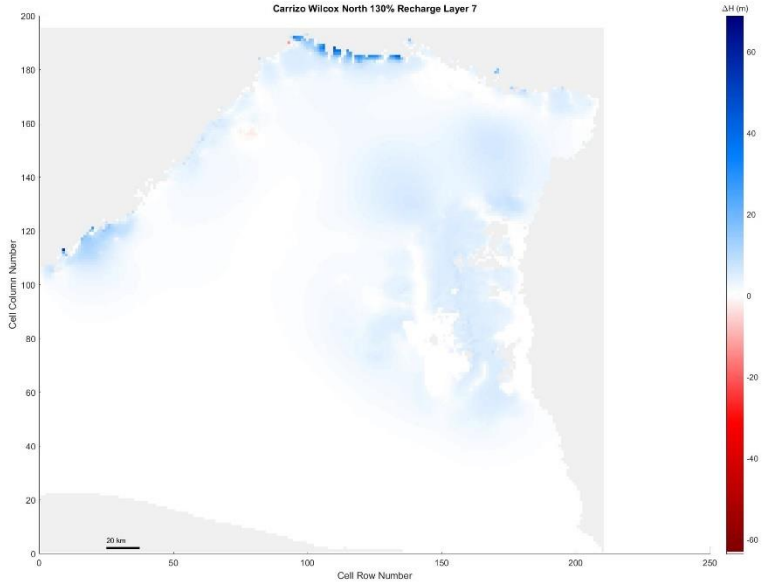

Figure 5. 228 Carrizo-Wilcox North, 130% original recharge hydraulic head spatial distribution of layer 7

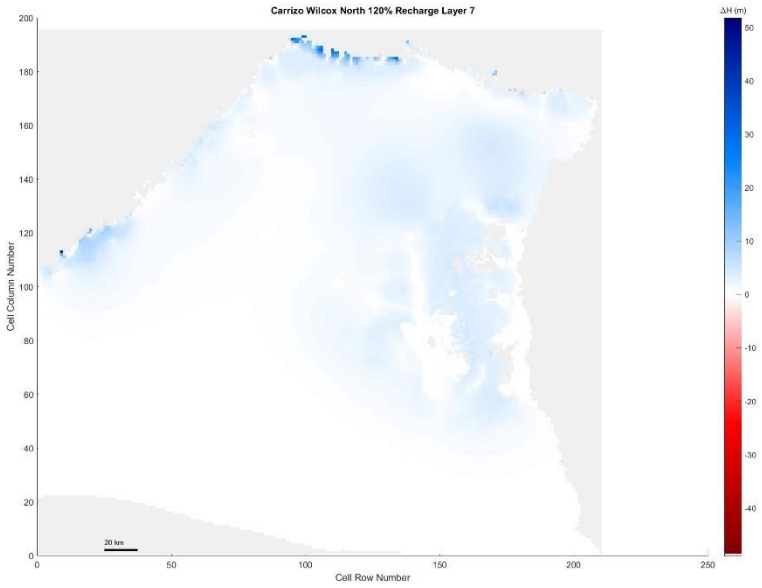

Figure 5. 229 Carrizo-Wilcox North, 120% original recharge hydraulic head spatial distribution of layer 7

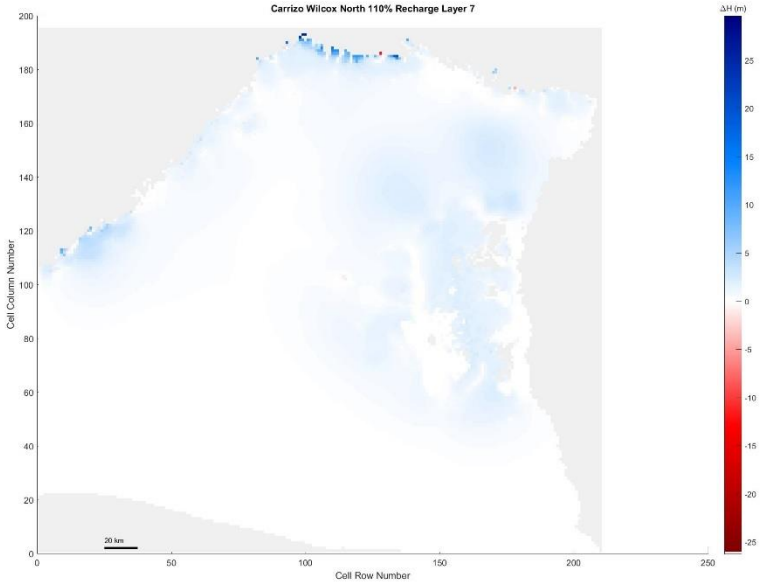

Figure 5. 230 Carrizo-Wilcox North, 110% original recharge hydraulic head spatial distribution of layer 7

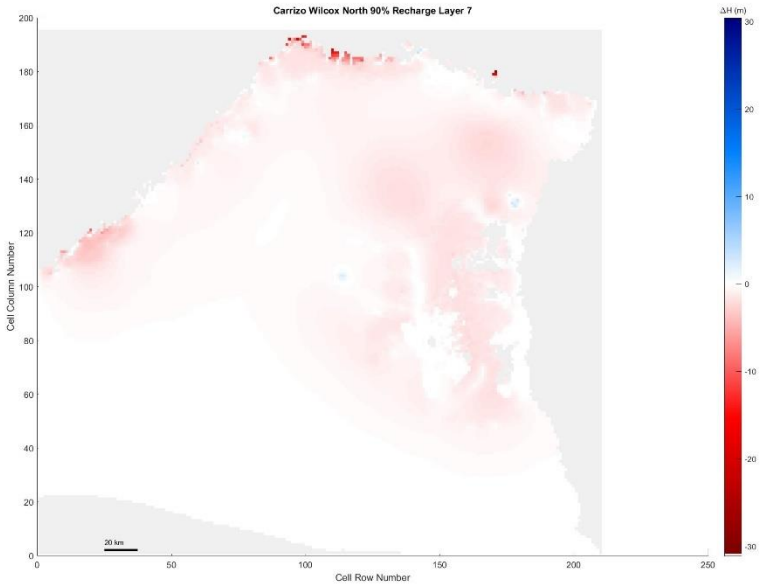

Figure 5. 231 Carrizo-Wilcox North, 90% original recharge hydraulic head spatial distribution of layer 7

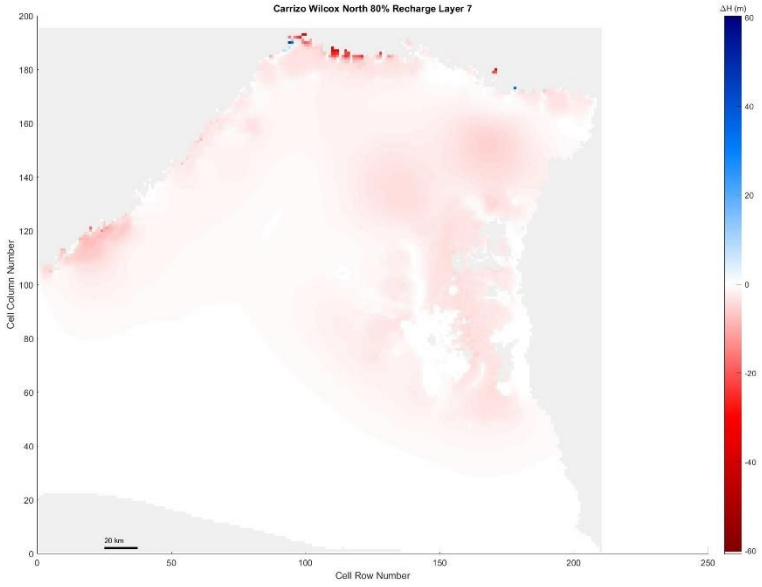

Figure 5. 232 Carrizo-Wilcox North, 80% original recharge hydraulic head spatial distribution of layer 7

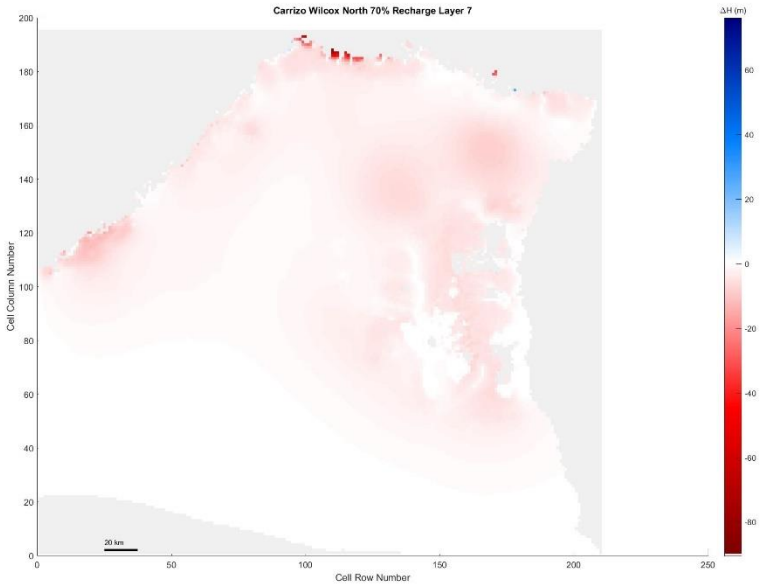

Figure 5. 233 Carrizo-Wilcox North, 70% original recharge hydraulic head spatial distribution of layer 7

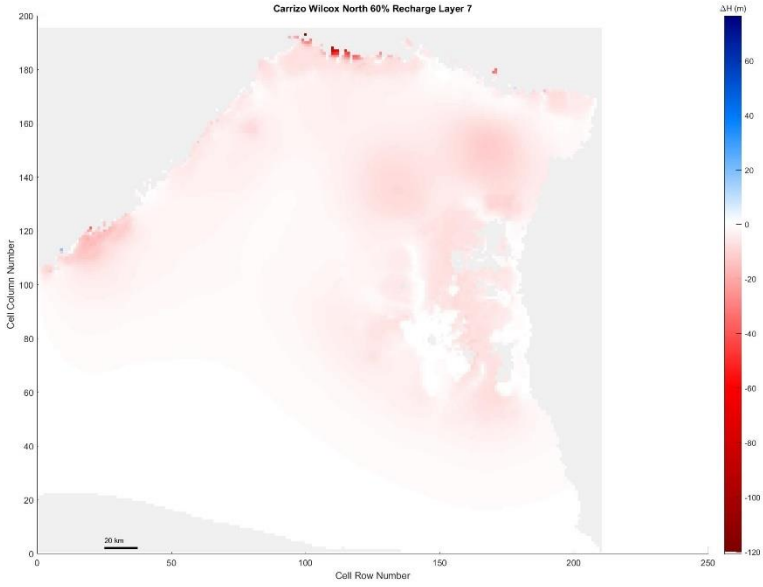

Figure 5. 234 Carrizo-Wilcox North, 60% original recharge hydraulic head spatial distribution of layer 7

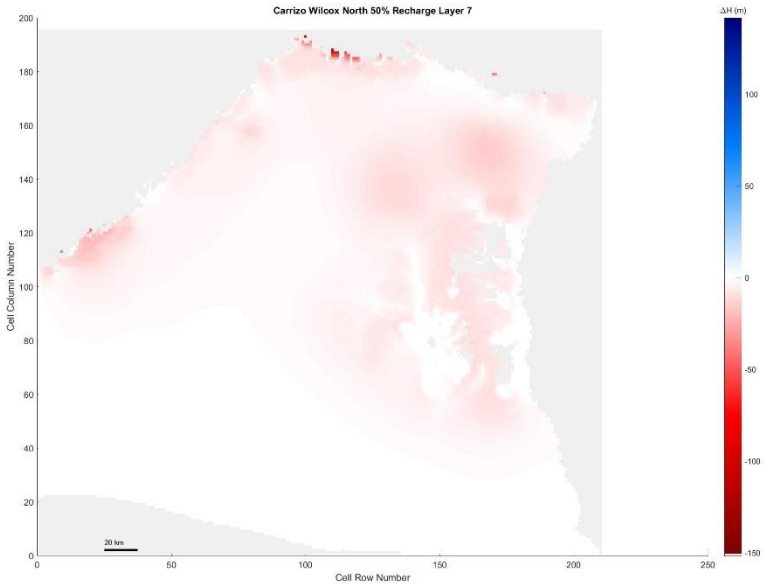

Figure 5. 235 Carrizo-Wilcox North, 50% original recharge hydraulic head spatial distribution of layer 7

Layer 8

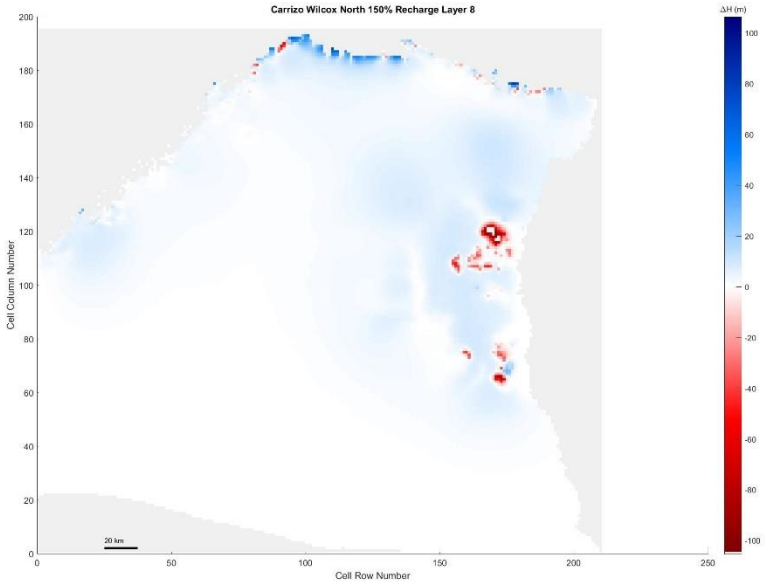

Figure 5. 236 Carrizo-Wilcox North, 150% original recharge hydraulic head spatial distribution of layer 8

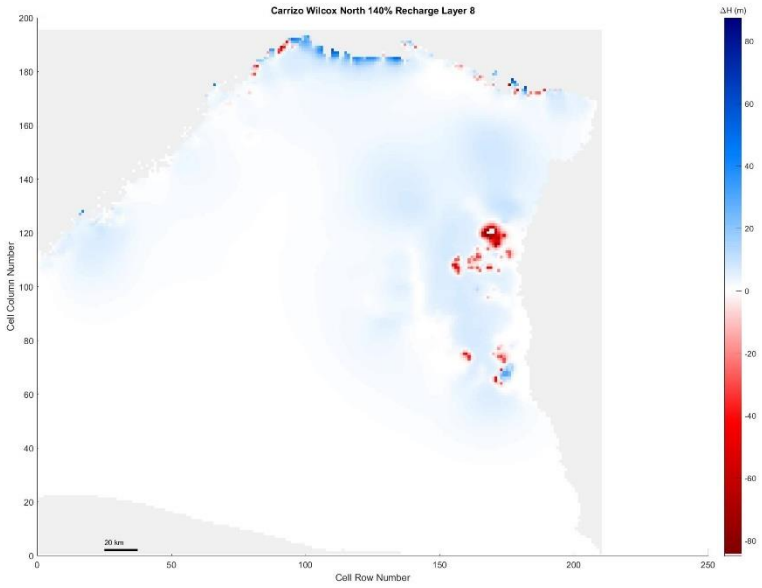

Figure 5. 237 Carrizo-Wilcox North, 140% original recharge hydraulic head spatial distribution of layer 8

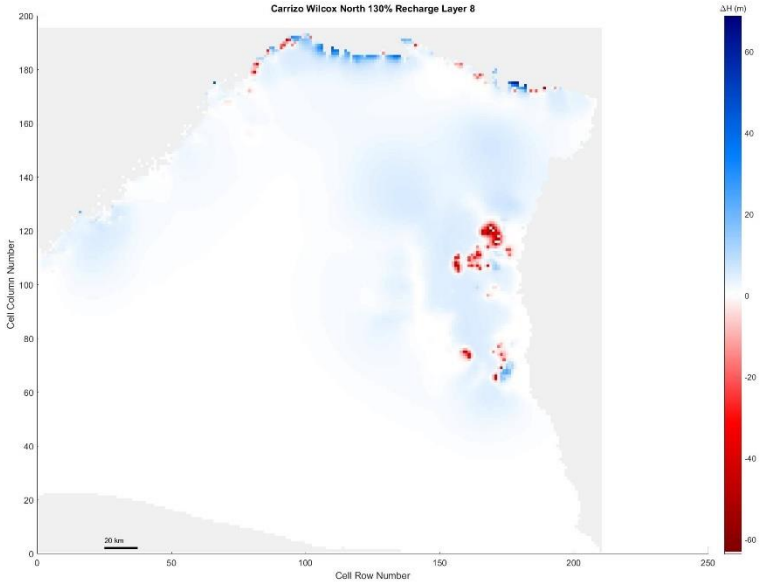

Figure 5. 238 Carrizo-Wilcox North, 130% original recharge hydraulic head spatial distribution of layer 8

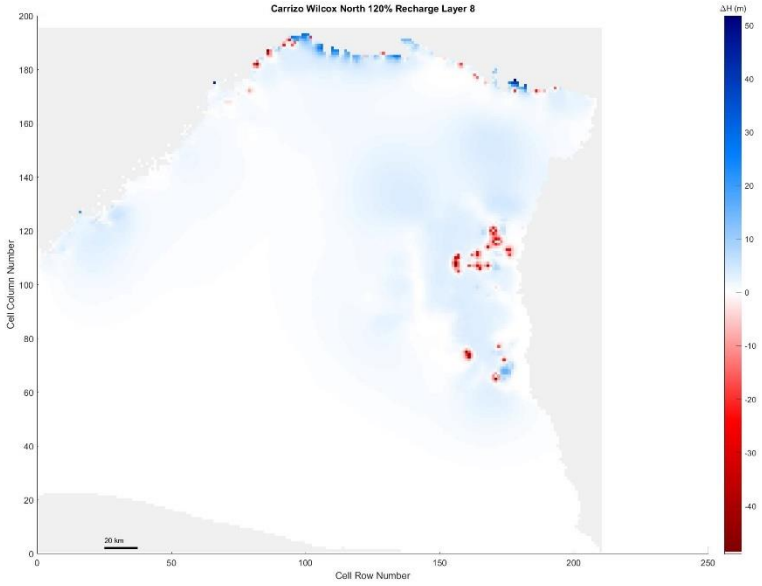

Figure 5. 239 Carrizo-Wilcox North, 120% original recharge hydraulic head spatial distribution of layer 8

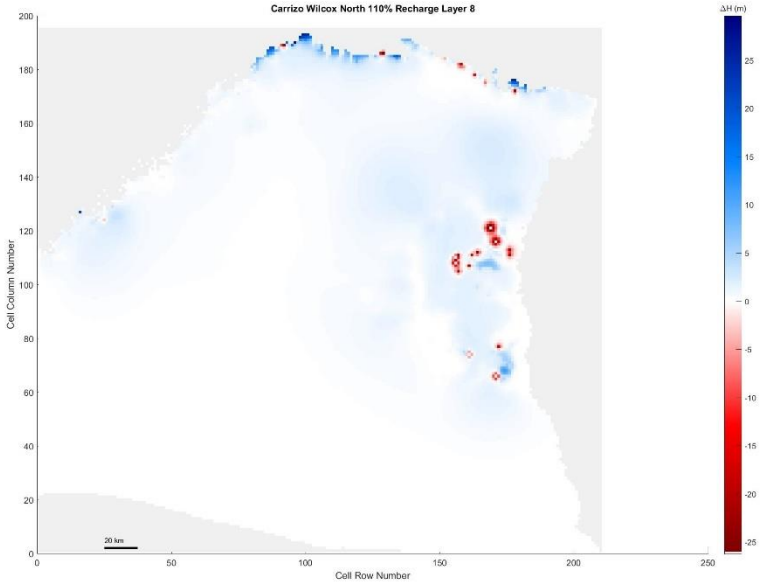

Figure 5. 240 Carrizo-Wilcox North, 110% original recharge hydraulic head spatial distribution of layer 8

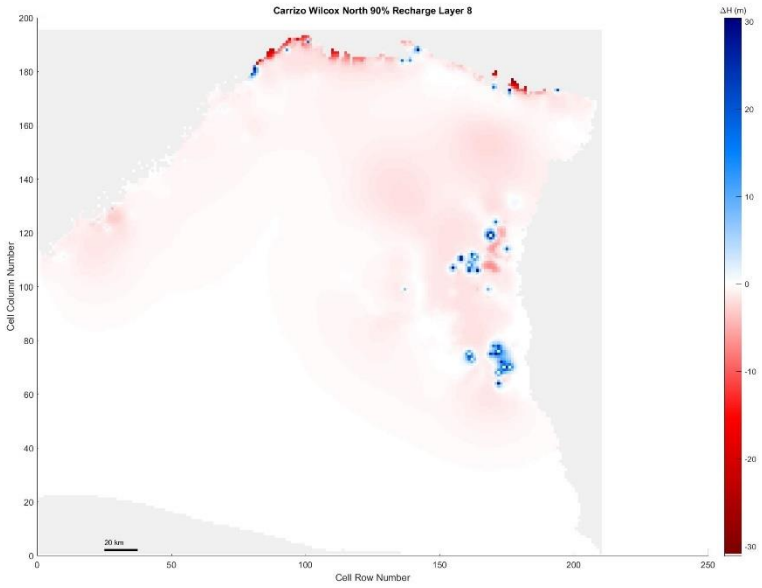

Figure 5. 241 Carrizo-Wilcox North, 90% original recharge hydraulic head spatial distribution of layer 8

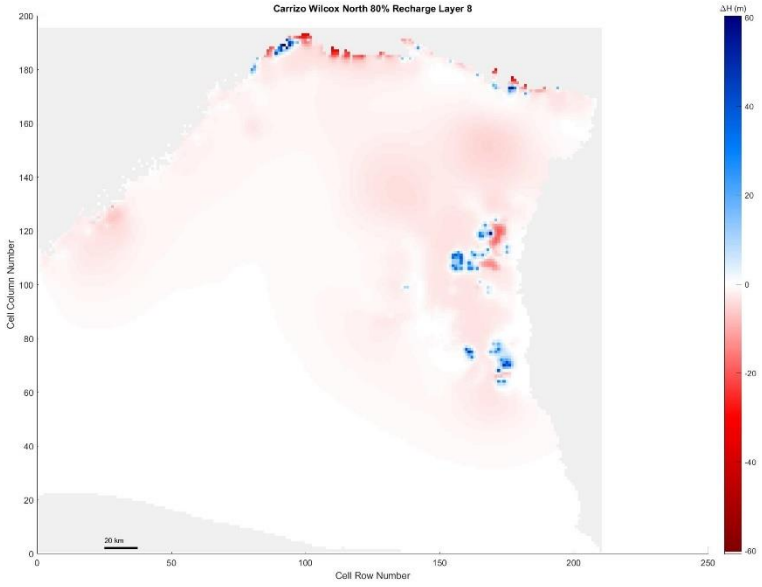

Figure 5. 242 Carrizo-Wilcox North, 80% original recharge hydraulic head spatial distribution of layer 8

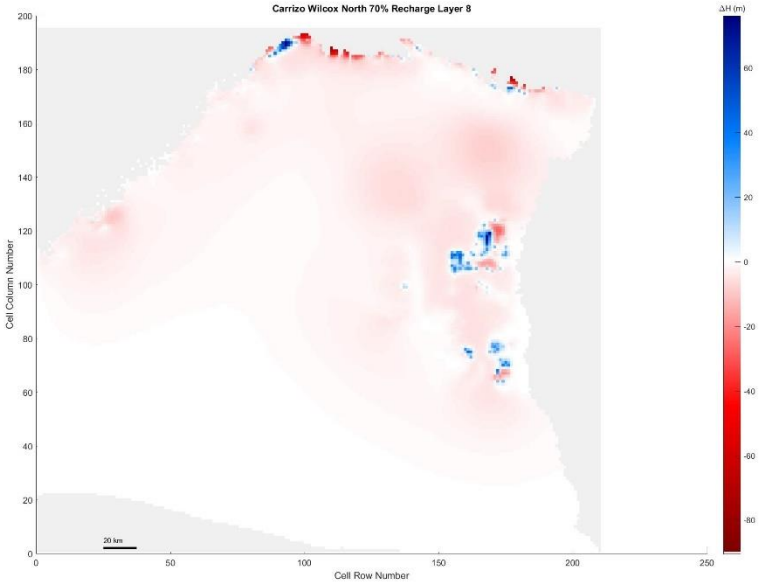

Figure 5. 243 Carrizo-Wilcox North, 70% original recharge hydraulic head spatial distribution of layer 8

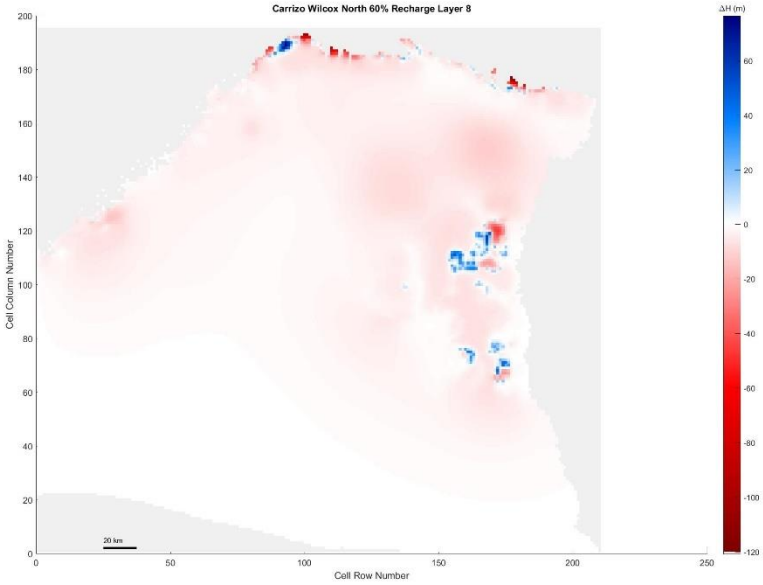

Figure 5. 244 Carrizo-Wilcox North, 60% original recharge hydraulic head spatial distribution of layer 8

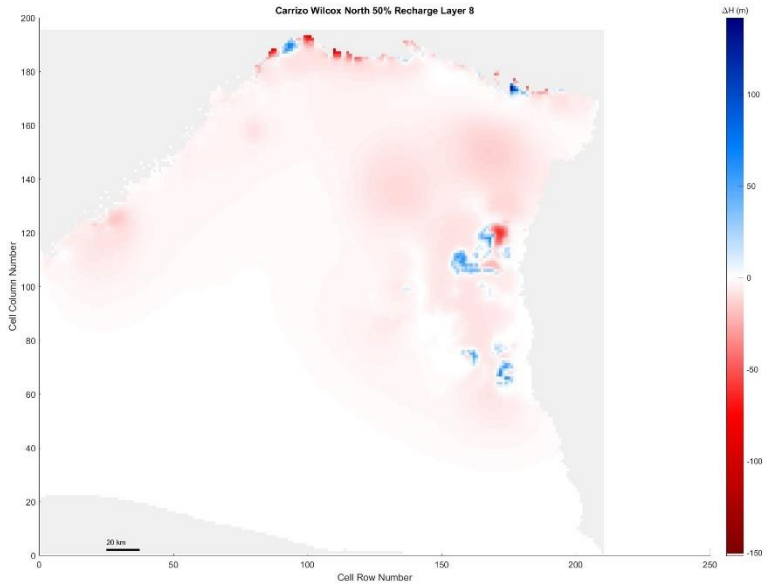

Figure 5. 245 Carrizo-Wilcox North, 50% original recharge hydraulic head spatial distribution of layer 8

Carrizo-Wilcox South

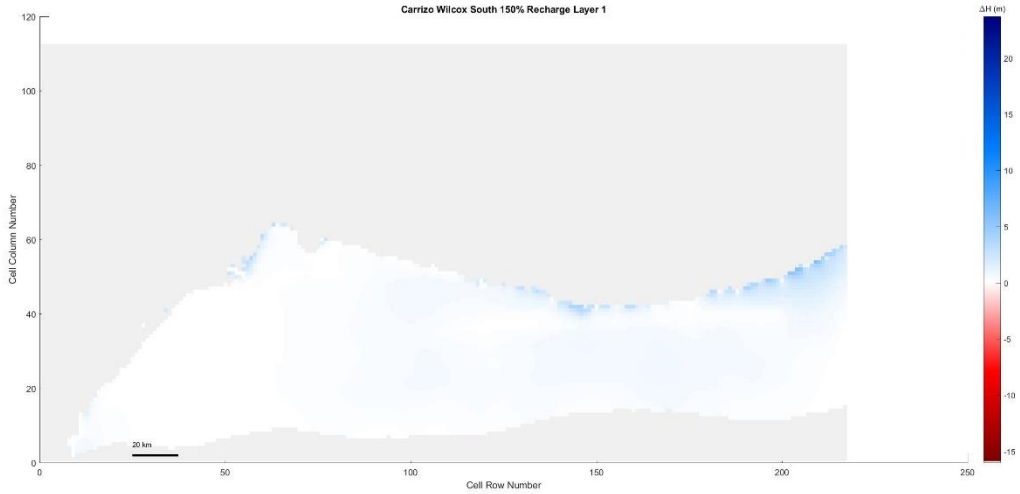

Figure 5. 246 Carrizo-Wilcox South, 150% original recharge hydraulic head spatial distribution of layer 1

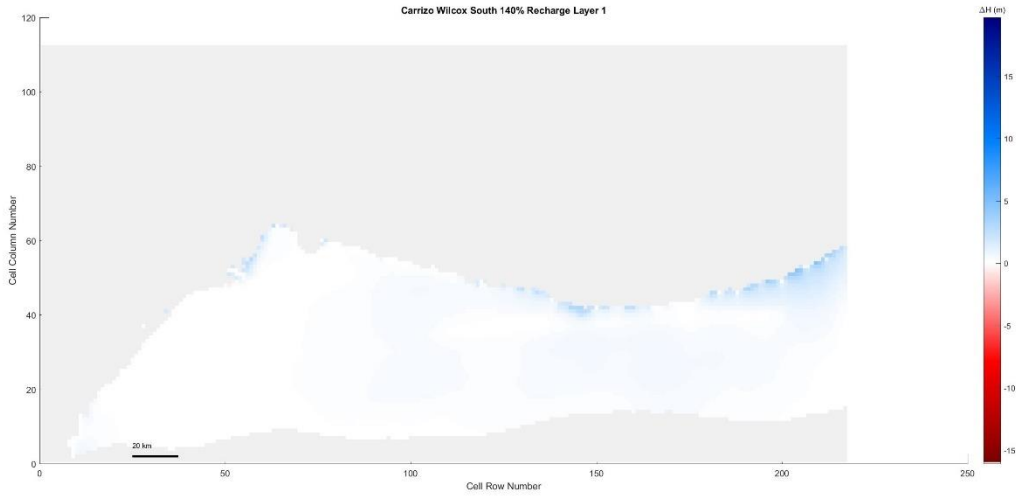

Figure 5. 247 Carrizo-Wilcox South, 140% original recharge hydraulic head spatial distribution of layer 1

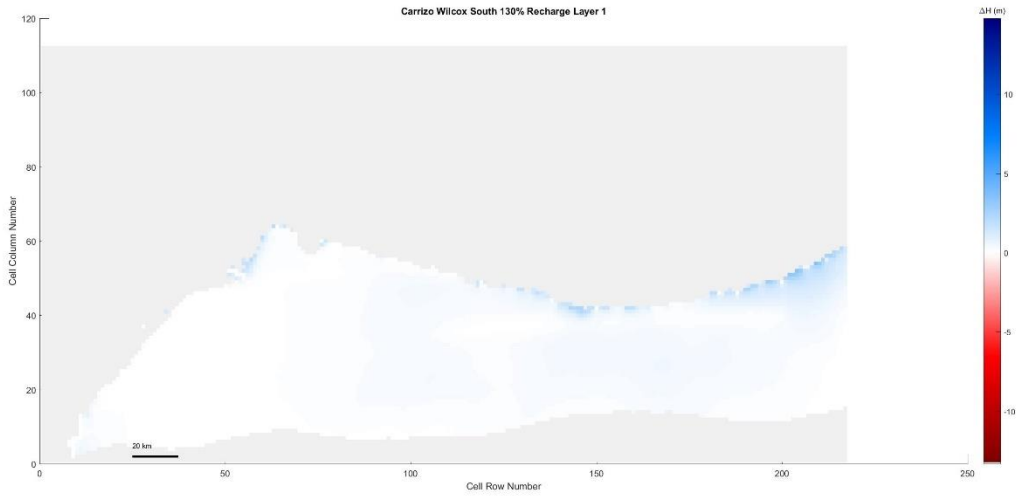

Figure 5. 248 Carrizo-Wilcox South, 130% original recharge hydraulic head spatial distribution of layer 1

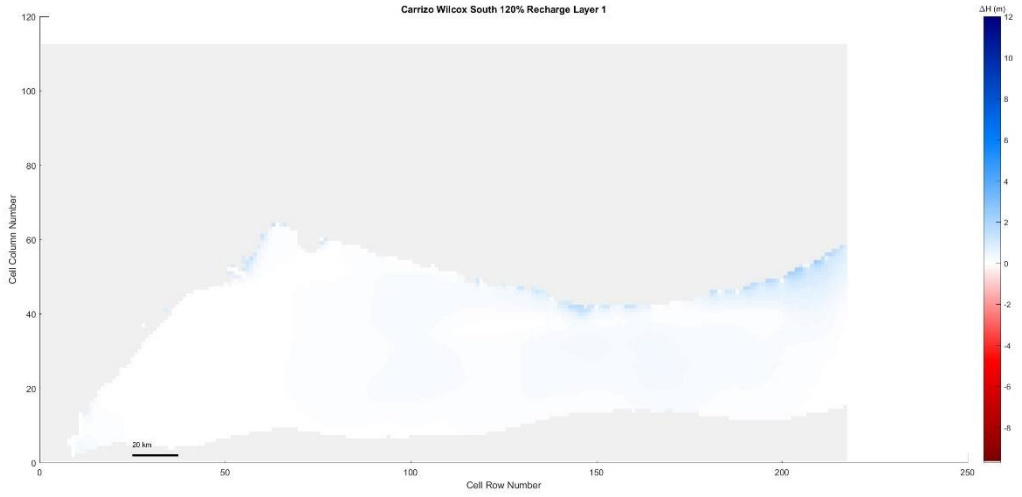

Figure 5. 249 Carrizo-Wilcox South, 120% original recharge hydraulic head spatial distribution of layer 1

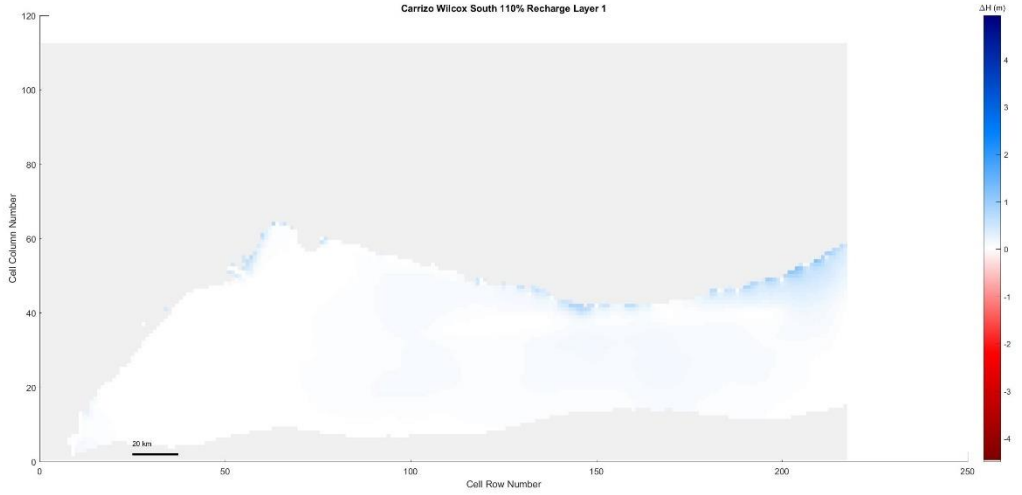

Figure 5. 250 Carrizo-Wilcox South, 110% original recharge hydraulic head spatial distribution of layer 1

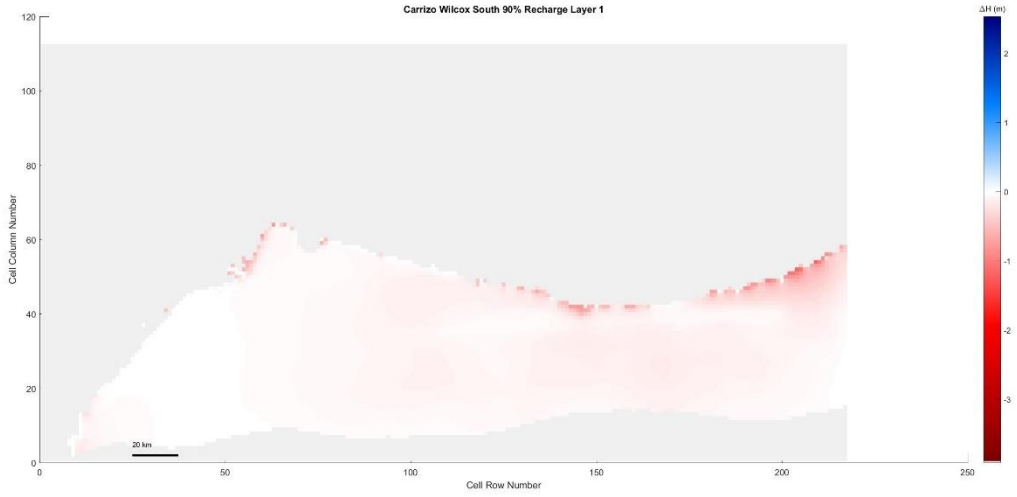

Figure 5. 251 Carrizo-Wilcox South, 90% original recharge hydraulic head spatial distribution of layer 1

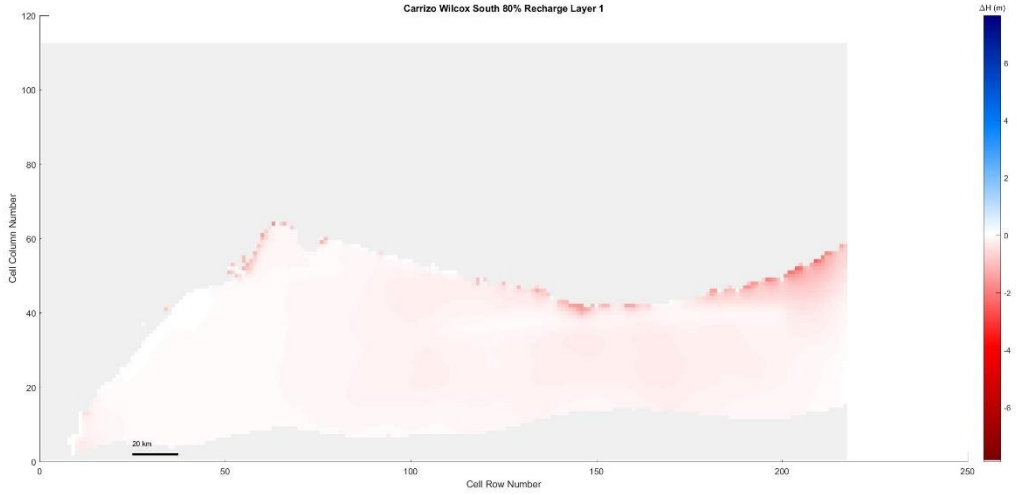

Figure 5. 252 Carrizo-Wilcox South, 80% original recharge hydraulic head spatial distribution of layer 1

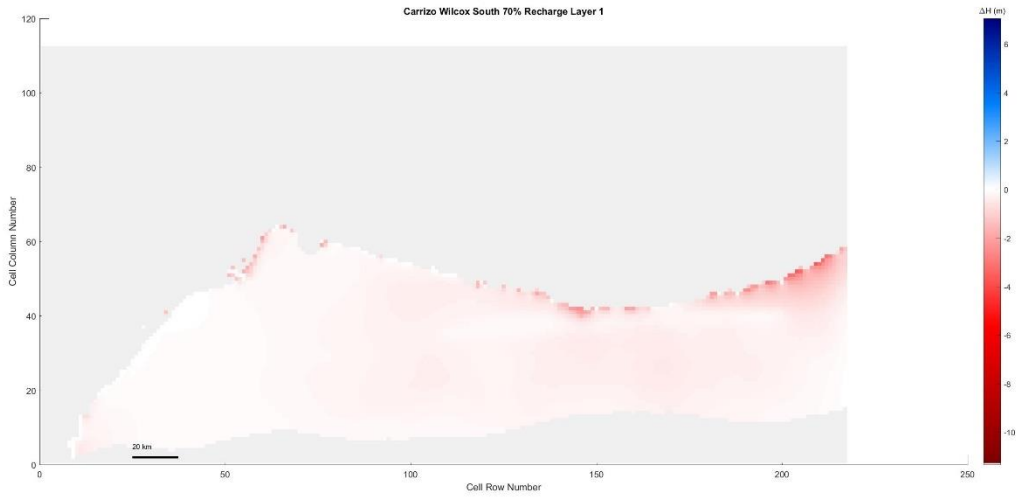

Figure 5. 253 Carrizo-Wilcox South, 70% original recharge hydraulic head spatial distribution of layer 1

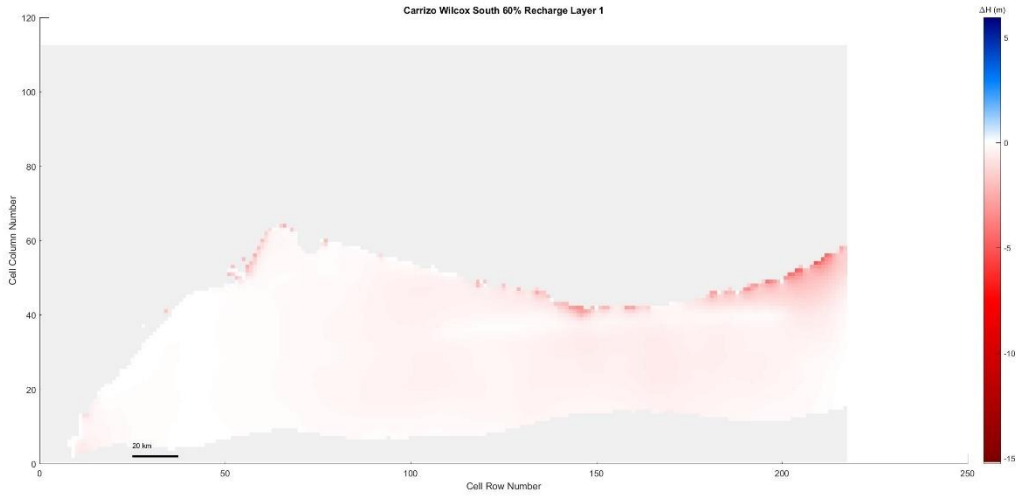

Figure 5. 254 Carrizo-Wilcox South, 60% original recharge hydraulic head spatial distribution of layer 1

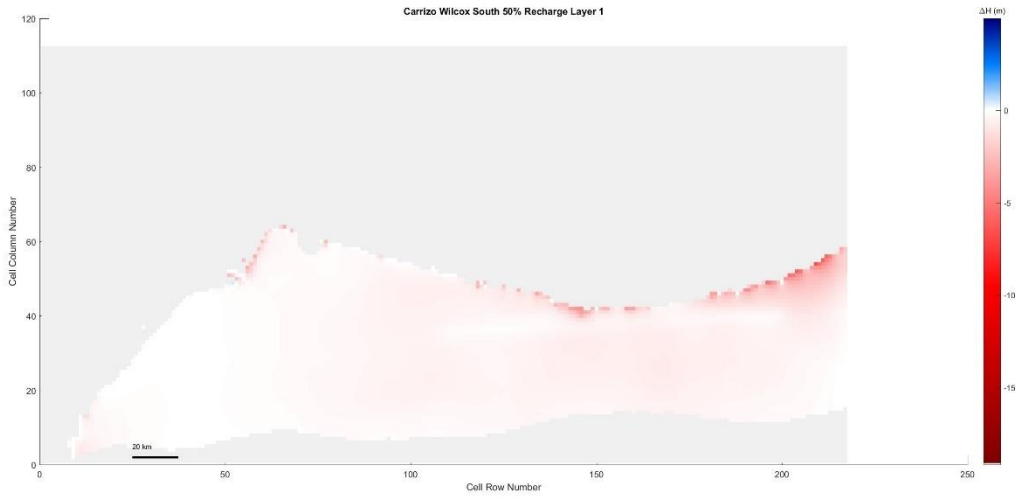

Figure 5. 255 Carrizo-Wilcox South, 50% original recharge hydraulic head spatial distribution of layer 1

Layer 2

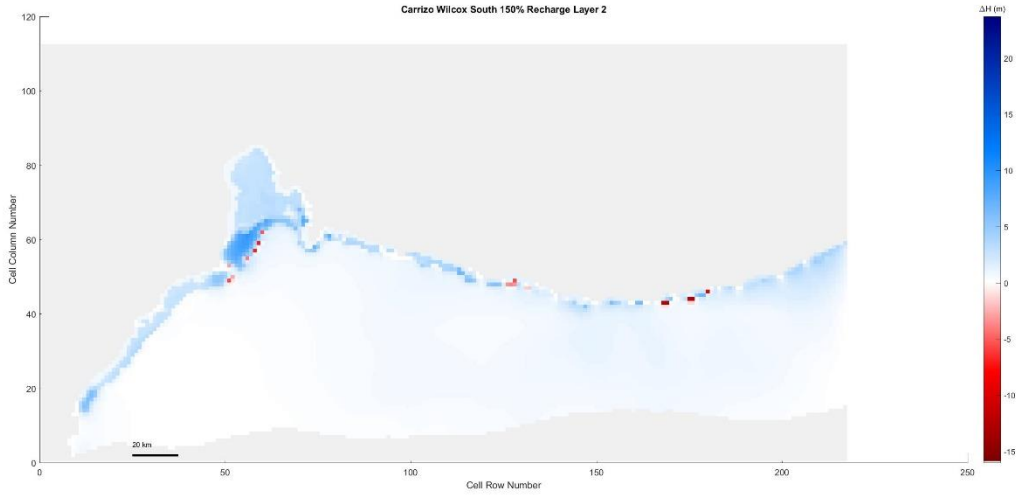

Figure 5. 256 Carrizo-Wilcox South, 150% original recharge hydraulic head spatial distribution of layer 2

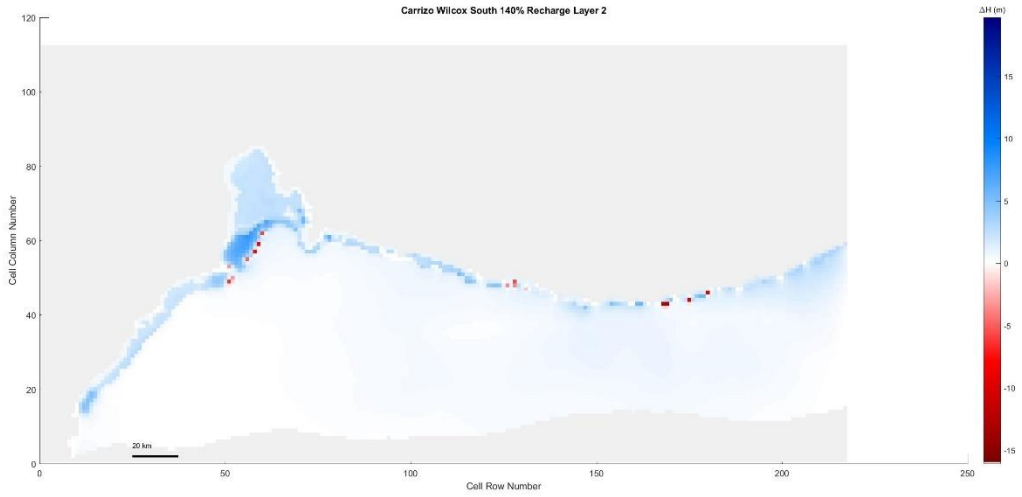

Figure 5. 257 Carrizo-Wilcox South, 140% original recharge hydraulic head spatial distribution of layer 2

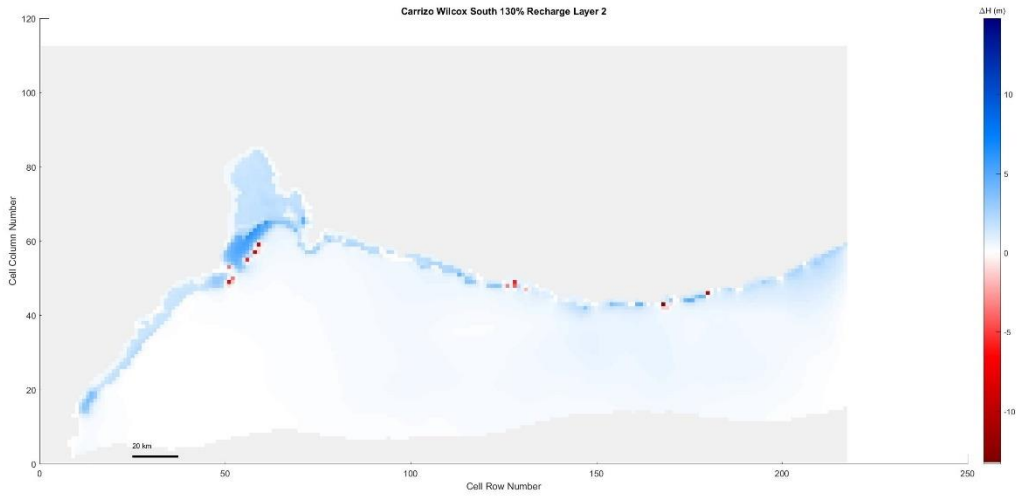

Figure 5. 258 Carrizo-Wilcox South, 130% original recharge hydraulic head spatial distribution of layer 2

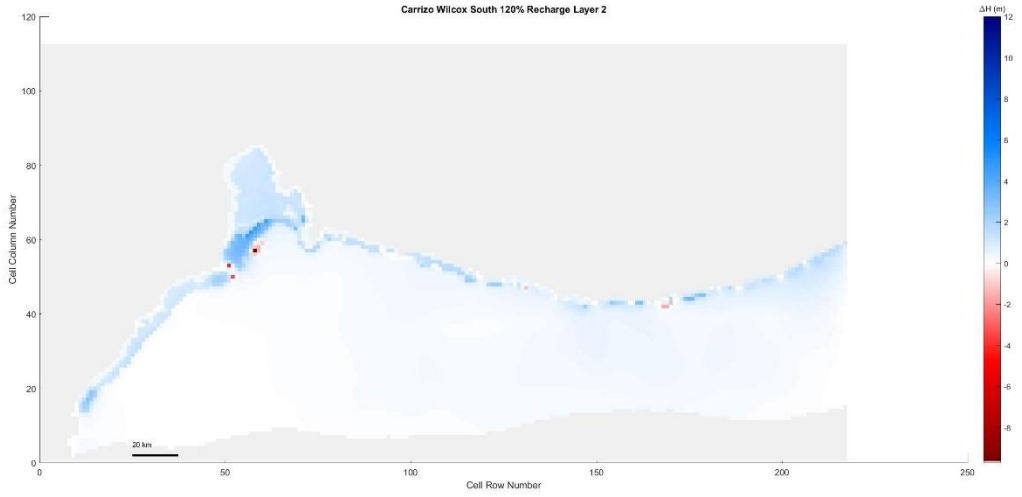

Figure 5. 259 Carrizo-Wilcox South, 120% original recharge hydraulic head spatial distribution of layer 2

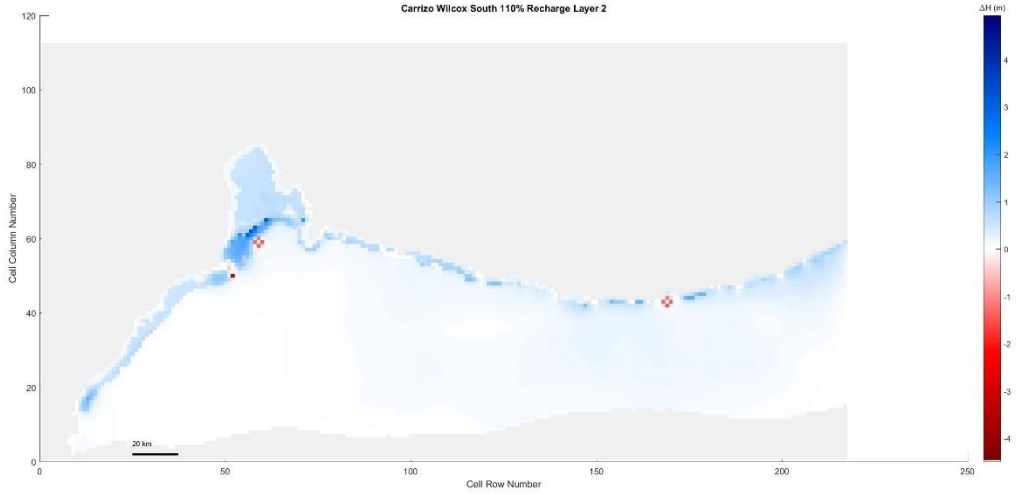

Figure 5. 260 Carrizo-Wilcox South, 110% original recharge hydraulic head spatial distribution of layer 2

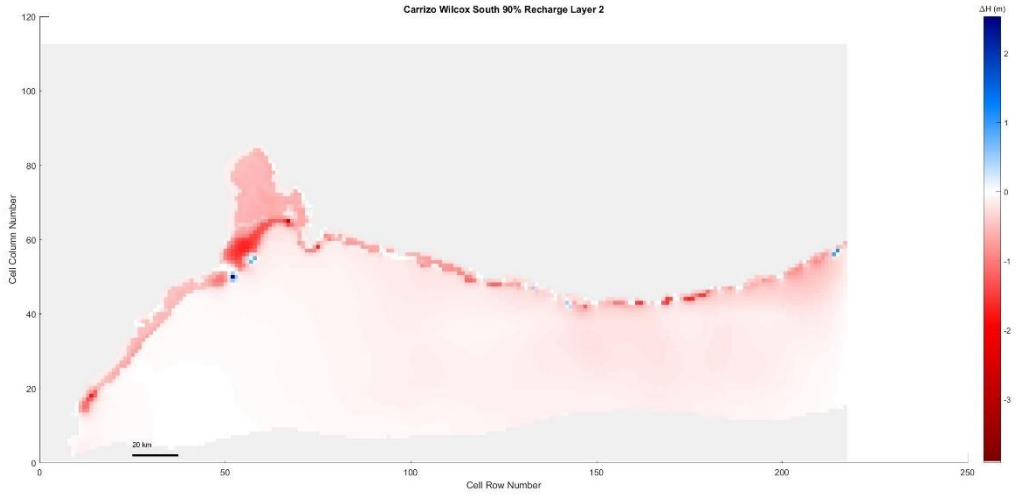

Figure 5. 261 Carrizo-Wilcox South, 90% original recharge hydraulic head spatial distribution of layer 2

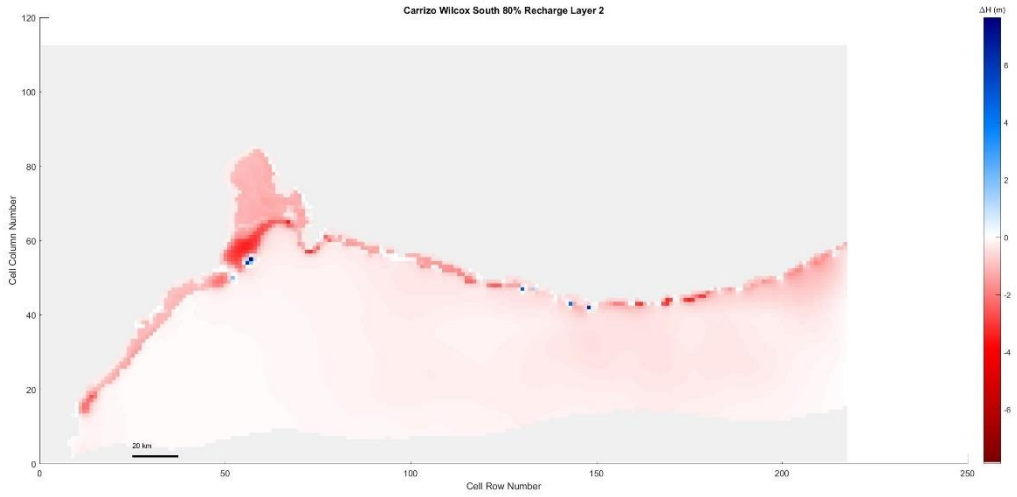

Figure 5. 262 Carrizo-Wilcox South, 80% original recharge hydraulic head spatial distribution of layer 2

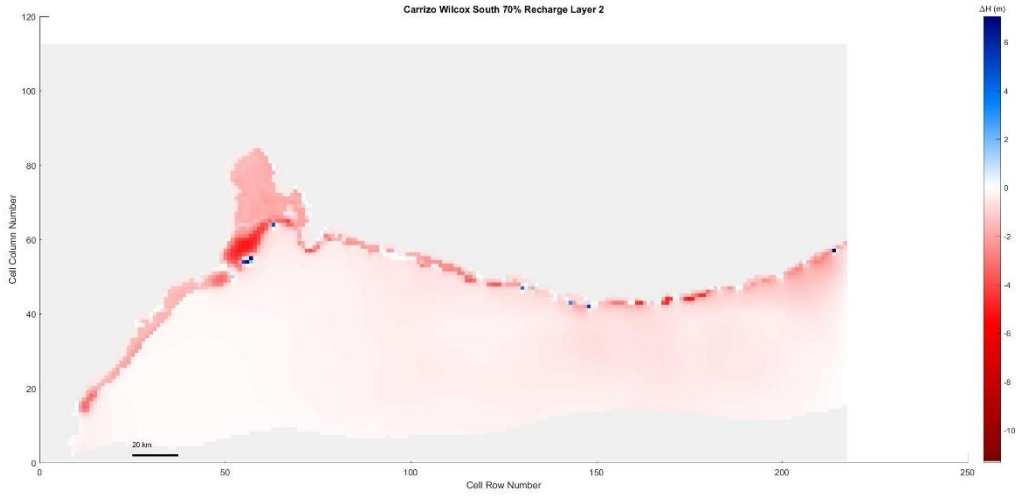

Figure 5. 263 Carrizo-Wilcox South, 70% original recharge hydraulic head spatial distribution of layer 2

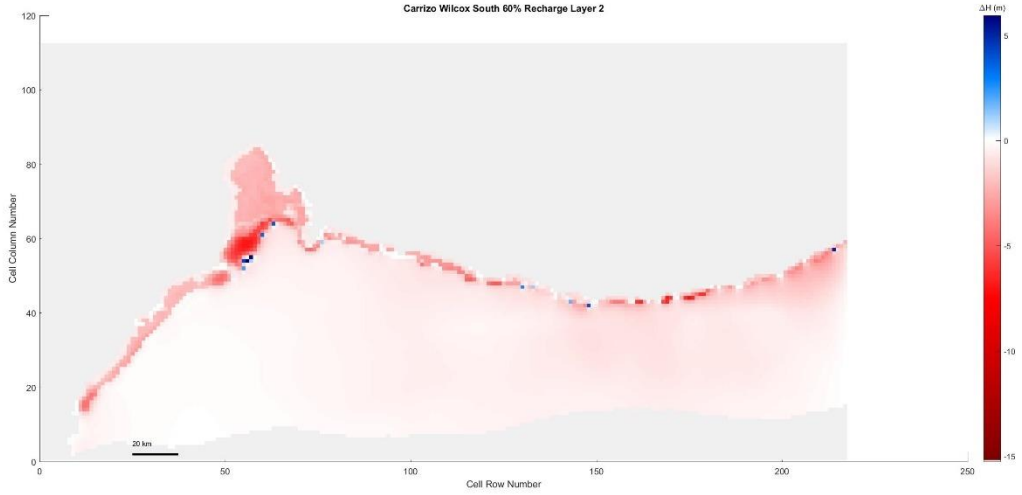

Figure 5. 264 Carrizo-Wilcox South, 60% original recharge hydraulic head spatial distribution of layer 2

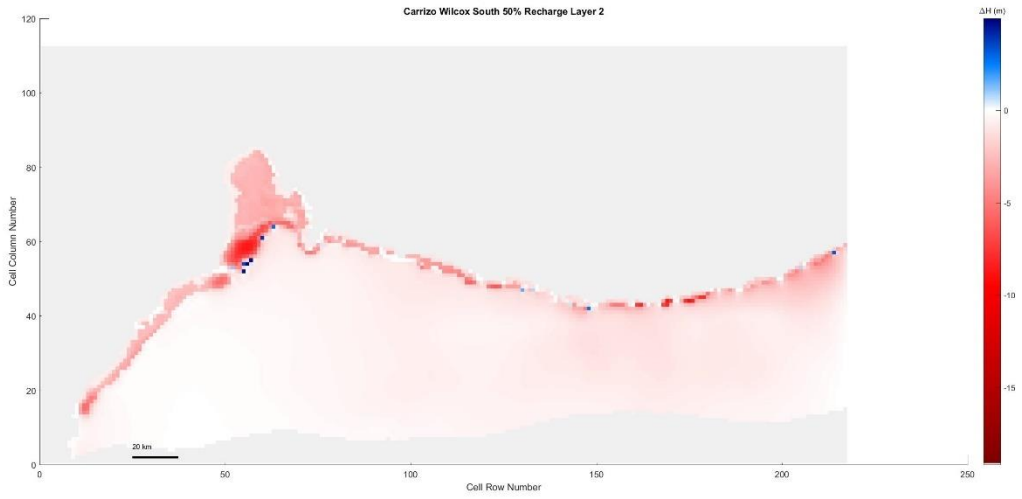

Figure 5. 265 Carrizo-Wilcox South, 50% original recharge hydraulic head spatial distribution of layer 2

Layer 3

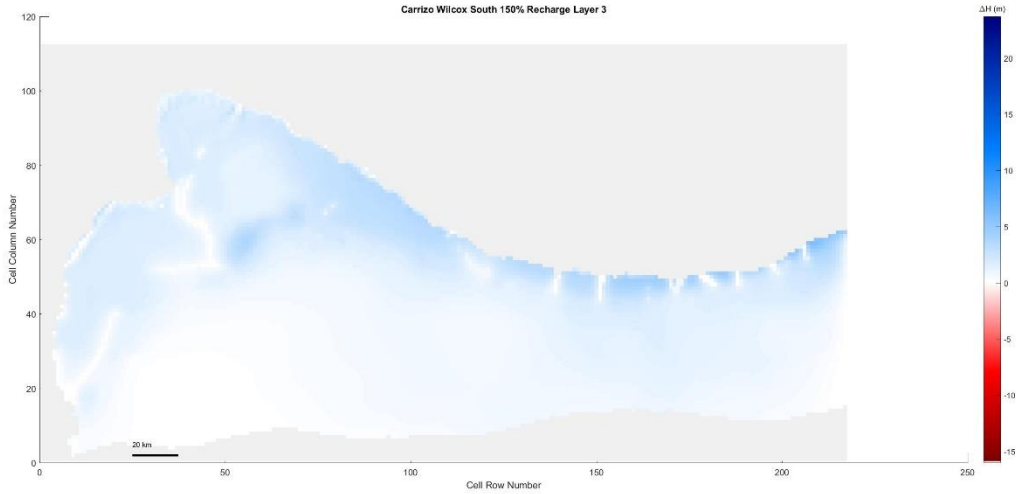

Figure 5. 266 Carrizo-Wilcox South, 150% original recharge hydraulic head spatial distribution of layer 3

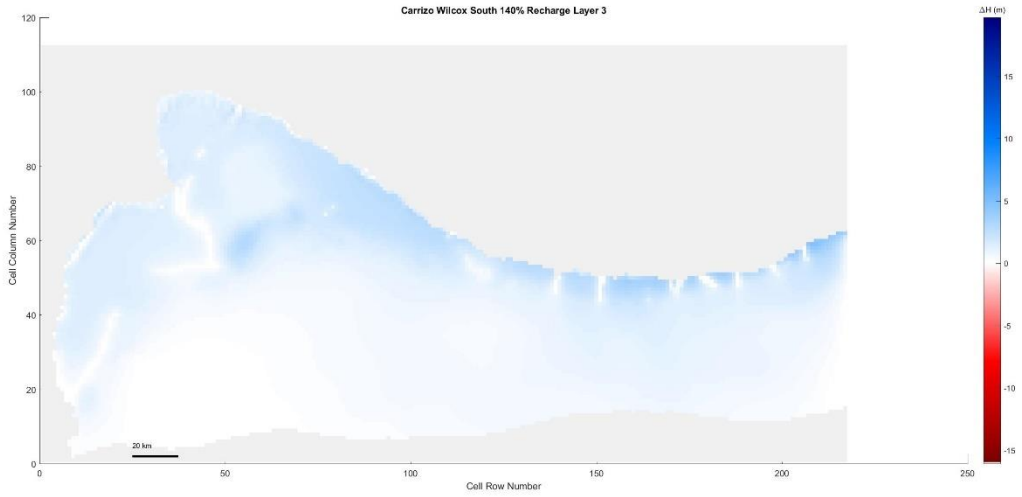

Figure 5. 267 Carrizo-Wilcox South, 140% original recharge hydraulic head spatial distribution of layer 3

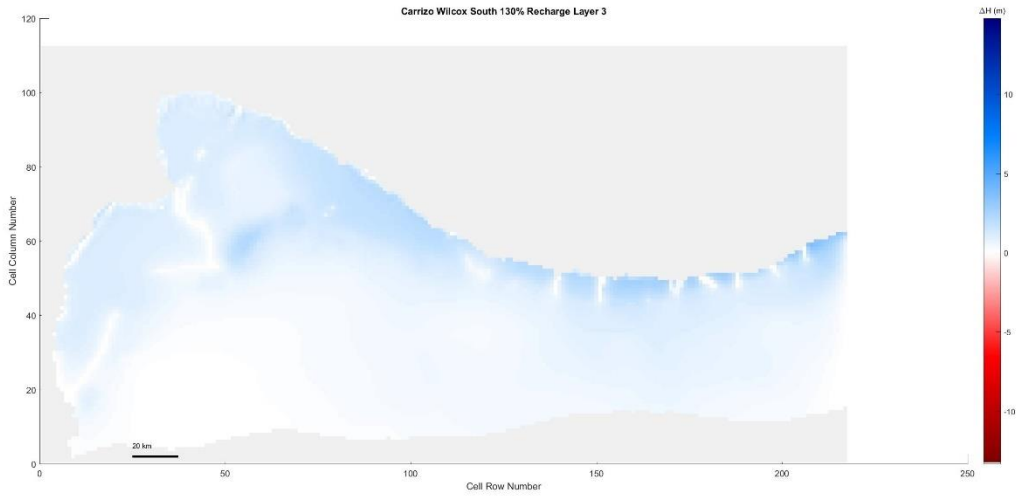

Figure 5. 268 Carrizo-Wilcox South, 130% original recharge hydraulic head spatial distribution of layer 3

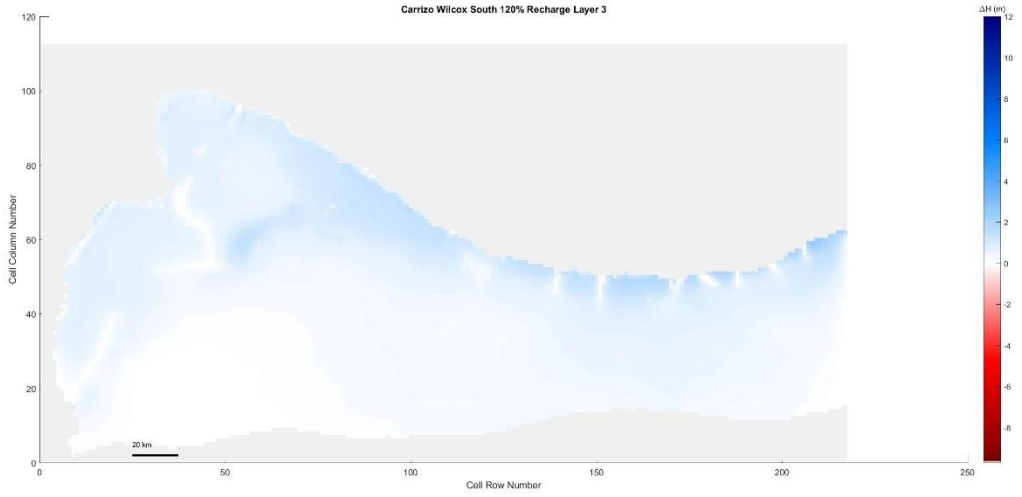

Figure 5. 269 Carrizo-Wilcox South, 120% original recharge hydraulic head spatial distribution of layer 3

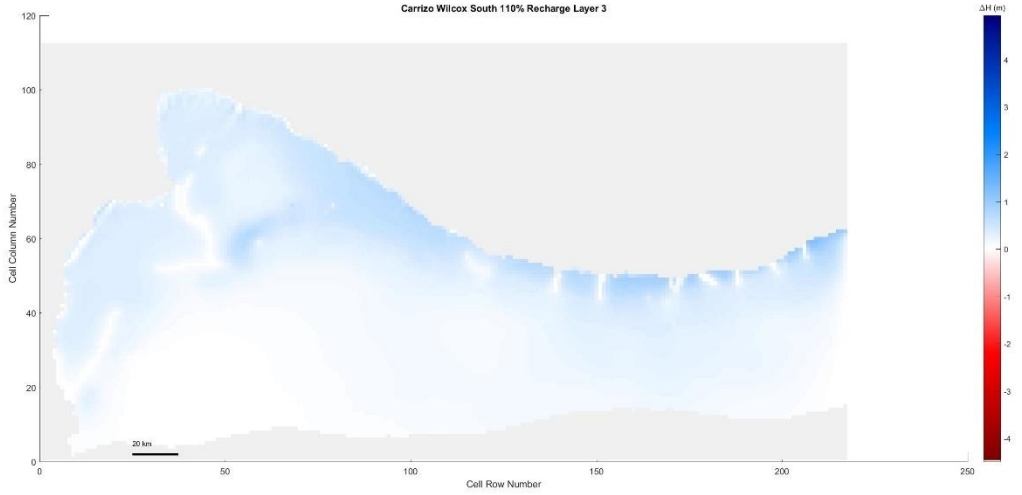

Figure 5. 270 Carrizo-Wilcox South, 110% original recharge hydraulic head spatial distribution of layer 3

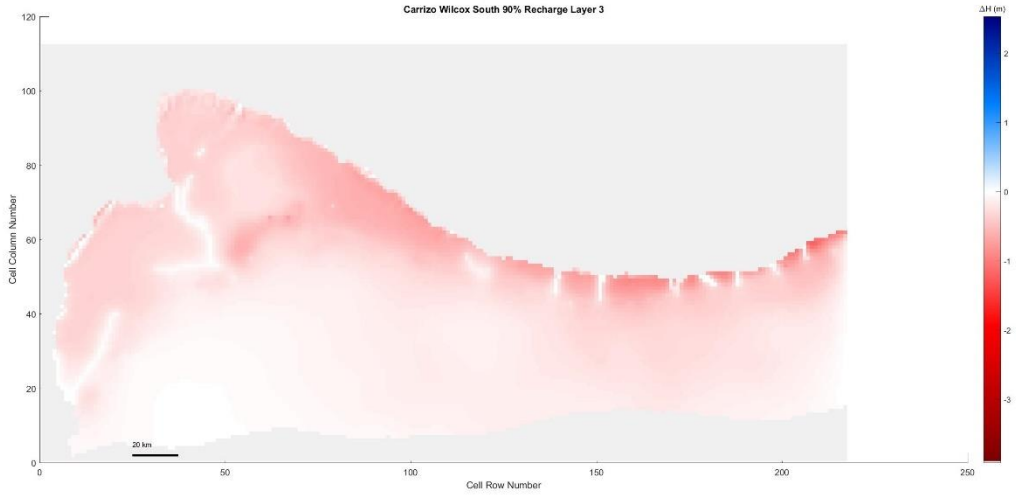

Figure 5. 271 Carrizo-Wilcox South, 90% original recharge hydraulic head spatial distribution of layer 3

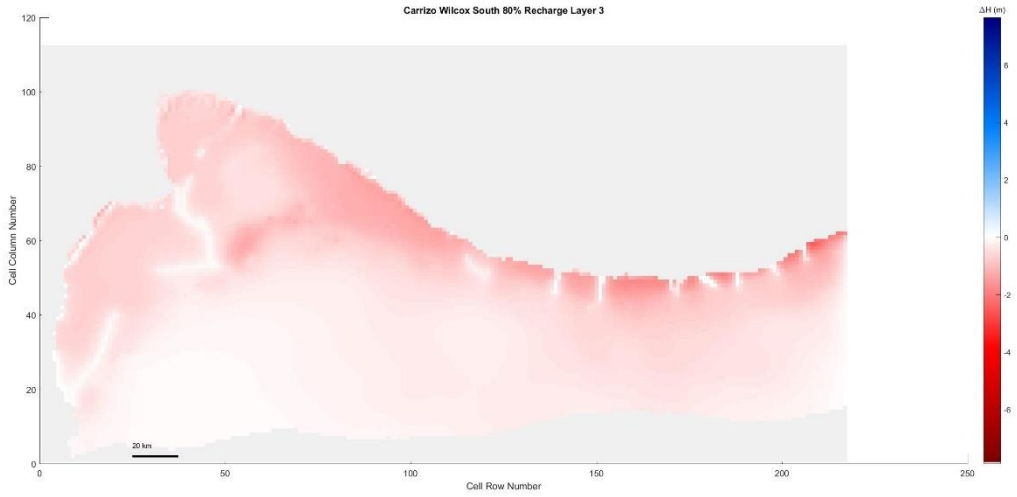

Figure 5. 272 Carrizo-Wilcox South, 80% original recharge hydraulic head spatial distribution of layer 3

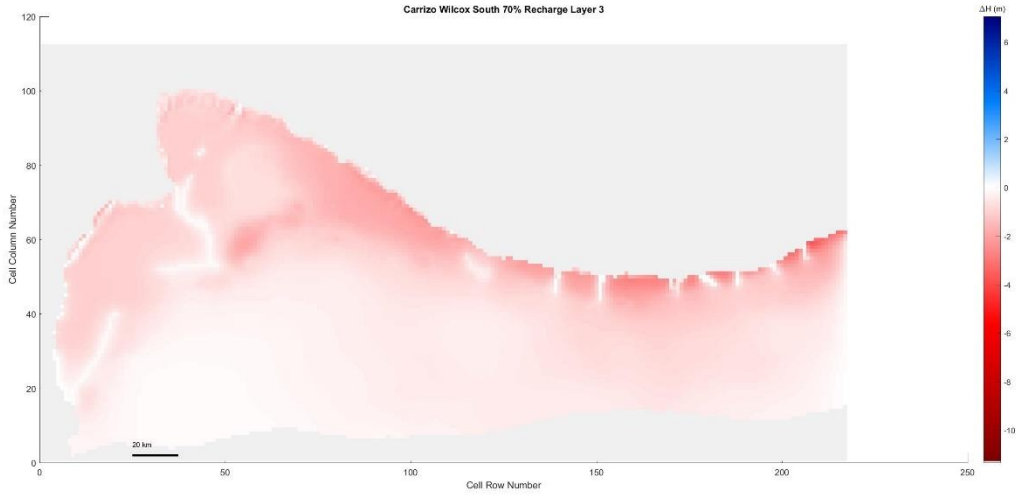

Figure 5. 273 Carrizo-Wilcox South, 70% original recharge hydraulic head spatial distribution of layer 3

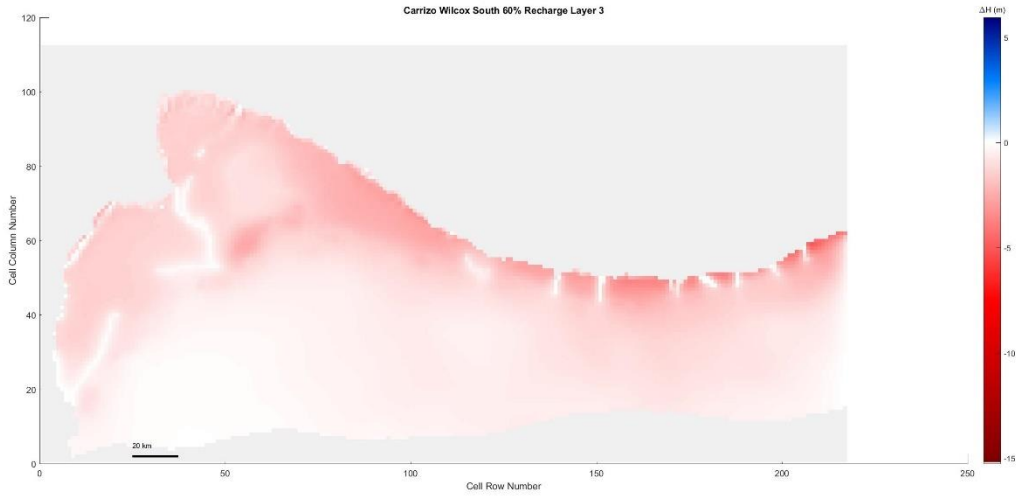

Figure 5. 274 Carrizo-Wilcox South, 60% original recharge hydraulic head spatial distribution of layer 3

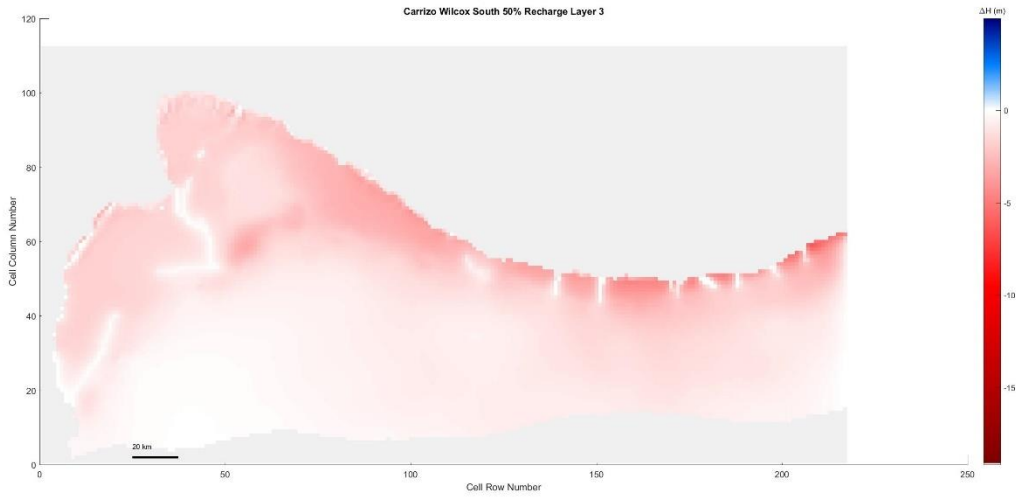

Figure 5. 275 Carrizo-Wilcox South, 50% original recharge hydraulic head spatial distribution of layer 3

Layer 4

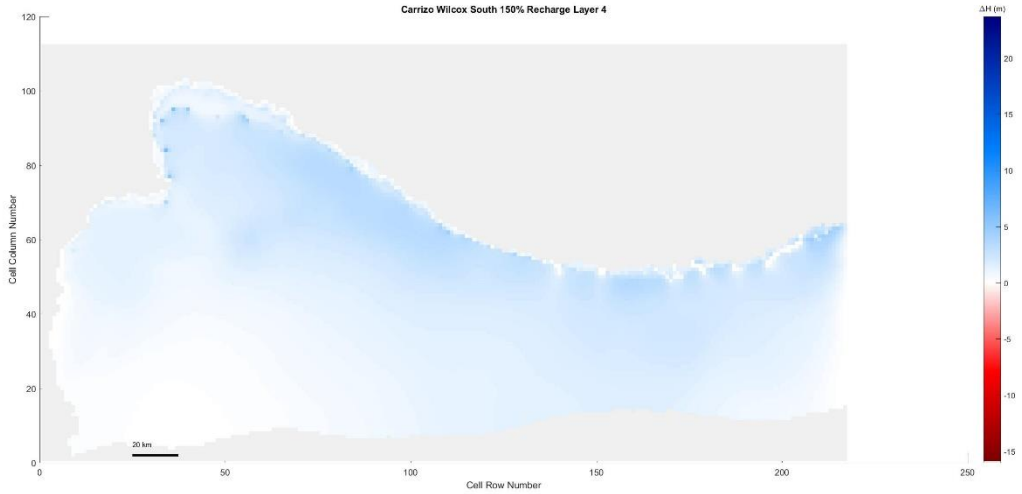

Figure 5. 276 Carrizo-Wilcox South, 150% original recharge hydraulic head spatial distribution of layer 4

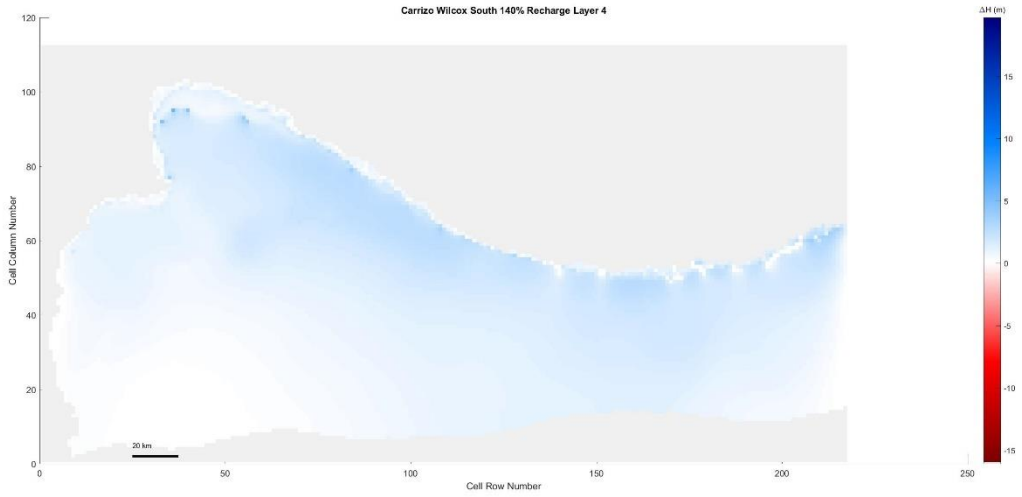

Figure 5. 277 Carrizo-Wilcox South, 140% original recharge hydraulic head spatial distribution of layer 4

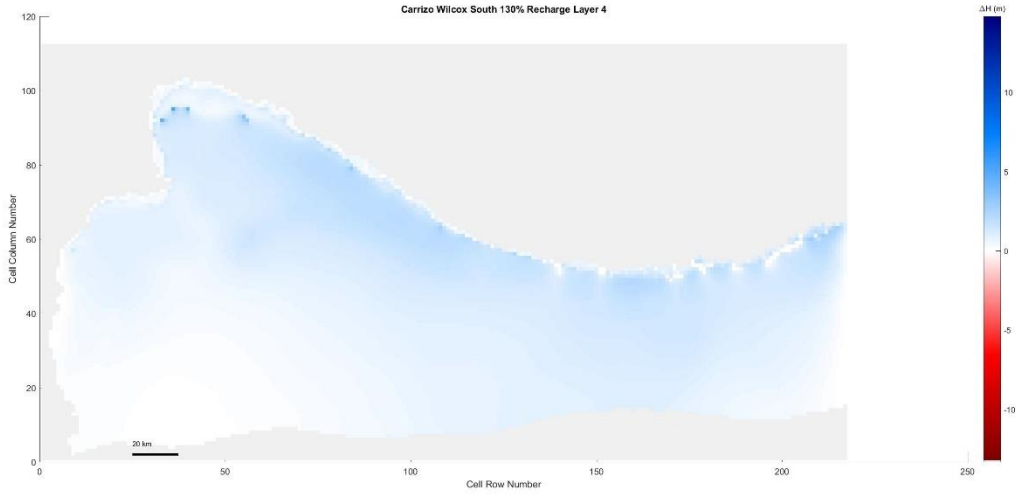

Figure 5. 278 Carrizo-Wilcox South, 130% original recharge hydraulic head spatial distribution of layer 4

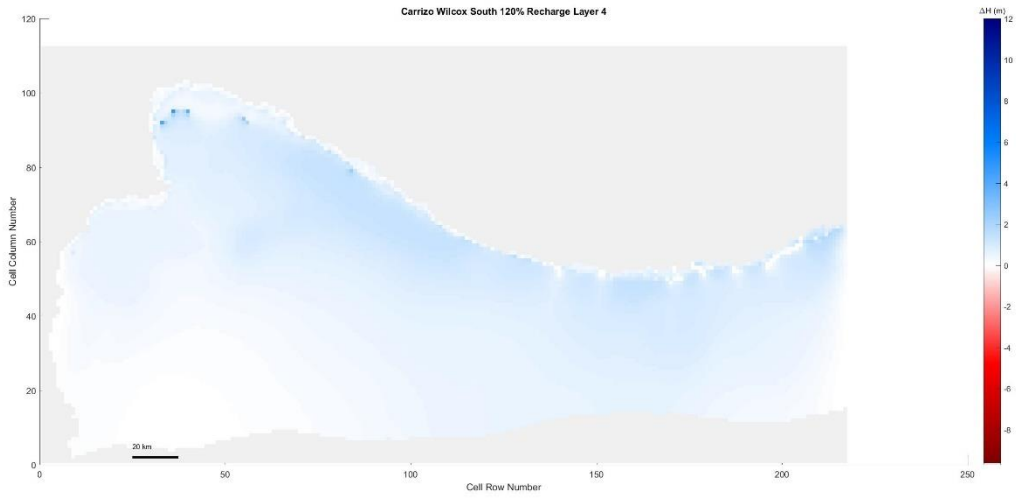

Figure 5. 279 Carrizo-Wilcox South, 120% original recharge hydraulic head spatial distribution of layer 4

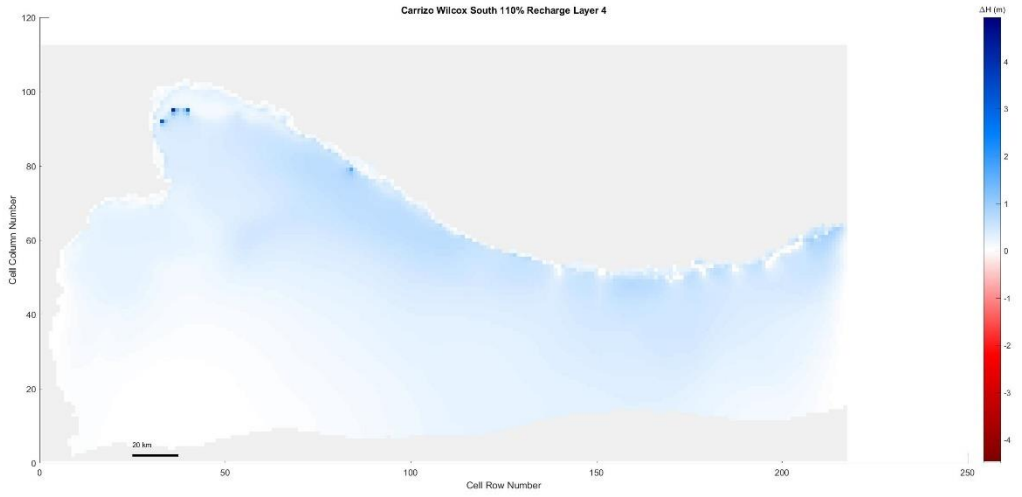

Figure 5. 280 Carrizo-Wilcox South, 110% original recharge hydraulic head spatial distribution of layer 4

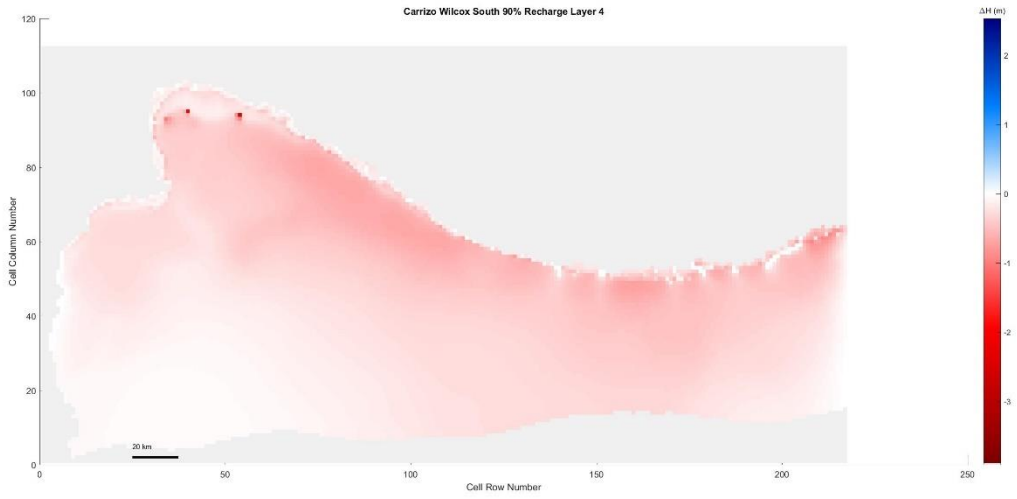

Figure 5. 281 Carrizo-Wilcox South, 90% original recharge hydraulic head spatial distribution of layer 4

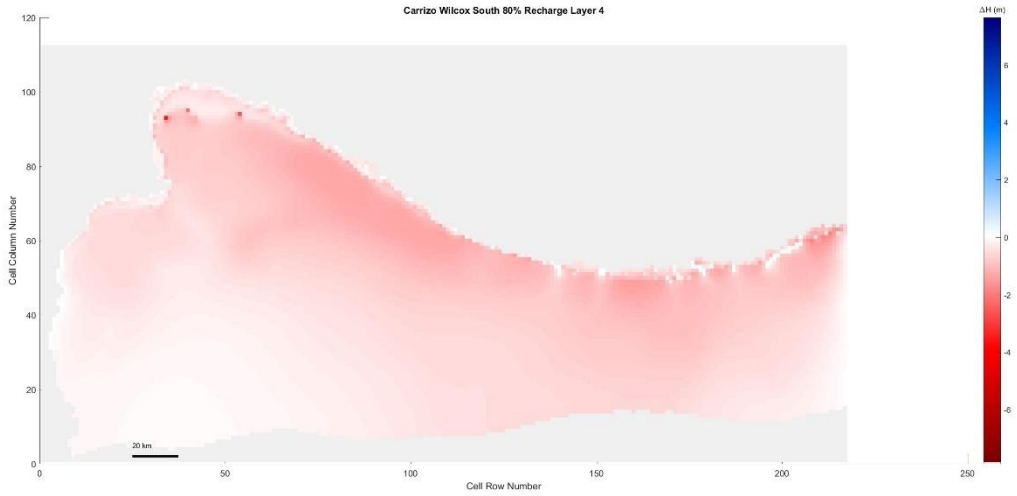

Figure 5. 282 Carrizo-Wilcox South, 80% original recharge hydraulic head spatial distribution of layer 4

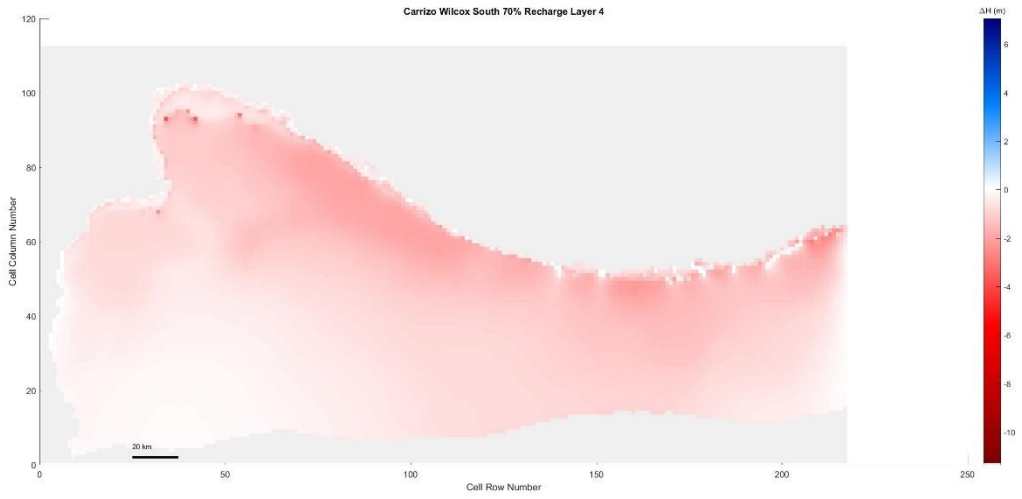

Figure 5. 283 Carrizo-Wilcox South, 70% original recharge hydraulic head spatial distribution of layer 4

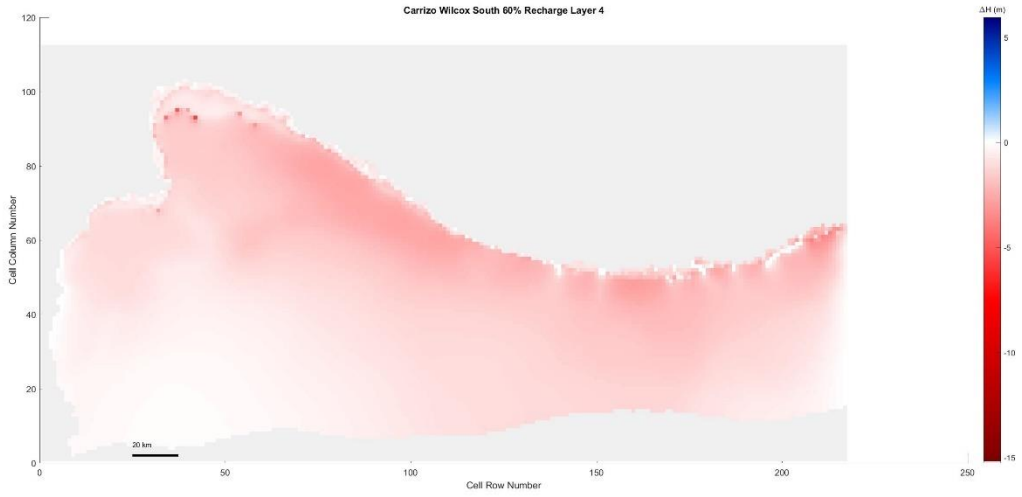

Figure 5. 284 Carrizo-Wilcox South, 60% original recharge hydraulic head spatial distribution of layer 4

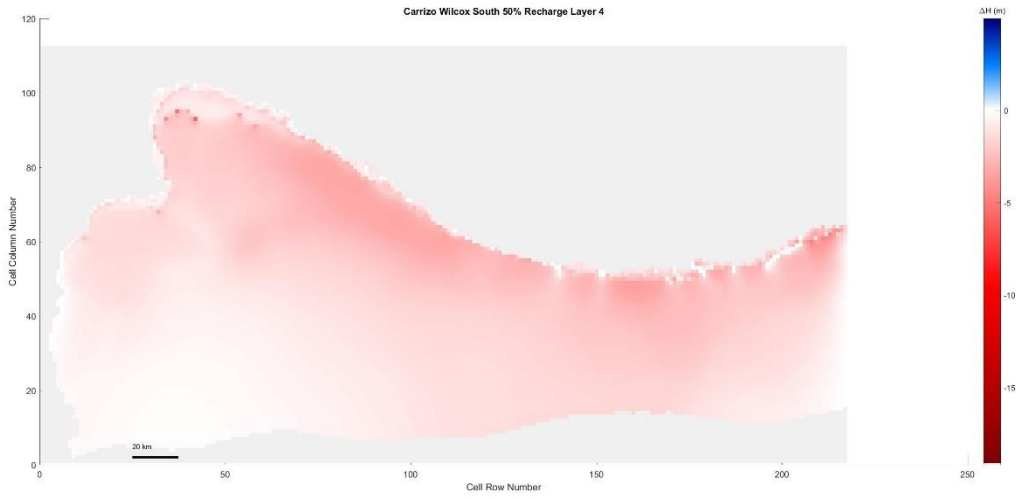

Figure 5. 285 Carrizo-Wilcox South, 50% original recharge hydraulic head spatial distribution of layer 4

Layer 5

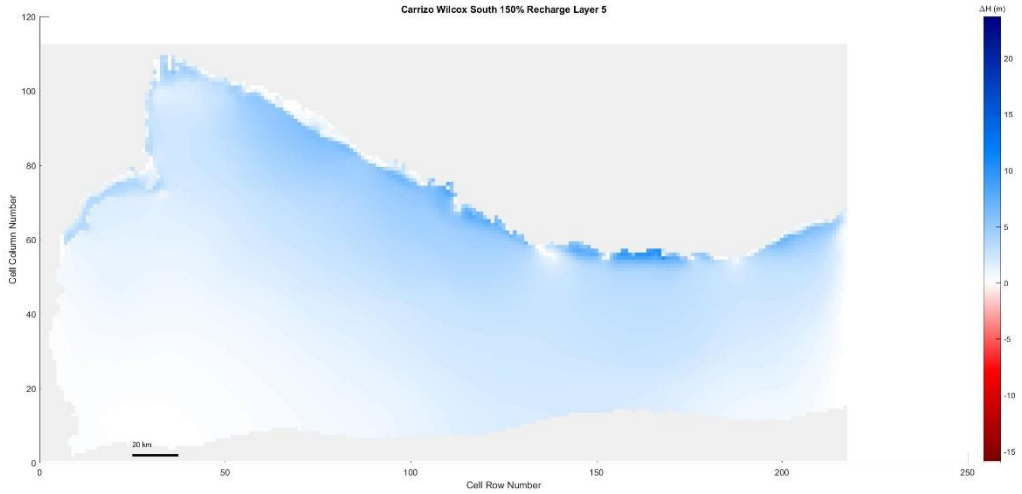

Figure 5. 286 Carrizo-Wilcox South, 150% original recharge hydraulic head spatial distribution of layer 5

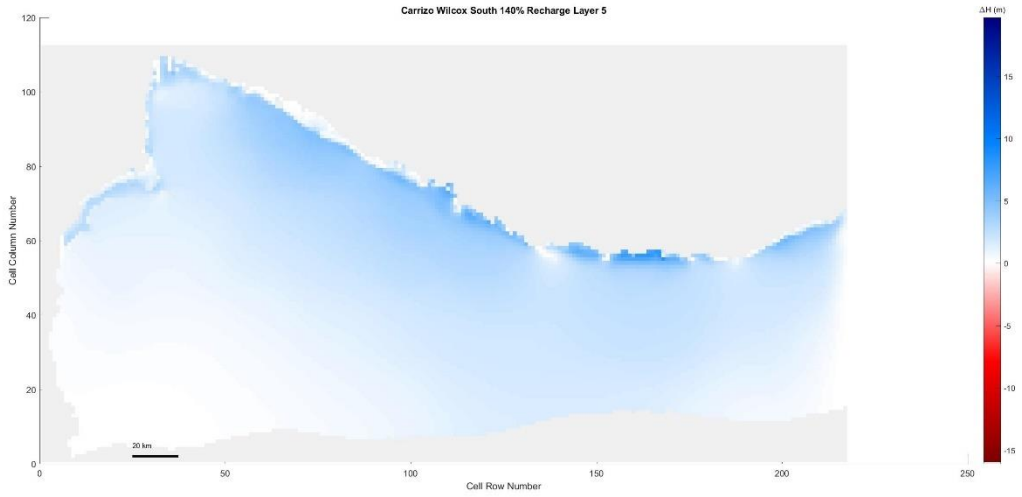

Figure 5. 287 Carrizo-Wilcox South, 140% original recharge hydraulic head spatial distribution of layer 5

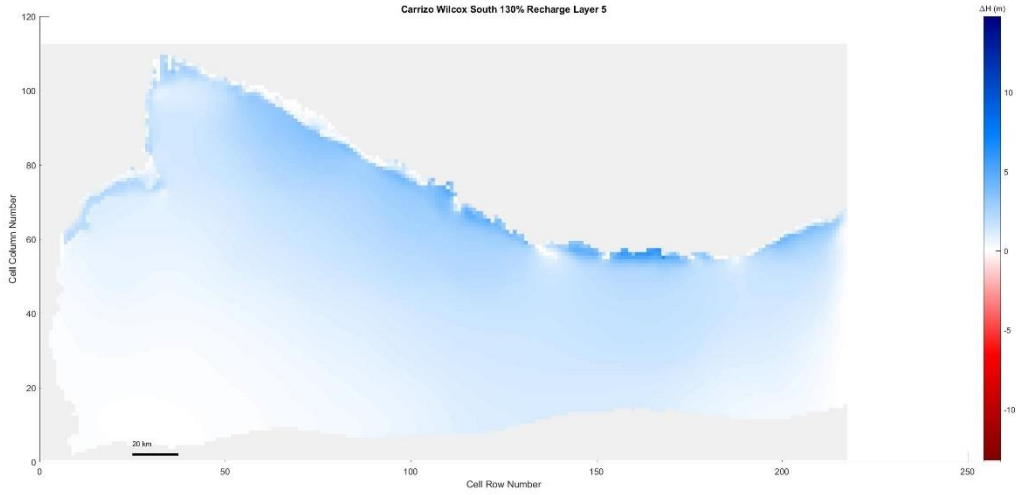

Figure 5. 288 Carrizo-Wilcox South, 130% original recharge hydraulic head spatial distribution of layer 5

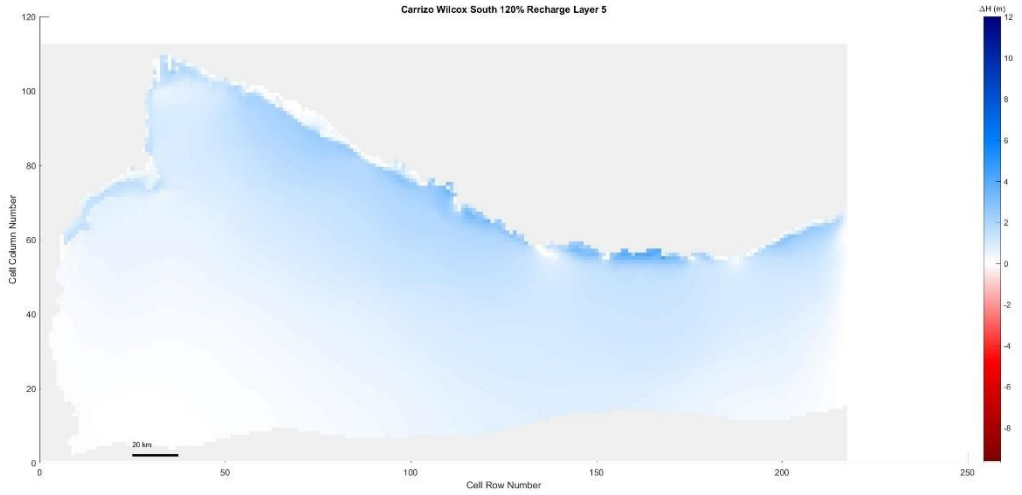

Figure 5. 289 Carrizo-Wilcox South, 120% original recharge hydraulic head spatial distribution of layer 5

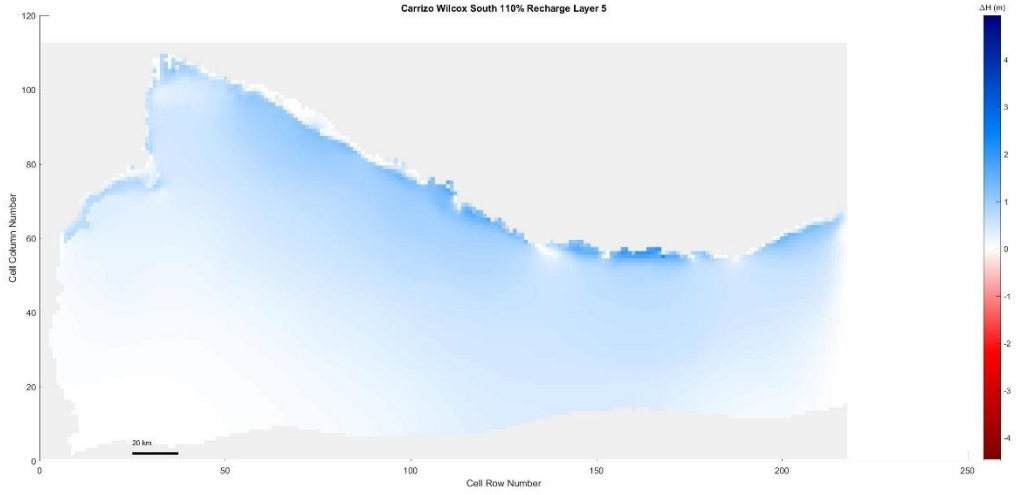

Figure 5. 290 Carrizo-Wilcox South, 110% original recharge hydraulic head spatial distribution of layer 5

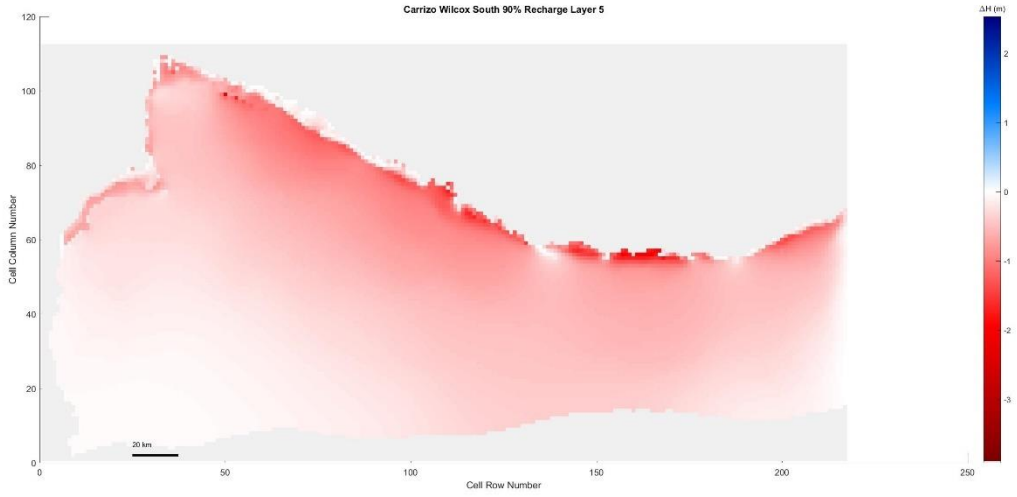

Figure 5. 291 Carrizo-Wilcox South, 90% original recharge hydraulic head spatial distribution of layer 5

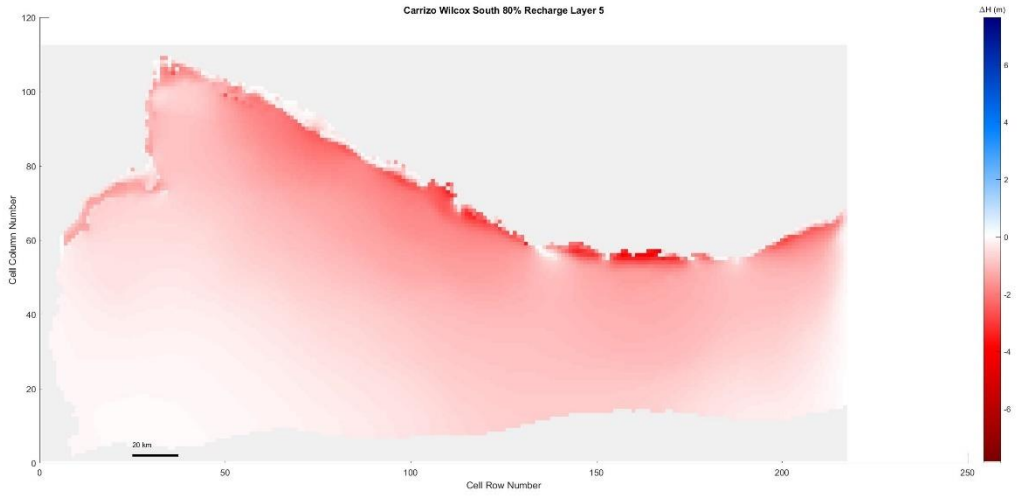

Figure 5. 292 Carrizo-Wilcox South, 80% original recharge hydraulic head spatial distribution of layer 5

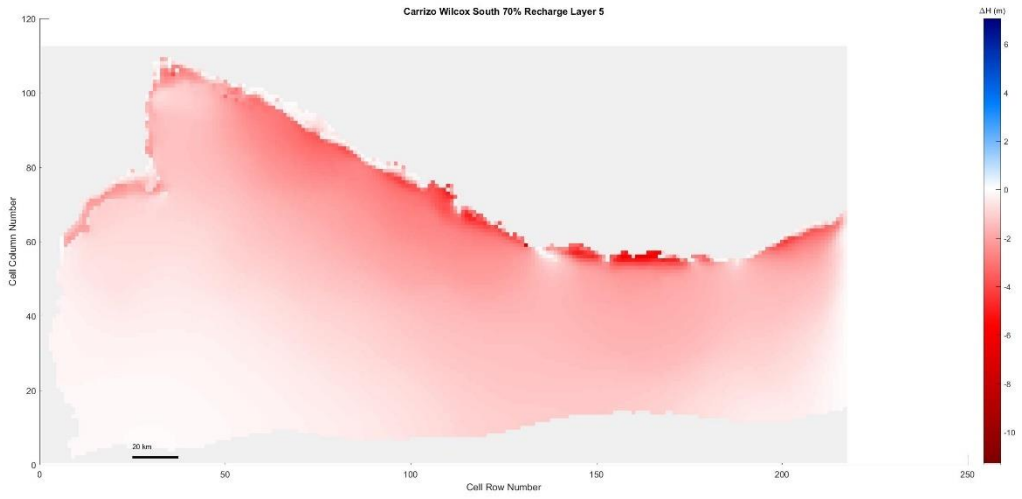

Figure 5. 293 Carrizo-Wilcox South, 70% original recharge hydraulic head spatial distribution of layer 5

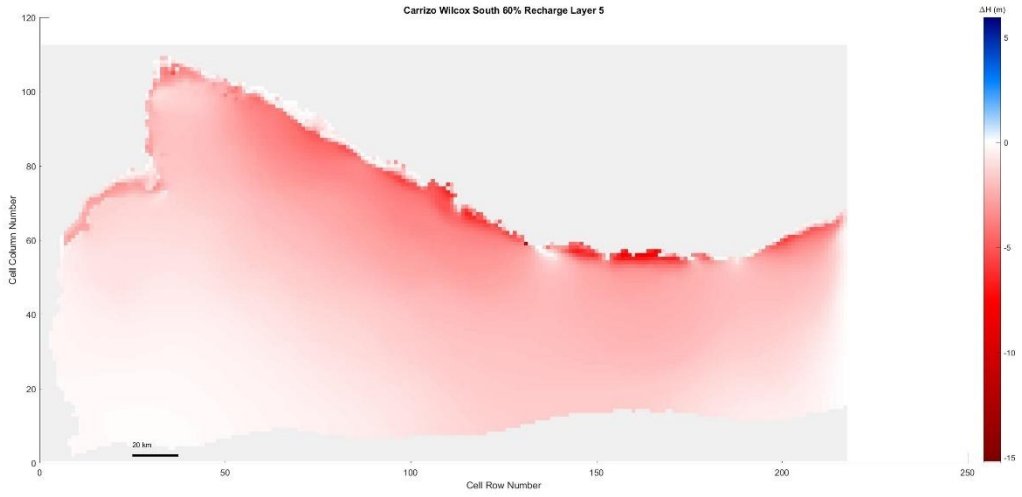

Figure 5. 294 Carrizo-Wilcox South, 60% original recharge hydraulic head spatial distribution of layer 5

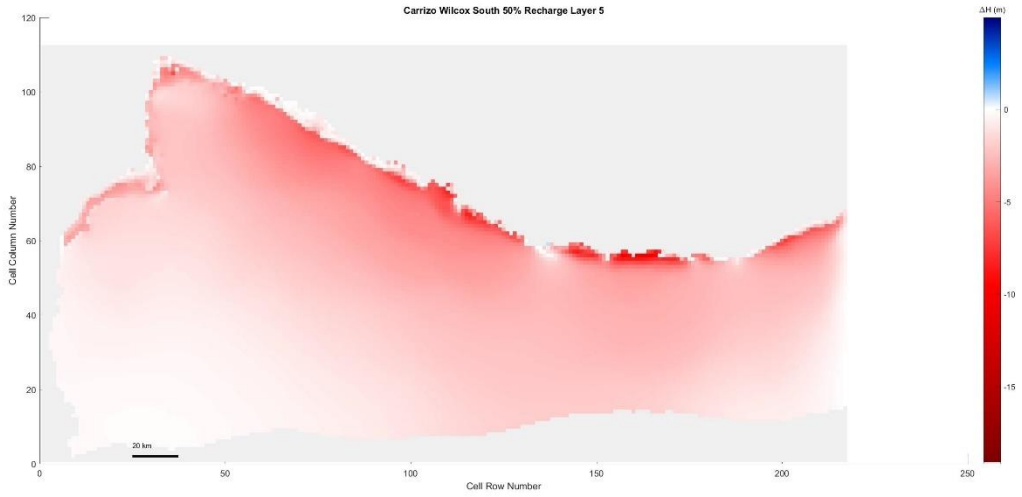

Figure 5. 295 Carrizo-Wilcox South, 50% original recharge hydraulic head spatial distribution of layer 5

Layer 6

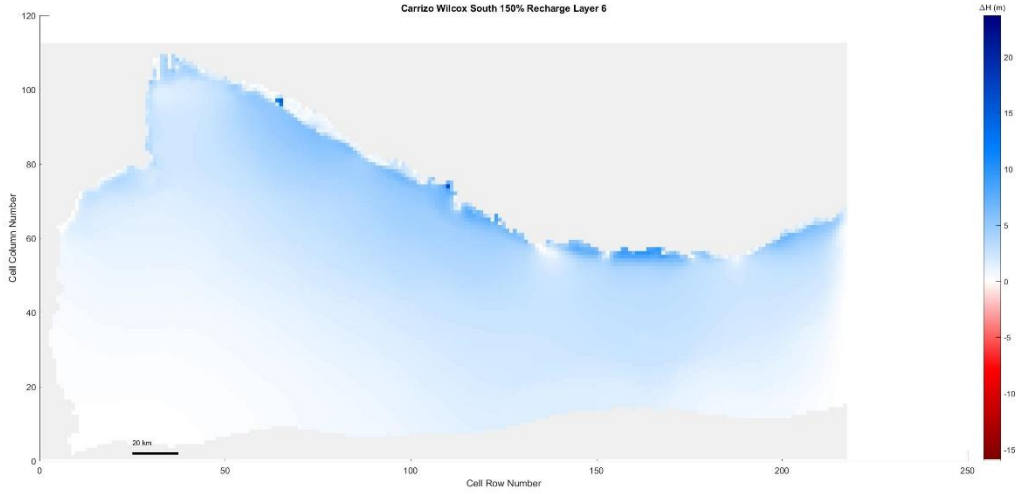

Figure 5. 296 Carrizo-Wilcox South, 150% original recharge hydraulic head spatial distribution of layer 6

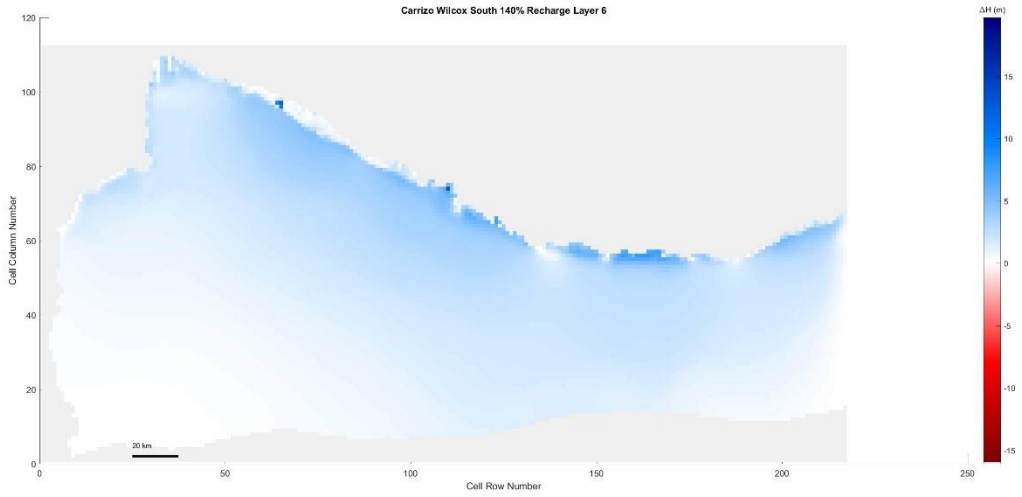

Figure 5. 297 Carrizo-Wilcox South, 140% original recharge hydraulic head spatial distribution of layer 6

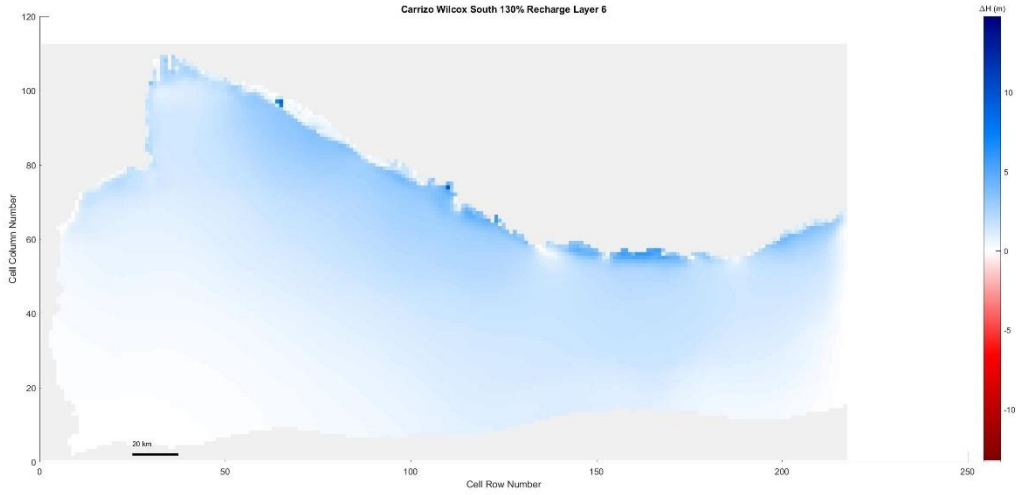

Figure 5. 298 Carrizo-Wilcox South, 130% original recharge hydraulic head spatial distribution of layer 6

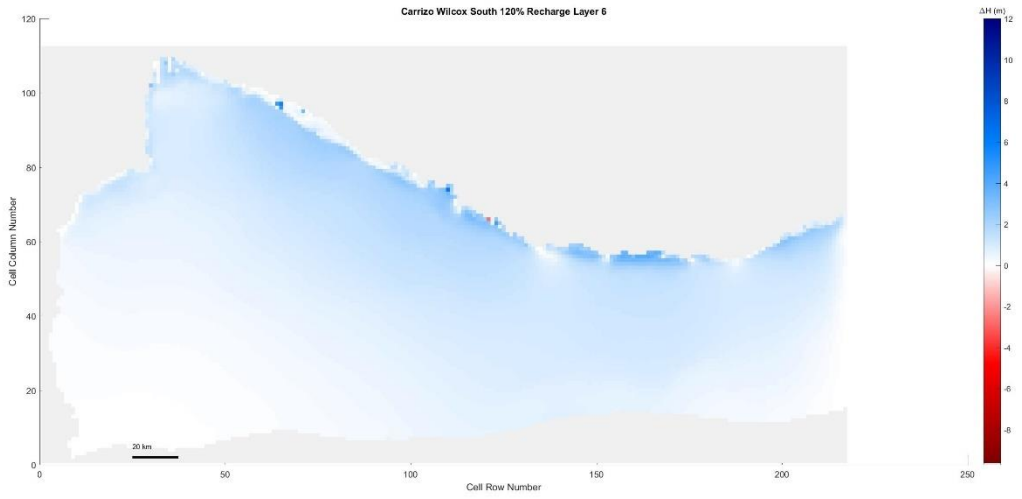

Figure 5. 299 Carrizo-Wilcox South, 120% original recharge hydraulic head spatial distribution of layer 6

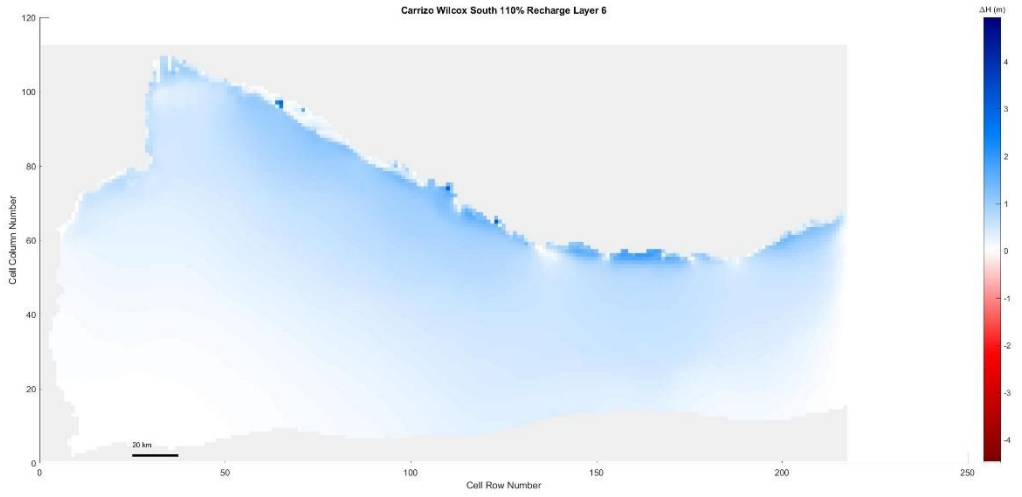

Figure 5. 300 Carrizo-Wilcox South, 110% original recharge hydraulic head spatial distribution of layer 6

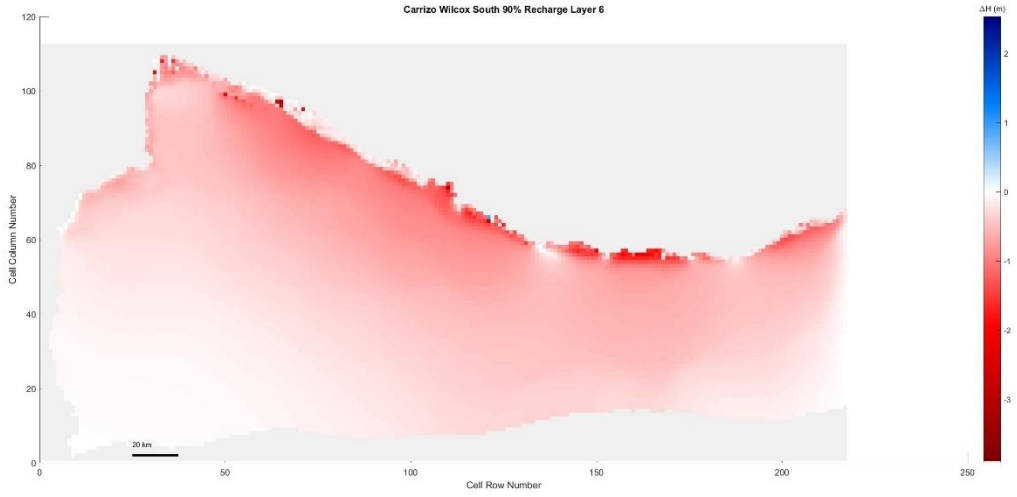

Figure 5. 301 Carrizo-Wilcox South, 90% original recharge hydraulic head spatial distribution of layer 6

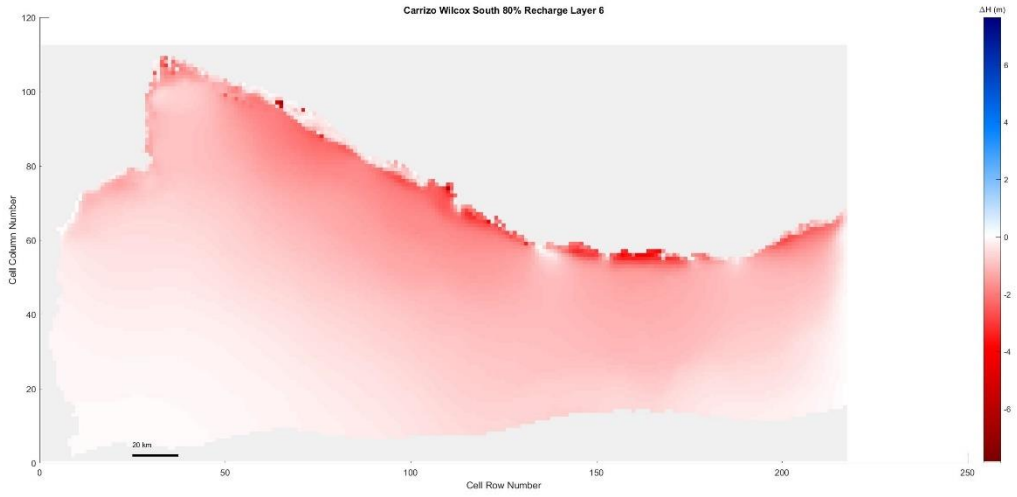

Figure 5. 302 Carrizo-Wilcox South, 80% original recharge hydraulic head spatial distribution of layer 6

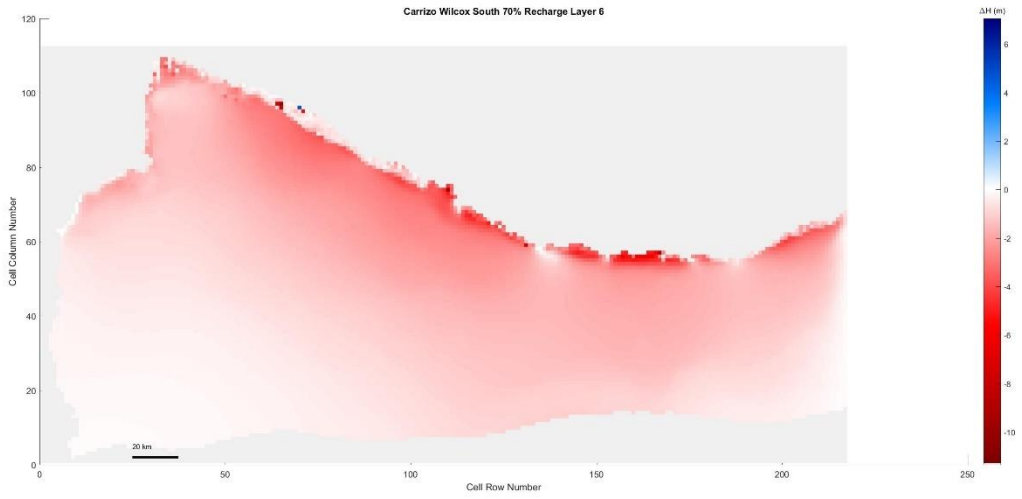

Figure 5. 303 Carrizo-Wilcox South, 70% original recharge hydraulic head spatial distribution of layer 6

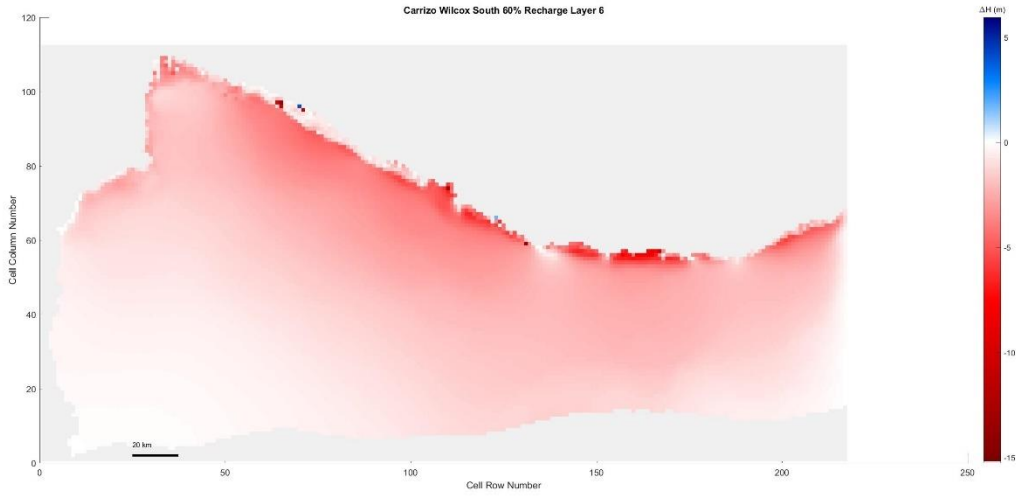

Figure 5. 304 Carrizo-Wilcox South, 60% original recharge hydraulic head spatial distribution of layer 6

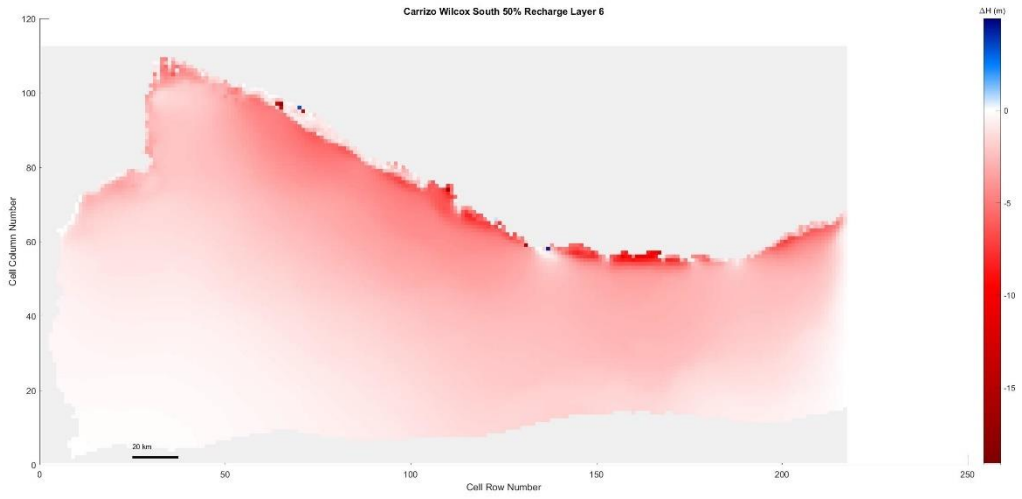

Figure 5. 305 Carrizo-Wilcox South, 50% original recharge hydraulic head spatial distribution of layer 6

Layer 7

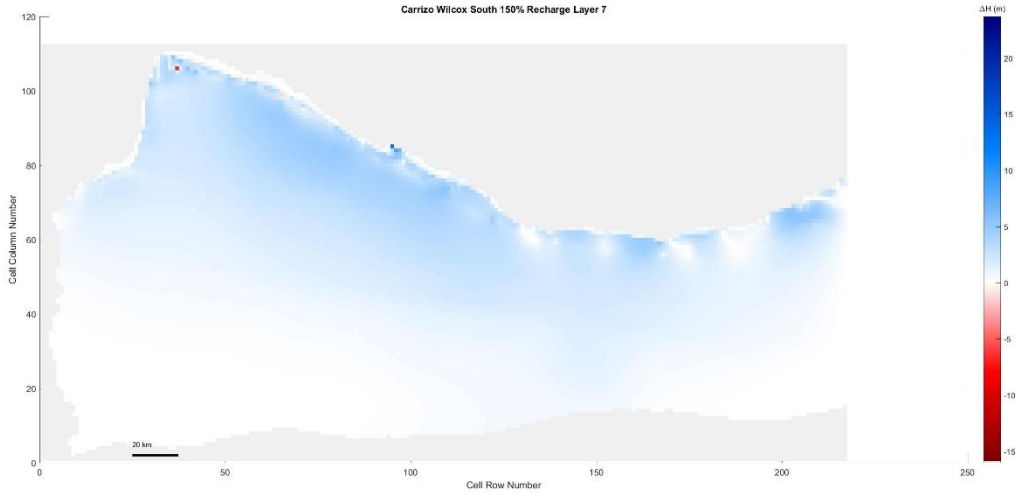

Figure 5. 306 Carrizo-Wilcox South, 150% original recharge hydraulic head spatial distribution of layer 7

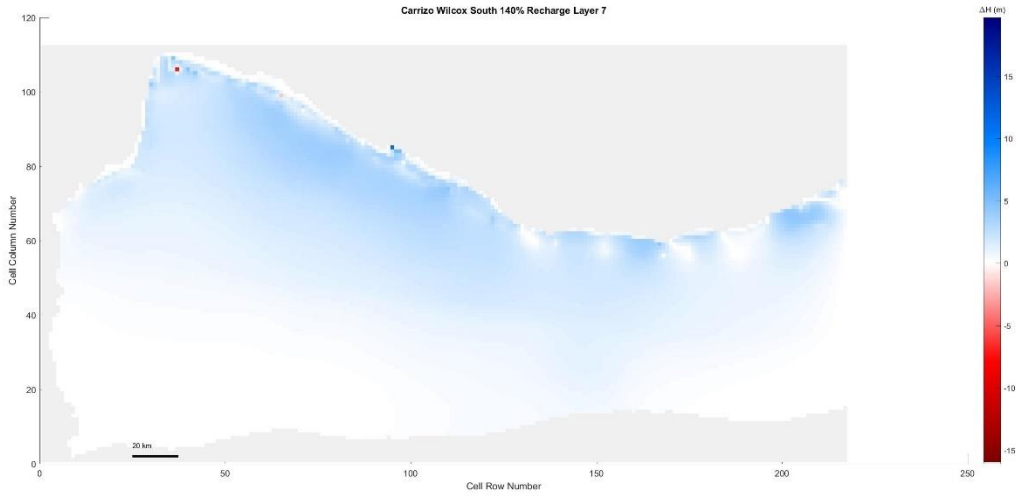

Figure 5. 307 Carrizo-Wilcox South, 140% original recharge hydraulic head spatial distribution of layer 7

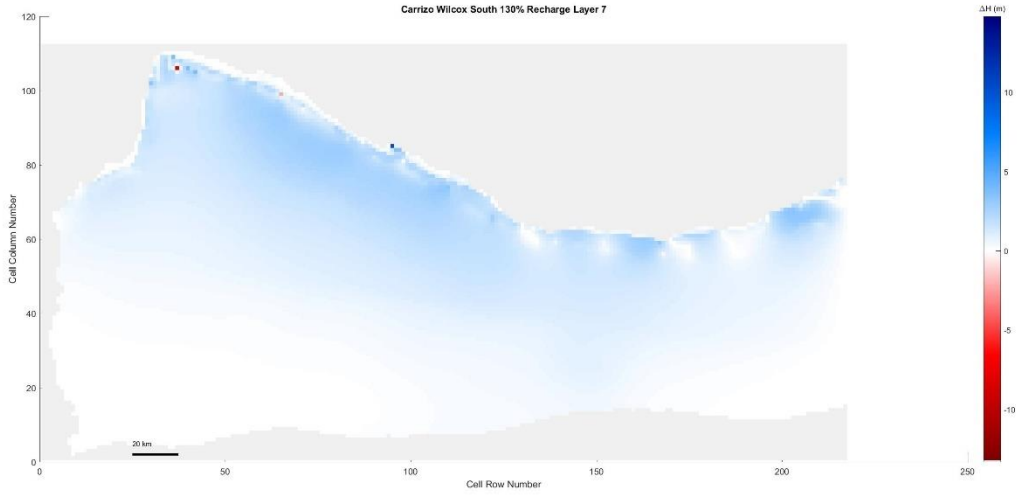

Figure 5. 308 Carrizo-Wilcox South, 130% original recharge hydraulic head spatial distribution of layer 7

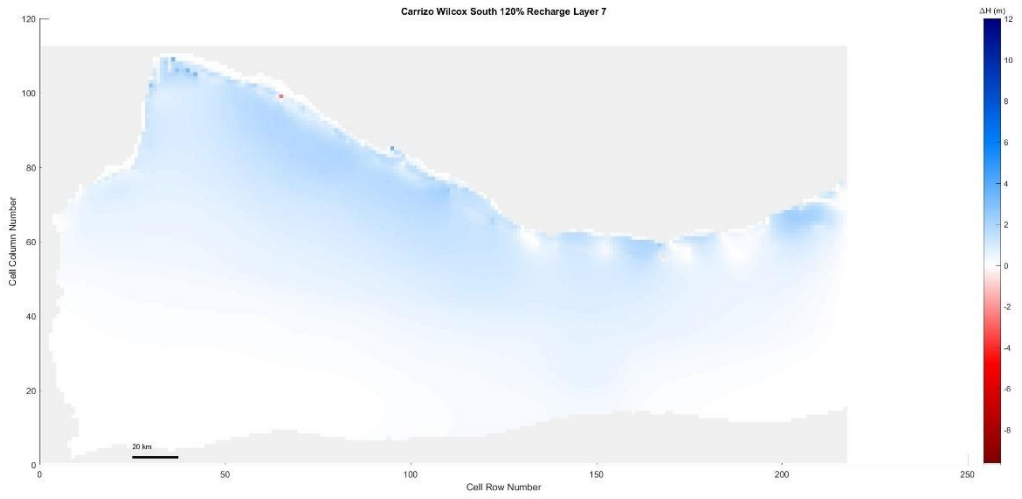

Figure 5. 309 Carrizo-Wilcox South, 120% original recharge hydraulic head spatial distribution of layer 7

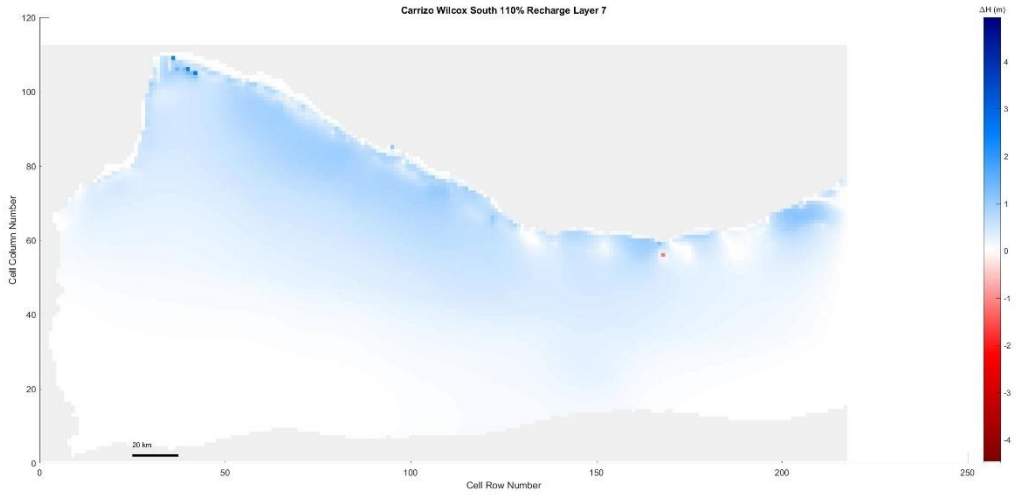

Figure 5. 310 Carrizo-Wilcox South, 110% original recharge hydraulic head spatial distribution of layer 7

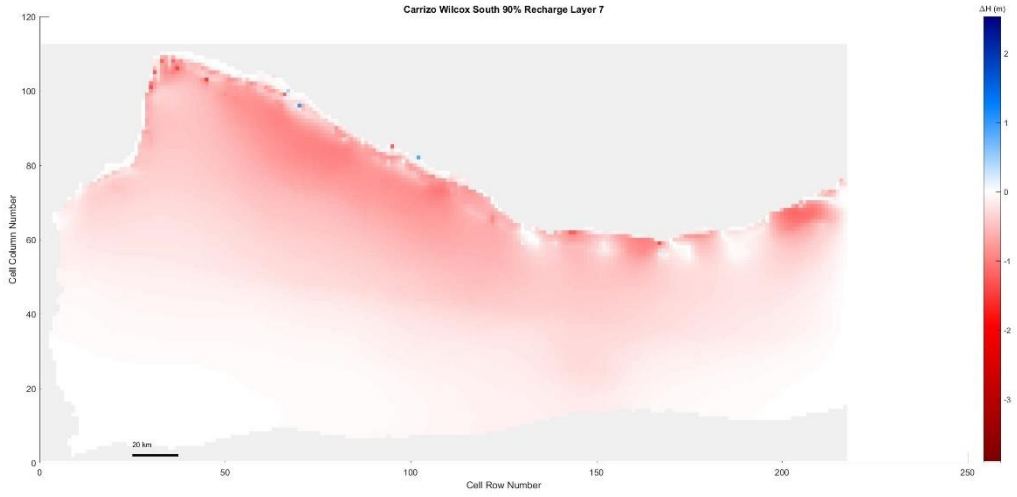

Figure 5. 311 Carrizo-Wilcox South, 90% original recharge hydraulic head spatial distribution of layer 7

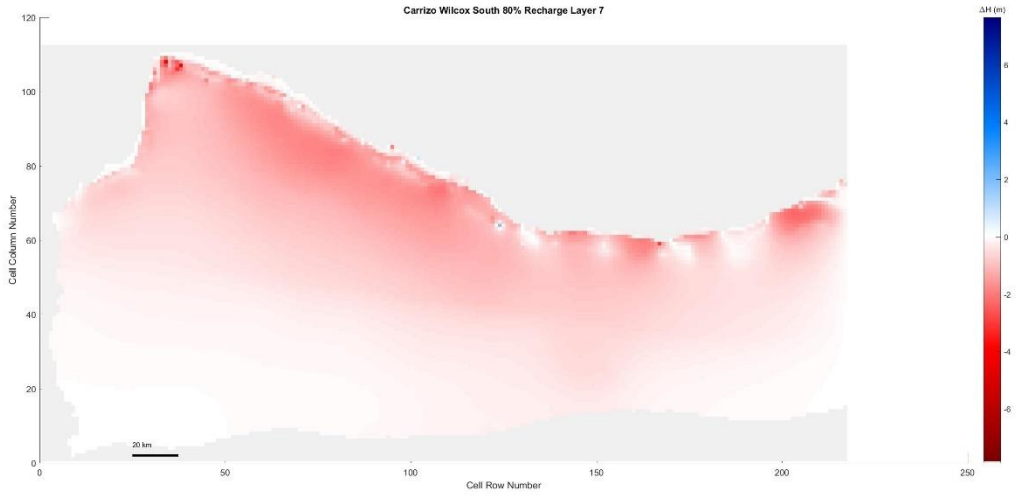

Figure 5. 312 Carrizo-Wilcox South, 80% original recharge hydraulic head spatial distribution of layer 7

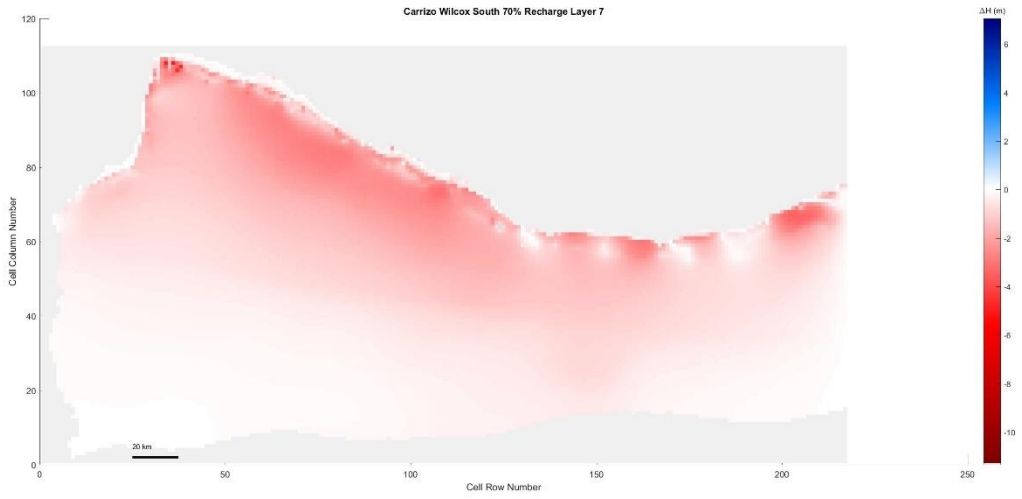

Figure 5. 313 Carrizo-Wilcox South, 70% original recharge hydraulic head spatial distribution of layer 7

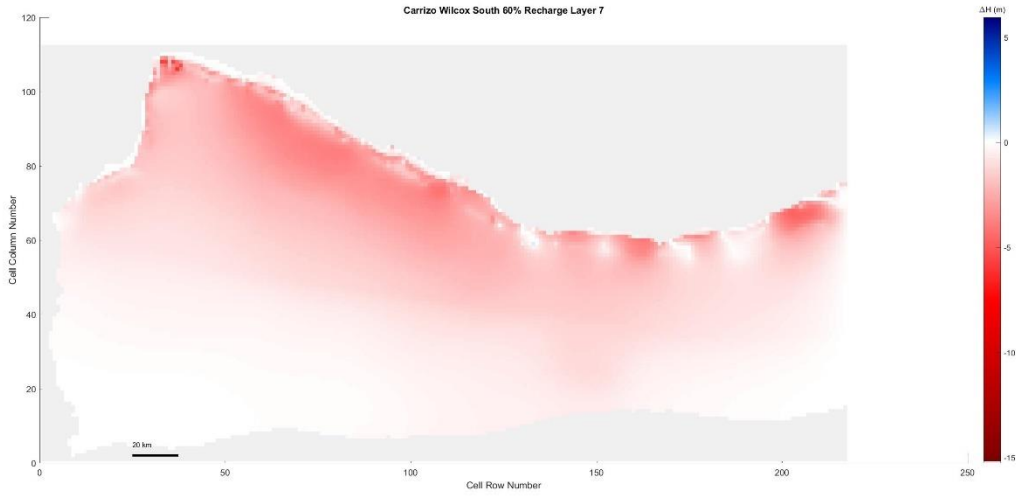

Figure 5. 314 Carrizo-Wilcox South, 60% original recharge hydraulic head spatial distribution of layer 7

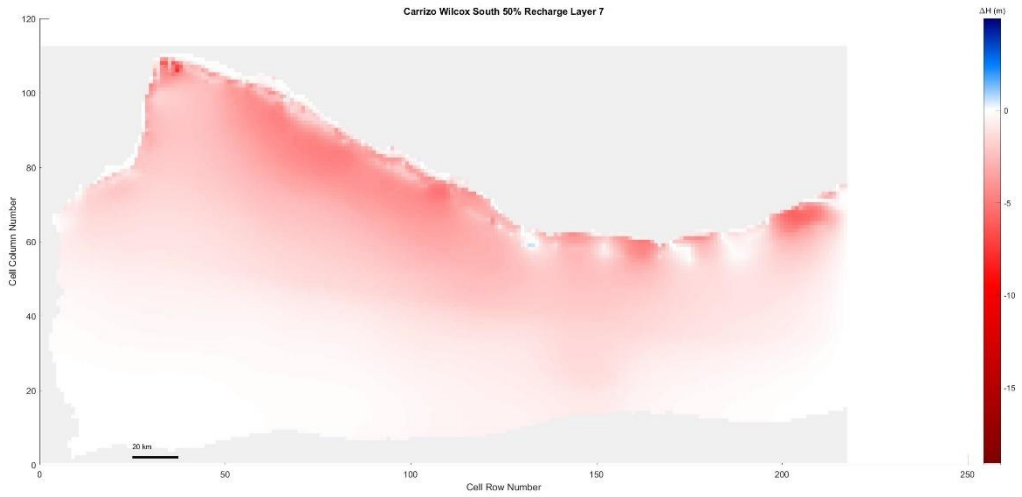

Figure 5. 315 Carrizo-Wilcox South, 50% original recharge hydraulic head spatial distribution of layer 7

Layer 8

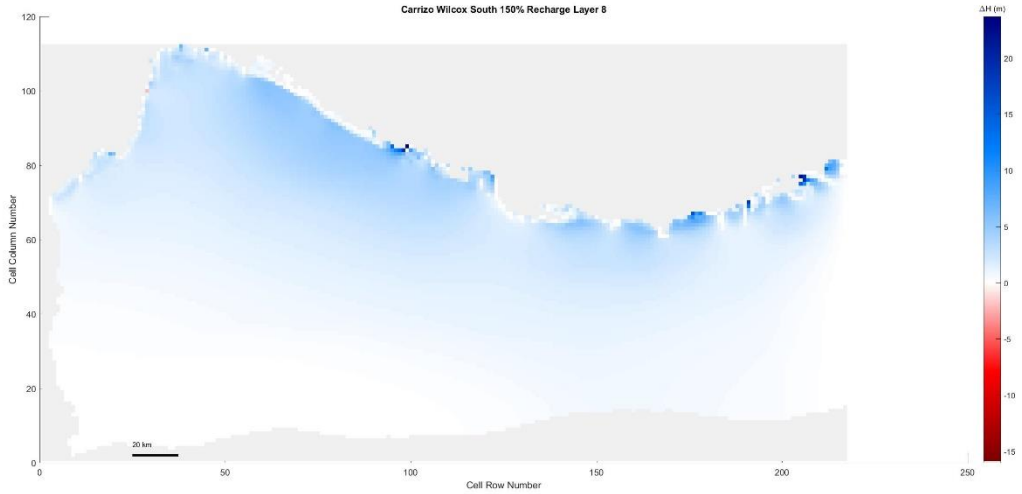

Figure 5. 316 Carrizo-Wilcox South, 150% original recharge hydraulic head spatial distribution of layer 8

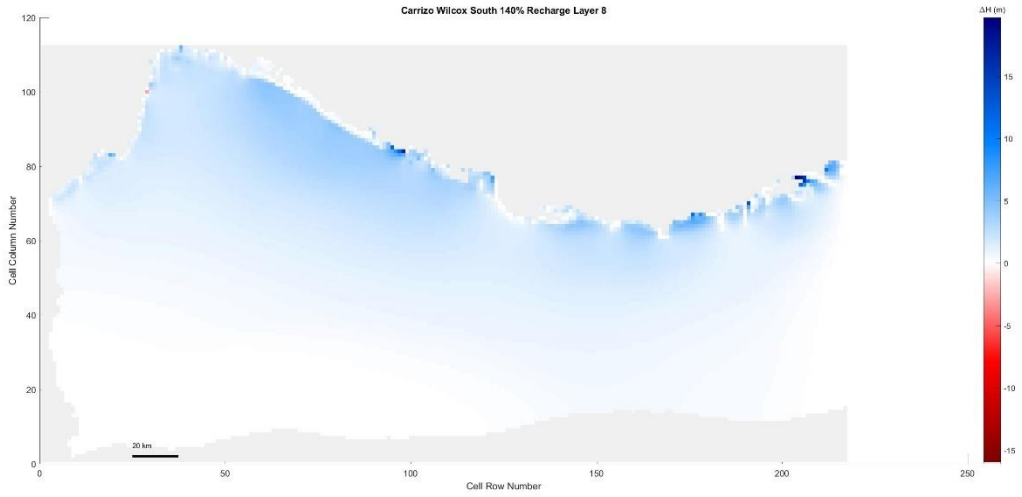

Figure 5. 317 Carrizo-Wilcox South, 140% original recharge hydraulic head spatial distribution of layer 8

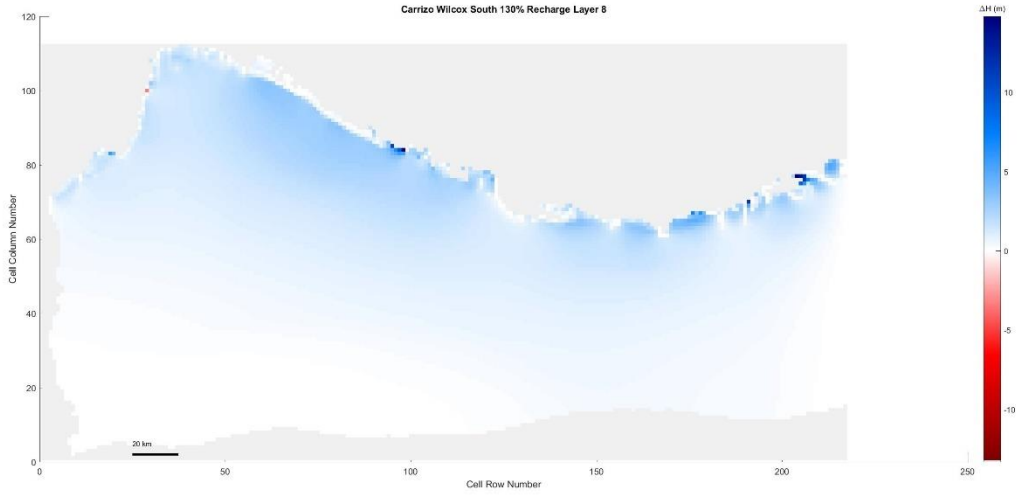

Figure 5. 318 Carrizo-Wilcox South, 130% original recharge hydraulic head spatial distribution of layer 8

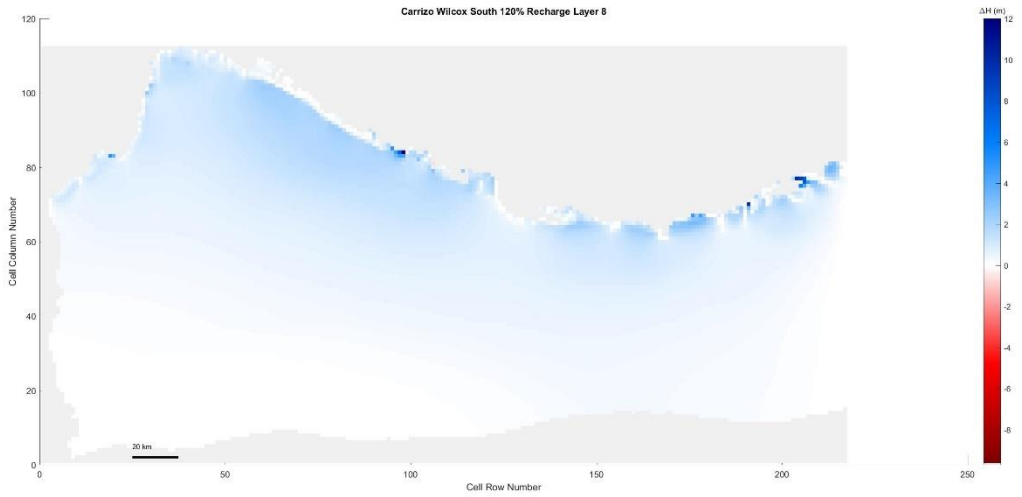

Figure 5. 319 Carrizo-Wilcox South, 120% original recharge hydraulic head spatial distribution of layer 8

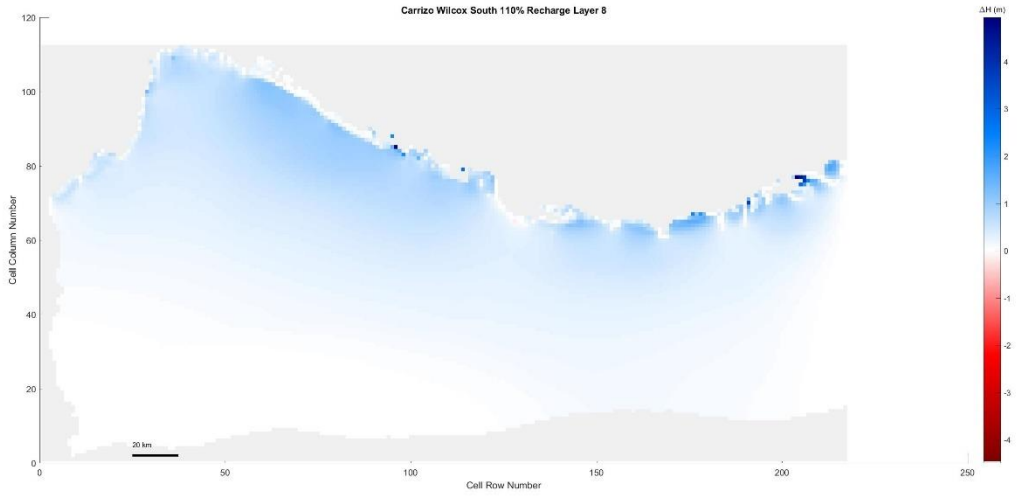

Figure 5. 320 Carrizo-Wilcox South, 110% original recharge hydraulic head spatial distribution of layer 8

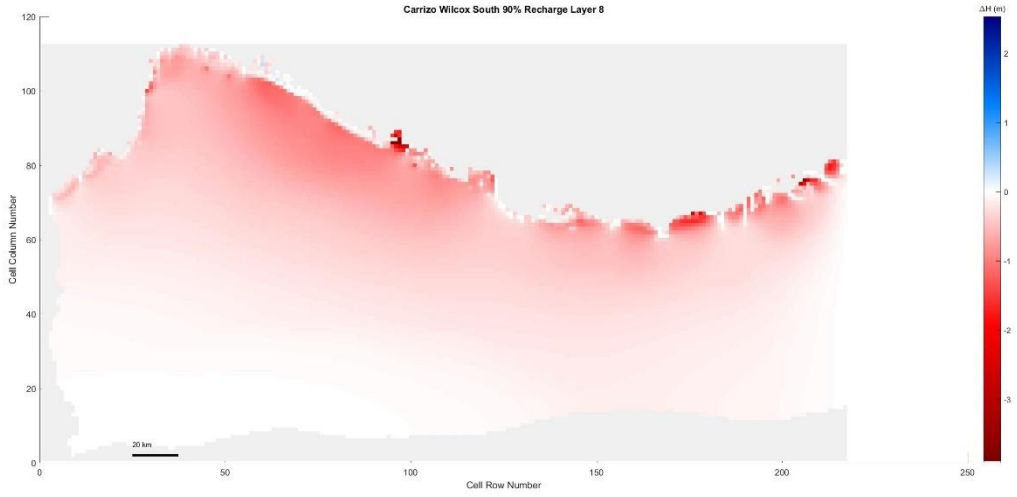

Figure 5. 321 Carrizo-Wilcox South, 90% original recharge hydraulic head spatial distribution of layer 8

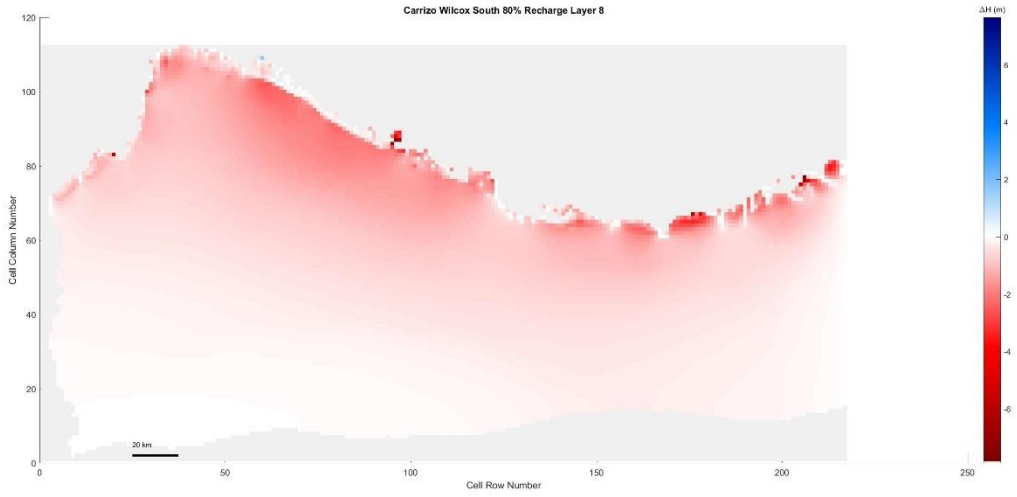

Figure 5. 322 Carrizo-Wilcox South, 80% original recharge hydraulic head spatial distribution of layer 8

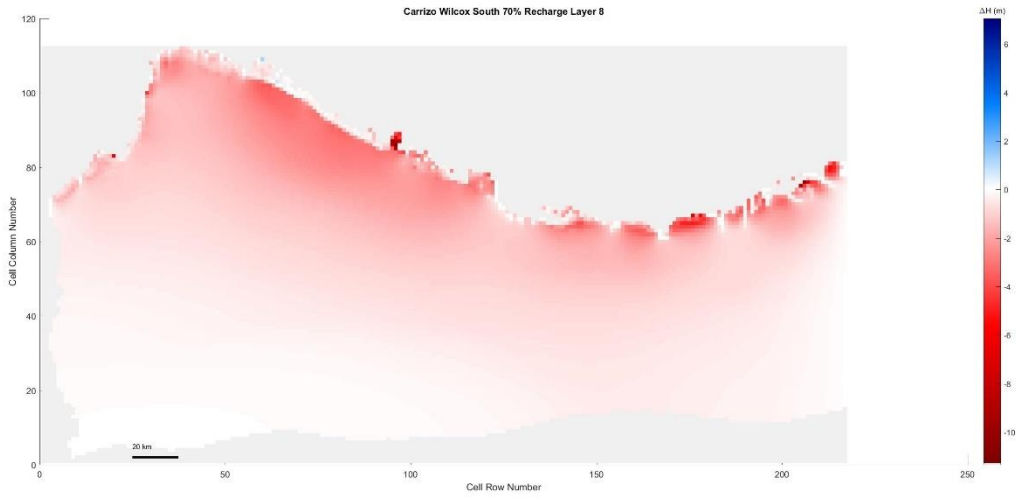

Figure 5. 323 Carrizo-Wilcox South, 70% original recharge hydraulic head spatial distribution of layer 8

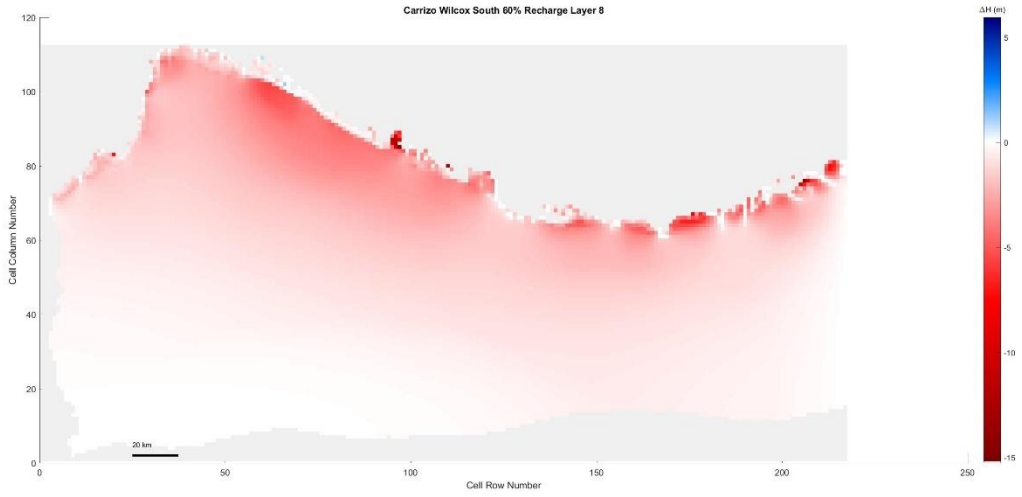

Figure 5. 324 Carrizo-Wilcox South, 60% original recharge hydraulic head spatial distribution of layer 8

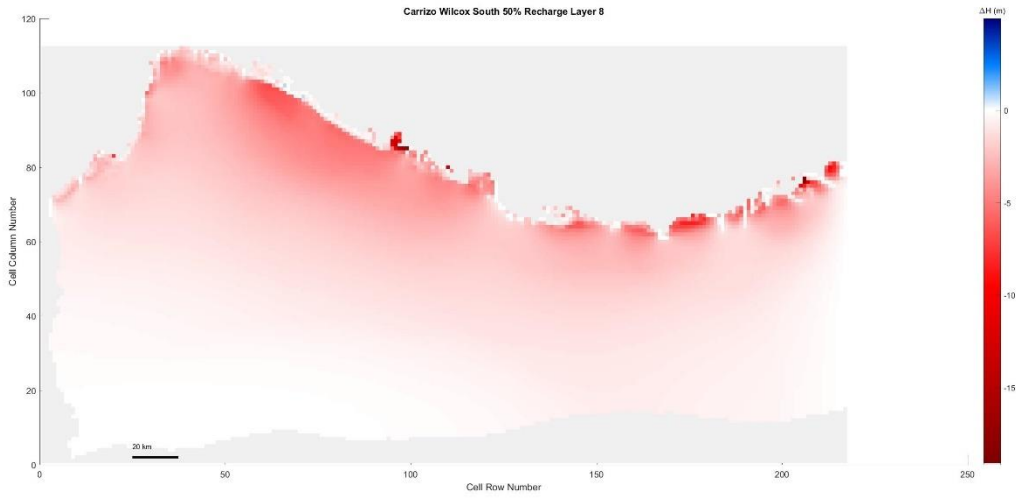

Figure 5. 325 Carrizo-Wilcox South, 50% original recharge hydraulic head spatial distribution of layer 8

Edwards Trinity Plateau

Layer 1

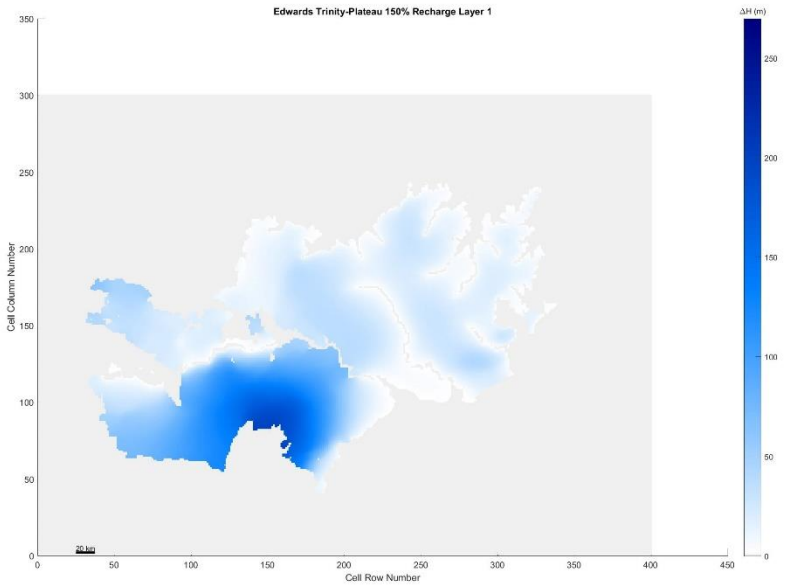

Figure 5. 326 Edwards Trinity Plateau, 150% original recharge hydraulic head spatial distribution of layer 1

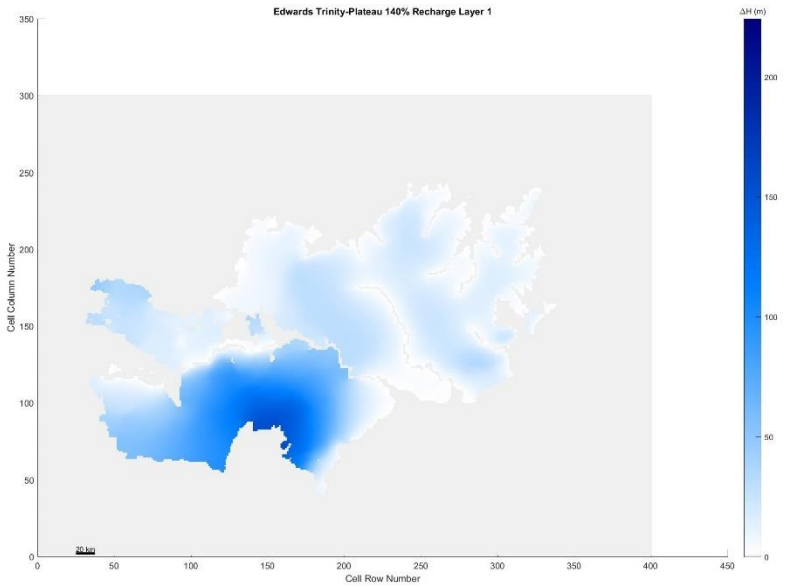

Figure 5. 327 Edwards Trinity Plateau, 140% original recharge hydraulic head spatial distribution of layer 1

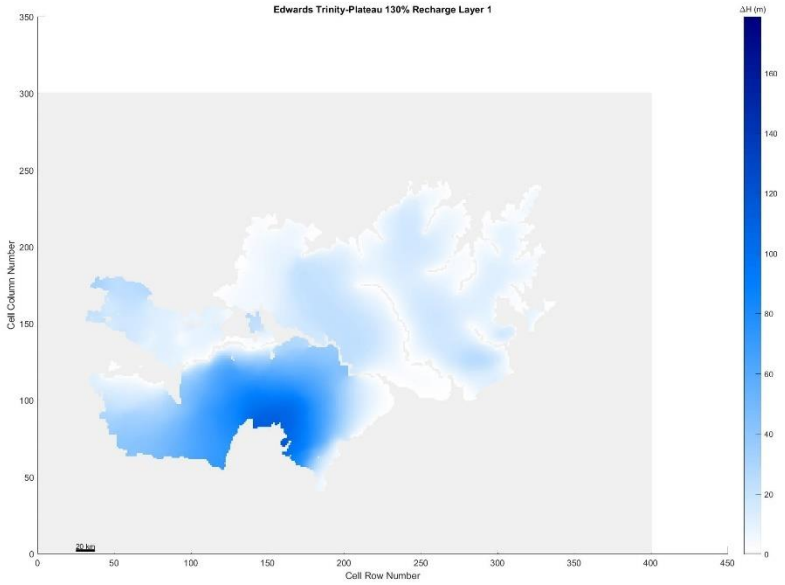

Figure 5. 328 Edwards Trinity Plateau, 130% original recharge hydraulic head spatial distribution of layer 1

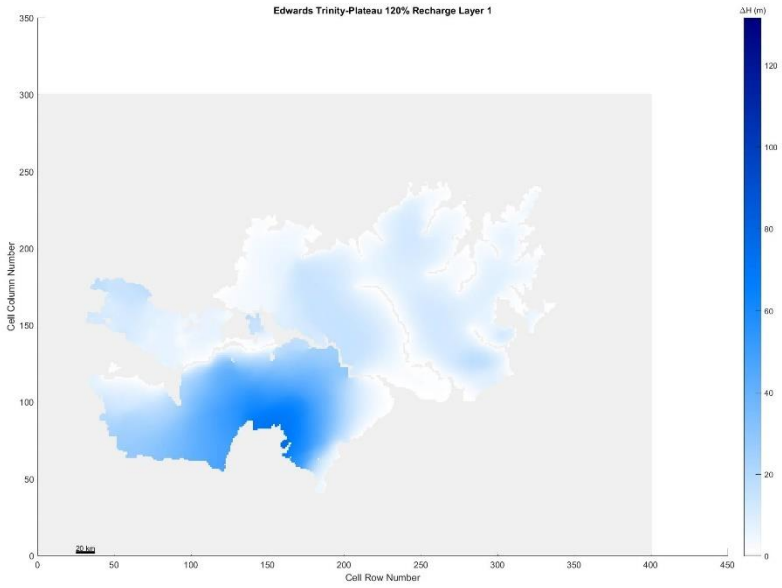

Figure 5. 329 Edwards Trinity Plateau, 120% original recharge hydraulic head spatial distribution of layer 1

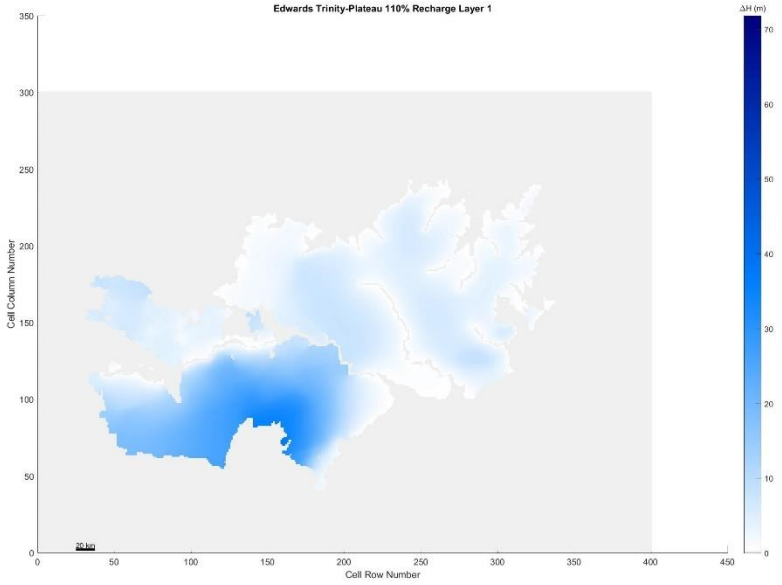

Figure 5. 330 Edwards Trinity Plateau, 110% original recharge hydraulic head spatial distribution of layer 1

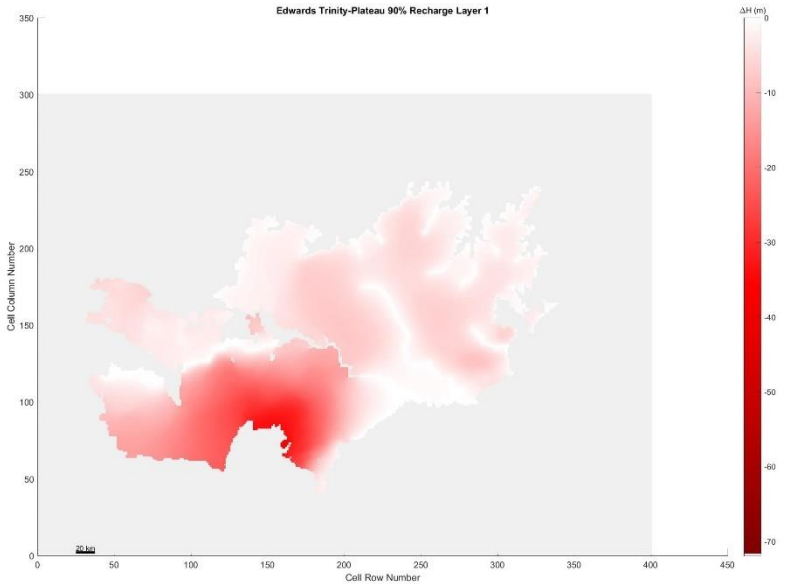

Figure 5. 331 Edwards Trinity Plateau, 90% original recharge hydraulic head spatial distribution of layer 1

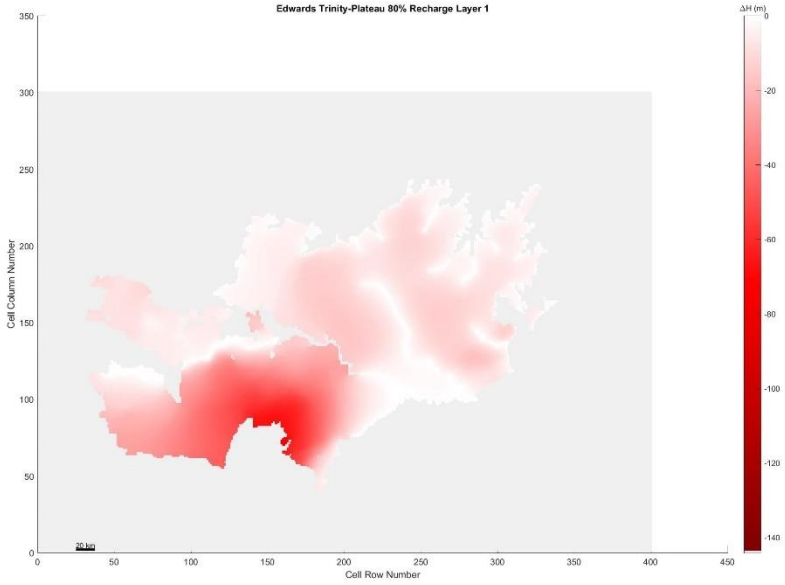

Figure 5. 332 Edwards Trinity Plateau, 80% original recharge hydraulic head spatial distribution of layer 1

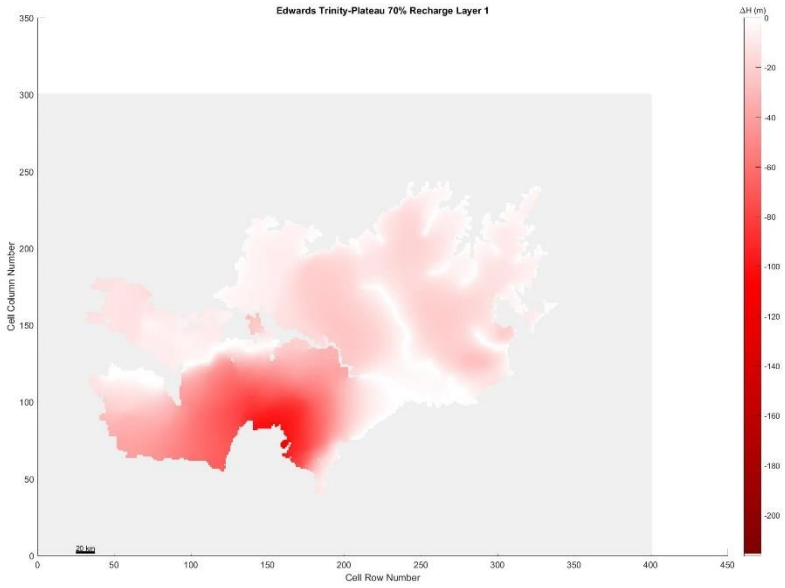

Figure 5. 333 Edwards Trinity Plateau, 70% original recharge hydraulic head spatial distribution of layer 1

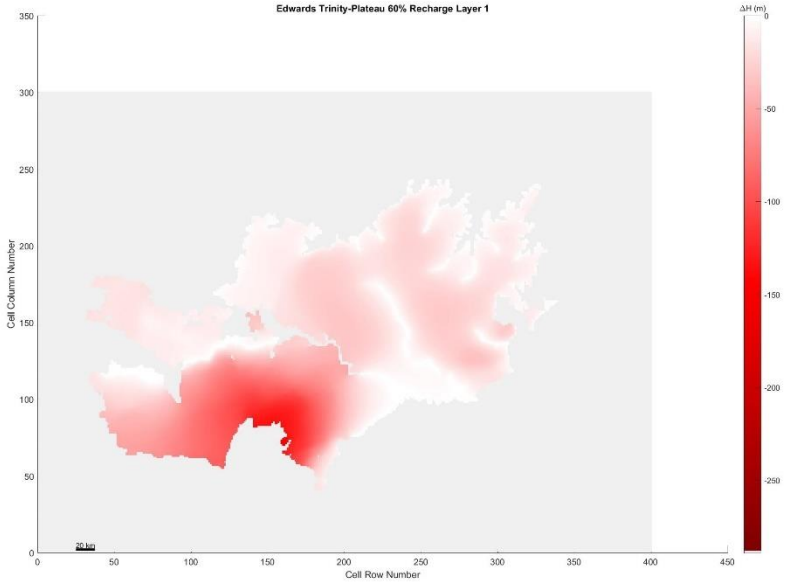

Figure 5. 334 Edwards Trinity Plateau, 60% original recharge hydraulic head spatial distribution of layer 1

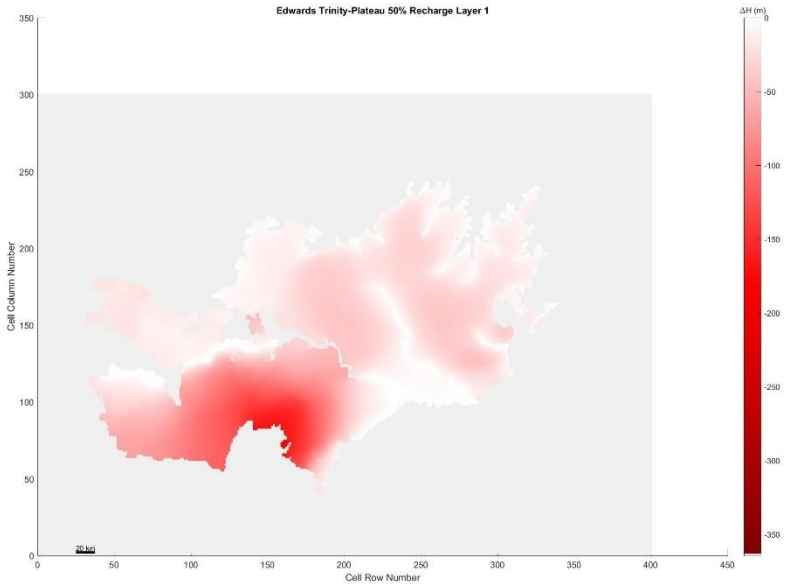

Figure 5. 335 Edwards Trinity Plateau, 50% original recharge hydraulic head spatial distribution of layer 1

Layer 2

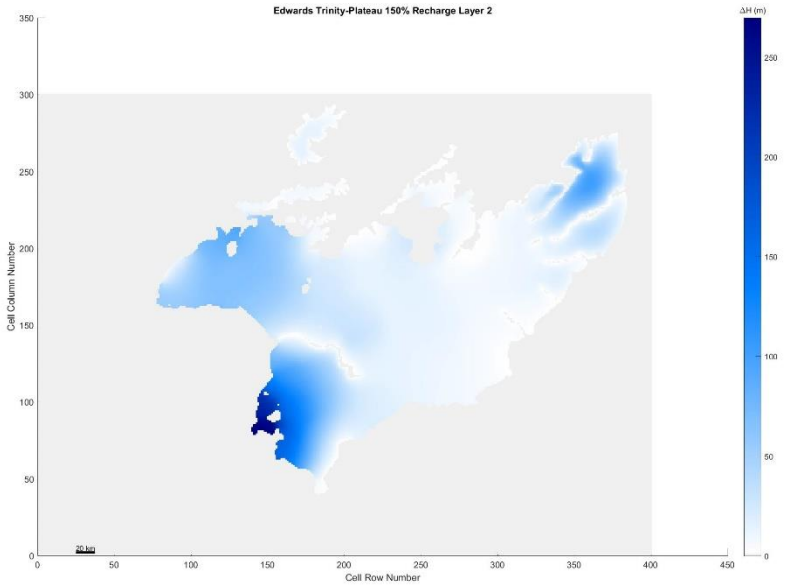

Figure 5. 336 Edwards Trinity Plateau, 150% original recharge hydraulic head spatial distribution of layer 2

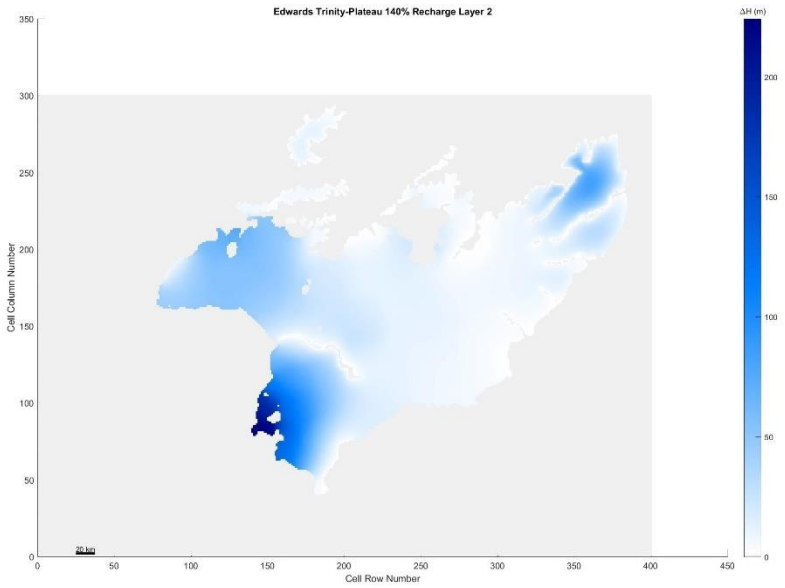

Figure 5. 337 Edwards Trinity Plateau, 140% original recharge hydraulic head spatial distribution of layer 2

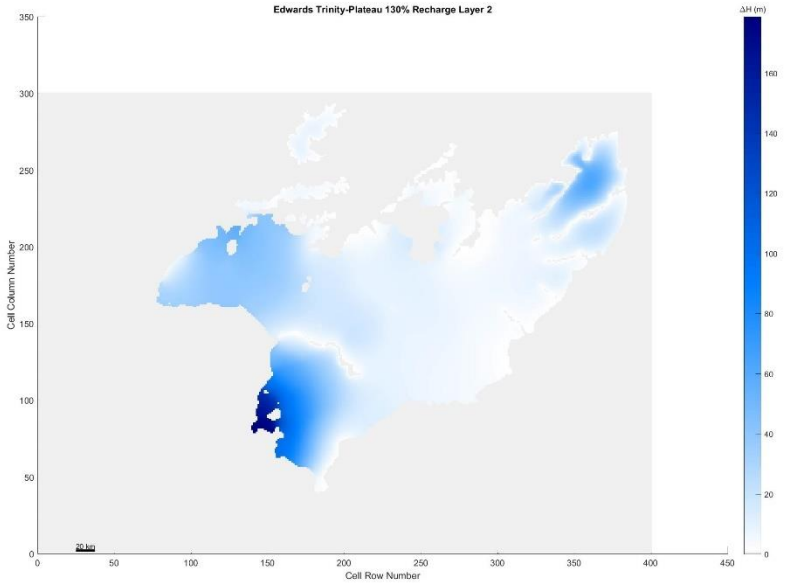

Figure 5. 338 Edwards Trinity Plateau, 130% original recharge hydraulic head spatial distribution of layer 2

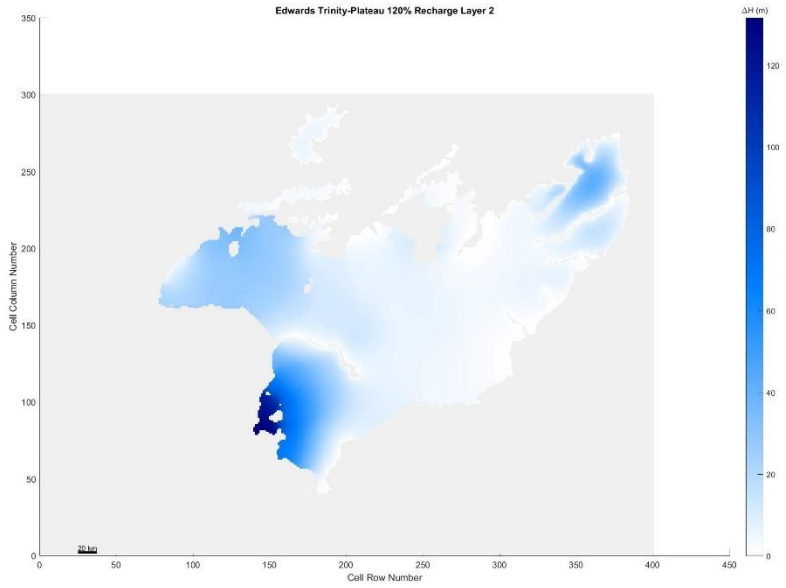

Figure 5. 339 Edwards Trinity Plateau, 120% original recharge hydraulic head spatial distribution of layer 2

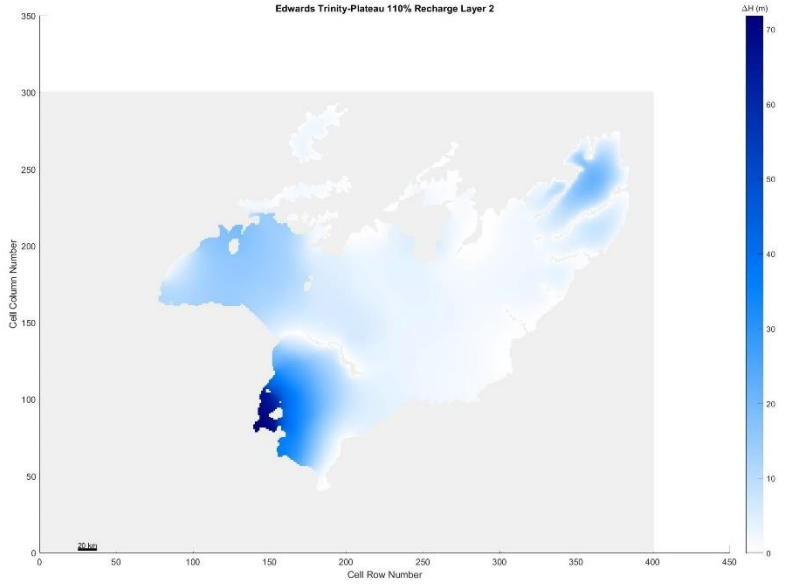

Figure 5. 340 Edwards Trinity Plateau, 110% original recharge hydraulic head spatial distribution of layer 2

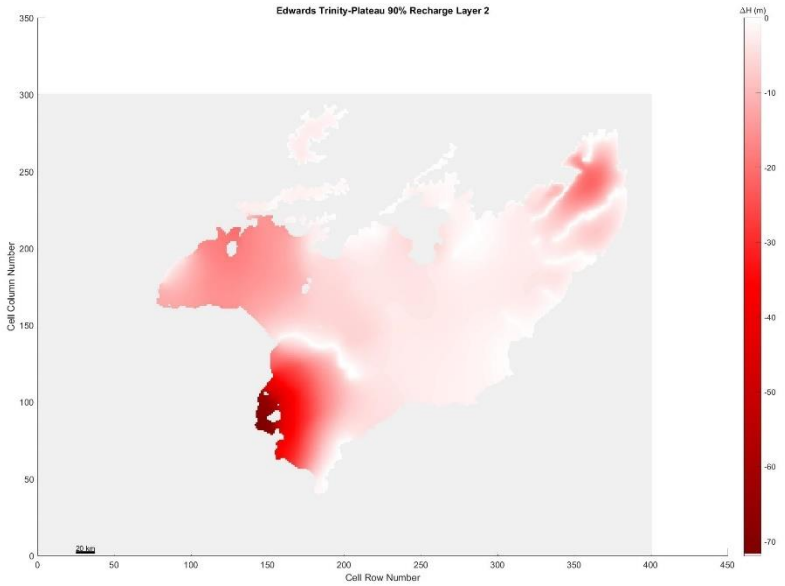

Figure 5. 341 Edwards Trinity Plateau, 90% original recharge hydraulic head spatial distribution of layer 2

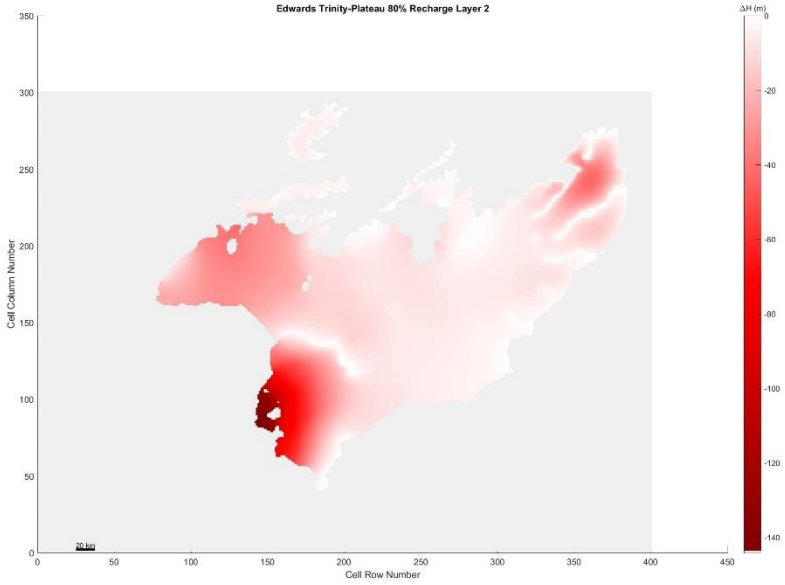

Figure 5. 342 Edwards Trinity Plateau, 80% original recharge hydraulic head spatial distribution of layer 2

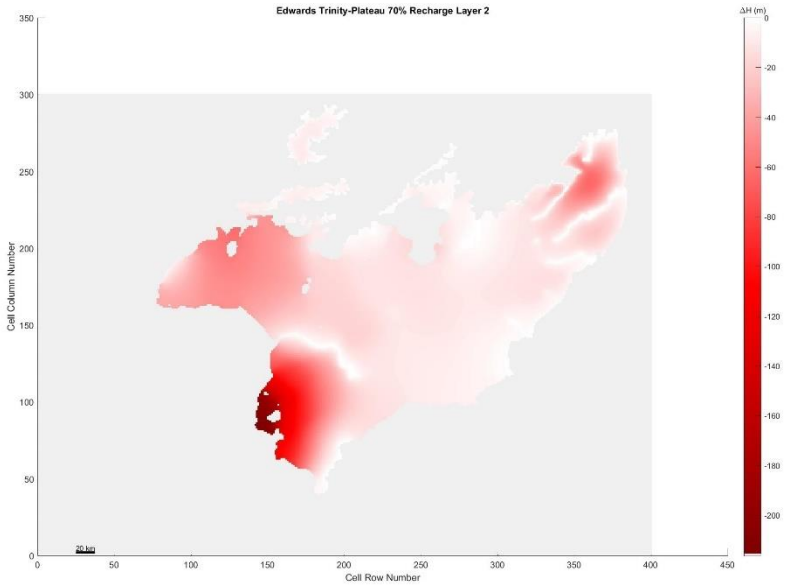

Figure 5. 343 Edwards Trinity Plateau, 70% original recharge hydraulic head spatial distribution of layer 2

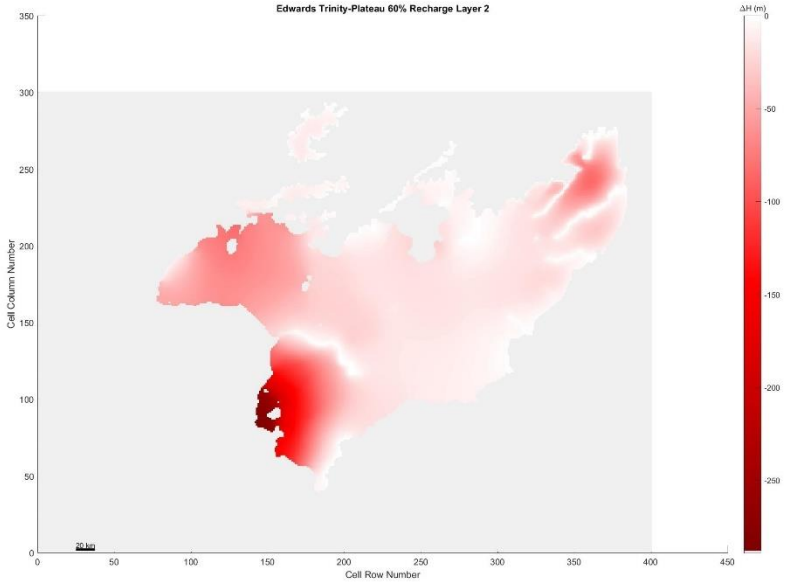

Figure 5. 344 Edwards Trinity Plateau, 60% original recharge hydraulic head spatial distribution of layer 2

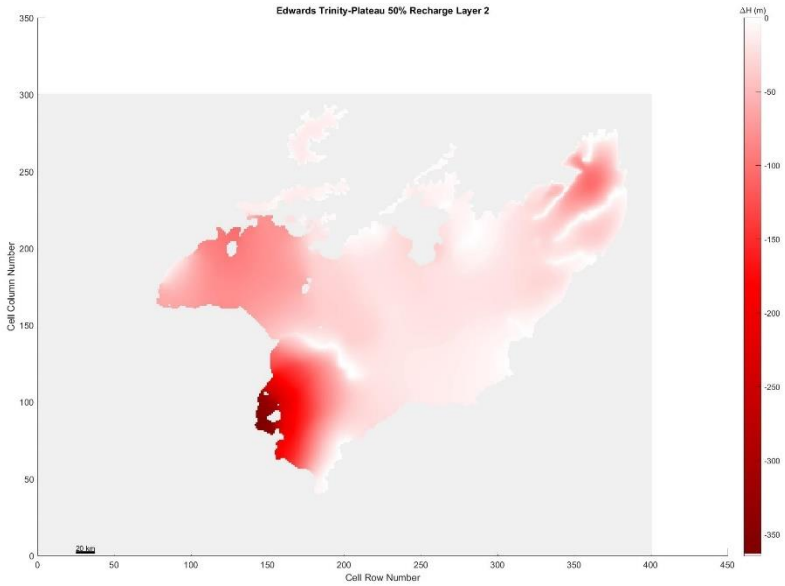

Figure 5. 345 Edwards Trinity Plateau, 50% original recharge hydraulic head spatial distribution of layer 2

Gulf Coast Central

Layer 1

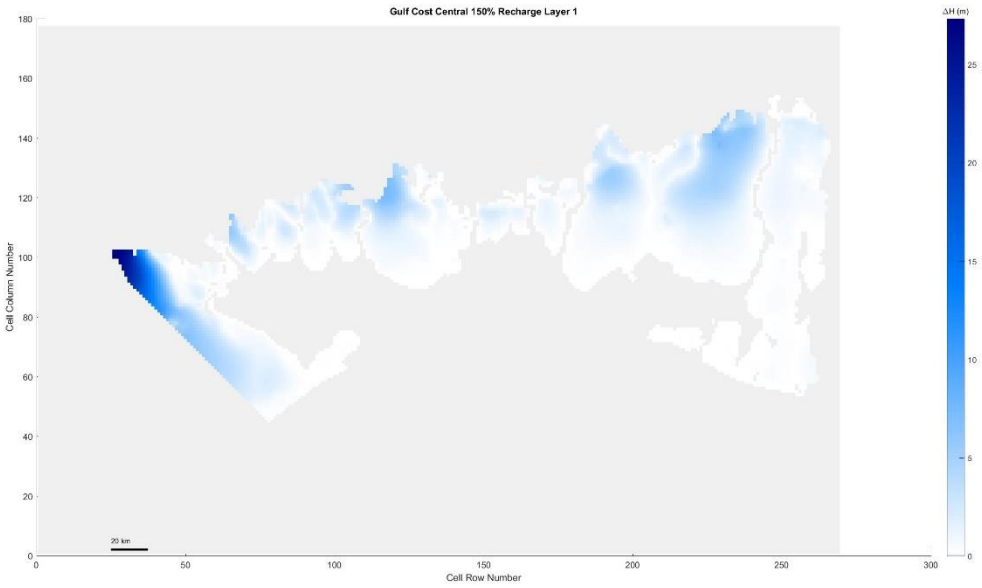

Figure 5. 346 Gulf Coast Central, 150% original recharge hydraulic head spatial distribution of layer 1

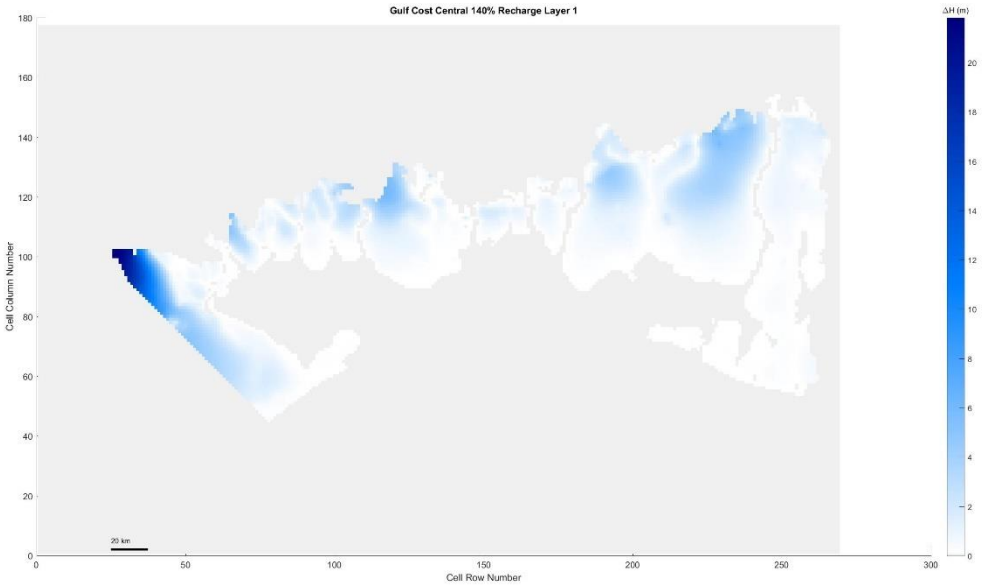

Figure 5. 347 Gulf Coast Central, 140% original recharge hydraulic head spatial distribution of layer 1

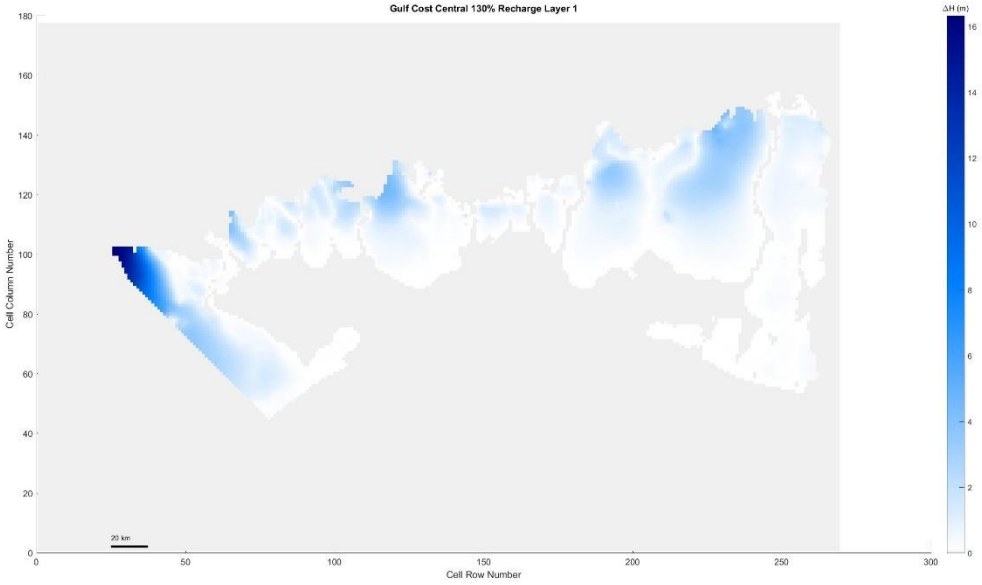

Figure 5. 348 Gulf Coast Central, 130% original recharge hydraulic head spatial distribution of layer 1

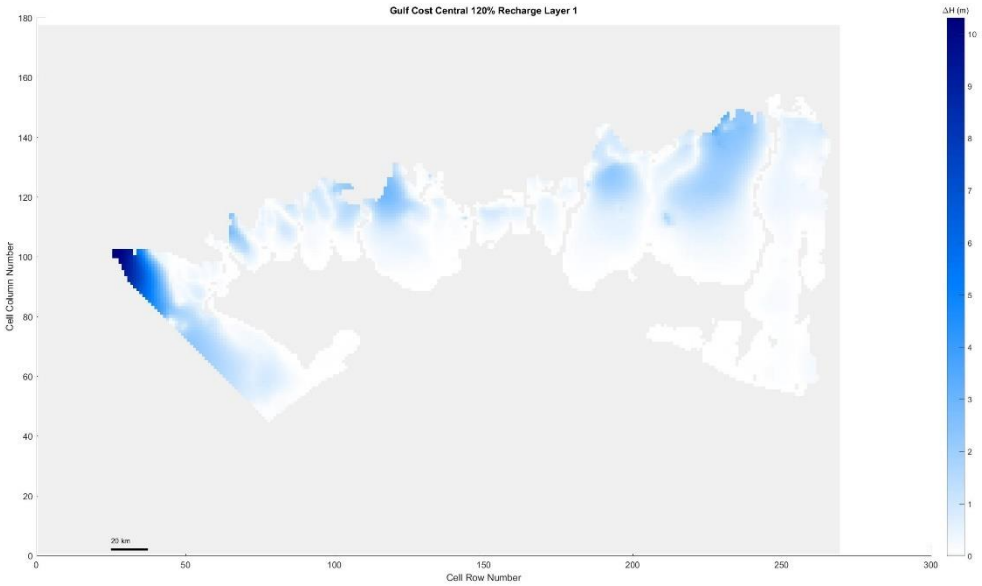

Figure 5. 349 Gulf Coast Central, 120% original recharge hydraulic head spatial distribution of layer 1

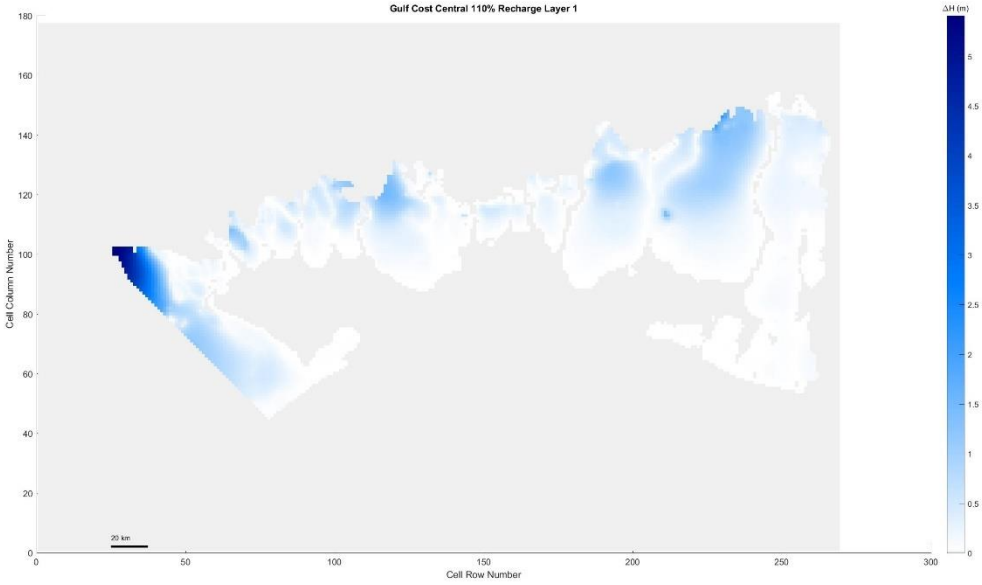

Figure 5. 350 Gulf Coast Central, 110% original recharge hydraulic head spatial distribution of layer 1

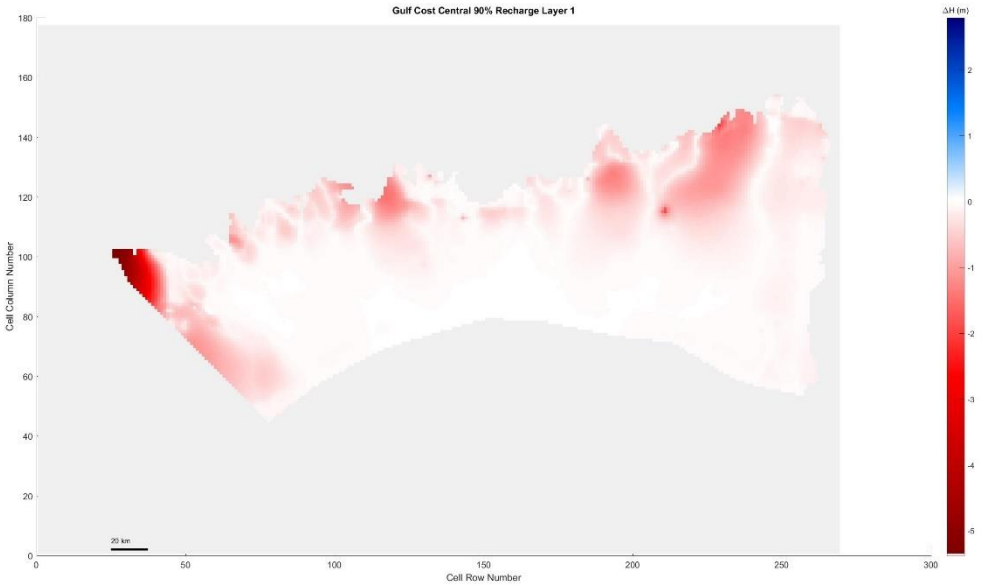

Figure 5. 351 Gulf Coast Central, 90% original recharge hydraulic head spatial distribution of layer 1

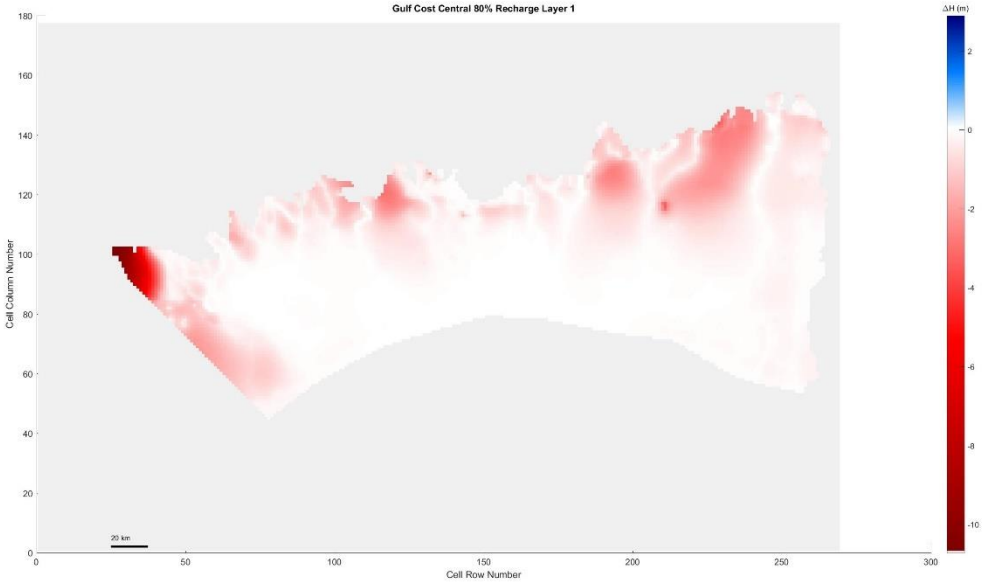

Figure 5. 352 Gulf Coast Central, 80% original recharge hydraulic head spatial distribution of layer 1

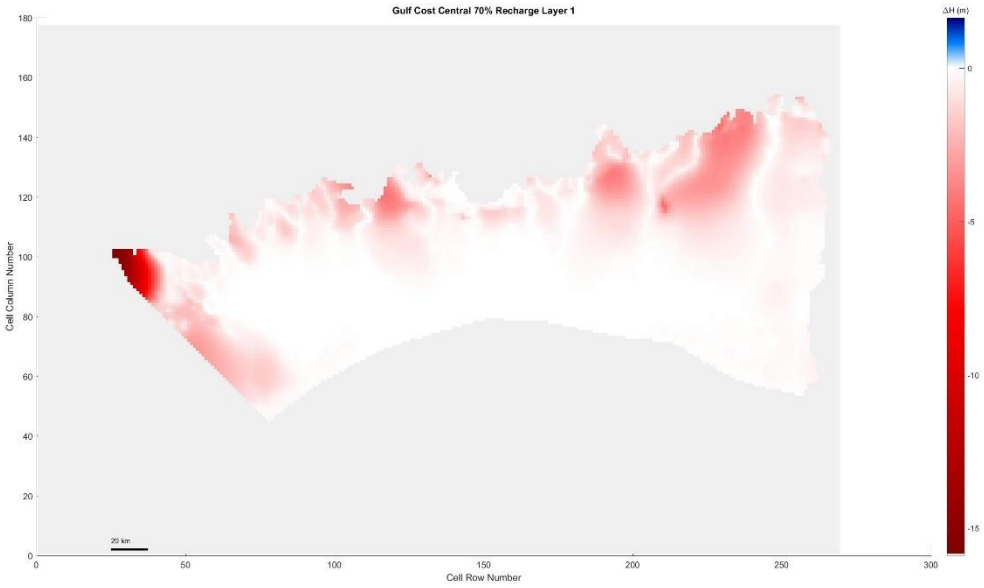

Figure 5. 353 Gulf Coast Central, 70% original recharge hydraulic head spatial distribution of layer 1

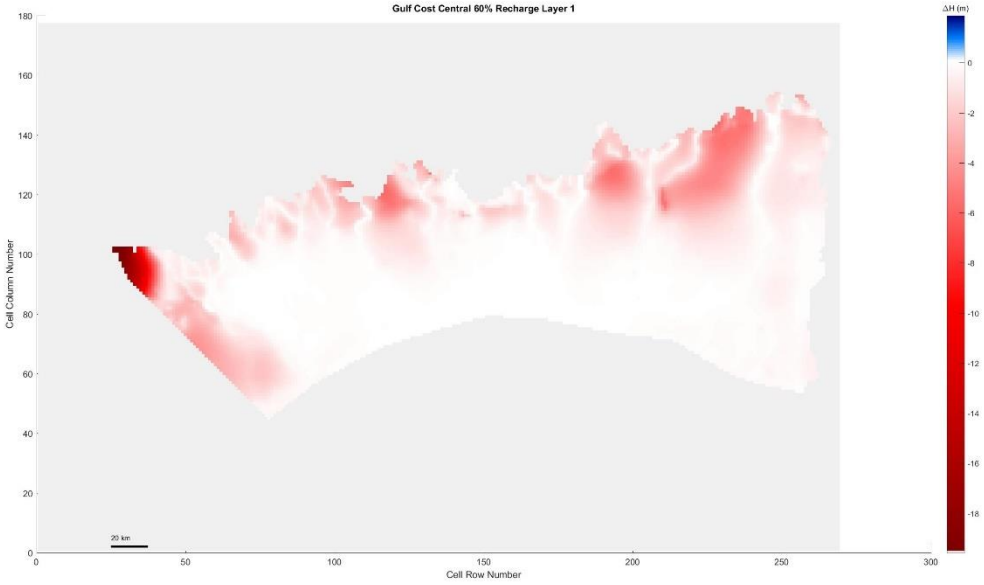

Figure 5. 354 Gulf Coast Central, 60% original recharge hydraulic head spatial distribution of layer 1

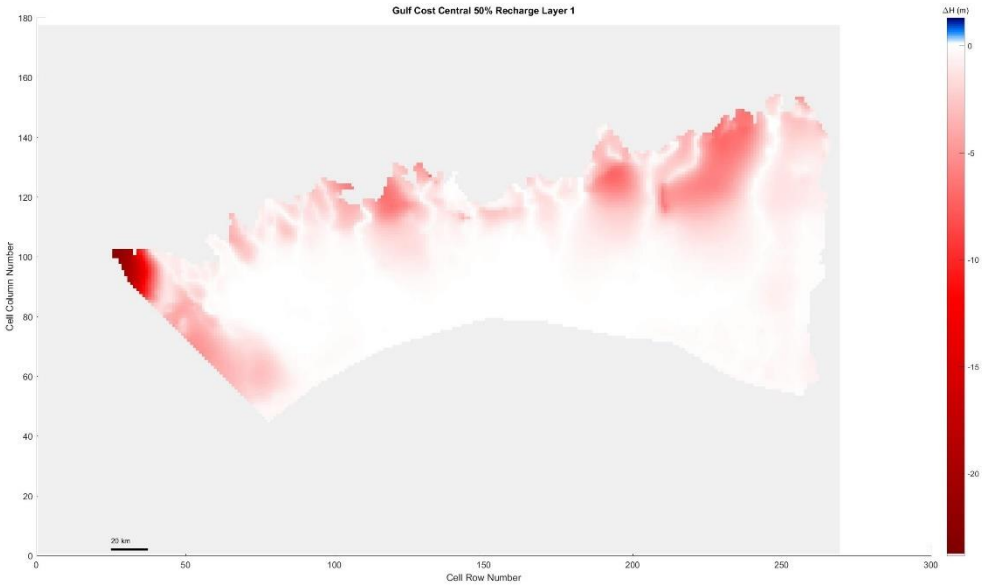

Figure 5. 355 Gulf Coast Central, 50% original recharge hydraulic head spatial distribution of layer 1

Layer 2

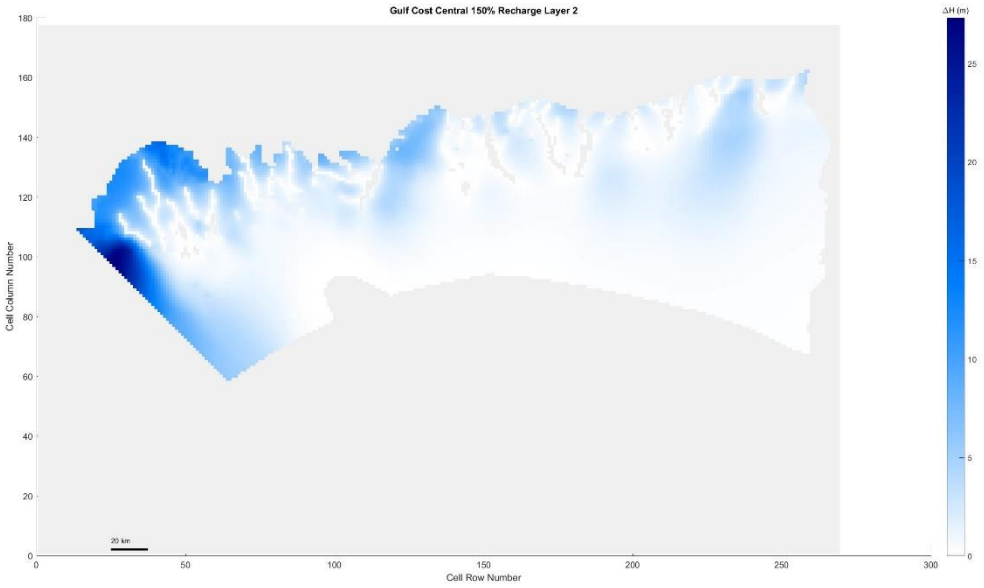

Figure 5. 356 Gulf Coast Central, 150% original recharge hydraulic head spatial distribution of layer 2

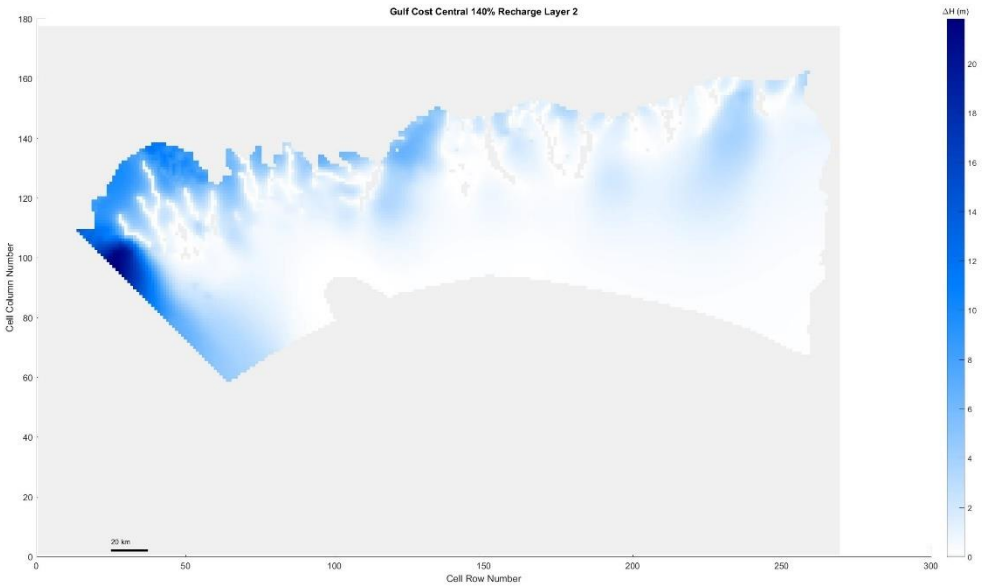

Figure 5. 357 Gulf Coast Central, 140% original recharge hydraulic head spatial distribution of layer 2

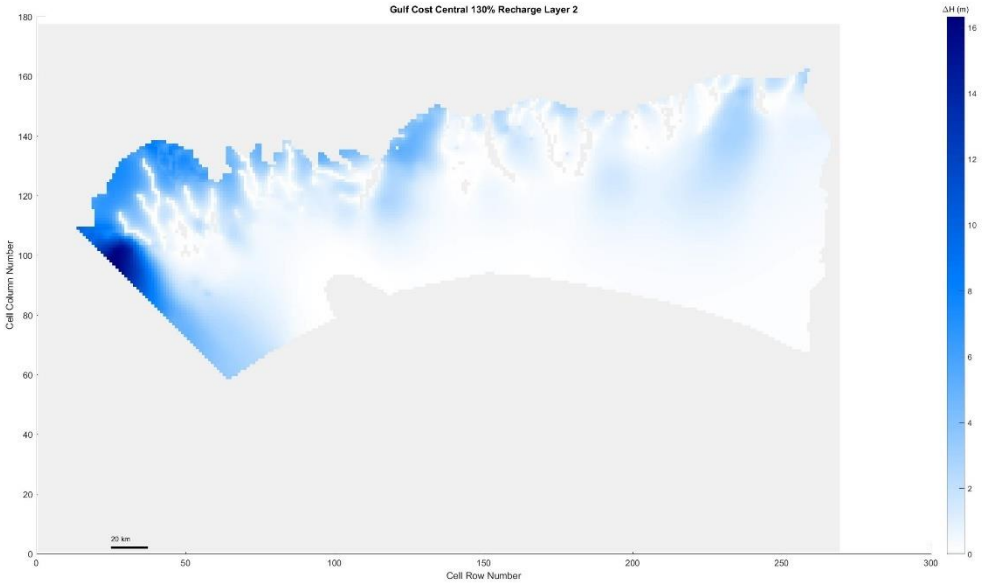

Figure 5. 358 Gulf Coast Central, 130% original recharge hydraulic head spatial distribution of layer 2

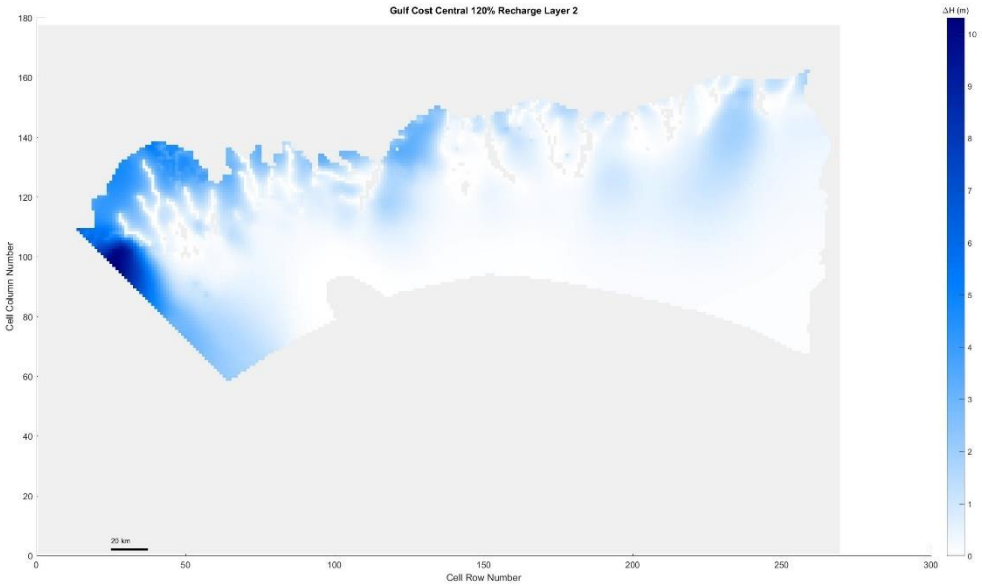

Figure 5. 359 Gulf Coast Central, 120% original recharge hydraulic head spatial distribution of layer 2

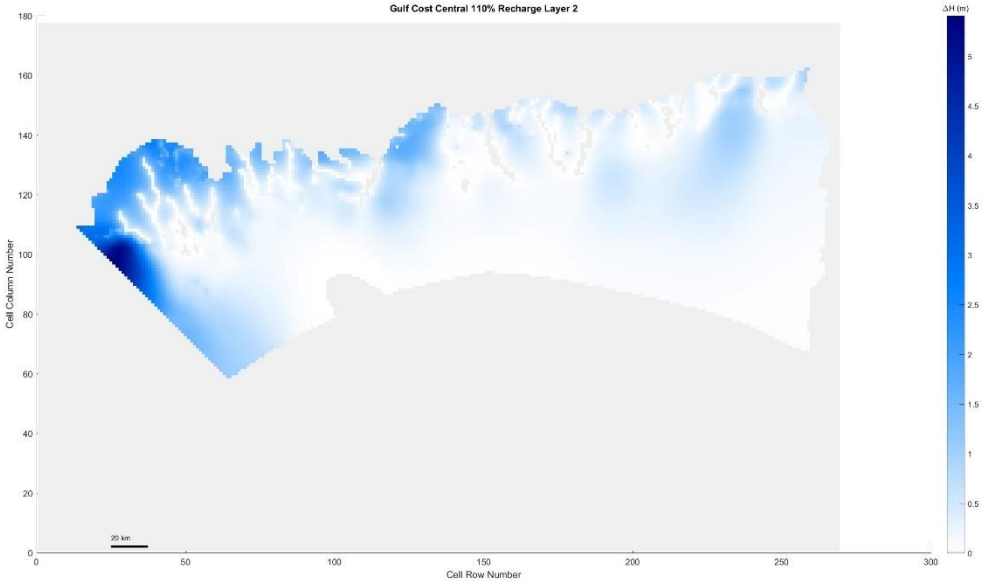

Figure 5. 360 Gulf Coast Central, 110% original recharge hydraulic head spatial distribution of layer 2

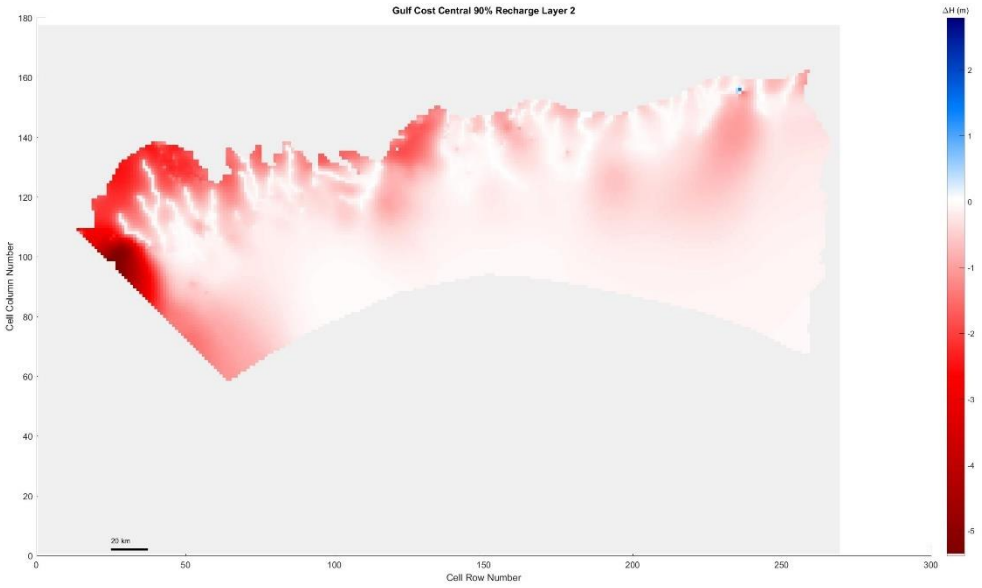

Figure 5. 361 Gulf Coast Central, 90% original recharge hydraulic head spatial distribution of layer 2

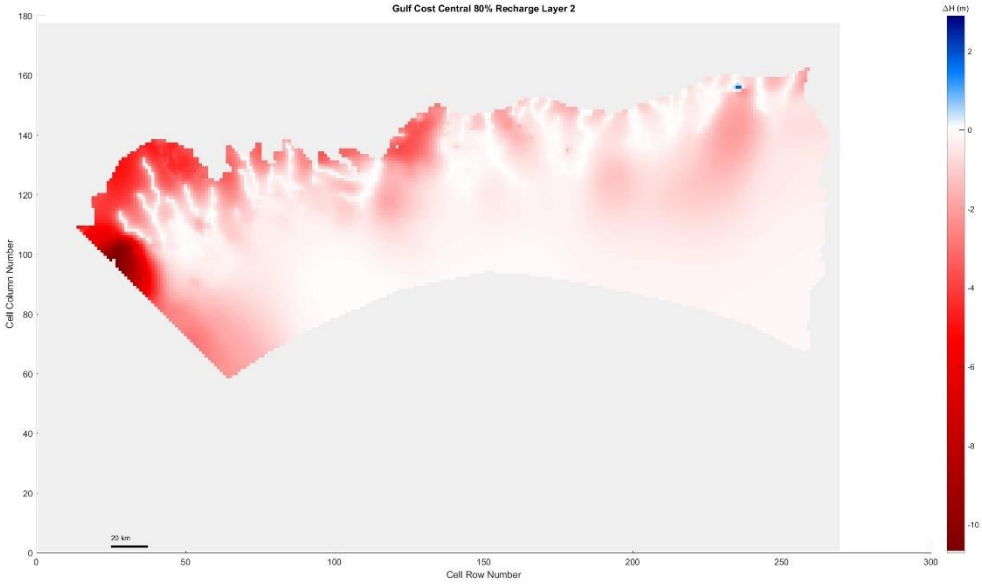

Figure 5. 362 Gulf Coast Central, 80% original recharge hydraulic head spatial distribution of layer 2

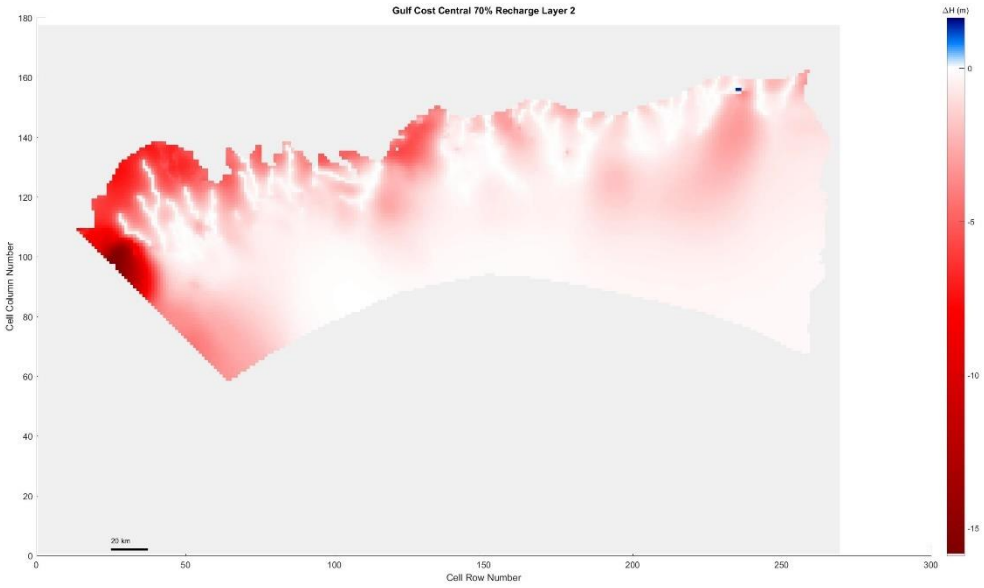

Figure 5. 363 Gulf Coast Central, 70% original recharge hydraulic head spatial distribution of layer 2

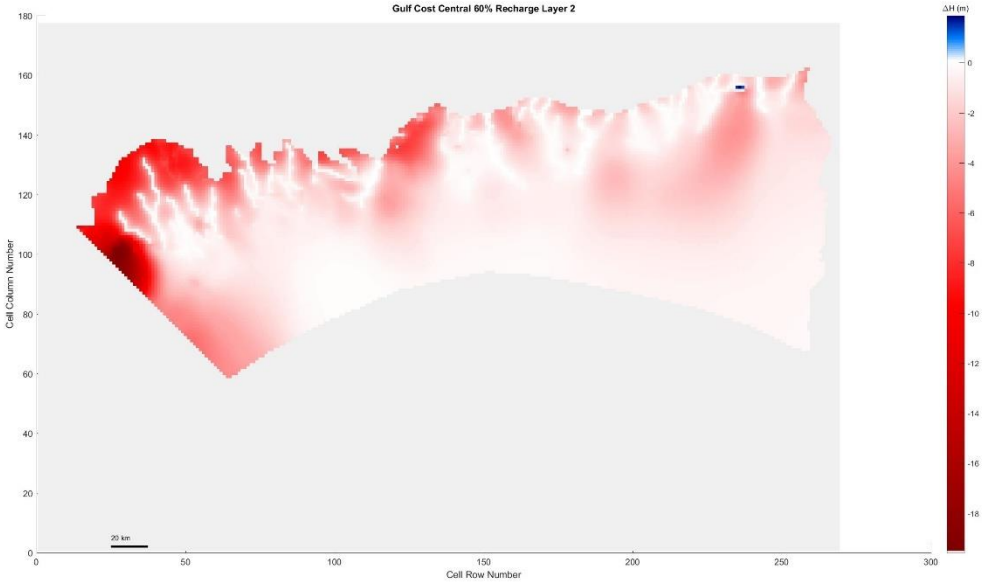

Figure 5. 364 Gulf Coast Central, 60% original recharge hydraulic head spatial distribution of layer 2

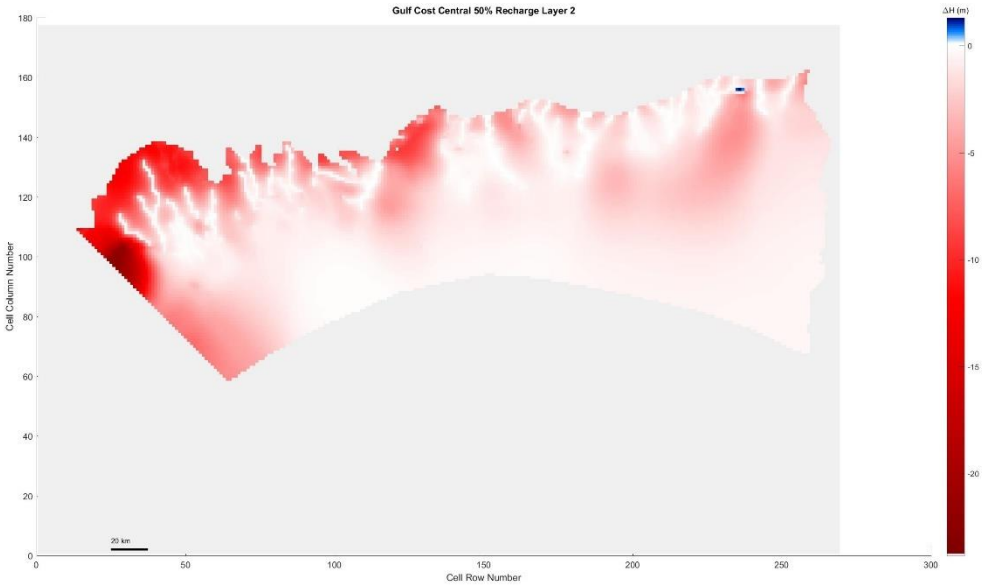

Figure 5. 365 Gulf Coast Central, 50% original recharge hydraulic head spatial distribution of layer 2

Layer 3

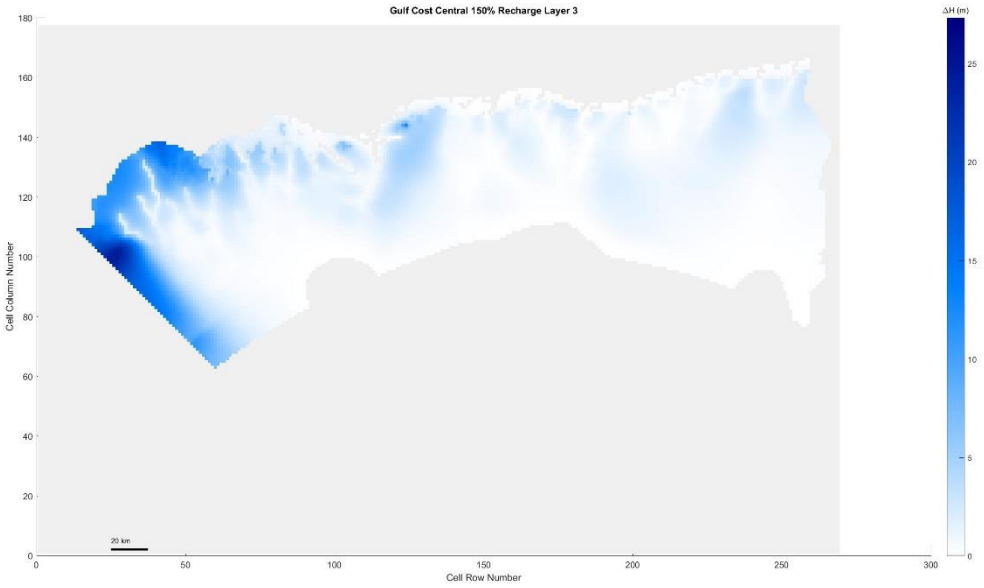

Figure 5. 366 Gulf Coast Central, 150% original recharge hydraulic head spatial distribution of layer 3

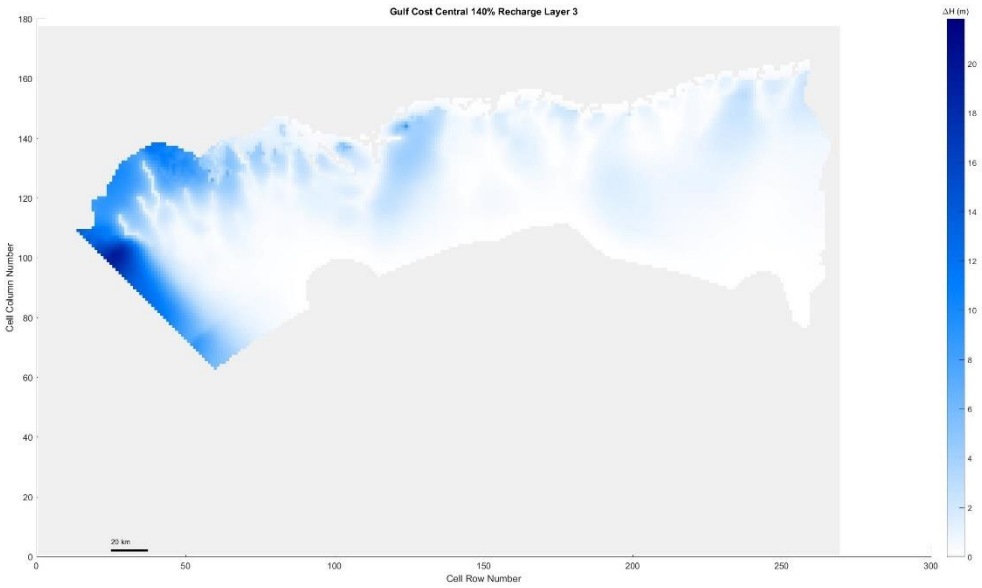

Figure 5. 367 Gulf Coast Central, 140% original recharge hydraulic head spatial distribution of layer 3

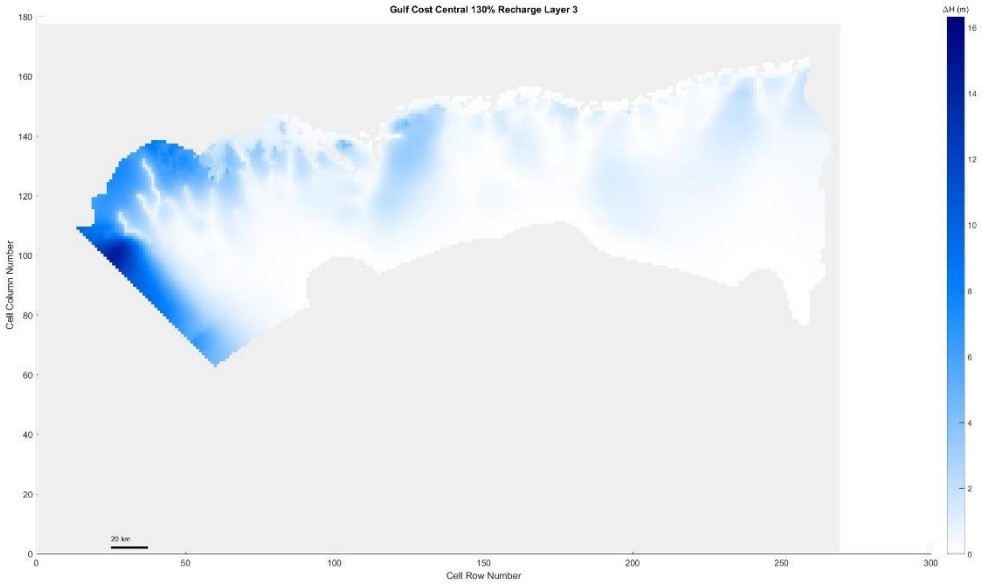

Figure 5. 368 Gulf Coast Central, 130% original recharge hydraulic head spatial distribution of layer 3

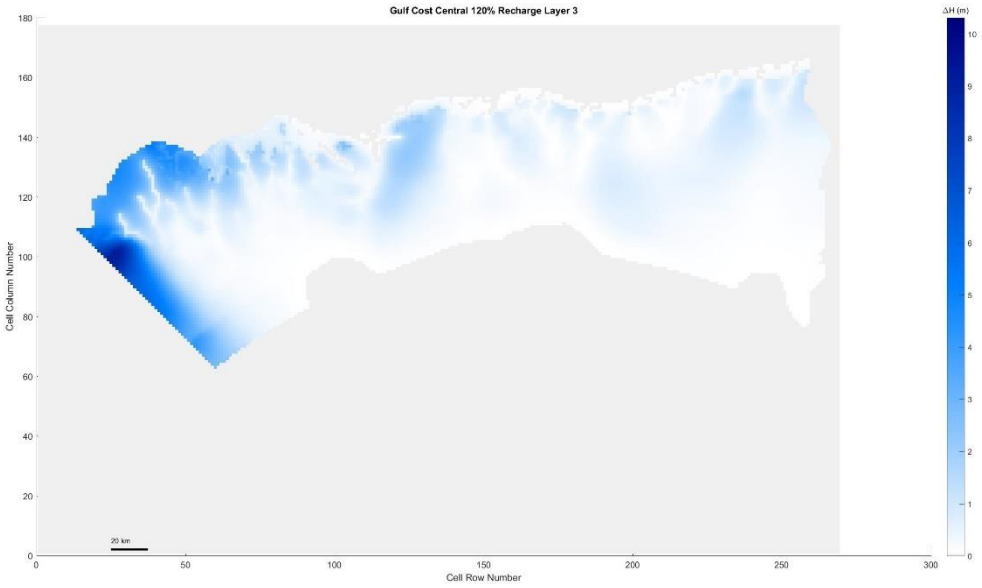

Figure 5. 369 Gulf Coast Central, 120% original recharge hydraulic head spatial distribution of layer 3

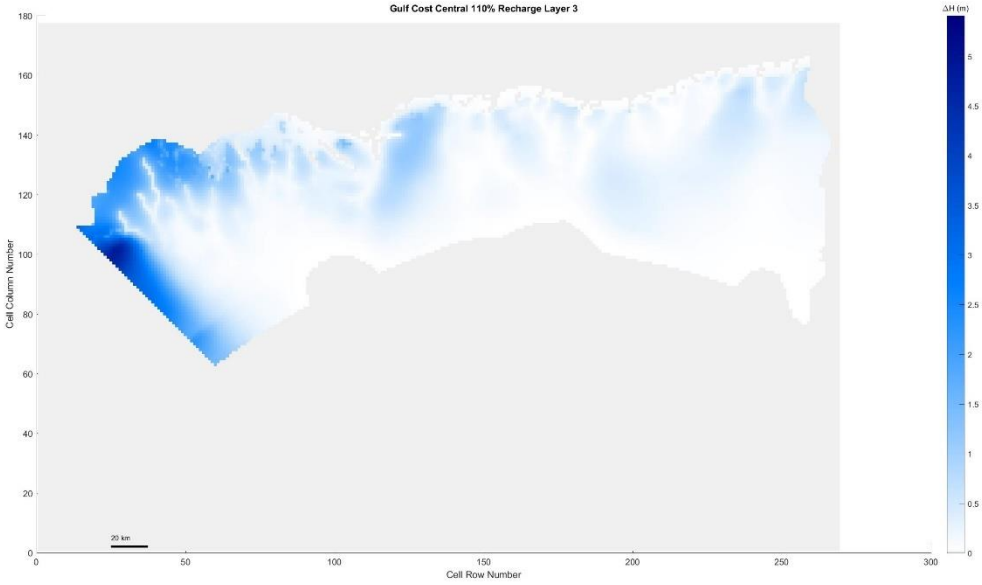

Figure 5. 370 Gulf Coast Central, 110% original recharge hydraulic head spatial distribution of layer 3

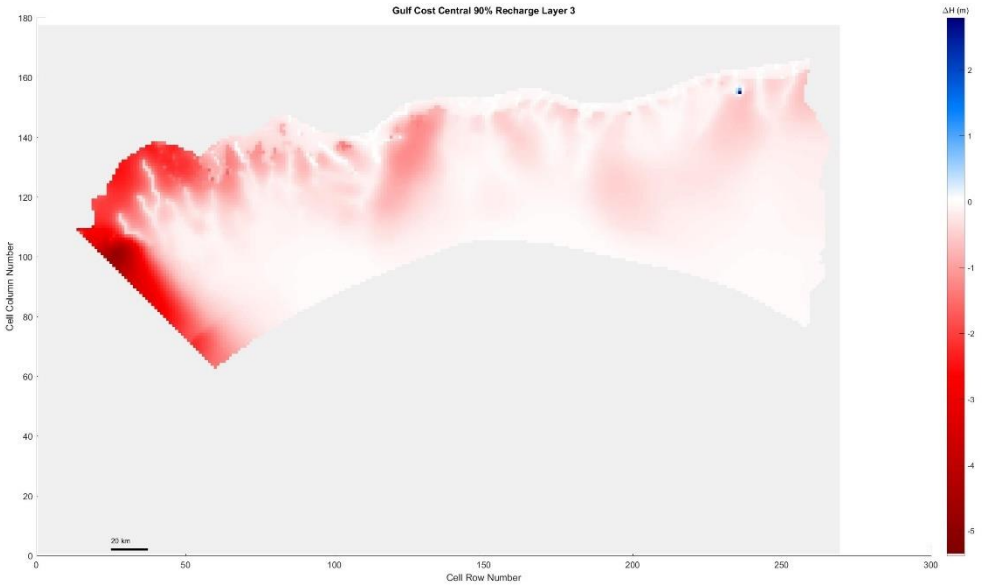

Figure 5. 371 Gulf Coast Central, 90% original recharge hydraulic head spatial distribution of layer 3

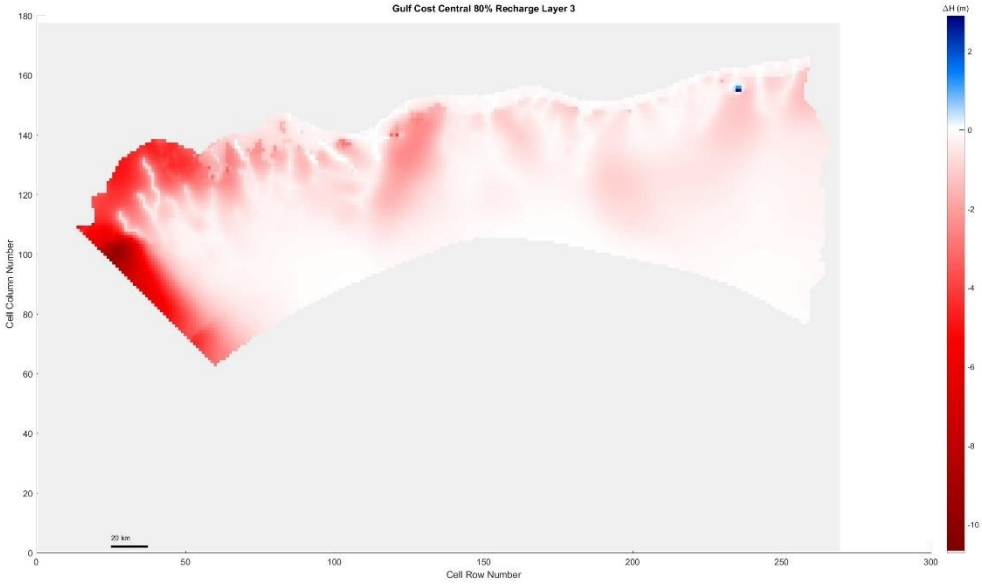

Figure 5. 372 Gulf Coast Central, 80% original recharge hydraulic head spatial distribution of layer 3

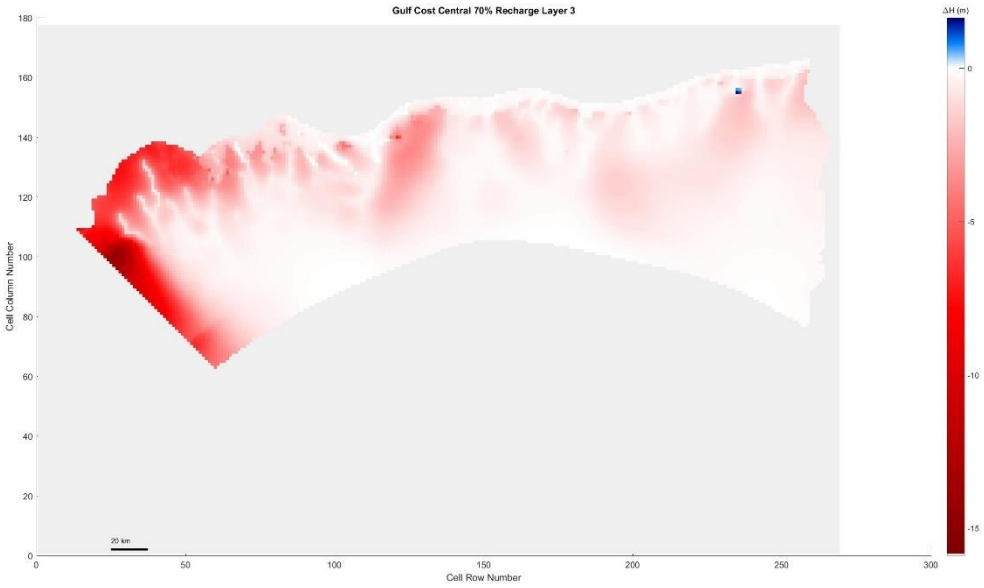

Figure 5. 373 Gulf Coast Central, 70% original recharge hydraulic head spatial distribution of layer 3

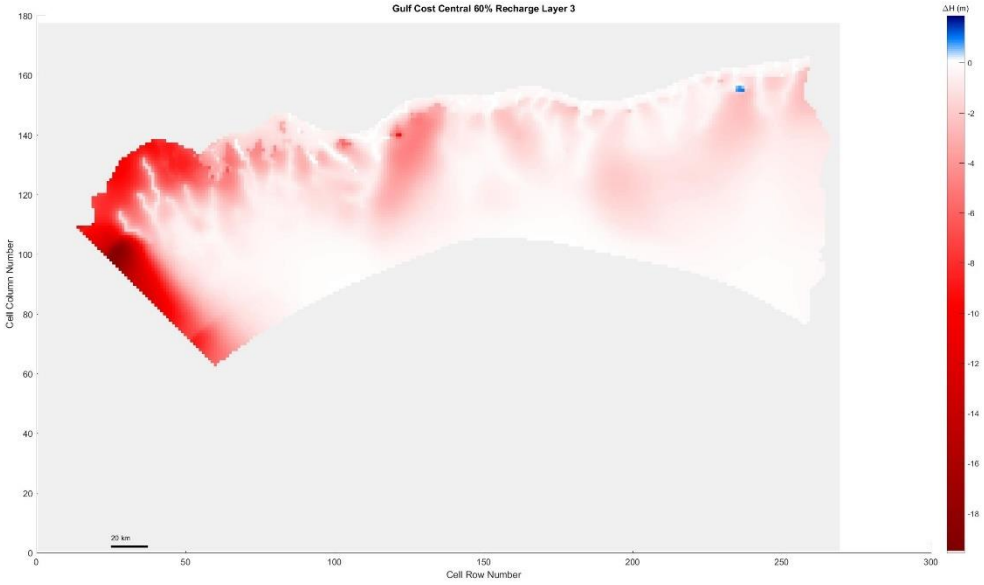

Figure 5. 374 Gulf Coast Central, 60% original recharge hydraulic head spatial distribution of layer 3

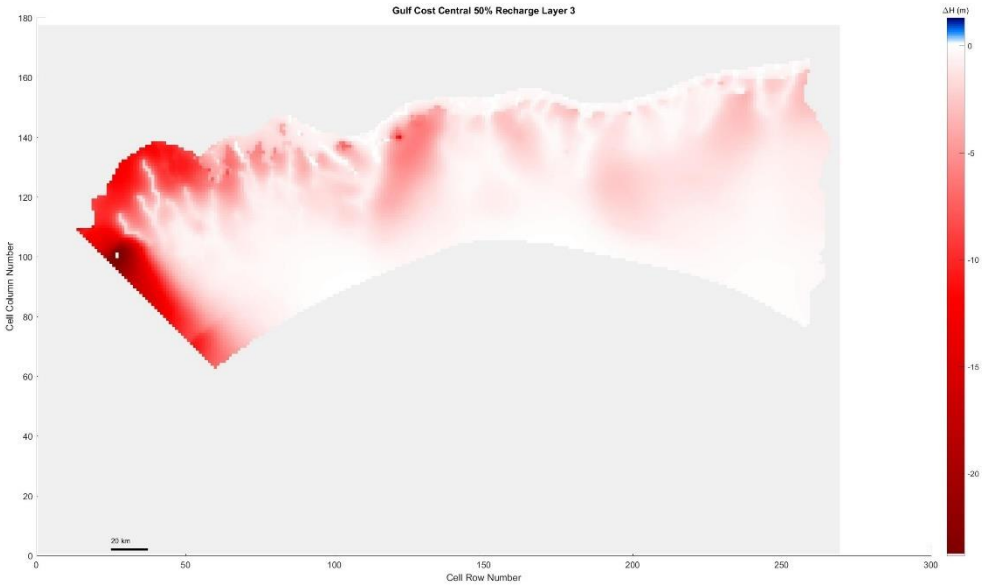

Figure 5. 375 Gulf Coast Central, 50% original recharge hydraulic head spatial distribution of layer 3

Layer 4

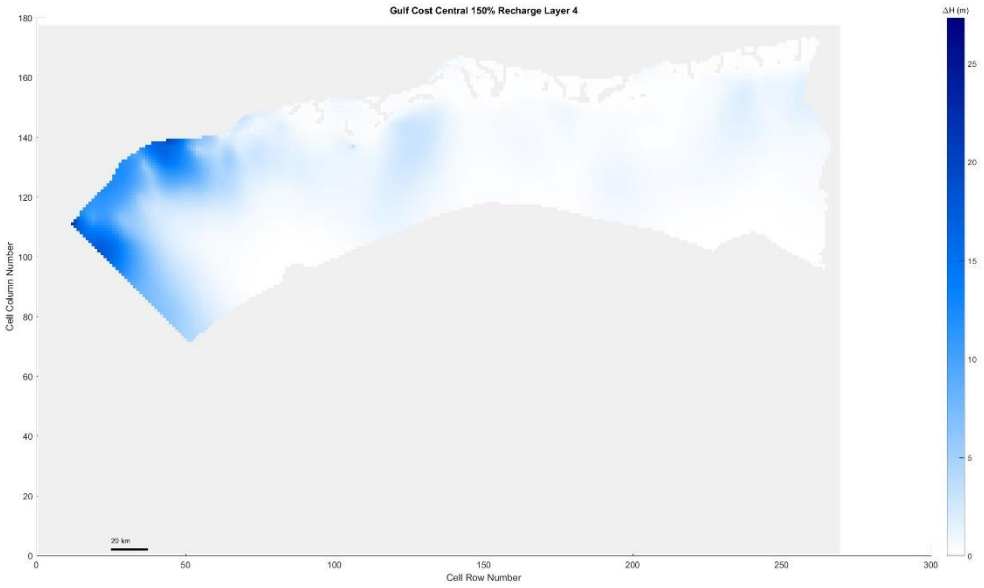

Figure 5. 376 Gulf Coast Central, 150% original recharge hydraulic head spatial distribution of layer 4

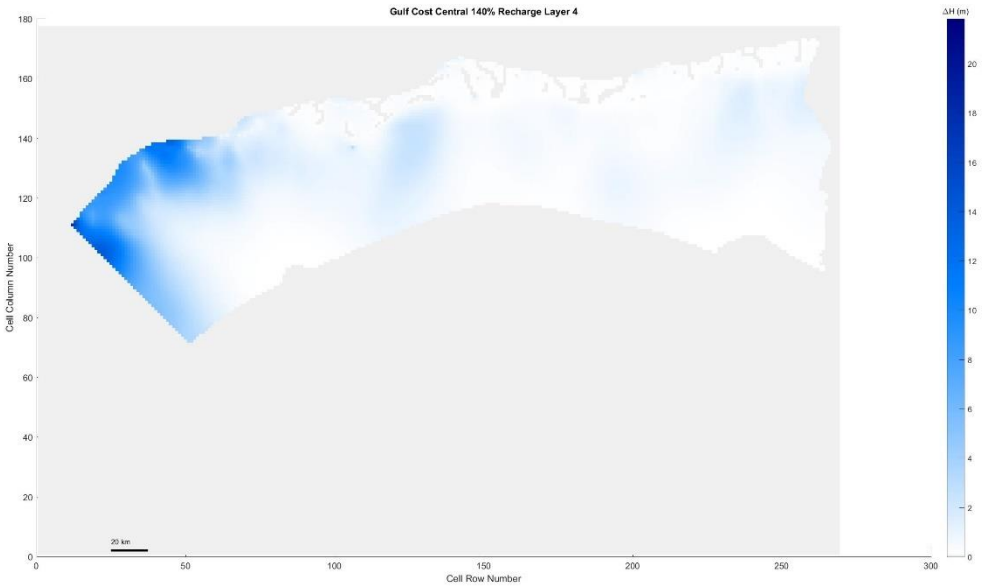

Figure 5. 377 Gulf Coast Central, 140% original recharge hydraulic head spatial distribution of layer 4

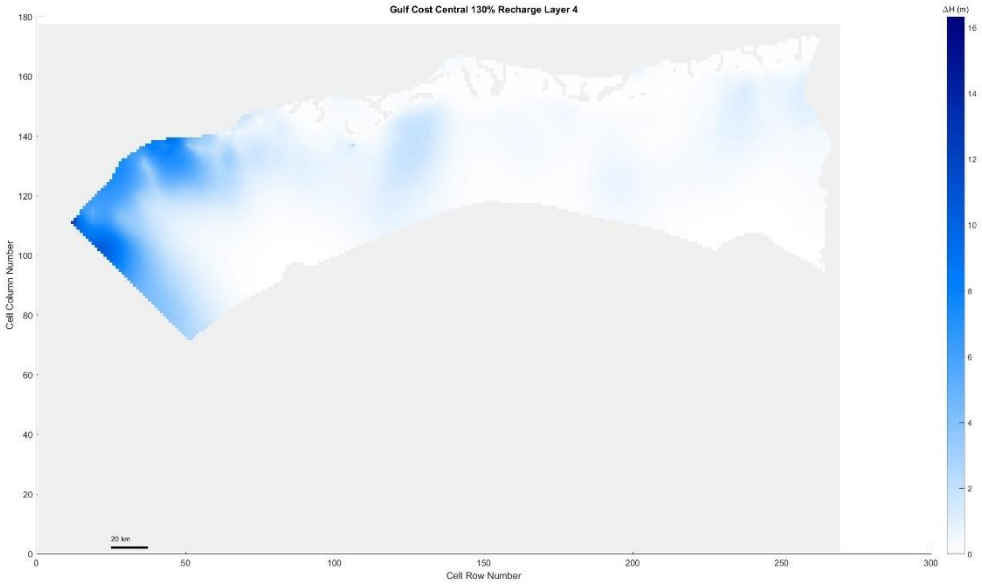

Figure 5. 378 Gulf Coast Central, 130% original recharge hydraulic head spatial distribution of layer 4

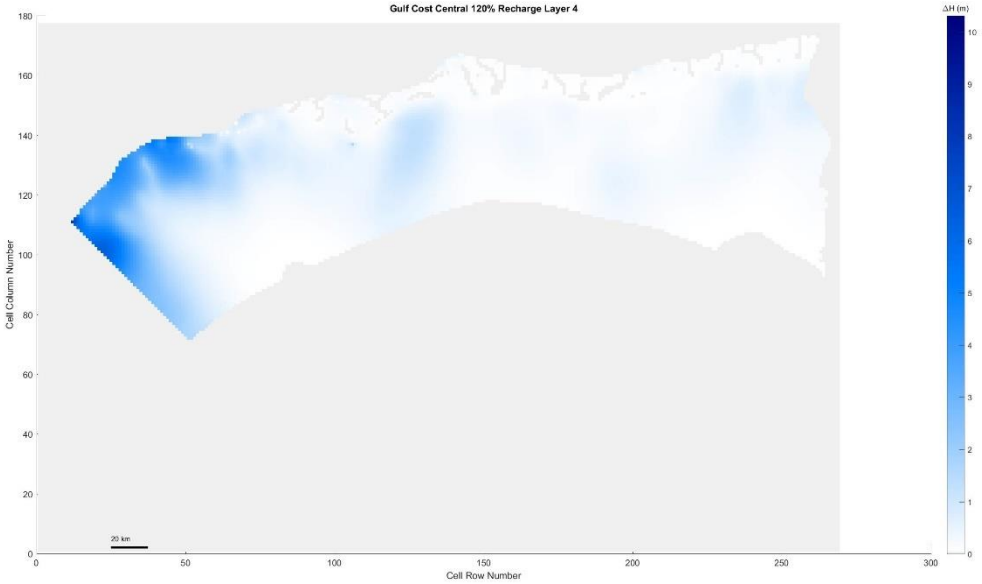

Figure 5. 379 Gulf Coast Central, 120% original recharge hydraulic head spatial distribution of layer 4

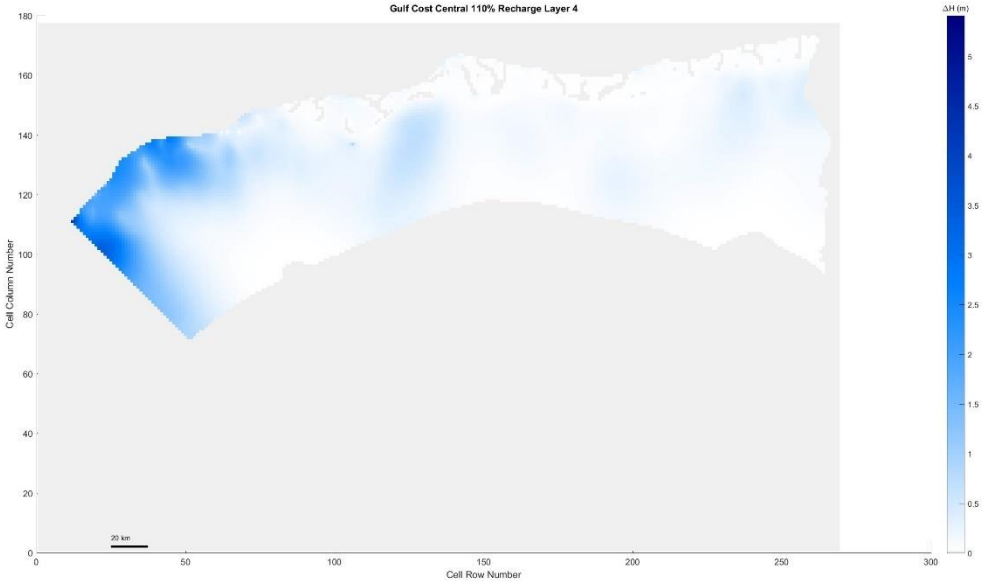

Figure 5. 380 Gulf Coast Central, 110% original recharge hydraulic head spatial distribution of layer 4

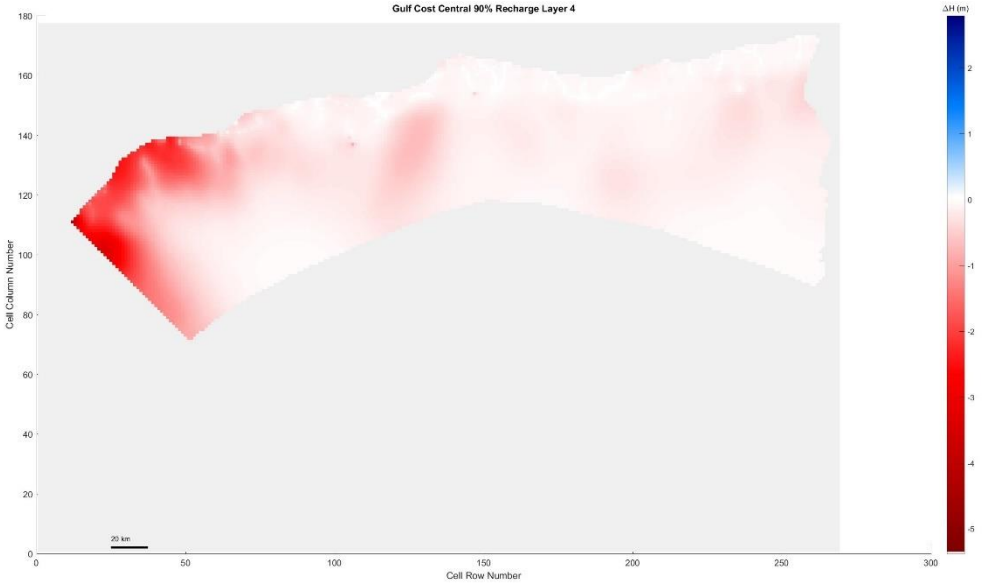

Figure 5. 381 Gulf Coast Central, 90% original recharge hydraulic head spatial distribution of layer 4

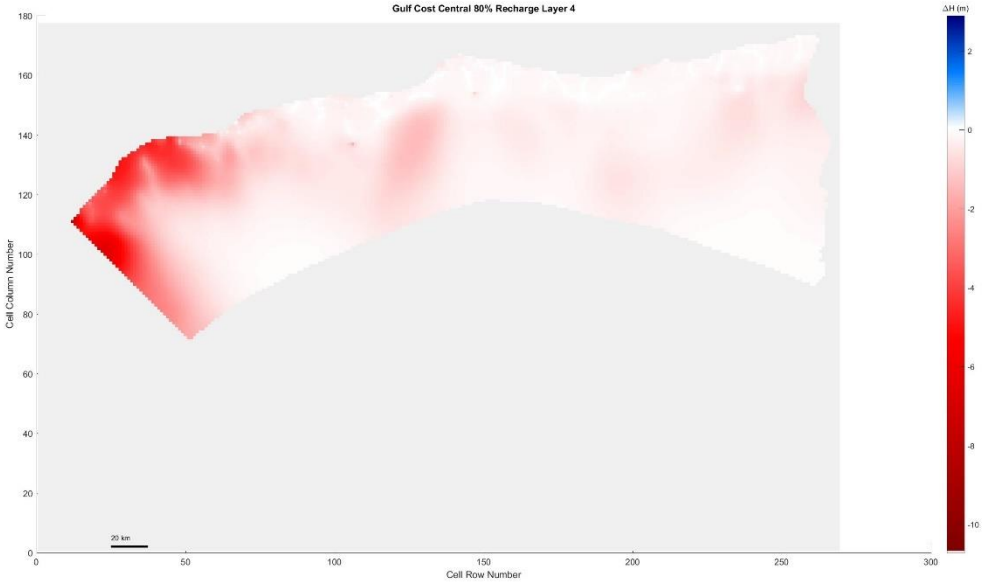

Figure 5. 382 Gulf Coast Central, 80% original recharge hydraulic head spatial distribution of layer 4

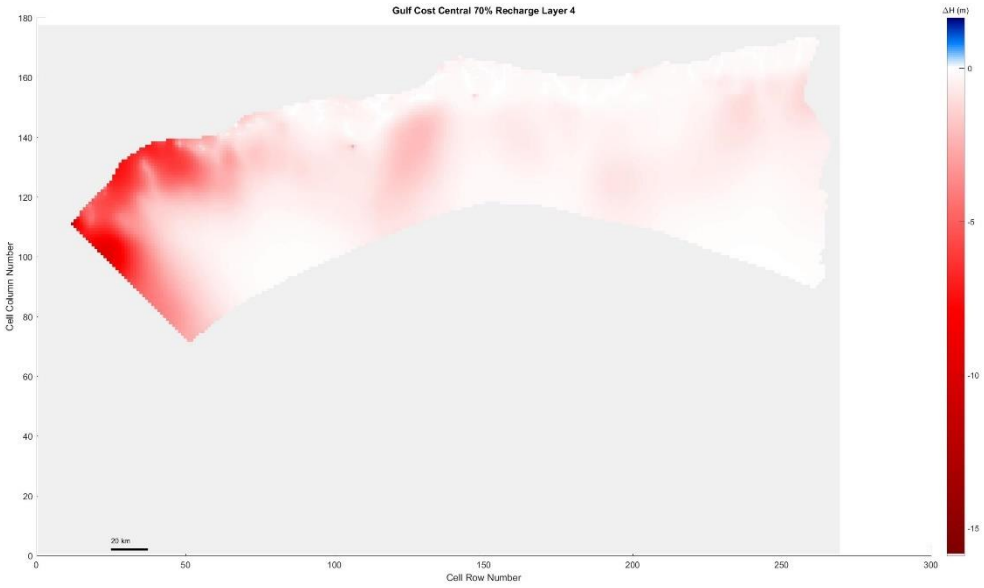

Figure 5. 383 Gulf Coast Central, 70% original recharge hydraulic head spatial distribution of layer 4

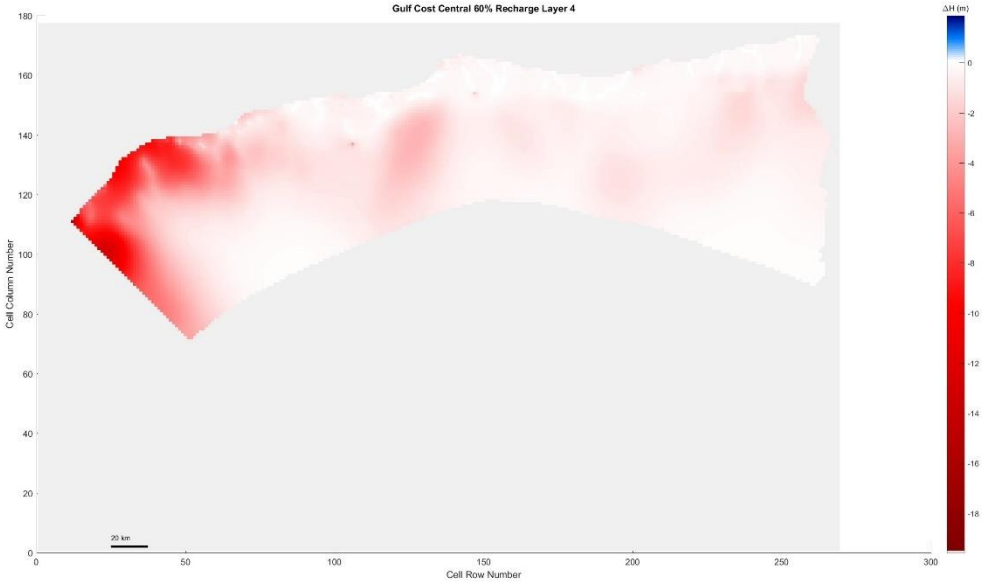

Figure 5. 384 Gulf Coast Central, 60% original recharge hydraulic head spatial distribution of layer 4

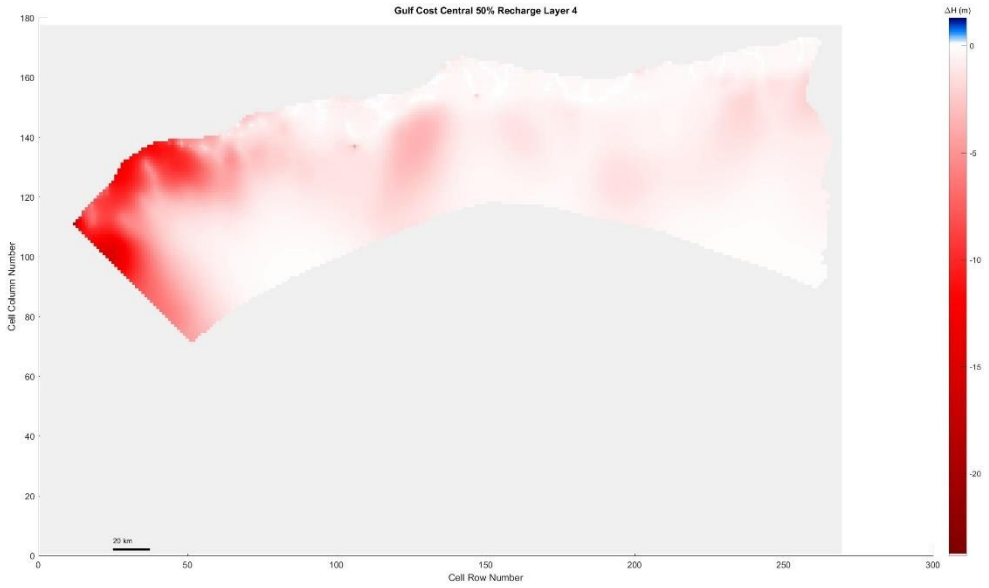

Figure 5. 385 Gulf Coast Central, 50% original recharge hydraulic head spatial distribution of layer 4

Gulf Coast North

Layer 1

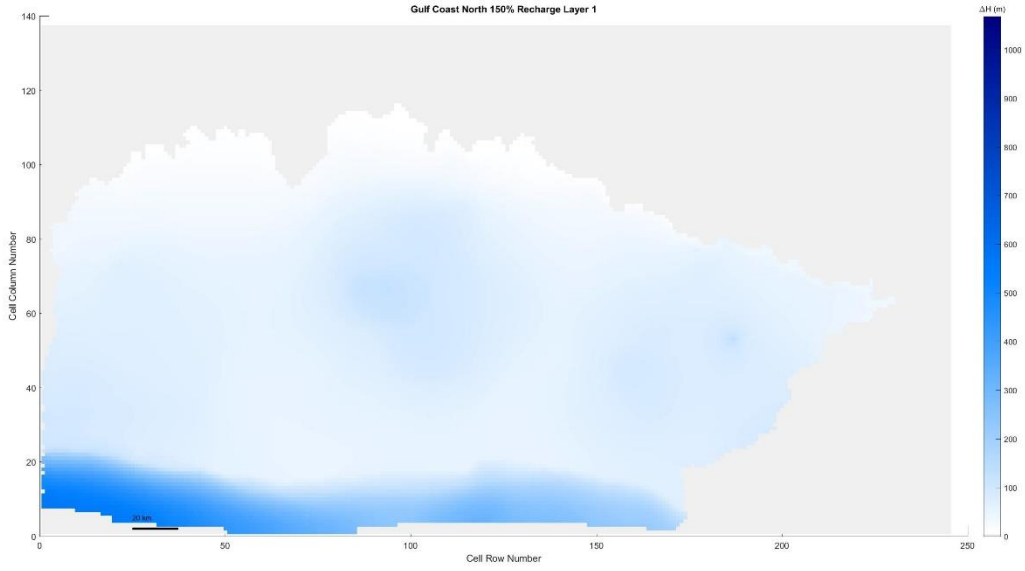

Figure 5. 386 Gulf Coast North, 150% original recharge hydraulic head spatial distribution of layer 1

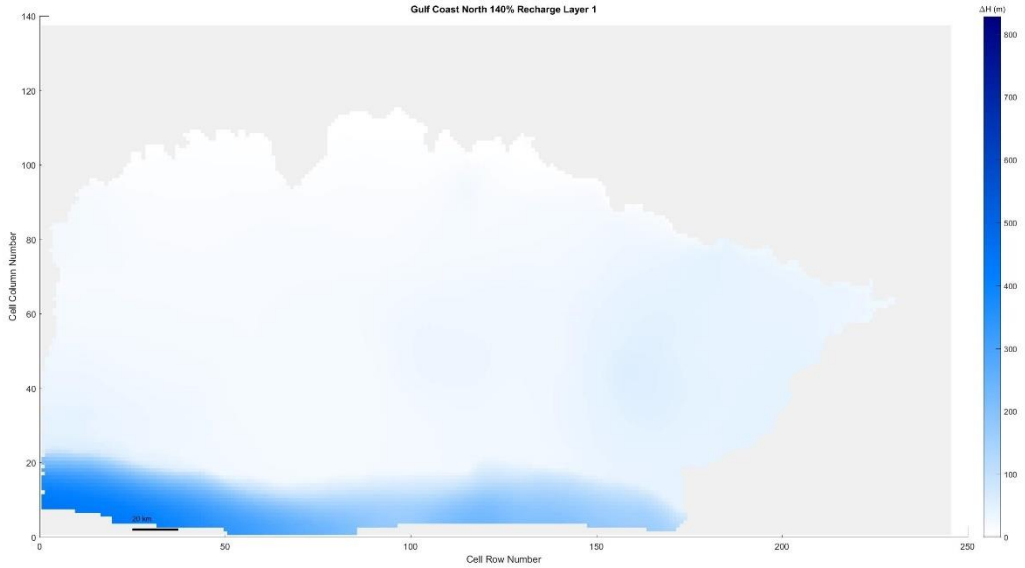

Figure 5. 387 Gulf Coast North, 140% original recharge hydraulic head spatial distribution of layer 1

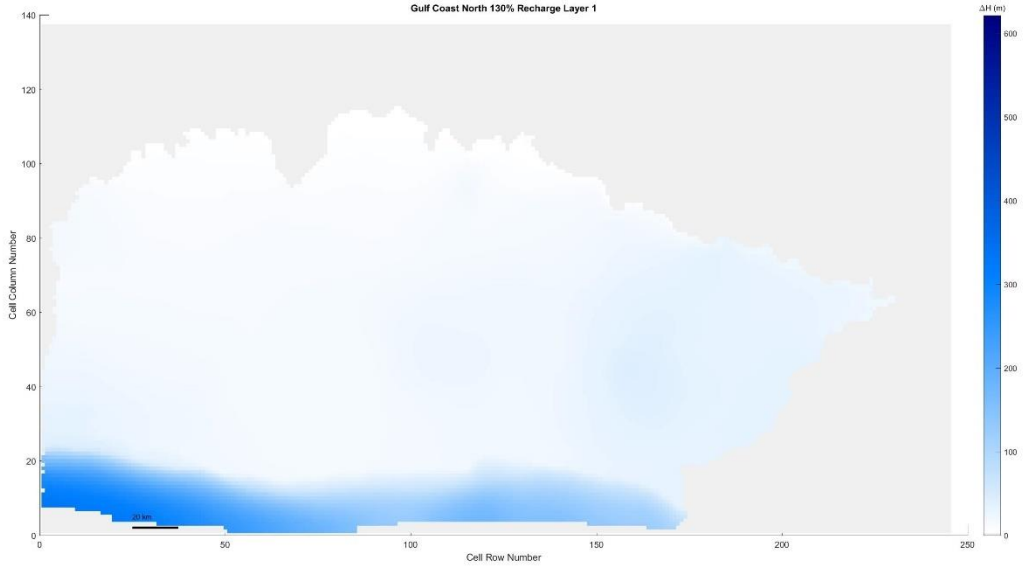

Figure 5. 388 Gulf Coast North, 130% original recharge hydraulic head spatial distribution of layer 1

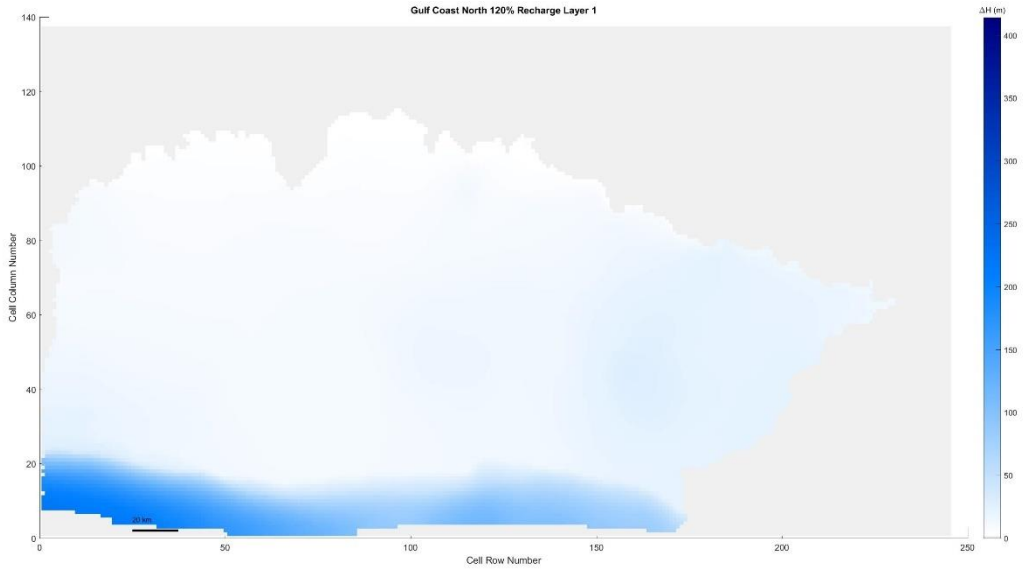

Figure 5. 389 Gulf Coast North, 120% original recharge hydraulic head spatial distribution of layer 1

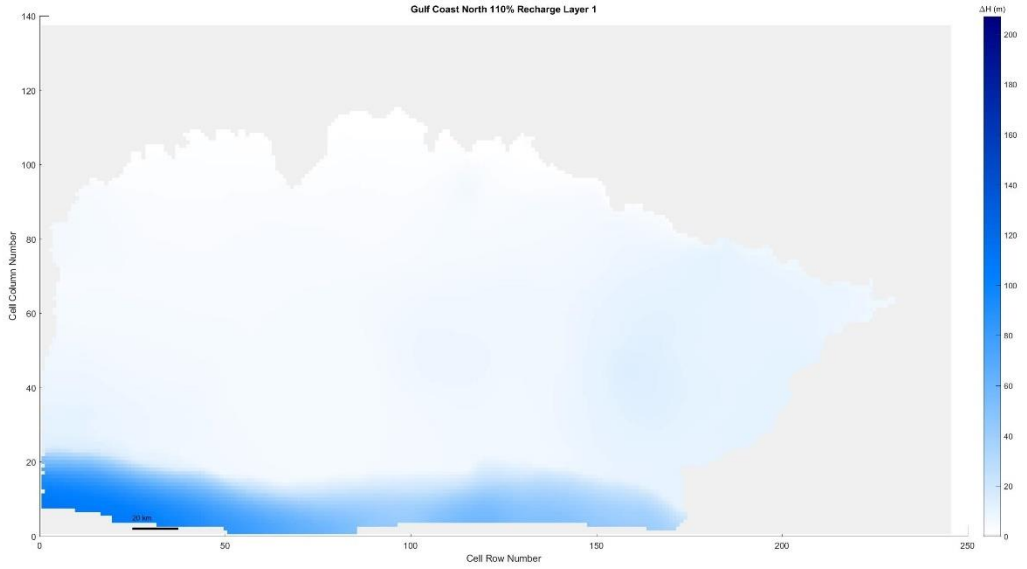

Figure 5. 390 Gulf Coast North, 110% original recharge hydraulic head spatial distribution of layer 1

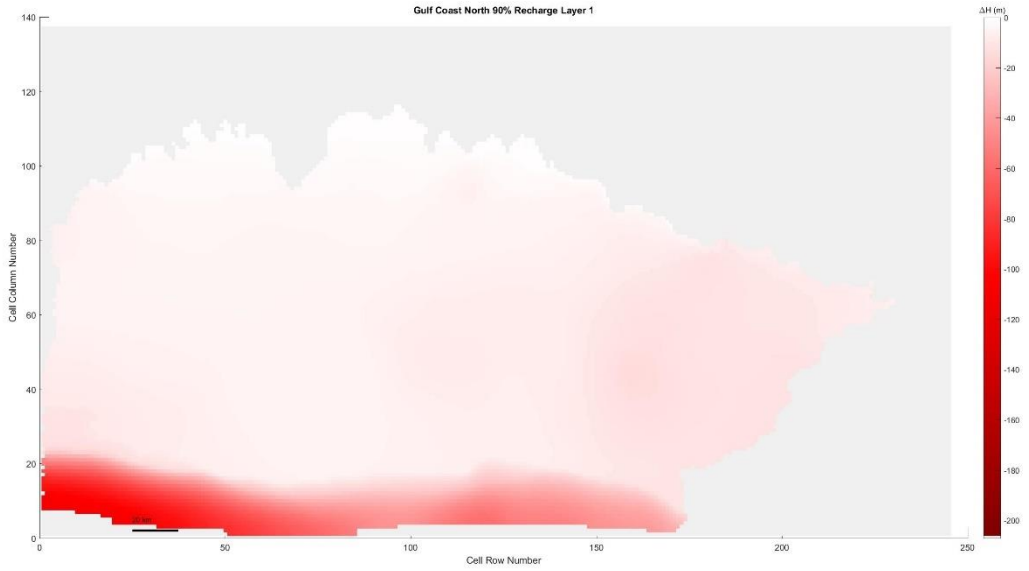

Figure 5. 391 Gulf Coast North, 90% original recharge hydraulic head spatial distribution of layer 1

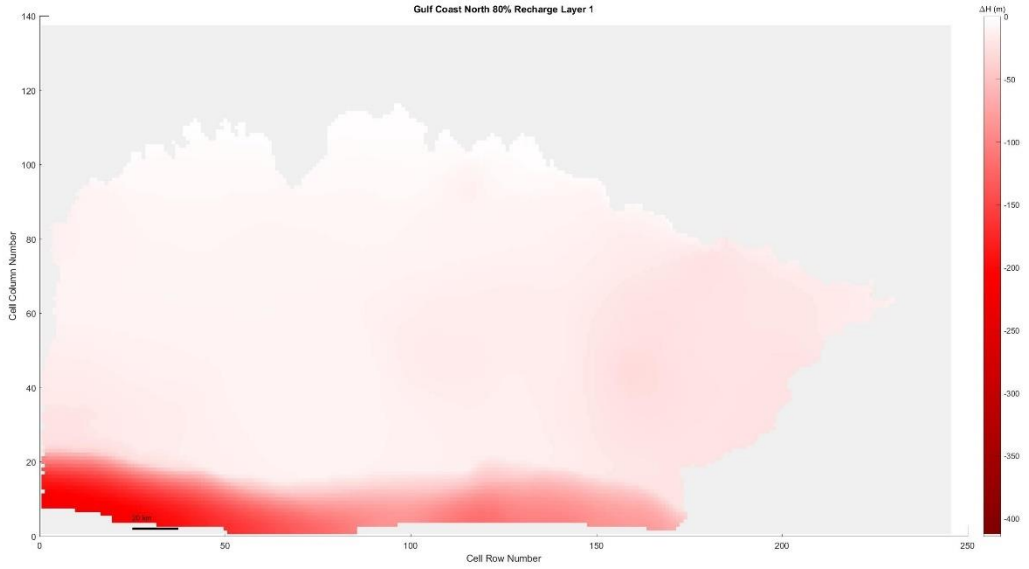

Figure 5. 392 Gulf Coast North, 80% original recharge hydraulic head spatial distribution of layer 1

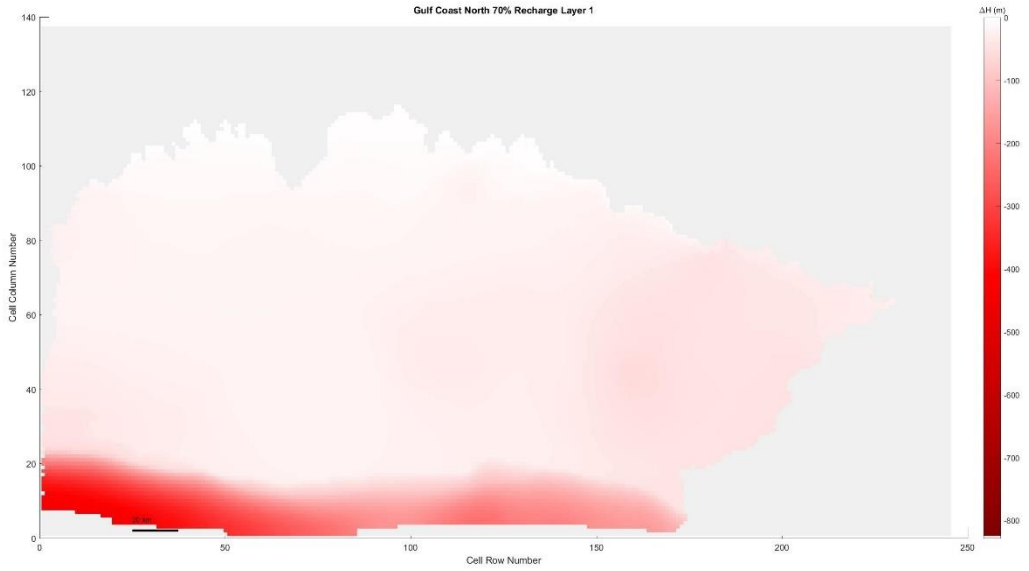

Figure 5. 393 Gulf Coast North, 70% original recharge hydraulic head spatial distribution of layer 1

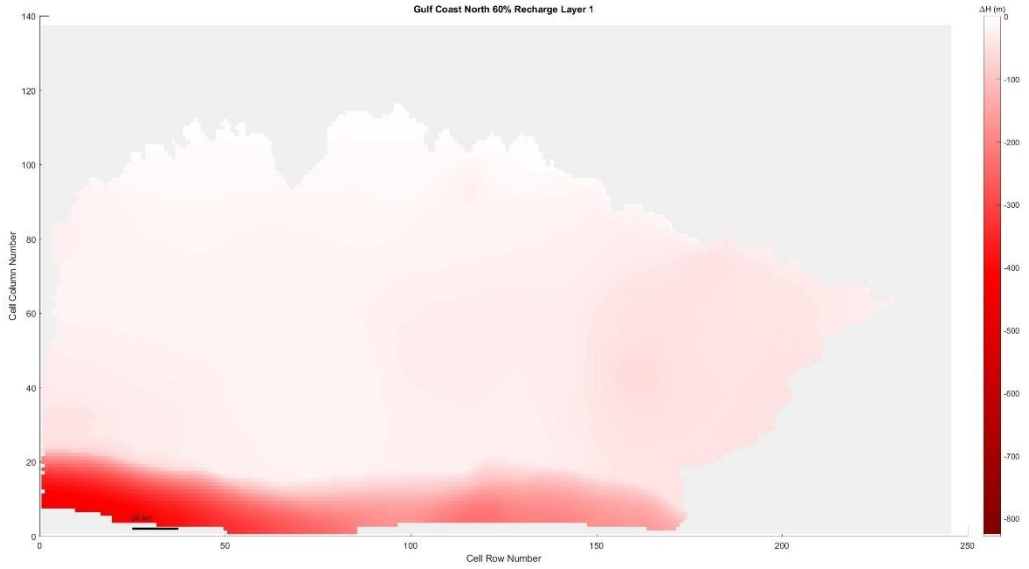

Figure 5. 394 Gulf Coast North, 60% original recharge hydraulic head spatial distribution of layer 1

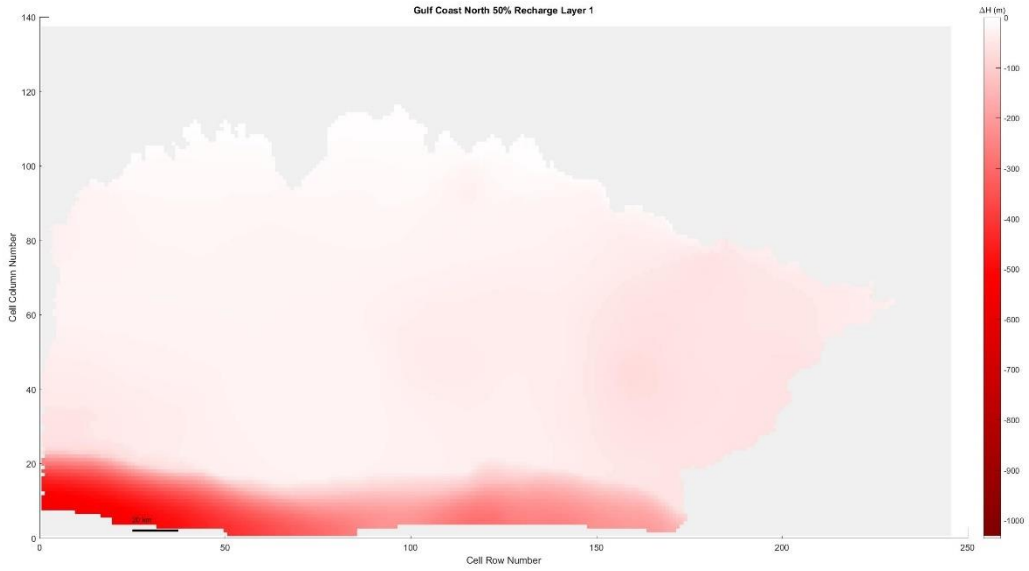

Figure 5. 395 Gulf Coast North, 50% original recharge hydraulic head spatial distribution of layer 1

Layer 2

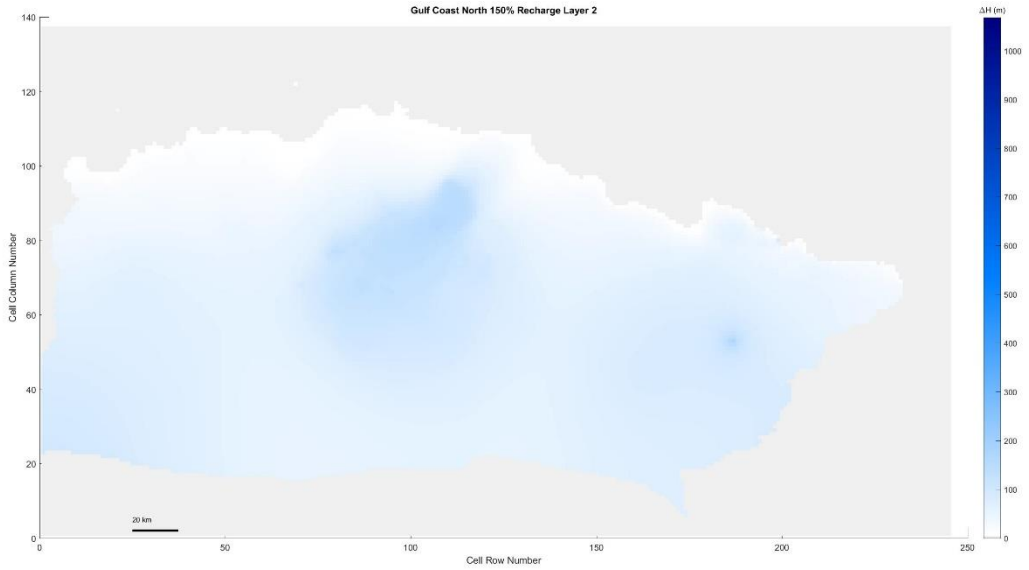

Figure 5. 396 Gulf Coast North, 150% original recharge hydraulic head spatial distribution of layer 2

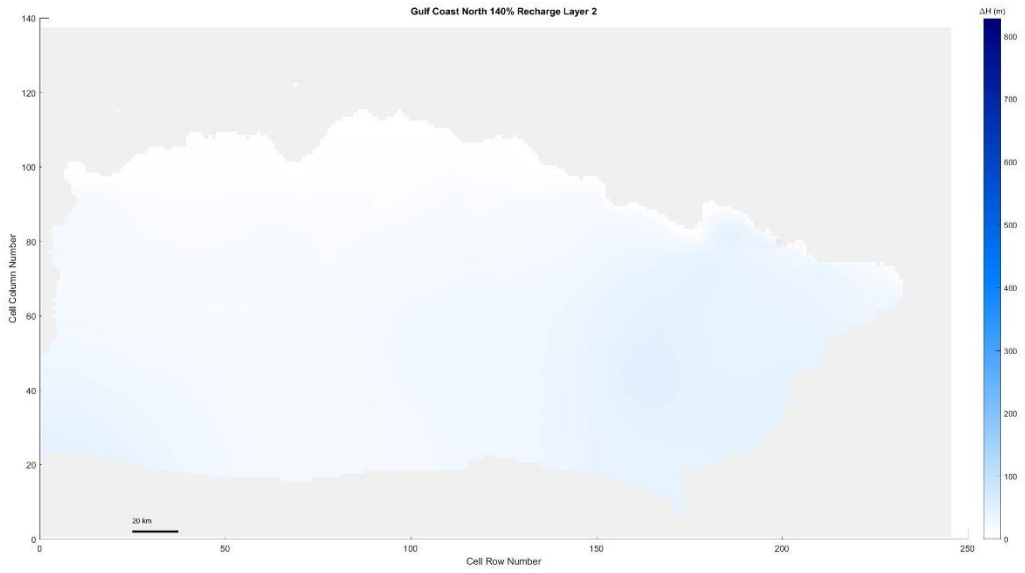

Figure 5. 397 Gulf Coast North, 140% original recharge hydraulic head spatial distribution of layer 2

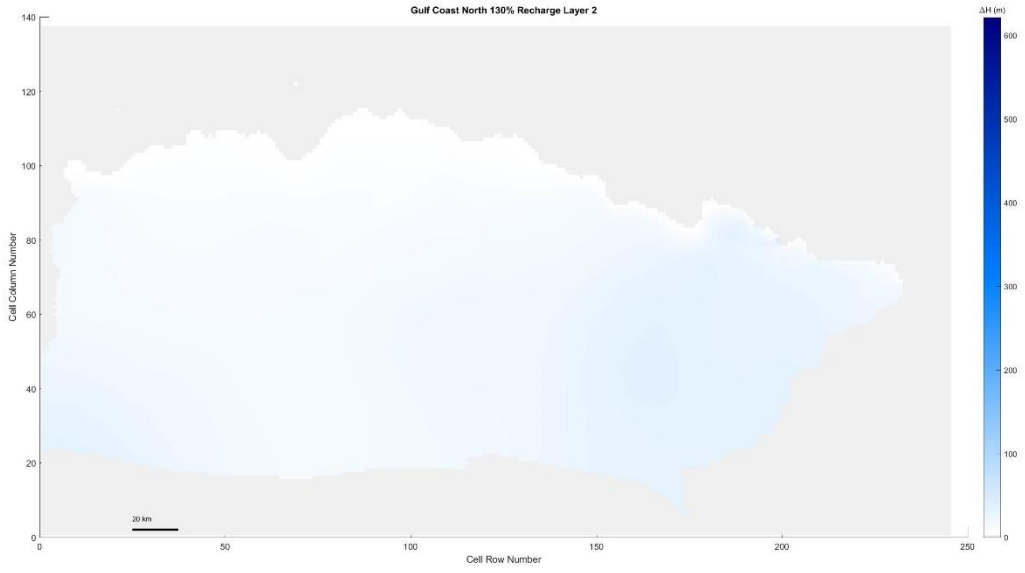

Figure 5. 398 Gulf Coast North, 130% original recharge hydraulic head spatial distribution of layer 2

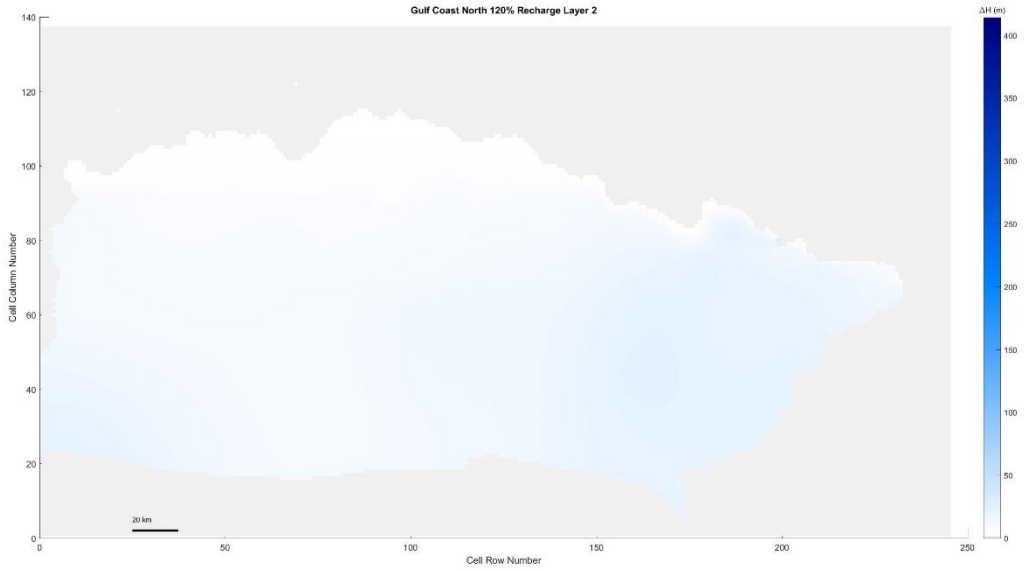

Figure 5. 399 Gulf Coast North, 120% original recharge hydraulic head spatial distribution of layer 2

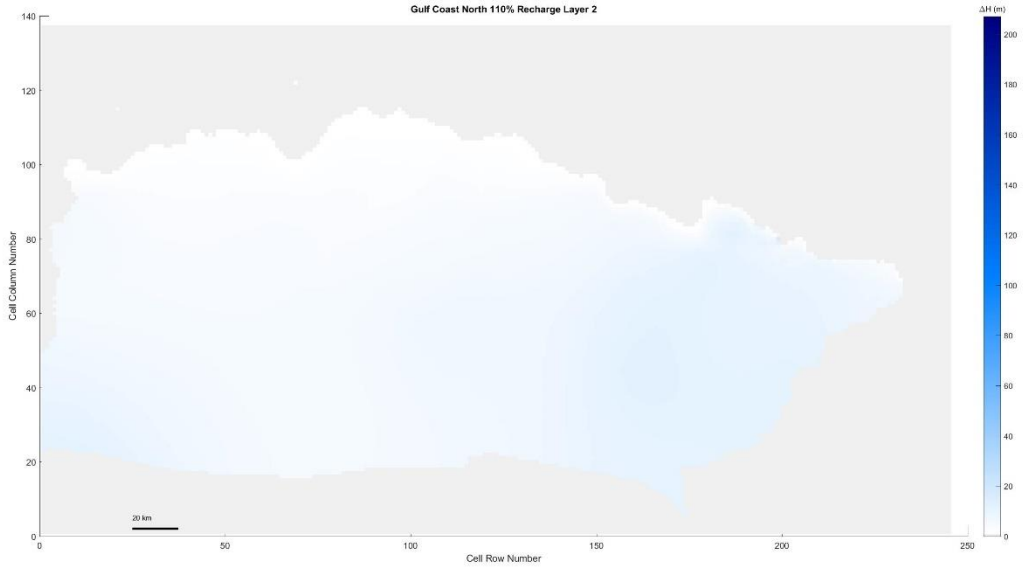

Figure 5. 400 Gulf Coast North, 110% original recharge hydraulic head spatial distribution of layer 2

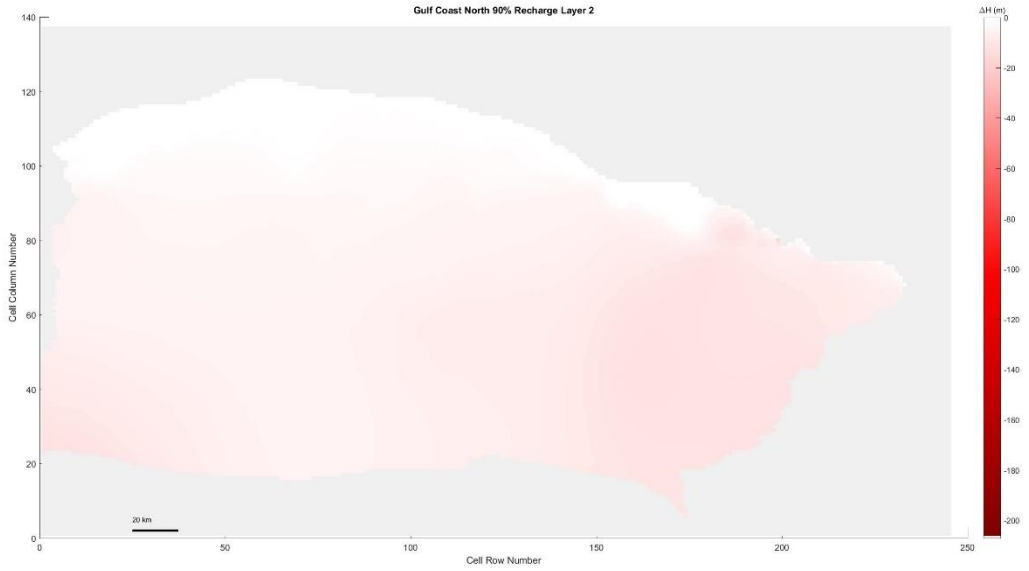

Figure 5. 401 Gulf Coast North, 90% original recharge hydraulic head spatial distribution of layer 2

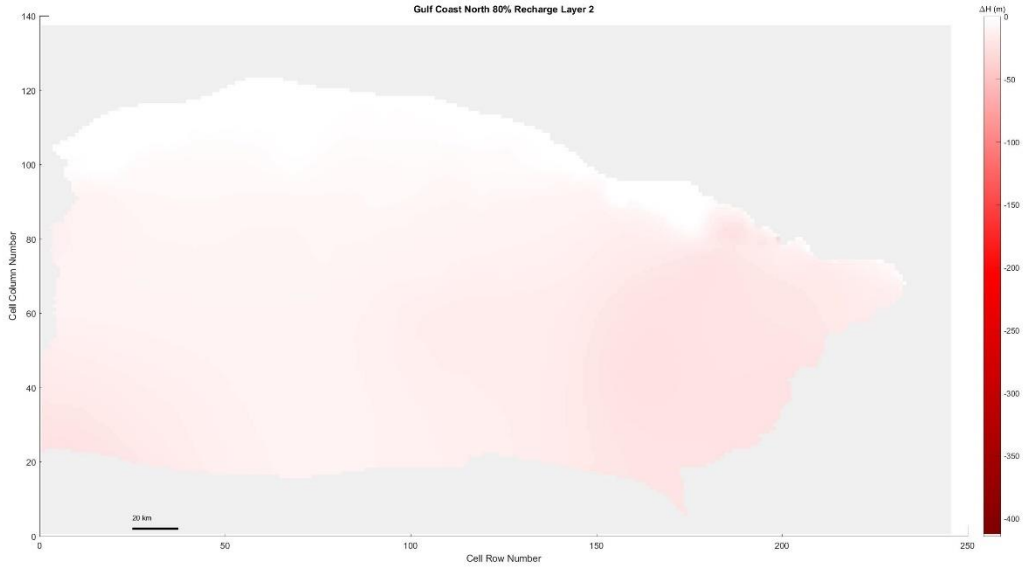

Figure 5. 402 Gulf Coast North, 80% original recharge hydraulic head spatial distribution of layer 2

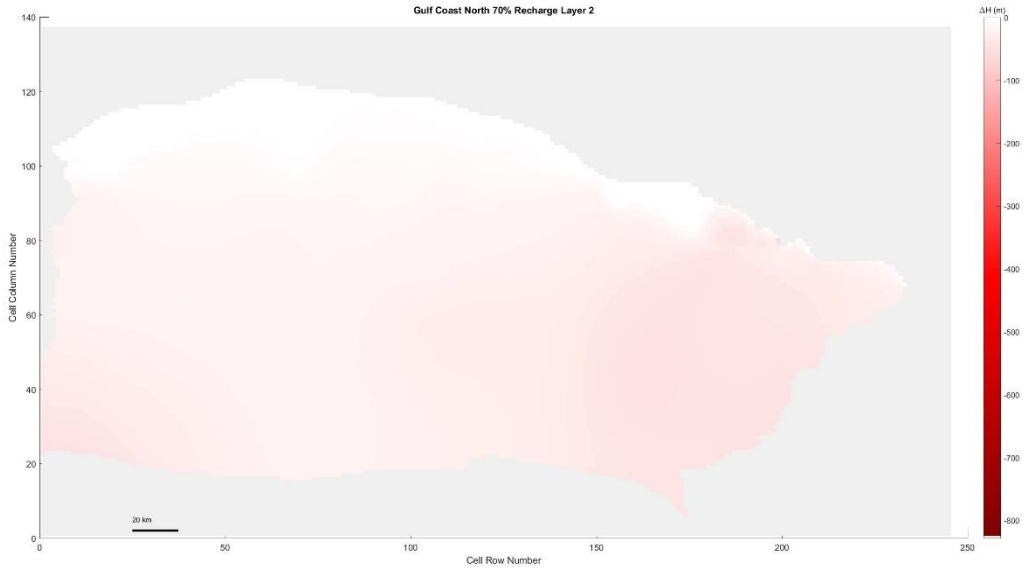

Figure 5. 403 Gulf Coast North, 70% original recharge hydraulic head spatial distribution of layer 2

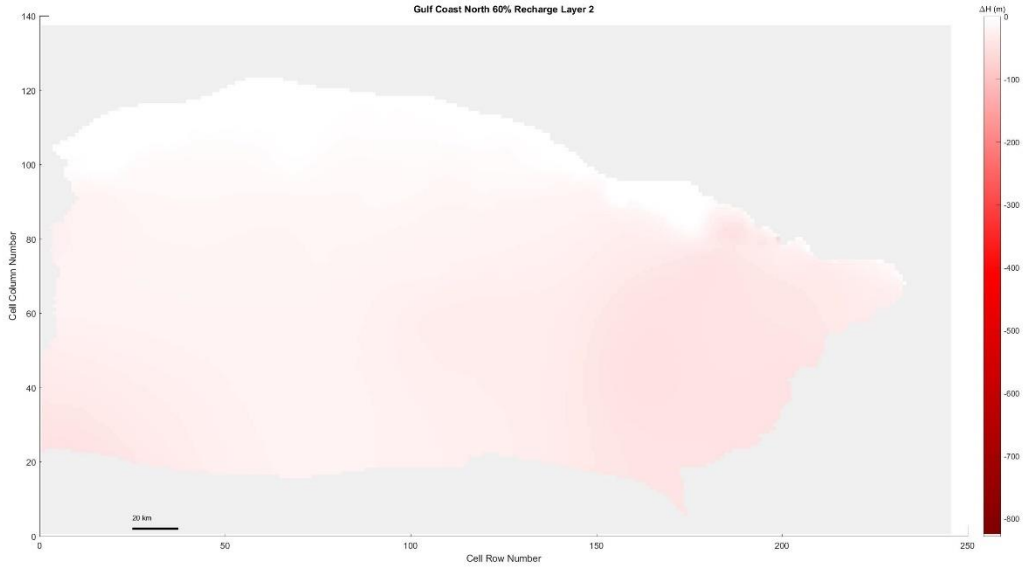

Figure 5. 404 Gulf Coast North, 60% original recharge hydraulic head spatial distribution of layer 2

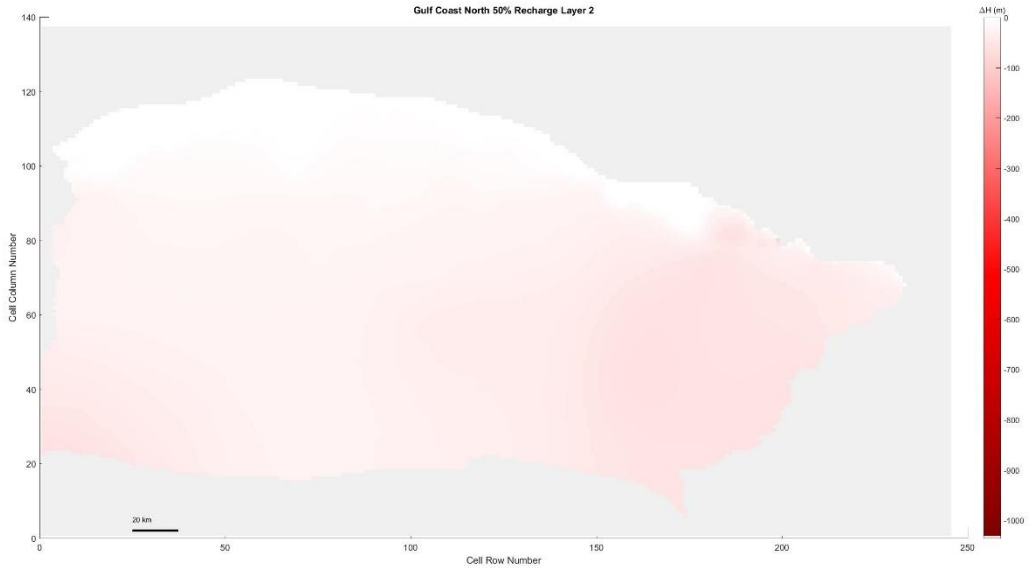

Figure 5. 405 Gulf Coast North, 50% original recharge hydraulic head spatial distribution of layer 2

Layer 3

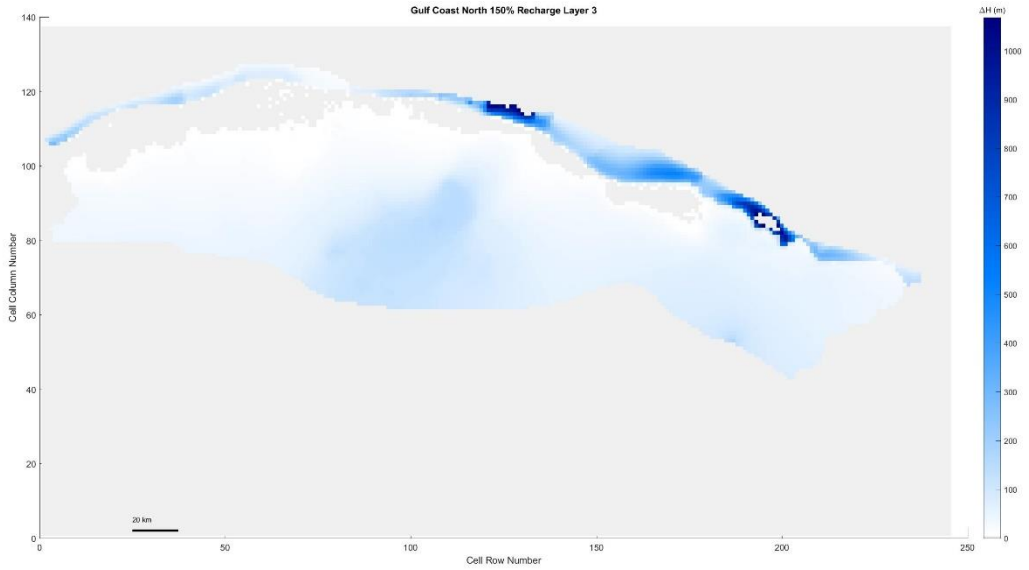

Figure 5. 406 Gulf Coast North, 150% original recharge hydraulic head spatial distribution of layer 3

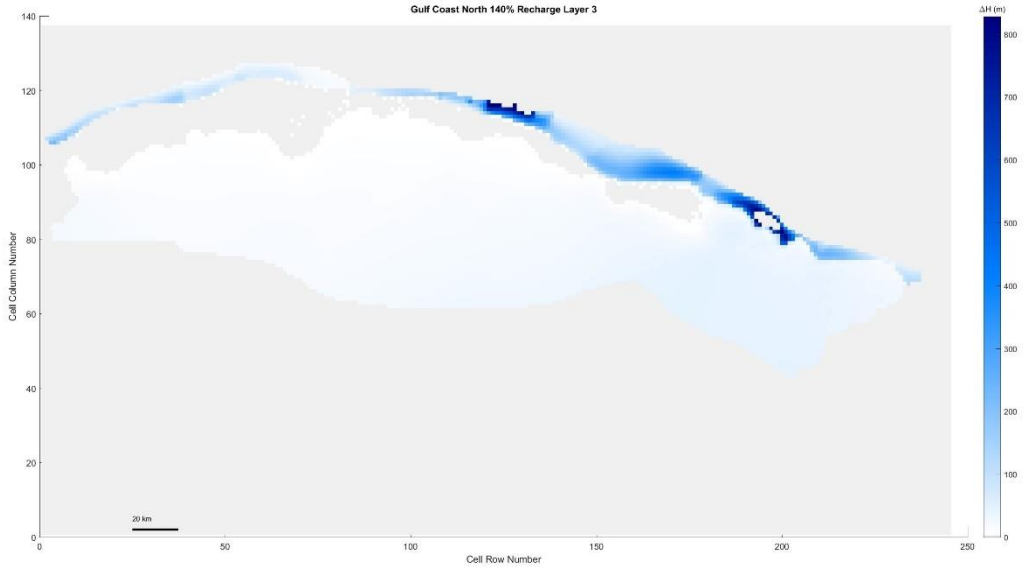

Figure 5. 407 Gulf Coast North, 140% original recharge hydraulic head spatial distribution of layer 3

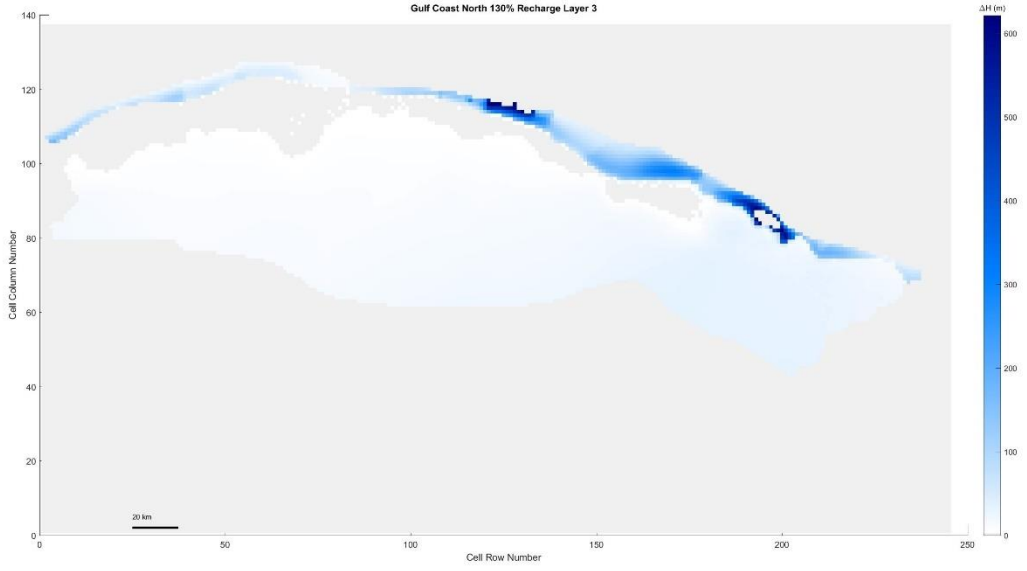

Figure 5. 408 Gulf Coast North, 130% original recharge hydraulic head spatial distribution of layer 3

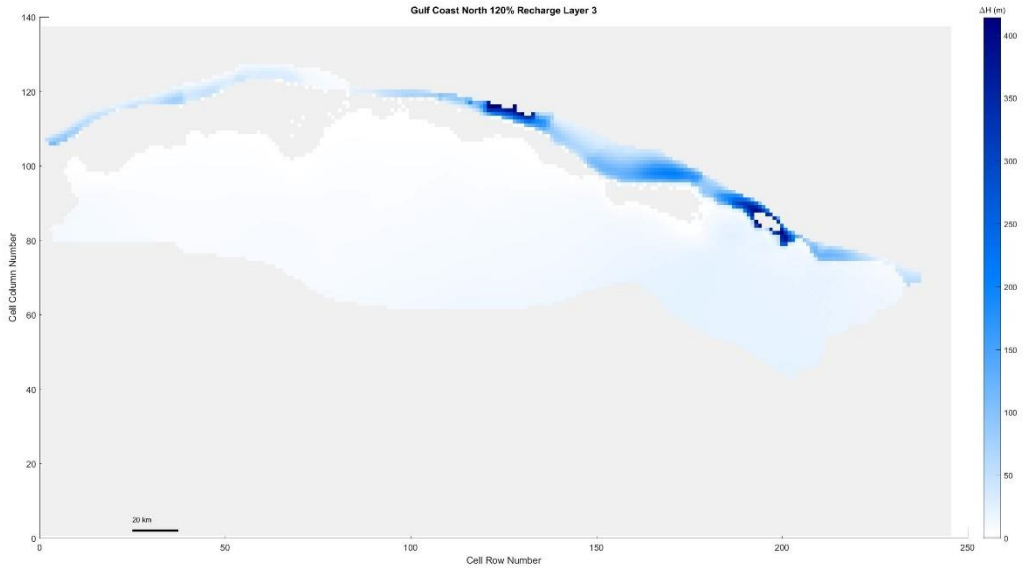

Figure 5. 409 Gulf Coast North, 120% original recharge hydraulic head spatial distribution of layer 3

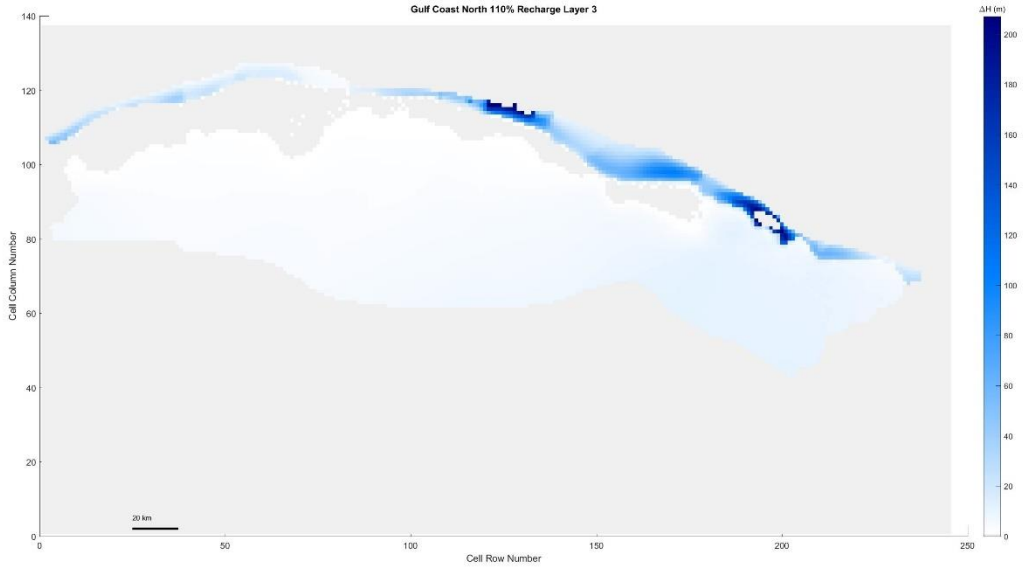

Figure 5. 410 Gulf Coast North, 110% original recharge hydraulic head spatial distribution of layer 3

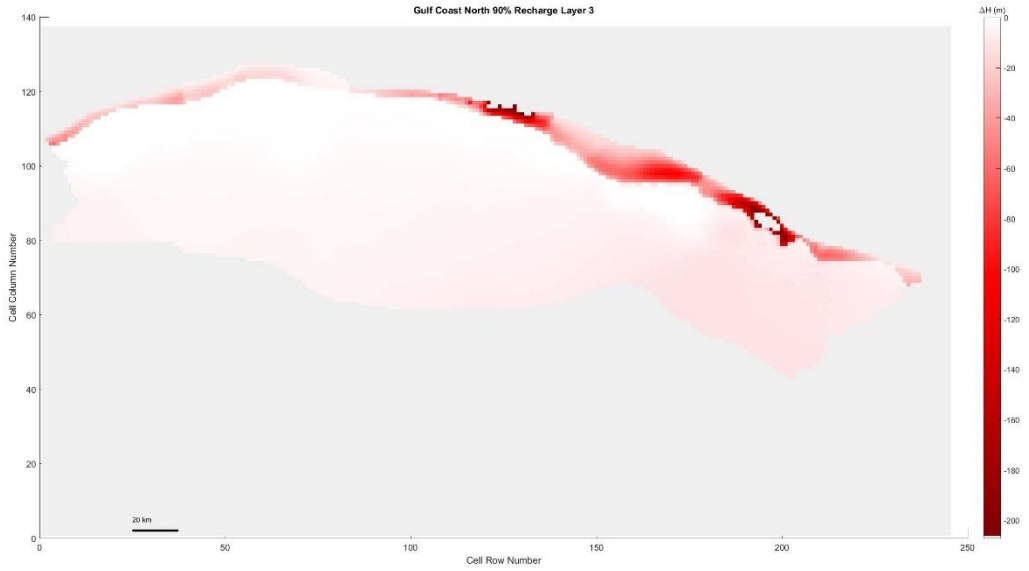

Figure 5. 411 Gulf Coast North, 90% original recharge hydraulic head spatial distribution of layer 3

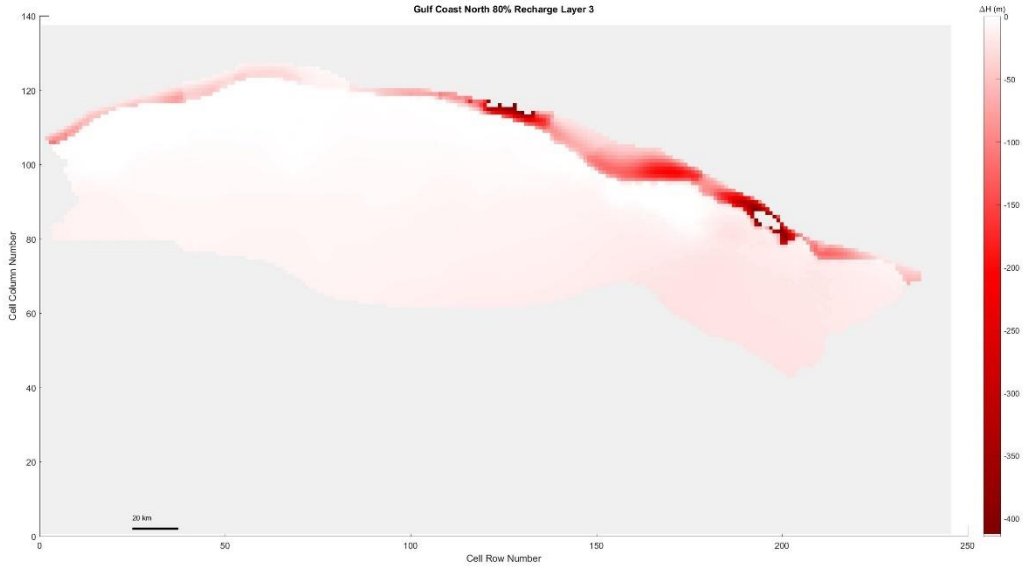

Figure 5. 412 Gulf Coast North, 80% original recharge hydraulic head spatial distribution of layer 3

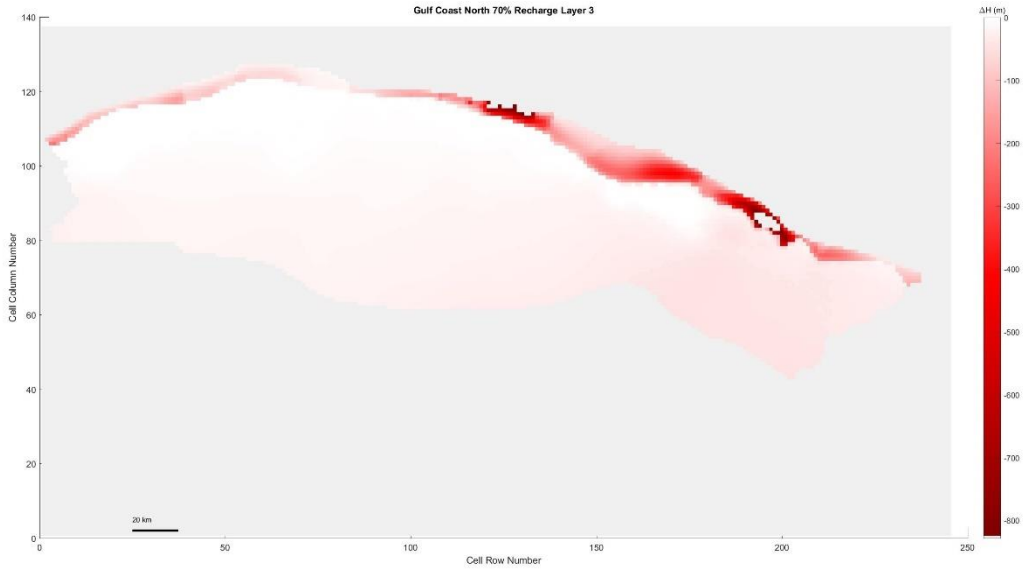

Figure 5. 413 Gulf Coast North, 70% original recharge hydraulic head spatial distribution of layer 3

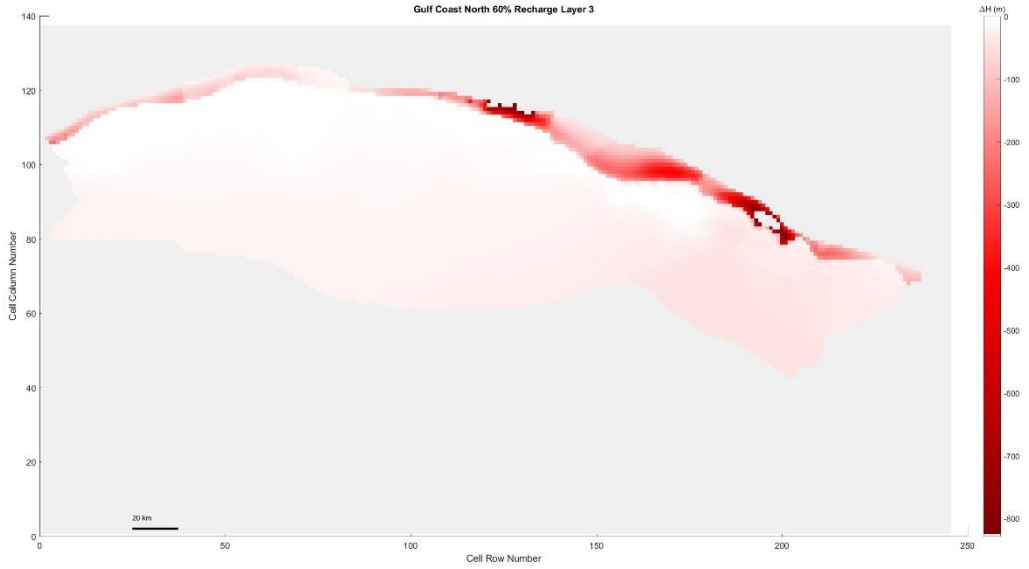

Figure 5. 414 Gulf Coast North, 60% original recharge hydraulic head spatial distribution of layer 3

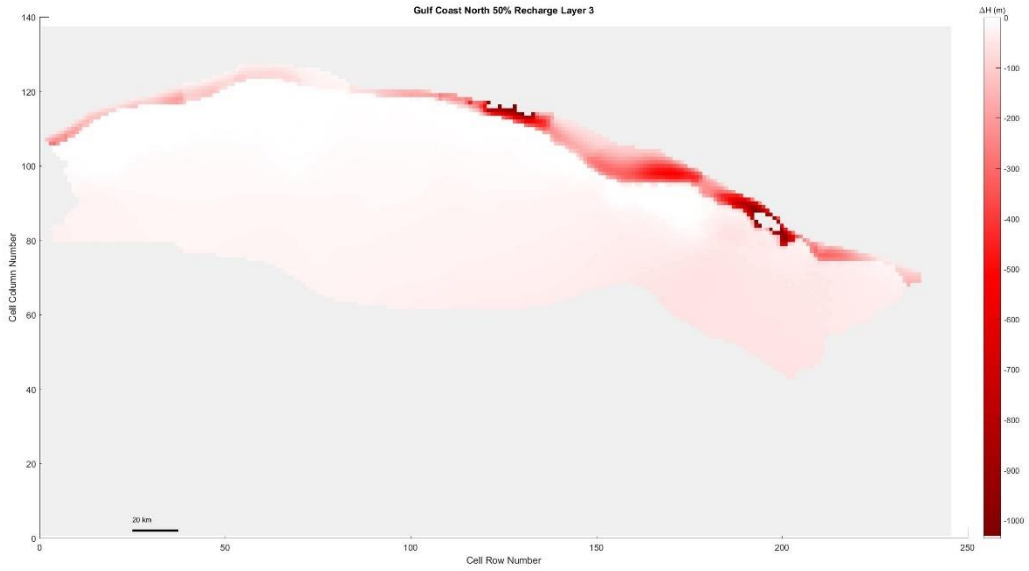

Figure 5. 415 Gulf Coast North, 50% original recharge hydraulic head spatial distribution of layer 3

Layer 4

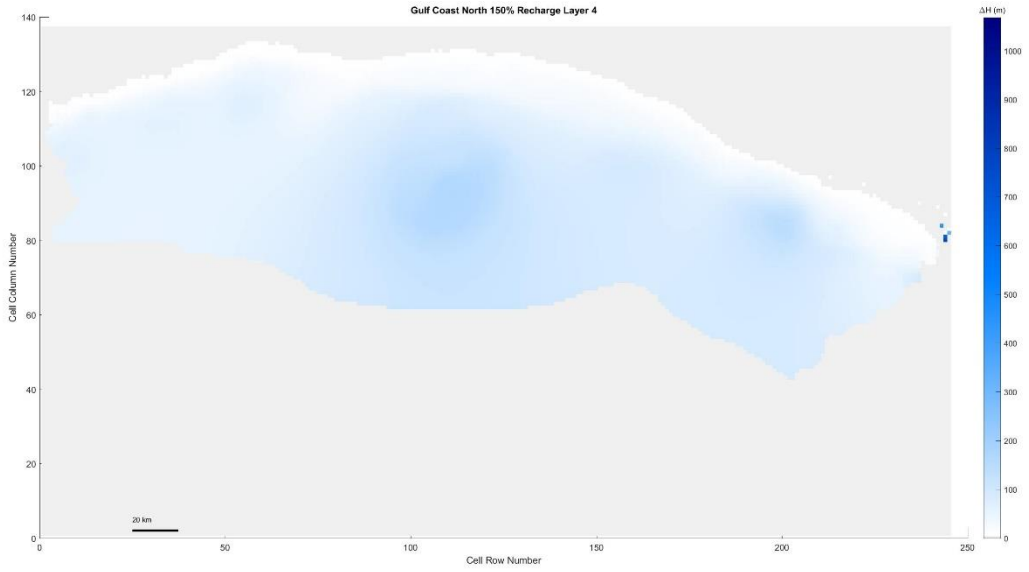

Figure 5. 416 Gulf Coast North, 150% original recharge hydraulic head spatial distribution of layer 4

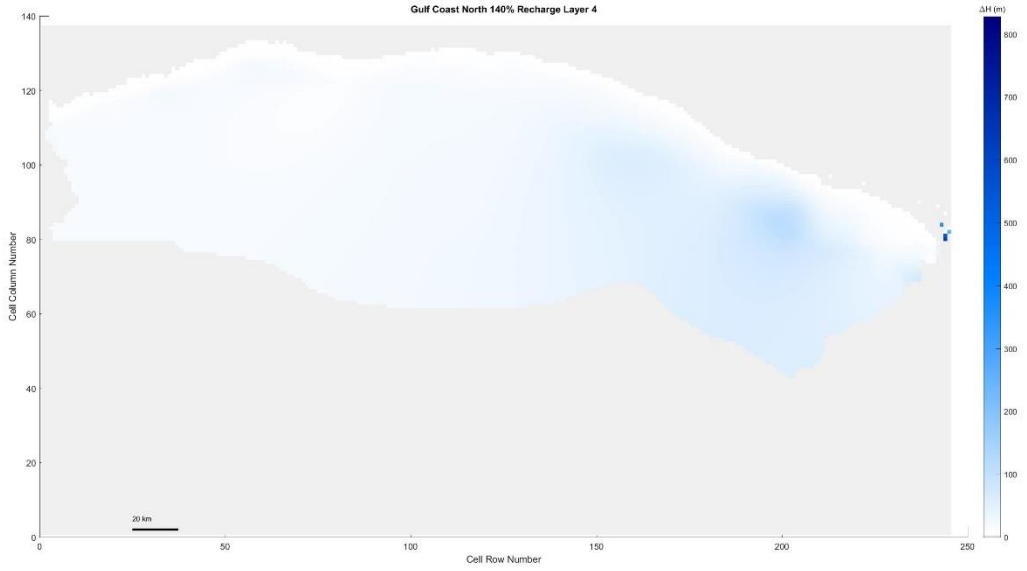

Figure 5. 417 Gulf Coast North, 140% original recharge hydraulic head spatial distribution of layer 4

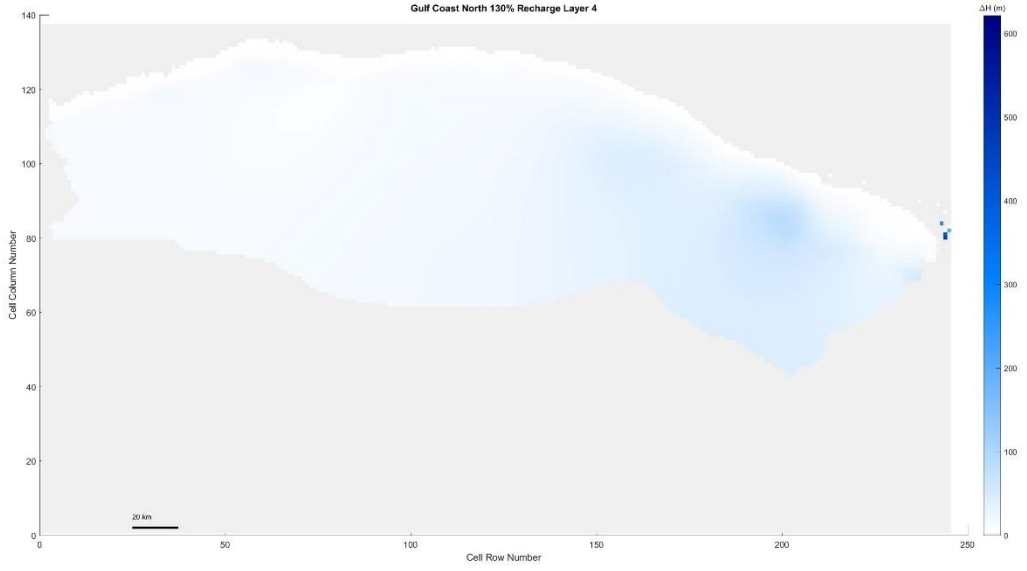

Figure 5. 418 Gulf Coast North, 130% original recharge hydraulic head spatial distribution of layer 4

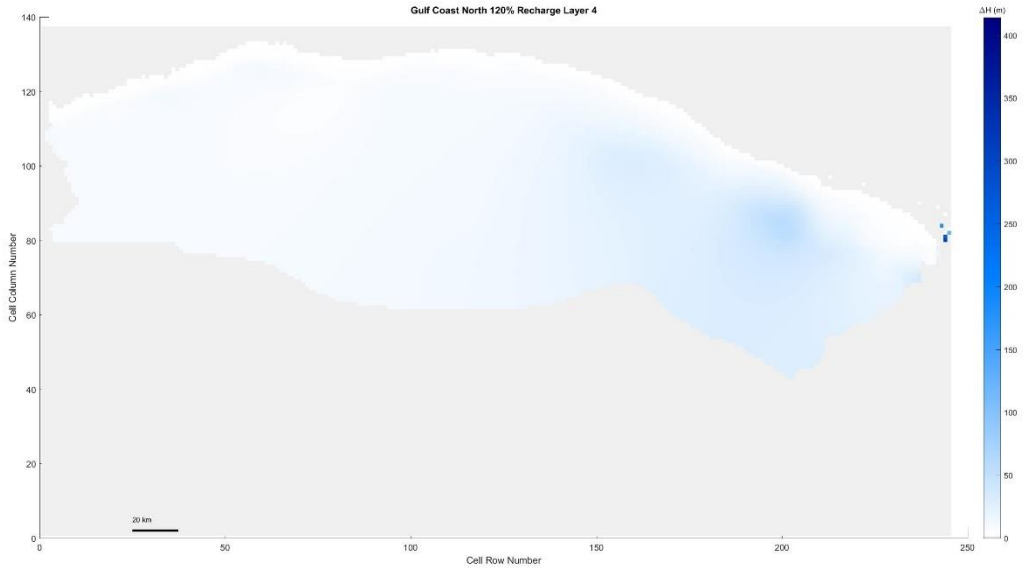

Figure 5. 419 Gulf Coast North, 120% original recharge hydraulic head spatial distribution of layer 4

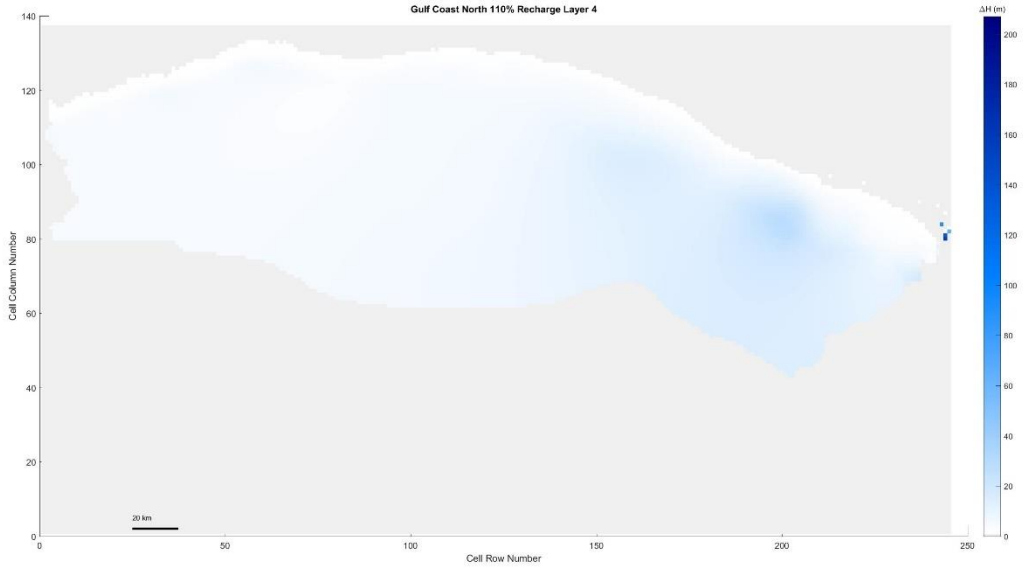

Figure 5. 420 Gulf Coast North, 110% original recharge hydraulic head spatial distribution of layer 4

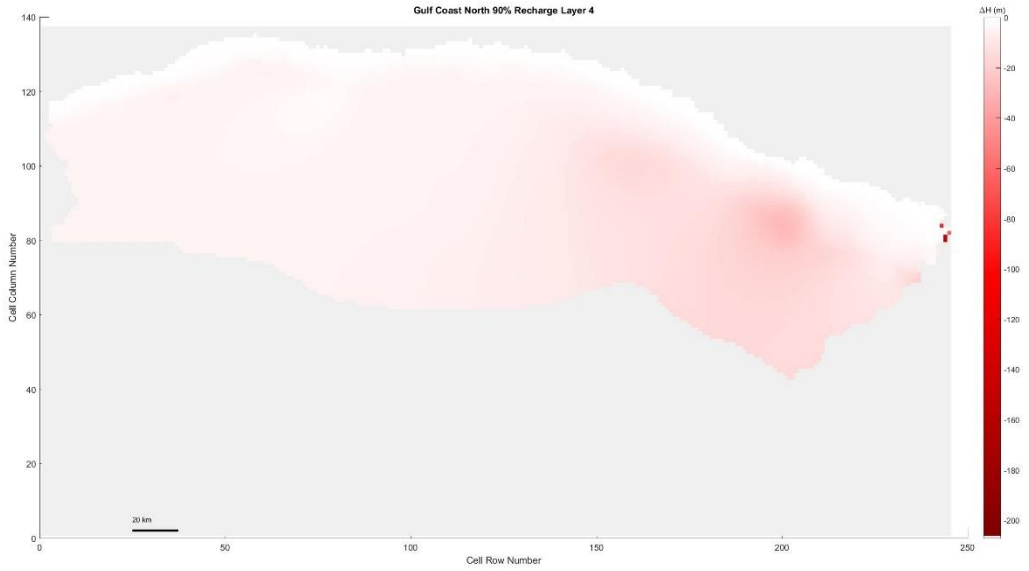

Figure 5. 421 Gulf Coast North, 90% original recharge hydraulic head spatial distribution of layer 4

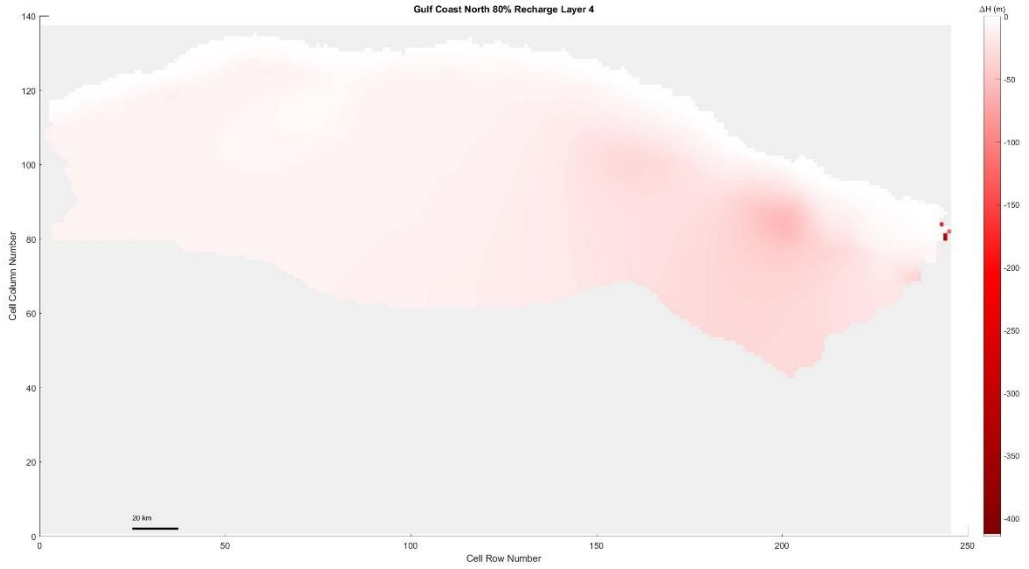

Figure 5. 422 Gulf Coast North, 80% original recharge hydraulic head spatial distribution of layer 4

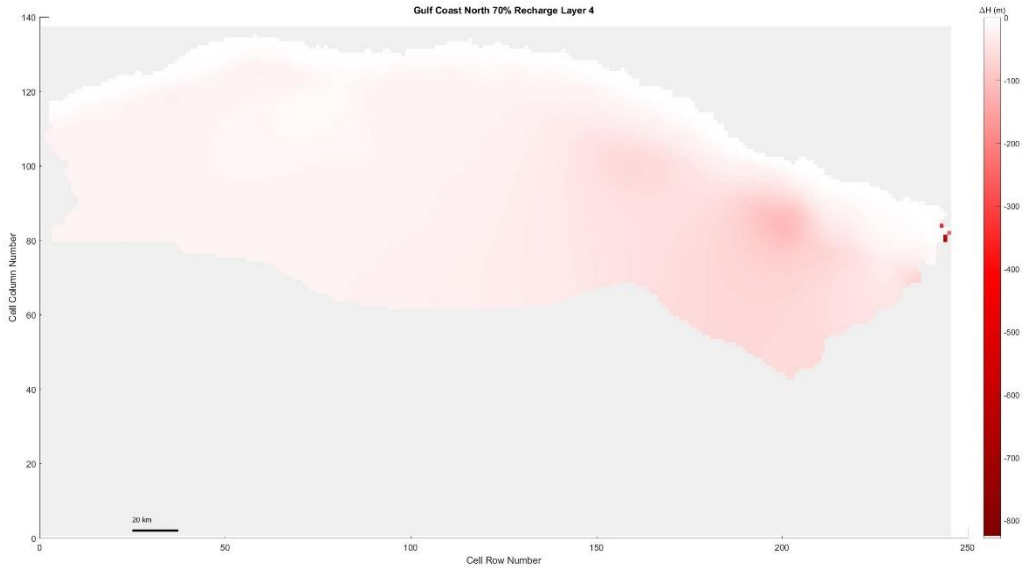

Figure 5. 423 Gulf Coast North, 70% original recharge hydraulic head spatial distribution of layer 4

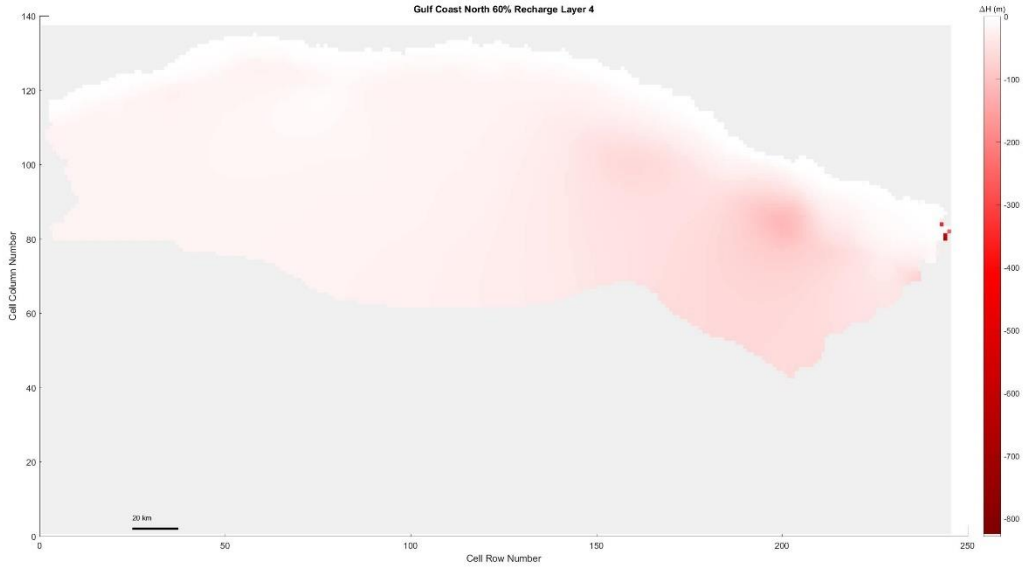

Figure 5. 424 Gulf Coast North, 60% original recharge hydraulic head spatial distribution of layer 4

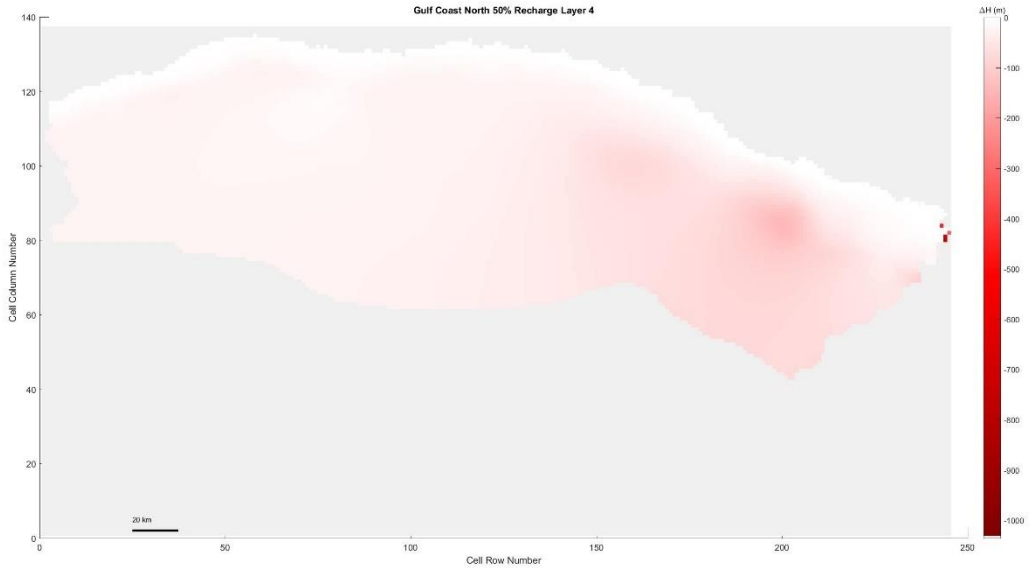

Figure 5. 425 Gulf Coast North, 50% original recharge hydraulic head spatial distribution of layer 4

Gulf Coast South

Layer 1

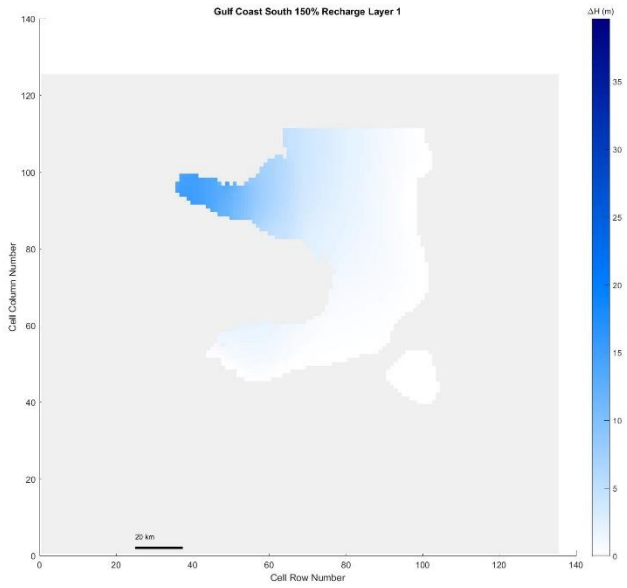

Figure 5. 426 Gulf Coast South, 150% original recharge hydraulic head spatial distribution of layer 1

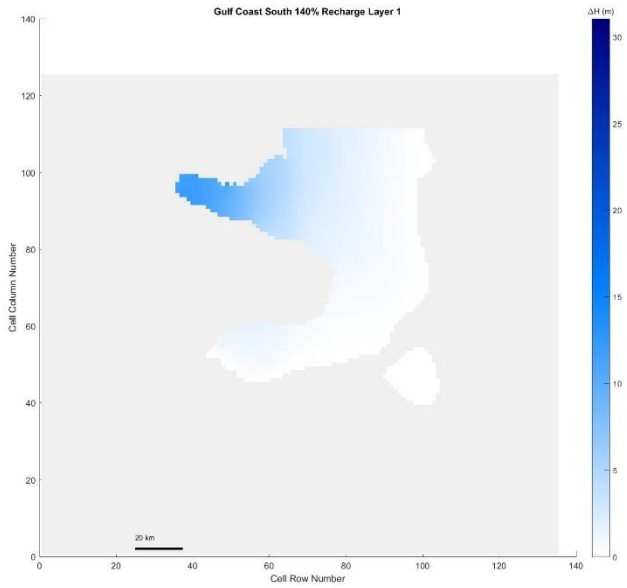

Figure 5. 427 Gulf Coast South, 140% original recharge hydraulic head spatial distribution of layer 1

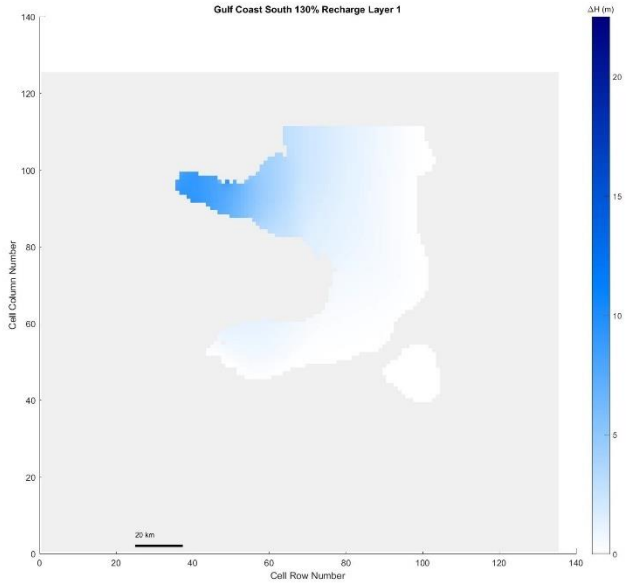

Figure 5. 428 Gulf Coast South, 130% original recharge hydraulic head spatial distribution of layer 1

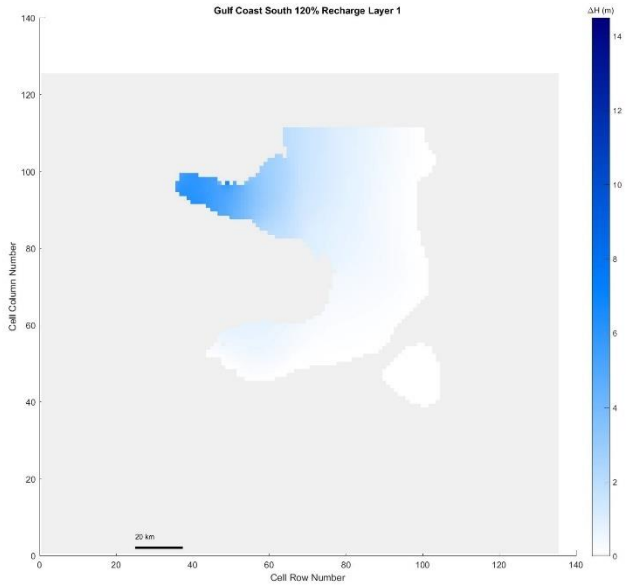

Figure 5. 429 Gulf Coast South, 120% original recharge hydraulic head spatial distribution of layer 1

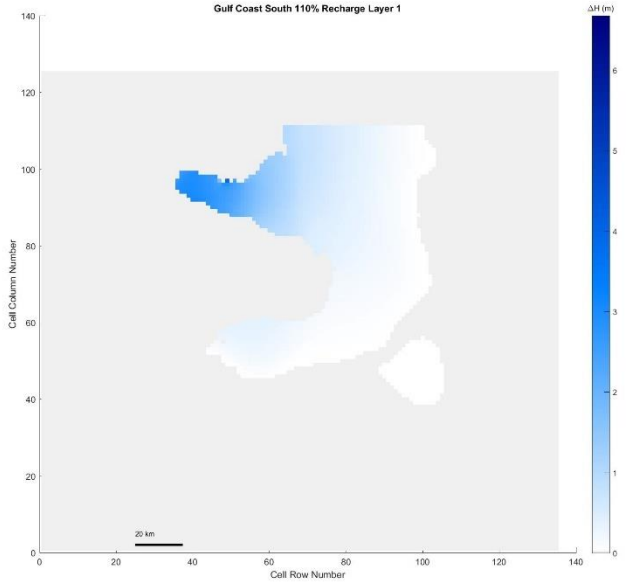

Figure 5. 430 Gulf Coast South, 110% original recharge hydraulic head spatial distribution of layer 1

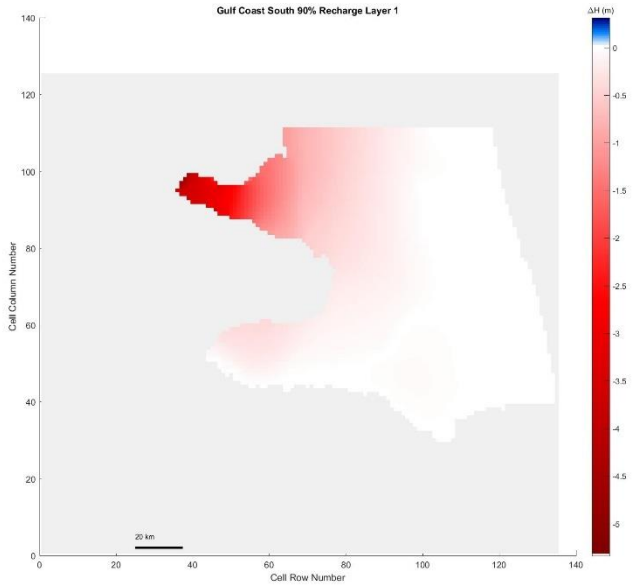

Figure 5. 431 Gulf Coast South, 90% original recharge hydraulic head spatial distribution of layer 1

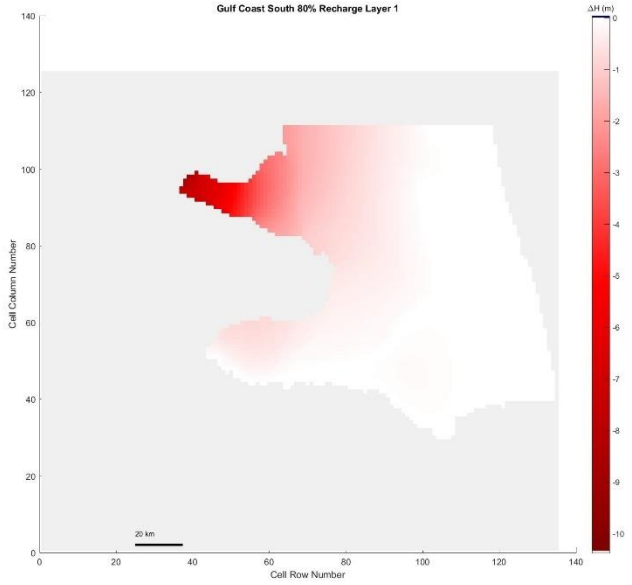

Figure 5. 432 Gulf Coast South, 80% original recharge hydraulic head spatial distribution of layer 1

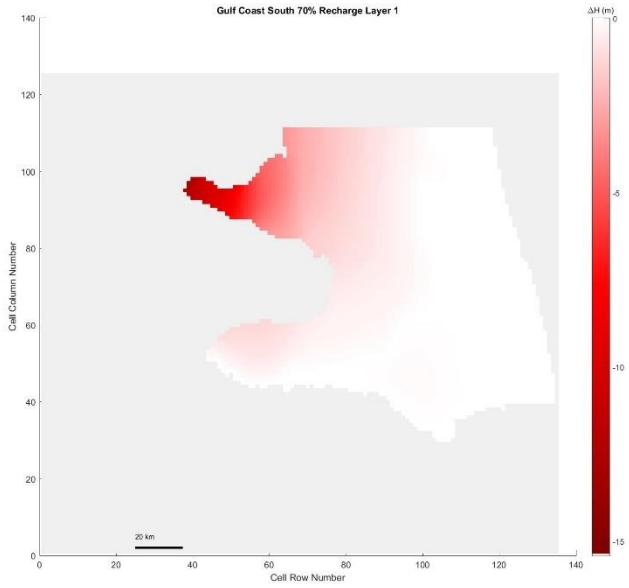

Figure 5. 433 Gulf Coast South, 70% original recharge hydraulic head spatial distribution of layer 1

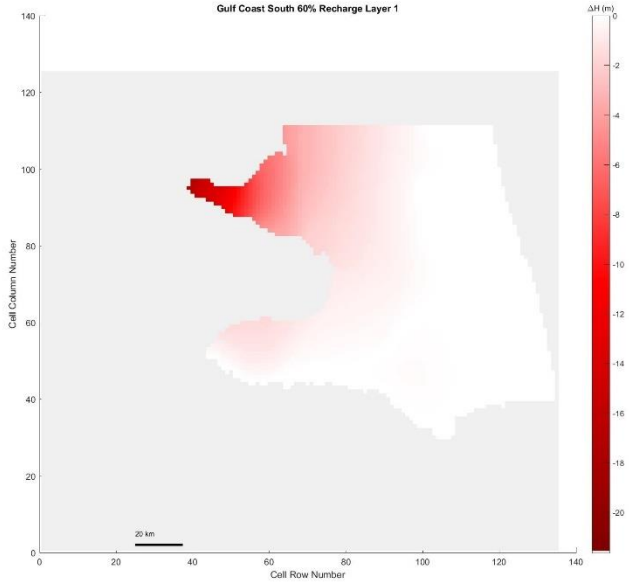

Figure 5. 434 Gulf Coast South, 60% original recharge hydraulic head spatial distribution of layer 1

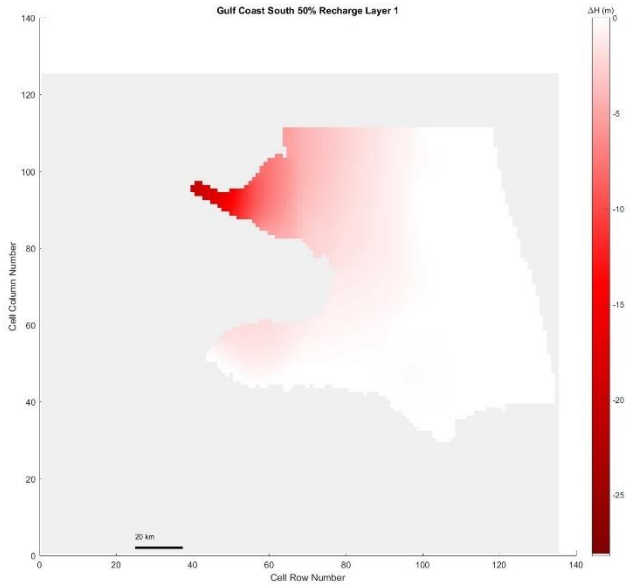

Figure 5. 435 Gulf Coast South, 50% original recharge hydraulic head spatial distribution of layer 1

Layer 2

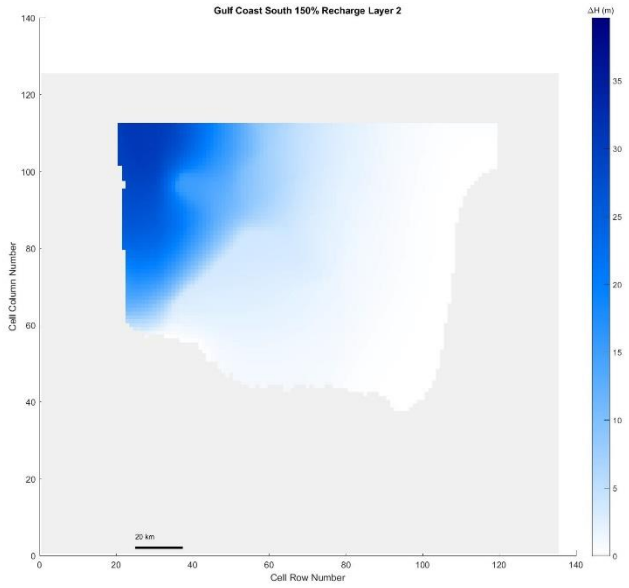

Figure 5. 436 Gulf Coast South, 150% original recharge hydraulic head spatial distribution of layer 2

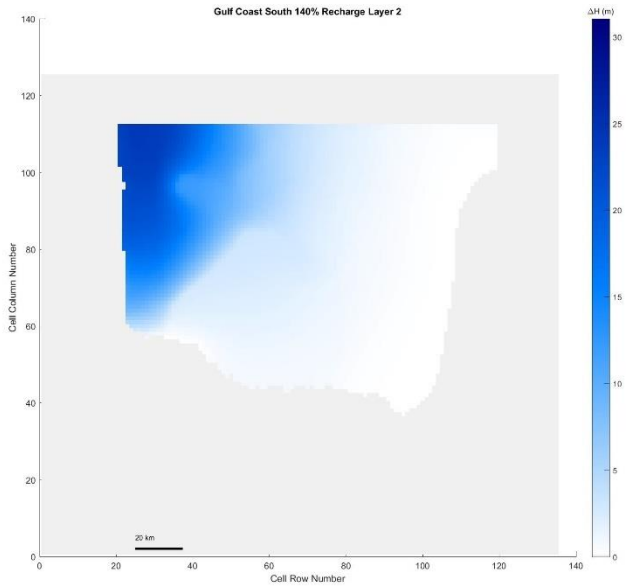

Figure 5. 437 Gulf Coast South, 140% original recharge hydraulic head spatial distribution of layer 2

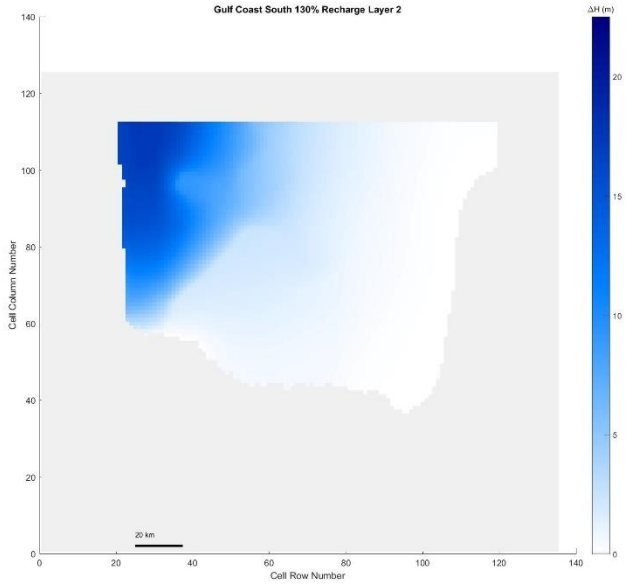

Figure 5. 438 Gulf Coast South, 130% original recharge hydraulic head spatial distribution of layer 2

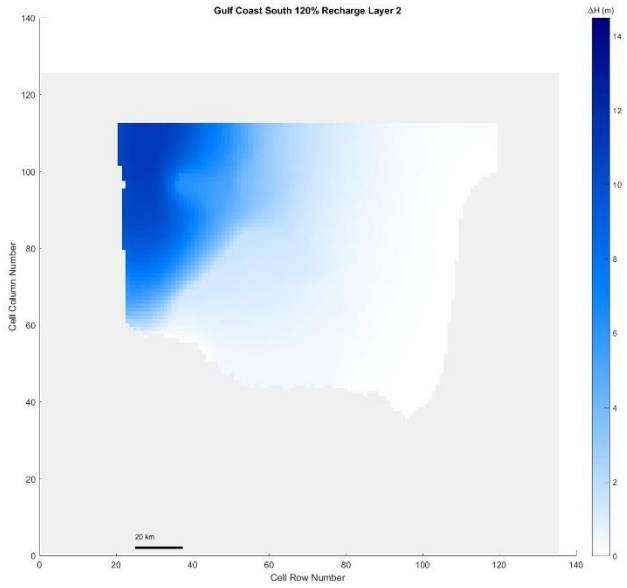

Figure 5. 439 Gulf Coast South, 120% original recharge hydraulic head spatial distribution of layer 2

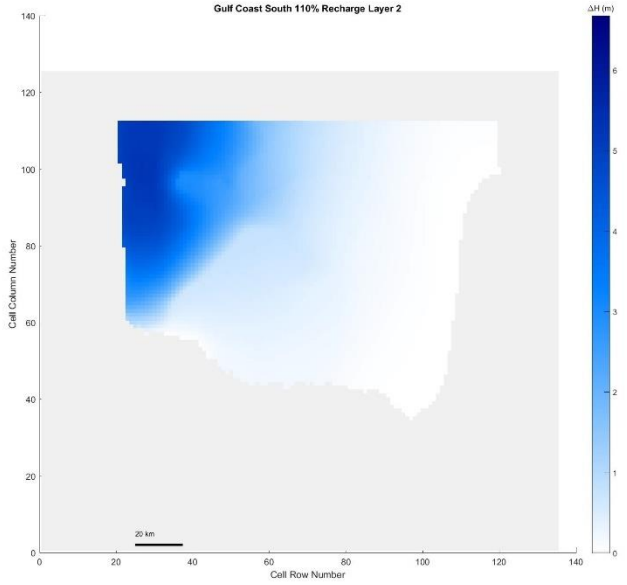

Figure 5. 440 Gulf Coast South, 110% original recharge hydraulic head spatial distribution of layer 2

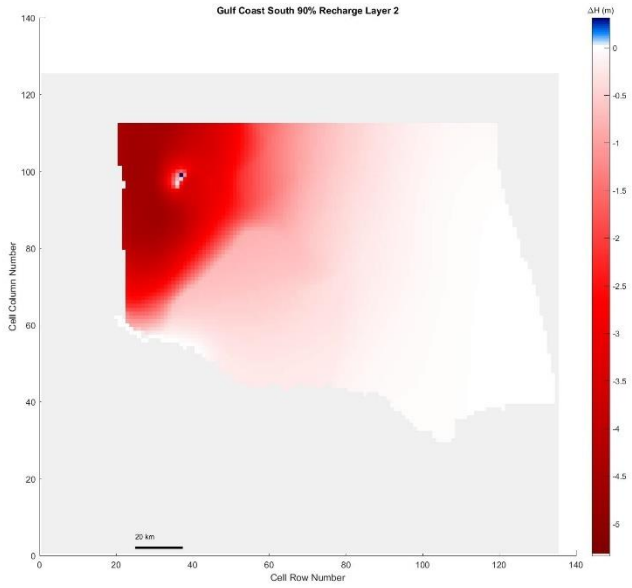

Figure 5. 441 Gulf Coast South, 90% original recharge hydraulic head spatial distribution of layer 2

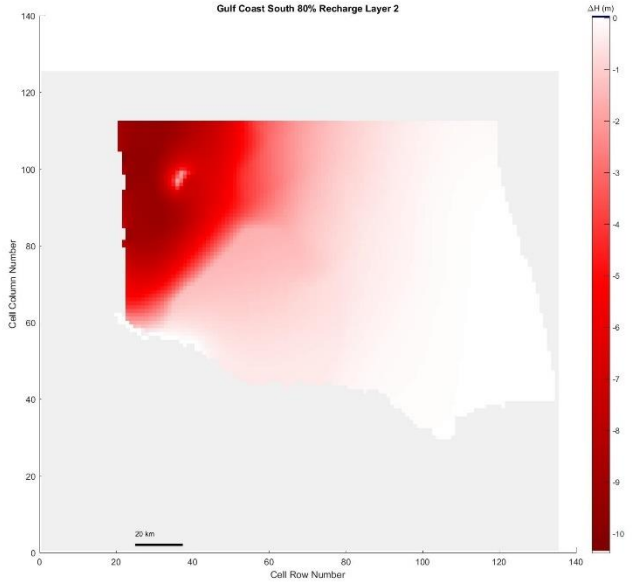

Figure 5. 442 Gulf Coast South, 80% original recharge hydraulic head spatial distribution of layer 2

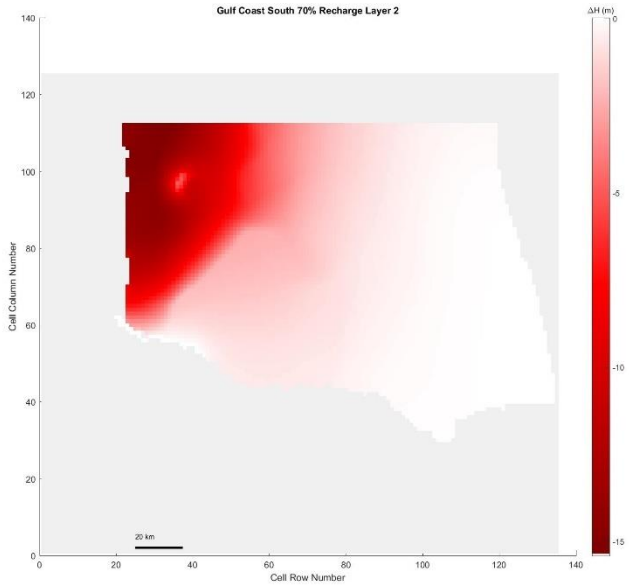

Figure 5. 443 Gulf Coast South, 70% original recharge hydraulic head spatial distribution of layer 2

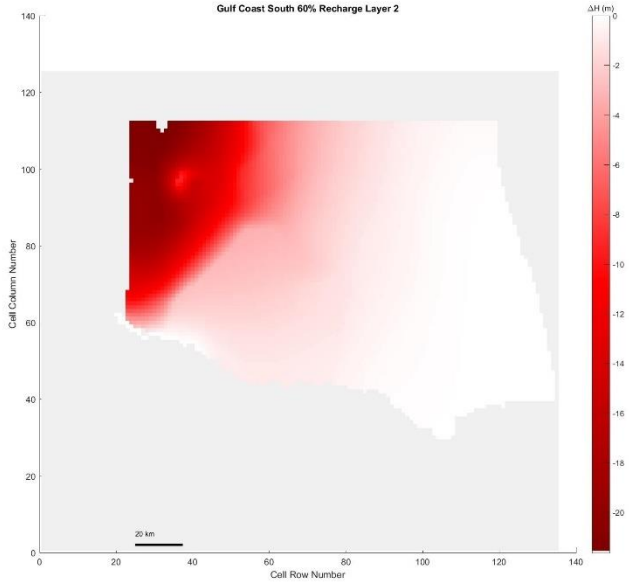

Figure 5. 444 Gulf Coast South, 60% original recharge hydraulic head spatial distribution of layer 2

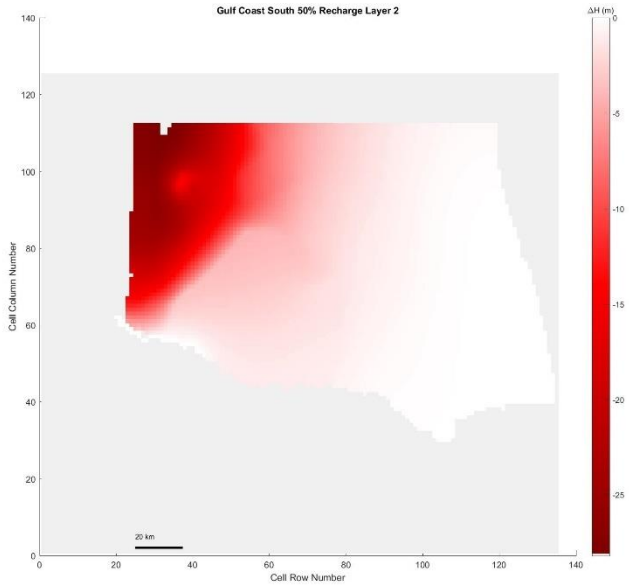

Figure 5. 445 Gulf Coast South, 50% original recharge hydraulic head spatial distribution of layer 2

Layer 3

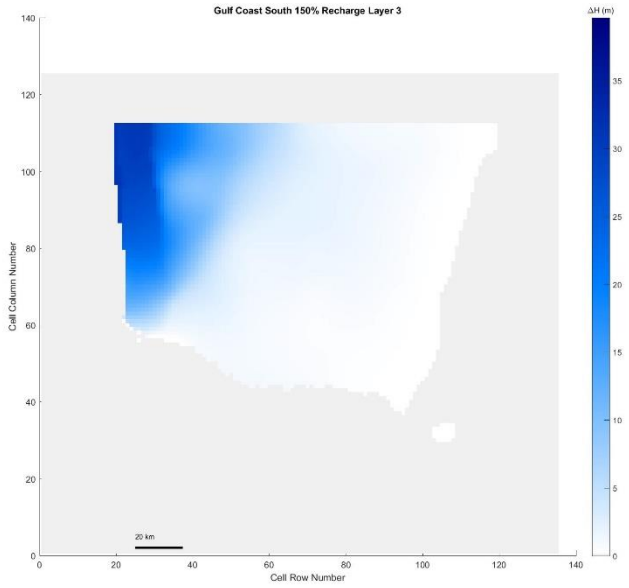

Figure 5. 446 Gulf Coast South, 150% original recharge hydraulic head spatial distribution of layer 3

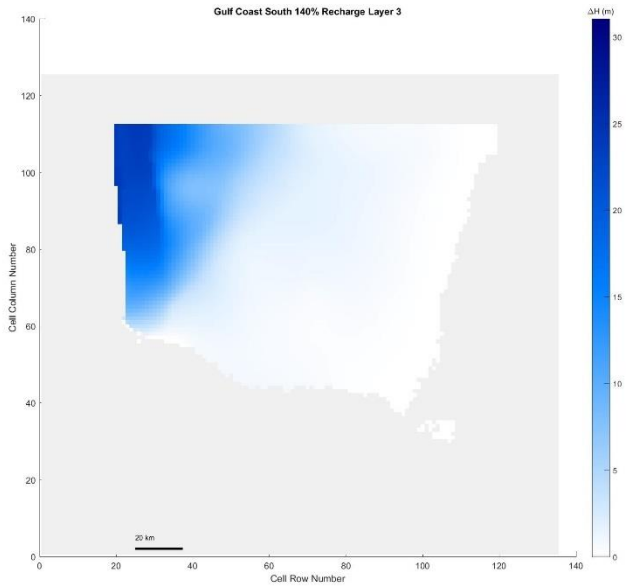

Figure 5. 447 Gulf Coast South, 140% original recharge hydraulic head spatial distribution of layer 3

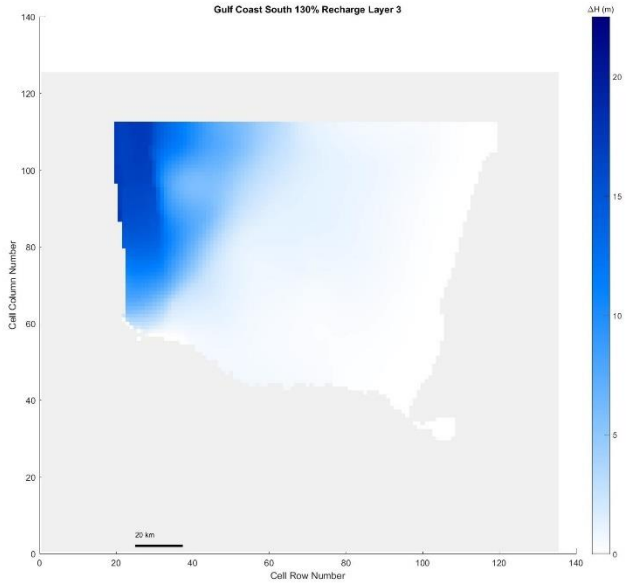

Figure 5. 448 Gulf Coast South, 130% original recharge hydraulic head spatial distribution of layer 3

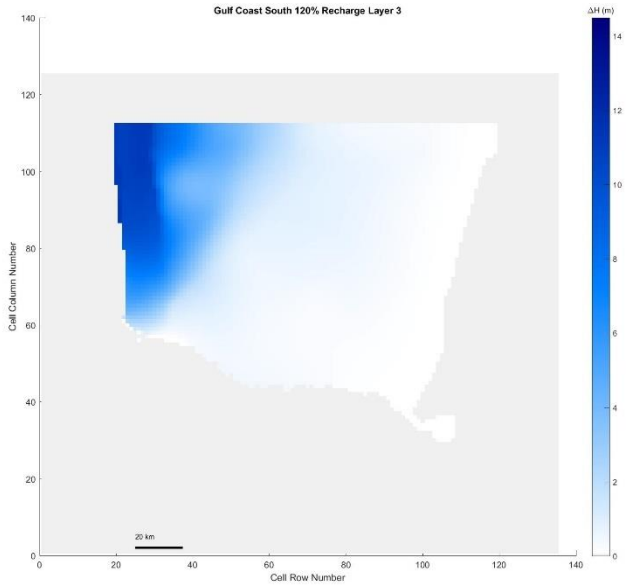

Figure 5. 449 Gulf Coast South, 120% original recharge hydraulic head spatial distribution of layer 3

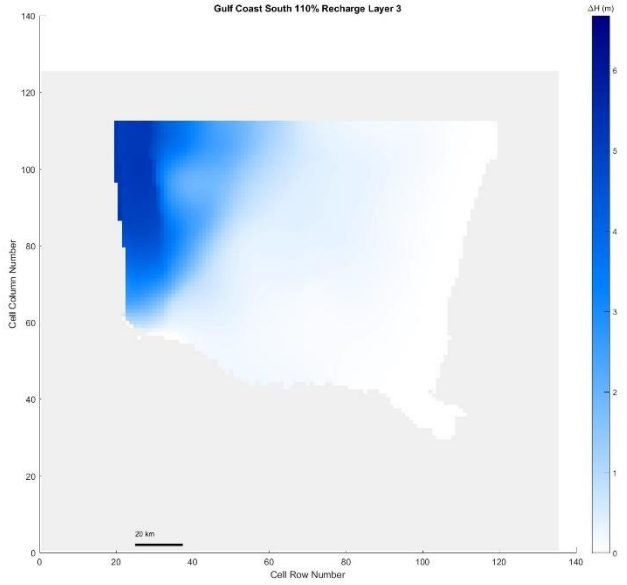

Figure 5. 450 Gulf Coast South, 110% original recharge hydraulic head spatial distribution of layer 3

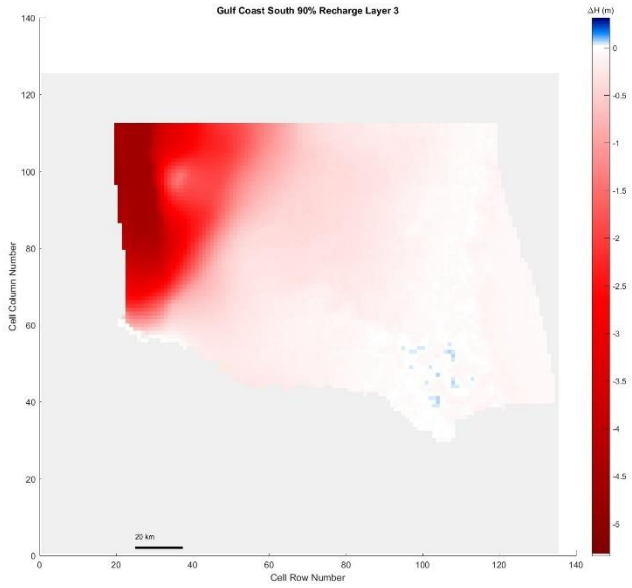

Figure 5. 451 Gulf Coast South, 90% original recharge hydraulic head spatial distribution of layer 3

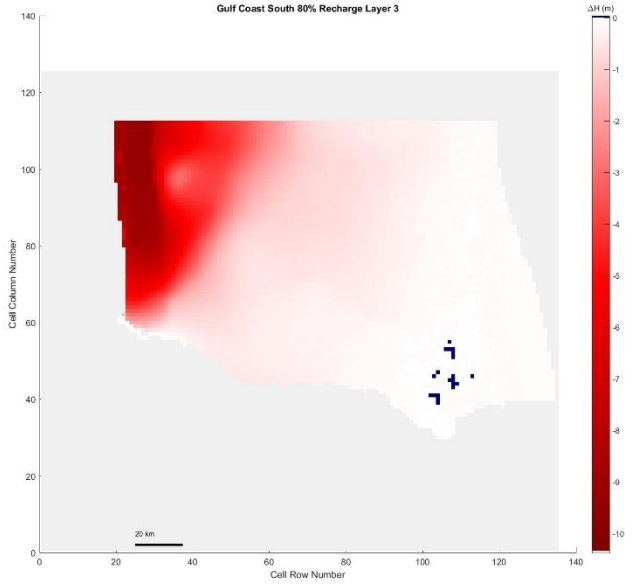

Figure 5. 452 Gulf Coast South, 80% original recharge hydraulic head spatial distribution of layer 3

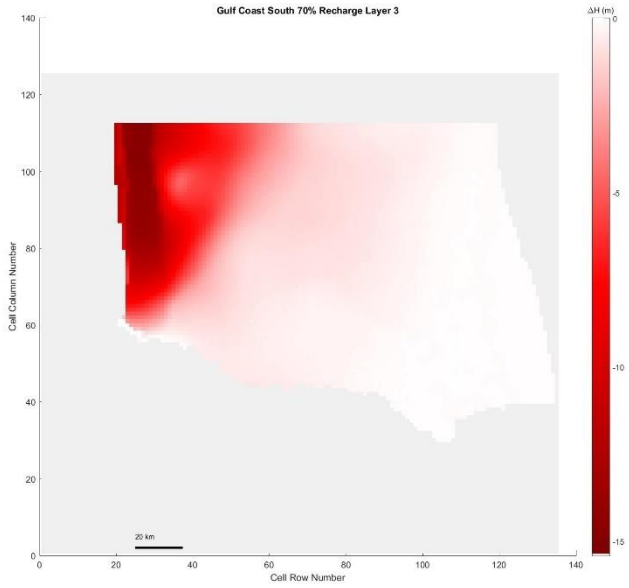

Figure 5. 453 Gulf Coast South, 70% original recharge hydraulic head spatial distribution of layer 3

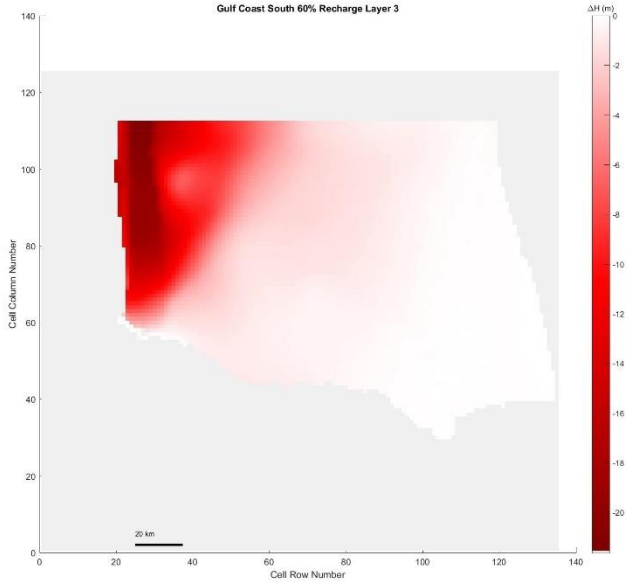

Figure 5. 454 Gulf Coast South, 60% original recharge hydraulic head spatial distribution of layer 3

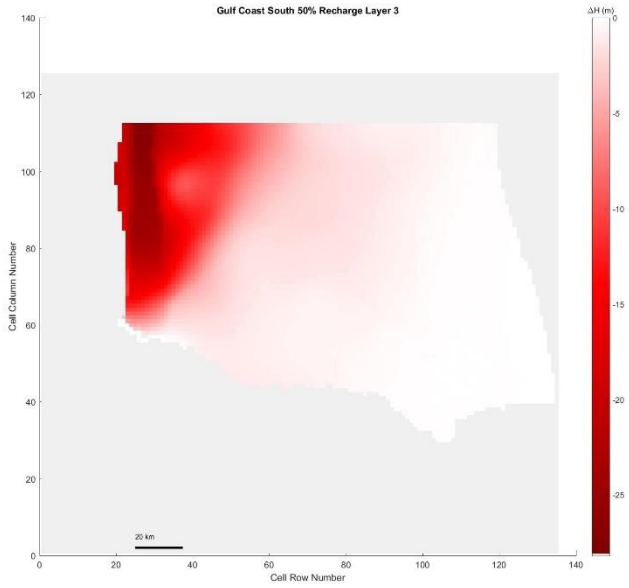

Figure 5. 455 Gulf Coast South, 50% original recharge hydraulic head spatial distribution of layer 3

Layer 4

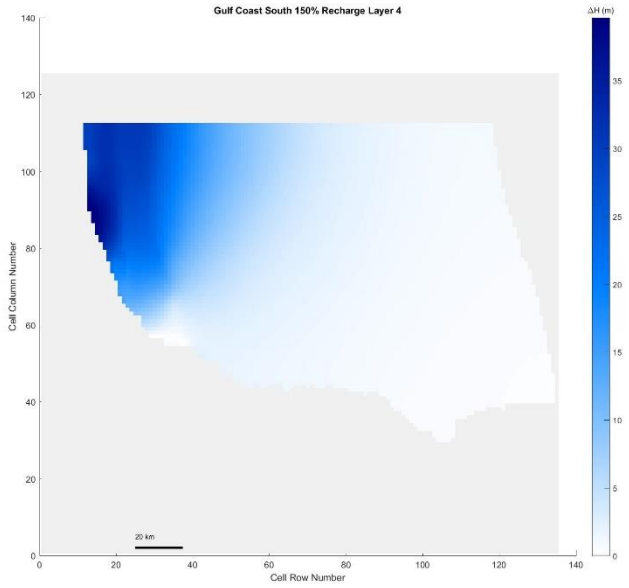

Figure 5. 456 Gulf Coast South, 150% original recharge hydraulic head spatial distribution of layer 4

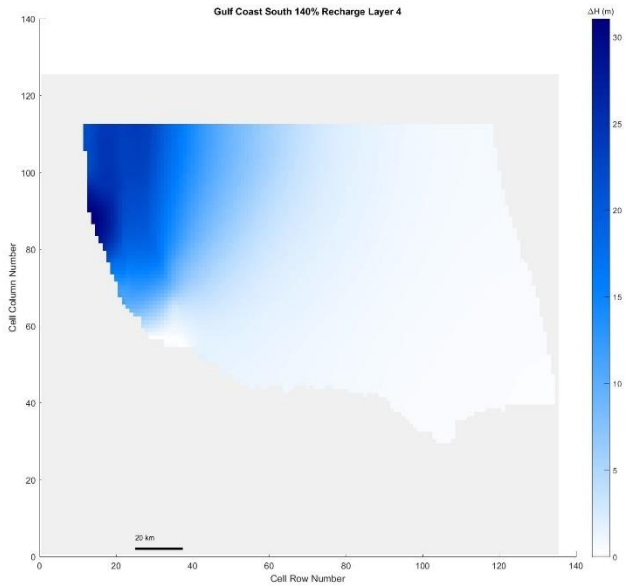

Figure 5. 457 Gulf Coast South, 140% original recharge hydraulic head spatial distribution of layer 4

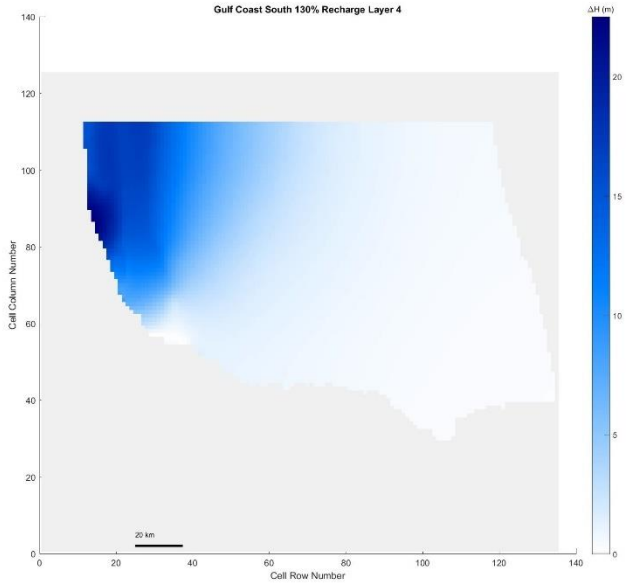

Figure 5. 458 Gulf Coast South, 130% original recharge hydraulic head spatial distribution of layer 4

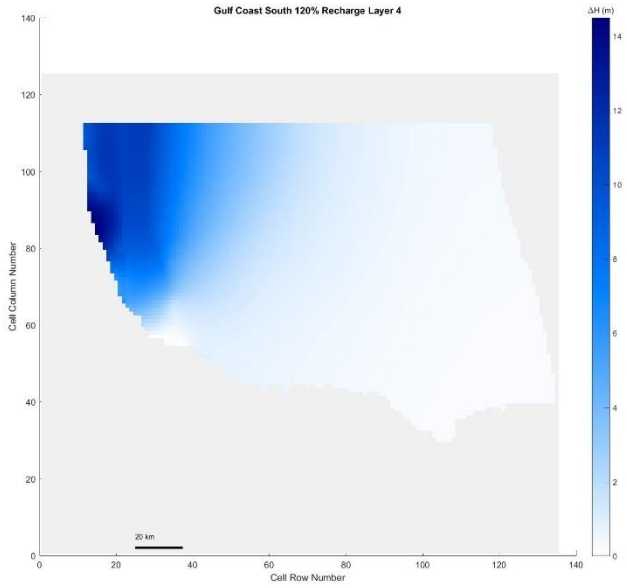

Figure 5. 459 Gulf Coast South, 120% original recharge hydraulic head spatial distribution of layer 4

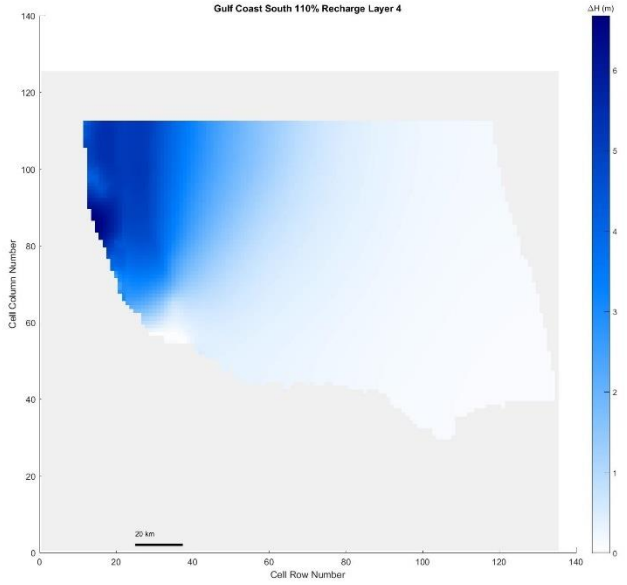

Figure 5. 460 Gulf Coast South, 110% original recharge hydraulic head spatial distribution of layer 4

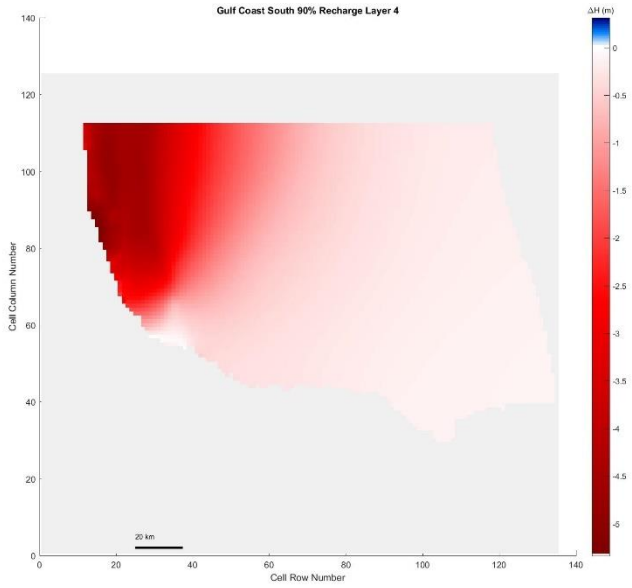

Figure 5. 461 Gulf Coast South, 90% original recharge hydraulic head spatial distribution of layer 4

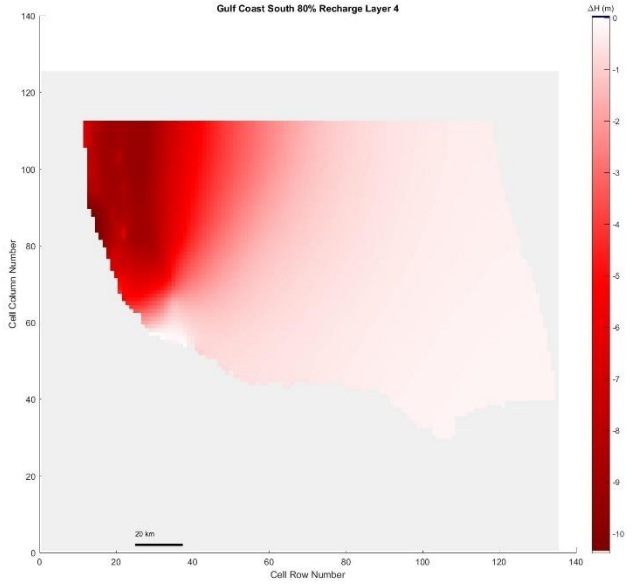

Figure 5. 462 Gulf Coast South, 80% original recharge hydraulic head spatial distribution of layer 4

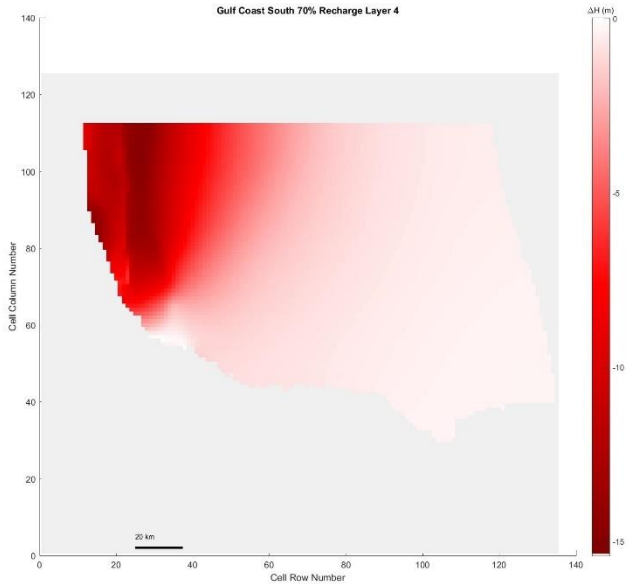

Figure 5. 463 Gulf Coast South, 70% original recharge hydraulic head spatial distribution of layer 4

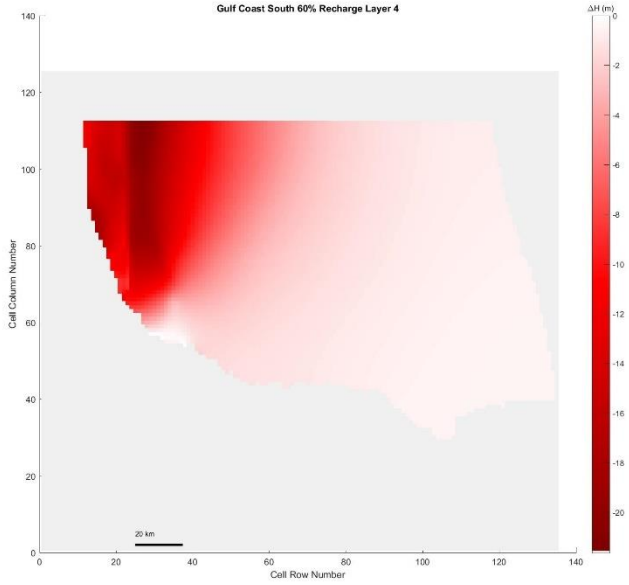

Figure 5. 464 Gulf Coast South, 60% original recharge hydraulic head spatial distribution of layer 4

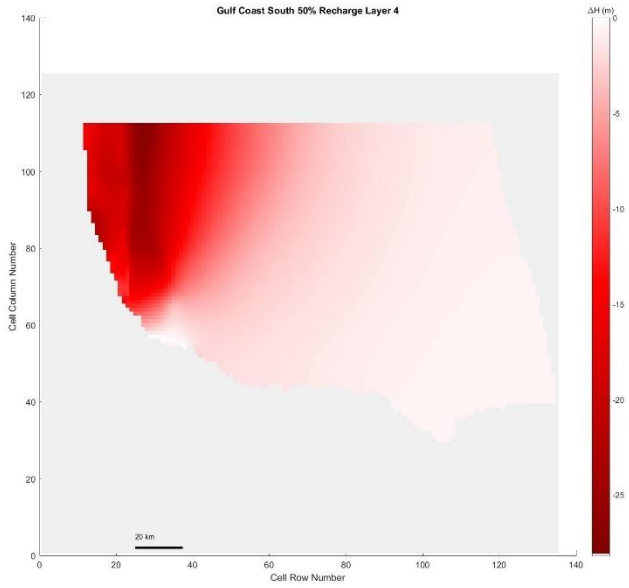

Figure 5. 465 Gulf Coast South, 50% original recharge hydraulic head spatial distribution of layer 4

Ogallala North

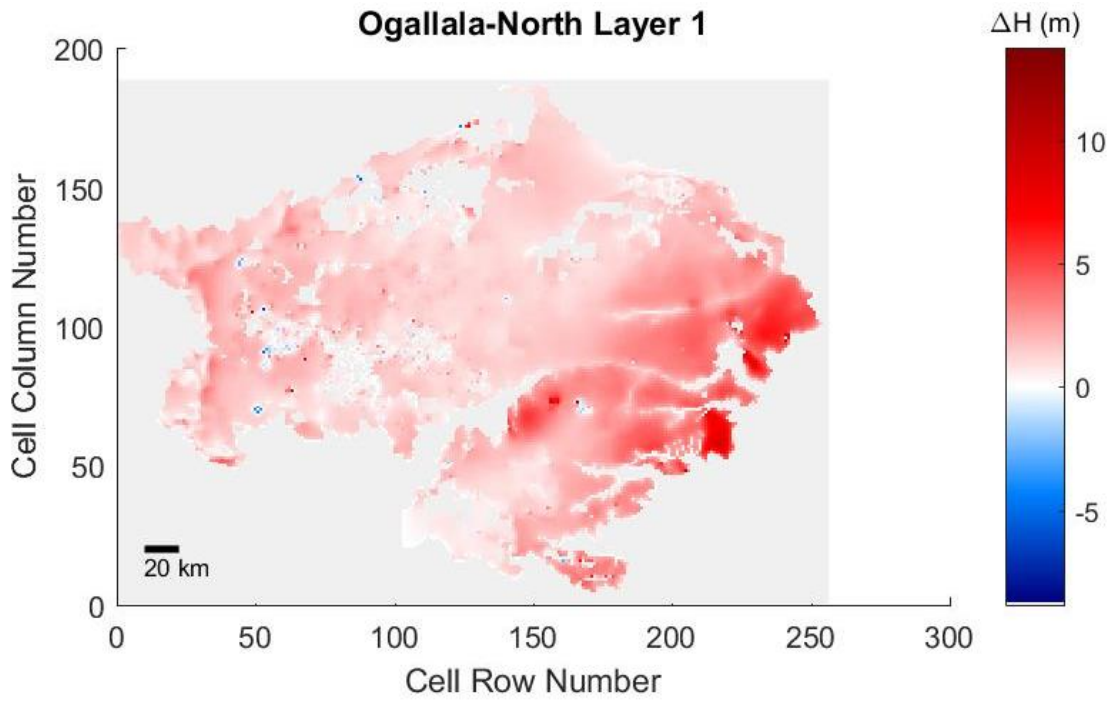

Figure 5. 466 Ogallala North, 150% original recharge hydraulic head spatial distribution of layer 1

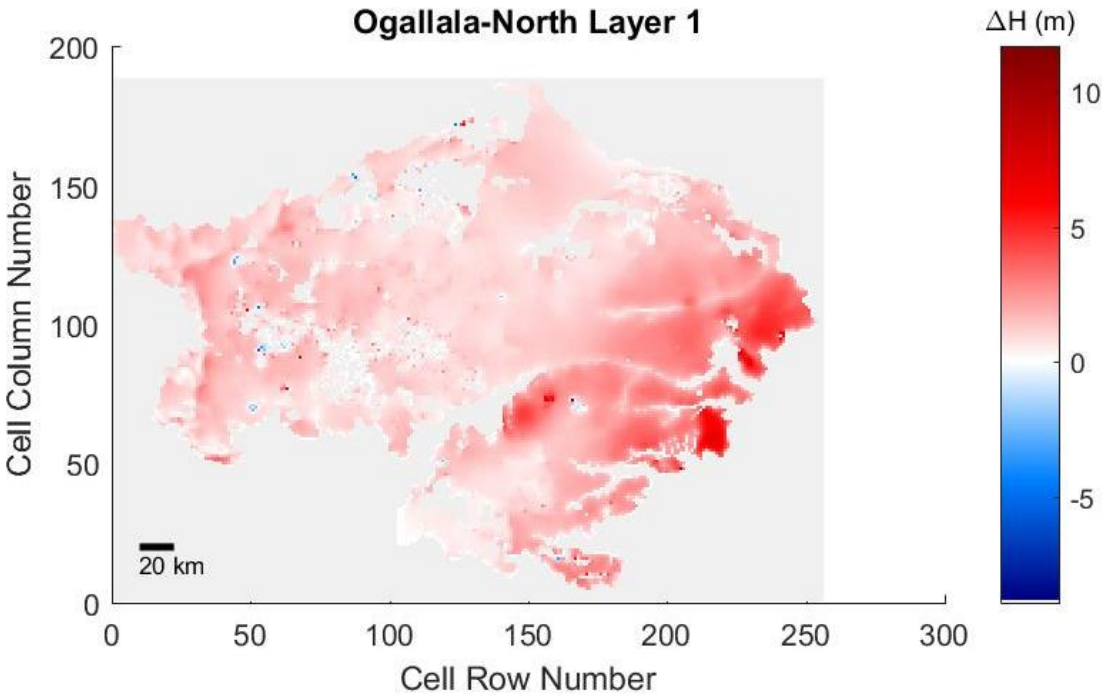

Figure 5. 467 Ogallala North, 140% original recharge hydraulic head spatial distribution of layer 1

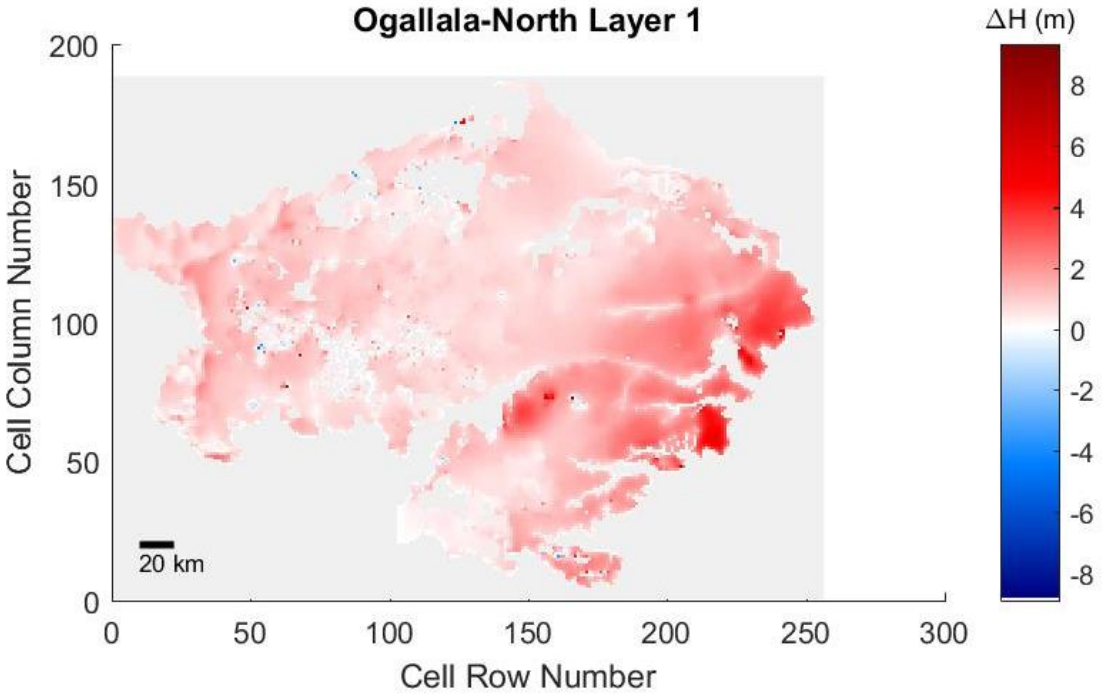

Figure 5. 468 Ogallala North, 130% original recharge hydraulic head spatial distribution of layer 1

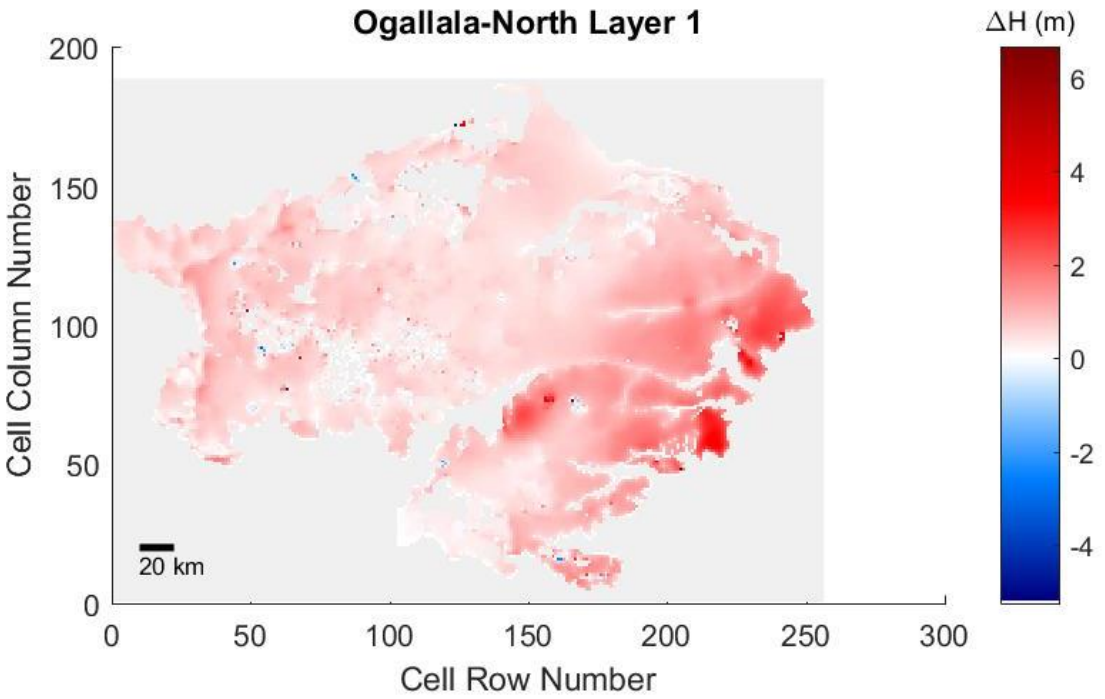

Figure 5. 469 Ogallala North, 120% original recharge hydraulic head spatial distribution of layer 1

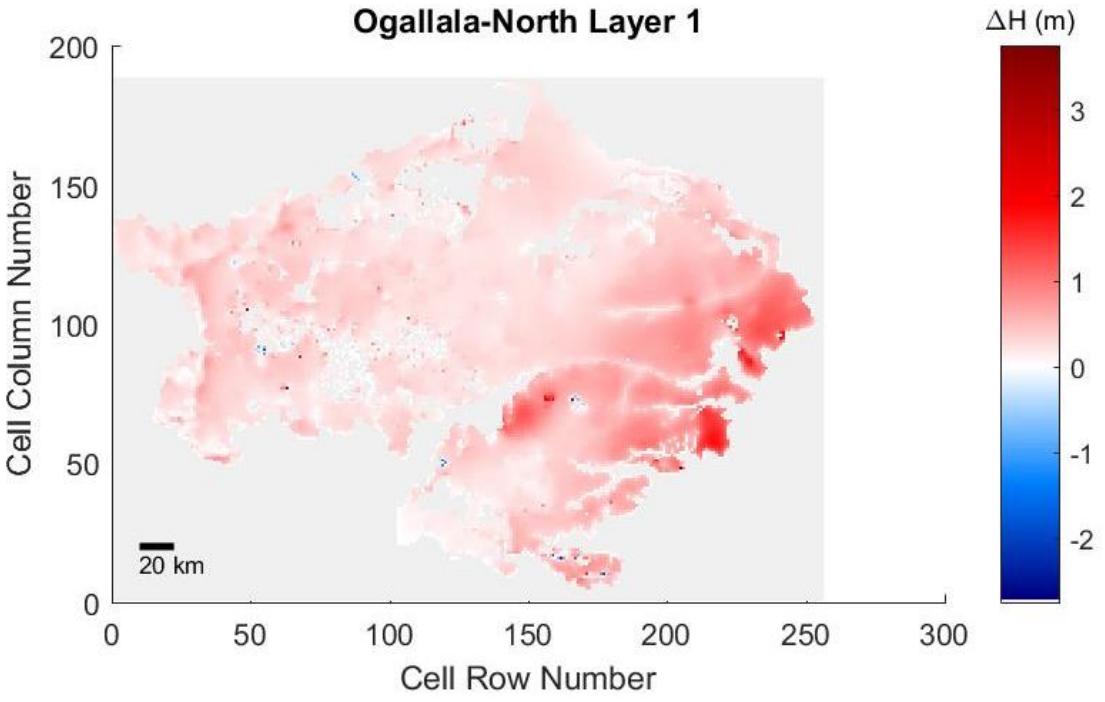

Figure 5. 470 Ogallala North, 110% original recharge hydraulic head spatial distribution of layer 1

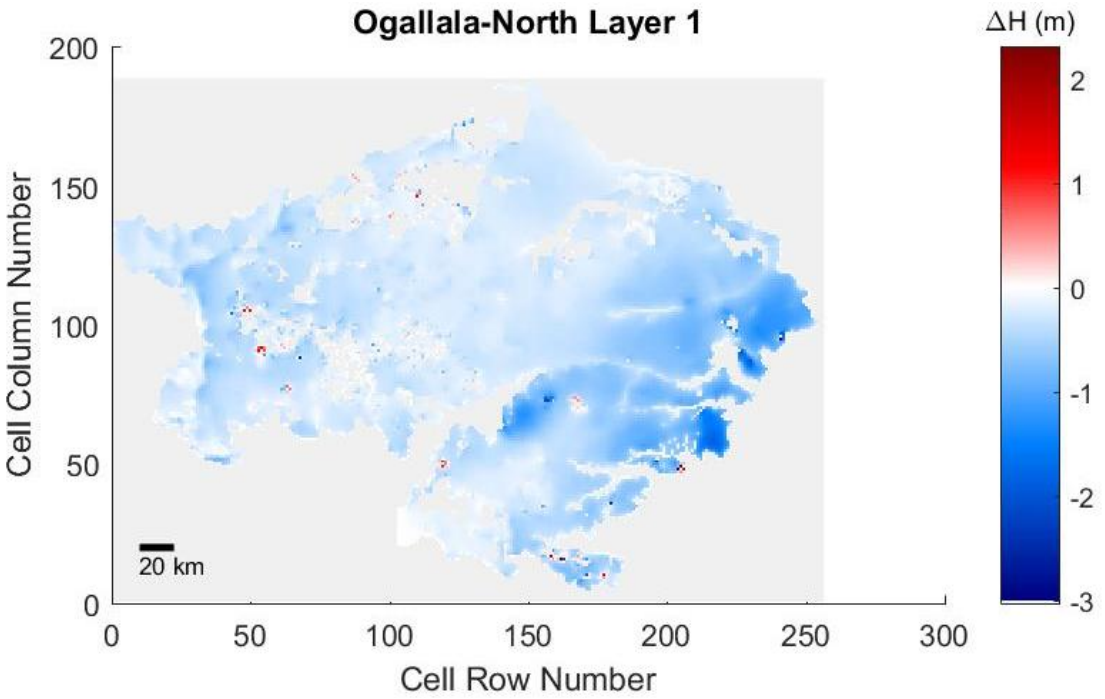

Figure 5. 471 Ogallala North, 90% original recharge hydraulic head spatial distribution of layer 1

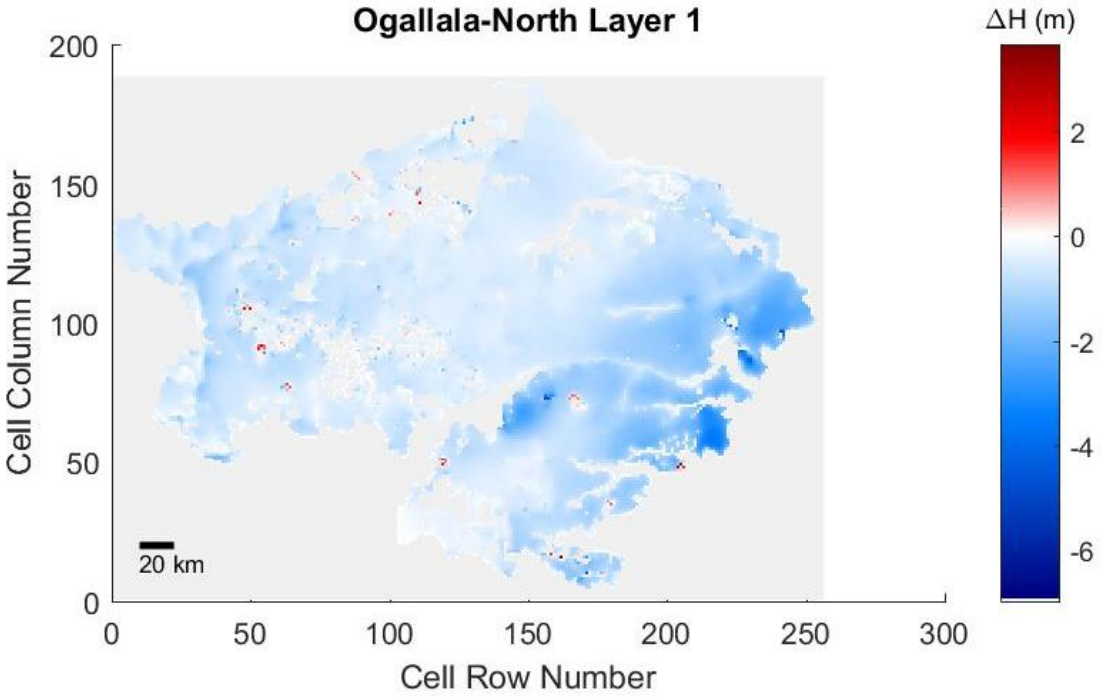

Figure 5. 472 Ogallala North, 80% original recharge hydraulic head spatial distribution of layer 1

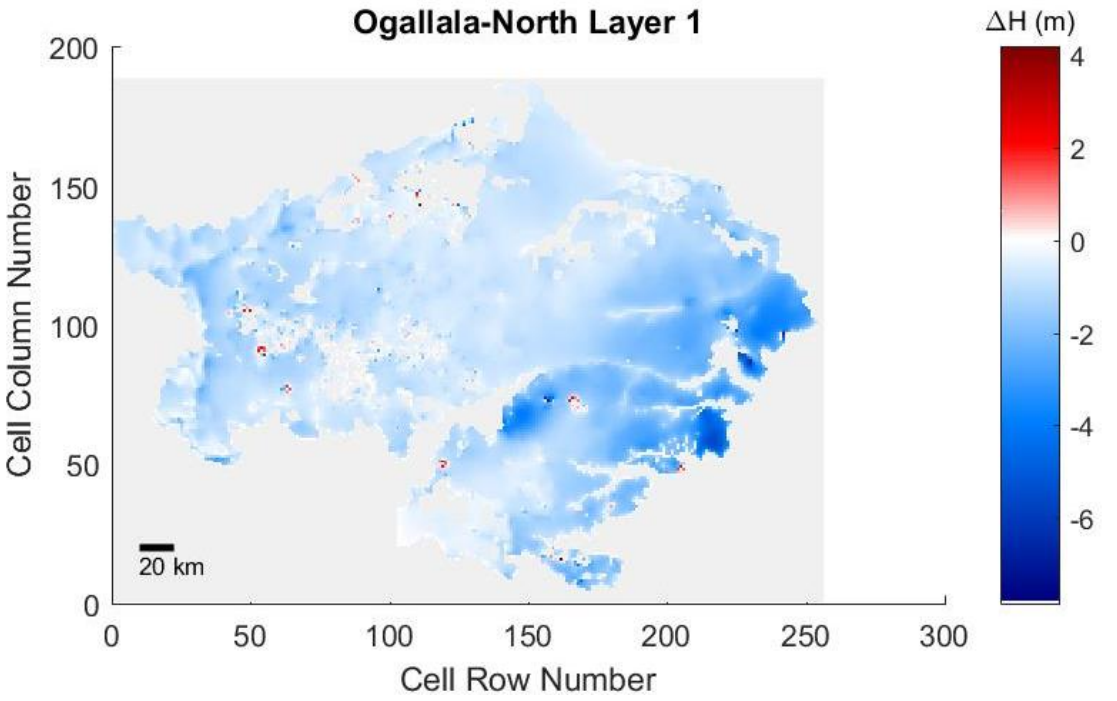

Figure 5. 473 Ogallala North, 70% original recharge hydraulic head spatial distribution of layer 1

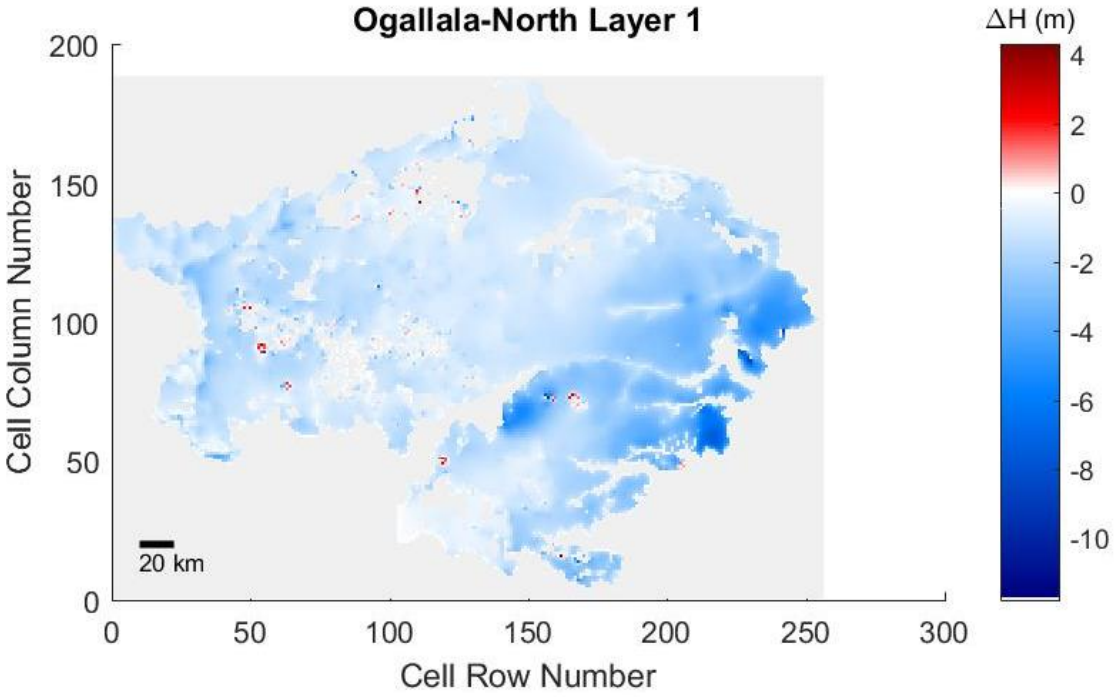

Figure 5. 474 Ogallala North, 60% original recharge hydraulic head spatial distribution of layer 1

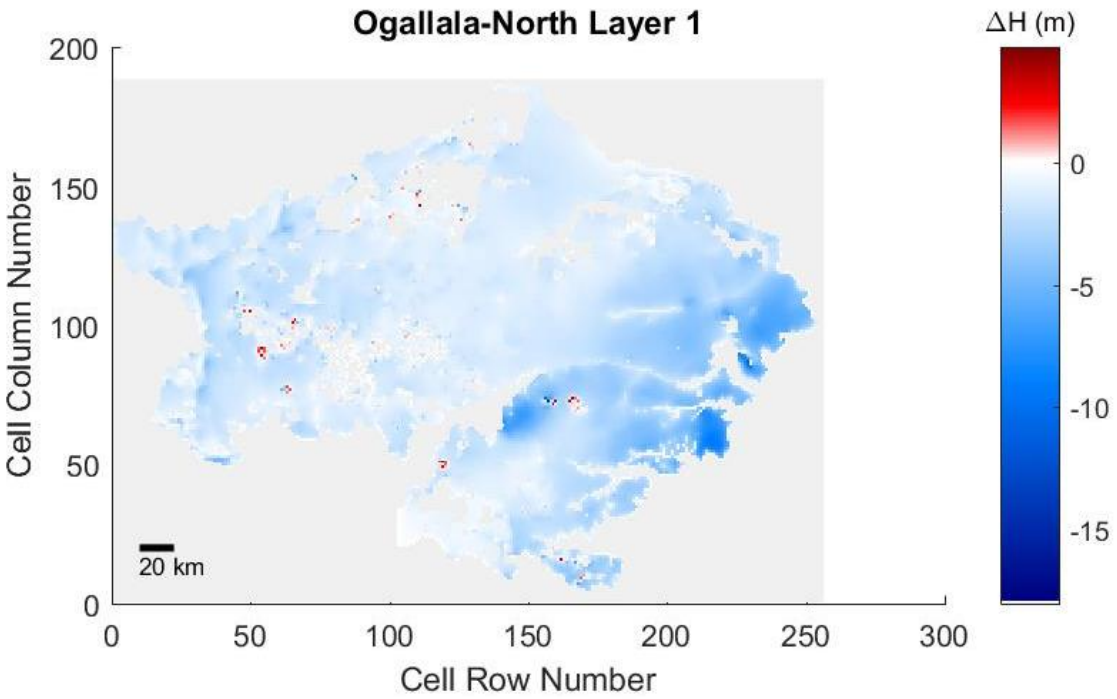

Figure 5. 475 Ogallala North, 50% original recharge hydraulic head spatial distribution of layer 1

Ogallala South

Layer 1

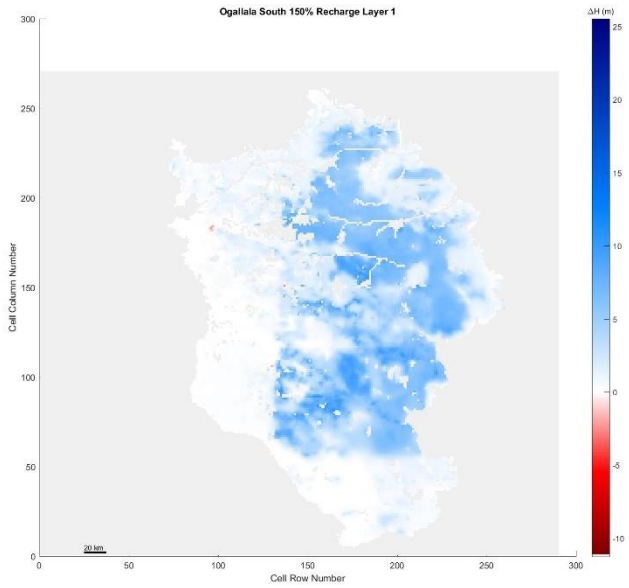

Figure 5. 476 Ogallala South, 150% original recharge hydraulic head spatial distribution of layer 1

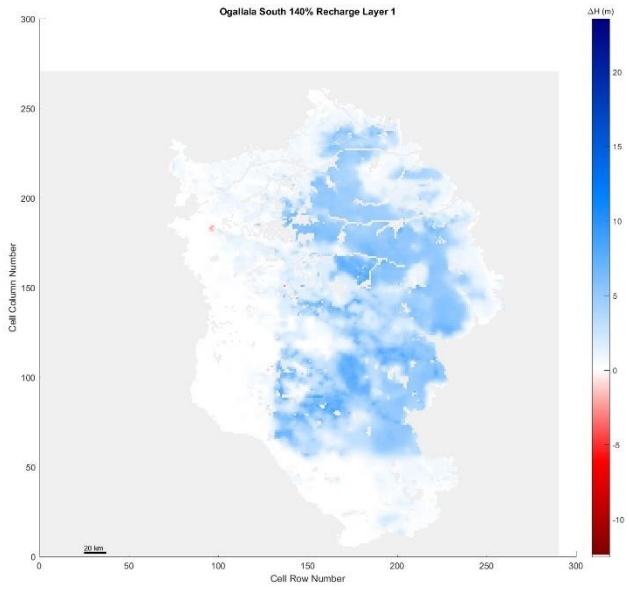

Figure 5. 477 Ogallala South, 140% original recharge hydraulic head spatial distribution of layer 1

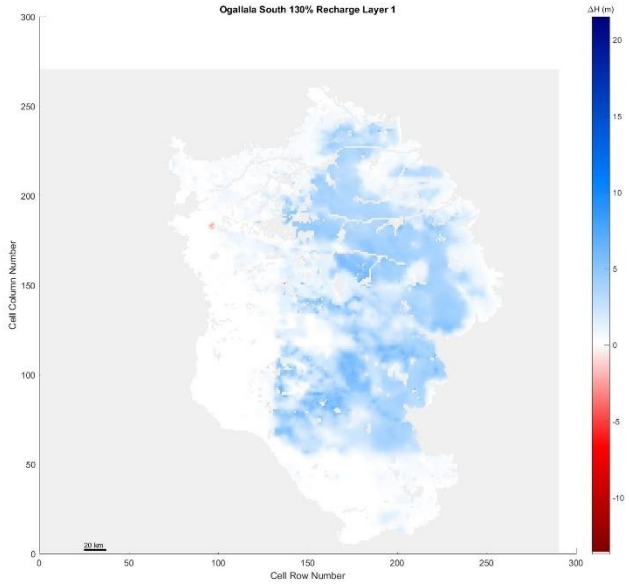

Figure 5. 478 Ogallala South, 130% original recharge hydraulic head spatial distribution of layer 1

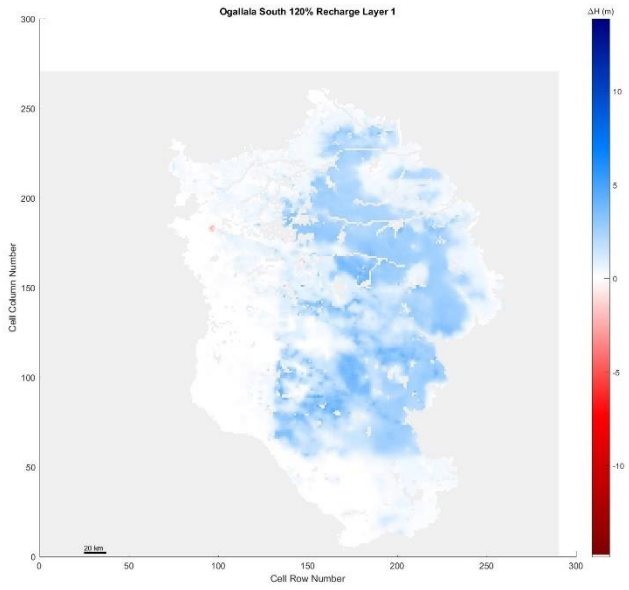

Figure 5. 479 Ogallala South, 120% original recharge hydraulic head spatial distribution of layer 1

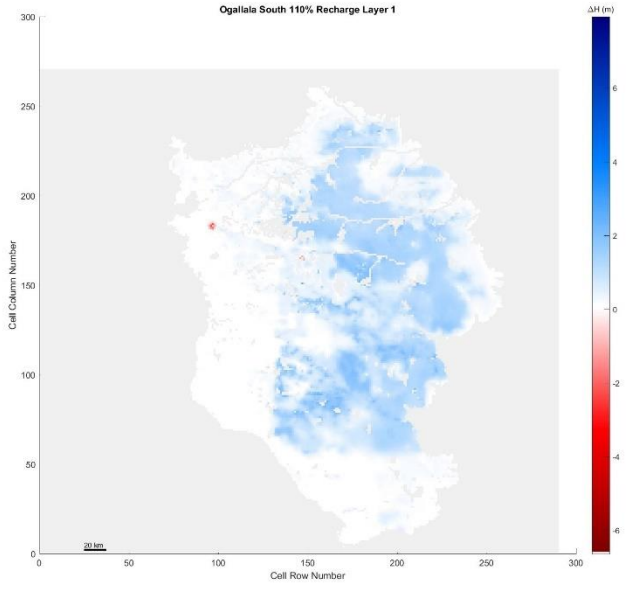

Figure 5. 480 Ogallala South, 110% original recharge hydraulic head spatial distribution of layer 1

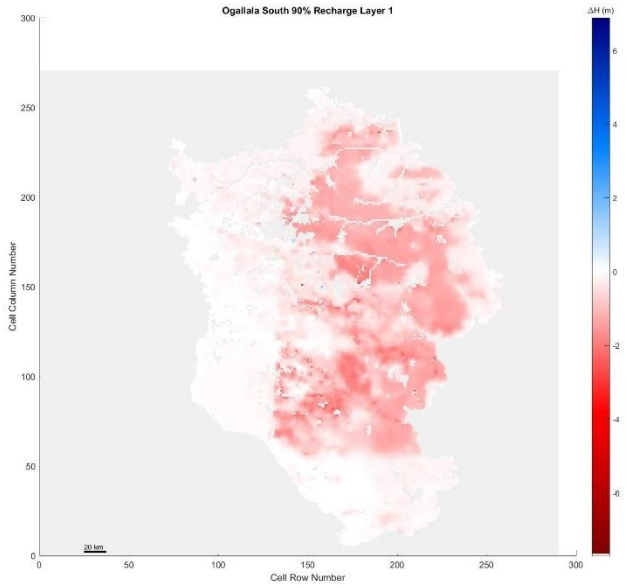

Figure 5. 481 Ogallala South, 90% original recharge hydraulic head spatial distribution of layer 1

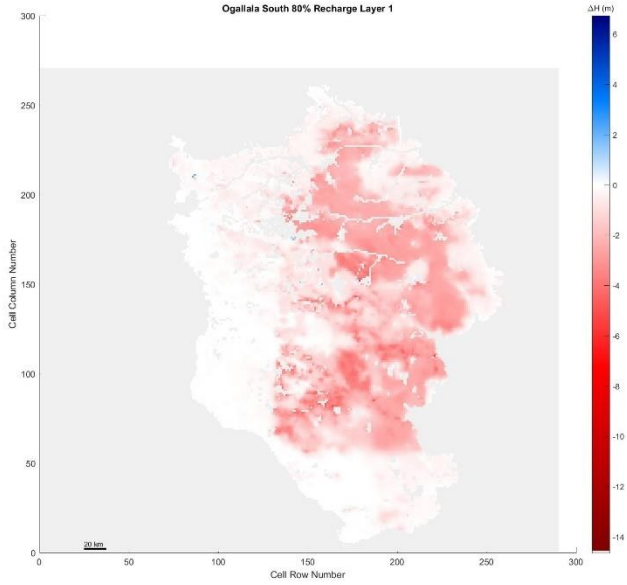

Figure 5. 482 Ogallala South, 80% original recharge hydraulic head spatial distribution of layer 1

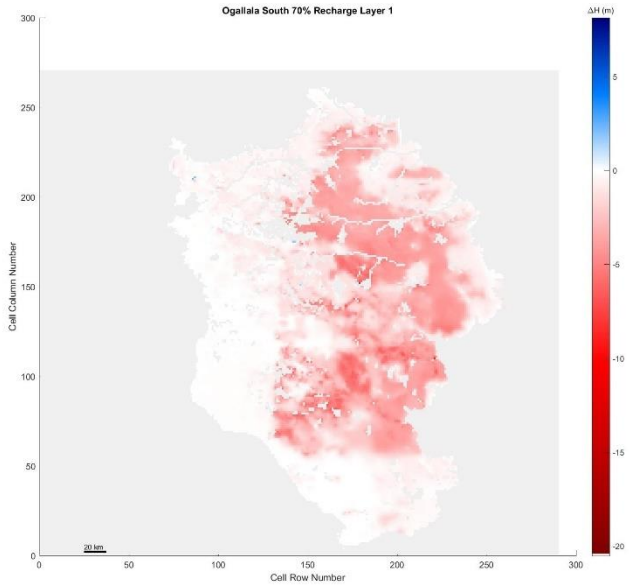

Figure 5. 483 Ogallala South, 70% original recharge hydraulic head spatial distribution of layer 1

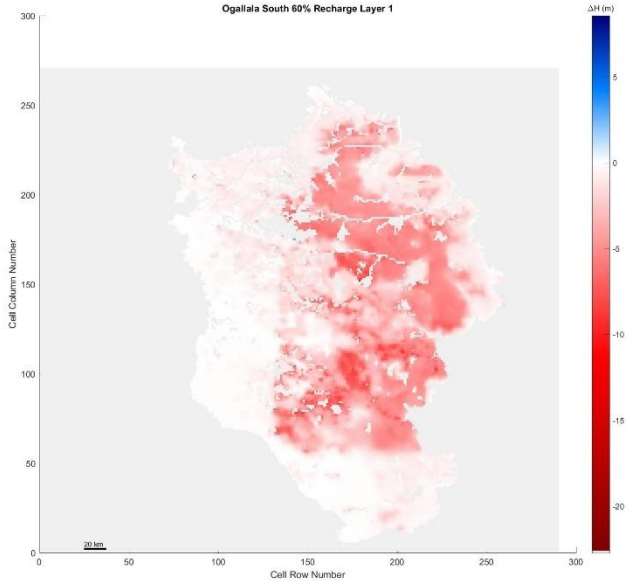

Figure 5. 484 Ogallala South, 60% original recharge hydraulic head spatial distribution of layer 1

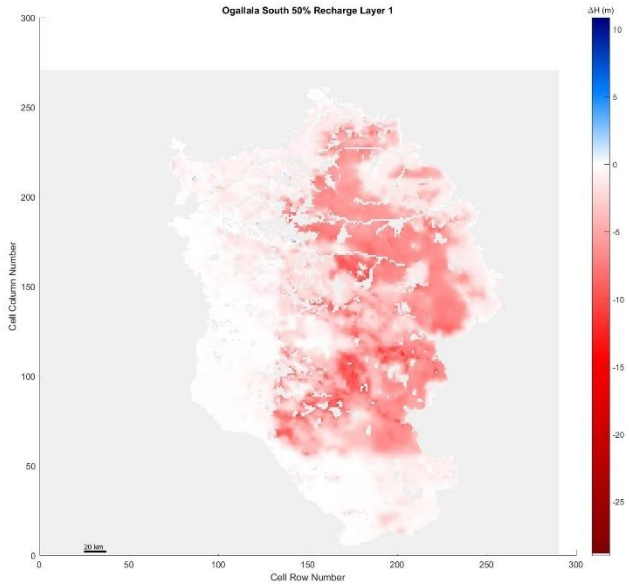

Figure 5. 485 Ogallala South, 50% original recharge hydraulic head spatial distribution of layer 1

Layer 2

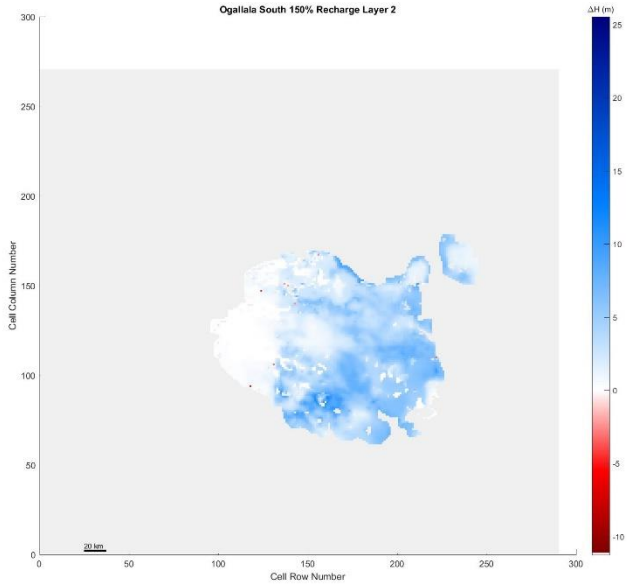

Figure 5. 486 Ogallala South, 150% original recharge hydraulic head spatial distribution of layer 2

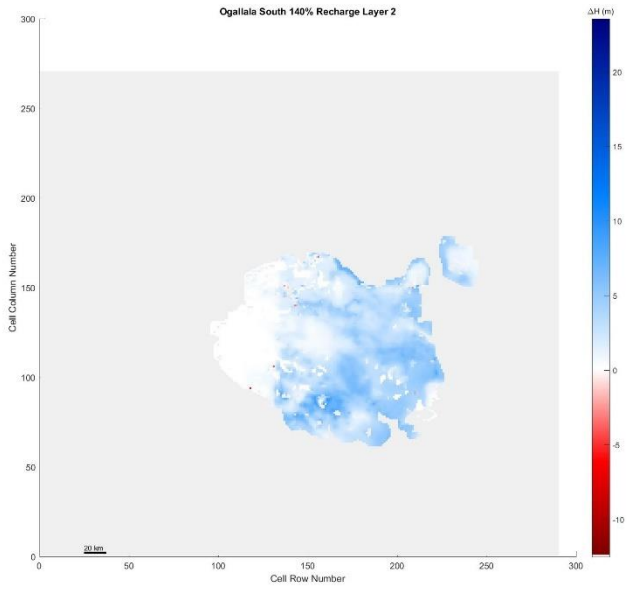

Figure 5. 487 Ogallala South, 140% original recharge hydraulic head spatial distribution of layer 2

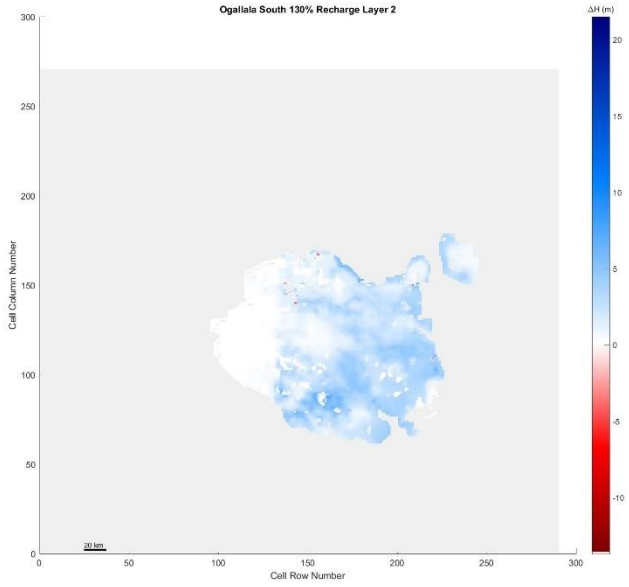

Figure 5. 488 Ogallala South, 130% original recharge hydraulic head spatial distribution of layer 2

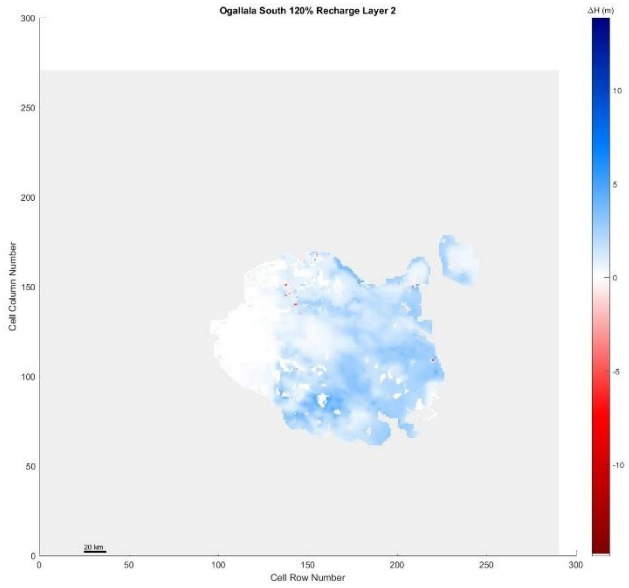

Figure 5. 489 Ogallala South, 120% original recharge hydraulic head spatial distribution of layer 2

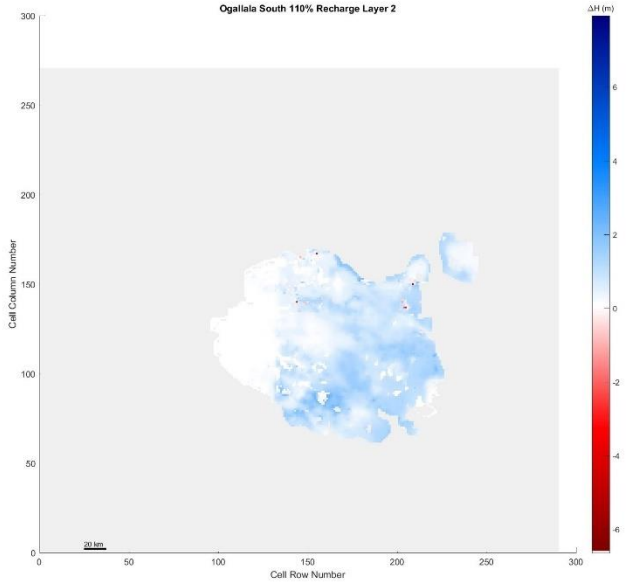

Figure 5. 490 Ogallala South, 110% original recharge hydraulic head spatial distribution of layer 2

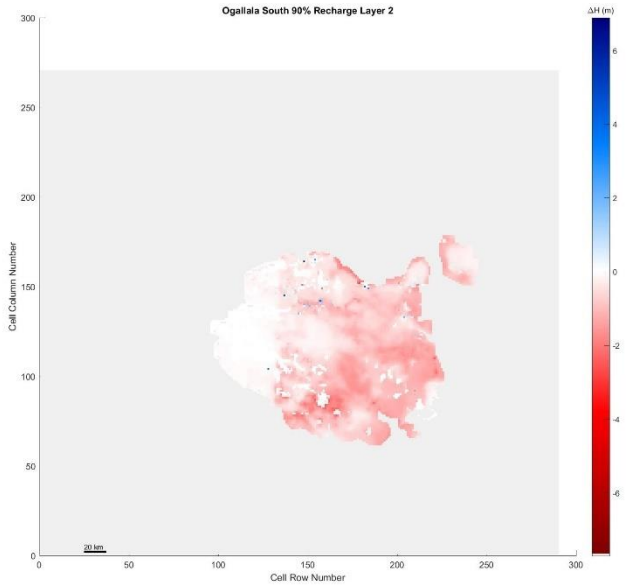

Figure 5. 491 Ogallala South, 90% original recharge hydraulic head spatial distribution of layer 2

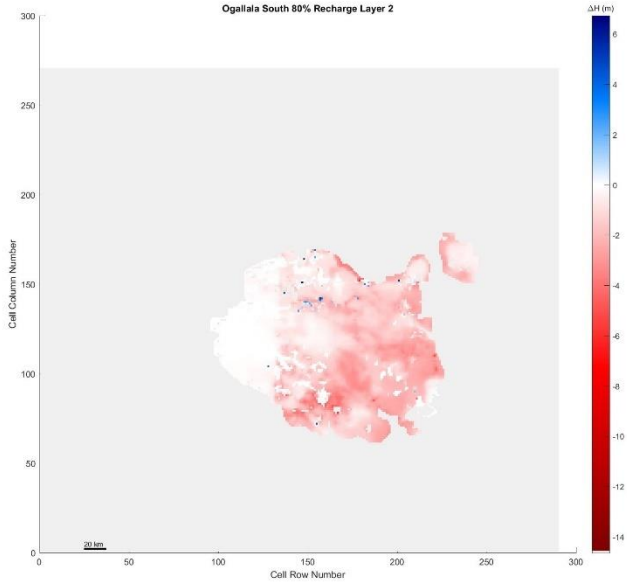

Figure 5. 492 Ogallala South, 80% original recharge hydraulic head spatial distribution of layer 2

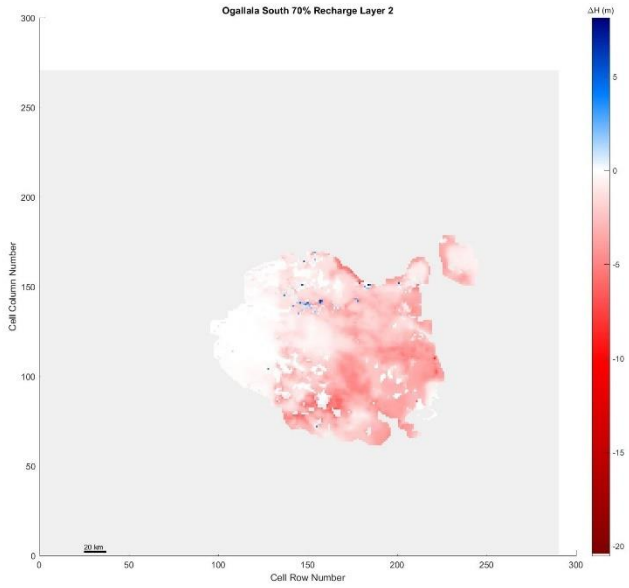

Figure 5. 493 Ogallala South, 70% original recharge hydraulic head spatial distribution of layer 2

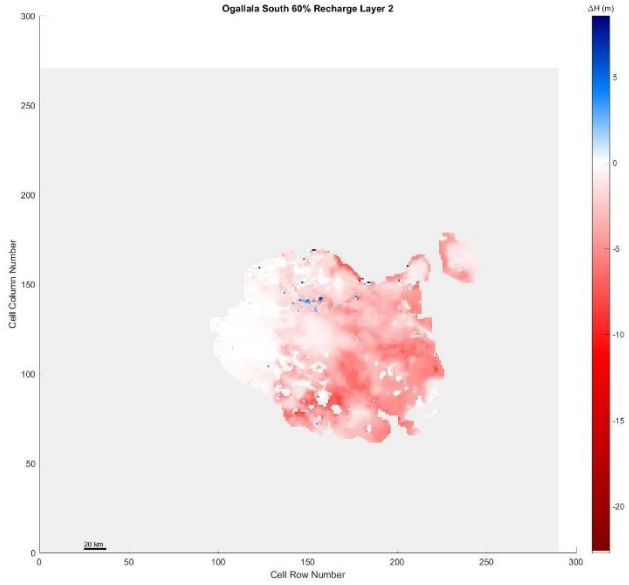

Figure 5. 494 Ogallala South, 60% original recharge hydraulic head spatial distribution of layer 2

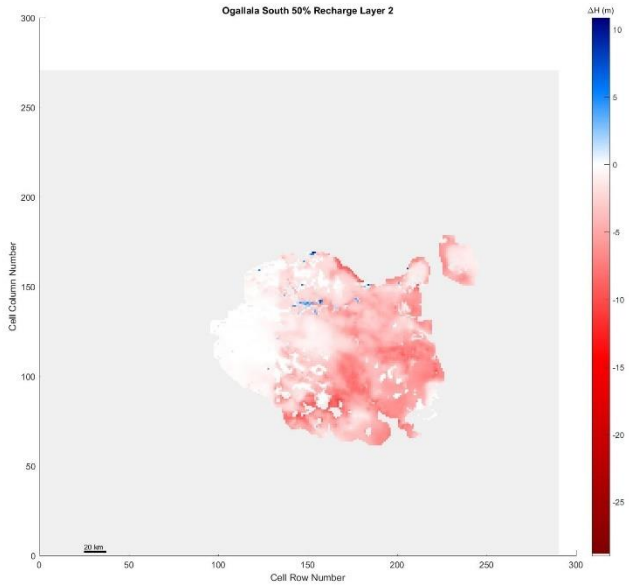

Figure 5. 495 Ogallala South, 50% original recharge hydraulic head spatial distribution of layer 2

Layer 3

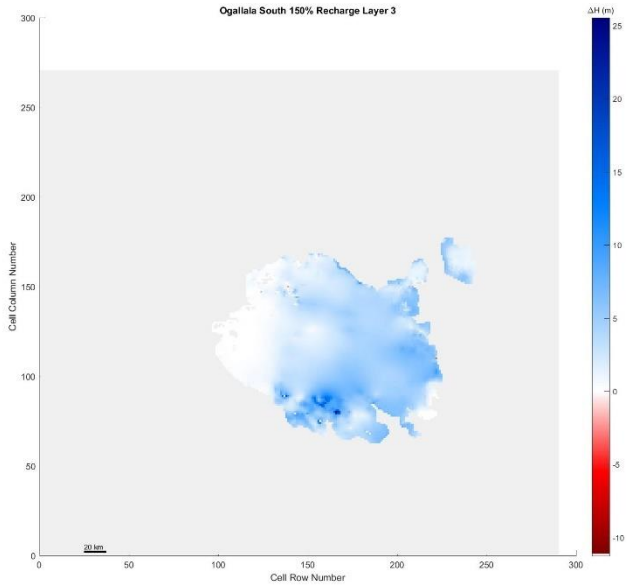

Figure 5. 496 Ogallala South, 150% original recharge hydraulic head spatial distribution of layer 3

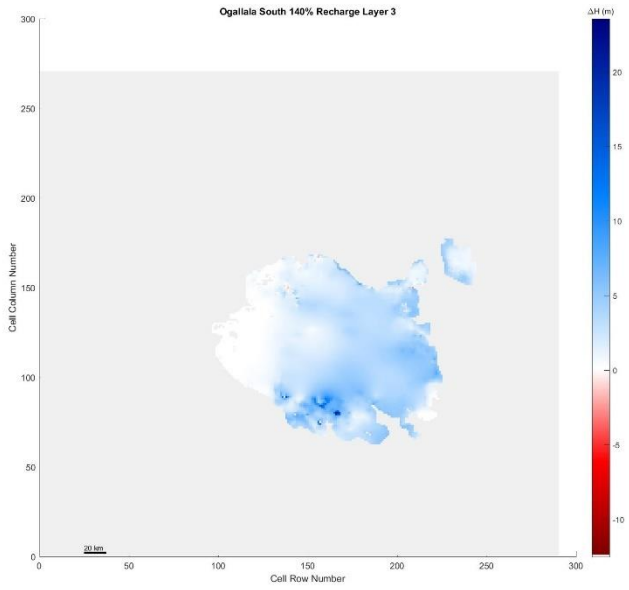

Figure 5. 497 Ogallala South, 140% original recharge hydraulic head spatial distribution of layer 3

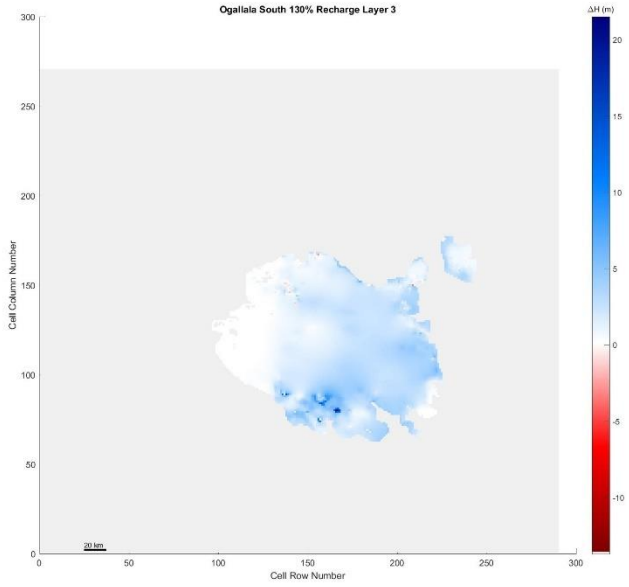

Figure 5. 498 Ogallala South, 130% original recharge hydraulic head spatial distribution of layer 3

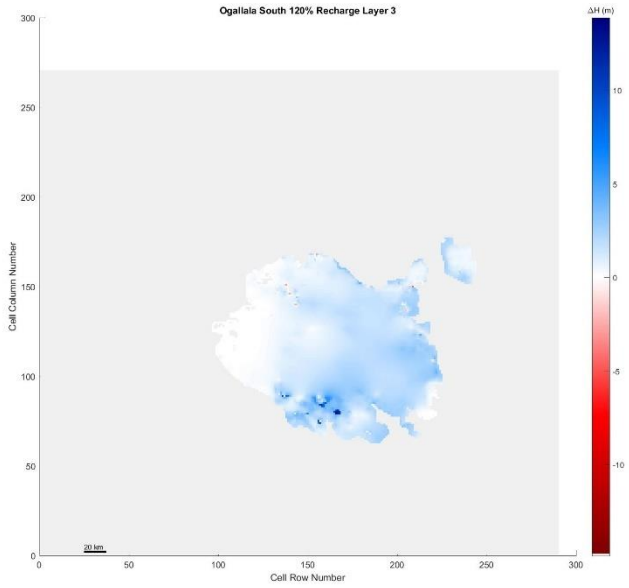

Figure 5. 499 Ogallala South, 120% original recharge hydraulic head spatial distribution of layer 3

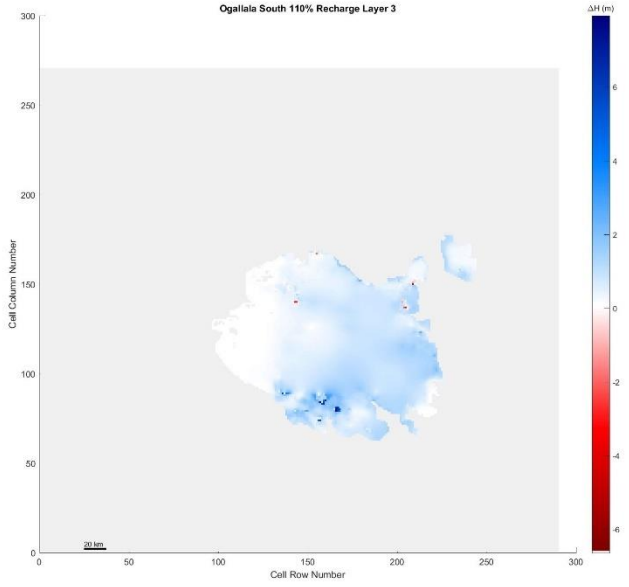

Figure 5. 500 Ogallala South, 110% original recharge hydraulic head spatial distribution of layer 3

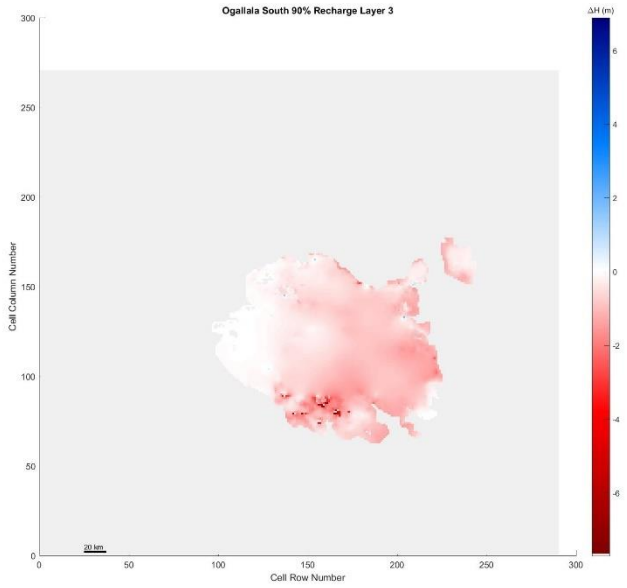

Figure 5. 501 Ogallala South, 90% original recharge hydraulic head spatial distribution of layer 3

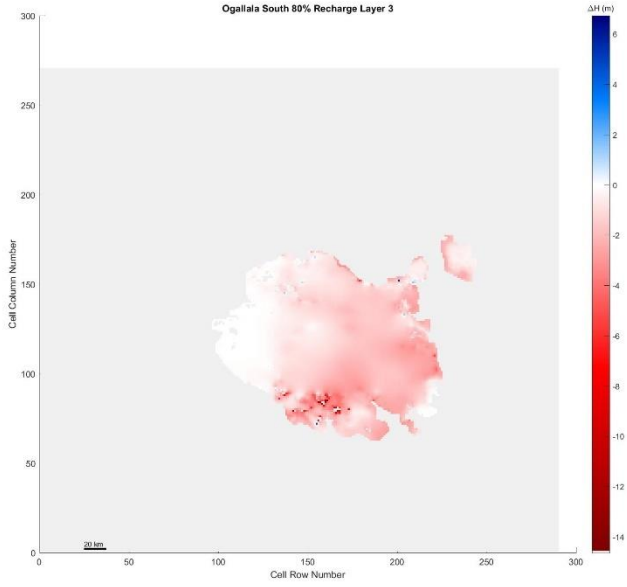

Figure 5. 502 Ogallala South, 80% original recharge hydraulic head spatial distribution of layer 3

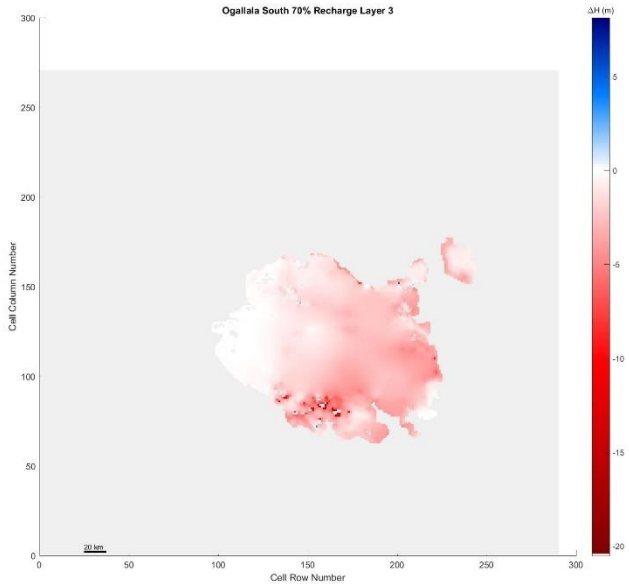

Figure 5. 503 Ogallala South, 70% original recharge hydraulic head spatial distribution of layer 3

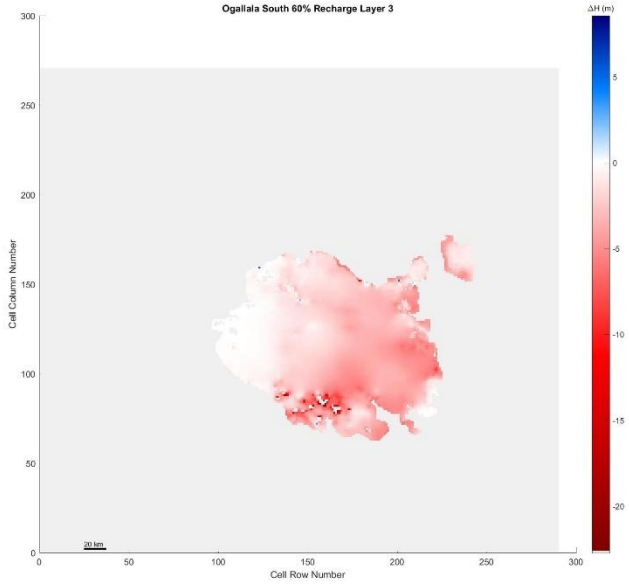

Figure 5. 504 Ogallala South, 60% original recharge hydraulic head spatial distribution of layer 3

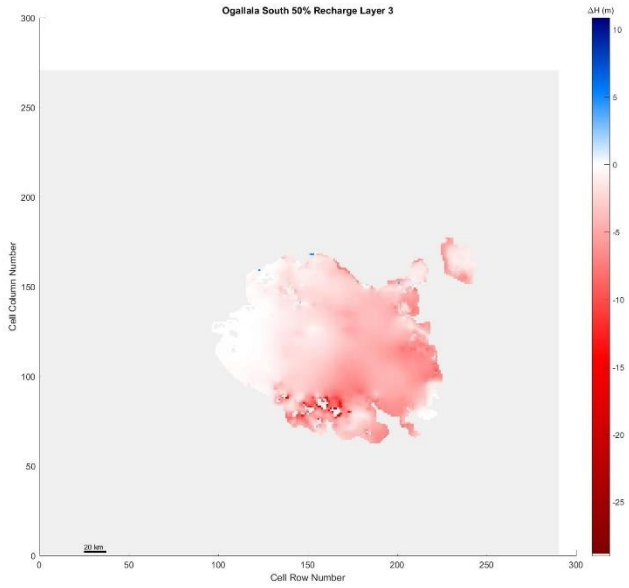

Figure 5. 505 Ogallala South, 50% original recharge hydraulic head spatial distribution of layer 3

Layer 4

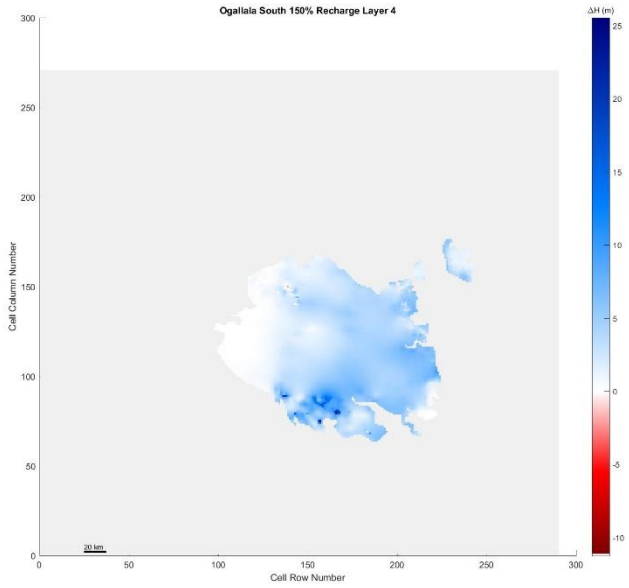

Figure 5. 506 Ogallala South, 150% original recharge hydraulic head spatial distribution of layer 4

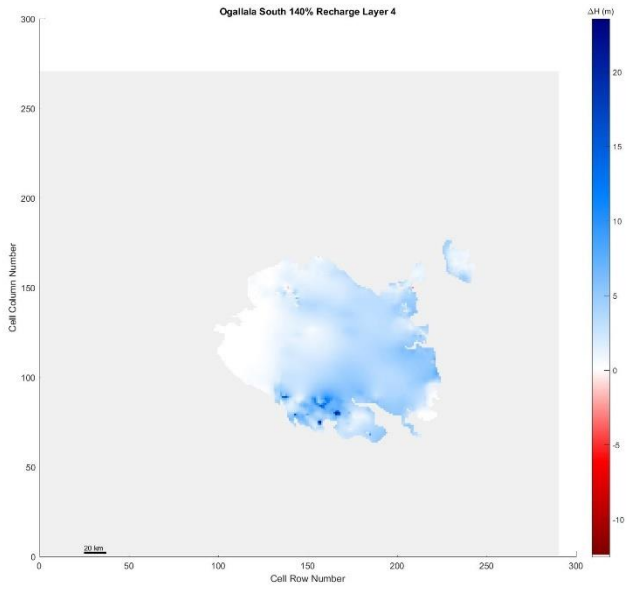

Figure 5. 507 Ogallala South, 140% original recharge hydraulic head spatial distribution of layer 4

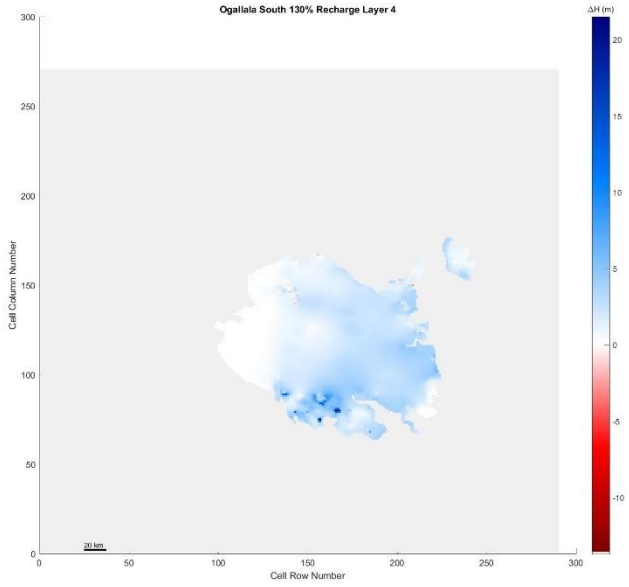

Figure 5. 508 Ogallala South, 130% original recharge hydraulic head spatial distribution of layer 4

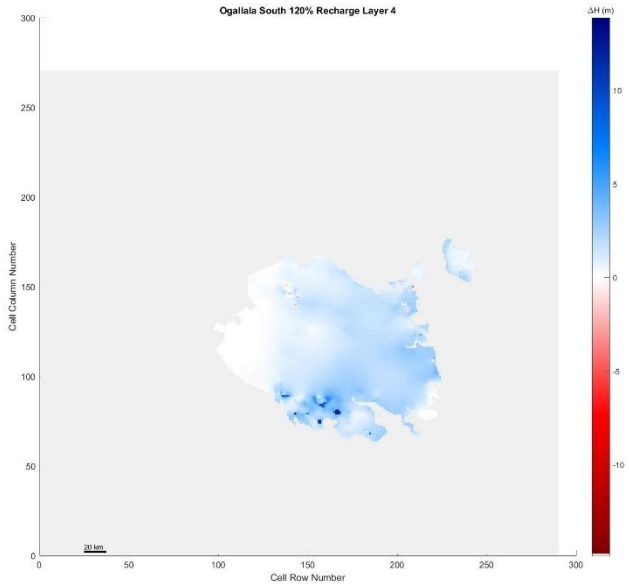

Figure 5. 509 Ogallala South, 120% original recharge hydraulic head spatial distribution of layer 4

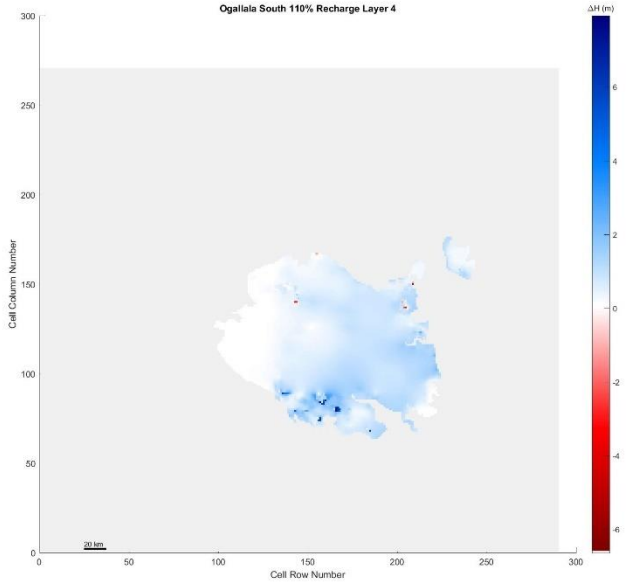

Figure 5. 510 Ogallala South, 110% original recharge hydraulic head spatial distribution of layer 4

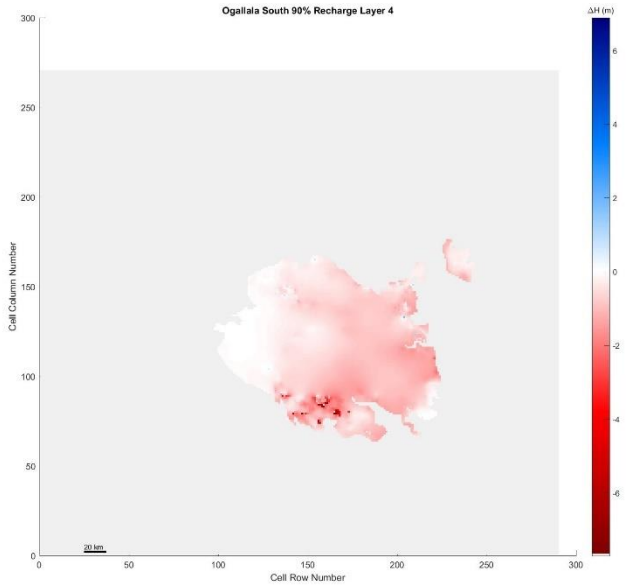

Figure 5. 511 Ogallala South, 90% original recharge hydraulic head spatial distribution of layer 4

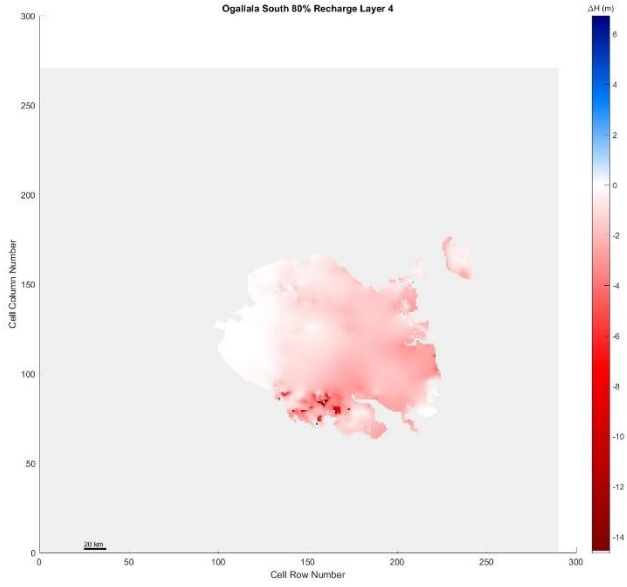

Figure 5. 512 Ogallala South, 80% original recharge hydraulic head spatial distribution of layer 4

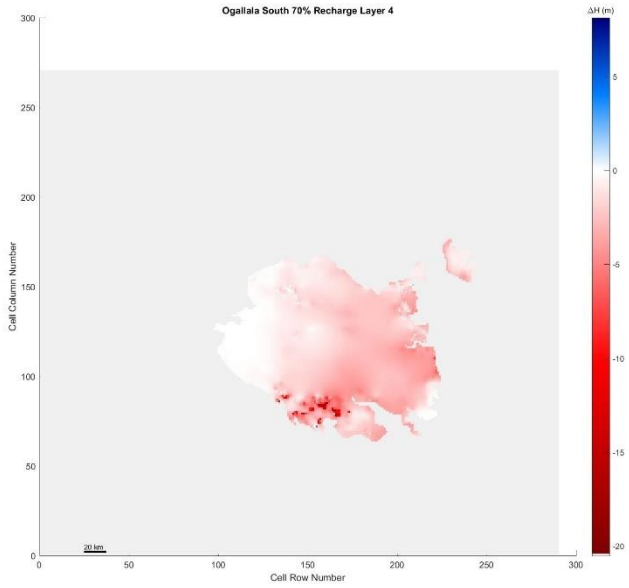

Figure 5. 513 Ogallala South, 70% original recharge hydraulic head spatial distribution of layer 4

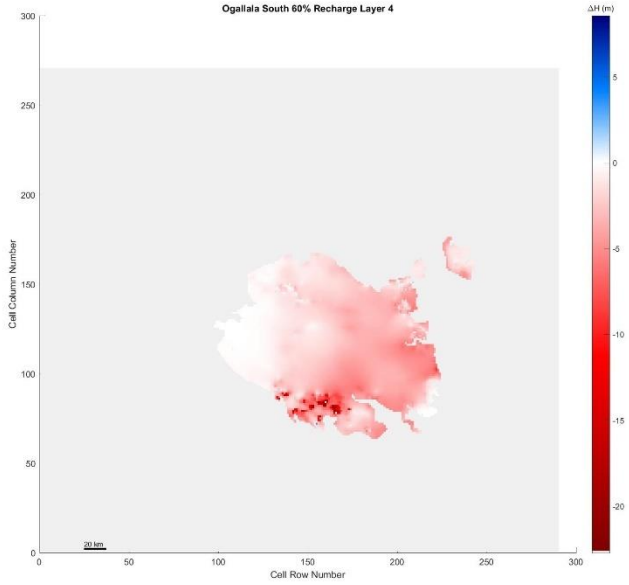

Figure 5. 514 Ogallala South, 60% original recharge hydraulic head spatial distribution of layer 4

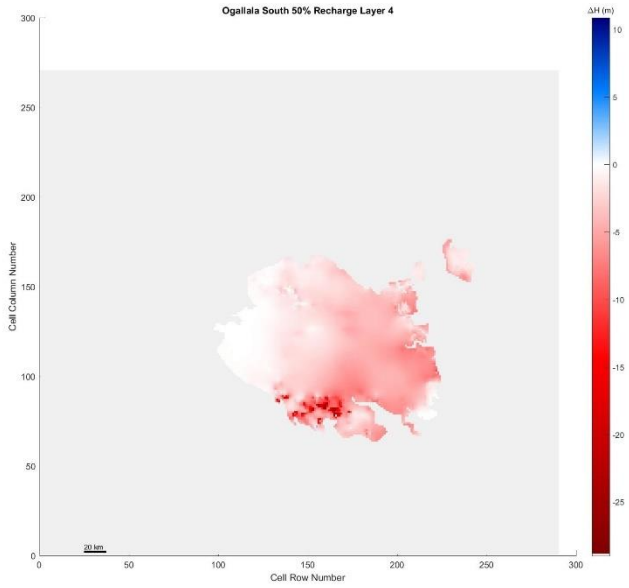

Figure 5. 515 Ogallala South, 50% original recharge hydraulic head spatial distribution of layer 4

Trinity Hill

Layer 1

Figure 5. 516 Trinity Hill, 150% original recharge hydraulic head spatial distribution of layer 1

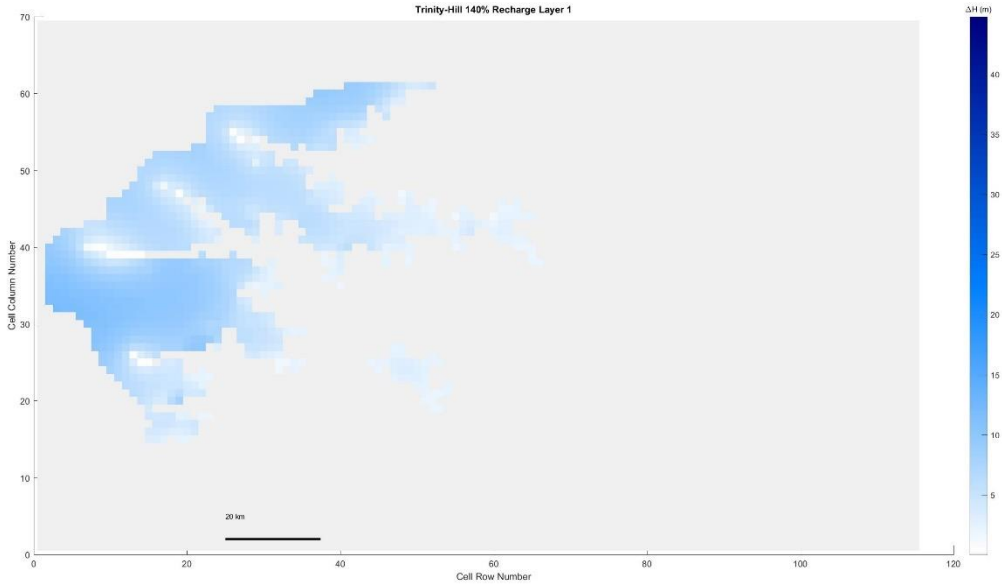

Figure 5. 517 Trinity Hill, 140% original recharge hydraulic head spatial distribution of layer 1

Figure 5. 518 Trinity Hill, 130% original recharge hydraulic head spatial distribution of layer 1

Figure 5. 519 Trinity Hill, 120% original recharge hydraulic head spatial distribution of layer 1

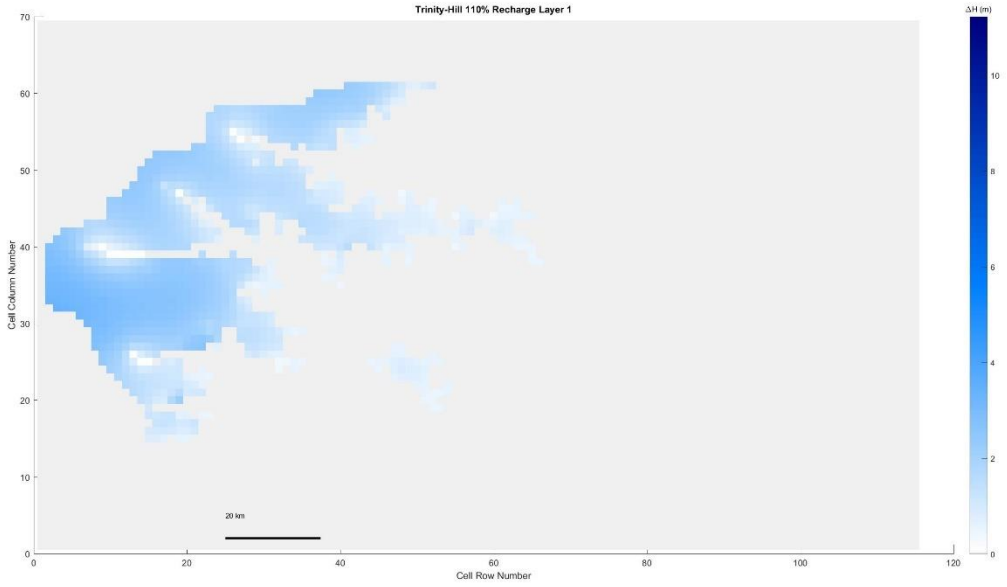

Figure 5. 520 Trinity Hill, 110% original recharge hydraulic head spatial distribution of layer 1

Figure 5. 521 Trinity Hill, 90% original recharge hydraulic head spatial distribution of layer 1

Figure 5. 522 Trinity Hill, 80% original recharge hydraulic head spatial distribution of layer 1

Figure 5. 523 Trinity Hill, 70% original recharge hydraulic head spatial distribution of layer 1

Figure 5. 524 Trinity Hill, 60% original recharge hydraulic head spatial distribution of layer 1

Figure 5. 525 Trinity Hill, 50% original recharge hydraulic head spatial distribution of layer 1

Layer 2

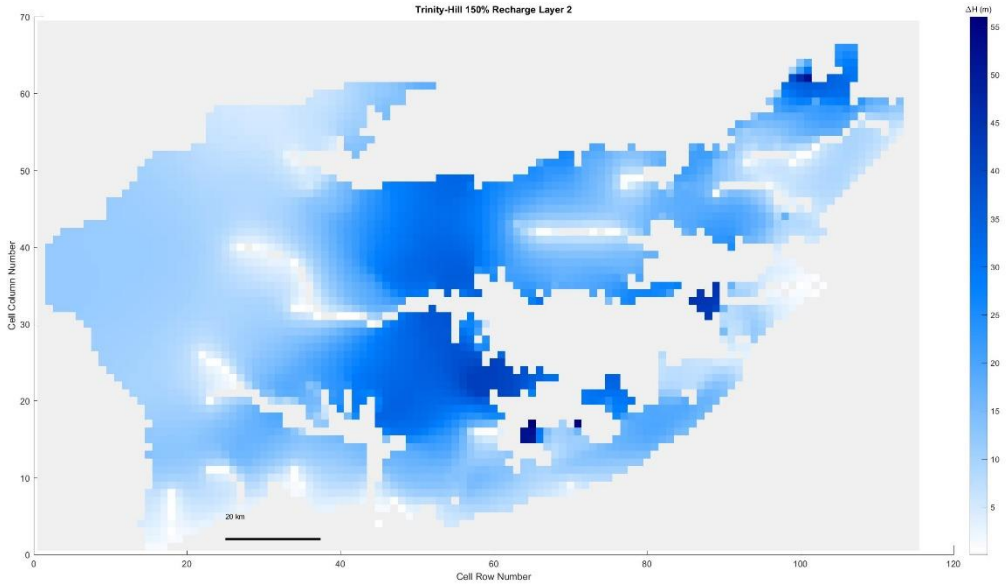

Figure 5. 526 Trinity Hill, 150% original recharge hydraulic head spatial distribution of layer 2

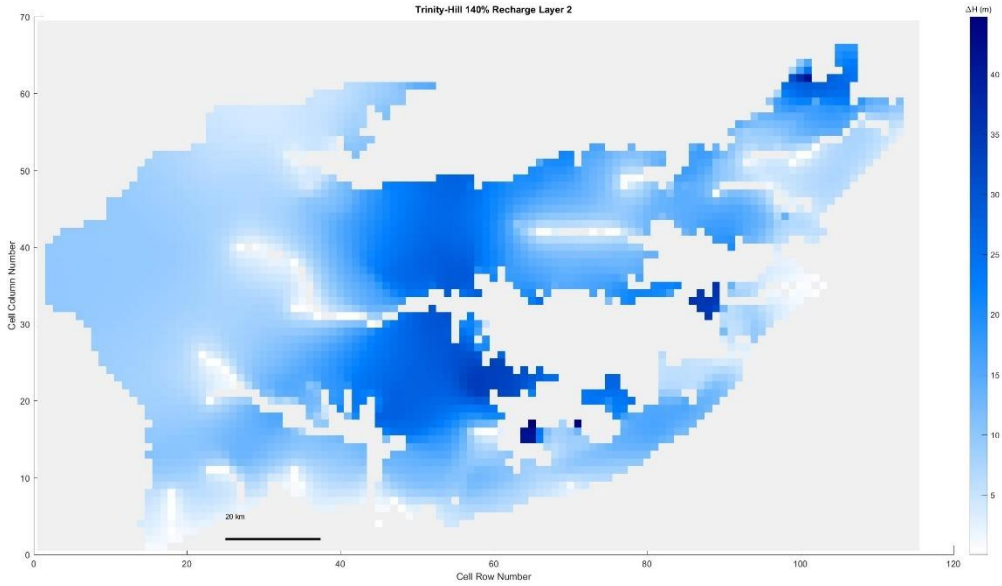

Figure 5. 527 Trinity Hill, 140% original recharge hydraulic head spatial distribution of layer 2

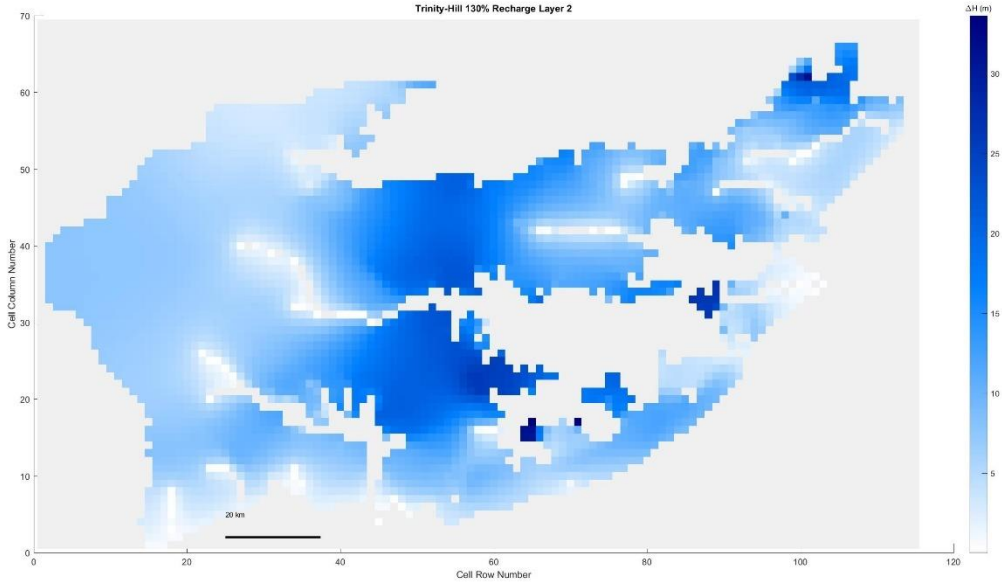

Figure 5. 528 Trinity Hill, 130% original recharge hydraulic head spatial distribution of layer 2

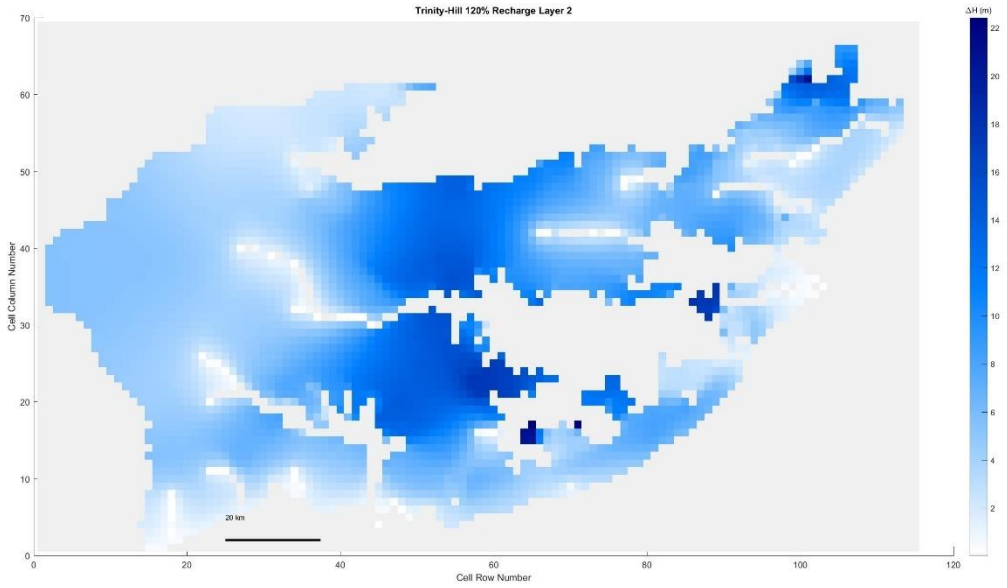

Figure 5. 529 Trinity Hill, 120% original recharge hydraulic head spatial distribution of layer 2

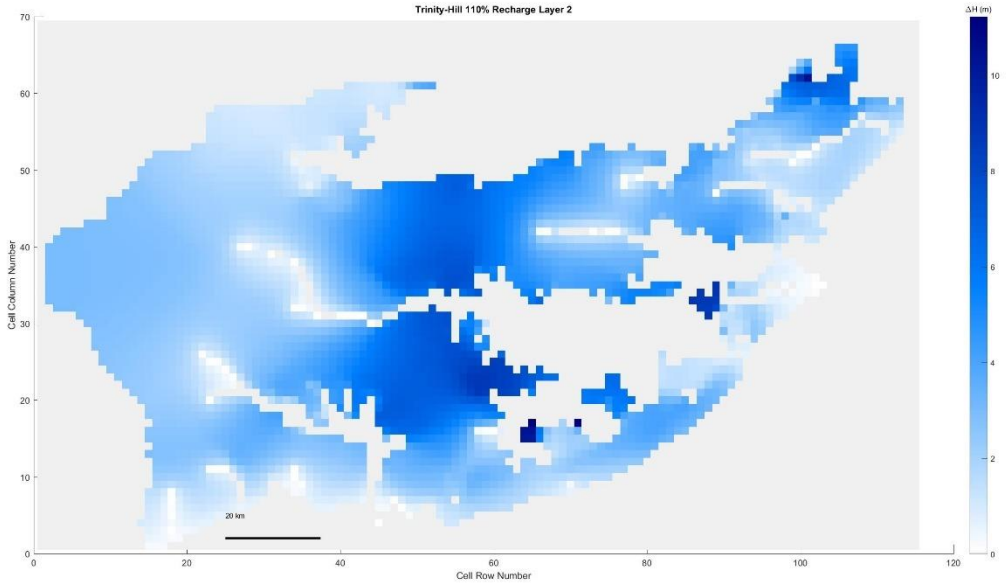

Figure 5. 530 Trinity Hill, 110% original recharge hydraulic head spatial distribution of layer 2

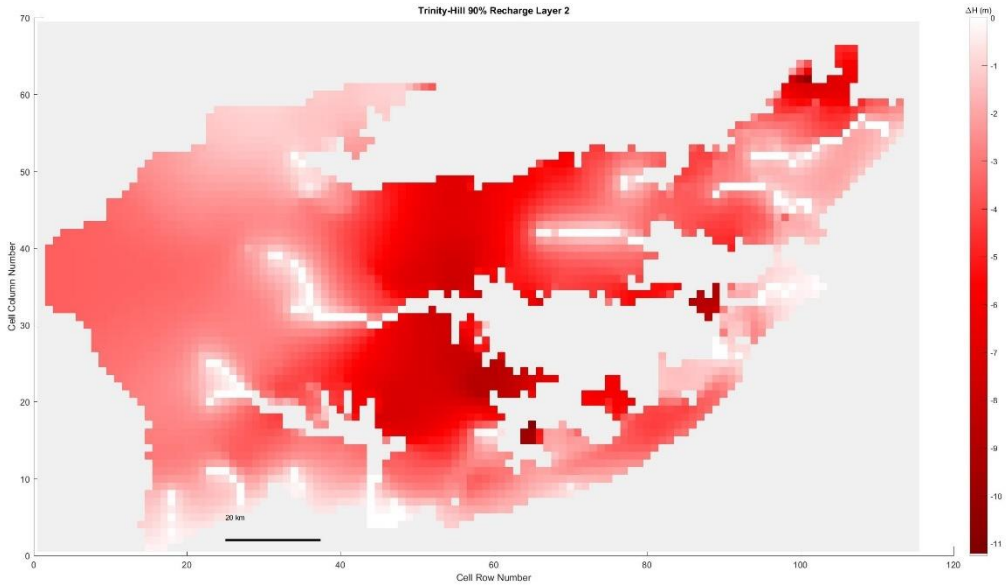

Figure 5. 531 Trinity Hill, 90% original recharge hydraulic head spatial distribution of layer 2

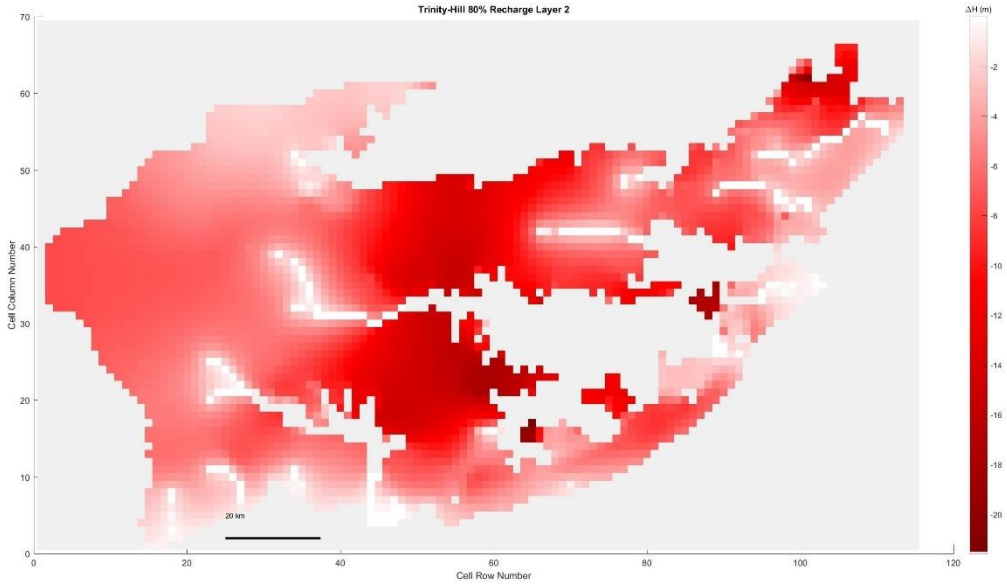

Figure 5. 532 Trinity Hill, 80% original recharge hydraulic head spatial distribution of layer 2

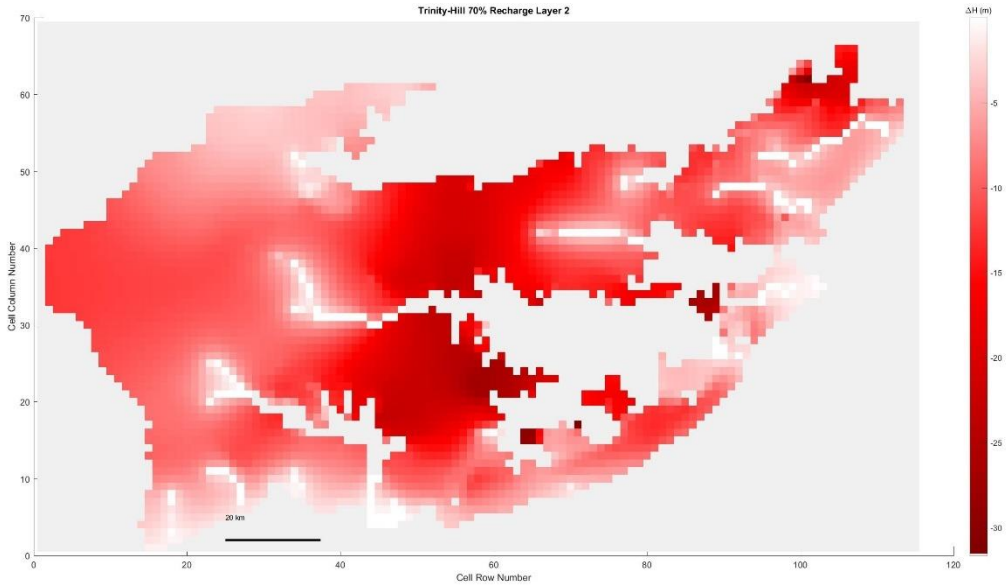

Figure 5. 533 Trinity Hill, 70% original recharge hydraulic head spatial distribution of layer 2

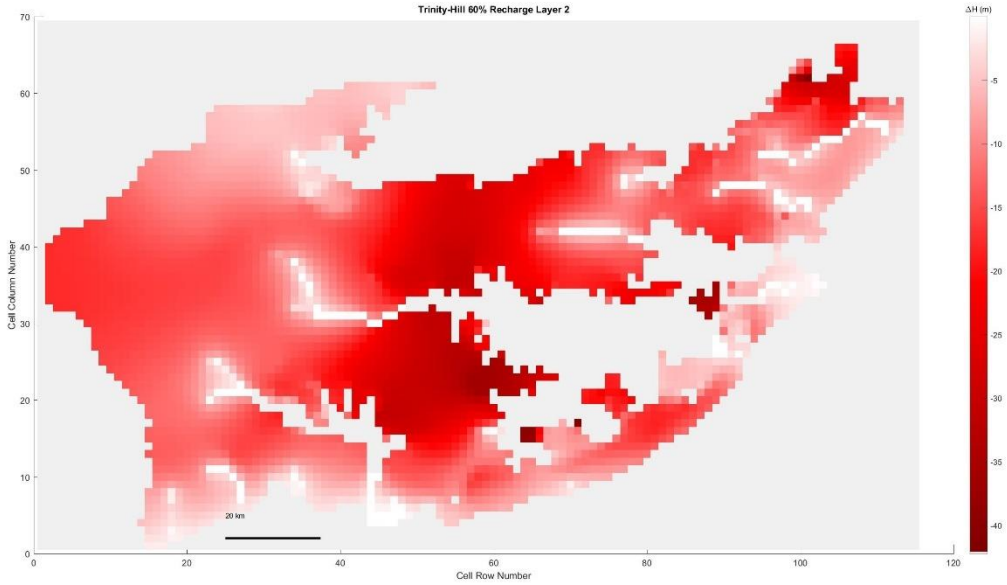

Figure 5. 534 Trinity Hill, 60% original recharge hydraulic head spatial distribution of layer 2

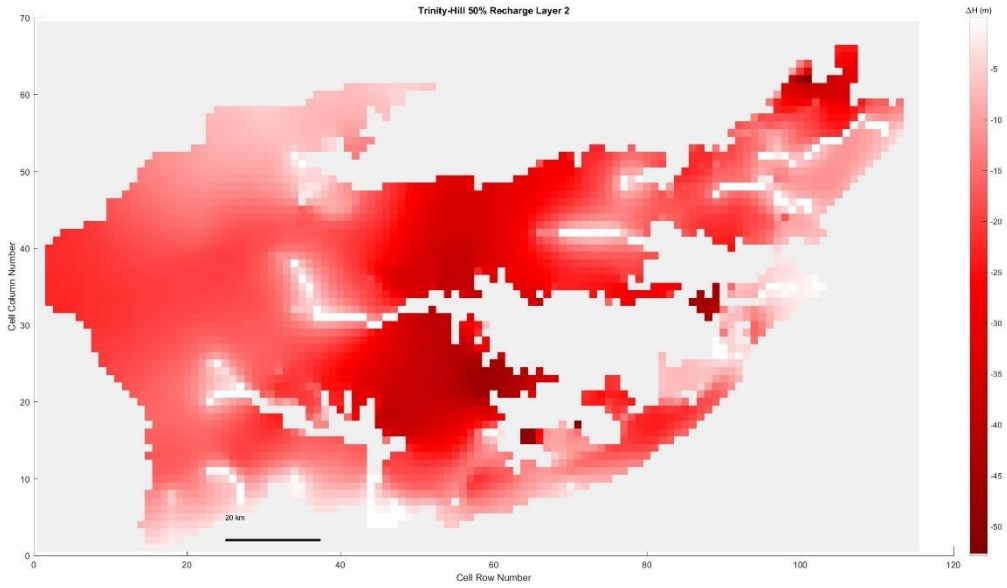

Figure 5. 535 Trinity Hill, 50% original recharge hydraulic head spatial distribution of layer 2

Layer 3

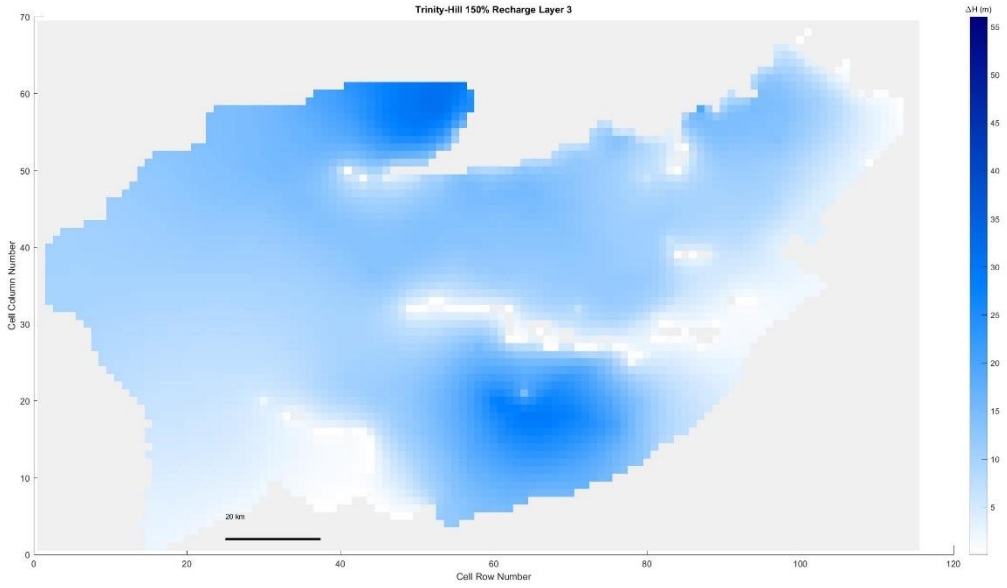

Figure 5. 536 Trinity Hill, 150% original recharge hydraulic head spatial distribution of layer 3

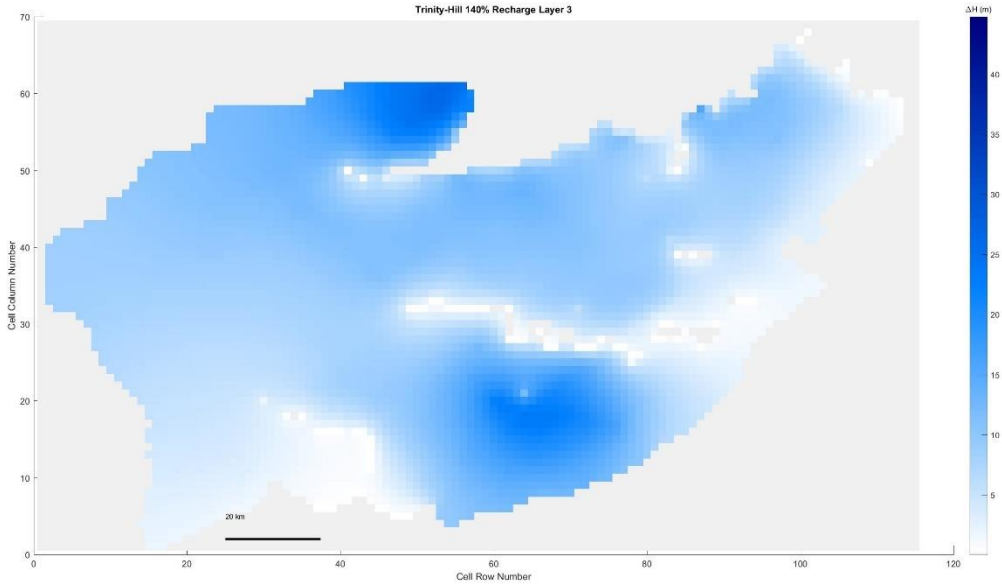

Figure 5. 537 Trinity Hill, 140% original recharge hydraulic head spatial distribution of layer 3

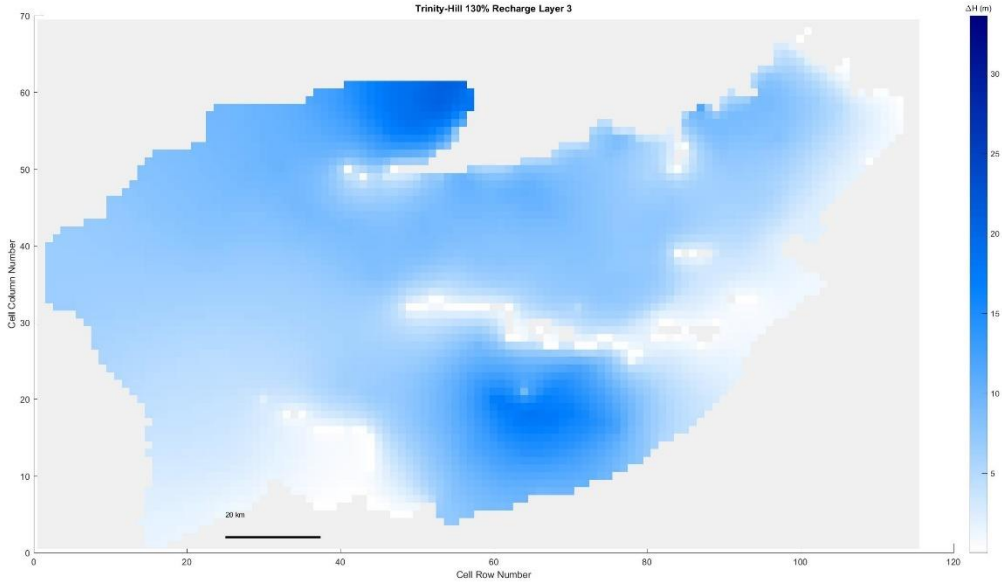

Figure 5. 538 Trinity Hill, 130% original recharge hydraulic head spatial distribution of layer 3

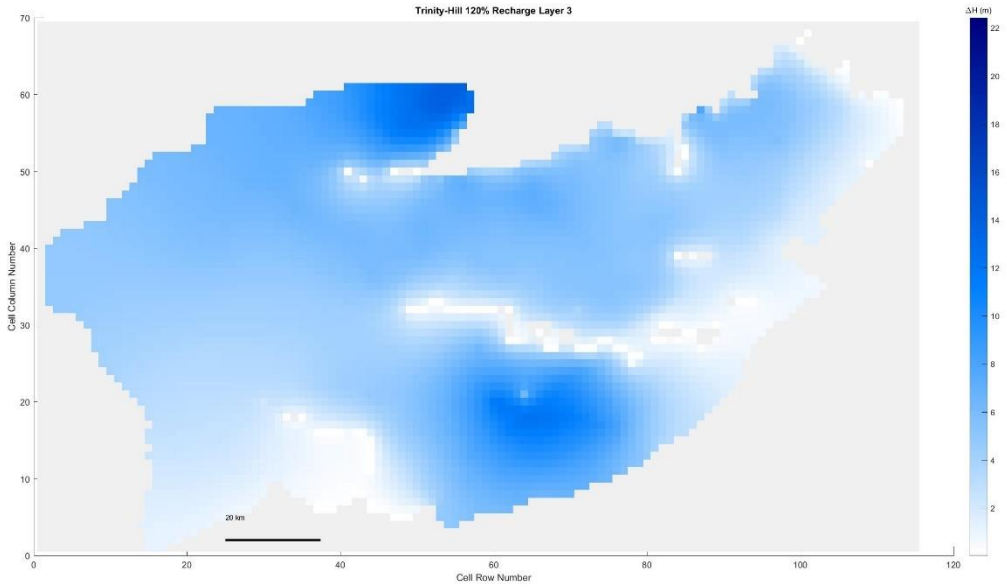

Figure 5. 539 Trinity Hill, 120% original recharge hydraulic head spatial distribution of layer 3

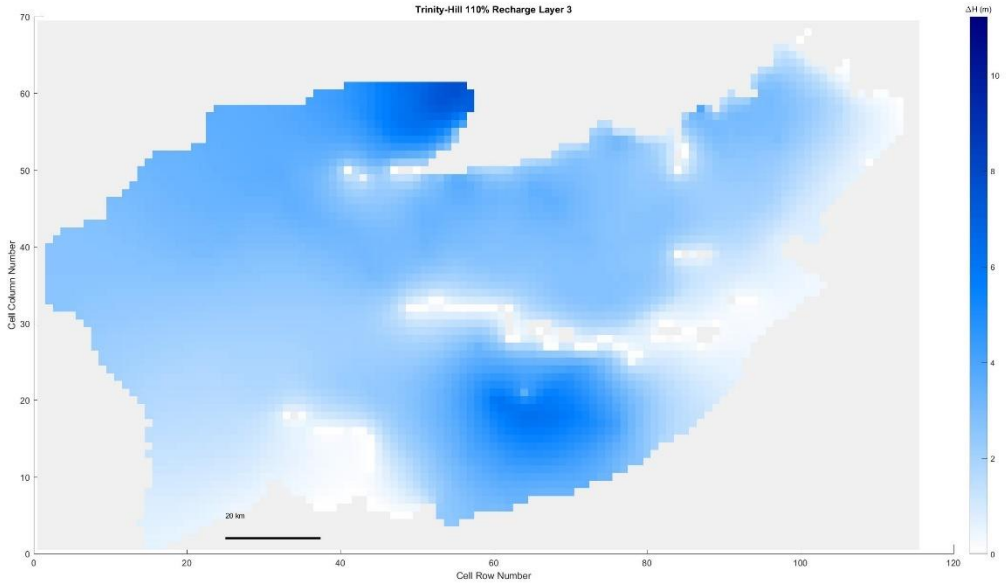

Figure 5. 540 Trinity Hill, 110% original recharge hydraulic head spatial distribution of layer 3

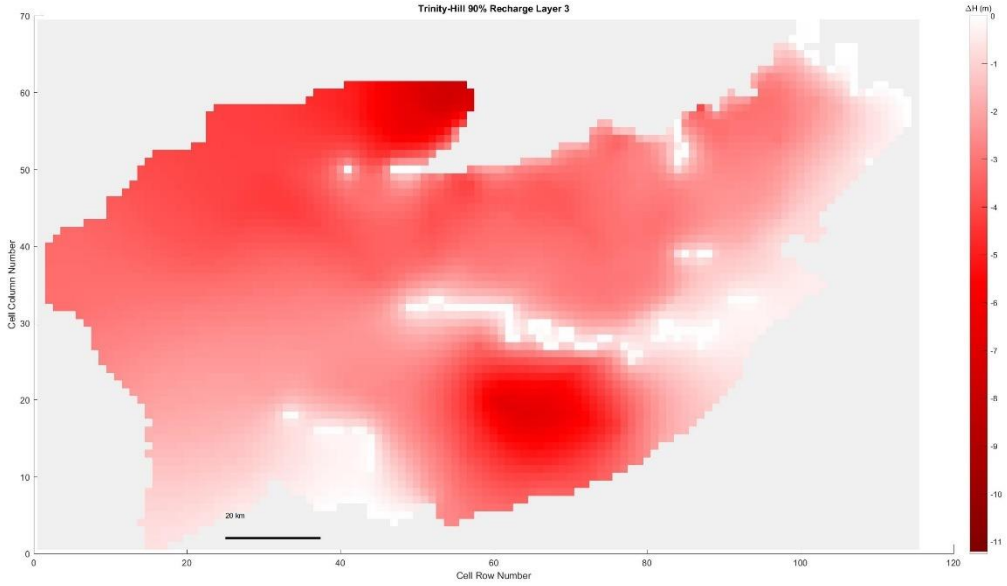

Figure 5. 541 Trinity Hill, 90% original recharge hydraulic head spatial distribution of layer 3

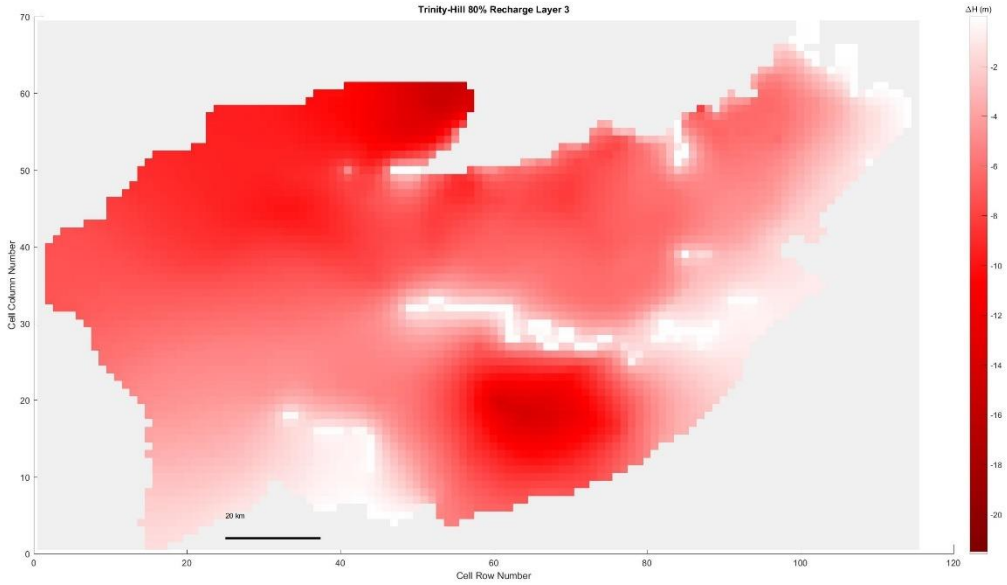

Figure 5. 542 Trinity Hill, 80% original recharge hydraulic head spatial distribution of layer 3

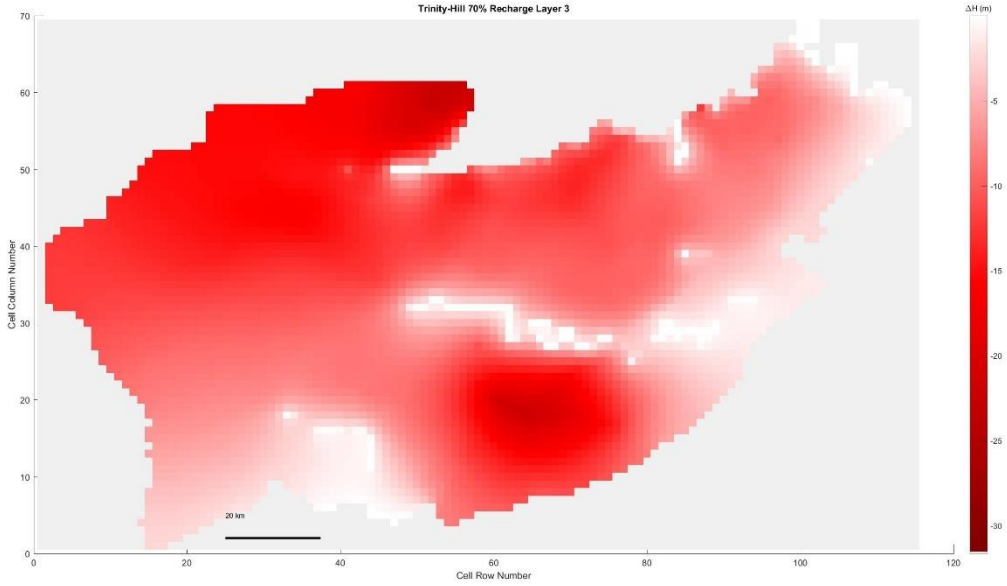

Figure 5. 543 Trinity Hill, 70% original recharge hydraulic head spatial distribution of layer 3

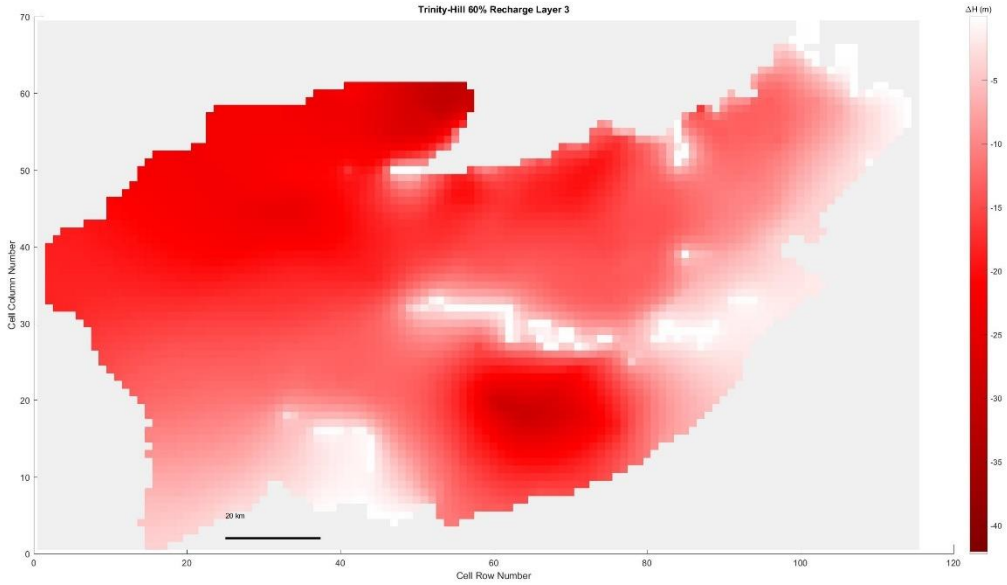

Figure 5. 544 Trinity Hill, 60% original recharge hydraulic head spatial distribution of layer 3

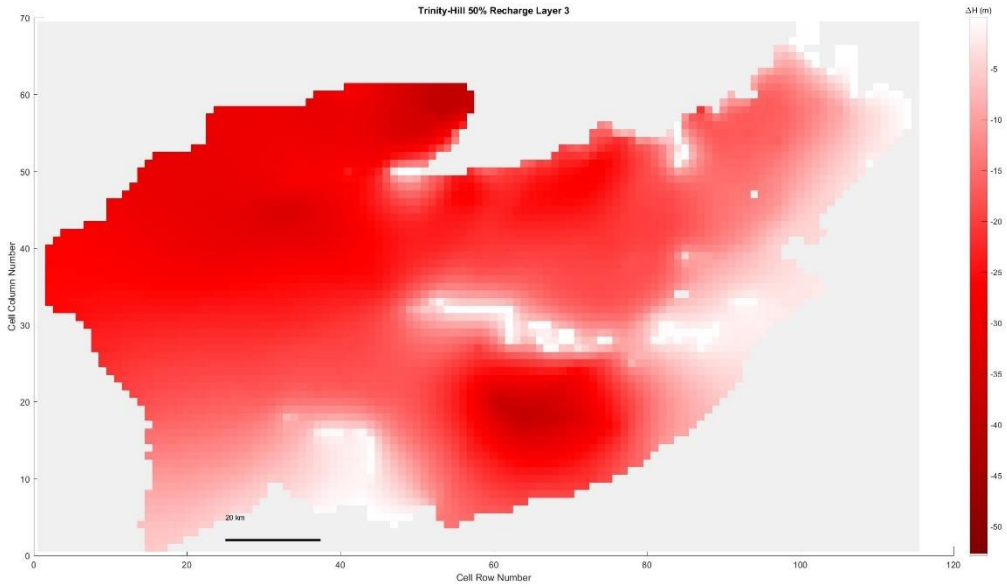

Figure 5. 545 Trinity Hill, 50% original recharge hydraulic head spatial distribution of layer 3

Layer 4

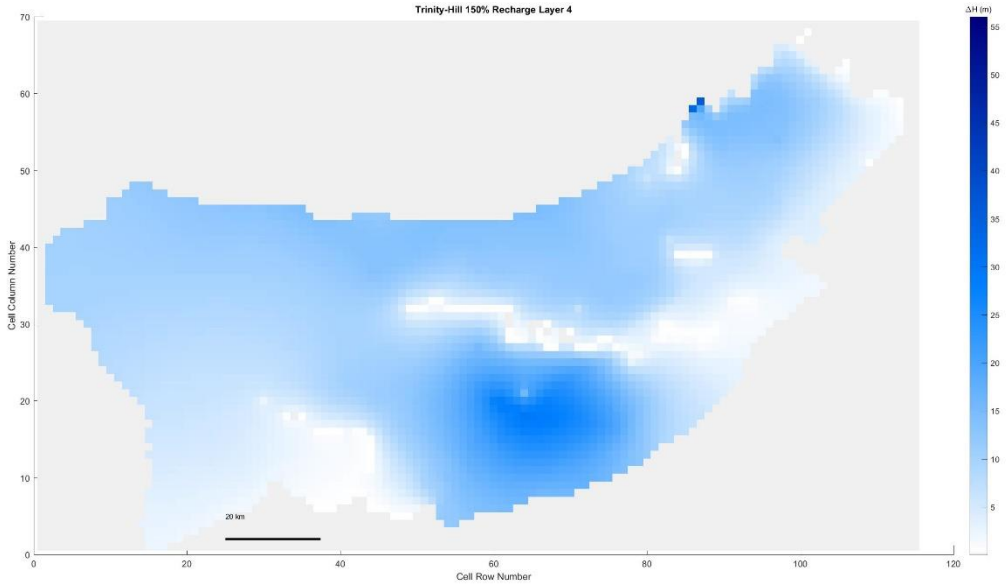

Figure 5. 546 Trinity Hill, 150% original recharge hydraulic head spatial distribution of layer 4

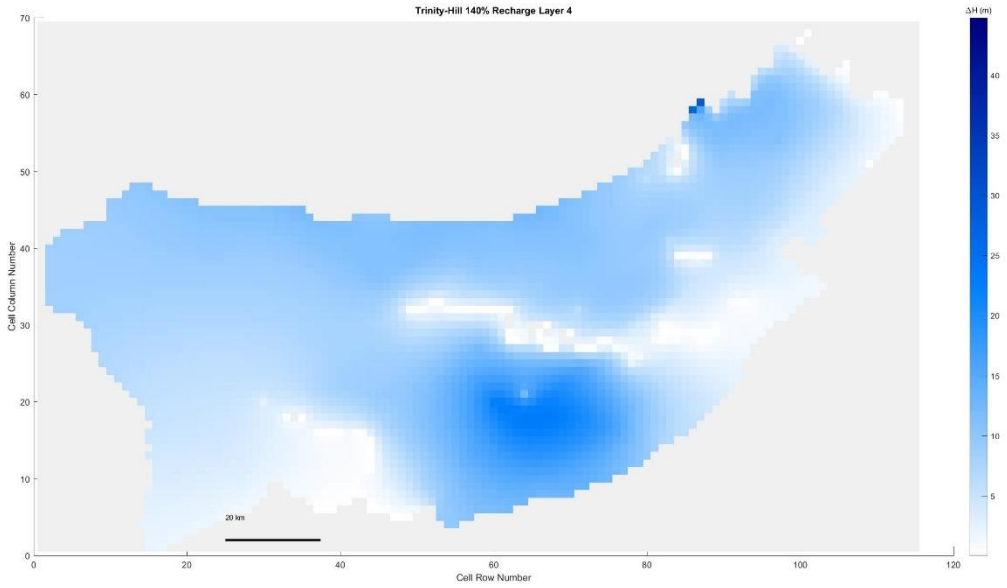

Figure 5. 547 Trinity Hill, 140% original recharge hydraulic head spatial distribution of layer 4

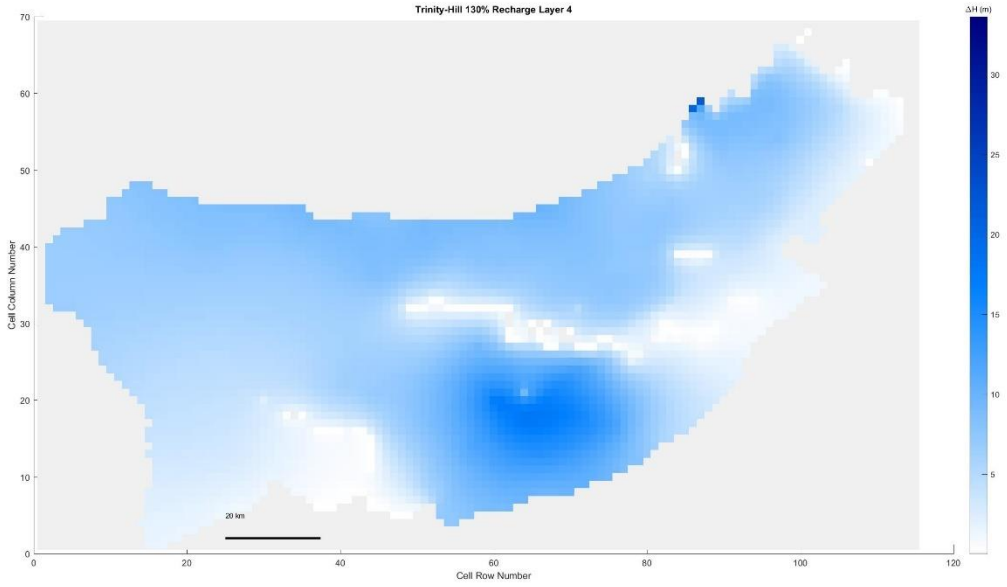

Figure 5. 548 Trinity Hill, 130% original recharge hydraulic head spatial distribution of layer 4

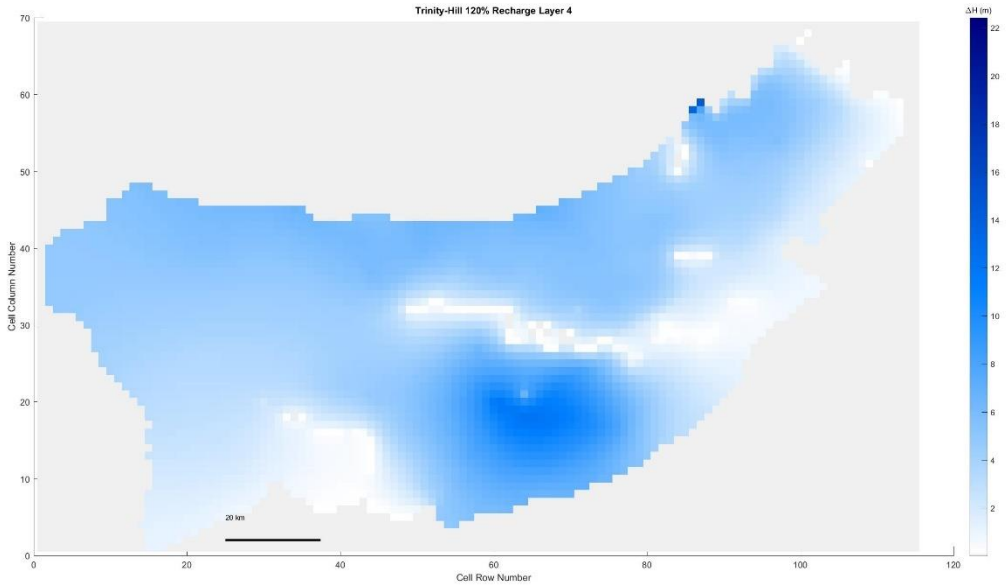

Figure 5. 549 Trinity Hill, 120% original recharge hydraulic head spatial distribution of layer 4

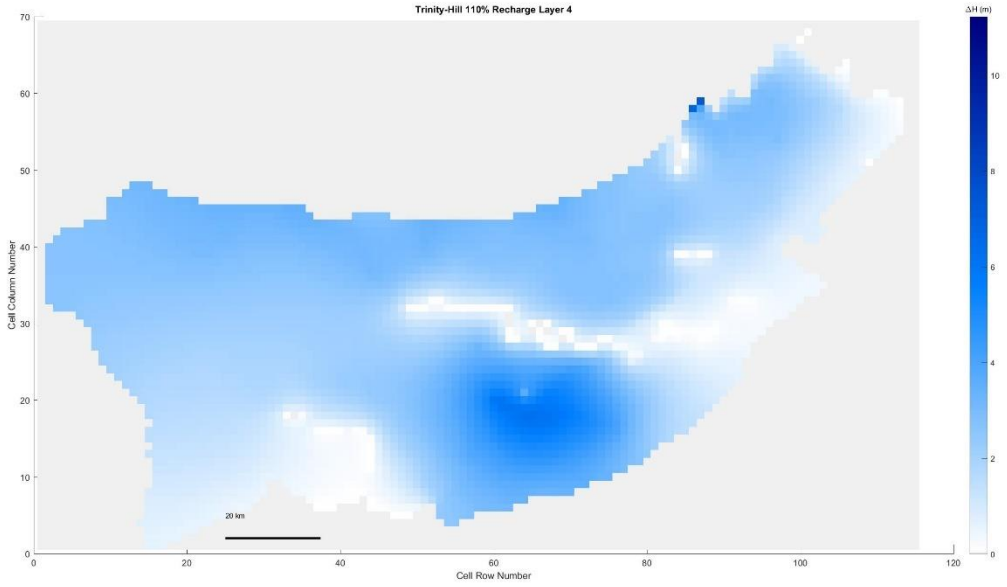

Figure 5. 550 Trinity Hill, 110% original recharge hydraulic head spatial distribution of layer 4

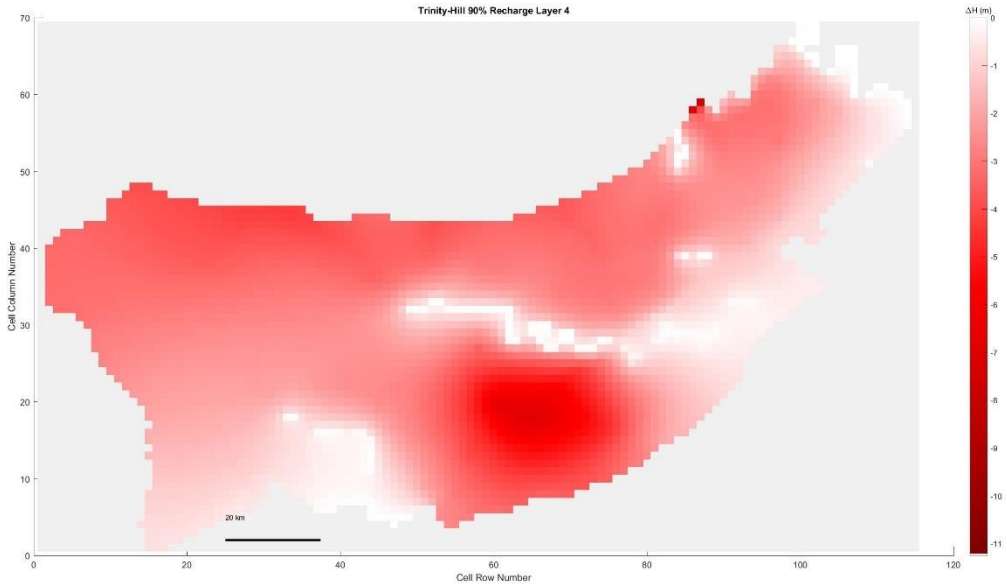

Figure 5. 551 Trinity Hill, 90% original recharge hydraulic head spatial distribution of layer 4

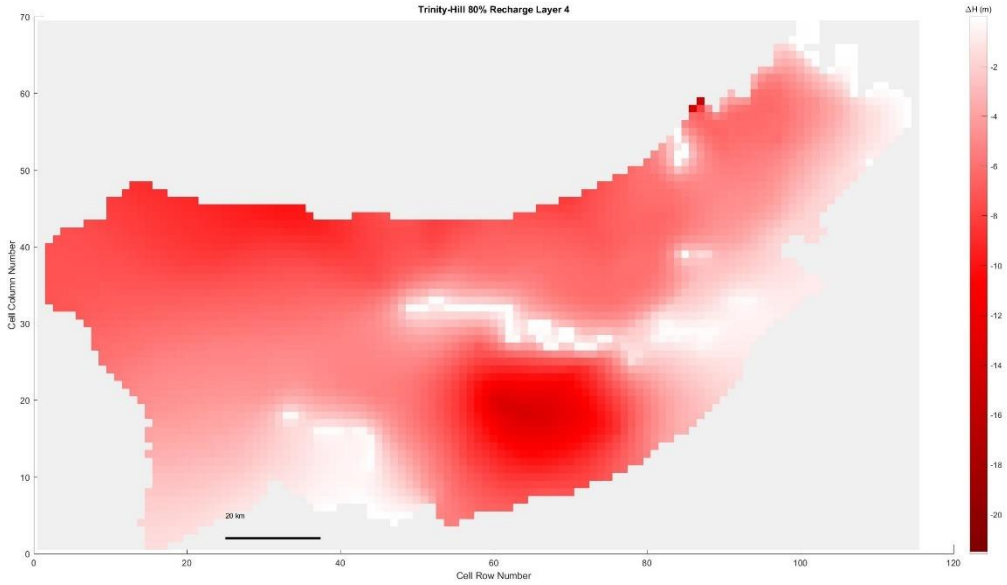

Figure 5. 552 Trinity Hill, 80% original recharge hydraulic head spatial distribution of layer 4

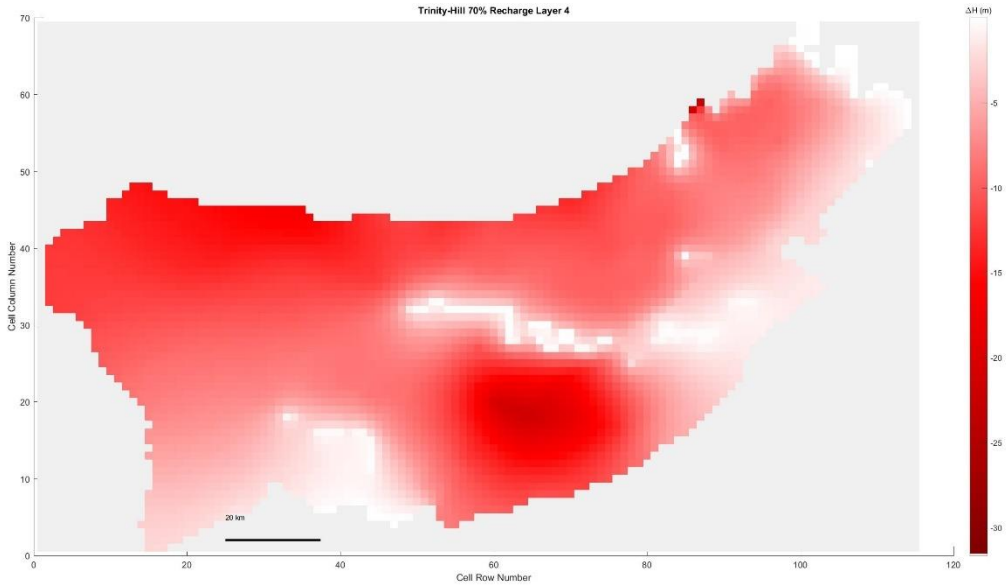

Figure 5. 553 Trinity Hill, 70% original recharge hydraulic head spatial distribution of layer 4

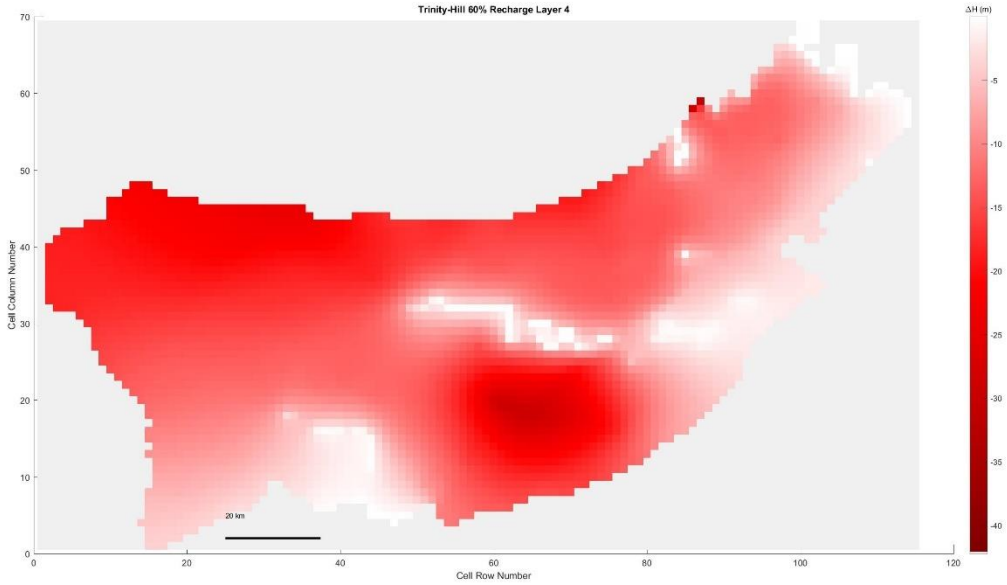

Figure 5. 554 Trinity Hill, 60% original recharge hydraulic head spatial distribution of layer 4

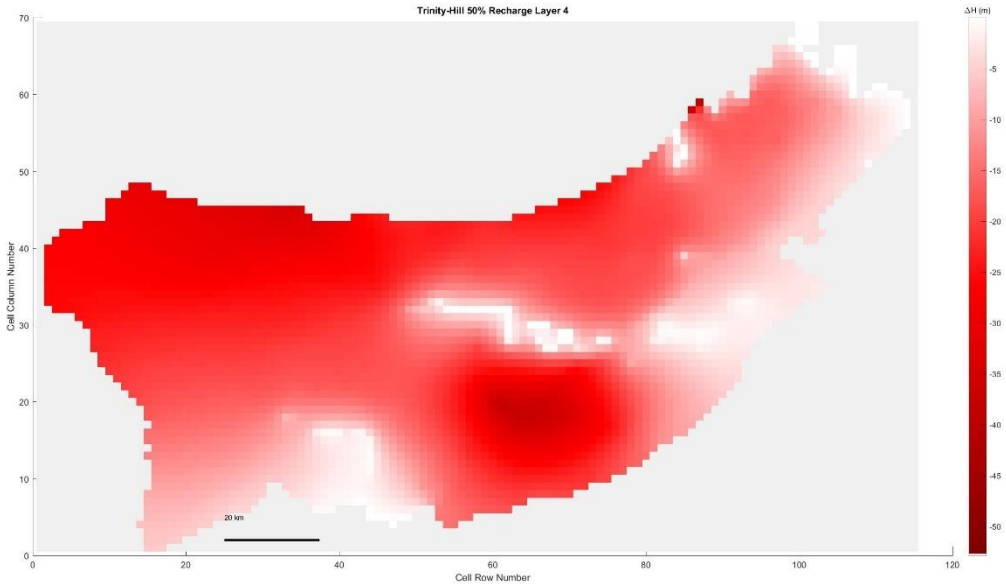

Figure 5. 555 Trinity Hill, 50% original recharge hydraulic head spatial distribution of layer 4